Supramolecular Architectures with Functionalised Host Ligands

James John Henkelis

Submitted in accordance with the requirements for the degree of

Doctor of Philosophy

The University of Leeds

School of Chemistry

July 2014

The candidate confirms that the work submitted is his/her own, except where work which has formed part of or jointly-authored publications has been included. The contribution of the candidate and the other authors to this work has been explicitly indicated below. The candidate confirms that appropriate credit has been given within the thesis where reference has been made to the work of others.

References for the jointly authored papers include:

J. J. Henkelis, T. K. Ronson, L. P. Harding and M. J. Hardie, 'M_3L_2 metallo-cryptophanes: [2]catenane and simple cages', *Chem. Commun*. **2011**, *47*, 6560-6562. Article published as part of a special issue on Supramolecular Chemistry.

J. J. Henkelis, L. P. Harding and M. J. Hardie, 'Coordination Polymers Utilizing *N*-Oxide Functionalised Host Ligands', *Inorg. Chem*. **2012**, *51*, 10657-10674.

J. J. Henkelis, T. K. Ronson and M. J. Hardie, 'Lanthanide coordination polymers with pyridyl-*N*-oxide or carboxylate functionalised host ligands', *CrystEngComm*. **2014**, *16*, 3688-3693. Article published as part of a special issue on Structural Macrocyclic Supramolecular Chemistry.

J. J. Henkelis, S. L. Warriner, J. Fisher and M. J. Hardie, 'Solvent-dependent chiral speciation behaviour and speciation control of Pd_6L_8 metallo-supramolecular cages', *Chem. Eur. J*. **2014**, *20*, 4117-4125.

J. J. Henkelis and M. J. Hardie, 'tuning the coordination chemistry of cyclotriveratrylene ligand pairs through alkyl chain aggregation', *CrystEngComm*, **2014**, DOI: 10.1039/C4CE00467A.

Acknowledgements

Firstly, I would like to thank Professor Michaele J. Hardie. It has been an absolute pleasure working for you on what has been a highly enjoyable and rewarding research project and I thank you for the opportunity. I am extremely grateful for all of the support given over the last three years and the invaluable training which you have provided.

I must also thank Dr Julie Fisher for all her help and advice given in the collection and interpretation of horribly broad NMR's, and to Drs Stuart Warriner and Lindsay Harding (University of Huddersfield) for their expertise in mass spectrometry.

I would also like to thank a few Hardie group veterans, with special mention to Tanya Ronson for much of my early practical training and to Tia Jacobs for keeping me in check and ensuring that the lab was run like the military. I must also thank Marc Albus Little for his talents as a laboratory manager and for helping us 'party' in Liverpool city centre.

A huge thank you is extended to all the current members of Lab 1.32. Especially to Flora and Vikki for making this lab a hilarious place of work, and who's unusual love of coins, flowers and the tour de France have made for good banter. Likewise, thanks go to Heba for deciphering the occasional hieroglyphic and to Mike and Jordan for being the broadest and tallest gentlemen to ever set foot in the office. You will all be missed.

Massive thanks go out to my homeboys, Ben and Jonny, it has been a great three-and-a-bit years working alongside you both. You certainly carried me along at times and it wouldn't have been the same without you. Jonny's ability to pull off moccasins and a cardigan without somebody noticing and Ben's ability to grow a sumptuous moustache will not be forgotten.

I also extend my thanks to all members of the Halcrow, Willans, McGowan and Wilson groups, in addition to all the technical staff here at Leeds and to the Charles Brotherton Trust for financial support.

I would like to thank all family members, especially Mum and Dad, for teaching me the value of hard work and for their unwavering support. I should also thank you for 'diverting' me away from a sports science degree all those years ago! I hope that I have made you proud.

My final and most important thanks are to my best friend and fiancée, Nic. Without you this PhD would have not been possible and I owe you more than you realise. I dedicate this achievement to you.

Abstract

This thesis concerns the rational design and controlled self-assembly of supramolecular architectures for application in areas such as molecular recognition. The research focuses on the cyclotriveratrylene family of molecular hosts, where their incorporation into both polyhedral and polymeric assemblies bestows hosting ability to the complexes isolated.

A novel pyridine-*N*-oxide ligand library has been prepared and the first examples of formal coordination polymers of the lanthanide(III) cations are subsequently reported. Their self-assembly was extended to the transition metals and a variety of coordination complexes were isolated that feature uncommon network topologies and structurally aesthetic motifs, such as large internal pore spaces.

The combined effects of ligand solubility and rigidity were investigated and used to rationalise the selective isolation of a homochiral, triply-interlocked [2]-catenane over simple capsular assemblies. This was further exemplified in the isolation of a metastable cage complex which underwent a symmetry-induced inter-cage transformation to afford a much larger, polyhedral complex. The solution-phase chemistry of these cages was further investigated and a sophisticated assembly/disassembly cycle was determined.

A stable family of cage complexes has been prepared using classical organometallic chemistry and self-assembly processes. Such cages were highly stable and their formation was observed to be cooperative. The solid state host-guest chemistry of these species was investigated, where they were observed to uptake various guests, including gaseous iodine, in a single-crystal-to-single-crystal manner.

Table of Contents

List of Figures

List of Schemes

List of Tables

List of Abbreviations

Å	Angstrom
Ar	Aryl
$^{13}C\{^{1}H\}$	Proton-decoupled Carbon (NMR)
^{o} C	Degrees Celcius
CTC	Cyclotricatechylene
CTG	Cyclotriguaiacylene
CTV	Cyclotriveratrylene
δ	Chemical shift
DCB	Dichlorobenzene
DMF	*N,N'*-dimethylformamide
DMSO	Dimethylsulfoxide
DOSY	Diffusion-Ordered NMR Spectroscopy
dppb	1,2-*bis*(diphenylphosphino)benzene
dppe	1,2-*bis*(diphenylphosphino)ethane
EDX	Energy Dispersive X-ray
en	Ethylenediamine
ES	Electrospray
e.s.d.	Estimated standard deviation
et al.	*et alia* (and others)
fac	Facial
Fc	Ferrocene
Hz	Hertz
IR	Infrared
J	Coupling constant (NMR)
K	Kelvin
L	Ligand
m	*meta*
m/z	Mass to charge ratio
MeCN	Acetonitrile
$MeNO_2$	Nitromethane
mer	Meridional
MOF	Metal-organic framework
MS	Mass spectrometry
NHC	*N*-heterocyclic carbene
NMP	*N*-methylpyrrolidone

NMR	Nuclear Magnetic Resonance
NOESY	Nuclear Overhauser Effect spectroscopy
o	*ortho*
p	*para*
Ph	Phenyl
ppm	parts per million
Py	Pyridine
S	Goodness of fit
T	Temperature
tert	Tertiary
TGA	Thermogravimetric analysis
THF	Tetrahydrofuran
TTF	Tetrathiafulvalene

Chapter 1

Introduction

1.1 Overview

Work presented in this thesis details the synthesis of novel cyclotriveratrylene (CTV) derivatives and their subsequent employment in the preparation of metallo-supramolecular assemblies. This chapter will introduce the reader to the field of supramolecular chemistry, outline the core principles and describe its development based on current, topical literature. It will provide context and indicate both the relevance and significance of the research reported to the field of supramolecular chemistry.

1.2 Supramolecular chemistry

The existence of forces between molecules was realised by Johannes van der Waals in 1873.[1] How they interact, with particular emphasis on complementarity and specificity, was later postulated by Herman E. Fischer in the late 19th century.[2] It wasn't until decades later, however, that Jean-Marie Lehn would pioneer the field of 'supramolecular chemistry' – the chemistry of the intermolecular bond.[3] Supramolecular chemistry (from the Latin *supra*, meaning beyond) uses these relatively weak and dynamic intermolecular interactions [4] to control the spatial arrangement of molecular components in a given *übermoleküle*, or supermolecule.[5] Lehn went on to summarise this phenomenon as "chemistry beyond the molecule, the science of non-covalent interactions", meaning: the spontaneous self-assembly of one or more molecular subunits to form a complex *via* weak but cooperative non-covalent interactions.[6] Following receipt of the Nobel Prize, shared by Cram, Lehn and Pedersen in 1987, supramolecular chemistry now represents a multidisciplinary field that encompasses both the physical and biological sciences that is targeted towards the construction of materials with both application and function.[7] Modern day supramolecular chemistry has grown in accordance with the availability of analytical techniques, where increasingly powerful instrumentation, such as X-ray diffraction from synchrotron sources [8] and novel solution-phase probes,[9] has enabled the elucidation of species that could not have been otherwise achieved.[10]

The formation of a supermolecule is directed by self-assembly processes.[11] George Whitesides regards this to be the "autonomous organisation of components into patterns or structures without human intervention". This is a general term that suggests self-assembly occurs on all scales and is responsible for the appearance of order from disorder, regardless of the system.[12] At the molecular level, self-assembly proceeds as the individual molecular subunits recognise one another in solution, through non-covalent interactions, to form intermediary kinetic

products that comprise the dynamic combinatorial library (DCL).[13] These form and dissipate reversibly, generally under thermodynamic control, and are recycled to form a single entity as the system spontaneously evolves towards the lowest energy conformation and a state of maximum entropy.[14] Solvation and solubility also direct self-assembly, which can lead to polymerisation and incomplete or unwanted self-assembly products. Thus, carefully pre-programming the molecular components and controlling their environment allows for some degree of predictability with regard to structural outcome.[15] For this to occur, careful consideration must be paid to the molecular components so that they interact in the manner that they were intended, otherwise the desired species may be inaccessible *via* self-assembly.[16] However, and despite meticulous efforts to control the way in which molecules interact, the results of self-assembly are often entirely serendipitous.[17]

Whilst scientists have become rather adept in "unnatural product synthesis", the most sophisticated and elegant examples of supramolecular self-assembly are found in Nature.[18] Single-stranded DNA (deoxyribose nucleic acid), for example, can locate and pair with its complementary strand with extremely high selectivity. Hydrogen bonding (A···T and C···G) and π-π stacking of nucleobases, alongside a minor solvophobic contribution, afford the double stranded helix with high fidelity.[19] Using these principles for design tools, Nadrian Seeman went on to establish the entirely new field of DNA nanotechnology.[20]

1.3 Metallo-supramolecular chemistry

Supramolecular interactions typically range from 5 to 300 kJ/mol and are cooperative. The ion-dipole coordination bond is regarded as one of the strongest intermolecular interactions, depending on the level of covalency, and therefore largely directs the formation of a metallo-supramolecular complex, with secondary interactions such as hydrogen bonding and π-π stacking attributable to structural fine tuning.[21] The degree of complementarity between metal cation and ligand, with respect to orbital suitability, preferred geometry and relative lability, allows for some amount of predictability when forming such complexes.[22]

Control over the coordination bond has allowed for a wide range of metallo-supramolecular architectures to be prepared, including coordination cages, polymers and topologically non-trivial constructs, each with unique properties and application. The field of metallo-supramolecular chemistry is now highly extensive. As such, the following is not intended to be a comprehensive review, but to introduce the pioneering research and illustrative examples that focus on host-guest chemistry, molecular recognition and catalysis.

Perhaps the first example of a well-defined architecture prepared through metal-directed self-assembly was a double-stranded helicate reported by Lehn.[23] The self-assembly of copper(I) trifluoroacetate ($CF_3CO_2^-$) and a linear *tris*(2,2'-bipyridine) ligand afforded the double-stranded helicate as a racemic mixture in near-quantitative yield, indicating the systems ability to self-sort through selection.[24] The complex was observed to possess an overall helical chirality (***Λ*** or ***Δ***) and crystallised as a racemate, with no evidence of the *meso* compound as a self-assembly product. Lehn remarked upon the conserved helical chirality and likened it to the DNA double helix discovered by Watson, Crick and Franklin.[25] The construction of metallo-helicates remains an active field in supramolecular chemistry which includes assemblies for guest binding [26] and in quantum information transfer as 'Qubits' (unit, quantum bit).[27]

Lehn went on to prepare higher order helical assemblies, including two circular double helicates formed through additional anion templation [28] that would later be used by Leigh as precursors to the topologically non-trivial pentafoil knot [29] and molecular Solomon's link [30] and also afford inspiration for Stoddart's Borromean rings [31] and other interlocked molecules.[32] Lehn's circular helicate and Leigh's pentafoil knot are particularly illustrative examples where choice of metal salt is crucial to the formation of the desired complex. Whilst it might be envisaged that a triple-stranded helicate would be afforded through the iron(II)-coordination of linear *tris*(2,2'-bipyridine) ligands, chloride anions act to template the formation of a cyclic structure through Cl···H-Ar hydrogen bonding interactions, **Figure 1.1**.

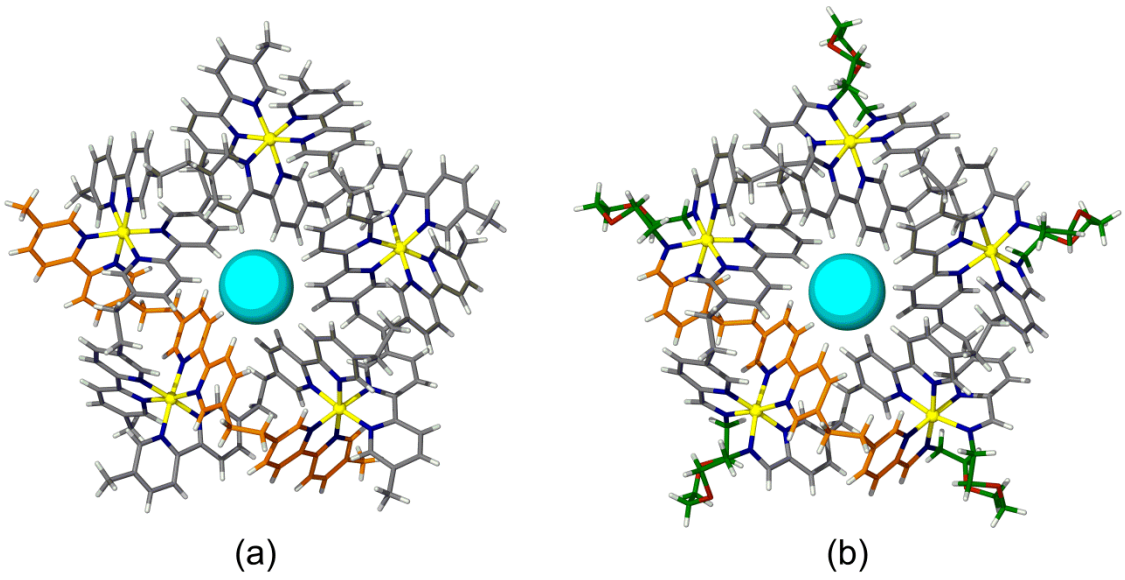

Figure 1.1 *Crystal structures of Lehn's cyclic double helicate (a) and Leigh's pentafoil knot (b). Chloride anions are coloured blue and shown in space-filling mode and one ligand from each example is coloured orange for clarity.*[28a, 29b]

Following Lehn's influential work on metallo-helicates, Fujita and co-workers succeeded in preparing the first geometrically well-defined 'square' complex.[33] The self-assembly of ditopic ligand 4,4'-bipyridine and an ethylenediamine-protected palladium(II) salt afforded the $[Pd_4L_4]^{8+}$ molecular square, where L = 4,4'-bipyridine, **Scheme 1.1**. The complex was prepared both rapidly and quantitatively, where the ^{1}H NMR spectra obtained were well resolved and symptomatic of a single and highly symmetric species present in solution. They concluded that, based on the 90 and 180 º bonding angles of the palladium(II) cation and ligand, respectively, only the $[Pd_4L_4]^{8+}$ complex would be accessible without inducing significant molecular strain. It was also noted that the species possessed an internal cavity of 6.5 × 7.8 × 7.8 Å which was able to reversibly bind 1,3,5-trimethoxybenzene in aqueous media; thus, confirming the ability for such complexes to recognise guests analogously to the organic cryptands and carcerands.[34]

The $[Pd_4L_4]^{8+}$ complex remained the focus of their attention for many years, during which time the crystal structure was obtained, confirming the metallo-rectangular form, **Scheme 1.1**.[35] Fujita *et al.* later extended these procedures to the preparation of the first [2]-catenanes formed through the spontaneous interlocking of two coordination 'square' complexes.[36] Such species differed from the earlier [2]-catenanes of Sauvage [37] and Stoddart [38] which employed classical synthetic procedures over dynamic self-assembly.

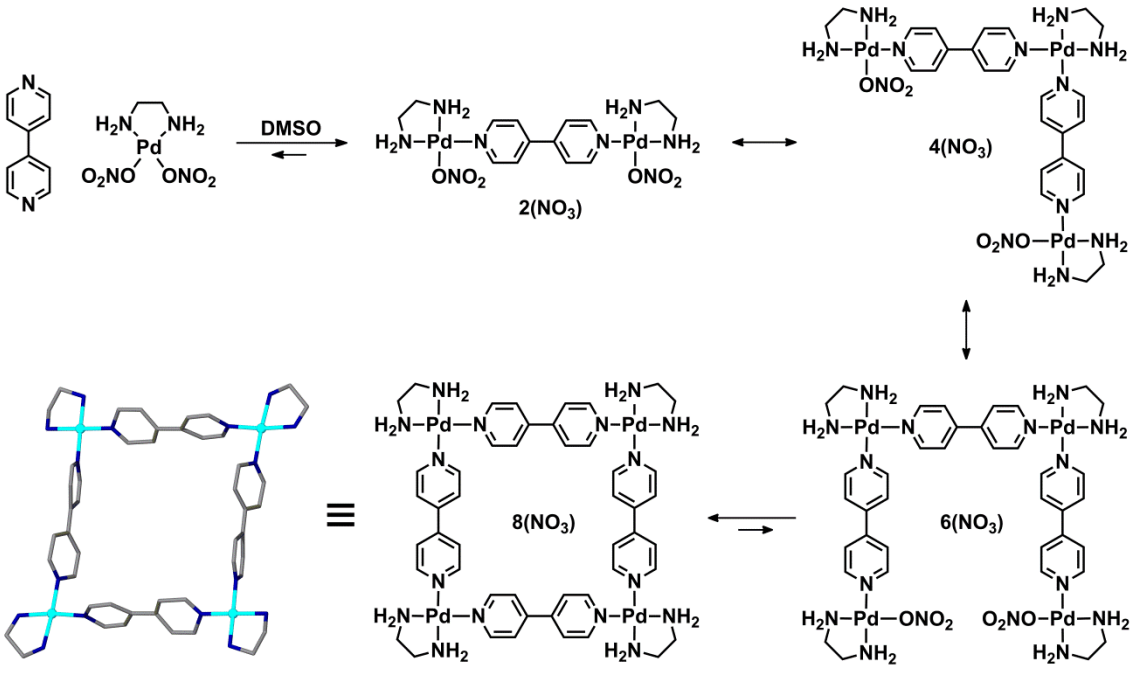

Scheme 1.1 *The formation of Fujita's 'molecular square' through self-assembly. The crystal structure is shown inset, highlighting the geometrically well-defined shape.*[33, 35a]

By using the predefined shapes of complementary molecular building blocks, chemists were able to predictably prepare a wide range of geometrically well-defined complexes, under

thermodynamic control. This methodology would later be termed the 'directional bonding' approach by Stang [39] and used to construct a plethora of cyclic nanostructures [40] that included rectangles [41] and polygons.[42] It was noted that as long as the molecular precursors were mixed in the appropriate stoichiometry and that the inherent symmetry and number of interactive sites were complementary, then a single self-assembly product would always be afforded.[43]

Whilst such species are structurally aesthetic, their potential application in host-guest and recognition chemistry is limited due to the lack of internal 'chemical space'.[44]

1.4 Coordination cages: Sophisticated molecular recognition and catalysis

The organic carcerands (from the Latin *carcer*, meaning prison) displayed an ability to strongly bind guests, generally solvents and other small molecules, in the formation of a carceplex, **Figure 1.2**.[45] Donald Cram likened the interior of such species to a new form of matter that was unlike the interior phases of zeolites or other clathrates and that their ability to exist in the solid, liquid or even gaseous bulk phases would be advantageous for the 'imprisonment' of molecules. He, and others, noted that such 'container compounds' were a prototype towards increasingly advanced molecular hosts that may offer application in the delivery of drugs and other useful products.[44]

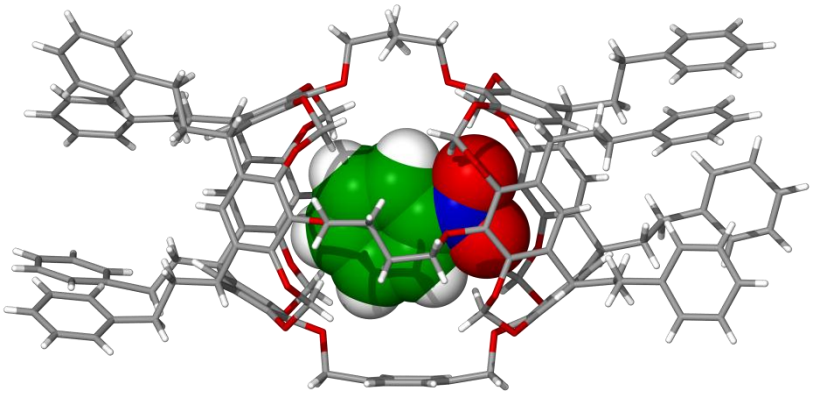

Figure 1.2 *Displaying the encapsulation of nitrobenzene by one of Cram's dissymmetric carcerands in the formation of a carceplex. The nitrobenzene molecule is distinguished in colour and displayed in space-filling mode for clarity.*[45]

Prior to their elucidation, Cram postulated that coordination cages would have an even greater impact on areas such as catalysis and cargo delivery and that by controlling the self-assembly of suitably pre-functionalised organic ligands and metal cations it would be possible to construct larger assemblies that would possess a similarly well-defined internal 'space'. Furthermore, it was predicted that the use of metal-directed self-assembly would negate the multi-step and often

pyrrhic syntheses required to construct a covalent analogue.[46] In the years that followed, research into coordination cages would be largely application driven.[47]

Coordination cages are often the entropically favoured product of self-assembly and therefore require suitably labile coordination bonds in order to facilitate their formation, ensuring that they may be isolated as the sole product, under thermodynamic control.[43, 48] Likewise, they are often highly symmetric and closely resemble Platonic and Archimedean solids.[49] Platonic solids represent the five regular polyhedra; the tetrahedron, cube, octahedron, dodecahedron and icosahedron, and are so named due to the incorporation of a single polygon at the faces. Archimedean solids consist of two or more regular polygons which meet at identical vertices and include the cuboctahedron, amongst many others.[50]

Possessing a well-defined exterior, some of the higher order solids may be likened to viral capsids, such as *Adenoviridae* (human Adenovirus; HAdV),[51] which consists of over one million amino acid residues in a manner that resembles an icosahedron.[52] The unusually high symmetry and large relative size make such species difficult to prepare synthetically; however, Atwood and Barbour have succeeded in mimicking icosahedral viral geometry in the crystalline solid state through the controlled crystallisation of *p*-sulfonatocalix[4]arene.[53]

The first three dimensional coordination cage, isolated by Saalfrank and co-workers in 1988, was prepared by the Grignard reaction of a substituted dimalonate ester with methylmagnesium bromide (MeMgBr) in tetrahydrofuran (THF) solvent, **Scheme 1.2**.[54] They noted that the ^{1}H NMR spectrum of the complex was "impressively simple", suggesting that the complex must therefore be of high molecular symmetry. Through single crystal diffraction analysis they discovered the complex to be a tetrahedral cage-type complex, $[Mg_4L_6]^{2-}$, where L = dimalonate ester ligand, that they likened to an expanded adamantane due to its T_d -symmetry. Despite its cage-like appearance, the complex featured no internal void space for which to bind guests (calculated volume, V = 10 Å^3).

Saalfrank and co-workers further exemplified their synthetic procedure to the formation of an expanded analogue that featured an internal cavity of 105 Å^3 but did not comment on its recognition properties.[55] In a similar approach to the early work of Saalfrank, Lindoy and co-workers have used functionalised *bis*(β-diketonate) ligands to prepare $[Fe_4L_6]^{n+}$ tetrahedral assemblies which can encapsulate up to four molecules of THF solvent,[56] in addition to complex architectures that include the universal 3-ravel.[57]

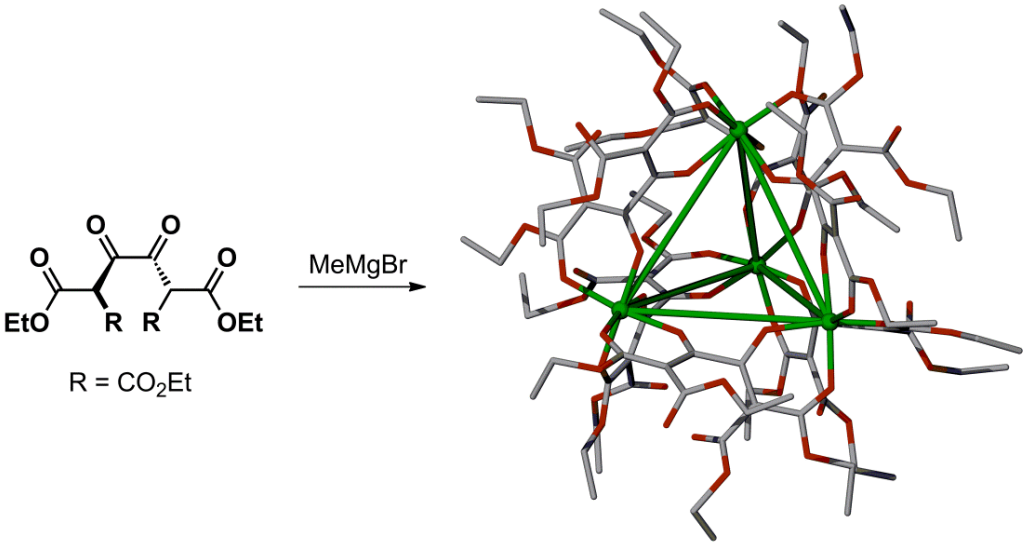

Scheme 1.2 *Preparation of the first tetrahedral coordination cage by Saalfrank and co-workers. The green lines between magnesium(II) centres indicate the tetrahedral framework.*[54]

It was the pioneering work of Raymond which first highlighted the potential of stable tetrahedral cages as molecular hosts. By controlling the helical chirality of the metal centre (***Δ*** or ***Λ***) at each vertex of the tetrahedron they succeeded in predictably preparing enantiopure $[M_4L_6]^{n-}$ and $[M_4L_4]^{n-}$ cages using functionalised *bis*- and *tris*(catechol)amide ligands, respectively.[58] Their so-called 'symmetry interaction' design principle proved to be rather general and structurally analogous tetrahedral cages were prepared using a wide range of metal salts.[59] The water-soluble and anionic tetrahedral cages displayed an affinity for cationic guests and were observed to bind similarly tetrahedral cations, such as tetra-*n*-alkylammonium cations from aqueous solution.[60]

Raymond and co-workers later indicated that such species were stimuli responsive and that cation binding could induce a structural change.[61] The reaction of a *bis*(catechol)amide ligand and gallium(III) cations afforded an equilibrium of $[Ga_4L_6]^{n-}$ tetrahedra and $[Ga_2L_3]^{n-}$ triple-stranded helicates, which could be quantitatively converted to the tetrahedral assembly upon treatment with tetramethylammonium (NMe_4^+) salts, **Figure 1.3a**.[61] Similar behaviour was noted by Ward and colleagues in the preparation of a $[Co_4L_6]^{n+}$ tetrahedral cage, where L = bidentate *bis*(pyridinepyrazolide) ligand.[62] Self-assembly initially afforded a dynamic mixture of interconverting products until a tetrahedral template was added. Treatment of the reaction mixture with a complementary anion, such as perchlorate (ClO_4^-), immediately afforded the tetrahedral cage through the formation of O···H-Ar hydrogen bonds between the anion and the cage interior, **Figure 1.3b**.[62-63]

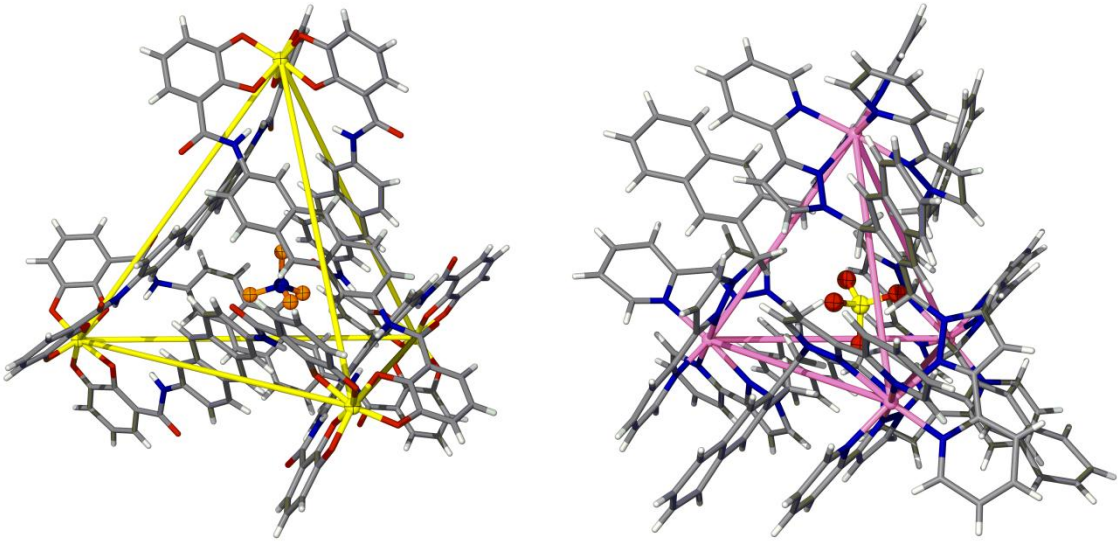

Figure 1.3 *Tetrahedral inclusion complexes, evidencing the binding of tetramethylammonium (NMe_4^+) cations by Raymond's anionic $[Ga_4L_6]^{n-}$ cage (a); and the perchlorate-templated formation of Ward's cationic $[Co_4L_6]^{n+}$ cage (b). Bound anions shown in the centre of each tetrahedral cage are displayed as hard spheres and the NMe_4^+ cation (a) coloured orange for clarity.*[60, 62]

Assessment into the application of tetrahedral cages began with Raymond and co-workers. They likened the interior of the $[Ga_4L_6]^{n-}$ cage to a chemical microenvironment which was dissimilar to the bulk solution and demonstrated the symmetry-driven encapsulation of a variety of guests in aqueous media. In doing so, they were able to use the tetrahedral cavities as micro-reactors to perform simple unimolecular chemical transformations, including an enantioselective 3-aza-Cope rearrangement [64] and Nazarov cyclisation of vinyl ketones,[65] where they noted enzymatic behaviour and a rate acceleration of up to 2100000 (k_{cat}/k_{uncat}). This was later extended to bimolecular reactions that included the C-H activation of alkenes through selective encapsulation of an iridium(III) guest and the subsequent addition, and co-encapsulation, of the alkene.[66]

Much of the recent research regarding the formation and application of tetrahedral cages involves Nitschke and co-workers. They have developed a subcomponent self-assembly methodology where imine bond formation and metal coordination occur simultaneously to afford $[Fe_4L_6]^{n+}$ tetrahedra with high fidelity.[67] They concluded that the cages could be both 'unlocked' and 'relocked' [68] and described them in terms of 'systems chemistry', meaning that the properties were emergent and only displayed as the sum of the interacting components.[69] The cages were decorated with sulfonate groups at the periphery and were therefore highly soluble in aqueous media. Similarly to the tetrahedral cages prepared by Ward and Raymond,

the cages had a well-defined internal cavity with a calculated volume of 140 $Å^3$ and were observed to selectively bind cyclohexane, acetone and acetonitrile, with sequential binding constants determined for each. Guest encapsulation could be modulated through the allosteric binding of other species, such as guanidinium cations, through hydrogen bonding at the cage windows, **Figure 1.4a**.[70]

The real breakthrough arrived with the incarceration of white phosphorus (P_4), which was shown to be stable to both water and oxygen when encapsulated within the hydrophobic interior of the cage, **Figure 1.4b**.[71] The rationale for which lies in molecular confinement, as the reaction between molecular oxygen (O_2) and P_4 would afford an intermediary which would be too large for the tetrahedral cavity without causing severe perturbations to the $[Fe_4L_6]^{n+}$ framework. Thus, the weak P-P bonds (200 kJ/mol) that usually offer little resistance to oxidation remain intact and the pyrophoric reaction to phosphorus oxide (P-O bonds in the range 356-650 kJ/mol) does not proceed.

Here, the pronounced interactive strength between cage and guest can be described in terms of hydrophobic specificity and in accordance with Rebek's proposed rule of '55% occupancy', which states that for a host and guest to interact favourably through only van der Waals interactions, the ideal packing coefficient for guest to host ought to be 55%.[72] Depending on the calculation used to estimate the cage volume,[73] the packing coefficient of this system remains between 50-60% and is therefore regarded as highly specific.

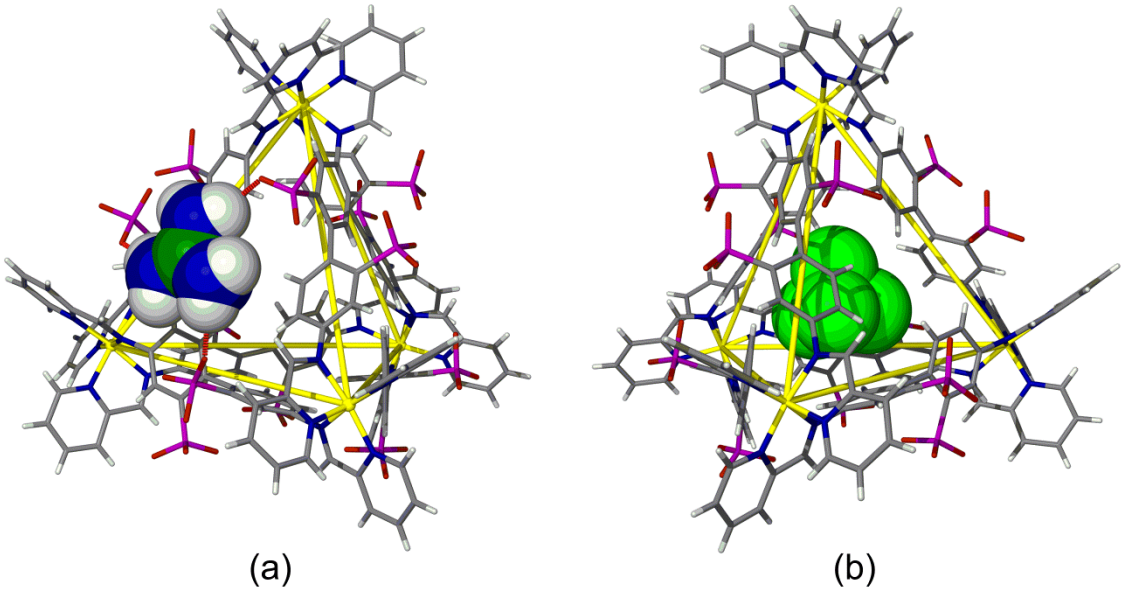

Figure 1.4 *Crystal structures of $[Fe_4L_6]^{n+}$ tetrahedral cages prepared by Nitschke and co-workers, displaying the allosteric binding of guanidinium at the cage windows (a) and the encapsulation of P_4, white phosphorus (b). Both guests are shown in space filling mode and hydrogen bonding between guanidinium and sulfonate is displayed using red, hashed lines.*[70-71]

Nitschke and co-workers further demonstrated the efficacy of the $[Fe_4L_6]^{n+}$ cage towards catalytic procedures that included Diels-Alder chemistry,[74] and in sophisticated anion [75] and small molecule binding.[76] Tetrahedral assemblies are now numerous in the literature and have even been prepared with the lanthanide(III) cations.[77] Likewise, there have also been reports of catenating tetrahedral cages [78] and those which display a physical response to an external stimulus, such as in Kruger's spin-crossover $[Fe_4L_4]^{n+}$ tetrahedral assembly, where L = *tris*(imine) ligand.[79]

Cubic coordination cages are a less common self-assembly product and are therefore not as frequently exemplified in their host-guest chemistry and application. The first example was prepared by Ward *et al.* through the self-assembly of *bis*(pyridylpyrazolide) ligands and cobalt(II) centres and isolated as a $[Co_8L_{12}]^{n+}$ octanuclear coordination cage.[80] The ligands associated through aromatic interactions at the faces of the cube to create a well-defined internal chemical environment; however, due to high levels of insolubility, the host-guest chemistry and recognition properties were not determined.[81]

As a collaborative effort, Ward and Hunter demonstrated the generality of cage formation and isolated a water soluble $[Co_8L_{12}]^{n+}$ analogue through the appendage of polyethyleneglycol (PEG) chains at the periphery of the ligands, **Figure 1.5a**. This allowed for the hydrophobic effect to be exploited and a wide range of polar guests were found to be selectively encapsulated by the cationic cubic framework.[82] The positively charged and paramagnetic $[Co_8L_{12}]^{n+}$ framework allowed for paramagnetic ^1H NMR studies to be undertaken, which afforded positional evidence of guest binding within the cage interior.

Using the same subcomponent self-assembly methodology as described above, Nitschke and co-workers were able to selectively isolate $[Fe_8L_{12}]^{n+}$ cubic structures from exactly linear *bis*(imine) ligands, **Figure 1.5b**.[83] Similarly to Ward, they found that solvophobics could induce guest binding and went on to encapsulate large aromatic guests, such as coronene and fullerenes,[84] and large anions.[85] They highlighted discriminative and regulative guest binding based on solvophobics and could selectively encapsulate ferrocene over 9-acetylanthracene, and *vice versa*, by switching the polarity of the solvent mixture.[86]

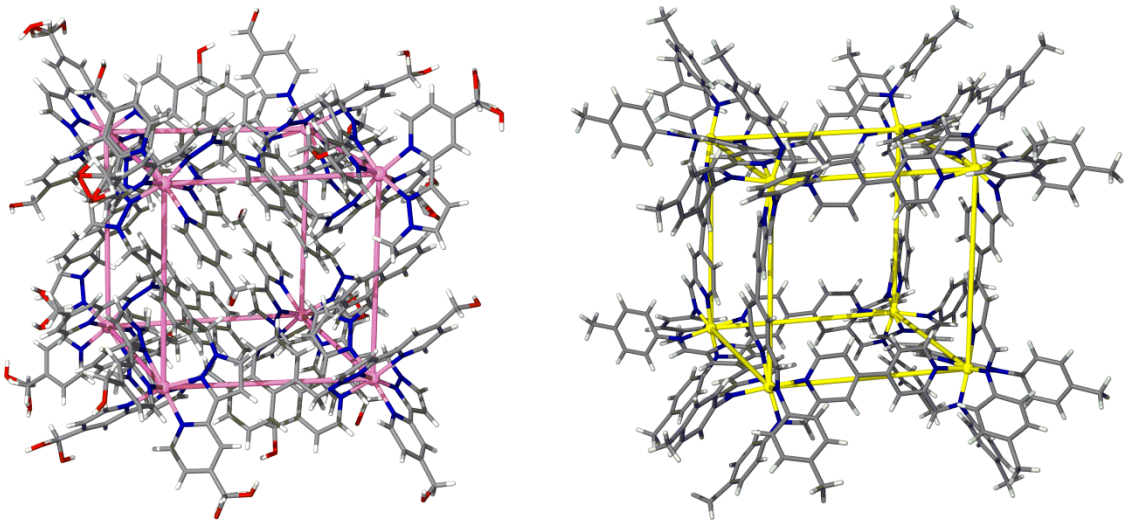

Figure 1.5 *Crystal structures of Ward's* $[Co_8L_{12}]^{n+}$ *(a) and Nitschke's* $[Fe_8L_{12}]^{n+}$ *(b) cubic coordination cages which each demonstrated sophisticated guest recognition properties in aqueous media through solvophobics. The coloured lines in each example denote the cubic arrangement of metal cations within the cage framework.*[82b, 86]

Perhaps the most well-exemplified coordination cages are derived from an octahedral framework of metal cations. The first nanometer-sized octahedral coordination cage was prepared by Fujita and co-workers in 1995 by use of a 'molecular panelling' design principle, **Figure 1.6**.[87] The $[Pd_6L_4]^{12+}$ cage complex, where L = 1,3,5-*tris*(4-pyridyl)triazine, utilised ethylenediamine as *cis*-protecting auxiliary as for the aforementioned $[Pd_4L_4]^{8+}$ 'square' complex and contained an exceptionally large interior cavity which they demonstrated could bind four molecules of adamantane-1-carboxylic acid, in aqueous media.[87]

In the two decades following, this particular $[Pd_6L_4]^{12+}$ coordination cage would go on to become a prized asset of the Fujita group, where its ability to not only host molecules, but facilitate chemical reactions between them, would introduce the moniker 'functional molecular flasks'.[88] The $[Pd_6L_4]^{12+}$ cage was observed to bind various small molecules, including fullerenes and tetrathiafulvalene (TTF, **Figure 1.6a**),[89] as well as allowing for the selective recognition of long-chained perfluorinated alcohols through a cage-induced self-aggregation mechanism, **Figure 1.6b**.[90]

Likewise, the $[Pd_6L_4]^{12+}$ cage was employed in the sensing and discrimination of aliphatics, in addition to the enablement of selective oxidation [91] and photodimerisation [92] of alkanes through irradiation. These represent the first examples where a chemical reaction has been sensitised by a self-assembled coordination cage. This procedure was further extended to metal complexes and shown to both encapsulate and provide stabilisation for a highly reactive and

coordinatively-unsaturated manganese [Cp'Mn(CO)$_2$] complex, where Cp' = η^5-methylcyclopentadienyl ligand, following the irradiation of the stable parent complex, [Cp'Mn(CO)$_3$].[93] Similarly, the cage has also allowed for the trapping of a highly unstable ruthenium dimer, [(η^5-indenyl)Ru(CO)$_2$]$_2$, which ordinarily undergoes photoinduced Ru-Ru bond cleavage and CO dissociation, yet is stabilised by the confines of the cage cavity.[94]

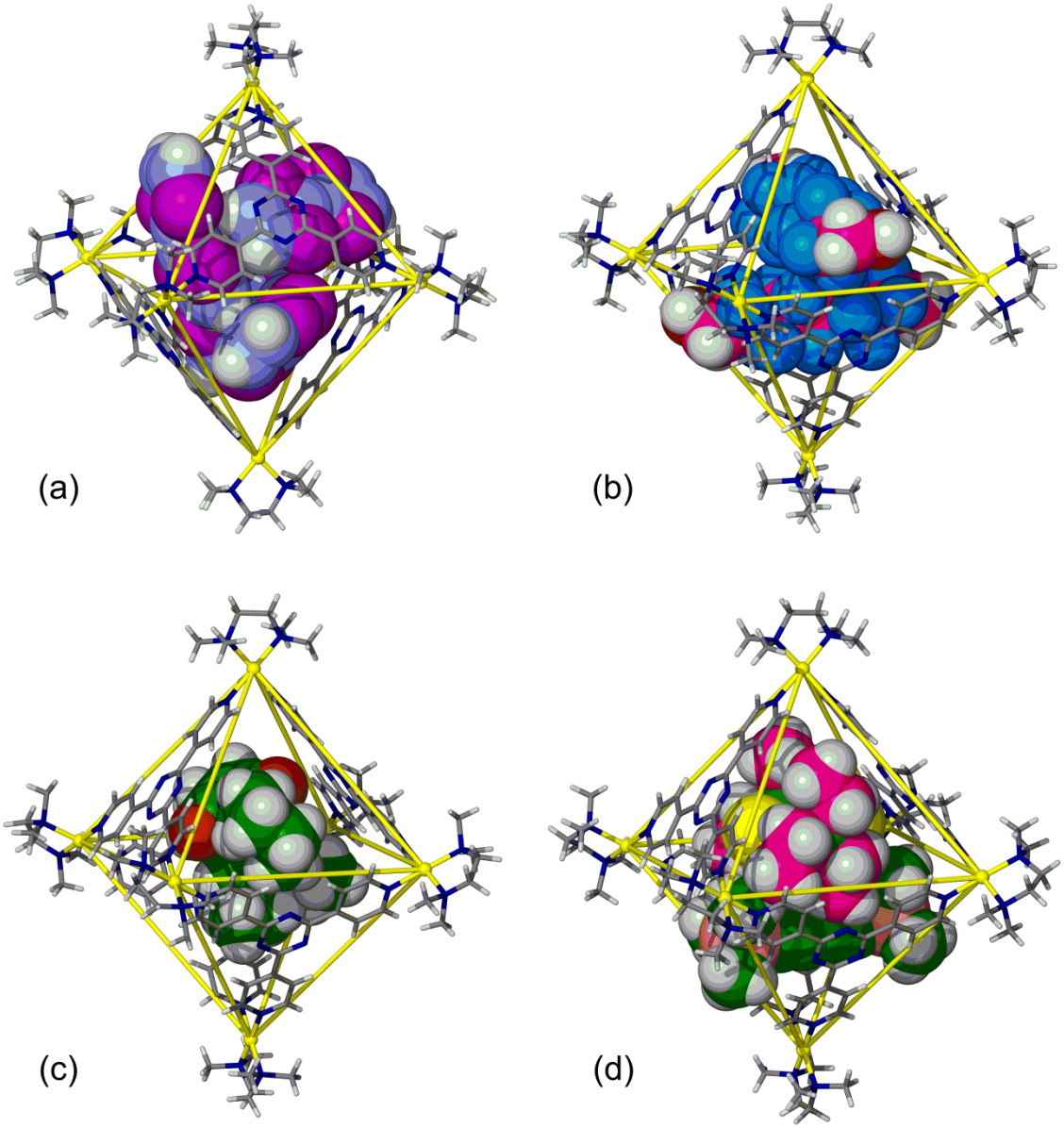

Figure 1.6 *The varied host-guest, recognition and catalytic chemistry of Fujita's [Pd$_6$L$_4$]$^{12+}$ octahedral coordination cage, displaying the encapsulation of four molecules of tetrathiafulvalene (TTF, a) and two molecules of a long-chained perfluorinated alcohol (b) into the cage cavity. The encapsulation of two independent and unreactive molecules (diene and dienophile) and enablement of Diels-Alder reactivity (c) and the encapsulation of pre-formed palladium(II) complex and substituted alkyne in the formation of σ-alkynylpalladium(II) complex (d). All 'guest' molecules in each example are distinguished by colour and displayed in space-filling mode for clarity.*[89-90, 95]

More impressive, are the catalytic abilities of the $[Pd_6L_4]^{12+}$ cage. Through the simultaneous encapsulation of 2,3-diethylnaphthalene and *N*-cyclohexylmaleimide from an aqueous suspension, Diels-Alder reactivity is achieved, **Figure 1.6c**.[95a] Ordinarily, this reaction does not proceed, especially in water, indicating the necessity of the cage host in generating the proximity and orientation factors required to facilitate the reaction. Rebek and co-workers have shown similar reaction prompting abilities in their hydrogen-bonded capsules [96] and were able to impart unusual regiochemical control by controlling the allowed reaction pathway.[97]

More recently, Fujita *et al*. have developed procedures to control metal-organic proximity through the binding of guests, akin to a metallo-enzyme. The selective co-encapsulation of a catalytically active palladium(II) complex and polyalkyne allowed for the facile C(*sp*)-H activation to form a σ-alkynylpalladium(II) complex within the cavity, **Figure 1.6d**.[95b] This is facilitated by the cage at room temperature, requires no additional base and will even proceed under acidic conditions. The rationale for such behaviour is due to proximity effects, where the co-encapsulation brings the two molecular components together in such a way as to force a reaction to occur, despite there being no interaction between the two in bulk solution.

The application of octahedral coordination cages is not limited to molecular recognition and catalysis. Shionoya and co-workers have used large, planar *tris*(phenyl-3-pyridyl) ligands to form giant $[M_6L_8]^{n+}$ octahedral cages from a wide range of metal centres, indicating its generality in self-assembly.[98] Through a molecular panelling approach, the large aromatic ligands were observed to effectively close off all windows of the octahedral framework, thus creating a chemically distinct interior cavity; however, they are yet to remark on its hosting abilities. Shionoya extended this metal-directed procedure to the preparation of an analogous $[Pd_6L_8]^{n+}$ octahedral assembly that was decorated with pendent alkene moieties at the cage periphery.[99] Through ring closing metathesis (RCM) they successfully sealed the cage at the ligand edges and sequestered the palladium(II) through addition of competing ligands, thus generating a 3 nanometer covalent assembly. Similar organically-linked octahedral assemblies, prepared through dynamic imine bond formation have been prepared by Warmuth.[100]

The preparation and host-guest chemistry of the higher order platonic coordination cages remains relatively rare. Research into uranyl chemistry by de Mendoza and co-workers has allowed for the isolation of a giant dodecahedral $[U_{20}L_{12}]^{20-}$ polyhedral assembly, where L = carboxylate functionalised calix[5]arene, **Figure 1.7a**.[101] Employment of the uranyl cation ($[UO_2]^{2+}$) is necessary in ensuring that the three calix[5]arene ligands remain equatorially coordinated about the uranium centre. The anionic cage measures approximately 4 nm in diameter and possesses an internal volume of 7000 $Å^3$ that was observed to encapsulate various *N*-protonated organics, such as pyridinium cations and a tetraprotonated 1,4,7,10-

tetraazacyclododecane (cylen) cation, **Figure 1.7a**. Similarly, Nitschke *et al.* have successfully prepared a homochiral icosahedral $[Fe_{12}L_{12}]^{n+}$ cage, where L = *tris*(pyridylimine) ligand, through subcomponent self-assembly, **Figure 1.7b**. The cage possesses *T*-symmetry and an internal cavity of 2800 $Å^3$ which was shown to reversibly bind the large and icosahedral carborane anion $[B_{12}F_{12}]^{2-}$ in acetonitrile solution.[102] Whilst such species do not display the highly sophisticated recognition or catalytic properties of some of the smaller coordination cages, they do represent a step towards the preparation of synthetic viral capsids.

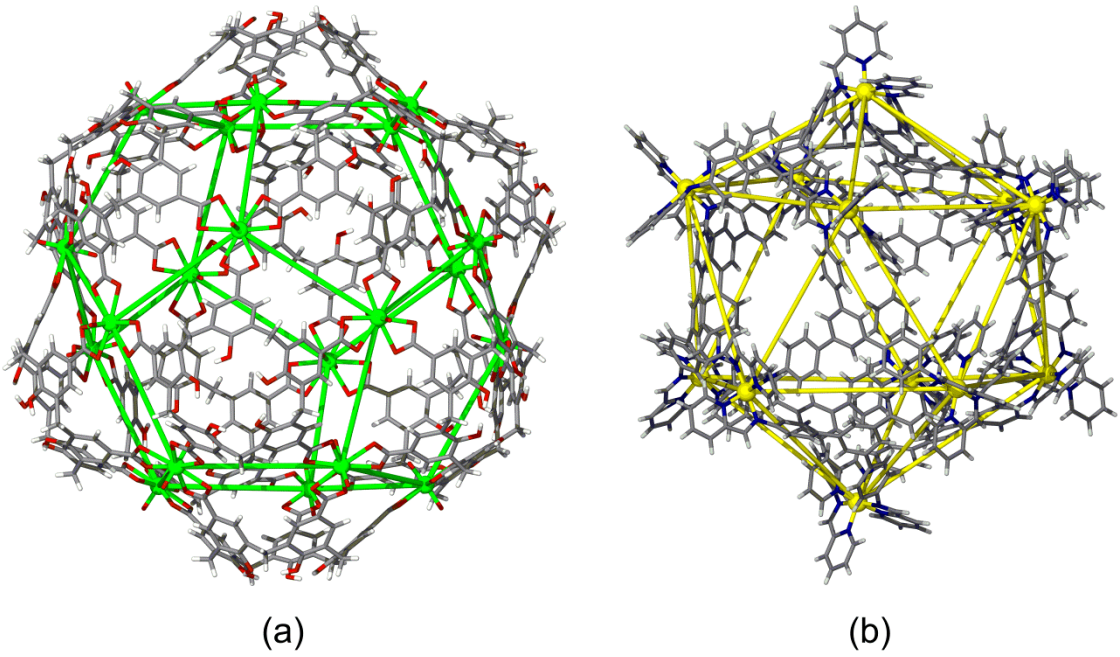

Figure 1.7 *Examples of higher order Platonic solids. The crystal structures of de Mendoza's* $[U_{20}L_{12}]^{20-}$ *dodecahedral assembly (a) and Nitschke's* $[Fe_{12}L_{12}]^{n+}$ *icoasahedral assembly (b). The coloured framework in each example is to indicate the Platonic solid framework.*[101-102]

The preparation of coordination cages that resemble the Archimedean solids began with Stang in 1999 with the isolation of heteroleptic $[Pt_{18}L_8L'_{12}]^{24+}$ cuboctahedral assembly, where L = *tris*(alkynylpyridyl)benzene and L' = *bis*(pyridyl) ligand.[103] He demonstrated that in order to prepare an Archimedean solid, where dissimilar polygons comprise the cage faces, that two complementary and geometrically predefined ligands must be used in conjunction with one another. Stang and co-workers went on to further exemplify the ability of classical 'directional bonding' self-assembly in the preparation of various heteroleptic cages and higher order Archimedean solids such as the truncated tetrahedron.[104]

Following the work of Stang, Fujita and colleagues succeeded in preparing a high-symmetry $[Pd_{12}L_{24}]^{24+}$ nanosphere, where L = *bis*(pyridyl) ligand, that closely resembles the Archimedean cuboctahedron.[105] The formation of the $[Pd_{12}L_{24}]^{24+}$ nanosphere was rather general, provided a

bis(pyridyl) ligand with a coordination bite angle of 125 º was used. They successfully prepared structurally analogous $[Pd_{12}L_{24}]^{24+}$ coordination cages which featured saccharide [106] and coronene [107] internal pendant moieties which were observed to facilitate the preparation of monodisperse silica nanoparticles and binding of fullerenes, respectively.

Fujita went on to prepare even larger $[Pd_{12}L_{24}]^{24+}$ coordination cages by use of an extended *bis*(pyridyl) ligand library. Through functionalisation with Biotin moieties they were able to bind and completely encapsulate the Gly76Cys-mutated protein Ubiquitin,[108] which represents the largest and perhaps most sophisticated example of host-guest chemistry yet reported. Furthermore, they successfully prepared the first formal cage-in-cage complex through orthogonal self-assembly, where the *bis*(pyridyl) ligand was further functionalised with a pendant *bis*(pyridine) moiety to allow for the formation of a smaller and symmetry matching cuboctahedral cage within the confines of the larger $[Pd_{12}L_{24}]^{24+}$ nanosphere, **Figure 1.8a**.[109] Whilst other cage-in-cage complexes are known, such as Raston's 'Russian doll' assembly,[110] this is the first reported example with a subdivided complex structure that closely resembles that of a double-shell viral capsid.[111]

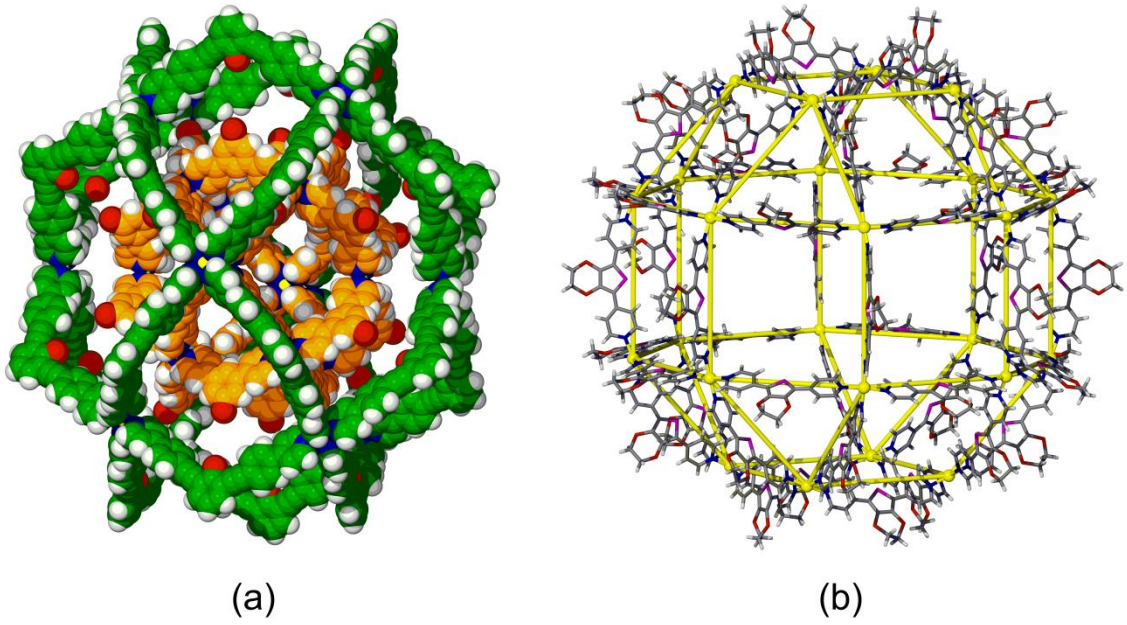

Figure 1.8 *Crystal structures of Archimedean coordination cages prepared by Fujita et al., displaying the orthogonal self-assembly of a sphere-in-sphere cuboctahedral complex (a) and giant* $[Pd_{24}L_{48}]^{48+}$ *rhombicuboctahedral coordination cage (b).*

Finally, Fujita and co-workers have also managed to prepare the first giant $[Pd_{24}L_{48}]^{48+}$ coordination cage using similar procedures as described above. By approximating the *bis*(pyridyl) ligands as the cage edges and the palladium(II) centres as the vertices the result is a 5 nm rhombicuboctahedron, consisting of 26 faces that comprise 8 triangles and 18 rectangles,

Figure 1.8b.[112] In this particular instance, the $[Pd_{24}L_{48}]^{48+}$ framework occupies less than 20% of the total unit cell volume and, with a calculated mass of 21946.73 Da (Daltons), is the first synthetic example that edges closer to the massive scale of biological self-assembly.

Whilst research in this area is dominated by the large research groups of Fujita and Stang, there are other elegant examples of large Archimedean coordination cages which display recognition properties. For example, research by Su and Zhang has lead to the isolation of a nanoscale assembly which closely resembles the rhombododecahedron, where the step-wise and orthogonal self-assembly of an unsymmetrical *bis*(pyridyl) ligand with palladium(II) and ruthenium(II) salts afforded the $[Pd_6(RuL_3)_8]^{n+}$ nanocage.[113] The $[Pd_6(RuL_3)_8]^{n+}$ coordination cage possessed an internal cavity of 5300 $Å^3$ and displayed an ability to encapsulate various conjugated aromatics, such as perylene and phenanthrene, in addition to providing stabilisation to photosensitive guests against UV radiation.

1.5 Coordination polymers: Synthesis and application

The host-guest and recognition properties of metal complexes are not limited to polyhedral assemblies. Many polymeric materials possess analogously well-defined internal pore spaces and therefore display the similarly sought after emergent properties.[114]

In the broadest sense, coordination polymers represent a class of materials in which multidentate ligands are bridged by metal cations to construct infinite, and often highly regular, networks.[115] This is a distinction from networked species that are formed through secondary interactions, such as hydrogen bonding, that link discrete, ligated metal centres.[116] The polymeric materials gained as a result of metal coordination are often classified by their dimensionality, and there are now thousands of polymeric structures known.[117] The simplest of which are 1D coordination chains, which are generally formed through the infinite bridging of ligands in a single direction.[118] Similarly, such materials can be expanded to 2D and 3D networks by considering the geometric and electronic requirements of ligand and metal.[119] This would be the basis for Desiraju's 'crystal engineering' design principle, where he noted that meticulous control over the preparation of polymeric materials often generated highly ordered frameworks with desirable physical and chemical properties.[120]

Whilst the polymers referred to here are regular, they need not be crystalline, and a variety of amorphous polymeric materials have been prepared which display electroluminescent [121] and mechanochemical [122] properties, leading to their incorporation into devices [123] and medical-based materials, respectively.[124]

The term ‘coordination polymer’ was coined by John C. Bailar in 1964 to describe the way in which certain metal cations would interact with ligands to create previously unreported inorganic structures. He remarked that such materials displayed dissimilar properties to their organic counterparts and went on to establish rules for their preparation and began to characterise their properties.[125]

The deliberate design and construction of polymeric networks was later developed by Robson and Hoskins in the realisation of ‘infinite frameworks’. By combining tetrahedral copper(I) centres with suitably tetrahedral ligands (4,4’,4’’,4’’’-tetracyano-tetraphenylmethane) they succeeded in preparing the first porous, 3D adamantoid network.[126] In additional experiments, they went on to exchange the existing tetrafluoroborate (BF_4^-) anion for hexafluorophosphate (PF_6^-).[127] These findings are considered to represent the birth of modern day coordination polymer research, which is now a mature and extensive field, in which a large proportion of research is directed towards application that seeks to utilise the pores within the polymeric frameworks. The key applications of coordination polymers, such as gas storage and catalysis, will be briefly summarised below.

A primary research aim for coordination polymers is towards gas storage, with particular emphasis on hydrogen (H_2) as its use as a fuel source cannot be implemented until safer methods for its storage are developed.[128] Yaghi and co-workers isolated the first metal-organic framework (MOF) in 1995 using a hydrothermal synthesis and noted the existence of large, rectangular pores within the network.[129] The term ‘MOF’ is now somewhat synonymous with ‘coordination polymer’ and the two are often used interchangeably.[130] Years later, they extended their synthetic procedure to isoreticular networks that included the famous ‘MOF-5’ - a high-symmetry cubic network prepared from the solvothermal synthesis of 1,4-benzenedicarboxylic acid and zinc(II) nitrate in the presence of hydroxide base.[129] They observed the structure to be highly regular, where the 1,4-benzenedicarboxylate ligands were bridged by $[Zn_4O]^{6+}$ tetrahedral nodes to generate large pores within the lattice, **Figure 1.9**.

They reported an extraordinarily high internal surface area of between 2500 and 3000 m^2g^{-1} and hydrogen adsorption of 5 weight *per* cent, when working at 78 K and 1 bar pressure.[131] In addition to the high surface areas, they rationalised that such high hydrogen adsorbance was due to the nature of the open framework, which provides exposed organic struts for the adsorption of molecules. This was later determined through inelastic neutron scattering (INS) which gave evidence for the adsorption sites within the network. Whilst MOF-5 boasted high thermal stability of between 300-400 ºC, the major limitation for its application was the extremely high sensitivity towards hydrolysis.

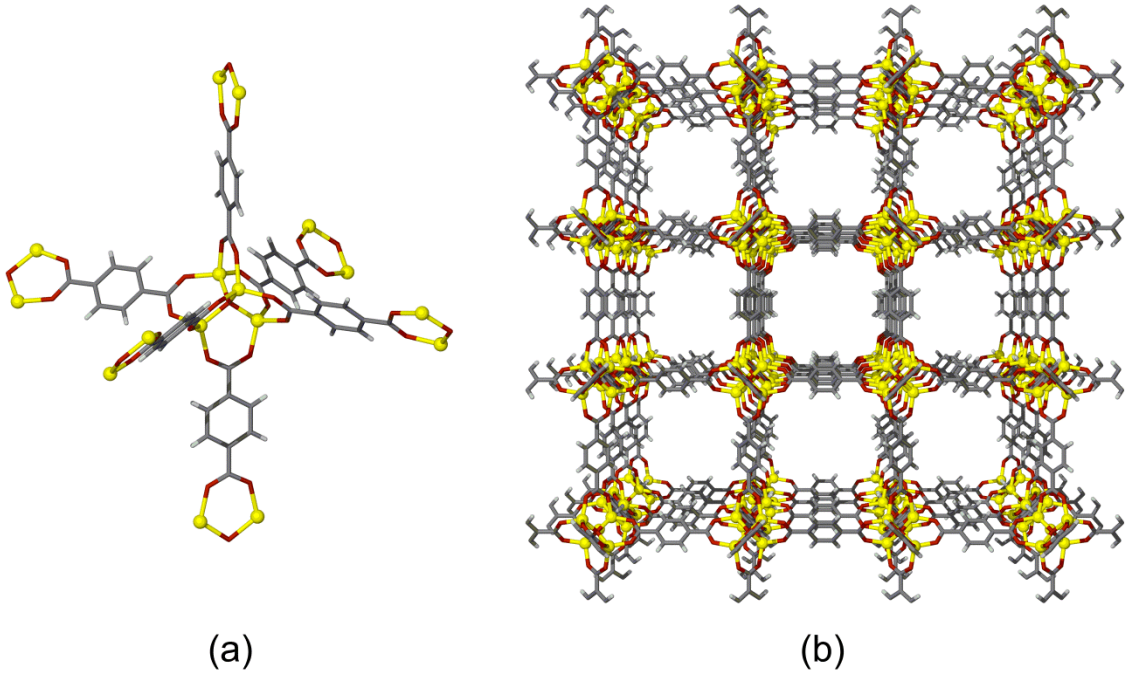

Figure 1.9 *From the crystal structure of Yaghi's MOF-5, displaying the binding modes of the terephthalate ligands about the* $[OZn_4]^{6+}$ *nodes (a) and the resultant high-symmetry cubic network (b). The Zinc(II) atoms are displayed as yellow spheres for clarity.*[131]

Yaghi and others went on to develop a series of isoreticular MOFs by expanding the length of struts between $[OZn_4]^{6+}$ nodes [132] and through the incorporation of C_3-symmetric carboxylate ligands, such as isophthalate.[133] They also successfully addressed their inherent susceptibility to hydrolysis [134] and prepared organic analogues which were completely resistant to hydrolysis.[135] More recently, in collaboration with Stoddart, they have demonstrated a way to incorporate catenated struts within the reticular framework as a route towards 'dynamic chemistry' and to provide mechanically interlocked components for selective guest binding.[136] Similar behaviour has been achieved by Loeb in the preparation of MO*R*Fs (metal-organic *rotaxane* frameworks) through the co-crystallisation of dibenzo crown ethers in the presence of a charged metal-organic framework.[137] Furthermore, they have extended the application to the selective uptake of carbon dioxide (CO_2) [138] and achieved 'ultrahigh porosity' of 10400 m^2g^{-1} without sacrificing the necessary robustness of the material.[139] The sheer volume of MOFs published over the last decade has resulted in much subject specific nomenclature and terminology.[140]

Other noteworthy examples which are able to reversibly adsorb gases are Chen's citrate-derived MOFs which are able to sequester CO_2 under ambient conditions and discriminate it from gaseous mixtures that include carbon monoxide (CO) and molecular nitrogen (N_2).[141] Chen and co-workers further exemplified this procedure in the practical separation of acetylene and

ethylene gases through the precise tailoring of the pore size within the potassium citrate network.[142]

The uptake of CO_2 is a pertinent research goal by many, owing to the link between anthropological CO_2 emissions and climate change.[143] Long and co-workers have developed a series of sophisticated MOFs for the selective uptake and subsequent degradation of CO_2 as a way to address this. They have successfully prepared a metal-organic framework featuring pendent amine functionalities, sited within well-defined pores, which was seen to significantly enhance the uptake of CO_2 from a Flue gas mixture.[144] The pendent amine moieties were observed to activate the adsorbed CO_2 through nucleophilic attack, facilitated by the close confines of the internal pores, in the formation of a carbamate intermediate.[145] Long and co-workers went on to exemplify this procedure in the selective sequestration of methane,[146] hydrogen [147] and mixtures of unsaturated aliphatics.[148]

Kitagawa has prepared a series of 'soft porous crystals' from the self-assembly of benzenedicarboxylate ligands with either copper(II) or zinc(II) metal centres which are both highly stable and mechanically durable.[149] Such materials were shown to facilitate the radical polymerisation of divinyl benzene by preventing disproportionation and controlling the orientation of the growing radical chain within the network.[150] This was achieved due to the well-defined 7.8 × 7.8 Å 1D channels present within the network; without which, unselective polymerisation to a mixture of cross-linked polymers was observed.[151] Interestingly, they could control both the rate and selectivity of radical polymerisation through substitution of the networks metal centre from copper(II) to zinc(II), with selective topotactic polymerisation afforded for the zinc(II)-based framework and no reaction observed with the copper(II)-derived framework.[152]

Kitagawa and co-workers went on to enable acetylene polymerisation within a 3D coordination polymer constructed from a heteroleptic mixture of pyrazine-2,3-dicarboxylate and 4,4'-bipyridine ligands, **Figure 1.10**.[153] This was achieved through phenoxide-assisted deprotonation and subsequent rapid polymerisation. Again, polymerisation proceeded in well-defined 1D channels within the network which facilitated the formation of a single *cis*-polyacetylene product, with no evidence for *trans*-polymerisation products. They went on to document highly selective recognition properties, where the uptake of pyrazine and expulsion of carbon disulfide proceeded with a structural reorganisation of the host network in order to form strong intermolecular interactions with the pyrazine guest.[152]

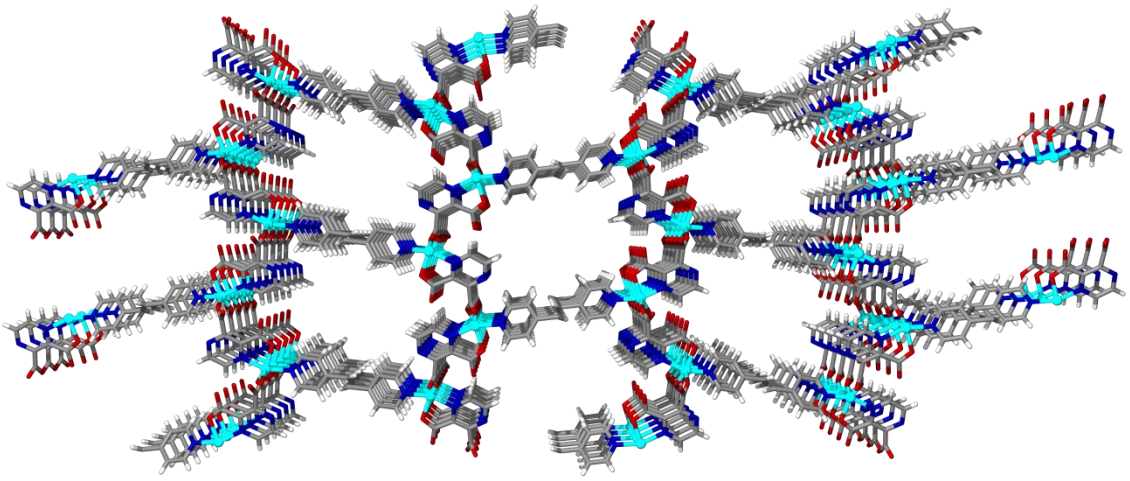

Figure 1.10 *From the crystal structure of Kitagawa's 'soft coordination polymer', as viewed down the crystallographic a axis to display the unidirectional channels. Copper(II) centres are shown as blue spheres.*[153]

The final application of coordination polymers to be discussed regards their employment as analytical tools. A collaborative effort between Fujita and Rissanen has recently developed a highly stable 3D coordination polymer consisting of 'networked cages' which enables the selective uptake of guests for crystallographic structure elucidation.[154] The 3D network, formed through the self-assembly of zinc(II) iodide and *tris*(4-pyridyl)triazine in a similar manner to the octahedral coordination cages described above, provides a well-defined and hydrophobic interior with which to bind guests. Guest uptake was effected at the nano- and microgram scale by submerging single crystals of the polymeric framework in solutions which contained various natural products, flavones and conformationally flexible compounds. For each example, single crystal diffraction analysis unambiguously evidenced the uptake of guest, and even allowed for the absolute structure determination of the natural product (3*R*, 14*S*, 26*R*)-miyakosyne A.[155] Moreover, the network was observed to act akin to 'nanoscale HPLC analyser' and was able to separate structural isomers of the flavone nobiletin, an extract from the peel of *Citrus unstitiu*.

Whilst the research received mixed reviews,[156] this procedure holds phenomenal potential with regards to the enablement of compound elucidation, particularly with species that are reluctant to crystallise,[157] or when there is too little material for conventional techniques, such as ^{1}H NMR spectroscopy.

1.6 Molecular hosts

Molecular hosts are distinct from both coordination cages and polymers and have intrinsic hosting abilities regardless of their assembly.[158] They are generally small organic compounds which can interact favourably with other molecules or ions in the formation of inclusion compounds.[159] Research in the field of molecular recognition is extensive and the many molecular hosts prepared include crown ethers,[160] cyclodextrins,[161] calix[*n*]arenes,[162] pillar[*n*]arenes,[163] asar[*n*]arenes,[164] cucurbit[*n*]urils [165] and other macrocyclic host molecules.[166]

Each particular molecular host generally displays a high affinity for a specific guest. For example, Zhao has determined the strength of interaction between hexane and other aliphatics with pillar[5]arene, in toluene solvent, **Figure 1.11a**.[163b] Likewise, the preparation of tetracationic 'ExBox' molecular receptors by Stoddart and co-workers has lead to their exemplification in various rotaxane [167] and catenane [168] assemblies, in addition to the isolation of conjugated aromatics from a crude oil mixture, **Figure 1.11c**.[169]

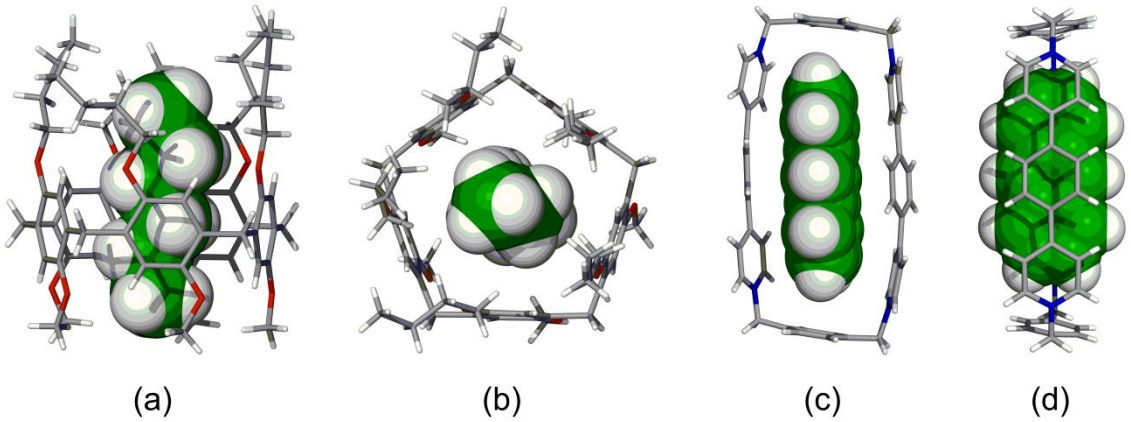

Figure 1.11 *Crystal structures of molecular host inclusion complexes. The encapsulation of hexane by Zhao's alkylated pillar[5]arene is shown from the side (a) and above (b).*[163b] *Anthracene binding by Stoddart's tetracationic 'ExBox' as viewed from the side (c) and above (d).*[166a] *The encapsulated guest in each example is distinguished by colour and displayed in space-filling mode for clarity.*

1.7 Cyclotriveratrylene

Cyclotriveratrylene (CTV) [170] and its analogues represent a class of relatively rigid and C_3-symmetric molecular hosts which feature an electronically rich and hydrophobic tribenzo[*a*,*d*,*g*]cyclononatriene core, closely resembling that of a shallow 'bowl'. They are known for their interesting host-guest properties and therefore much of their chemistry is targeted towards molecular recognition.[171]

In solution, CTV exists in an equilibrium of two molecular conformations, comprising the favoured C_3-symmetric 'crown' and the unstable C_1-symmetric 'saddle', **Figure 1.12**.[172] Conversion between the two proceeds *via* a ring flipping mechanism, where partial inversion of the crown conformer generates a strained species in which the three aromatic rings are orientated orthogonally with respect to one another. The inherent instability associated with the saddle conformation results in rapid regeneration of the crown conformer and is therefore generally considered as a transition state. Whilst energetically unfavourable, the saddle conformation can be isolated through the rapid quenching of a melt.[172a]

The half-life for inversion was determined to be *ca*. one month (at 20 ºC) based on the racemisation of deuterated CTV analogues, although this varies with the functional groups appended.[173] Nevertheless, the large rotational energy barrier renders interconversion slow at room temperature and thus immeasurable on the NMR timescale. As such, CTV and its analogues are easily identifiable by the diastereotopic protons attributable to the methylene linker. These characteristic *endo* and *exo* protons typically resonate at δ = 3.8 and 4.9 ppm, respectively, and display a large geminal coupling constant of approximately 15 Hz.[174]

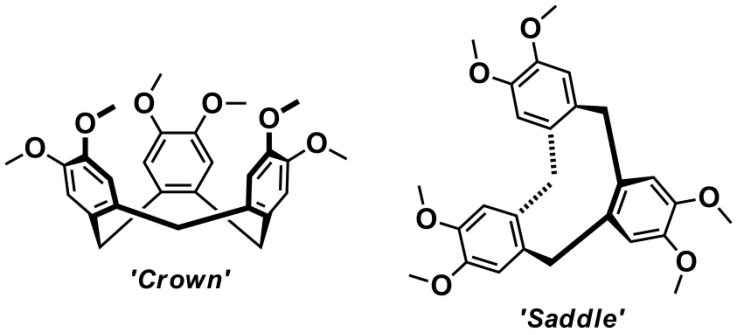

Figure 1.12 *The crown and saddle conformations of cyclotriveratrylene (CTV).*

CTV can be both partially and fully demethylated to afford the chiral, *tris*-hydroxy derivative, cyclotriguaiacylene (CTG) [175] and hexa-hydroxy derivative, cyclotricatechylene (CTC),[176] respectively, **Figure 1.13**. Both species feature phenolic functionalities atop the tribenzo[*a*,*d*,*g*]cyclononatriene framework that are easily *O*-functionalised and have each been used to prepare a variety of compounds, including ligands.[177] Other derivatives, including *tris*-amino,[178] hexaalkyl [179] and hexasulfanyl [180] analogues of CTV have been prepared.

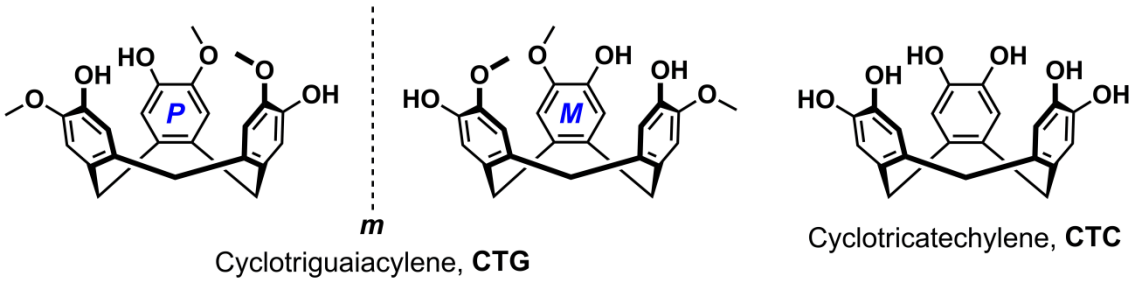

Figure 1.13 *The molecular structures of CTG and CTC. The two enantiomers of CTG are denoted with the helical chirality descriptors* ***P*** *and* ***M****.*

CTV has well documented host-guest properties and has been seen to bind globular guests, including carboranes [181] and fullerenes, **Figure 1.14a**.[182] Recently, de Mendoza and co-workers have prepared functionalised CTVs as scavengers for the higher fullerenes (C_{80} and C_{84}) [183] and succeeded in selectively isolating individual fullerenes from a fullerite mixture.[184] Likewise, many of the networked structures of CTV display inclusion properties,[185] with a variety of clathrate compounds characterised.[176]

One of the major research areas in CTV chemistry is in the preparation of cryptophanes.[186] These represent C_3-symmetric 'container compounds' that comprise two covalently-linked CTV units in a head-to-head manner, thus creating a well-defined internal cavity for guest binding.[187] Cryptophanes are versatile hosts and have been observed to strongly bind various small molecules [188] and even gases, including methane [189] and xenon,[190] for hyperpolarised ^{129}Xe biological NMR.[191] Holman and co-workers have extended this to the encapsulation of anions by a metallated cryptophane with a π-acidic interior, **Figure 1.14b**.[192]

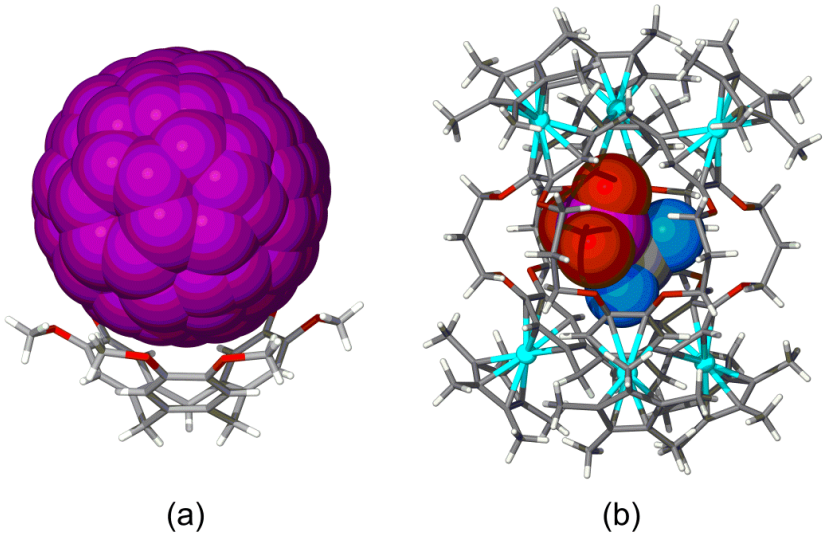

Figure 1.14 *Crystal structures of CTV-based inclusion complexes. Displaying fullerene-C_{60} binding by CTV (a) and the binding of a trifluoromethanesulfonate ($CF_3SO_3^-$) anion by Holman's π-acidic cryptophane.*[192]

Another prominent research area is in the self-assembly of ligand-functionalised CTVs to construct metallo-supramolecular architectures, with a view to isolating materials that amplify the hosting abilities of the tribenzo[*a*,*d*,*g*]cyclononatriene core through its inclusion into either a well-defined polymer,[193] or coordination cage.[194]

Research by Hardie and co-workers demonstrated the potential of such ligands in the preparation of $[Ag_2L_2]^{2+}$ capsules and $[Ag_4L_4]^{4+}$ tetrahedra through the self assembly of *tris*(3-pyridylmethylamino) and *tris*(4-pyridylmethylamino)CTG, respectively, **Figure 1.15**.[195] The two complexes were solvent templated, as evidenced through examination of their crystal structures, which displayed acetonitrile solvent acting as both ligand and guest within each cage.[196] Interestingly, use of ligand *tris*(2-pyridylmethylamino)CTG under similar conditions did not afford a discrete cage and instead gave rise to an 'entangled' coordination polymer that featured host-guest interactions between hexafluorophosphate (PF_6^-) anion and ligand cavity.[197] The same coordination network could be prepared in the presence of *ortho*-carborane which was observed to replace the PF_6^- anion, thus indicating is applicability in host-guest and recognition chemistry.[198]

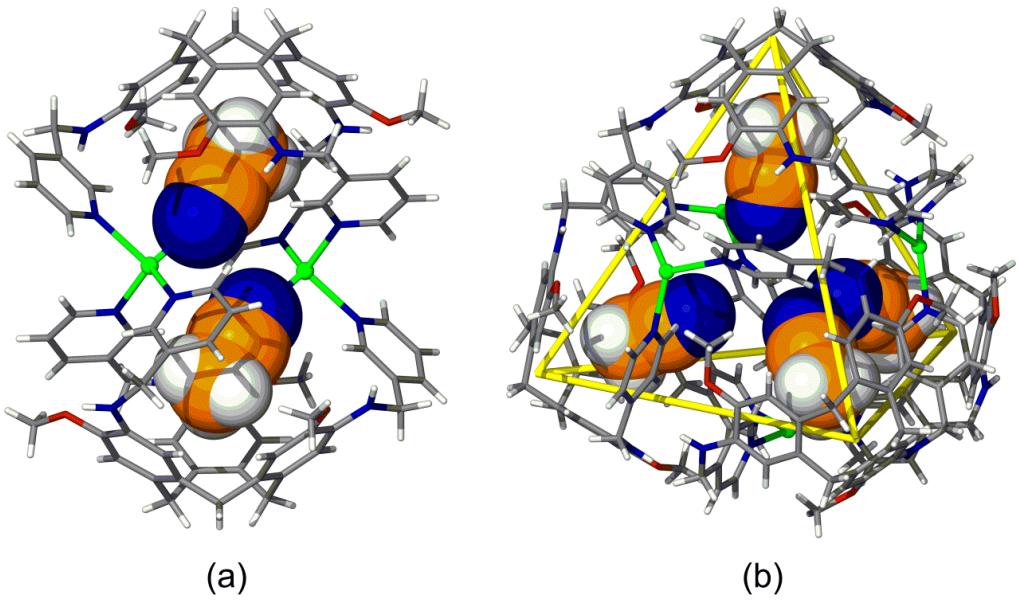

Figure 1.15 *Crystal structures of the $[Ag_2L_2]^{2+}$ capsule (a) and $[Ag_4L_4]^{4+}$ tetrahedron (b) prepared by Hardie and co-workers. Green spheres represent the silver(I) cations and the acetonitrile guests are distinguished by colour and shown in space-filling mode for clarity.*[195]

By exploring the self-assembly of ligand-functionalised CTVs with labile transition metal cations Hardie and colleagues went on to prepare a variety of discrete coordination cages, including an $[Ag_4L_4]^{4+}$ cube [199] and $[Pd_6L_8]^{12+}$ octahedron,[200] in addition to a variety of coordination polymers.[201] However, and despite the documented hosting abilities of the

tribenzo[*a*,*d*,*g*]cyclononatriene core, the coordination cages prepared did not exhibit recognition properties as predicted.

The metallo-supramolecular chemistry of ligand-functionalised CTVs is not limited to coordination cages and polymers. Hardie and co-workers went on to prepare a variety of interlocked structures that comprised a [2]-catenane and topologically complex $[Pd_4L_4]^{8+}$ 'Solomon's cube', where L = *tris*(3-pyridyl-4-pyridyl)CTG.[202]

Here, the interweaving and twisting of the ligands affords the Solomon's link within the interlocked assembly through formation of two figure-of-eight ring motifs which feature alternating over and under crossing points within the structure, **Figure 1.16**. What is most interesting is its controlled formation by self-assembly processes, unlike the template-directed procedures of Leigh and Stoddart.[30,31] The Solomon's cube represents the most complex architecture yet identified with derivatised CTVs and packs in the solid state to afford a hollow spheroid which closely resembles an Archimedean truncated hexahedron.[202] Whilst the complex was evidenced in the solution phase, its hosting abilities were severely impeded by high levels of insolubility.

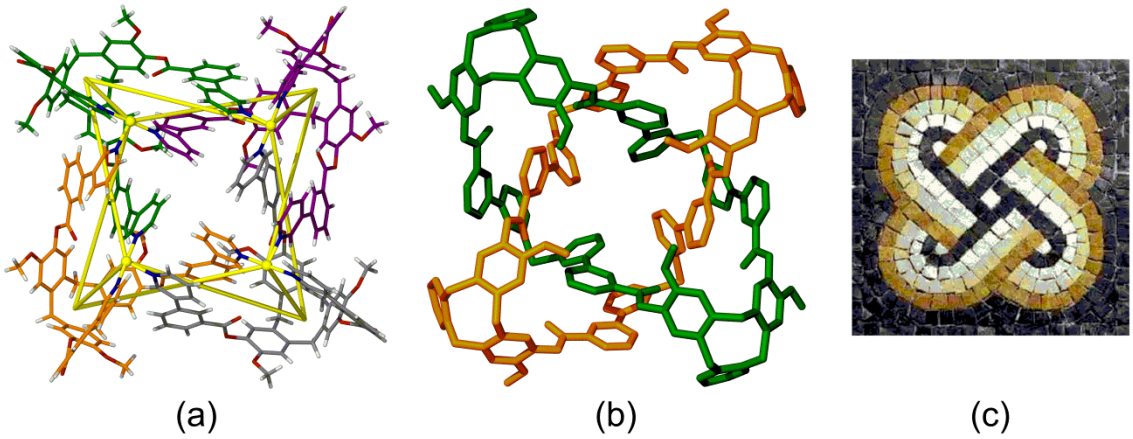

Figure 1.16 *Taken from the crystal structure of Hardie's 'Solomon's cube' (a), where the yellow lines represent the topological crossing points between individual palladium(II) centres.*[202] *The molecular Solomon's link motif (b) within the complex is colour-coded to depict the over and under relationship of the two interlocking components, which is also shown graphically (c) by means of a mural, taken from the Basilica di Aquilera, Italy.*[203]

1.8 Project outline

Aims of the research can be broadly categorised into two parts. Firstly, is the preparation of novel donor-functionalised CTV ligands for the construction of metallo-supramolecular architectures through self-assembly, both discrete and polymeric, which feature inwardly orientated host ligands. Secondly, is the detailed examination of the recognition and guest binding properties of the constructs gained, both in solution and in the crystalline solid state.

Such donor-functionalised CTV ligands will be rationally designed as to facilitate their metal-mediated self-assembly towards a single, predetermined outcome. Following their synthesis, and by considering the stereoelectronic requirements of all molecular components, it should be possible to predictably install the CTV molecular host into the aforementioned metallo-supramolecular architectures as to enhance their hosting ability.

Whilst metal-organic constructs of functionalised CTVs are known, their post-synthetic application in areas such as guest storage and separation has yet to be developed. The construction of coordination polymers that incorporate the lanthanide(III) cations will be targeted as a route towards potentially photoluminescent materials for guest sensing. Likewise, the isolation of robust and potentially porous materials bearing inwardly orientated CTV ligands may offer a suitable chemical platform for the binding and separation of gases.

The ability to control the solution-phase self-assembly of ligand-functionalised CTVs remains challenging. A principal aim is to prepare discrete metallo-cages that possess a well-defined internal void space for application in sophisticated host-guest chemistry and which are capable of the selective sequestration of guest molecules, molecular cargo delivery and the facilitation of chemical reactions.

1.9 Bibliography

[1] (a) J. D. van der Waals, *Verhand. Kon. Akad.* **1880**, *20*, 1; (b) K.-T. Tang, J. P. Toennies, *Angew. Chem. Int. Ed.* **2010**, *49*, 9574-9579; (c) F. London, *Z. Physik* **1930**, *63*, 245-279; (d) F. London, *J. Chem. Soc., Faraday Trans.* **1937**, *33*, 8-26.

[2] (a) H. E. Fischer, *Ber. Deutsch. Chem. Ges.* **1894**, *27*, 2985-2992; (b) H. Kunz, *Angew. Chem. Int. Ed.* **2002**, *41*, 4439-4451.

[3] (a) J. M. Lehn, *Angew. Chem. Int. Ed.* **1988**, *27*, 89-112; (b) J. M. Lehn, *Science* **1993**, *260*, 1762-1763.

[4] (a) A. Werner, *Zeitschr. Anorg. Chem.* **1893**, *3*, 267-271; (b) W. M. Latimer, W. H. Rodebush, *J. Am. Chem. Soc.* **1920**, *42*, 1419-1433; (c) C. A. Hunter, J. K. M. Sanders, *J. Am. Chem. Soc.* **1990**, *112*, 5525-5534; (d) T. Steiner, *Angew. Chem. Int. Ed.* **2002**, *41*, 48-76; (e) F. J. M. Hoeben, P. Jonkheijm, E. W. Meijer, A. P. H. J. Schenning, *Chem. Rev.* **2005**, *105*, 1491-1546.

[5] K. L. Wolf, *Z. Phys. Chem. B.* **1937**, *36*, 237-287.

[6] G. R. Desiraju, *Nature* **2001**, *412*, 397-400.

[7] (a) J.-M. Lehn, *Science* **2002**, *295*, 2400-2403; (b) C. J. Pedersen, *J. Am. Chem. Soc.* **1967**, *89*, 7017-7036; (c) D. J. Cram, *Angew. Chem. Int. Ed.* **1988**, *27*, 1009-1020; (d) J.-M. Lehn, *Angew. Chem. Int. Ed.* **2013**, *52*, 2836-2850.

[8] (a) W. H. Bragg, W. L. Bragg, *Proc. R. Soc. A* **1913**, *88*, 428-438; (b) W. L. Bragg, *Proc. R. Soc. A* **1913**, *89*, 248-277; (c) J. A. K. Howard, M. R. Probert, *Science* **2014**, *343*, 1098-1102.

[9] (a) J.-C. Hierso, *Chem. Rev.* **2014**, *114*, 4838-4867; (b) M. Nilsson, *J. Mag. Reson.* **2009**, *200*, 296-302; (c) Y. Cohen, L. Avram, L. Frish, *Angew. Chem. Int. Ed.* **2005**, *44*, 520-554; (d) A. Pastor, E. Martínez-Viviente, *Coord. Chem. Rev.* **2008**, *252*, 2314-2345.

[10] D. Shechtman, I. Blech, D. Gratias, J. W. Cahn, *Phys. Rev. Lett.* **1984**, *53*, 1951-1953.

[11] G. M. Whitesides, M. Boncheva, *Proc. Natl. Acad. Sci. USA* **2002**, *99*, 4769-4774.

[12] G. M. Whitesides, B. Grzybowski, *Science* **2002**, *295*, 2418-2421.

[13] (a) M. Malakoutikhah, J. J. P. Peyralans, M. Colomb-Delsuc, H. Fanlo-Virgós, M. C. A. Stuart, S. Otto, *J. Am. Chem. Soc.* **2013**, *135*, 18406-18417; (b) J. W. Steed, J. L. Atwood, *Wiley* **2009**.

[14] (a) C. Piguet, *Dalton Trans.* **2011**, *40*, 8059-8071; (b) C. Piguet, *Chem. Commun.* **2010**, *46*, 6209-6231; (c) J. Hamacek, M. Borkovec, C. Piguet, *Dalton Trans.* **2006**, 1473-1490.

[15] G. W. Orr, L. J. Barbour, J. L. Atwood, *Science* **1999**, *285*, 1049-1052.

[16] D. Philp, J. F. Stoddart, *Angew. Chem. Int. Ed.* **1996**, *35*, 1154-1196.

[17] R. W. Saalfrank, H. Maid, A. Scheurer, *Angew. Chem. Int. Ed.* **2008**, *47*, 8794-8824.

[18] (a) Q. Wang, E. Kaltgrad, T. Lin, J. E. Johnson, M. G. Finn, *Chemistry & biology* **2002**, *9*, 805-811; (b) C. Helgstrand, W. R. Wikoff, R. L. Duda, R. W. Hendrix, J. E. Johnson, L. Liljas, *J. Mol. Biol.* **2003**, *334*, 885-899; (c) J. F. Stoddart, *Nature* **1988**, *334*, 10-11.

[19] (a) J. D. Watson, F. H. D. Crick, *Nature* **1953**, *171*, 737-738; (b) M. Mandelkern, J. G. Elias, D. Eden, D. M. Crothers, *J. Mol. Biol.* **1981**, *152*, 153-161; (c) P. Yakovchuk, E. Protozanova, M. D. Frank-Kamenetskii, *Nucleic Acids Res.* **2006**, *34*, 564-574.

[20] (a) C. Mao, W. Sun, Z. Shen, N. C. Seeman, *Nature* **1999**, *397*, 144-146; (b) H. Yan, X. Zhang, Z. Shen, N. C. Seeman, *Nature* **2002**, *415*, 62-65; (c) P. S. Weiss, *ACS Nano* **2008**, *2*, 1089-1096; (d) C. K. McLaughlin, G. D. Hamblin, H. F. Sleiman, *Chem. Soc. Rev.* **2011**, *40*, 5647-5656; (e) H. Yang, C. K. McLaughlin, F. A. Aldaye, G. D. Hamblin, A. Z. Rys, I. Rouiller, H. F. Sleiman, *Nat. Chem.* **2009**, *1*, 390-396; (f) I. Severcan, C. Geary, A. Chworos, N. Voss, E. Jacovetty, L. Jaeger, *Nat. Chem.* **2010**, *2*, 772-779.

[21] M. Albrecht, *Naturwissenschaften* **2007**, *94*, 951-966.

[22] N. J. Young, B. P. Hay, *Chem. Commun.* **2013**, *49*, 1354-1379.

[23] J. M. Lehn, A. Rigault, J. Siegel, J. Harrowfield, B. Chevrier, D. Moras, *Proc. Natl. Acad. Sci. USA* **1987**, *84*, 2565-2569.

[24] J. R. Nitschke, J.-M. Lehn, *Proc. Natl. Acad. Sci. USA* **2003**, *100*, 11970-11974.

[25] B. Maddox, *Nature* **2003**, *421*, 407-408.

[26] A. Sørensen, A. M. Castilla, T. K. Ronson, M. Pittelkow, J. R. Nitschke, *Angew. Chem. Int. Ed.* **2013**, *52*, 11273-11277.

[27] Y. Morita, Y. Yakiyama, S. Nakazawa, T. Murata, T. Ise, D. Hashizume, D. Shiomi, K. Sato, M. Kitagawa, K. Nakasuji, T. Takui, *J. Am. Chem. Soc.* **2010**, *132*, 6944-6946.

[28] (a) B. Hasenknopf, J.-M. Lehn, B. O. Kneisel, G. Baum, D. Fenske, *Angew. Chem. Int. Ed.* **1996**, *35*, 1838-1840; (b) P. N. W. Baxter, J. M. Lehn, K. Rissanen, *Chem. Commun.* **1997**, 1323-1324; (c) D. P. Funeriu, K. Rissanen, J.-M. P. Lehn, *Proc. Natl. Acad. Sci. USA* **2001**, *98*, 10546-10551.

[29] (a) M. J. Hardie, *Nat. Chem.* **2012**, *4*, 7-8; (b) J.-F. Ayme, J. E. Beves, D. A. Leigh, R. T. McBurney, K. Rissanen, D. Schultz, *Nat. Chem.* **2012**, *4*, 15-20.

[30] (a) C. D. Pentecost, K. S. Chichak, A. J. Peters, G. W. V. Cave, S. J. Cantrill, J. F. Stoddart, *Angew. Chem. Int. Ed.* **2007**, *46*, 218-222; (b) J. E. Beves, C. J. Campbell, D. A. Leigh, R. G. Pritchard, *Angew. Chem. Int. Ed.* **2013**, *52*, 6464-6467.

[31] (a) K. S. Chichak, S. J. Cantrill, A. R. Pease, S.-H. Chiu, G. W. V. Cave, J. L. Atwood, J. F. Stoddart, *Science* **2004**, *304*, 1308-1312; (b) K. S. Chichak, S. J. Cantrill, J. F. Stoddart, *Chem. Commun.* **2005**, 3391-3393.

[32] (a) C. D. Meyer, C. S. Joiner, J. F. Stoddart, *Chem. Soc. Rev.* **2007**, *36*, 1705-1723; (b) M. E. Belowich, J. F. Stoddart, *Chem. Soc. Rev.* **2012**, *41*, 2003-2024; (c) J. E. Beves, B. A. Blight, C. J. Campbell, D. A. Leigh, R. T. McBurney, *Angew. Chem. Int. Ed.* **2011**, *50*, 9260-9327; (d) J.-F. Ayme, J. E. Beves, C. J. Campbell, D. A. Leigh, *Chem. Soc. Rev.* **2012**, *42*, 1700-1712; (e) P. E. Barran, H. L. Cole, S. M. Goldup, D. A. Leigh, P. R. McGonigal, M. D. Symes, J. Wu, M. Zengerle, *Angew. Chem. Int. Ed.* **2011**, *50*, 12280-12284.

[33] M. Fujita, J. Yazaki, K. Ogura, *J. Am. Chem. Soc.* **1990**, *112*, 5645-5647.

[34] J. C. Sherman, D. J. Cram, *J. Am. Chem. Soc.* **1989**, *111*, 4527-4528.

[35] (a) M. Fujita, O. Sasaki, T. Mitsuhashi, T. Fujita, J. Yazaki, K. Yamaguchi, K. Ogura, *Chem. Commun.* **1996**, 1535-1536; (b) M. Fujita, M. Tominaga, A. Hori, B. Therrien, *Acc. Chem. Res.* **2005**, *38*, 369-378.

[36] (a) M. Fujita, F. Ibukuro, H. Hagihara, K. Ogura, *Nature* **1994**, *367*, 720-723; (b) M. Fujita, *Acc. Chem. Res.* **1998**, *32*, 53-61; (c) M. Fujita, N. Fujita, K. Ogura, K. Yamaguchi, *Nature* **1999**, *400*, 52-55; (d) A. Hori, K. Kumazawa, T. Kusukawa, D. K. Chand, M. Fujita, S. Sakamoto, K. Yamaguchi, *Chem. Eur. J.* **2001**, *7*, 4142-4149.

[37] C. O. Dietrich-Buchecker, J. P. Sauvage, J. P. Kintzinger, *Tetrahedron Lett.* **1983**, *24*, 5095-5098.

[38] (a) P. R. Ashton, T. T. Goodnow, A. E. Kaifer, M. V. Reddington, A. M. Z. Slawin, N. Spencer, J. F. Stoddart, C. Vicent, D. J. Williams, *Angew. Chem. Int. Ed.* **1989**, *28*, 1396-1399; (b) P. R. Ashton, C. L. Brown, E. J. T. Chrystal, T. T. Goodnow, A. E. Kaifer, K. P. Parry, A. M. Z. Slawin, N. Spencer, J. F. Stoddart, D. J. Williams, *Angew. Chem. Int. Ed.* **1991**, *30*, 1039-1042; (c) C. P. Collier, G. Mattersteig, E. W. Wong, Y. Luo, K. Beverly, J. Sampaio, F. M. Raymo, J. F. Stoddart, J. R. Heath, *Science* **2000**, *289*, 1172-1175.

[39] (a) P. J. Stang, B. Olenyuk, *Acc. Chem. Res.* **1997**, *30*, 502-518; (b) M. D. Levin, P. J. Stang, *J. Am. Chem. Soc.* **2000**, *122*, 7428-7429.

[40] B. Olenyuk, A. Fechtenkotter, P. J. Stang, *J. Chem. Soc., Dalton Trans.* **1998**, 1707-1728.

[41] (a) C. J. Kuehl, C. L. Mayne, A. M. Arif, P. J. Stang, *Org. Lett.* **2000**, *2*, 3727-3729; (b) C. J. Kuehl, S. D. Huang, P. J. Stang, *J. Am. Chem. Soc.* **2001**, *123*, 9634-9641; (c) S. Shanmugaraju, V. Vajpayee, S. Lee, K.-W. Chi, P. J. Stang, P. S. Mukherjee, *Inorg. Chem.* **2012**, *51*, 4817-4823.

[42] (a) S. Leininger, M. Schmitz, P. J. Stang, *Org. Lett.* **1999**, *1*, 1921-1923; (b) Y.-R. Zheng, P. J. Stang, *J. Am. Chem. Soc.* **2009**, *131*, 3487-3489; (c) J. Lee, K. Ghosh, P. J. Stang, *J. Am. Chem. Soc.* **2009**, *131*, 12028-12029; (d) S. Li, J. Huang, F. Zhou, T. R. Cook, X. Yan, Y. Ye, B. Zhu, B. Zheng, P. J. Stang, *J. Am. Chem. Soc.* **2014**, *136*,

5908-5911; (e) Y.-R. Zheng, W.-J. Lan, M. Wang, T. R. Cook, P. J. Stang, *J. Am. Chem. Soc.* **2011**, *133*, 17045-17055.

[43] R. Chakrabarty, P. S. Mukherjee, P. J. Stang, *Chem. Rev.* **2011**, *111*, 6810-6918.

[44] D. J. Cram, *Nature* **1992**, *356*, 29-36.

[45] J. Yoon, C. B. Knobler, E. F. Maverick, D. J. Cram, *Chem. Commun.* **1997**, 1303-1304.

[46] C. Seel, F. Vögtle, *Angew. Chem. Int. Ed.* **1992**, *31*, 528-549.

[47] (a) L. Pirondini, F. Bertolini, B. Cantadori, F. Ugozzoli, C. Massera, E. Dalcanale, *Proc. Natl. Acad. Sci. USA* **2002**, *99*, 4911-4915; (b) A. L. Balch, *Inorg. Chem.* **2014**, *53*, 3921-3925.

[48] (a) S.-K. Lin, *J. Chem. Inf. Comp. Sci.* **1996**, *36*, 367-376; (b) P. Skowronek, B. Warzajtis, U. Rychlewska, J. Gawronski, *Chem. Commun.* **2013**, *49*, 2524-2526.

[49] (a) S. Leininger, J. Fan, M. Schmitz, P. J. Stang, *Proc. Natl. Acad. Sci. USA* **2000**, *97*, 1380-1384; (b) M. M. J. Smulders, I. A. Riddell, C. Browne, J. R. Nitschke, *Chem. Soc. Rev.* **2013**, *42*, 1728-1754.

[50] A. F. Wells, *Three Dimensional Nets and Polyhedra*, Wiley, Chichester, **1997**.

[51] S. C. Harrison, *Science* **2010**, *329*, 1026-1027.

[52] (a) V. S. Reddy, S. K. Natchiar, P. L. Stewart, G. R. Nemerow, *Science* **2010**, *329*, 1071-1075; (b) H. Liu, L. Jin, S. B. S. Koh, I. Atanasov, S. Schein, L. Wu, Z. H. Zhou, *Science* **2010**, *329*, 1038-1043.

[53] J. L. Atwood, L. J. Barbour, S. J. Dalgarno, M. J. Hardie, C. L. Raston, H. R. Webb, *J. Am. Chem. Soc.* **2004**, *126*, 13170-13171.

[54] R. W. Saalfrank, A. Stark, K. Peters, H. G. von Schnering, *Angew. Chem. Int. Ed.* **1988**, *27*, 851-853.

[55] R. W. Saalfrank, B. Hörner, D. Stalke, J. Salbeck, *Angew. Chem. Int. Ed.* **1993**, *32*, 1179-1182.

[56] (a) J. K. Clegg, F. Li, K. A. Jolliffe, G. V. Meehan, L. F. Lindoy, *Chem. Commun.* **2011**, *47*, 6042-6044; (b) C. R. K. Glasson, G. V. Meehan, C. A. Motti, J. K. Clegg, P. Turner, P. Jensen, L. F. Lindoy, *Dalton Trans.* **2011**, *40*, 10481-10490.

[57] F. Li, J. K. Clegg, L. F. Lindoy, R. B. Macquart, G. V. Meehan, *Nat. Commun.* **2011**, *2*, 205.

[58] (a) B. A. Borgias, S. R. Cooper, Y. B. Koh, K. N. Raymond, *Inorg. Chem.* **1984**, *23*, 1009-1016; (b) C. Brückner, R. E. Powers, K. N. Raymond, *Angew. Chem. Int. Ed.* **1998**, *37*, 1837-1839.

[59] (a) D. L. Caulder, K. N. Raymond, *Acc. Chem. Res.* **1999**, *32*, 975-982; (b) D. L. Caulder, C. Brückner, R. E. Powers, S. König, T. N. Parac, J. A. Leary, K. N. Raymond, *J. Am. Chem. Soc.* **2001**, *123*, 8923-8938.

[60] T. N. Parac, D. L. Caulder, K. N. Raymond, *J. Am. Chem. Soc.* **1998**, *120*, 8003-8004.

[61] M. Scherer, D. L. Caulder, D. W. Johnson, K. N. Raymond, *Angew. Chem. Int. Ed.* **1999**, *38*, 1587-1592.

[62] J. S. Fleming, K. L. V. Mann, C. A. Carraz, E. Psillakis, J. C. Jeffery, J. A. McCleverty, M. D. Ward, *Angew. Chem. Int. Ed.* **1998**, *37*, 1279-1281.

[63] (a) R. L. Paul, Z. R. Bell, J. S. Fleming, J. C. Jeffery, J. A. McCleverty, M. D. Ward, *Heteroatom Chem.* **2002**, *13*, 567-573; (b) R. L. Paul, Z. R. Bell, J. C. Jeffery, J. A. McCleverty, M. D. Ward, *Proc. Natl. Acad. Sci. USA* **2002**, *99*, 4883-4888.

[64] D. Fiedler, H. van Halbeek, R. G. Bergman, K. N. Raymond, *J. Am. Chem. Soc.* **2006**, *128*, 10240-10252.

[65] C. J. Hastings, M. D. Pluth, R. G. Bergman, K. N. Raymond, *J. Am. Chem. Soc.* **2010**, *132*, 6938-6940.

[66] D. H. Leung, R. G. Bergman, K. N. Raymond, *J. Am. Chem. Soc.* **2006**, *128*, 9781-9797.

[67] J. R. Nitschke, *Angew. Chem. Int. Ed.* **2004**, *43*, 3073-3075.

[68] P. Mal, D. Schultz, K. Beyeh, K. Rissanen, J. R. Nitschke, *Angew. Chem. Int. Ed.* **2008**, *47*, 8297-8301.

[69] (a) J. R. Nitschke, *Nature* **2009**, *462*, 736-738; (b) J. R. Nitschke, *Chem. Soc. Rev.* **2014**, *43*, 1798-1799.

[70] S. Zarra, M. M. J. Smulders, Q. Lefebvre, J. K. Clegg, J. R. Nitschke, *Angew. Chem. Int. Ed.* **2012**, *51*, 6882-6885.

[71] P. Mal, B. Breiner, K. Rissanen, J. R. Nitschke, *Science* **2009**, *324*, 1697-1699.

[72] (a) S. Mecozzi, J. J. Rebek, *Chem. Eur. J.* **1998**, *4*, 1016-1022; (b) F. Hof, S. L. Craig, C. Nuckolls, J. J. Rebek, *Angew. Chem. Int. Ed.* **2002**, *41*, 1488-1508.

[73] Swiss PDBviewer: *spdbv.vital-it.ch*.

[74] M. M. J. Smulders, J. R. Nitschke, *Chem. Sci.* **2012**, *3*, 785-788.

[75] (a) J. K. Clegg, J. Cremers, A. J. Hogben, B. Breiner, M. M. J. Smulders, J. D. Thoburn, J. R. Nitschke, *Chem. Sci.* **2013**, *4*, 68-76; (b) J. Mosquera, S. Zarra, J. R. Nitschke, *Angew. Chem. Int. Ed.* **2013**, *53*, 1556-1559.

[76] (a) T. K. Ronson, C. Giri, N. Kodiah Beyeh, A. Minkkinen, F. Topić, J. J. Holstein, K. Rissanen, J. R. Nitschke, *Chem. Eur. J.* **2013**, *19*, 3374-3382; (b) A. Jiménez, R. A. Bilbeisi, T. K. Ronson, S. Zarra, C. Woodhead, J. R. Nitschke, *Angew. Chem. Int. Ed.* **2014**, *53*, 4556-4560.

[77] (a) B. El Aroussi, N. Dupont, G. Bernardinelli, J. Hamacek, *Inorg. Chem.* **2009**, *49*, 606-615; (b) B. El Aroussi, L. Guénée, P. Pal, J. Hamacek, *Inorg. Chem.* **2011**, *50*, 8588-8597; (c) J. Hamacek, C. Besnard, T. Penhouet, P.-Y. Morgantini, *Chem. Eur. J.* **2011**, *17*, 6753-6764; (d) Y. Jiao, J. Wang, P. Wu, L. Zhao, C. He, J. Zhang, C. Duan, *Chem. Eur. J.* **2014**, *20*, 2224-2231.

[78] S. P. Black, A. R. Stefankiewicz, M. M. J. Smulders, D. Sattler, C. A. Schalley, J. R. Nitschke, J. K. M. Sanders, *Angew. Chem. Int. Ed.* **2013**, *52*, 5749-5752.

[79] P. Kruger, A. Ferguson, M. A. Squire, R. Clerac, C. Mathoniere, D. Mitcov, D. Siretanu, *Chem. Commun.* **2013**, *49*, 1597-1599.

[80] (a) S. P. Argent, H. Adams, T. Riis-Johannessen, J. C. Jeffery, L. P. Harding, M. D. Ward, *J. Am. Chem. Soc.* **2006**, *128*, 72-73; (b) S. P. Argent, H. Adams, T. Riis-Johannessen, J. C. Jeffery, L. P. Harding, W. Clegg, R. W. Harrington, M. D. Ward, *Dalton Trans.* **2006**, 4996-5013.

[81] (a) I. S. Tidmarsh, T. B. Faust, H. Adams, L. P. Harding, L. Russo, W. Clegg, M. D. Ward, *J. Am. Chem. Soc.* **2008**, *130*, 15167-15175; (b) M. D. Ward, *Chem. Commun.* **2009**, 4487-4499.

[82] (a) S. Turega, M. Whitehead, B. R. Hall, A. J. H. M. Meijer, C. A. Hunter, M. D. Ward, *Inorg. Chem.* **2013**, *52*, 1122-1132; (b) M. Whitehead, S. Turega, A. Stephenson, C. A. Hunter, M. D. Ward, *Chem. Sci.* **2013**, *4*, 2744-2751.

[83] M. M. J. Smulders, A. Jiménez, J. R. Nitschke, *Angew. Chem. Int. Ed.* **2012**, *51*, 6681-6685.

[84] W. Meng, B. Breiner, K. Rissanen, J. D. Thoburn, J. K. Clegg, J. R. Nitschke, *Angew. Chem. Int. Ed.* **2011**, *50*, 3479-3483.

[85] W. J. Ramsay, T. K. Ronson, J. K. Clegg, J. R. Nitschke, *Angew. Chem. Int. Ed.* **2013**, *52*, 13439-13443.

[86] C. Browne, S. Brenet, J. K. Clegg, J. R. Nitschke, *Angew. Chem. Int. Ed.* **2013**, *125*, 1998-2002.

[87] M. Fujita, D. Oguro, M. Miyazawa, H. Oka, K. Yamaguchi, K. Ogura, *Nature* **1995**, *378*, 469-471.

[88] M. Yoshizawa, J. K. Klosterman, M. Fujita, *Angew. Chem. Int. Ed.* **2009**, *48*, 3418-3438.

[89] Y. Inokuma, T. Arai, M. Fujita, *Nat. Chem.* **2011**, *2*, 780-783.

[90] H. Takezawa, T. Murase, G. Resnati, P. Metrangolo, M. Fujita, *J. Am. Chem. Soc.* **2014**, *136*, 1786-1788.

[91] M. Yoshizawa, S. Miyagi, M. Kawano, K. Ishiguro, M. Fujita, *J. Am. Chem. Soc.* **2004**, *126*, 9172-9173.

[92] Y. Inokuma, M. Kawano, M. Fujita, *Nat. Chem.* **2011**, *3*, 349-358.

[93] M. Kawano, Y. Kobayashi, T. Ozeki, M. Fujita, *J. Am. Chem. Soc.* **2006**, *128*, 6558-6559.

[94] S. Horiuchi, T. Murase, M. Fujita, *J. Am. Chem. Soc.* **2011**, *133*, 12445-12447.

[95] (a) T. Murase, S. Horiuchi, M. Fujita, *J. Am. Chem. Soc.* **2010**, *132*, 2866-2867; (b) Y. Kohyama, T. Murase, M. Fujita, *J. Am. Chem. Soc.* **2014**, *136*, 2966-2969.

[96] F. Hof, J. Rebek, *Proc. Natl. Acad. Sci. USA* **2002**, *99*, 4775-4777.

[97] (a) R. S. Meissner, J. J. Rebek, J. De Mendoza, *Science* **1995**, *270*, 1485-1488; (b) J. Kang, J. Rebek, *Nature* **1997**, *385*, 50-52.

[98] S. Hiraoka, K. Harano, M. Shiro, Y. Ozawa, N. Yasuda, K. Toriumi, M. Shionoya, *Angew. Chem. Int. Ed.* **2006**, *45*, 6488-6491.

[99] S. Hiraoka, Y. Yamauchi, R. Arakane, M. Shionoya, *J. Am. Chem. Soc.* **2009**, *131*, 11646-11647.

[100] (a) D. Xu, R. Warmuth, *J. Am. Chem. Soc.* **2008**, *130*, 7520-7521; (b) J. Sun, R. Warmuth, *Chem. Commun.* **2011**, *47*, 9351-9353.

[101] S. Pasquale, S. Sattin, E. C. Escudero-Adán, M. Martínez-Belmonte, J. de Mendoza, *Nat. Commun.* **2012**, *3*, 785.

[102] R. A. Bilbeisi, T. K. Ronson, J. R. Nitschke, *Angew. Chem. Int. Ed.* **2013**, *52*, 9027-9030.

[103] B. Olenyuk, J. A. Whiteford, A. Fechtenkotter, P. J. Stang, *Nature* **1999**, *398*, 796-799.

[104] (a) U. Radhakrishnan, M. Schweiger, P. J. Stang, *Org. Lett.* **2001**, *3*, 3141-3143; (b) C. J. Kuehl, Y. K. Kryschenko, U. Radhakrishnan, S. R. Seidel, S. D. Huang, P. J. Stang, *Proc. Natl. Acad. Sci. USA* **2002**, *99*, 4932-4936; (c) S. R. Seidel, P. J. Stang, *Acc. Chem. Res.* **2002**, *35*, 972-983; (d) H.-B. Yang, K. Ghosh, A. M. Arif, P. J. Stang, *J. Org. Chem.* **2006**, *71*, 9464-9469.

[105] D. Fujita, A. Takahashi, S. Sato, M. Fujita, *J. Am. Chem. Soc.* **2011**, *133*, 13317-13319.

[106] K. Suzuki, S. Sato, M. Fujita, *Nat. Chem.* **2010**, *2*, 25-29.

[107] K. Suzuki, K. Takao, S. Sato, M. Fujita, *J. Am. Chem. Soc.* **2010**, *132*, 2544-2545.

[108] D. Fujita, K. Suzuki, S. Sato, M. Yagi-Utsumi, Y. Yamaguchi, N. Mizuno, T. Kumasaka, M. Takata, M. Noda, S. Uchiyama, K. Kato, M. Fujita, *Nat. Commun.* **2012**, *3*, 1093.

[109] Q.-F. Sun, T. Murase, S. Sato, M. Fujita, *Angew. Chem. Int. Ed.* **2011**, *50*, 10318-10321.

[110] M. J. Hardie, C. L. Raston, *J. Chem. Soc., Dalton Trans.* **2000**, 2483-2492.

[111] S. Casjens, *Virus Structure and Assembly, Jones and Bartlett, Boston, MA*, **1985**.

[112] Q.-F. Sun, J. Iwasa, D. Ogawa, Y. Ishido, S. Sato, T. Ozeki, Y. Sei, K. Yamaguchi, M. Fujita, *Science* **2010**, *328*, 1144-1147.

[113] K. Li, L.-Y. Zhang, C. Yan, S.-C. Wei, M. Pan, L. Zhang, C.-Y. Su, *J. Am. Chem. Soc.* **2014**, *136*, 4456-4459.

[114] T. R. Cook, Y.-R. Zheng, P. J. Stang, *Chem. Rev.* **2012**, *113*, 734-777.

[115] R. Robson, *J. Chem. Soc., Dalton Trans.* **2000**, 3735-3744.

[116] (a) A. Schoedel, M. J. Zaworotko, *Chem. Sci.* **2014**, *5*, 1269-1282; (b) N. Rigby, T. Jacobs, J. P. Reddy, M. J. Hardie, *Cryst. Growth Des.* **2012**, *12*, 1871-1881.

[117] The Cambridge Crystallographic Database (CCDC), *www.ccdc.cam.ac.uk*.

[118] (a) P. Gamez, P. d. Hoog, O. Roubeau, M. Lutz, W. L. Driessen, A. L. Spek, J. Reedijk, *Chem. Commun.* **2002**, 1488-1489; (b) D. Dutta, A. D. Jana, M. Debnath, A. Bhaumik, J. Marek, M. Ali, *Dalton Trans.* **2010**, *39*, 11551-11559.

[119] (a) Y. B. Go, X. Wang, A. J. Jacobson, *Inorg. Chem.* **2007**, *46*, 6594-6600; (b) K. Biradha, M. Fujita, *Chem. Commun.* **2001**, 15-16; (c) A. M. P. Peedikakkal, Y. M. Song, R. G. Xiong, S. Gao, J. J. Vittal, *Eur. J. Inorg. Chem.* **2010**, *24*, 3856-3865; (d) L. L. Wen, D. B. Dang, C. Y. Duan, Y. Z. Li, Z. F. Tian, Q. J. Meng, *Inorg. Chem.* **2005**, *44*, 7161-7170; (e) S. J. Dalgarno, M. J. Hardie, J. L. Atwood, J. E. Warren, C. L. Raston, *New J. Chem.* **2005**, *29*, 649-652; (f) Q. Zhu, T. Sheng, R. Fu, C. Tan, S. Hu, X. Wu, *Chem. Commun.* **2010**, *46*, 9001-9003; (g) D.-S. Li, F. Fu, J. Zhao, Y.-P. Wu, M. Du, K. Zou, W.-W. Dong, Y.-Y. Wang, *Dalton Trans.* **2010**, *39*, 11522-11525; (h) Y. Y. Zhang, S. X. Liu, K. K. Du, M. X. Xue, *Inorg. Chem. Commun.* **2010**, *13*, 641-644; (i) L. J. Zhang, D. H. Xu, Y. S. Zhou, F. Jiang, *New J. Chem.* **2010**, *34*, 2470-2478; (j) F. Dai, D. Sun, D. Sun, *Cryst. Growth Des.* **2011**, *11*, 5670-5675; (k) F. Meng, L. Qin, M. Zhang, H. Zheng, *CrystEngComm* **2014**, *16*, 698-706.

[120] G. R. Desiraju, *Angew. Chem. Int. Ed.* **1995**, *34*, 2311-2327.

[121] R. H. Friend, R. W. Gymer, A. B. Holmes, J. H. Burroughes, R. N. Marks, C. Taliani, D. D. C. Bradley, D. A. D. Santos, J. L. Bredas, M. Logdlund, W. R. Salaneck, *Nature* **1999**, *397*, 121-128.

[122] C. Weder, *Nature* **2009**, *459*, 45-46.

[123] G. D. Stucky, *Nature* **2001**, *410*, 885-886.

[124] T. F. A. de Greef, E. W. Meijer, *Nature* **2008**, *453*, 171-173.

[125] (a) J. C. Bailar, Jr., *Prep. Inorg. React.* **1964**, *1*, 1-57; (b) G. S. Girolami, *Inorg. Chem.* **1992**, *31*, 3183-3184.

[126] B. F. Hoskins, R. Robson, *J. Am. Chem. Soc.* **1989**, *111*, 5962-5964.

[127] B. F. Hoskins, R. Robson, *J. Am. Chem. Soc.* **1990**, *112*, 1546-1554.

[128] (a) B. Panella, M. Hirscher, *Adv. Mater.* **2005**, *17*, 538-541; (b) K. Sanderson, *Nature* **2007**, *448*, 746-748.

[129] O. M. Yaghi, H. Li, *J. Am. Chem. Soc.* **1995**, *117*, 10401-10402.

[130] A. J. Blake, N. R. Champness, T. L. Easun, D. R. Allan, H. Nowell, M. W. George, J. Jia, X.-Z. Sun, *Nat. Chem.* **2010**, *2*, 688-694.

[131] N. L. Rosi, J. Eckert, M. Eddaoudi, D. T. Vodak, J. Kim, M. O'Keeffe, O. M. Yaghi, *Science* **2003**, *300*, 1127-1129.

[132] (a) O. M. Yaghi, M. O'Keeffe, N. W. Ockwig, H. K. Chae, M. Eddaoudi, J. Kim, *Nature* **2003**, *423*, 705-714; (b) J. L. C. Rowsell, A. R. Millward, K. S. Park, O. M.

Yaghi, *J. Am. Chem. Soc.* **2004**, *126*, 5666-5667; (c) A. C. Sudik, A. P. Côté, A. G. Wong-Foy, M. O'Keeffe, O. M. Yaghi, *Angew. Chem. Int. Ed.* **2006**, *45*, 2528-2533.

[133] H. K. Chae, J. Kim, O. D. Friedrichs, M. O'Keeffe, O. M. Yaghi, *Angew. Chem. Int. Ed.* **2003**, *42*, 3907-3909.

[134] S. S. Kaye, A. Dailly, O. M. Yaghi, J. R. Long, *J. Am. Chem. Soc.* **2007**, *129*, 14176-14177.

[135] (a) A. P. Côté, A. I. Benin, N. W. Ockwig, M. O'Keeffe, A. J. Matzger, O. M. Yaghi, *Science* **2005**, *310*, 1166-1170; (b) S. S. Han, H. Furukawa, O. M. Yaghi, W. A. Goddard, *J. Am. Chem. Soc.* **2008**, *130*, 11580-11581.

[136] (a) Q. W. Li, C. H. Sue, S. Basu, A. K. Shveyd, W. Y. Zhang, G. Barin, L. Fang, A. A. Sarjeant, J. F. Stoddart, O. M. Yaghi, *Angew. Chem. Int. Ed.* **2010**, *49*, 6751-6755; (b) H. Deng, M. A. Olson, J. F. Stoddart, O. M. Yaghi, *Nat. Chem.* **2010**, *2*, 439-443; (c) A. Coskun, M. Hmadeh, G. Barin, F. Gándara, Q. Li, E. Choi, N. L. Strutt, D. B. Cordes, A. M. Z. Slawin, J. F. Stoddart, J.-P. Sauvage, O. M. Yaghi, *Angew. Chem. Int. Ed.* **2012**, *51*, 2160-2163; (d) Q. Li, W. Zhang, O. Š. Miljanić, C.-H. Sue, Y.-L. Zhao, L. Liu, C. B. Knobler, J. F. Stoddart, O. M. Yaghi, *Science* **2009**, *325*, 855-859.

[137] (a) S. J. Loeb, *Chem. Commun.* **2005**, 1511-1518; (b) D. J. Hoffart, S. J. Loeb, *Supramol. Chem.* **2007**, *19*, 89-93; (c) H.-Y. Gong, B. M. Rambo, W. Cho, V. M. Lynch, M. Oh, J. L. Sessler, *Chem. Commun.* **2011**, *47*, 5973-5975.

[138] A. R. Millward, O. M. Yaghi, *J Am Chem Soc* **2005**, *127*, 17998-17999.

[139] (a) H. Furukawa, N. Ko, Y. B. Go, N. Aratani, S. B. Choi, E. Choi, A. O. Yazaydin, R. Q. Snurr, M. O'Keeffe, J. Kim, O. M. Yaghi, *Science* **2010**, *329*, 424-428; (b) H. Deng, S. Grunder, K. E. Cordova, C. Valente, H. Furukawa, M. Hmadeh, F. Gándara, A. C. Whalley, Z. Liu, S. Asahina, H. Kazumori, M. O'Keeffe, O. Terasaki, J. F. Stoddart, O. M. Yaghi, *Science* **2012**, *336*, 1018-1023.

[140] (a) N. W. Ockwig, O. Delgado-Friedrichs, M. O'Keeffe, O. M. Yaghi, *Acc. Chem. Res.* **2005**, *38*, 176-182; (b) M. O'Keeffe, M. A. Peskov, S. J. Ramsden, O. M. Yaghi, *Acc. Chem. Res.* **2008**, *41*, 1782-1789; (c) O. Delgado-Friedrichs, M. O'Keeffe, *J. Solid State Chem.* **2005**, *178*, 2480-2485; (d) V. A. Blatov, M. O'Keeffe, D. M. Proserpio, *CrystEngComm* **2010**, *12*, 44-48; (e) S. R. Batten, N. R. Champness, X.-M. Chen, J. Garcia-Martinez, S. Kitagawa, L. Ohrstrom, M. O'Keeffe, M. P. Suh, J. Reedijk, *Pure Appl. Chem.* **2013**, *85*, 1715-1724; (f) O. Delgado-Friedrichs, M. O'Keeffe, O. M. Yaghi, *PhysChemChemPhys* **2007**, *9*, 1035-1043.

[141] S. Xiang, Y. He, Z. Zhang, H. Wu, W. Zhou, R. Krishna, B. Chen, *Nat. Commun.* **2012**, *3*, 954.

[142] S.-C. Xiang, Z. Zhang, C.-G. Zhao, K. Hong, X. Zhao, D.-R. Ding, M.-H. Xie, C.-D. Wu, M. C. Das, R. Gill, K. M. Thomas, B. Chen, *Nat. Commun.* **2011**, *2*, 204.

[143] K. Caldeira, P. B. Duffy, *Science* **2000**, *287*, 620-622.

[144] A. Demessence, D. M. D'Alessandro, M. L. Foo, J. R. Long, *J. Am. Chem. Soc.* **2009**, *131*, 8784-8786.

[145] T. M. McDonald, D. M. D'Alessandro, R. Krishna, J. R. Long, *Chem. Sci.* **2011**, *2*, 2022-2028.

[146] J. A. Mason, M. Veenstra, J. R. Long, *Chem. Sci.* **2014**, *5*, 32-51.

[147] K. Sumida, S. Horike, S. S. Kaye, Z. R. Herm, W. L. Queen, C. M. Brown, F. Grandjean, G. J. Long, A. Dailly, J. R. Long, *Chem. Sci.* **2010**, *1*, 184-191.

[148] S. J. Geier, J. A. Mason, E. D. Bloch, W. L. Queen, M. R. Hudson, C. M. Brown, J. R. Long, *Chem. Sci.* **2013**, *4*, 2054-2061.

[149] S. Kitagawa, R. Kitaura, S.-i. Noro, *Angew. Chem. Int. Ed.* **2004**, *43*, 2334-2375.

[150] T. Uemura, N. Yanai, S. Kitagawa, *Chem. Soc. Rev.* **2009**, *38*, 1228-1236.

[151] T. Uemura, D. Hiramatsu, Y. Kubota, M. Takata, S. Kitagawa, *Angew. Chem. Int. Ed.* **2007**, *46*, 4987-4990.

[152] S. Horike, S. Shimomura, S. Kitagawa, *Nat. Chem.* **2009**, *1*, 695-704.

[153] T. Uemura, R. Kitaura, Y. Ohta, M. Nagaoka, S. Kitagawa, *Angew. Chem. Int. Ed.* **2006**, *45*, 4112-4116.

[154] Y. Inokuma, S. Yoshioka, J. Ariyoshi, T. Arai, Y. Hitora, K. Takada, S. Matsunaga, K. Rissanen, M. Fujita, *Nature* **2013**, *495*, 461-466.

[155] Y. Inokuma, S. Yoshioka, J. Ariyoshi, T. Arai, Y. Hitora, K. Takada, S. Matsunaga, K. Rissanen, M. Fujita, *Nature* **2013**, *501*, 262-262.

[156] (a) P. Stallforth, J. Clardy, *Nature* **2013**, *495*, 456-457; (b) A. Stoddart, *Nat. Mater.* **2013**, *12*, 378-378.

[157] A. Doerr, *Nat. Methods* **2013**, *10*, 460-461.

[158] (a) J. L. Atwood, L. J. Barbour, A. Jerga, B. L. Schottel, *Science* **2002**, *298*, 1000-1002; (b) A. Szumna, *Chem. Soc. Rev.* **2010**, *39*, 4274-4285.

[159] J. L. Atwood, L. J. Barbour, A. Jerga, *Science* **2002**, *296*, 2367-2369.

[160] (a) R. S. Forgan, D. C. Friedman, C. L. Stern, C. J. Bruns, J. F. Stoddart, *Chem. Commun.* **2010**, *46*, 5861-5863; (b) C. J. Bruns, S. Basu, J. Fraser Stoddart, *Tetrahedron Lett.* **2010**, *51*, 983-986.

[161] Z. Liu, M. Frasconi, J. Lei, Z. J. Brown, Z. Zhu, D. Cao, J. Iehl, G. Liu, A. C. Fahrenbach, Y. Y. Botros, O. K. Farha, J. T. Hupp, C. A. Mirkin, J. Fraser Stoddart, *Nat. Commun.* **2013**, *4*, 1855.

[162] (a) S. Shinkai, K. Araki, O. Manabe, *J. Am. Chem. Soc.* **1988**, *110*, 7214-7215; (b) S. J. Dalgarno, C. L. Raston, *Chem. Commun.* **2002**, 2216-2217.

[163] (a) C. Ke, N. L. Strutt, H. Li, X. Hou, K. J. Hartlieb, P. R. McGonigal, Z. Ma, J. Iehl, C. L. Stern, C. Cheng, Z. Zhu, N. A. Vermeulen, T. J. Meade, Y. Y. Botros, J. F. Stoddart,

J. Am. Chem. Soc. **2013**, *135*, 17019-17030; (b) H. Zhang, Y. Zhao, *Chem. Eur. J.* **2013**, *19*, 16862-16879.

[164] S. T. Schneebeli, C. Cheng, K. J. Hartlieb, N. L. Strutt, A. A. Sarjeant, C. L. Stern, J. F. Stoddart, *Chem. Eur. J.* **2013**, *19*, 3860-3868.

[165] J. Černochová, P. Branná, M. Rouchal, P. Kulhánek, I. Kuřitka, R. Vícha, *Chem. Eur. J.* **2012**, *18*, 13633-13637.

[166] (a) J. C. Barnes, M. Juríček, N. L. Strutt, M. Frasconi, S. Sampath, M. A. Giesener, P. L. McGrier, C. J. Bruns, C. L. Stern, A. A. Sarjeant, J. F. Stoddart, *J. Am. Chem. Soc.* **2012**, *135*, 183-192; (b) J. C. Barnes, M. Juríček, N. A. Vermeulen, E. J. Dale, J. F. Stoddart, *J. Org. Chem.* **2013**, *78*, 11962-11969; (c) M. Juricek, J. C. Barnes, N. L. Strutt, N. A. Vermeulen, K. C. Ghooray, E. J. Dale, P. R. McGonigal, A. K. Blackburn, A.-J. Avestro, J. F. Stoddart, *Chem. Sci.* **2014**, *5*, 2724-2731.

[167] R. S. Forgan, C. Wang, D. C. Friedman, J. M. Spruell, C. L. Stern, A. A. Sarjeant, D. Cao, J. F. Stoddart, *Chem. Eur. J.* **2012**, *18*, 202-212.

[168] J. C. Barnes, A. C. Fahrenbach, D. Cao, S. M. Dyar, M. Frasconi, M. A. Giesener, D. Benítez, E. Tkatchouk, O. Chernyashevskyy, W. H. Shin, H. Li, S. Sampath, C. L. Stern, A. A. Sarjeant, K. J. Hartlieb, Z. Liu, R. Carmieli, Y. Y. Botros, J. W. Choi, A. M. Z. Slawin, J. B. Ketterson, M. R. Wasielewski, W. A. Goddard, J. F. Stoddart, *Science* **2013**, *339*, 429-433.

[169] (a) M. Juríček, J. C. Barnes, E. J. Dale, W.-G. Liu, N. L. Strutt, C. J. Bruns, N. A. Vermeulen, K. C. Ghooray, A. A. Sarjeant, C. L. Stern, Y. Y. Botros, W. A. Goddard, J. F. Stoddart, *J. Am. Chem. Soc.* **2013**, *135*, 12736-12746; (b) R. M. Young, S. M. Dyar, J. C. Barnes, M. Juríček, J. F. Stoddart, D. T. Co, M. R. Wasielewski, *J. Phys. Chem. A* **2013**, *117*, 12438-12448.

[170] (a) M. J. Hardie, *Chem. Soc. Rev.* **2010**, *39*, 516-527; (b) J. L. Scott, D. R. MacFarlane, C. L. Raston, C. M. Teoh, *Green Chem.* **2000**, *2*, 123-126.

[171] O. Taratula, P. A. Hill, N. S. Khan, P. J. Carroll, I. J. Dmochowski, *Nat. Commun.* **2010**, *1*, 148.

[172] (a) H. Zimmermann, P. Tolstoy, H.-H. Limbach, R. Poupko, Z. Luz, *J. Phys. Chem. B* **2004**, *108*, 18772-18778; (b) A. Collet, *Tetrahedron* **1987**, *43*, 5725-5759.

[173] J. W. Steed, H. Zhang, J. L. Atwood, *Supramol. Chem.* **1996**, *7*, 37-45.

[174] J. Costante, C. Garcia, A. Collet, *Chirality* **1997**, *9*, 446-453.

[175] J. Canceill, J. Gabard, A. Collet, *J. Am. Chem. Soc.* **1983**, 122-123.

[176] J. J. Loughrey, C. A. Kilner, M. J. Hardie, M. A. Halcrow, *Supramol. Chem.* **2011**, *24*, 2-13.

[177] M. J. Hardie, R. M. Mills, C. J. Sumby, *J. Org. Biol. Chem.* **2004**, *2*, 2958-2964.

[178] C. Garcia, J. Malthete, A. Collet, *Bull. Soc. Chim. Fra.* **1993**, 93-95.

[179] M. J. Hardie, R. Ahmad, C. J. Sumby, *New J. Chem.* **2005**, *29*, 1231-1240.

[180] M. A. Little, J. J. Loughrey, A. Santoro, M. A. Halcrow, M. J. Hardie, *Tetrahedron Lett*. **2014**, *55*, 2530-2533.

[181] (a) C. Carruthers, J. Fisher, L. P. Harding, M. J. Hardie, *Dalton Trans.* **2010**, *39*, 355-357; (b) M. J. Hardie, C. L. Raston, *Chem. Commun.* **1999**, 1153-1163.

[182] J. L. Atwood, M. J. Barnes, M. G. Gardiner, C. L. Raston, *Chem. Commun.* **1996**, 1449-1450.

[183] (a) E. Huerta, H. Isla, E. M. Perez, C. Bo, N. Martin, J. d. Mendoza, *J. Am. Chem. Soc.* **2010**, *132*, 5351-5353; (b) E. Huerta, G. A. Metselaar, A. Fragoso, E. Santos, C. Bo, J. de Mendoza, *Angew. Chem. Int. Ed.* **2007**, *46*, 202-205.

[184] E. Huerta, E. Cequier, J. d. Mendoza, *Chem. Commun.* **2007**, 5016-5018.

[185] R. Ahmad, I. Dix, M. J. Hardie, *Inorg. Chem.* **2003**, *42*, 2182-2184.

[186] T. Brotin, J.-P. Dutasta, *Chem. Rev.* **2008**, *109*, 88-130.

[187] K. T. Holman, *Encyclopedia of Supramolecular Chemistry. CRC Press* **2004**, 340-348.

[188] (a) C. E. O. Roesky, E. Weber, T. Rambusch, H. Stephan, K. Gloe, M. Czugler, *Chem. Eur. J.* **2003**, *9*, 1104-1112; (b) J. Canceill, L. Lacombe, A. Collet, *J. Chem. Soc., Chem. Commun.* **1987**, 219-221.

[189] M. A. Little, J. Donkin, J. Fisher, M. A. Halcrow, J. Loder, M. J. Hardie, *Angew. Chem. Int. Ed.* **2011**, *51*, 764-766.

[190] T. Brotin, T. Devic, A. Lesage, L. Emsley, A. Collet, *Chem. Eur. J.* **2001**, *7*, 1561-1573.

[191] (a) P. Berthault, H. Desvaux, T. Wendlinger, M. Gyejacquot, A. Stopin, T. Brotin, J.-P. Dutasta, Y. Boulard, *Chem. Eur. J.* **2010**, *16*, 12941-12946; (b) L. Schröder, T. J. Lowery, C. Hilty, D. E. Wemmer, A. Pines, *Science* **2006**, *314*, 446-449.

[192] R. M. Fairchild, K. T. Holman, *J. Am. Chem. Soc.* **2005**, *127*, 16364-16365.

[193] S. T. Mough, K. T. Holman, *Chem. Commun.* **2008**, 1407-1409.

[194] M. J. Hardie, *Israel J. Chem.* **2011**, *51*, 807-816.

[195] C. J. Sumby, M. J. Hardie, *Angew. Chem. Int. Ed.* **2005**, *44*, 6395-6399.

[196] (a) C. J. Sumby, J. Fisher, T. J. Prior, M. J. Hardie, *Chem. Eur. J.* **2006**, *12*, 2945-2959; (b) C. J. Sumby, M. J. Carr, A. Franken, J. D. Kennedy, C. A. Kilner, M. J. Hardie, *New J. Chem.* **2006**, *30*, 1390-1396.

[197] C. J. Sumby, M. J. Hardie, *Cryst. Growth Des.* **2005**, *5*, 1321-1324.

[198] M. J. Hardie, *J. Chem. Crystallogr*. **2007**, *37*, 69-80.

[199] C. Carruthers, T. K. Ronson, C. J. Sumby, A. Westcott, L. P. Harding, T. J. Prior, P. Rizkallah, M. J. Hardie, *Chem. Eur. J.* **2008**, *14*, 10286-10296.

[200] (a) T. K. Ronson, C. Carruthers, J. Fisher, T. Brotin, L. P. Harding, P. J. Rizkallah, M. J. Hardie, *Inorg. Chem.* **2010**, *49*, 675-685; (b) T. K. Ronson, J. Fisher, L. P. Harding, M. J. Hardie, *Angew. Chem. Int. Ed.* **2007**, *46*, 9086-9088.

[201] (a) M. A. Little, T. K. Ronson, M. J. Hardie, *Dalton Trans.* **2011**, *40*, 12217-12227; (b) M. A. Little, M. A. Halcrow, L. P. Harding, M. J. Hardie, *Inorg. Chem.* **2010**, *49*, 9486-9496; (c) T. K. Ronson, M. J. Hardie, *CrystEngComm* **2008**, *10*, 1731-1734.

[202] T. K. Ronson, J. Fisher, L. P. Harding, P. J. Rizkallah, J. E. Warren, M. J. Hardie, *Nat. Chem.* **2009**, *1*, 212-216.

[203] (a) Image taken of the 4th Century King Solomon's knot from the mosaic pavement of Basilica di Aquilera, Italy; (b) L. Rose, *Seeing Solomon's Knot. Stone and Scott Publishers* **2005**, 1-160.

Chapter 2

Lanthanide(III) coordination polymers of hard-oxygen-functionalised host ligands

2.1 Introduction

The lanthanide cations represent attractive building blocks for supramolecular self-assembly and generate much interest due to their characteristic physicochemical properties, such as photoluminescence and magnetism.[1] As a result, a great deal of their chemistry is focussed towards imaging and sensing,[2] yet the ability to form complexes with high coordination numbers offers a route towards the construction of novel architectures that would be otherwise inaccessible with the transition series. For similar reasons, the coordination chemistry of the actinides is also an emergent field.[3]

Coordination complexes afforded through lanthanide(III) coordination include chelates, helicates and cages,[4] with their application spanning the areas of molecular recognition, sensing and catalysis.[5] Such accounts include Hamacek's $[Eu_4L_4]^{12+}$ and Duan's $[Ce_4L_4]^{12+}$ tetrahedral assemblies, which highlight anion binding and catalytic properties, respectively, **Figure 2.1**.[5] The employment of lanthanide(III) cations as an active template in the construction of topologically complex systems has been realised by Gunnlaugsson and co-workers in the preparation of both [2]- and [3]-catenanes.[6]

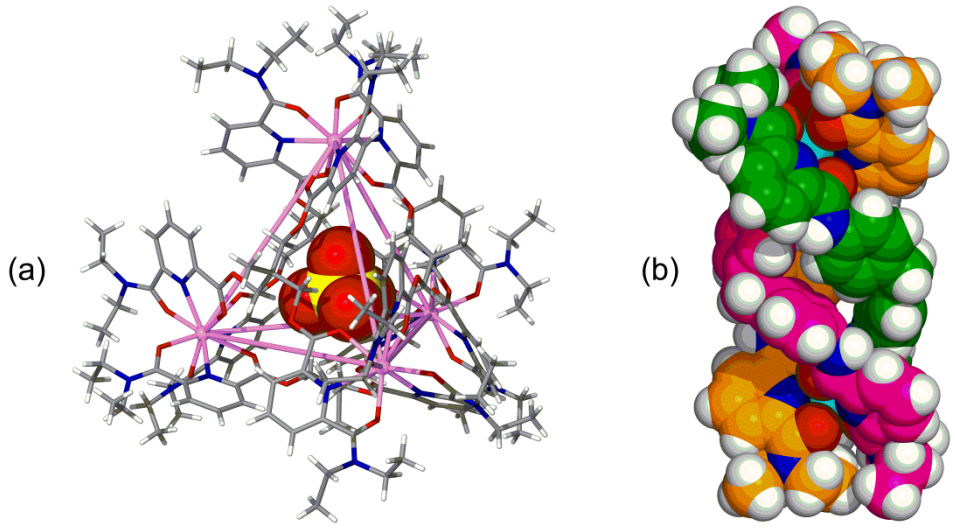

Figure 2.1 *From the crystal structures of (a) Hamacek's $[Eu_4L_4]^{12+}$ tetrahedron with encapsulated perchlorate (ClO_4^-) anion; and (b) a representative $[Nd_2L_3]^{6+}$ helicate, shown in space-filling view and with individual ligands colour-coded for clarity.*

The physical properties of the lanthanide series can be transferred to the bulk crystalline solid by inclusion into coordination polymers.[7] For example, a ratiometric and colorimetric

luminescent thermometer has been prepared by Qian and co-workers, which produces a distinctive luminescent response with a change in temperature.[8] Similarly, Dalgarno's metal-organic calixarene nanotubes display interesting magnetic properties as a result of their molecular packing in the crystalline solid state.[9]

Whilst metal-organic complexes of functionalised cyclotriveratrylenes (CTVs) and the transition metals are well exemplified in the literature,[10] coordination polymers resulting from lanthanide(III) coordination are somewhat less developed and, thus far, limited to hydrogen-bonded superstructures featuring formally uncoordinated lanthanide(III) aquo ions.[11] Structurally similar complexes have also been identified with derivatised calixarenes,[12] and lanthanide(III)-complexes of other tripodal C_3-symmetric ligands have been reported by Hamacek *et al*.[13]

Hard-oxygen-functionalised CTVs, such as carboxylate and catecholates, are known; however, their coordination chemistry is limited and the handful of complexes isolated have shown no emergent properties.[14] For example, the $[Cu_4L_4]$ tetrahedral assemblies prepared by Robson and co-workers utilising cyclotricatechylene (CTC) as ligand were plagued by oxygen sensitivity, impeding their ability to potentially host molecules.[15] An aim of this research was in the *N*-oxidation of pyridyl-functionalised CTVs to their corresponding pyridine-*N*-oxides as suitable ligands for the construction of polyhedral and polymeric assemblies with the lanthanide(III) cations.

2.2 Ligand synthesis

The preparation of (±)-2,7,12-trimethoxy-3,8,13-*tris*(hydroxy)-10,15-dihydro-5*H*-tribenzo[*a*,*d*,*g*]cyclononatriene (CTG, **2.4**) was conducted on multi-gram scale and in accordance with literature procedures, **Scheme 2.1**.[16] Alkylation of 3-hydroxy-4-methoxy benzyl alcohol (**2.1**) with allyl bromide in the presence of carbonate base generated 3-propenoxy-4-methoxy benzyl alcohol (**2.2**) in quantitative yields. Cyclisation of **2.2** to trimeric intermediate **2.3** was carried out in the melt, with a catalytic amount of phosphoric acid driving the condensation. The low yields obtained (~ 30 %) are expected for such solventless reactions, whereby the product precipitates with time and impedes stirring. Deprotection of **2.3** with palladium(II) acetate, triphenyl phosphine and diethylamine, under anhydrous and anoxic conditions, furnished **2.4** in 45% yield. As for all CTV derivatives, a characteristic ^{1}H NMR spectrum was obtained and conclusive of CTG (**2.4**) formation, with the diastereotopic *endo* and *exo* methylene protons of the tribenzo[*a*,*d*,*g*]cyclononatriene core resonating at 3.4 and 4.6 ppm, respectively, **Figure 2.2**.

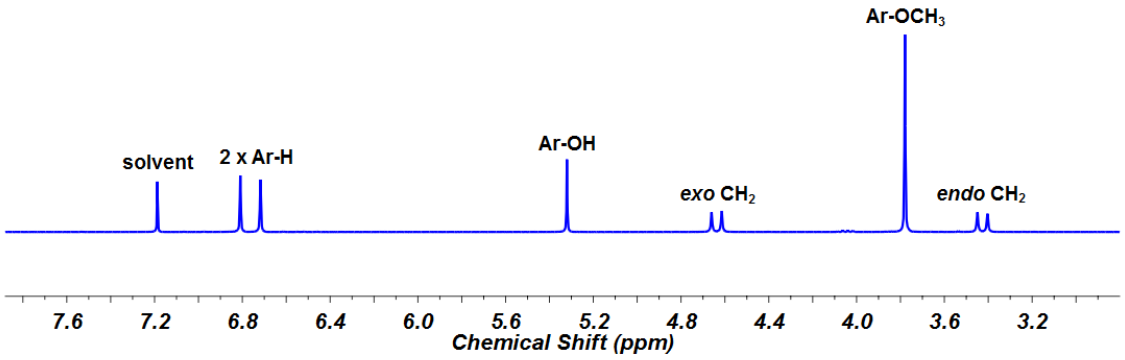

Figure 2.2 *Interpreted ^{1}H NMR spectrum of CTG (**2.4**) recorded in $CDCl_3$, noting the characteristic endo and exo diastereotopic methylene protons of the tribenzo[a,d,g]cyclononatriene core.*

CTG (**2.4**) was not chirally resolved and employed as a racemic mixture for all subsequent syntheses. Ligand precursors (±)-2,7,12-trimethoxy-3,8,13-*tris*(2-pyridylmethyloxy)-10,15-dihydro-5*H*-tribenzo[*a*,*d*,*g*]cyclononatriene (**2.5**) and (±)-2,7,12-trimethoxy-3,8,13-*tris*(3-pyridylmethyloxy)-10,15-dihydro-5*H*-tribenzo[*a*,*d*,*g*]cyclononatriene (**2.6**) were prepared through reaction of CTG with the necessary bromomethyl pyridine, **Scheme 2.1**. Ligand **2.5** was quantitatively prepared on a multi-gram scale, according to literature procedures, employing potassium carbonate base and acetone solvent.[17] Conversely, and owing to the inherent instability of 3-bromomethyl pyridine, ligand **2.6** was only accessible on a small scale and in low yield.[18] As such, reactions were conducted at low temperatures with sodium hydride (NaH) base and anhydrous and anoxic DMF solvent, in an attempt to minimize polymerisation of the electrophile.

Ligand precursors (±)-2,7,12-trimethoxy-3,8,13-*tris*(3-carboxypyridyl)-10,15-dihydro-5*H*-tribenzo[*a*,*d*,*g*]cyclononatriene (**2.7**), (±)-2,7,12-trimethoxy-3,8,13-*tris*(4-carboxypyridyl)-10,15-dihydro-5*H*-tribenzo[*a*,*d*,*g*]cyclononatriene (**2.8**), and (±)-2,7,12-trimethoxy-3,8,13-*tris*(4-pyridyl-4-carboxyphenyl)-10,15-dihydro-5*H*-tribenzo[*a*,*d*,*g*]cyclononatriene (**2.9**) were each prepared according to adapted literature procedures,[19] through substitution of the corresponding pyridine carbonyl chloride, using triethylamine as scavenger base and anhydrous tetrahydrofuran (THF) as solvent, **Scheme 2.1**.

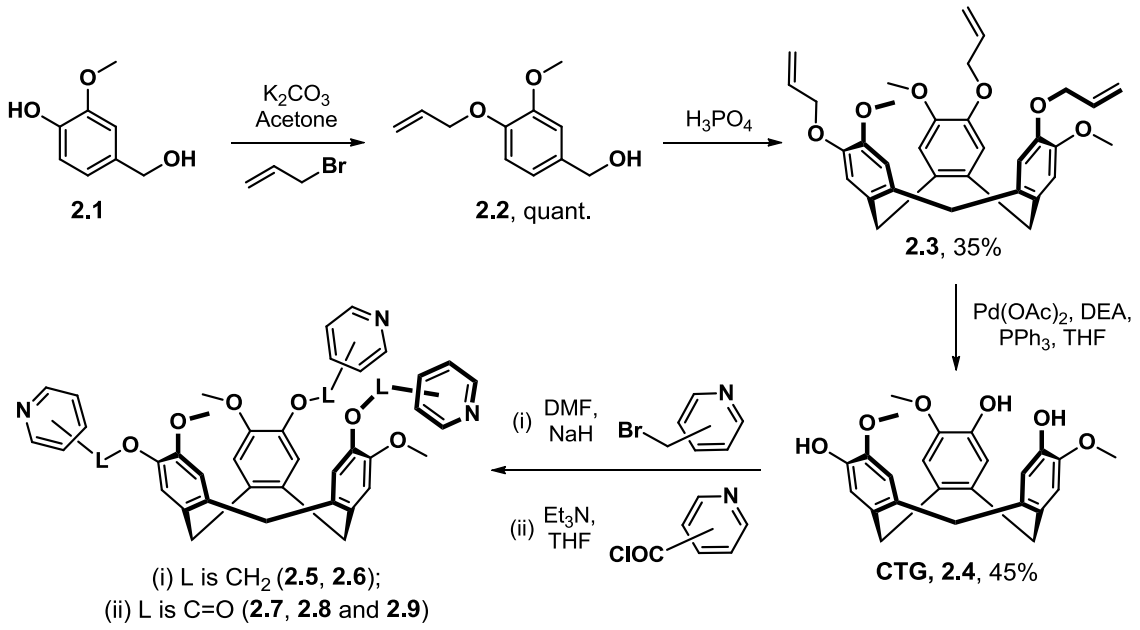

Scheme 2.1 *Three-step literature preparation of CTG (**2.4**) and the subsequent general synthesis of ether-linked (**2.5**, **2.6**) and ester-linked (**2.7**, **2.8** and **2.9**) ligands.*

Following, the novel pyridine-*N*-oxide ligand library, comprising (±)-2,7,12-trimethoxy-3,8,13-*tris*(2-pyridylmethyloxy-*N*-oxide)-10,15-dihydro-5*H*-tribenzo[*a*,*d*,*g*]cyclononatriene (**2.10**), (±)-2,7,12-trimethoxy-3,8,13-*tris*(3-pyridylmethyloxy-*N*-oxide)-10,15-dihydro-5*H*-tribenzo[*a*,*d*,*g*]cyclononatriene (**2.11**), (±)-2,7,12-trimethoxy-3,8,13-*tris*(3-carboxypyridine-*N*-oxide)-10,15-dihydro-5*H*-tribenzo[*a*,*d*,*g*]cyclononatriene (**2.12**), (±)-2,7,12-trimethoxy-3,8,13-*tris*(4-carboxypyridine-*N*-oxide)-10,15-dihydro-5*H*-tribenzo[*a*,*d*,*g*]cyclononatriene (**2.13**) and (±)-2,7,12-trimethoxy-3,8,13-*tris*(4-pyridine-*N*-oxide-4-carboxyphenyl)-10,15-dihydro-5*H*-tribenzo[*a*,*d*,*g*]cyclononatriene (**2.14**) were synthesised from their corresponding pyridyl precursors using an excess of *meta*-chloroperoxybenzoic acid (*m*-CPBA) in anhydrous dichloromethane and isolated as racemic mixtures in high yields, **Scheme 2.2**.

Their formation is facile and occurs by nucleophilic attack at the activated peracid, which proceeds through a five membered transition state to afford the benign and water-soluble carboxylic acid and corresponding pyridine-*N*-oxide. A representative mechanism of their formation is shown below in **Scheme 2.3**. Alternative synthetic procedures using hydrogen peroxide/glacial acetic acid or oxone (potassium peroxymonosulfate) proved ineffective, with only partial *N*-oxidation observed or an inseparable mixture of products obtained.[20]

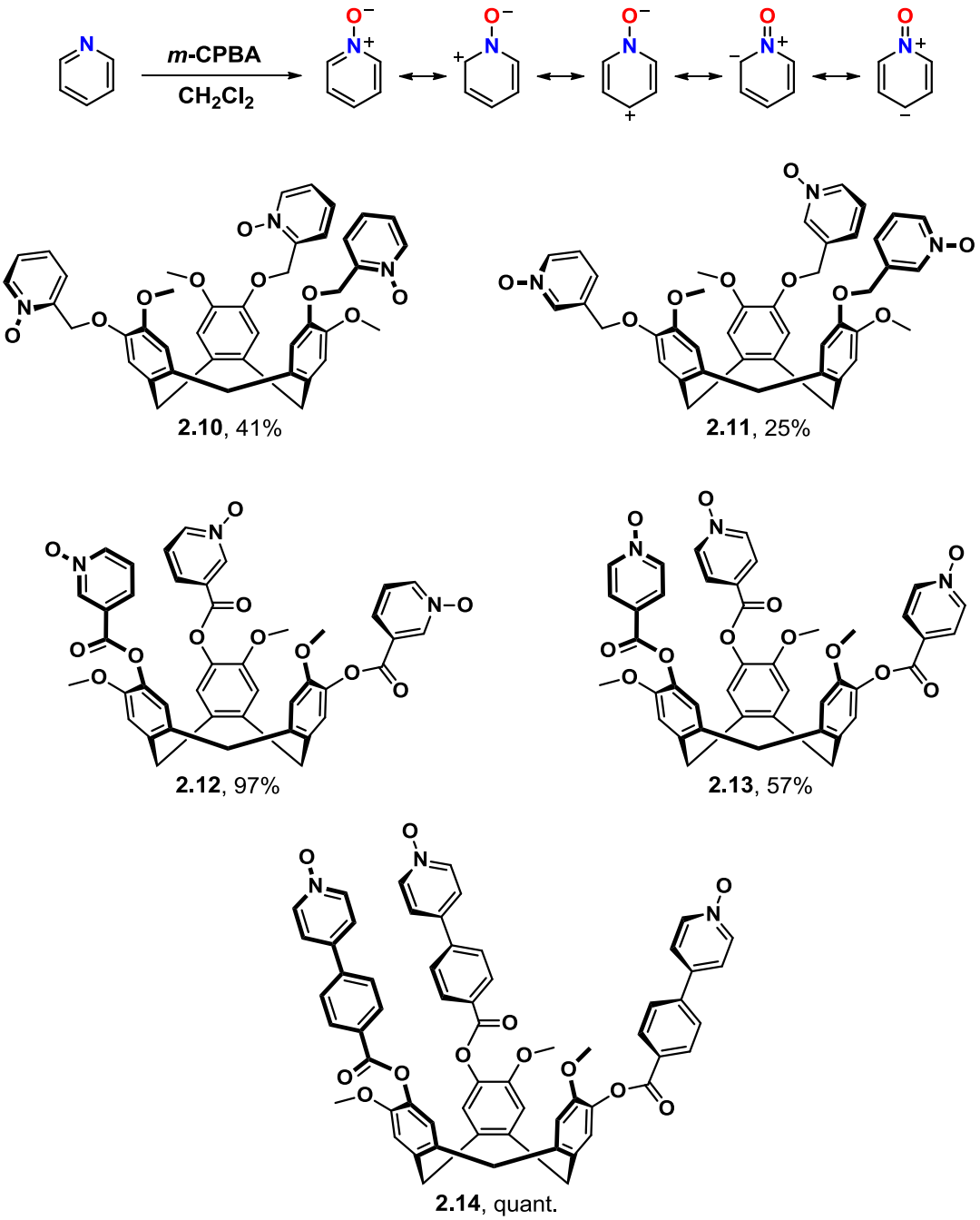

Scheme 2.2 *The novel pyridine-N-oxide ligand library (**2.10-2.14**) prepared and utilised through the study. Stable resonance forms are also displayed.*

Ligands **2.10**-**2.14** were fully analysed and their purity and composition were confirmed with combustion analyses and infrared spectroscopy; the latter indicating a successful *N*-oxidation with the N-O bond stretches at ~ 1520 and 1340 cm^{-1}. Electrospray mass spectrometry afforded incontrovertible evidence for their formation with mass peaks of (*m/z*) 730.3759, 730.3756, 772.2137, 772.2138 and 1022.2913 observed, which corresponded to the molecular ions {**2.10**·H}$^+$, {**2.11**·H}$^+$, {**2.12**·H}$^+$, {**2.13**·H}$^+$ and {**2.14**·Na}$^+$, respectively. Likewise, all ^{1}H and ^{13}C NMR spectra procured were consistent with the proposed structures of the ligands.

The recorded ^{1}H NMR spectra displayed characteristic resonances attributable to the tribenzo[*a*,*d*,*g*]cyclononatriene core, alongside a marked shift in the protons of the pyridine ring. Such protons experienced a shielding effect due to strong magnetic anisotropy and electric field of the *N*-oxide moiety.[21] This effect was especially evident for the protons sited *ortho* and *para* and in accordance with the resonance structures available upon *N*-oxidation, **Figure 2.2**. The representative ^{1}H NMR spectra of ligand **2.8** and the corresponding pyridine-*N*-oxide **2.13** are shown below in **Figure 2.3**.

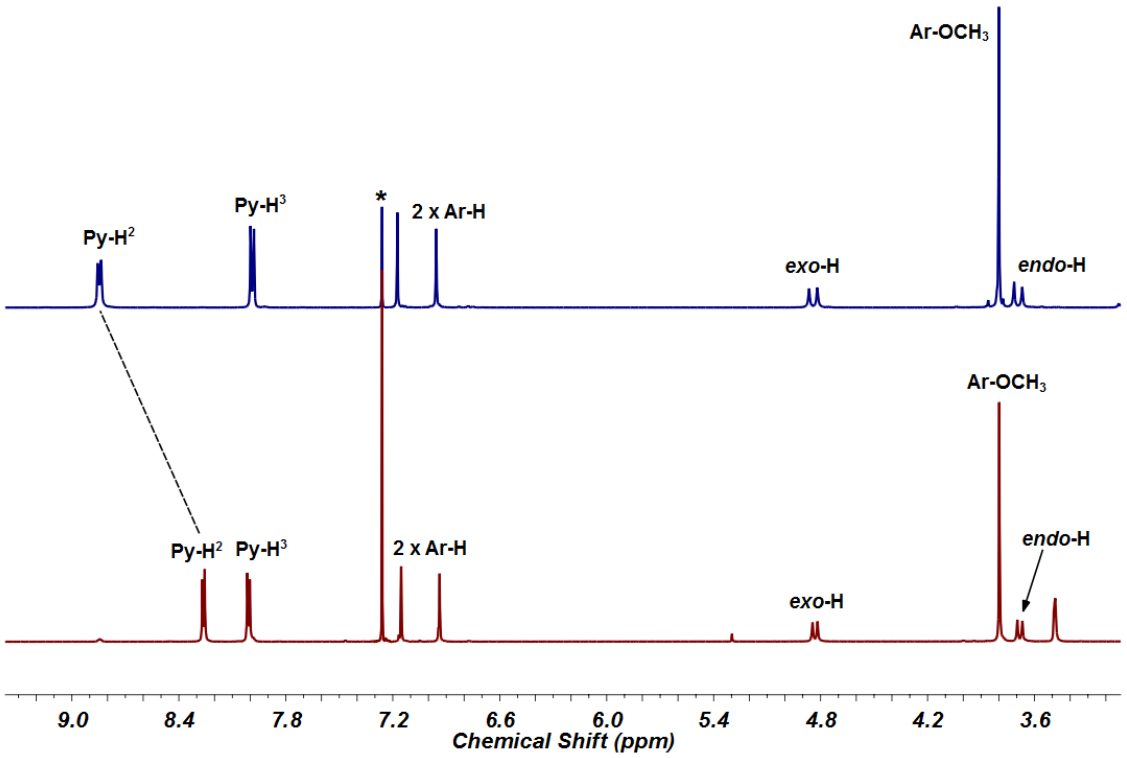

Figure 2.3 *Interpreted ^{1}H NMR spectra of ligand **2.8** (blue trace) and corresponding N-oxide **2.13** (red trace) in $CDCl_3$.*

Ligand **2.20** was prepared *via* a multi-step synthesis, **Scheme 2.4**, where the precursor 4-bromomethyl-dimethyl-2,6-pyridinedicarboxylate **(2.18)** was synthesised according to a literature procedure.[22] Esterification of pyridine-1,2-dicarboxylic acid (**2.15**) in the presence of acidic methanol afforded the diester (**2.16**) in quantitative yield, which was subsequently reacted with hydrogen peroxide, iron(II) sulfate and sulphuric acid, in methanol, to afford 4-hydroxymethyl-dimethyl-2,6-pyridinedicarboxylate (**2.17**) in 19 % yield. This reaction is likely to proceed through an *in situ N*-oxidation, followed by *para*-directed electrophilic aromatic substitution with formaldehyde, again generated *in situ* by the strongly oxidising Caro's acid (H_2SO_5), **Scheme 2.3**.

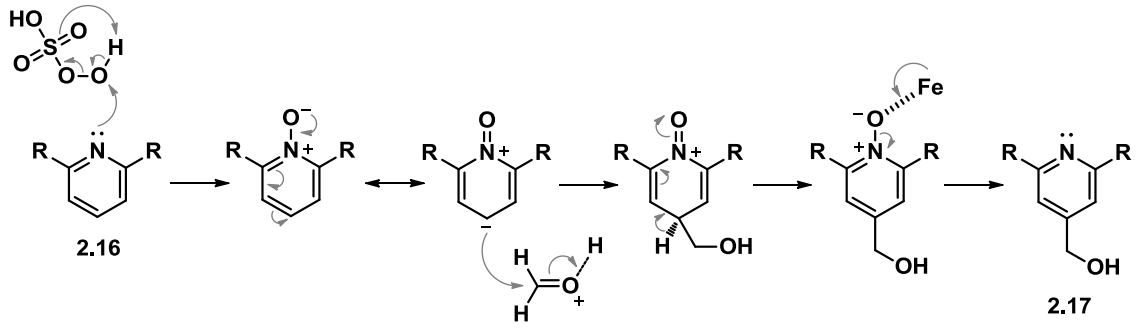

Scheme 2.3 *Proposed mechanism for the electrophilic aromatic substitution of starting material* ***2.16*** *to afford the desired product* ***2.17****.*

Initial attempts to prepare ligand precursor **2.19** directly from the primary alcohol **2.17** utilising standard Mitsunobu conditions were attempted, yet resulted in an inseparable mixture of products.[22b] Rather, bromination of **2.17** with phosphorus tribromide in anhydrous dichloromethane furnished the active electrophile **2.18** in quantitative yield. Reaction of CTG (**2.4**) with **2.18** in the presence of potassium carbonate base and acetonitrile solvent afforded the novel ligand precursor **2.19** in 97% yield, **Scheme 2.4**.

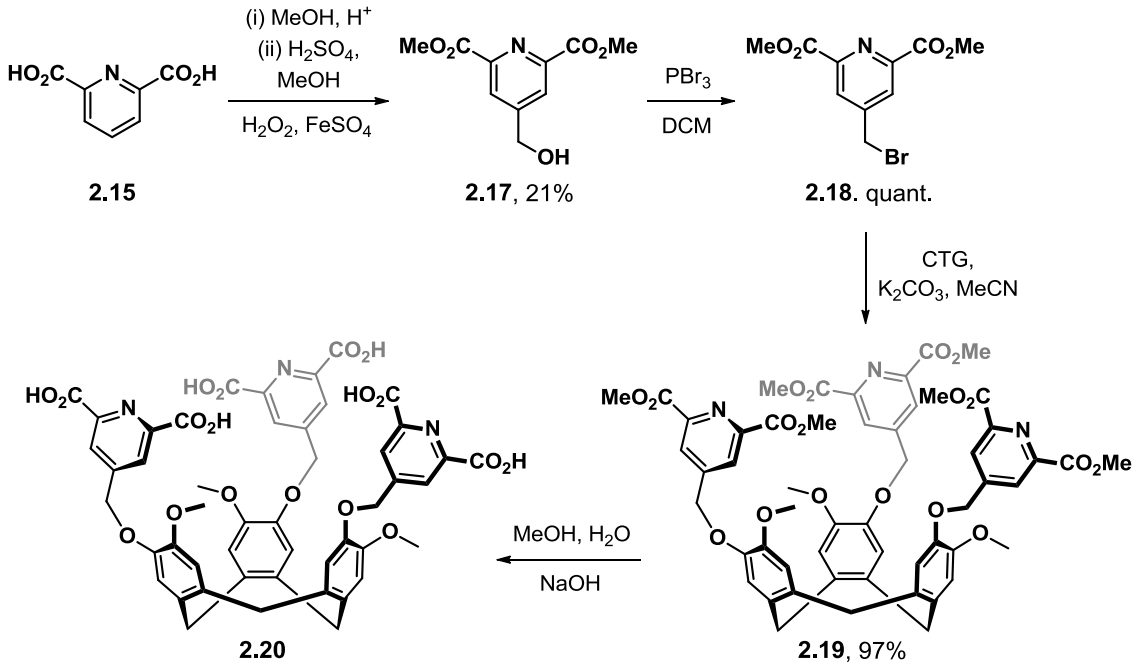

Scheme 2.4 *The formation of* ***2.20*** *from its precursors.*

The mass spectrum of ligand **2.19** in acetonitrile indicated the mass peak (*m/z*) 1052.3039, which was attributed to $\{MH\}^+$ and calculated for 1052.3022. Purity and composition were confirmed by combustion analysis and infrared spectroscopy and seen to be consistent with the proposed structure of ligand **2.19**. The successful substitution of CTG (**2.4**) to afford compound **2.19** was easily envisaged through examination of its ^{1}H NMR spectrum, **Figure 2.4**.

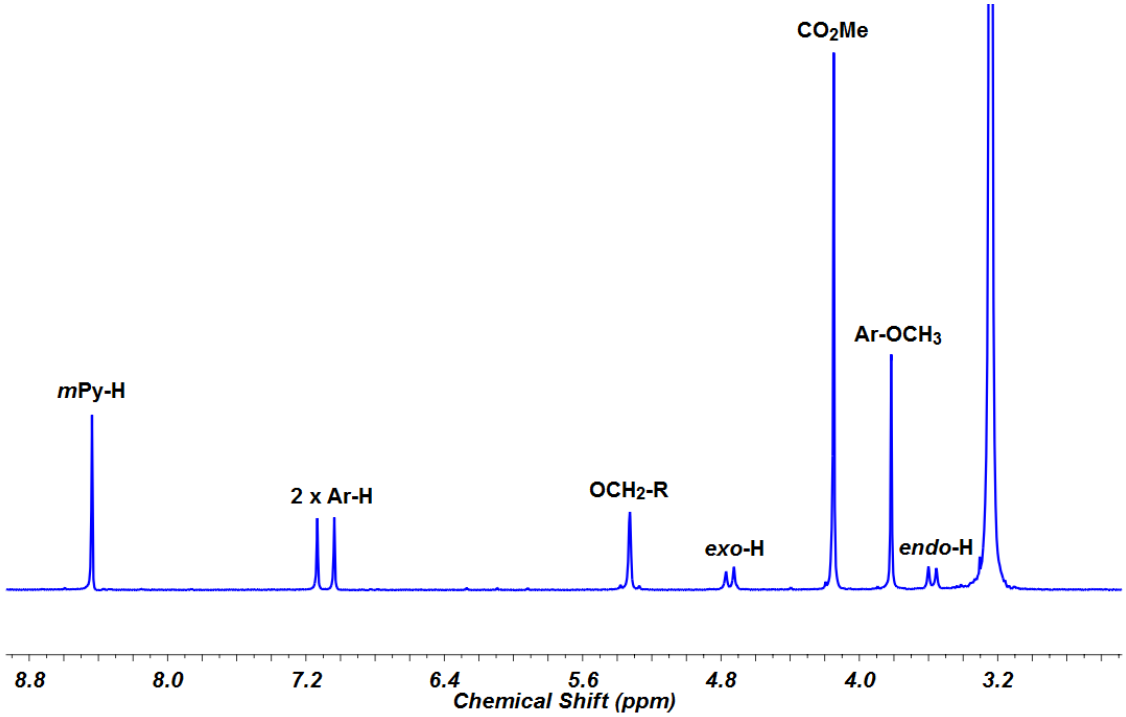

Figure 2.4 *Interpreted ^{1}H NMR spectrum of compound* ***2.19*** *in d_3-MeCN.*

Deprotection of **2.19** to afford ligand **2.20** was undertaken in a 7:1 mixture of methanol:water with hydroxide base at reflux. The insolubility of the resultant solid meant that its solution-phase chemistry could not be probed; however, infrared analysis confirmed the generation of a carboxylic acid with a broad and hydrogen-bonded O-H bond stretch at 3300 cm^{-1}. Combustion analysis of the product analysed as the sodium salt of the acid, which could not be purified by any means.

2.2.1 Clathrate complexes of pyridine-*N*-oxide ligands

Single crystals of ligands **2.10**, **2.12** and **2.13** were obtained and their clathrate complexes determined crystallographically, **Table 2.3**. Three forms of clathrate behaviour were noted, comprising both the inclusion and exclusion of hetero-guest (solvent) molecules, alongside reciprocal self-inclusion motifs between individual ligands.

Ligand **2.10** displayed a solvent-dependent isomorphism, or solvatomorphism, with crystals grown from both water and *N,N'*-dimethylformamide (DMF) solutions. Crystals of complex **2.10**·2(H_2O) were grown from the slow evaporation of water and a solution was obtained in the triclinic space group *P*1 to display perfectly aligned columns of **2.10** ligands in a bowl-in-bowl arrangement and water molecules occupying the interstitial sites, **Figure 2.5a**. The water molecules bridge individual **2.10** ligands through hydrogen bonding and link the ligands into a *pseudo* 2D sheet. Each lattice water molecule connects two **2.10** ligands across the polar *N*-

oxide moiety, **Figure 2.5a**, with N-O···H-O separations of 1.882 and 1.870 Å.[23] Hydrogen bonding in derivatised CTVs is commonplace, and is well documented with the relatively acidic C-H proton of *ortho*-carborane.[24] A particularly elegant example of hydrogen bonding in the solid state is that of Sasaki and colleagues, where an aqueous mixture of achiral molecular components was observed to transfer supramolecular chirality upon the creation of hydrogen-bonded helices, consisting of 21 individual interactions.[25] Likewise, Ward and co-workers have remarked upon the importance of water-mediated hydrogen bonding in the determination and quantification of isoquinoline-*N*-oxide binding in a polyhedral coordination cage host.[26]

Individual **2.10** ligands stack in a columnar array with inter-aromatic distances of 4.55 Å, which is too long to suggest the presence of aromatic interaction.[27] This inter-ligand distance is proportional to the crystallographic unit cell *a* axis, 4.5584(6), and represents a β-form of CTV, as determined by Steed and Atwood.[28] Each column of **2.10** ligands is homochiral and features the inclusion of only one ligand enantiomer; however, the overall lattice composition is that of a racemate.

Crystals of complex **2.10**·2(DMF) were grown from the diffusion of diethyl ether vapours into a DMF solution of the complex and a solution was obtained in the triclinic space group $P\bar{1}$. Conversely to exclusion complex **2.10**·2(H_2O), the inclusion complex **2.10**·2(DMF) displays host-guest interactions between the hydrophobic tribenzo[*a,d,g*]-cyclononatriene core and a DMF solvent molecule. The non-polar *N,N'*-dimethyl moiety is orientated towards the ligand cavity with the polar carboxy function forming a weak hydrogen bond with a proximal pyridyl proton, displaying an O···H-Py separation of 2.627 Å. However, in doing so, the ligand loses its molecular C_3-symmetry, **Figure 2.5b**. This type of clathrate behaviour is common with CTV and its derivatives, and inclusion complexes have been isolated with acetone, acetonitrile, dimethylsulfoxide (DMSO), ethanol and tetrahydrofuran (THF) solvents.[29]

Individual **2.10** ligands pack in a columnar manner that is supported through back-to-back aromatic interactions, with π-π centroid separation of 3.568 Å. Furthermore, reciprocal hydrogen bonding motifs are present between two polar *N*-oxide moieties and its *ortho*-proton, with O···H-C separations of 2.358 Å.

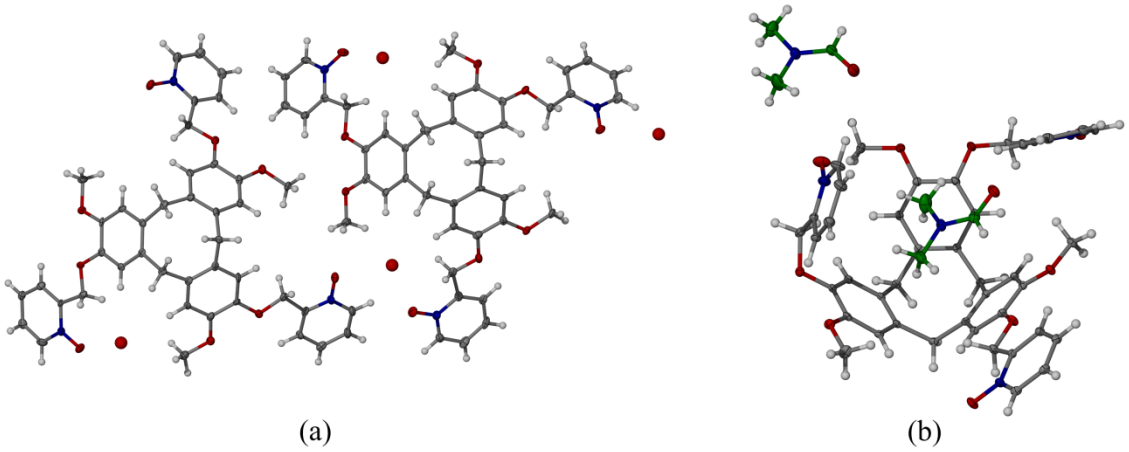

Figure 2.5 *(a) From the crystal structure of complex* ***2.10****·2(H_2O), displaying the asymmetric unit, as viewed down the crystallographic a-b plane; (b) from the crystal structure of complex* ***2.10****·2(DMF) highlighting the host-guest interactions between ligand and DMF. Anisotropic displacement parameters are at 30 % and solvent DMF coloured green for clarity.*

Single crystals of complex **2.12**·2(NMP) were grown from the diffusion of diethyl ether vapours into an *N*-methylpyrrolidone (NMP) solution of the ligand and isolated as large, colourless blocks. The structure solved in the triclinic space group $P\bar{1}$ to display the asymmetric unit as one molecule of **2.12** and two NMP solvent molecules, **Figure 2.6a**. The NMP solvent molecules form no interactions between themselves or the ligand and simply fill interstitial sites within the lattice. Such exclusion behaviour has been observed by Loughrey and co-workers in the formation of donor:acceptor charge transfer complexes with CTC with tetracyanoethylene (TCNE) and tetracyanoquinodimethyl (TCNQ) lattice guests.[30]

Individual **2.12** ligands pack in a self-complementary manner, where the ligand arm of one is reciprocally and non-covalently bound by the tribenzo[*a,d,g*]cyclononatriene core of a neighbour. This dimeric unit is supported by aromatic interactions between the aromatic core and pyridyl moiety of the two interacting **2.12** ligands, with aromatic centroid separation of 3.793 Å, **Figure 2.6b**. Hardie and colleagues have assigned the appropriate moniker of 'handshake' to this supramolecular interaction, which is specific to *tris*-functionalised CTVs and has been observed in the solid state between various quinalyl- and pyridyl-substituted ligands and their metal complexes.[31]

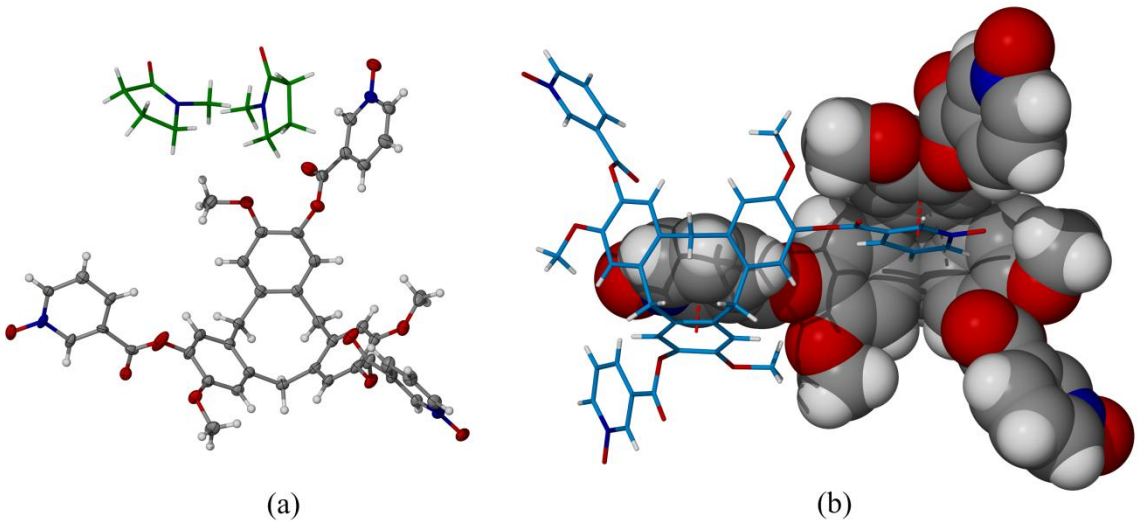

Figure 2.6 *From the crystal structure of* ***2.12****·2(NMP). (a) The asymmetric unit: solvent NMP coloured green and anisotropic displacement parameters set at 30 % probability; (b) reciprocal hand-shake motif between two molecules of ligand* ***2.12****. Individual ligands are colour coded, shown in space filling where appropriate and aromatic interactions displayed using red hashed lines. Positional disorder about the pyridine-N-oxide moiety is not shown.*

Single crystals of complex **2.13**·DMF were obtained from the slow evaporation of a DMF solution of **2.13** and collected using synchrotron radiation at station I19 at Diamond Light Source. The structure solved in the monoclinic space group $P2_1/n$ to display the asymmetric unit as one molecule of ligand **2.13** and one molecule of solvent DMF. Ligands display narcissistic chiral discrimination and pack to afford homochiral columns of only one enantiomer of ligand, **Figure 2.7**. This is an often observed but not well understood phenomenon of CTV and its analogues which is likely due to symmetry restriction,[32] similar to the molecular chiral recognition as described by McBride.[33] Aromatic separations between ligands are 4.70 Å and therefore their formation is not supported by aromatic interactions. Whilst each column of ligands is homochiral, the extended structure is a racemate, where the opposing columns propagate either up, or down. Such opposing ligands interact across their respective columns through hydrogen bonding between the ethereal moieties of the tribenzo[*a*,*d*,*g*]cyclononatriene core, displaying O···H-C separations of 1.985 Å.

The packing of **2.13** ligands in the extended lattice affords small, interstitial sites which are filled with solvent DMF. However, rather than classical clathrate behaviour, DMF molecules form weak associations with proximal **2.13** ligands through hydrogen bonding, **Figure 2.7a**. A dimeric interaction is afforded between the pyridine-*N*-oxide and formyl moieties, with Py-H···O=C and N-O···H-C separations of 2.387 and 2.434 Å, respectively, **Figure 2.7a**.

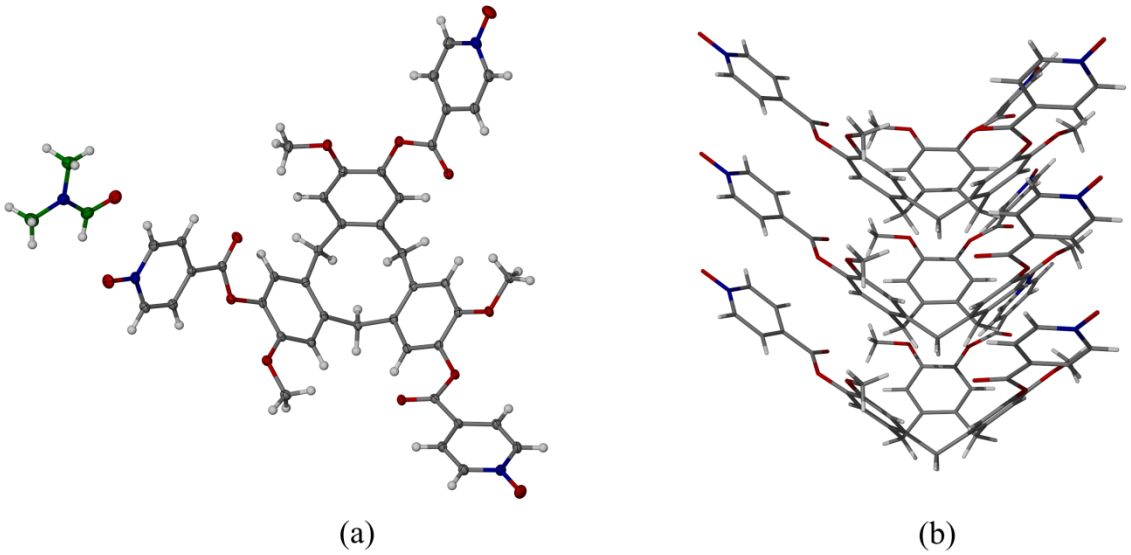

Figure 2.7 *From the crystal structure of complex* ***2.13****·DMF. (a) The asymmetric unit, as viewed down the crystallographic a axis. DMF guest coloured green for clarity and anisotropic displacement parameters set at 30 %; (b) characteristic bowl-in-bowl stacking behaviour of individual* ***2.13*** *ligands, as viewed down the crystallographic b axis.*

2.3 Coordination polymers with the lanthanide(III) series

Owing to the insolubility of ligand **2.20**, conventional complexation reactions undertaken at room temperature were unsuccessful. Instead, solvothermal syntheses in Parr-acid digestion bombs were attempted, through superheating a suspension of **2.20** and LnX_3, where X = halide, nitrate (NO_3^-), perchlorate (ClO_4^-) and trifluoromethanesulfonate (triflate, $CF_3SO_3^-$) in a polar, aprotic solvent. Despite the extensive range of conditions employed,[34] crystals suitable for single crystal diffraction were not obtained. Subsequently, attempts towards the ester hydrolysis of ligand **2.19** were undertaken solvothermally in the presence of suitable lanthanide salts in a bid to facilitate complex formation *in situ*. Again, crystalline material was not obtained and so complexation studies of ligand **2.20** were not pursued further.

Ligands **2.10**-**2.14** were of significantly lower solubility than the corresponding pyridyl precursors; thus, the solvents DMF, DMAC (*N,N'*-dimethylacetamide), DMSO and NMP were required in order to promote self-assembly at room temperature. The coordination polymers gained from their self-assembly with the lanthanide(III) cations were testament to the coordinating nature of the solvents employed, where crystallographic analysis showed their tendency to act as ligands. Likewise, coordinating anions were observed to facilitate similar behaviour.[35]

Solution-phase experiments of ligands **2.10**-**2.14** with available diamagnetic lanthanide metal salts displayed only broadened resonances in their ^{1}H NMR spectra which did not sharpen with

time. The use of d_6-DMSO, d_7-DMF and D_2O solvents did not improve the spectra procured and their broadness and asymmetry were symptomatic of polymerisation. Stable constructs could not be identified in the gas phase either, with the electrospray mass spectra of these complex mixtures displaying only a sequential increase in ligand:metal adducts, supporting the notion of oligomerisation. Despite the range of conditions tried, crystalline samples were only obtained from a select few samples.

The stoichiometric reaction of ligand **2.10** with gadolinium(III) nitrate (NO_3^-) in DMF solvent afforded a 1D polymer, $\{[Gd(\mathbf{2.10})(NO_3)_3]\cdot DMF\}_\infty$, complex **2.21**. Yellow needles were isolated by diffusing diethyl ether vapours into a solution of the complex in DMF and analysed by single crystal diffraction methods. The structure solved in the monoclinic space group *C*2/*c* to display the asymmetric unit as one Gd(III) centre, which is coordinated by a molecule of ligand **2.10** and three chelating nitrate anions, in addition to one molecule of uncoordinated DMF, disordered over two positions, **Figure 2.8**. Selected bond metrics are given in **Table 2.1**.

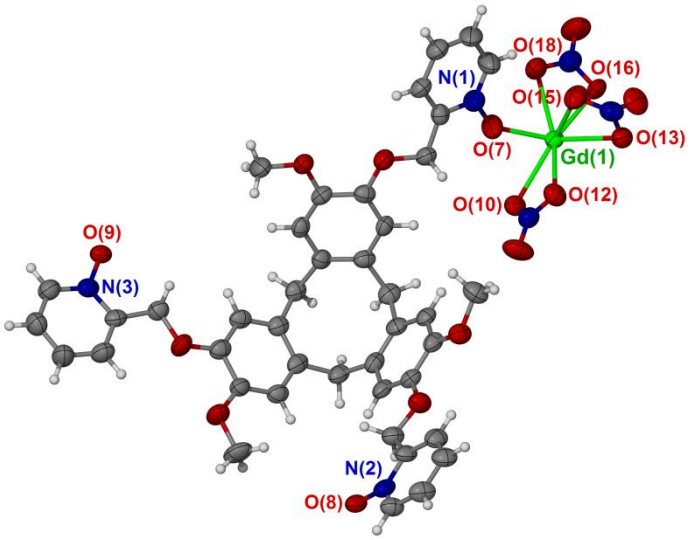

Figure 2.8 *The asymmetric unit from the crystal structure of complex* ***2.21****. Solvent DMF omitted for clarity and anisotropic displacement parameters are shown at 50 % probability.*

Gd(1)-O(7)	2.370(6)	Gd(1)-O(15)	2.511(6)
Gd(1)-O(10)	2.550(6)	Gd(1)-O(16)	2.505(6)
Gd(1)-O(12)	2.539(6)	Gd(1)-O(18)	2.517(7)
Gd(1)-O(13)	2.539(6)		

Table 2.1 *Selected bond lengths (Å) from the crystal structure of complex* ***2.21***

Each ligand **2.10** coordinates to three symmetry-equivalent Gd(III) centres, each of which are 9-coordinate with a tricapped trigonal-prismatic geometry. Furthermore, each Gd(III) centre is

meridonially coordinated by three independent **2.10** ligands and chelating nitrate anions. Gd-O(ligand) distances range from 2.358(5) to 2.390(6) Å, with equatorial and axial O(ligand)-Gd-O(ligand) bond angles of 80.63(19), 90.6(2) and 149.9(2)˚, respectively, thus forming a near T-shape arrangement of **2.10** around the Gd(III) centre. Weak intramolecular interactions are present between an un-bound oxygen of a chelating nitrate anion and adjacent methyl group, with O···H-C separation of 2.54 Å. The ligand retains non-crystallographic C_3-symmetry and displays a propensity to coordinate away from the hydrophobic bowl, as to prevent steric crowding upon coordination, which is facilitated by the flexible ether linkage.

Symmetry expansion leads to the formation of a 3-connected 1D ladder, where the ligands assemble linearly in an alternate up-down arrangement, assisted by back-to-back π-interactions between core CTG aromatics, with centroid separations of 3.85(6) Å. Individual 1-D ladders were observed to be homo-chiral, with only one enantiomer of the ligand included in their formation; however, the overall structure exists as a racemate, **Figure 2.9**.

Some of the earliest 1D ladder-type polymers were prepared by Fujita and co-workers, through the self-assembly of 1,4-*bis*(4-pyridylmethyl)benzene and cadmium(II) nitrate. They too remarked upon the necessity of coordinating anion and solvent in order to promote polymerisation.[36] Examples more commonly related to complex **2.21** are those prepared by Reedijk and Zheng,[37] where analogues of *tris*(4-pyridyl)benzenes have afforded 3-connected ladders, which display porosity for guest binding and an ability to undergo remarkable crystallographic phase transitions, respectively. Examples which incorporate the lanthanide(III) cations into 3-connected polymers include Chen's coordination chains resulting from the self-assembly of pyridine-2,6-dicarboxylates with promethium(III) or cerium(III) metal centres, which display both magnetic and fluorescent properties.[38] The shear wealth of such coordination polymers has made them the subject of a number of recent and extensive review articles.[39]

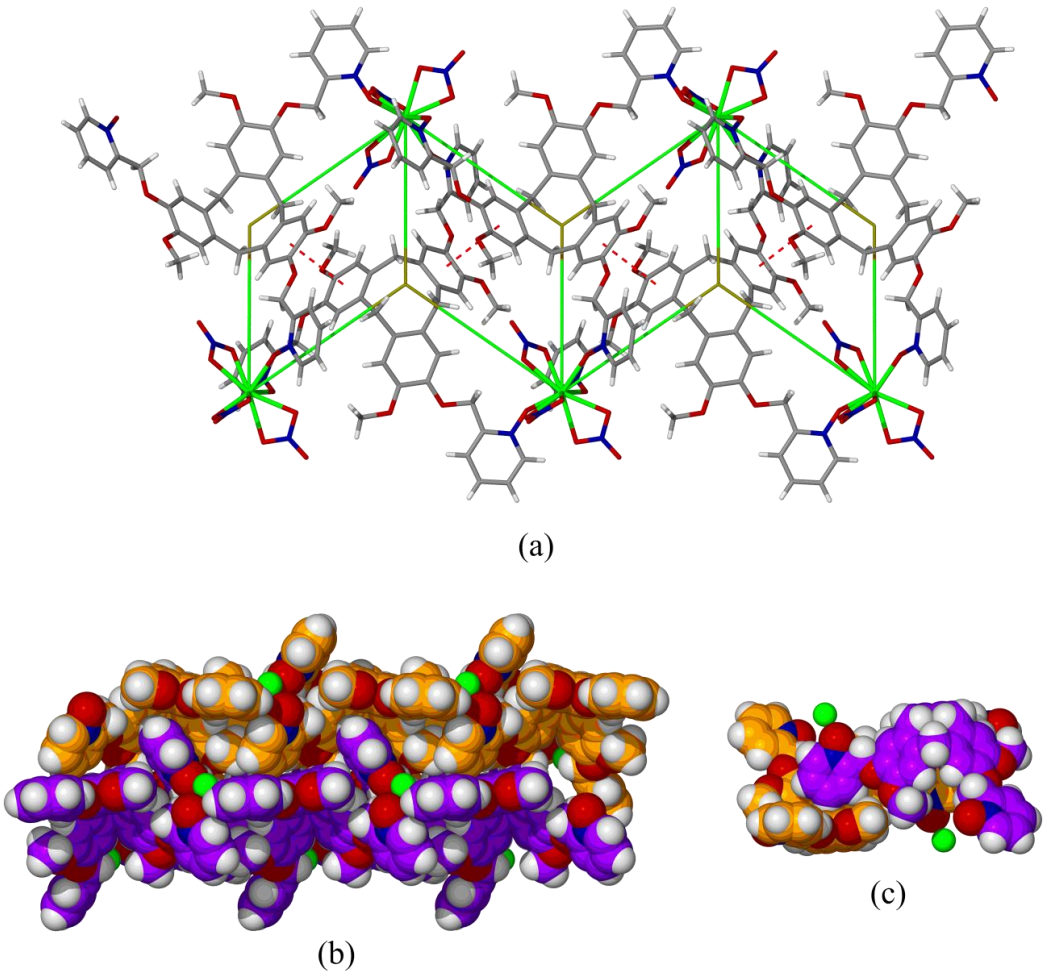

Figure 2.9 *From the crystal structure of complex* ***2.21****. (a) The resultant 3-connected, homochiral, 1-D chain formed through metal coordination and back-to-back stacking of ligands. Aromatic π-interactions displayed as red, hashed lines and chain connectivity displayed as green lines; (b) aggregation of 1-D chains, facilitated by hydrophobic self-inclusion. Solvent DMF omitted and chains colour coded for clarity; (c) reciprocal hand-shake motif present between two distinct ligands.*[40]

The extended structure depends strongly on synergistic self inclusion and features the reciprocal 'handshake' motif, as introduced for clathrate complex **2.12**·2(NMP), above, **Figure 2.9c**.[31] This 2-D aggregation of 1-D chains proceeds with the hydrophobic cavity of a ligand **2.10**, of a given 1-D ladder, playing host to a ligand arm from an adjacent 1-D ladder and *vice versa*. The polar *N*-oxide moiety of the reciprocating arm is orientated away from the hydrophobic bowl and coordinates a Gd(III) cation to complete the structural motif, **Figure 2.9b**.

The 3-D lattice is afforded through interdigitation of parallel 1-D ladders between proximal aromatic groups, **Figure 2.10**. Once formed, complex **2.21** was observed to be insoluble in all common laboratory solvents and therefore an examination of its solution-phase chemistry was not undertaken; however, the composition and purity of the bulk crystalline solid were confirmed by infrared spectroscopy and combustion analysis, respectively.

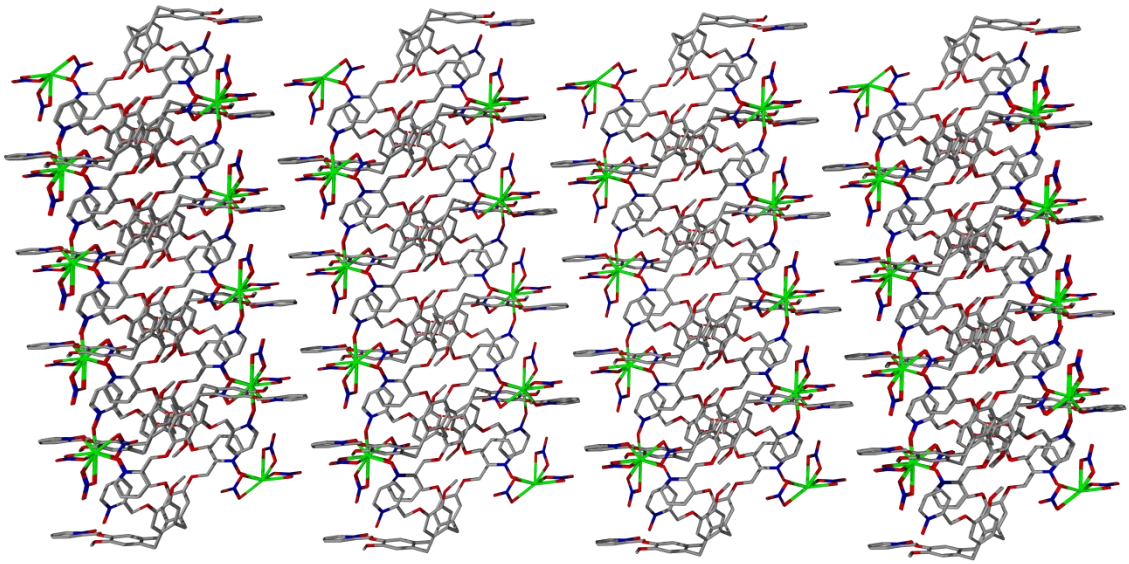

Figure 2.10 *From the crystal structure of complex* ***2.21****. The extended packing diagram, highlighting the intercalation of associated 2-D layers. Solvent DMF and ligand protons are omitted for clarity.*[40]

The reaction of ligand **2.13** with two equivalents of samarium(III) chloride in DMF also resulted in the formation of a complex with a 1D ladder structure, of composition $\{[Sm(\mathbf{2.13})Cl(DMF)_3]\cdot[SmCl_5(DMF)]\cdot 1.5(DMF)\}_\infty$, complex **2.22**. Although fundamentally similar to complex **2.21**, the orientation of the pyridyl-*N*-oxide moiety and rigidity of the ester linkage generate a different structural outcome. Crystals of the complex were grown as described for complex **2.21** and were isolated as large, yellow needles. The structure was solved in the triclinic space group $P\bar{1}$ to display the asymmetric unit as two crystallographically and chemically distinct Sm(III) containing units: $[Sm(\mathbf{2.13})Cl(DMF)_3]^{2+}$ and $[SmCl_5(DMF)]^{2-}$, the latter being a simple, anionic octahedral lattice guest, **Figure 2.11**.

Complex 2.22 was not seen to form when stoichiometric amounts of ligand **2.13** and metal salt were used, confirming that two equivalents of metal salt, and hence the presence of anionic lattice guest, are integral in its formation. The anionic Sm(III) guest displays Sm-Cl and Sm-O(DMF) bond distances of 2.6707(17)-2.7286(16) and 2.406(6) Å, respectively and Cl-Sm-Cl bond angles ranging 865.99(6)-97.89(5) for the *cis*- and 161.78(6)-176.40(6)˚ for the *trans*-chlorides. Anionic lanthanide pentachlorides are uncommon, but have been reported with Nd(III), Ce(III) and Eu(III) as methanol, pyridine and tetrahydrofuran solvates, respectively.[41]

The cationic unit, $[Sm(\mathbf{2.13})Cl(DMF)_3]^{2+}$, contains a central Sm(III) cation that is coordinated by three crystallographically related molecules of ligand **2.13**, three molecules of coordinating DMF and a chloride ligand. Each 8-coordinate Sm(III) centre has square antiprismatic geometry with the three **2.13** ligands coordinating in a pseudo-*fac* orientation. Bond distances range

2.398(4)-2.430(4) Å for the Sm-O(ligand), 2.7724(17) Å for Sm-Cl and between 2.414(4) and 2.508(4) Å for the Sm-O(DMF) bonds. Selected bond metrics for complex **2.22** are stated below in **Table 2.2**.

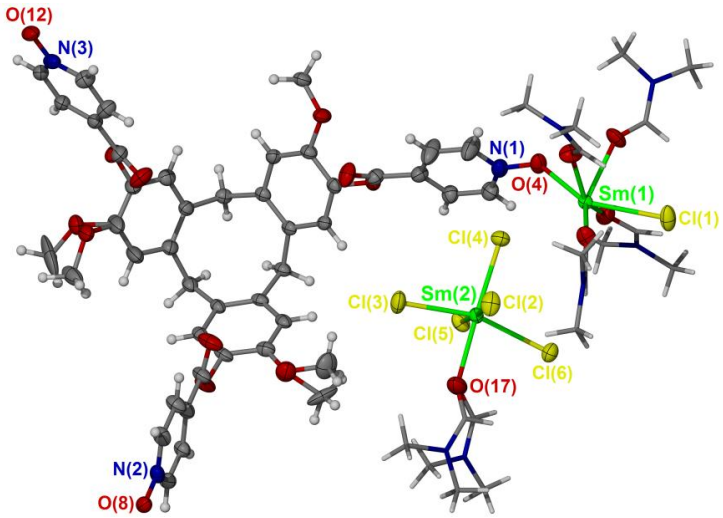

Figure 2.11 *The asymmetric unit from the crystal structure of complex* ***2.22****. Anisotropic displacement parameters are set at 40 % probability.*

Sm(1)-O(4)	2.399(4)	O(4)-Sm(1)-Cl(1)	142.03(11)
Sm(1)-Cl(1)	2.7724(17)	O(17)-Sm(2)-Cl(2)	94.70(15)
Sm(2)-Cl(2)	2.6952(17)	O(17)-Sm(2)-Cl(3)	83.11(15)
Sm(2)-Cl(3)	2.6707(17)	O(17)-Sm(2)-Cl(5)	88.44(15)
Sm(2)-Cl(4)	2.6912(16)	O(17)-Sm(2)-Cl(6)	79.37(15)
Sm(2)-Cl(5)	2.6883(16)	Cl(2)-Sm(2)-Cl(3)	85.99(6)
Sm(2)-Cl(6)	2.7286(16)	Cl(2)-Sm(2)-Cl(6)	90.46(5)
Sm(2)-O(17)	2.406(6)	O(17)-Sm(2)-Cl(4)	174.80(16)

Table 2.2 *Selected bond lengths (Å) and angles (°) from the crystal structure of complex* ***2.22***

Symmetry expansion of the $[Sm(\mathbf{2.13})Cl(DMF)_3]^{2+}$ unit affords a 3-connected 1D ladder with a quasi-cylindrical conformation and an off-set, head-to-head assembly of **2.13** with respect to one another. The rigidity and outwardly orientated pyridyl-*N*-oxide donor moieties of **2.13** are essential in achieving such a conformation, which would not be accessible with a more flexible ligand such as **2.10** or **2.11**. In this case, and unlike complex **2.21**, the inclusion of both ligand enantiomers renders each 1-D ladder a racemate. There are no interactions to note within the 1D ladders, nor any significant free space, despite their cylindrical shape. In addition to the examples listed above, similar 1D 'open framework' complexes have been afforded with derivatised CTVs, including Holman's infinitely linked cryptophane complex and Zheng's 1D nanotube, which both display an ability to host molecules in the solid state.[42]

The structure extends 2-dimensionally through association of individual 1-D chains *via* intermolecular host-guest interactions; where, in this case, the *N,N'*-dimethyl moiety of a coordinated DMF molecule are orientated within the hydrophobic cavity of **2.13** and *vice versa*, **Figure 2.12a**.

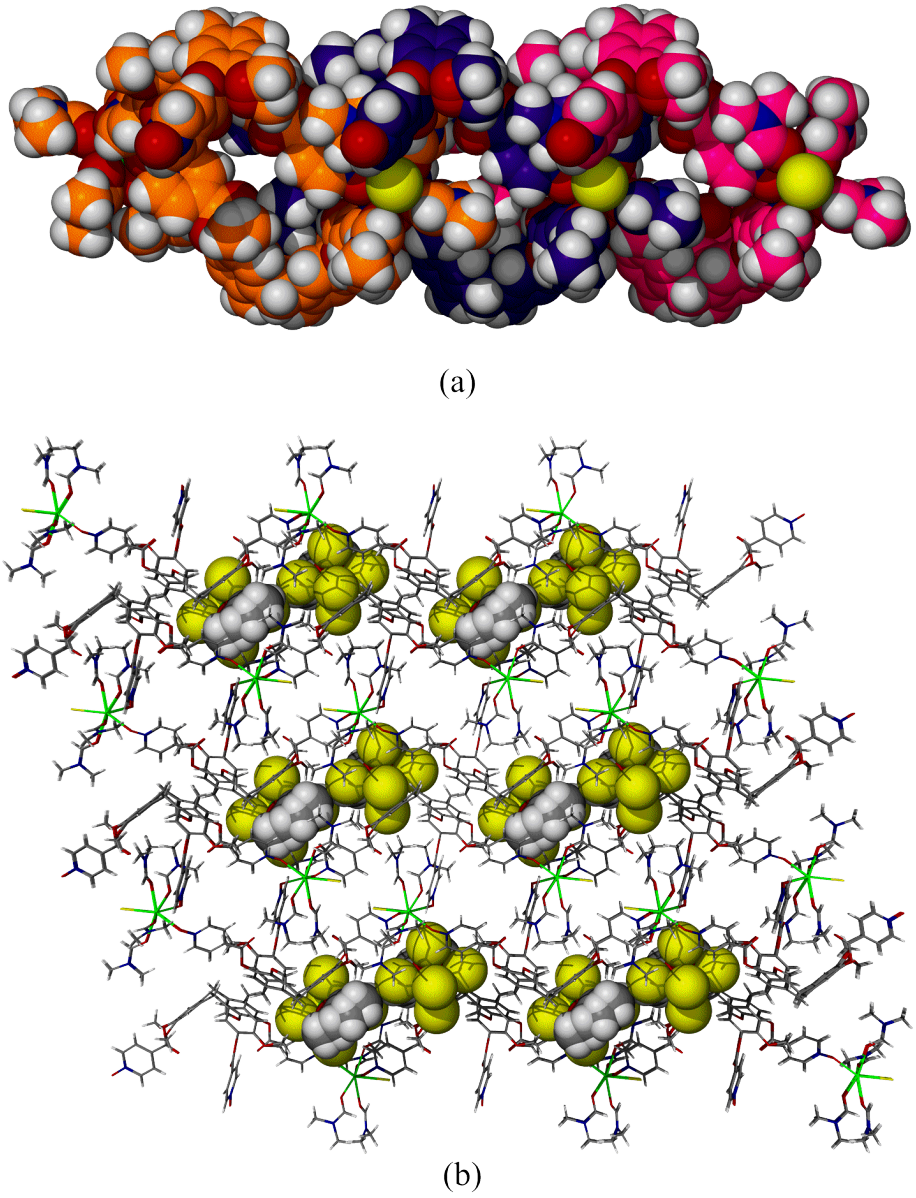

Figure 2.12 *From the crystal structure of complex* ***2.22****. (a) As viewed down the crystallographic c axis, depicting the interdigitation of individual 1D cylinders. Shown in space filling mode and colour coded for clarity; (b) extended crystal lattice, highlighting the positions of octahedral lattice guest,* $[SmCl_5(DMF)]^{2-}$*, displayed in space filling mode.*[40]

The extended lattice proceeds *via* the stacking of resultant sheets, facilitated by back-to-back π-interactions, with staggered centroid separations of 3.85 Å. This affords proton-rich, electropositive pockets which are filled with the aforementioned anionic $[SmCl_5(DMF)]^{2-}$ guests. Close contacts were recorded for each of the five bound chlorides,[43] with Cl···H-C

interactions ranging from 2.54 to 3.06 Å. The result is a dense extended lattice, with no void space to note, **Figure 2.12b**. As with complex **2.21**, complex **2.22** was found to be highly insoluble once formed and only solid state analysis sought. Purity of the complex was confirmed with combustion analysis and the composition was supported with infrared spectroscopy.

Extended ligand **2.14** was also seen to form complexes with the lanthanide(III) series. Single crystals from both NMP and DMF solutions of the ligand and cerium(III) trifluoromethanesulfonate ($CF_3SO_3^-$) were isolated; however, a data collection of suitable strength could not be determined – even with a synchrotron source. The cell indexed as trigonal, *a*, *b* = 60.25, *c* = 38.97 Å which was in good agreement for each crystal trialled. Data were weak and a resolution of only 2 Å was achieved (~ 2θ = 18.11 º) for the full data collection and a reliable solution could not be obtained. Mass spectrometry did not aid complex elucidation and highlighted only $\{Ce_2(\mathbf{2.14})_2(OTf)_4\}^{2+}$ at (*m/z*) 1438.12. The ^{1}H NMR spectrum of the analogous diamagnetic lanthanum complex in d_7-DMF did not display shifts to the ligand resonances, suggesting that the complex gained may be a phenomenon of the solid state.

2.4 Conclusions and future work

A novel ligand library comprising pyridine-*N*-oxide and pyridine-carboxylate donor moieties was synthesised and their clathrate complexes determined crystallographically. The pyridine-*N*-oxide ligands prepared proved effective in forming complexes with the lanthanide(III) series, with crystalline samples being isolated. Furthermore, the first examples of coordination polymers of functionalised CTVs and the lanthanide(III) cations were structurally elucidated.

Despite the larger coordination numbers of the lanthanides, higher dimensionality networks were not obtained due to the presence of coordinating solvent and anions. To improve solubility and perhaps allow for discrete complexes to be made, flexible and chelating derivatives built on a more solubilised CTG core would be essential, in addition to the employment of weakly coordinating solvent and anions. Nevertheless, these findings represent a step towards the construction of increasingly complex and robust network and cage structures comprising the CTV framework and the lanthanide(III) series.

In addition to addressing the inherent insolubility of ligands already prepared, future work should focus on synthesising both macrocyclic and chelating CTV-derived ligands towards the preparation of functional molecular hosts for the photoluminescent sensing of small molecules in the solution-phase. It would be envisaged that the strength and degree of guest binding by the CTV molecular cavity could be probed by various photophysical measurements.

2.5 Experimental

2.5.1 Instrumentation

NMR spectra were recorded by automated procedures on a Bruker Avance 500 or DPX 300 MHz NMR spectrometer. All deuterated solvents were purchased from Euriso-top. All ^{1}H and $^{13}C\{^{1}H\}$ spectra were referenced relative to an internal standard. High resolution electrospray mass spectra (ESI-MS) were measured on a Bruker MicroTOF-Q or Bruker MaXis Impact spectrometer in either positive or negative ion mode by Ms. Tanya Marinko-Covell of the University of Leeds Mass Spectrometry Service and Dr. Lindsay P. Harding of the University of Huddersfield. Low resolution mass spectra were recorded on an open-access Bruker Micromass LCT spectrometer with simultaneous HPLC using an acetonitrile/water eluent and sodium formate calibrant. FT-IR spectra were recorded as solid phase samples on a Perkin-Elmer Spectrum One spectrophotometer. Samples for microanalysis were dried under vacuum before analysis and the elemental composition determined by Mr Ian Blakeley of the University of Leeds Microanalytical Service using a Carlo Erba elemental analyser MOD 1106 spectrometer.

2.5.2 Synthesis

Unless otherwise stated, all chemicals were obtained from commercial sources and used without further purification. Ligands were employed as racemic mixtures for all complexation studies listed herein.

Synthesis of 3-methoxy-4-(propenyloxy)benzyl alcohol (2.2). 4-Hydroxy-3-methoxybenzyl alcohol (30.74 g, 195 mmol), allyl bromide (19.1 mL, 218 mmol) and potassium carbonate (27.26 g, 194 mmol) were heated at reflux in acetone (200 mL), for 24 hours under an inert atmosphere. The solvent was removed *in vacuo*, the residue extracted with dichloromethane (3 × 300 mL), washed with water (2 × 300 mL) and the chlorinated extracts dried over magnesium sulfate. Solvent was removed *in vacuo* to give **2.2** as a white solid. Yield 37.5 g: quantitative (Lit. 99 %). M.pt 68–70 °C (Lit. 69 °C); HR MS (ES^{+}): *m/z* 177.0910 $\{M\text{-}OH\}^{+}$; calculated for $C_{11}H_{13}O_2$ 177.0916; ^{1}H NMR (500 MHz, $CDCl_3$) δ (ppm) = 6.93 (s, 1H, Ar-H^6), 6.85 (s, 2H, Ar-H^2, Ar-H^3), 6.08 (m, 1H, C=CH-), 5.40 (d, 1H, *trans*-C=CH_2, *J* = 17.1 Hz), 5.28 (d, 1H, *cis*-C=CH_2, *J* = 10.3 Hz), 4.61 (m, 4H, CH_2-OH, Ar-OCH_2-), 3.88 (s, 3H, Ar-OCH_3); $^{13}C\{^{1}H\}$ NMR (75 MHz, $CDCl_3$) δ (ppm) = 150.1, 147.9, 134.5, 133.7, 119.8, 118.4, 113.9, 111.3, 70.4, 65.7, 56.4; Analysis for $C_{11}H_{14}O_3$ (calculated, found) C (68.02, 68.12), H (7.27, 7.31). All data are consistent with the literature.[16]

Synthesis of (±)-2,7,12-trimethoxy-3,8,13-*tris*(propenyloxy)-10,15-dihydro-5*H*-tribenzo[*a,d,g*]cyclononatriene (2.3). 3-Methoxy-4-(propenyloxy)benzyl alcohol (42.0 g, 216.6 mmol) was heated and stirred at 70 °C. A catalytic quantity of phosphoric acid (spatula tip) was added, and the reaction stirred for sixteen hours, during which time it solidified. This solid was triturated in methanol (400 mL) before the solid was collected by filtration, washed with further methanol and dried *in vacuo* to afford **2.3** as a white solid. Yield 14.75 g: 39% (Lit. 41%). M.pt 176–178 °C (Lit. 175 °C); ^{1}H NMR (500 MHz, $CDCl_3$) δ (ppm) = 6.86 (s, 3H, Ar-H), 6.80 (s, 3H, Ar-H), 6.08 (m, 3H, C=CH-), 5.36 (d, 3H, *trans*-C=CH_2, *J* = 17.2 Hz), 5.23 (d, 3H, *cis*-C=CH_2, *J* = 10.5 Hz), 4.73 (d, 3H, CTG *exo*-H, *J* = 13.7 Hz), 4.59 (m, 6H, Ar-OCH_2-), 3.83 (s, 9H, Ar-OCH_3), 3.51 (d, 3H, CTG *endo*-H, *J* = 13.7 Hz); ^{13}C{^{1}H} NMR (75 MHz, $CDCl_3$) δ (ppm) = 148.2, 146.7, 133.7, 132.3, 131.7, 117.5, 115.6, 113.6, 70.2, 56.1, 36.5. All data are consistent with the literature.[16]

Synthesis of (±)-2,7,12-trimethoxy-3,8,13-*tris*(hydroxy)-10,15-dihydro-5*H*-tribenzo[*a,d,g*]cyclononatriene (CTG, 2.4). (±)-2,7,12-Trimethoxy-3,8,13-*tris*(propenyloxy)-10,15-dihydro-5*H*-tribenzo[*a,d,g*]cyclononene (10.0 g, 18.8 mmol) and triphenylphosphene (950 mg, 3.62 mmol) were heated for 3 hours at 80 °C in a mixture of dry tetrahydrofuran (250 mL), diethylamine (91 mL) and water (77 mL). The system was degassed for three hours with argon; after which, palladium(II) acetate (315 mg, 1.40 mmol) was added, and stirred at reflux, in which time the mixture turned dark brown. The reaction was cooled to room temperature, the solvent removed *in vacuo* and the resulting residue extracted with ethyl acetate (3 × 300 mL). The ethyl acetate extracts were filtered, washed with water (300 mL), brine (3 × 300 mL), dried over magnesium sulfate and the solvent removed *in vacuo*. The resulting oily solid was triturated with ether (100 mL) and collected to yield **2.4** as an off-white solid. Yield 3.66 g: 49% (Lit. 67 %). M.pt > 300 °C (Lit. > 300); HR MS (ES^{+}): *m/z* 431.1462 {MNa}$^{+}$; calculated for $C_{24}H_{24}O_6Na$ 431.1471; ^{1}H NMR (500 MHz, $CDCl_3$) δ (ppm) = 6.87 (s, 3H, Ar-H), 6.79 (s, 3H, Ar-H), 5.39 (bs, 3H, Ar-OH), 4.73 (d, 3H, CTG *exo*-H, *J* = 13.7 Hz), 3.89 (s, 9H, Ar-OCH_3), 3.52 (d, 3H, CTG *endo*-H, *J* = 13.7 Hz); ^{13}C{^{1}H} NMR (75 MHz, $CDCl_3$) δ (ppm) = 145.6, 144.5, 132.9, 131.6, 115.8, 112.7, 56.5, 36.7; Analysis for $C_{24}H_{24}O_6$ (calculated, found) C (70.57, 70.84), H (5.92, 6.08). All data are consistent with the literature.[43]

Synthesis of (±)-2,7,12-trimethoxy-3,8,13-*tris*(2-pyridylmethyloxy)-10,15-dihydro-5*H*-tribenzo[*a,d,g*]cyclononatriene (2.5). A suspension of CTG (1.21 g, 2.94 mmol) and potassium carbonate (3.32 g, 24.0 mmol) were stirred at reflux in acetone (400 mL) for 30 minutes, under argon. 2-bromomethylpyridine hydrobromide (2.90 g, 11.47 mmol) was added and the reaction held at reflux for a further 96 hours, during which time the reaction mixture turned from colourless to orange and darkened further over time. After cooling, the acetone was removed *in*

vacuo, water (300 mL) was added and the suspension extracted with dichloromethane (4 × 300 mL). The combined extracts were dried over magnesium sulfate and concentrated *in vacuo*, resulting in a brown oil that solidified upon standing. Trituration in methanol yielded **2.5** as a bright white solid. Yield 1.78 g: 89 % (Lit. 85 %); M.pt 162–164 °C (Lit. 162 °C); HRMS (ES^+): *m/z* 682.2939 $\{MH\}^+$; calculated for $C_{42}H_{39}O_6N_3$ 682.2917; ^1H NMR (500 MHz, $CDCl_3$) δ (ppm) = 8.59 (d, 3H, Py-H^6, *J* = 4.6 Hz), 7.68 (td, 3H, Py-H^4, *J* = 7.7, 1.3 Hz), 7.49 (d, 3H, Py-H^3, *J* = 7.8 Hz), 7.19 (dd, 3H, Py-H^5, *J* = 7.2, 5.1 Hz), 6.83 (s, 3H, Ar-H), 6.66 (s, 3H, Ar-H), 5.28 (m, 6H, Ar-OCH_2-), 4.67 (d, 3H, CTG *exo*-H, *J* = 12.8 Hz), 3.79 (s, 9H, Ar-OCH_3), 3.42 (d, 3H, CTG *endo*-H, *J* = 12.8 Hz); $^{13}C\{^1H\}$ NMR (75 MHz, $CDCl_3$) δ (ppm) = 157.7, 148.9, 148.2, 146.6, 137.1, 132.6, 131.7, 122.6, 121.3, 115.3, 113.7, 71.7, 56.3, 36.5. All data are consistent with the literature.[17]

Synthesis of (±)-2,7,12-trimethoxy-3,8,13-*tris*(3-pyridylmethyloxy)-10,15-dihydro-5*H*-tribenzo[*a,d,g*]cyclononatriene (2.6). Sodium hydride (60% NaH dispersed in mineral oil, 145 mg, 3.57 mmol) was added in small portions to a stirred solution of CTG (145 mg, 0.355 mmol) in anhydrous DMF (6 mL). The reaction mixture was stirred for 30 minutes under an argon atmosphere. A solution of 3-bromomethyl pyridine‡ (2.45 mmol) in dichloromethane (30 mL) added via syringe and the reaction mixture stirred for a further 48 hours. Water (100 mL) and dichloromethane (100 mL) were added and the aqueous layer washed with dichloromethane (2 × 100 mL). The combined organic layers were washed with water (5 × 100 mL), brine (2 × 100 mL), dried over magnesium sulfate and solvent removed *in vacuo*. The residue was purified by column chromatography (silica, 5% methanol in dichloromethane), and triturated in ether to afford the target ligand as a white solid. Yield 146 mg: 44.1%. [‡ 3-bromomethyl pyridine was freshly prepared before use by the following method: Saturated aqueous sodium carbonate (~10 mL) added dropwise to a stirred solution of 3-bromomethyl pyridine hydrobromide (620 mg, 2.45 mmol) in distilled water (20 mL) at 0 °C to reach pH 7. The 3-bromomethyl pyridine was extracted with dichloromethane (30 mL), dried over magnesium sulfate and filtered. The filtrate was used rapidly, without further purification]. M.pt 149–151 °C; HR MS (ES^+): *m/z* 682.2938 $\{MH\}^+$; calculated for $C_{42}H_{39}O_6N_3$ 682.2917; ^1H NMR (500 MHz, $CDCl_3$) δ (ppm) = 8.69 (s, 3H, Py-H^2), 8.58 (d, 3H, Py-H^6, *J* = 4.3 Hz), 7.76 (d, 3H, Py-H^4, *J* = 7.7 Hz), 7.29 (dd, 3H, Py-H^5, *J* = 7.7, 5.1 Hz), 6.85 (s, 3H, Ar-H), 6.72 (s, 3H, Ar-H), 5.11 (s, 6H, Ar-OCH_2-), 4.71 (d, 3H, CTG *exo*-H, *J* = 13.7 Hz), 3.76 (s, 9H, Ar-OCH_3), 3.50 (d, 3H, CTG *endo*-H, *J* = 13.7 Hz); $^{13}C\{^1H\}$ NMR (75 MHz, $CDCl_3$) δ (ppm) = 149.4, 148.7, 148.7, 146.6, 135.2, 133.2, 132.9, 131.7, 123.6, 116.8, 113.8, 69.4, 56.2, 36.5; Analysis for **2.6** (% calculated; found) C (73.88; 74.09), H (5.90; 6.10), N (6.15; 5.85); Infrared analysis (FT-IR, cm^{-1}) 3006, 2932, 1668, 1517, 1129.

Synthesis of (±)-2,7,12-trimethoxy-3,8,13-*tris*(3-carboxypyridyl)-10,15-dihydro-5*H*-tribenzo[*a,d,g*]cyclononene (2.7). Anhydrous triethylamine (4.0 mL, 29.3 mmol) was added to a stirred solution of CTG (1.0 g, 2.46 mmol) in dry tetrahydrofuran (100 mL) at -78 °C, under an argon atmosphere. After one hour, nicotinoyl chloride hydrochloride (1.37 g, 7.62 mmol) was added to the reaction mixture and held at -78 °C for a further two hours, before being left at room temperature for 48 hours. A second portion of nicotinoyl chloride hydrochloride (1.37 g, 7.62 mmol) was added, and left to stir for a further 96 hours. The solvent was removed *in vacuo*, and the resultant residue triturated in ethanol to afford **2.7** as a white solid. Yield 1.45 g: 75 % (Lit. 42 %); M.pt 256-257 °C (Lit. 254-256 °C); HR MS (ES^+): *m/z* 762.2003 $\{MK\}^+$; calculated for $C_{42}H_{33}O_9N_3K$ 768.1854; ^1H NMR (500 MHz, $CDCl_3$) δ (ppm) = 9.39 (s, 3H, Py-H^2), 8.84 (d, 3H, Py-H^6, *J* = 4.8 Hz), 8.44 (d, 3H, Py-H^4, *J* = 7.9 Hz), 7.46 (dd, 3H, Py-H^5, *J* = 7.9, 4.9 Hz), 7.19 (s, 3H, Ar-H), 6.96 (s, 3H, Ar-H), 4.82 (d, 3H, CTG *exo*-H, *J* = 13.8 Hz), 3.81 (s, 9H, Ar-OCH_3), 3.67 (d, 3H, CTG *endo*-H, *J* = 13.8 Hz). All data are consistent with the literature.[17]

Synthesis of (±)-2,7,12-trimethoxy-3,8,13-*tris*(4-carboxypyridyl)-10,15-dihydro-5*H*-tribenzo[*a,d,g*]cyclononatriene (2.8). Anhydrous triethylamine (2.1 mL, 15 mmol) was added to a stirred solution of CTG (500 mg, 1.22 mmol) in dry tetrahydrofuran (50 mL) at -78 °C, under an argon atmosphere. After one hour, isonicotinoyl chloride hydrochloride (675 mg, 3.79 mmol) was added to the reaction mixture and held at -78 °C for a further two hours, before being stirred at room temperature for 48 hours. A second portion of isonicotinoyl chloride hydrochloride (300 mg, 1.69 mmol) was added and left to stir for a further 48 hours. The solvent was removed *in vacuo*, and the resultant residue triturated in ethanol to afford **2.8** as a white solid. Yield 701 mg: 80 % (Lit. 83 %); M.pt 261-262 °C (Lit. 259-261 °C); HR MS (ES^+): *m/z* 724.2822 $\{MH\}^+$; calculated for $C_{42}H_{34}O_9N_3$ 724.2802; ^1H NMR (500 MHz, $CDCl_3$) δ (ppm) = 8.85 (d, 6H, Py-H^2, *J* = 6.0 Hz), 7.99 (d, 6H, Py-H^3, *J* = 6.0 Hz), 7.17 (s, 3H, Ar-H), 6.96 (s, 3H, Ar-H), 4.84 (d, 3H, CTG *exo*-H, *J* = 13.9 Hz), 3.81 (s, 9H, Ar-OCH_3), 3.70 (d, 3H, CTG *endo*-H, *J* = 13.9 Hz). All data are consistent with the literature.[19]

Synthesis of 4-(4-pyridyl)benzoyl chloride hydrochloride. Under an argon atmosphere, 4-(4-pyridyl)benzoic acid hydrochloride (1.83 g, 7.77 mmol) was held at reflux in thionyl chloride (10 mL) containing a few drops of DMF for 24 hours. The thionyl chloride was removed *in vacuo* and the off-white solid washed with diethyl ether to give 4-(4-pyridyl)benzoyl chloride hydrochloride in quantitative yield which was used without further purification. All data are consistent with the literature.[29c]

Synthesis of (±)-2,7,12-trimethoxy-3,8,13-*tris*(4-pyridyl-4-carboxyphenyl)-10,15-dihydro-5*H*-tribenzo[*a,d,g*]cyclononatriene (2.9). CTG (153 mg, 0.375 mmol) was dissolved in anhydrous tetrahydrofuran (30 mL) under an inert atmosphere and cooled to -78°C in an ice bath. Anhydrous triethylamine (0.65 mL, 6 eq.) was added to the reaction mixture, which was then stirred for a further 30 minutes. 4-(4-Pyridyl)benzoyl chloride hydrochloride (320 mg, 1.26 mmol) was added to the solution, which was stirred at -78°C for one hour, and then at room temperature for 2 days. A further portion of 4-(4-pyridyl)benzoyl chloride hydrochloride (320 mg, 1.26 mmol) was added and the mixture stirred for a further 2 days. The solution was taken to dryness *in vacuo* and the residue triturated with ethanol to give **2.9** as a white solid. Yield 287 mg: 80%. HR MS (ES^+): *m/z* 952.3232 $\{MH\}^+$; calculated for $C_{60}H_{46}N_3O_9$ 952.3229; ^1H NMR (500 MHz, $CDCl_3$) δ (ppm) = 8.73 (d, 6H, Py-H^2, J = 5.9 Hz), 8.31 (d, 6H, Ph-H^3, J = 8.4 Hz), 7.77 (d, 6H, Ph-H^2, J = 8.4 Hz), 7.56 (d, 6H, Py-H^3, J = 5.9 Hz), 7.20 (s, 3H, Ar-H), 6.98 (s, 3H, Ar-H), 4.86 (d, 3H, CTG *exo*-H, J = 13.8 Hz), 3.82 (s, 9H, Ar-OCH_3), 3.71 (d, 3H, CTG *endo*-H, J = 13.8 Hz); $^{13}C\{^1H\}$ NMR (75 MHz, $CDCl_3$): δ (ppm) 164.2, 150.5, 150.0, 147.1, 143.1, 138.6, 138.1, 131.6, 131.1, 130.0, 127.2, 124.1, 121.7, 114.3, 56.3, 36.6. All data are consistent with the literature.[29c]

Synthesis of (±)-2,7,12-trimethoxy-3,8,13-*tris*(2-pyridylmethyloxy-*N*-oxide)-10,15-dihydro-5*H*- tribenzo[*a,d,g*]cyclononatriene (2.10). (±)-2,7,12-Trimethoxy-3,8,13-*tris*(2-pyridylmethyloxy)-10,15-dihydro-5*H*- tribenzo[*a,d,g*]cyclononatriene (250 mg, 0.367 mmol) was dissolved in dichloromethane (50 mL) at -78 °C and *Meta*-chloroperoxybenzoic acid (*m*-CPBA. 380 mg, 2.2 mmol) added under an inert atmosphere. The reaction mixture was stirred for 24 hours, during which time it yellowed, and sodium hydrogen carbonate was added to quench the reaction. The organic layer was removed, washed with water (2 × 75 mL) and sat. sodium hydrogen carbonate (2 × 50 mL), dried over magnesium sulfate and solvent removed *in vacuo*. The resulting crude solid was purified by recrystallisation in acetone (50 mL) and diethyl ether (30 mL), where colourless crystals of **2.10** were obtained after 48 hours. Yield 110 mg: 41%. M.pt 142–145 °C; HR MS (ES^+): *m/z* 730.3759 $\{MH\}^+$; calculated for $C_{42}H_{40}N_3O_9$ 730.3765; ^1H NMR (500Mhz, d_6-DMSO) δ (ppm) = 8.34 (d, 3H, Py-H^6, J = 6.0 Hz), 7.48 (d, 3H, Py-H^3, J = 7.7 Hz), 7.42 (m, 3H, Py-H^5), 7.36 (m, 3H, Py-H^4), 7.23 (s, 3H, Ar-H), 7.08 (s, 3H, Ar-H), 5.22 (m, 6H, CH_2-Py), 4.68 (d, 3H, CTG *exo*-H, J = 13.7 Hz), 3.67 (s, 9H, Ar-OCH_3), 3.54 (d, 3H, CTG *endo*-H, J = 13.7 Hz); $^{13}C\{^1H\}$ NMR (75 MHz, DMSO) δ (ppm) = 147.8, 147.6, 145.9, 139.3, 133.6, 132.3, 125.7, 125.3, 123.9, 115.6, 114.3, 65.2, 56.2, 35.2; Analysis for **2.10**·1.5(H_2O) (% calculated, found) C (66.66, 66.95), H (5.59, 5.55), N (5.55, 5.40); Infrared analysis (FT-IR, cm^{-1}) = 3107, 2920, 1643, 1585, 1518, 1334.

Synthesis of (±)-2,7,12-trimethoxy-3,8,13-*tris*(3-pyridylmethoxy-*N*-oxide)-10,15-dihydro-5*H*-tribenzo[*a,d,g*]cyclononatriene (2.11). (±)-2,7,12-Trimethoxy-3,8,13-*tris*(3-pyridylmethyloxy)-10,15-dihydro-5*H*-tribenzo[*a*,*d*,*g*]cyclononatriene (150 mg, 0.22 mmol) was dissolved in dichloromethane (~ 20 mL) at -78 °C and *Meta*-chloroperoxybenzoic acid (*m*-CPBA. 227 mg, 1.32 mmol) added under an inert atmosphere. The reaction mixture was stirred for one hour, before sodium hydrogen carbonate being added to quench the reaction. The organic layer was removed, washed with water (2 × 50 mL), dried over magnesium sulfate and the solvent removed *in vacuo*. The resulting yellow oily solid was triturated in methanol to yield **2.11** as a yellow powder. Yield 37.6 mg: 25 %. HR MS (ES^+): *m/z* 730.2756 $\{MH\}^+$; calculated for $C_{42}H_{40}N_3O_9$ 730.3765; ^1H NMR (500MHz, CD_2Cl_2) δ (ppm) = 7.94 (s, 3H, Py-H^2), 7.86 (d, 3H, Py-H^6, *J* = 4.2 Hz), 7.47 (d, 3H, Py-H^4, *J* = 7.8 Hz), 7.30 (m, 3H, Py-H^5), 6.84 (s, 3H, Ar-H), 6.77 (s, 3H, Ar-H), 4.95 (s, 6H, CH_2-Py), 4.66 (d, 3H, CTG *exo*-H, *J* = 12.1 Hz), 3.72 (s, 9H, Ar-OCH_3), 3.48 (d, 3H, CTG *endo*-H, *J* = 12.1 Hz); Infrared analysis (FT-IR, cm^{-1}) = 3106, 2912, 1658, 1559, 1521, 1342. Ligand **2.11** could not be sufficiently purified for complete analysis and was not employed in coordination studies.

Synthesis of (±)-2,7,12-trimethoxy-3,8,13-*tris*(3-carboxypyridine-*N*-oxide)-10,15-dihydro-5*H*- tribenzo[*a,d,g*]cyclononatriene (2.12). (±)-2,7,12-Trimethoxy-3,8,13-*tris*(3-carboxypyridyl)-10,15-dihydro-5*H*- tribenzo[*a*,*d*,*g*]cyclononatriene (500 mg, 0.690 mmol) was dissolved in dichloromethane (120 mL) and stirred under an argon atmosphere at -78 °C. *Meta*-chloroperoxybenzoic acid (*m*-CPBA. 600 mg, 2.75 mmol) was added to the reaction mixture and stirred at -78 °C for two hours, followed by 48 hours at room temperature. The reaction was quenched with sodium metabisulfite (spatula tip), washed with sat. aqueous sodium bicarbonate (2 × 200 mL) and brine (200 mL), dried over magnesium sulfate and concentrated *in vacuo*. The resultant off-white solid was triturated in methanol, affording **2.12** as a bright white solid. Yield 514 mg: 97 %; M.pt > 270 °C; HR MS (ES^+): *m/z* 772.2137 $\{MH\}^+$; calculated for $C_{42}H_{34}N_3O_{12}$ 772.2142; ^1H NMR (500 MHz, d_6-DMSO) δ (ppm) = 8.67 (s, 3H, Py-H^2), 8.53 (d, 3H, Py-H^6, *J* = 4.8 Hz), 7.93 (d, 3H, Py-H^4, *J* = 7.9 Hz), 7.63 (dd, 3H, Py-H^5, *J* = 7.9, 4.9 Hz), 7.57 (s, 3H, Ar-H), 7.32 (s, 3H, Ar-H), 4.90 (d, 3H, CTG *exo*-H, *J* = 13.5 Hz), 3.75 (s, 9H, Ar-OCH_3), 3.71 (d, 3H, CTG *endo*-H, *J* = 13.5 Hz); $^{13}C\{^1H\}$ NMR (75 MHz, $CDCl_3$) δ (ppm) = 161.4, 149.4, 143.3, 139.5, 139.3, 137.7, 132.2, 128.9, 127.5, 126.2, 124.3, 114.9, 56.7, 35.3; Analysis for **2.12**·0.5(H_2O) (% calculated, found) C (64.61, 64.45), H (4.39, 4.60), N (5.38, 5.30); Infrared analysis (FT-IR, cm^{-1}) = 3346, 2986, 1737, 1611, 1508, 1482, 1435, 1397, 1293, 1213, 1133, 1018, 966, 928, 887, 833, 742, 664, 562.

Synthesis of (±)-2,7,12-trimethoxy-3,8,13-*tris*(4carboxypyridine-*N*-oxide)-10,15-dihydro-5*H*-tribenzo[*a,d,g*]cyclononatriene (2.13). (±)-2,7,12-Trimethoxy-3,8,13-*tris*(4-carboxypyridyl)-10,15-dihydro-5*H*-tribenzo[*a,d,g*]cyclononatriene (100 mg, 0.138 mmol) was dissolved in dichloromethane (20 mL), and stirred under an argon atmosphere at -78 °C. *Meta*-chloroperoxybenzoic acid (*m*-CPBA. 96 mg, 0.552 mmol) was added to the reaction mixture and stirred at -78 °C for an hour, followed by 24 hours at room temperature. The reaction was quenched with sat. sodium bicarbonate (3 × 65 mL), washed with water (50 mL) and brine (50 mL), dried over magnesium sulfate and concentrated *in vacuo*. The resultant yellow oily solid was triturated in ethanol to afford **2.13** as a fine, off-white solid. Yield 61 mg: 57 %; M.pt > 300 °C; HR MS (ES^+): *m/z* 772.2137 $\{MH\}^+$; calculated for $C_{42}H_{34}N_3O_{12}$ 772.2142; ^1H NMR (500 MHz, $CDCl_3$) δ (ppm) = 8.27 (d, 6H, Py-H^2, *J* = 7.7 Hz), 8.01 (d, 6H, Py-H^3, *J* = 7.7 Hz), 7.16 (s, 3H, Ar-H), 6.94 (s, 3H, Ar-H), 4.84 (d, 3H, CTG *exo*-H, *J* = 13.7 Hz), 3.80 (s, 9H, Ar-OCH_3), 3.69 (d, 3H, CTG *endo*-H, *J* = 13.7 Hz); $^{13}C\{^1H\}$ NMR (75 MHz, d_6-DMSO) δ (ppm) = 161.9, 149.6, 140.1, 139.2, 137.9, 132.3, 127.4, 124.4, 124.4, 114.9, 56.6, 35.4; Analysis for **2.13**·0.5(H_2O) (% calculated, found) C (64.61, 64.30), H (4.39, 4.35), N (5.38, 5.30); Infrared analysis (FT-IR, cm^{-1}) = 3117, 2936, 1738, 1612, 1506, 1478, 1399.

Synthesis of (±)-2,7,12-trimethoxy-3,8,13-*tris*(4-pyridine-*N*-oxide-4-carboxyphenyl)-10,15-dihydro-5*H*-tribenzo[*a,d,g*]cyclononatriene (2.14). (±)-2,7,12-Trimethoxy-3,8,13-*tris*(4-pyridyl-4-carboxyphenyl)-10,15-dihydro-5*H*-tribenzo[*a,d,g*]cyclononatriene (305 mg, 0.748 mmol) was dissolved in dichloromethane (100 mL) at -78℃. *Meta*-chloroperoxybenzoic acid (*m*-CPBA. 227 mg, 1.313 mmol) was added to the flask, under argon, and stirred for 2 hours at -78, followed by 48 hours at room temperature. The dichloromethane layer was washed with mildly basic aqueous sodium bicarbonate (3 × 100 mL), dried over magnesium sulphate and reduced *in vacuo* to yield a yellow oil. Trituration of the crude product in methanol afforded **2.14** as a white solid. Yield 318 mg: quant. M.pt > 300 °C; HR MS (ES^+): *m/z* 1022.2913 $\{MNa\}^+$; calculated for $C_{60}H_{45}O_{12}N_3Na$ 1022.2901; ^1H NMR (500 MHz, d_6-DMSO) δ (ppm) = 8.32 (d, 6H, Py-H^2, *J* = 7.2 Hz), 8.18 (d, 6H, Ph-H^2, *J* = 8.3 Hz), 8.01 (d, 6H, Ph-H^3, *J* = 8.3 Hz), 7.88 (d, 6H, Py-H^3, *J* = 7.2 Hz), 6.56 (s, 3H, Ar-H), 6.34 (s, 3H, Ar-H), 4.90 (d, 3H, CTG *exo*-H, *J* = 13.1 Hz), 3.73 (s, 9H, Ar-OCH_3), 3.70 (d, 3H, CTG *endo*-H, *J* = 13.1 Hz); $^{13}C\{^1H\}$ NMR (75 MHz, $CDCl_3$) δ (ppm) = 163.7, 149.3, 140.6, 139.13, 138.6, 137.8, 134.5, 131.9, 130.6, 128.5, 126.7, 124.1, 114.4, 56.2, 34.9; Analysis for **2.14**·2(H_2O) (% calculated; found) C (69.90, 69.56), H (4.77, 4.65), N (4.06, 3.95); Infrared analysis (FT-IR, cm^{-1}) = 3422, 2940, 1728, 1607, 1505, 1177.

Synthesis of dimethyl-2,6-pyridinedicarboxylate (2.16). 2,6-Pyridinedicarboxylic acid (40.0 g, 239 mmol) was held at reflux in methanol (350 mL) with a catalytic amount of concentrated sulphuric acid for 24 hours. The reaction mixture was allowed to cool and the solvent removed *in vacuo*. The crude solid was taken up into dichloromethane (100 mL) and neutralized to pH 7 with sat. aqueous sodium hydrogen carbonate, dried over magnesium sulfate and reduced *in vacuo* to give **2.16** as a white crystalline solid. Yield 46.7 g: quantitative; M.pt 122 - 124 °C (Lit. 121 – 124 °C); LC MS (ES^+): *m/z* 196.1 $\{MH\}^+$; calculated for $C_9H_9NO_4$ 196.1024; ^1H NMR (500 MHz, $CDCl_3$) δ (ppm) = 8.29 (d, 2H, Py-H^3, *J* = 7.5 Hz), 8.02 (t, 1H, Py-H^4, *J* = 8.0 Hz), 4.02 (s, 6H, O-CH_3). All data are consistent with the literature.[22a]

Synthesis of 4-hydroxymethyl-dimethyl-2,6-pyridinedicarboxylate (2.17). Dimethyl-2,6-pyridinedicarboxylate (5.61 g, 28.7 mol) was added to a stirring solution of sulphuric acid (30 % v/v, 30 mL) and methanol (30 mL) at 0 ℃. The temperature was allowed to slowly reach room temperature. Hydrogen peroxide (30 %, 24 mL) and iron(II) sulfate (sat. aqueous, 30 mL) were added drop-wise and simultaneously to keep the temperature between 20-25℃. Once the addition was complete, the reaction mixture was allowed to stir at room temperature for a further 30 minutes. Potassium carbonate was added slowly to reach pH 7 and the precipitate filtered. The filtrate was extracted with ethyl acetate (4 × 55 mL), dried over magnesium sulfate and concentrated *in vacuo* to give **2.17** as an off-white solid. The crude solid was purified by column chromatography (silica, 30% hexane in ethyl acetate), affording the desired compound as a white solid. Yield 1.23 g: 21 % (Lit. 19 %). M.pt 154–157 °C (Lit. 154-158 °C); LC MS (ES^+): *m/z* 226.2 $\{MH\}^+$; calculated for $C_{10}H_{12}O_5N$ 226.1689; ^1H NMR (500 MHz, $CDCl_3$) δ (ppm) = 8.32 (s, 2H, Py-H^3), 4.91 (s, 2H, -CH_2-), 4.03 (s, 6H, O-CH_3), 2.18 (m, 1H, -OH). All data are consistent with the literature.[22]

Synthesis of 4-bromomethyl-dimethyl-2,6-pyridinedicarboxylate (2.18). Phosphorus tribromide (12.1 g, 44.7 mmol) was dissolved in dichloromethane (100 mL) and added drop-wise to a vigorously stirring solution of 4-hydroxymethyl-dimethyl-2,6-pyridinedicarboxylate (2.04 g, 8.89 mmol) in dichloromethane (70 mL) at 0℃. Once complete, the mixture was allowed to stir at room temperature for a further 45 minutes. Water (100 mL) and aqueous sodium bicarbonate were added slowly to pH 7, which was subsequently extracted into dichloromethane (5 × 125 mL). The organic layers were combined, dried over magnesium sulfate and concentrated *in vacuo* to yield **2.18** as a white powder. Yield 2.43 g: 96 % (Lit. unreported). M.pt 110-113 °C (Lit. 110-113 °C); HR MS (ES^+): *m/z* 309.9695 $\{MNa\}^+$; calculated for $C_{10}H_{10}O_4NBrNa$ 309.9691; ^1H NMR (500 MHz, $CDCl_3$) δ (ppm) = 8.33 (s, 2H, Py-H^3), 4.51 (s, 2H, CH_2Br), 4.03 (s, 6H, O-CH_3). All data are consistent with the literature.[22]

Synthesis of (±)-2,7,12-trimethoxy-3,8,13-*tris*(dimethyl-2,6-pyridinedicarboxylatemethyloxy)-10,15-dihydro-5*H*-tribenzo[*a,d,g*]cyclononatriene (2.19). (±)-2,7,12-Trimethoxy-3,8,13-*tris*(hydroxy)-10,15-dihydro-5*H*-tribenzo[*a,d,g*]cyclononatriene (CTG. 305 mg, 0.748 mmol) and potassium carbonate (625 mg, 4.52 mmol) were dissolved in acetonitrile (125 mL) and the mixture held at reflux for 30 minutes. 4-bromomethyl-dimethyl-2,6-pyridinedicarboxylate (1.30 g, 4.51 mol) was added to the reaction mixture, which was held at reflux for a further 48 hours, affording a white precipitate. The reaction was allowed to cool and all solvent removed *in vacuo*. The resultant residue was taken up into dichloromethane and washed with water (3 × 100 mL), dried over magnesium sulfate and concentrated *in vacuo*. Trituration of the impure product in cold methanol afforded **2.19** as a white solid. Yield 748 mg: 97 %. M.pt 133-136 °C; HR MS (ES^+): *m/z* 1052.3039 $\{MNa\}^+$; calculated for $C_{54}H_{51}O_{18}N_3Na$ 1052.3022; ^1H NMR (500 MHz, $CDCl_3$) δ (ppm) = 8.40 (s, 6H, Py-H^3), 6.91 (s, 3H, Ar-H), 6.80 (s, 3H, Ar-H), 5.18 (m, 6H, CH_2-Py), 4.73 (d, 3H, CTG *exo*-H, *J* = 13.9 Hz), 4.03 (s, 18H, Ar-CO_2CH_3), 3.82 (s, 9H, Ar-OCH_3), 3.52 (d, 3H, CTG *endo*-H, *J* = 13.9 Hz); $^{13}C\{^1H\}$ NMR (75 MHz, $CDCl_3$) δ (ppm) = 165.0, 150.2, 149.2, 148.5, 146.3, 134.3, 131.7, 125.8, 118.3, 114.1, 70.4, 56.2, 53.3, 36.4; Analysis for **2.19**·3(H_2O) (% calculated; found) C (59.83, 59.65), H (5.30, 5.00), N (3.88, 3.70); Infrared analysis (FT-IR, cm^{-1}) = 3002, 2910, 1713, 1599, 1440, 1129.

Synthesis of (±)-2,7,12-trimethoxy-3,8,13-*tris*(2,6-pyridinedicarboxylatemethyloxy)-10,15-dihydro-5*H*-tribenzo[*a,d,g*]cyclononatriene (2.20). (±)-2,7,12-Trimethoxy-3,8,13-*tris*(dimethyl-2,6-pyridinedicarboxylatemethyloxy)-10,15-dihydro-5*H*-tribenzo[*a,d,g*]cyclononatriene (100 mg, 0.0798 mmol) was dissolved in a 7:1 mixture of methanol and water and heated to reflux in the presence of sodium hydroxide (235 mg, 60 eq.) overnight. The reaction mixture was cooled and the highly insoluble white solid collected by filtration. Infrared analysis (FT-IR, cm^{-1}) = 3536, 2999, 2910, 1707, 1569, 1128.

Preparation of $\{[Gd(2.10)(NO_3)_3]\cdot(DMF)\}_\infty$ (Complex 2.21). $Gd(NO_3)_3\cdot 6(H_2O)$ (10.15 mg, 0.0225 mmol) and **2.10** (5.11 mg, 0.0075 mmol) were dissolved in DMF (~ 1 mL) and diethyl ether vapours were diffused into the solution. Small colourless needles formed after 14 days which were analyzed *via* single crystal X-ray analysis. Yield 9.8 mg. Analysis for $\{[Gd(\mathbf{2.10})(NO_3)_3]\cdot(DMF)\cdot(H_2O)\}_\infty$ $C_{45}H_{48}GdN_7O_{20}$ (% calculated, found) C (46.13, 46.15), H (4.16, 3.90), N (8.42, 8.15); Infrared analysis (FT-IR, cm^{-1}) = 3458 (broad), 3140, 2985, 2328, 1672, 1609, 1518, 1454, 1384, 1295, 1266, 1212, 1142, 1090, 1058, 1029, 1011, 950, 858, 816, 766, 741, 698, 600, 569, 550.

Preparation of {[Sm(2.13)Cl(DMF)$_3$]·[SmCl$_5$(DMF)]·1.5(DMF)}$_\infty$ (Complex 2.22). $SmCl_3 \cdot 6(H_2O)$ (11.41 mg, 0.0225 mmol) and **2.13** (5.09 mg, 0.0075 mmol) were dissolved in DMF (~ 1 mL) and diethyl ether vapours were diffused into the solution. Yellow needles formed after 21 days which were analyzed *via* single crystal X-ray analysis. Yield 5.9 mg. Analysis for $\{[Sm(\mathbf{2.13})Cl(DMF)_3]\cdot[SmCl_5(DMF)]\cdot 3(H_2O)\}_\infty$ $C_{57}H_{74}Cl_6N_{8.5}O_{20}Sm_2$: (% calculated, found) C (39.53, 39.75), H (4.01, 4.35), N (5.71, 5.35); Infrared analysis (FT-IR, cm^{-1}) = 3119, 2938, 1745, 1628, 1505, 1484, 1443, 1404, 1252, 1163, 1139, 1052, 927, 861, 830, 746, 679, 630, 581, 497, 484, 470.

Preparation of {[Ce$_a$(2.14)$_b$·(DMF)$_c$]·(OTf)$_{3a}$} (Complex 2.23). $Ce(OTf)_3$ (11.41 mg, 0.0225 mmol) and **2.14** (8.49 mg, 0.0075 mmol) were dissolved in DMF (~ 2 mL) and diethyl ether vapours were diffused into the solution. Yellow blocks formed after 28 days which were analyzed *via* single crystal X-ray analysis. Yield 5.9 mg. HR MS (ES^+): *m/z* 1000.3009 {**2.14**H}$^+$, 1481.7302 $\{Ce_2(\mathbf{2.14})_2(OTf)_4\}^{2+}$ and 1580.8012 {Ce(**2.14**)(OTf)$_2$(NMP)}$^+$; calculated for 1001.3012, 1481.7306 and 1580.7991, respectively; Analysis for (% calculated, found) C (*n/a*, 45.95), H (*n/a*, 4.45), N (*n/a*, 5.80); Infrared analysis = (FT-IR, cm^{-1}) 3300-2900 (broad), 1735, 1645, 1513, 1274, 847; Crystal data (Matrix only, synchrotron radiation): Trigonal, *a*,*b* = 60.1516, *c* = 39.0232 Å, α,β = 90, γ = 120°, *V* = 122274.44 Å^3.

2.5.3 X-ray crystallography

Crystals were mounted under inert oil on a MiTeGen tip and flash frozen to 150(1) K using an Oxford Cryosystems cryostream low temperature device. X-ray diffraction data were collected using graphite-monochromated Mo-*K* radiation (λ = 0.71073 Å) using a Bruker-Nonius X-8 diffractometer with ApexII detector and FR591 rotating anode generator; or using synchrotron radiation (λ = 0.6889 Å) with a Crystal Logic 4-circle Kappa goniometer and Rigaku Saturn 724 CCD diffractometer at station I19 of Diamond Light Source. Data were corrected for Lorenztian and polarization effects and absorption corrections were applied using multi-scan methods. The structures were solved by direct methods using SHELXS-97 and refined by full-matrix on F^2 using SHELXL-97, interfaced through the X-seed interface.[44] Unless otherwise specified, all non-hydrogen atoms were refined as anisotropic, and hydrogen positions were included at geometrically estimated positions. Molecular graphics were obtained using POV-RAY through the X-Seed interface.[45] Additional details are given below and data collections and refinements summarised in **Table 2.3**.

Crystals of clathrate complex **2.10**·2(H_2O) were twinned and the data reduced and corrected for absorption using the programs TWINABS and Cell_now, interfaced as part of the Bruker ApexII suite.[46] Crystals of clathrate complex **2.12**·2(NMP) were weakly diffracting. One 3-

carboxypyridine-*N*-oxide moiety was modelled with two-fold molecular disorder and its positions refined at 40:60 occupancies. This disordered group, along with two NMP solvent molecules, were refined isotropically. Additionally, the bond lengths of one NMP solvent molecule were restrained to be chemically reasonable. Crystals of clathrate complex **2.13**·(DMF) were weakly diffracting and collected using synchrotron radiation at station I19 of Diamond Light Source. Complex **2.21**: A solvent DMF molecule was refined isotropically and modelled as disordered across two positions, each at 50% occupancy, and the C-O bond lengths of the disordered DMF were restrained to be chemically reasonable. Complex **2.22**: Two methyl groups of ligand **2.13** were refined as being disordered across two positions, one with the OMe moiety in two positions, each at 50% occupancy, and the other with the CH_3 group across two positions at 75:25 occupancy. The coordinated DMF ligand of the $[SmCl_5(DMF)]^{2-}$ unit was refined as disordered across two positions, each at 50% occupancy. The two uncoordinated solvent DMF molecules were refined isotropically and one modelled with symmetry-related disorder that was refined at 50% occupancy. Additionally, the bond lengths of this DMF molecule were restrained to be chemically reasonable.

Table 2.3 *Details of collection and structure refinements for clathrate and inclusion complexes (**2.10**, **2.12** and **2.13**) and metal complexes (**2.21** and **2.22**).*

	2.10·2(H_2O)	**2.10**·2(DMF)	**2.12**·2(NMP)	**2.13**·DMF *	**2.21**	**2.22**
Formula	$C_{84}H_{86}N_6O_{22}$	$C_{48}H_{53}N_5O_{11}$	$C_{52}H_{51}N_5O_{14}$	$C_{45}H_{40}N_4O_{13}$	$C_{45}H_{45}GdN_7O_{19}$	$C_{61.5}H_{78.5}Cl_6N_{9.5}O_{18.5}Sm_2$
Mr	1531.59	875.95	969.98	844.81	1146.14	1760.24
Crystal colour and shape	Colourless, fragment	Colourless, needle	Colourless, block	Colourless, plate	Yellow, needle	Yellow, block
Crystal size (mm)	0.08 x 0.05 x 0.05	0.12 x 0.08 x 0.08	0.20 x 0.12 x 0.12	0.18 x 0.15 x 0.09	0.10 x 0.08 x 0.01	0.24 x 0.18 x 0.14
Crystal system	Triclinic	Triclinic	Triclinic	Monoclinic	Monoclinic	Triclinic
Space group	*P*1	$P\bar{1}$	$P\bar{1}$	$P2_1/n$	*C*2/*c*	$P\bar{1}$
a (Å)	4.5584(6)	9.2161(5)	13.1282(13)	4.6996(16)	44.860(4)	12.7326(12)
b (Å)	16.3294(18)	11.1018(7)	14.0590(15)	21.173(7)	15.1635(14)	16.1047(13)
c (Å)	24.986(3)	22.8800(15)	15.0060(13)	39.052(14)	15.6748(14)	19.7002(17)
α (^{0})	99.660(4)	85.589(4)	92.776(6)	90	90	103.648(2)
β (^{0})	92.270(4)	81.494(3)	95.507(7)	91.286(4)	97.550(4)	94.159(3)
γ (^{0})	92.770(4)	75.676(3)	95.507(7)	90	90	94.159(3)
V (Å^3)	1829.2(4)	2241.3(2)	2447.2 (4)	3885(2)	10570.2(17)	3911.0(6)
Z	1	2	2	4	8	2
ρ_{calc} (g.cm^{-3})	1.390	1.298	1.316	1.444	1.440	1.495
θ range (^{0})	2.25 – 24.98	1.80 – 30.10	1.6– 25.00	1.78 – 31.70	1.42 – 26.73	1.06– 27.28
No. data collected	22009	44701	20244	36804	34505	61774
No. unique data	11097	12918	8581	12838	10958	17431
R_{int}	0.0813	0.0564	0.0586	0.0510	0.0958	0.0517
No. obs. Data ($I > 2\sigma(I)$)	6454	6881	4367	8287	6048	12627
No. parameters	1016	584	567	564	633	933
No. restraints	3	0	1	0	2	4
R_1 (obs data)	0.0876	0.0554	0.1075	0.0652	0.0698	0.0504
wR_2 (all data)	0.2440	0.1312	0.3754	0.1653	0.2194	0.1494
S	0.988	0.995	1.192	1.083	1.006	1.038

* Data collected using synchrotron radiation.

2.6 Bibliography

[1] (a) M. D. Ward, *Coord. Chem. Rev.* **2010**, *254*, 2634-2642; (b) A. P. de Silva, H. Q. N. Gunaratne, T. Gunnlaugsson, A. J. M. Huxley, C. P. McCoy, J. T. Rademacher, T. E. Rice, *Chem. Rev.* **1997**, *97*, 1515-1566; (c) T. Lazarides, H. Adams, D. Sykes, S. Faulkner, G. Calogero, M. D. Ward, *Dalton Trans.* **2008**, 691-698; (d) T. K. Ronson, H. Adams, L. P. Harding, S. J. A. Pope, D. Sykes, S. Faulkner, M. D. Ward, *Dalton Trans.* **2007**, 1006-1022; (e) Z.-M. Zhang, Y.-G. Li, S. Yao, E.-B. Wang, *Dalton Trans.* **2011**, *40*, 6465-6479.

[2] (a) C. M. G. dos Santos, A. J. Harte, S. J. Quinn, T. Gunnlaugsson, *Coord. Chem. Rev.* **2008**, *252*, 2512-2527; (b) J. Feng, H. Zhang, *Chem. Soc. Rev.* **2013**, *42*, 387-410; (c) J.-F. Lemonnier, L. Guénée, C. Beuchat, T. A. Wesolowski, P. Mukherjee, D. H. Waldeck, K. A. Gogick, S. Petoud, C. Piguet, *J. Am. Chem. Soc.* **2011**, *133*, 16219-16234.

[3] S. Pasquale, S. Sattin, E. C. Escudero-Adán, M. Martínez-Belmonte, J. de Mendoza, *Nat. Commun.* **2012**, *3*, 785.

[4] (a) J. P. Leonard, P. Jensen, T. McCabe, J. E. O'Brien, R. D. Peacock, P. E. Kruger, T. Gunnlaugsson, *J. Am. Chem. Soc.* **2007**, *129*, 10986-10987; (b) B. E. Aroussi, S. Zebret, C. Besnard, P. Perrottet, J. Hamacek, *J. Am. Chem. Soc.* **2011**, *133*, 10764-10767; (c) S. Zebret, C. Besnard, G. Bernardinelli, J. Hamacek, *Eur. J. Inorg. Chem.* **2012**, *14*, 2409-2417; (d) Y.-B. Dong, P. Wang, J.-P. Ma, X.-X. Zhao, H.-Y. Wang, B. Tang, R.-Q. Huang, *J. Am. Chem. Soc.* **2007**, *129*, 4872-4873.

[5] (a) B. El Aroussi, L. Guénée, P. Pal, J. Hamacek, *Inorg. Chem.* **2011**, *50*, 8588-8597; (b) Y. Jiao, J. Wang, P. Wu, L. Zhao, C. He, J. Zhang, C. Duan, *Chem. Eur. J.* **2014**, *20*, 2224-2231; (c) T. Gunnlaugsson, J. P. Leonard, *Dalton Trans.* **2005**, 3204-3212.

[6] C. Lincheneau, B. Jean-Denis, T. Gunnlaugsson, *Chem. Commun.* **2014**, *50*, 2857-2860.

[7] (a) M.-S. Chen, J. Fan, T.-A. Okamura, G.-C. L, W.-Y. Sun, *Inorg. Chim. Acta.* **2011**, *366*, 268-274; (b) F. Dai, D. Sun, D. Sun, *Cryst. Growth Des.* **2011**, *11*, 5670-5675; (c) Y. Jin, F. Luo, Y. X. Che, J. M. Zheng, *Inorg. Chem. Commun.* **2008**, *11*, 711-713; (d) S. Muniappan, S. Lipstman, S. George, I. Goldberg, *Inorg. Chem.* **2007**, *46*, 5544-5554; (e) J. M. Herrera, S. G. Baca, H. Adams, M. D. Ward, *Polyhedron* **2006**, *25*, 869-875.

[8] Y. Cui, W. Zou, R. Song, J. Yu, W. Zhang, Y. Yang, G. Qian, *Chem. Commun.* **2014**, *50*, 719-721.

[9] (a) S. Kennedy, G. Karotsis, C. M. Beavers, S. J. Teat, E. K. Brechin, S. J. Dalgarno, *Angew. Chem. Int. Ed.* **2010**, *49*, 4205-4208; (b) S. J. Dalgarno, M. J. Hardie, J. L. Atwood, J. E. Warren, C. L. Raston, *New J. Chem.* **2005**, *29*, 649-652.

[10] (a) M. J. Hardie, *Chem. Soc. Rev.* **2010**, *39*, 516-527; (b) J. J. Henkelis, S. A. Barnett, L. P. Harding, M. J. Hardie, *Inorg. Chem.* **2012**, *51*, 10657-10674; (c) M. A. Little, T. K. Ronson, M. J. Hardie, *Dalton Trans.* **2011**, *40*, 12217-12227.

[11] (a) M. J. Hardie, C. L. Raston, A. Salinas, *Chem. Commun.* **2001**, 1850-1851; (b) R. Ahmad, I. Dix, M. J. Hardie, *Inorg. Chem.* **2003**, *42*, 2182-2184.

[12] (a) S. J. Dalgarno, M. J. Hardie, J. E. Warren, C. L. Raston, *Dalton Trans.* **2004**, 2413-2416; (b) S. J. Dalgarno, C. L. Raston, *Chem. Commun.* **2002**, 2216-2217.

[13] (a) J. Hamacek, C. Besnard, T. Penhouet, P.-Y. Morgantini, *Chem. Eur. J.* **2011**, *17*, 6753-6764; (b) B. El Aroussi, N. Dupont, G. R. Bernardinelli, J. Hamacek, *Inorg. Chem.* **2009**, *49*, 606-615.

[14] (a) S. T. Mough, K. T. Holman, *Chem. Commun.* **2008**, 1407-1409; (b) T. K. Ronson, H. Nowell, A. Westcott, M. J. Hardie, *Chem. Commun.* **2010**, *47*, 176-178.

[15] (a) B. F. Abrahams, B. A. Boughton, N. J. FitzGerald, J. L. Holmes, R. Robson, *Chem. Commun.* **2011**, *47*, 7404-7406; (b) B. F. Abrahams, N. J. FitzGerald, R. Robson, *Angew. Chem. Int. Ed.* **2010**, *49*, 2896-2899.

[16] (a) J. Canceill, J. Gabard, A. Collet, *J. Chem. Soc., Chem. Commun.* **1983**, 122-123; (b) J. L. Scott, D. R. MacFarlane, C. L. Raston, C. M. Teoh, *Green Chem.* **2000**, *2*, 123-126; (c) J. Canceill, A. Collet, G. Gottarelli, *J. Am. Chem. Soc.* **1984**, *106*, 5997-6003; (d) T. Brotin, J.-P. Dutasta, *Chem. Rev.* **2008**, *109*, 88-130.

[17] M. J. Hardie, R. M. Mills, C. J. Sumby, *J. Org. Biol. Chem.* **2004**, *2*, 2958-2964.

[18] J. J. Henkelis, T. K. Ronson, L. P. Harding, M. J. Hardie, *Chem. Commun.* **2011**, *47*, 6560-6562.

[19] M. J. Hardie, C. J. Sumby, *Inorg. Chem.* **2004**, *43*, 6872-6874.

[20] N. Rigby, T. Jacobs, J. P. Reddy, M. J. Hardie, *Cryst. Growth Des.* **2012**, *12*, 1871-1881.

[21] G. Barbieri, R. Benassi, P. Lazzeretti, L. Schenetti, F. Taddei, *Org. Magn. Resonance* **1975**, *7*, 451-454.

[22] (a) X.-C. Su, B. Man, S. Beeren, H. Liang, S. Simonsen, C. Schmitz, T. Huber, B. A. Messerle, G. Otting, *J. Am. Chem. Soc.* **2008**, *130*, 10486-10487; (b) E. Huerta, H. Isla, E. M. Perez, C. Bo, N. Martin, J. de Mendoza, *J. Am. Chem. Soc.* **2010**, *132*, 5351-5353.

[23] T. Steiner, *Angew. Chem. Int. Ed.* **2002**, *41*, 48-76.

[24] M. J. Hardie, P. D. Godfrey, C. L. Raston, *Chem. Eur. J.* **1999**, *5*, 1828-1833.

[25] T. Sasaki, I. Hisaki, T. Miyano, N. Tohnai, K. Morimoto, H. Sato, S. Tsuzuki, M. Miyata, *Nat. Commun.* **2013**, *4*, 1787.

[26] M. Whitehead, S. Turega, A. Stephenson, C. A. Hunter, M. D. Ward, *Chem. Sci.* **2013**, *4*, 2744-2751.

[27] M. Alonso, T. Woller, F. J. Martín-Martínez, J. Contreras-García, P. Geerlings, F. De Proft, *Chem. Eur. J.* **2014**, *20*, 4931-4941.

[28] (a) J. W. Steed, H. Zhang, J. L. Atwood, *Supramol. Chem.* **1996**, *7*, 37-45; (b) C. A. Hunter, J. K. M. Sanders, *J. Am. Chem. Soc.* **1990**, *112*, 5525-5534.

[29] (a) C. J. Sumby, M. J. Hardie, *Acta. Crystallogr. Sect. E* **2007**, *E63*, O1537-O1539; (b) R. Ahmad, M. J. Hardie, *Supramol. Chem.* **2006**, *18*, 29-38; (c) T. K. Ronson, C. Carruthers, J. Fisher, T. Brotin, L. P. Harding, P. J. Rizkallah, M. J. Hardie, *Inorg. Chem.* **2010**, *49*, 675-685.

[30] J. J. Loughrey, C. A. Kilner, M. J. Hardie, M. A. Halcrow, *Supramol. Chem.* **2011**, *24*, 2-13.

[31] C. Carruthers, T. K. Ronson, C. J. Sumby, A. Westcott, L. P. Harding, T. J. Prior, P. Rizkallah, M. J. Hardie, *Chem. Eur. J.* **2008**, *14*, 10286-10296.

[32] J.-T. Yu, Y.-Y. Shi, J. Sun, J. Lin, Z.-T. Huang, Q.-Y. Zheng, *Sci. Rep.* **2013**, *3*, 2947.

[33] J. M. McBride, R. L. Carter, *Angew. Chem. Int. Ed.* **1991**, *30*, 293-295.

[34] H.-C. Zhou, J. R. Long, O. M. Yaghi, *Chem. Rev.* **2012**, *112*, 673-674.

[35] (a) G. M. Whitesides, B. Grzybowski, *Science* **2002**, *295*, 2418-2421; (b) C. Piguet, *Dalton Trans.* **2011**, *40*, 8059-8071; (c) C. Piguet, *Chem. Commun.* **2010**, *46*, 6209-6231; (d) J. Hamacek, M. Borkovec, C. Piguet, *Dalton Trans.* **2006**, 1473-1490.

[36] M. Fujita, O. Sasaki, K.-Y. Watanabe, K. Ogura, K. Yamaguchi, *New J. Chem.* **1998**, *22*, 189-191.

[37] (a) P. Gamez, P. d. Hoog, O. Roubeau, M. Lutz, W. L. Driessen, A. L. Spek, J. Reedijk, *Chem. Commun.* **2002**, 1488-1489; (b) F. Meng, L. Qin, M. Zhang, H. Zheng, *CrystEngComm* **2014**, *16*, 698-706.

[38] M.-X. Hu, Y.-G. Chen, C.-J. Zhang, Q.-J. Kong, *CrystEngComm* **2010**, *12*, 1454-1460.

[39] T. R. Cook, Y.-R. Zheng, P. J. Stang, *Chem. Rev.* **2012**, *113*, 734-777.

[40] J. J. Henkelis, T. K. Ronson, M. J. Hardie, *CrystEngComm* **2013**, *16*, 3688-3693.

[41] (a) J.-S. Li, B. Neumuller, K. Dehniche, *Z. Anorg. Allg. Chem.* **2002**, *628*, 2785; (b) F. Bravard, Y. Bretonnaire, R. Wietzke, C. Gateau, M. Mazzanti, P. Delangle, J. Pecaut, *Inorg. Chem.* **2003**, *42*, 7978; (c) J. S. Jin, S. C. Jin, X. Y. Wang, W. Q. Chen, *Chin. J. Struct. Chem.* **1988**, *181*, 561-564.

[42] J.-T. Yu, J. Sun, Z.-T. Huang, Q.-Y. Zheng, *CrystEngComm* **2012**, *14*, 112-115.

[43] T. Brotin, T. Devic, A. Lesage, L. Emsley, A. Collet, *Chem. Eur. J.* **2001**, *7*, 1561-1573.

[44] (a) G. Sheldrick, *Acta. Crystallogr. Sect. A* **2008**, *A64*, 112-122; (b) L. J. Barbour, *Supramol. Chem.* **2001**, *1*, 189-191.

[45] Persistence of Vision Raytracer Pty. Ltd. Williamstown, 2004.

[46] G. M. Sheldrick, T. R. Schneider, *Macromolecular Crystallography,. Pt. B* **1997**, *277*, 319-343.

Chapter 3

Coordination polymers featuring pyridyl-*N*-oxide functionalised host ligands

3.1 Introduction

Whilst J. C. Bailar [1] may lay claim to the first 'coordination polymer', it was Robson's 'infinite frameworks' that first highlighted their potential.[2] Since Yaghi's realisation of the 'MOF' (Metal Organic Framework),[3] research into the chemistry of coordination polymers remains largely application driven.[4] In fact, the sheer volume of such systems prepared over the last decade has resulted in an IUPAC-published guide regarding their correct nomenclature,[5] and brought about the necessity of 'grammar' and 'taxonomy' in order to classify their topology.[6] Coordination polymers are of such interest that they have been the topic of a number of recent review articles.[7]

A primary goal in coordination polymer chemistry is in the construction of porous materials. Owing to their large internal surface areas, many of these materials can reversibly bind gases of environmental concerns, such as CO_2 and CH_4,[8] as well as those associated with energy production, namely H_2.[9] Other prominent areas are in small molecule catalysis [10] and in the additional incorporation of electronic [11] and mechanical [12] components for sensing and switching, respectively. A detailed review of the construction of such materials, followed by an assessment of their properties and applications, is found in Chapter 1 of this thesis.

The majority of coordination polymers and MOFs are formed from carboxylate or pyridyl ligands,[13] yet their construction using derivatised pyridine-*N*-oxides remains somewhat underdeveloped. *N*-oxides are hard-oxygen donors that form strong metal-ligand bonds due to a relatively high charge density of the *N*-oxide donor moiety. Generally, complexes of pyridine-*N*-oxides result from the coordination of suitably hard metal centres, such as the early transition metals and lanthanide cations.[14] They are, however, capable of forming complexes with almost all transition metals, and have afforded a variety of coordination complexes.[15] For example, work by Schröder and Champness, utilising the simple ligand 4,4'-bipyridyl-*N,N'*-dioxide, has afforded a wide range of 1- and 2D coordination polymers, where altering the metal salt is enough to effect structural change.[16]

The ability to incorporate dynamic components into coordination networks potentially affords switchable materials.[17] Loeb and co-workers have constructed various MORFs (Metal Organic Rotaxane Frameworks) which contain electron deficient pillared 'struts' encased with electron rich crown ethers.[18] They have demonstrated the formation of a [2]-pseudorotaxane, from the ditopic ligand 1,2-*bis*-(4,4'-bipyridinium-*N,N'*-dioxide)ethane and dibenzo-24-crown-8 ether,

which then undergoes complexation with cadmium(II) cations to afford an interlocked 2D network, **Figure 3.1**.[19] Because the ligand and crown ether are chemically independent of one another, yet remain mechanically interlocked within the network, they offer a truly coherent switch, where all components operate in phase with one another.[20] This is distinct from solution-phase chemical switches, based on catenanes and rotaxanes, where motion and relative orientation is effectively random.[21]

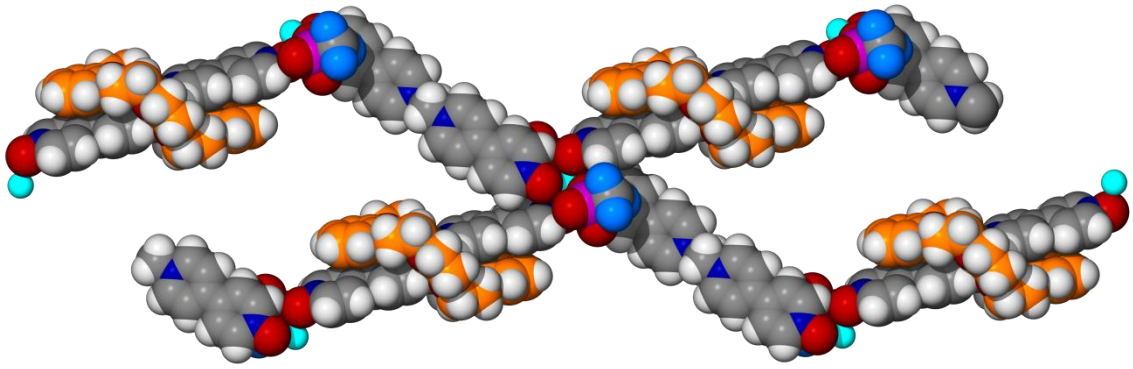

Figure 3.1 *Loeb's Metal Organic Rotaxane Framework (MORF), displaying part of the mechanically interlocked 2D network formed through cadmium(II) complexation.*[19]

Other notable accounts of coordination polymers constructed from functionalised pyridine-*N*-oxides are in the field of molecular electronics. Porphyrins are well-known for their electronic [22] and catalytic [23] properties, as well as their ability to interact with guest molecules.[24] Hosseini and co-workers have developed a 'metallo-tecton' approach to the construction of coordination polymers from *N*-oxide functionalised tetrapyridyl metallo-porphyrins.[25] In these systems, self-complexation forms both 1- and 2- coordination polymers, where the *N*-oxide moiety coordinates the chelated zinc(II) cation at the centre of a neighbouring metallo-porphyrin.[26] However, the presence of additional metal centres, such as Hg(II) or Pb(II), affords heterobimetallic conjugated 3D networks.[27] These systems display extensive conjugation and π-intercalation that result in interesting electronic properties.

The ability for many coordination networks to 'host' certain molecules is generally as a result of their supramolecular structure, not the individual components. Molecular hosts, such as cyclodextrins,[28] calix[*n*]arenes,[29] pillar[*n*]arenes,[30] and cyclotriveratrylenes (CTVs) [31] all possess an intrinsic ability to non-covalently and reversibly bind guests; however, coordination polymers bearing these motifs that are capable of sophisticated function are yet to be realised. Much of the reported host-guest chemistry of functionalised CTVs is solution-phase [32] or as a result of co-crystallisation,[33] yet the ability to selectively preorganise the tribenzo[*a*,*d*,*g*]cyclononatriene core into a highly robust network would be advantageous for post-synthetic application.

Coordination polymers featuring hard-oxygen-functionalised CTVs are generally restricted to catecholates and carboxylates, such as in Robson's tetrahedral assemblies [34] and Zheng's porous 1D copper(II) nanotube, **Figure 3.2**,[35] respectively. Likewise, Holman has prepared a 'soft' coordination polymer resulting from a carboxylate-functionalised cryptophane that is shown to bind various solvent molecules in the solid state.[36] Other transition metal examples of carboxylate-functionalised CTVs are discrete complexes.[37]

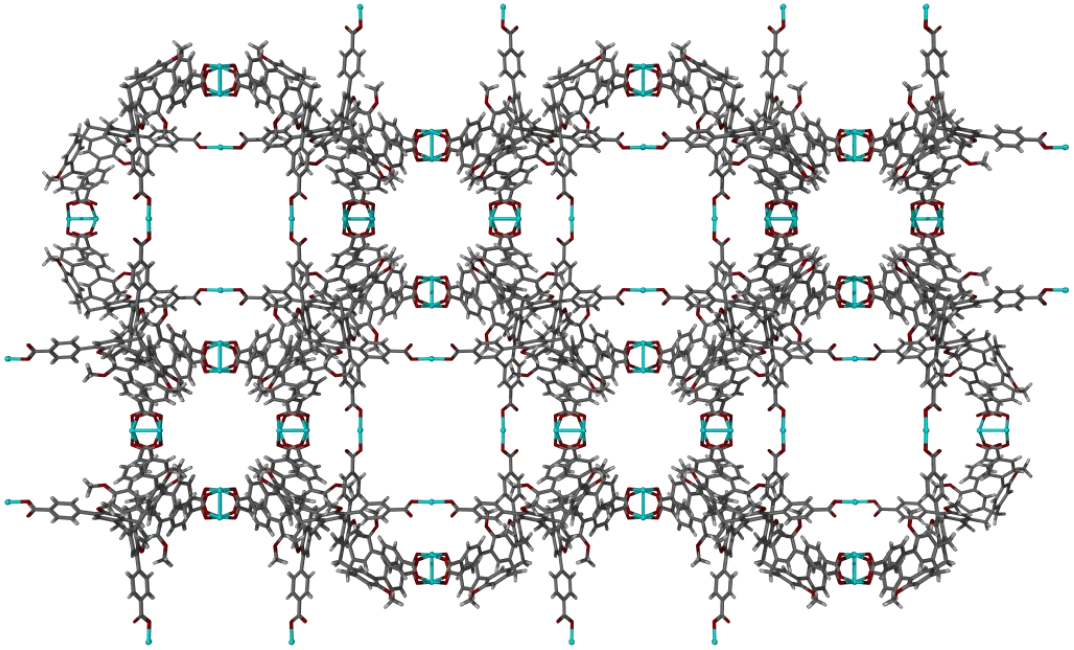

Figure 3.2 *Displaying the large void spaces present in the extended crystal structure of Zheng's copper(II)-containing nanotube, as viewed down the crystallographic c axis.*[35]

As reported in Chapter 2, ligands (±)-2,7,12-trimethoxy-3,8,13-*tris*(2-pyridylmethyloxy-*N*-oxide)-10,15-dihydro-5*H*-tribenzo[*a*,*d*,*g*]cyclononatriene (**2.10**), (±)-2,7,12-trimethoxy-3,8,13-*tris*(3-carboxypyridine-*N*-oxide)-10,15-dihydro-5*H*-tribenzo[*a*,*d*,*g*]cyclononatriene (**2.12**) and (±)-2,7,12-trimethoxy-3,8,13-*tris*(4-carboxypyridine-*N*-oxide)-10,15-dihydro-5*H*-tribenzo[*a*,*d*,*g*]cyclononatriene (**2.13**), **Figure 3.3**, afforded coordination polymers with the lanthanide(III) cations; however, their coordination chemistry was limited and the structures gained were not identified as potential candidates for further application. An aim of this research was to utilise ligands **2.10**, **2.12** and **2.13** for transition metal complexation to prepare robust coordination networks that may display the aforementioned properties and post-synthetic applications; such as in gas storage, catalysis and sophisticated host-guest chemistry. For these properties to become emergent, the networks were designed to feature the inwardly orientated tribenzo[*a*,*d*,*g*]cyclononatriene core within either cavities or channels to provide a binding platform for guests and afford a hydrophobic surface for gas sorption.

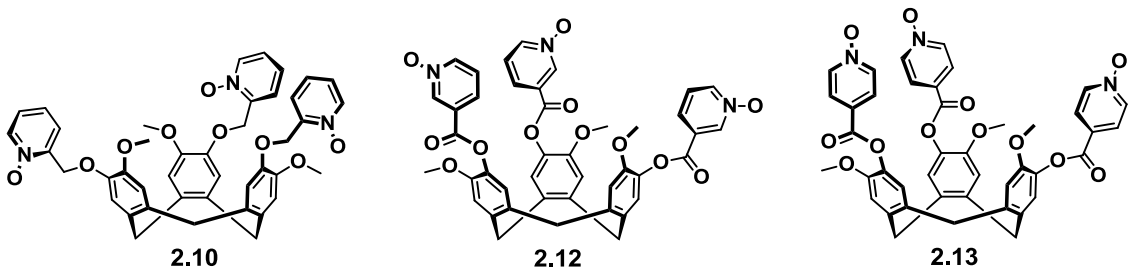

Figure 3.3 *Molecular structures of pyridine-N-oxides used in the following study.*

3.2 Coordination polymers of 3,6-connectivity

Ligand **2.13** affords coordination polymers of 3,6-connectivity upon self-assembly with selected transition metal cations. In these examples the network connectivity is determined by infinitely linked 3- and 6-connecting nodes (ligand and metal centres, respectively) within the framework. The self-assembly of ligand **2.13** with silver(I) cations results in the formation of a 3D network of pyrite (***pyr***) topology that features a linear, ligand-unsupported argentophilic interaction. Its self-assembly when M = copper(II), cobalt(II) or zinc(II) metal centres results in the formation of 2D coordination networks of general composition $\{[M(\mathbf{2.13})_2]\cdot(BF_4)_2\}_\infty$ and with the relatively rare kagome dual (***kgd***) topology.[6c-e]

3.2.1 $\{[Ag_3(NMP)_6(\mathbf{2.13})_2]\cdot 3(ClO_4)\cdot n(NMP)\}_\infty$ 3D network of pyrite (*pyr*) topology

The reaction of ligand **2.13** and silver(I) perchlorate (ClO_4^-) in *N*-methylpyrrolidone (NMP) afforded a 3D network of pyrite (***pyr***) topology, $\{[Ag_3(NMP)_6(\mathbf{2.13})_2]\cdot 3(ClO_4)\cdot n(NMP)\}_\infty$, complex **3.1**. Crystals were obtained by diffusing diethyl ether vapours into a solution of the complex in NMP and analysed by single crystal X-ray diffraction methods. The structure solved in the cubic space group $Pa\bar{3}$ to display the asymmetric unit as two crystallographically distinct silver(I) centres, along with one third of an **2.13** ligand, an NMP ligand and a disordered perchlorate counter anion, **Figure 3.4**. Selected bond lengths and angles for complex **3.1** are displayed in **Table 3.1**.

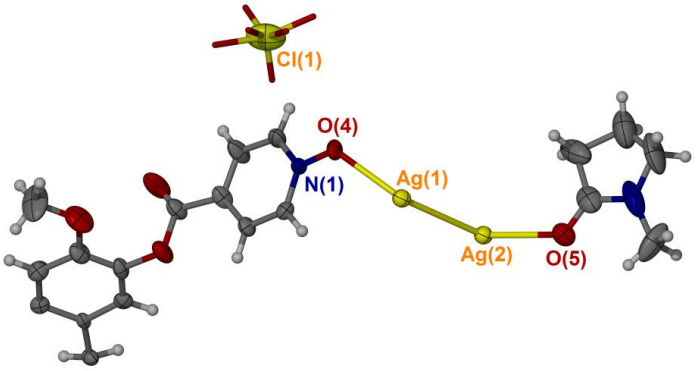

Figure 3.4 *The asymmetric unit of complex* ***3.1****. Aside from the disordered perchlorate anion, all anisotropic displacement parameters are set at 35 %.*

The central silver(I) cation, Ag(1), is located on a 3-fold inversion site and is coordinated by six, symmetry-equivalent **2.13** ligands in a *pseudo*-octahedral manner, **Figure 3.5**, with *cis* O-Ag(1)-O bond angles at 88.46(16) and 91.54(16) Å. There are further interactions to two symmetry-related Ag(2) centres that are sited on a 3-fold rotation axis, which gives rise to a ligand unsupported argentophilic trimer, displaying Ag···Ag separation of 3.2753(9) Å. Typical argentophillic interactions are in the range of 2.9-3.3 Å;[38] however, this instance is particularly rare as it is ligand unsupported and exactly linear. There are examples in the literature which are structurally similar,[39] however they are usually in a cyclical motif,[40] or ligand supported.[41] The largest coinage metal pyrazolide cluster yet reported contains a Ag_{10} cluster, supported by bridging pyridine-pyrazolide ligands;[42] although more complex silver-containing assemblies have been shown to exist in the gas-phase.[43]

Ag(1)-O(4)	2.436(5)	O(4)-Ag(1)-O(4^{ii-iii})	88.46(16)
Ag(1)-O(4^{i-v})	2.436(5)	O(4)-Ag(1)-O(4^{iv})	91.54(16)
Ag(2)-O(5)	2.414(6)	O(4^{ii})-Ag(1)-O(4^{v})	180
Ag(2)-O(5^{i-v})	2.414(6)	O(4)-Ag(1)-Ag(2)	126.35(11)
Ag(1)-Ag(2)	3.2753(9)	O(4)-Ag(1)-Ag(2^{i})	53.65(11)
Ag(1)-Ag(2^{i})	3.2753(9)	O(5)-Ag(2)-Ag(1)	119.23(11)
O(4)-Ag(1)-O(4^{i})	180.0(3)	O(5)-Ag(2)-O($5^{ii/iii}$)	98.18(16)

Symmetry operations: **i** 1-*x*, 1-*y*, -*z*; **ii** 1-*y*, *z* + ½, -*x* + ½; **iii** –*z* + ½, 1-*x*, *y* – ½; **iv** *z* + ½, *x*, -*y* + ½; **v** *y*, -*z* + ½, *x* – ½.

Table 3.1 *Selected bond lengths (Å) and angles (°) from the crystal structure of complex* ***3.1***

The terminal and approximately tetrahedral silver(I) centres, Ag(2), do not play a role in network topology and are coordinated by three symmetry-related NMP ligands, **Figure 3.5**. The central silver(I) centre, Ag(1), is coordinated by six **2.13** ligands, all of which are 3-connected within the extended lattice, resulting in a 3,6-connectivity.

The extended lattice of complex **3.1** is a 3D network of high symmetry. The 3,6-connectivity and lattice symmetry affords a pyrite (***pyr***) topology [6c-e] with Schlälfi symbol $(6^3)_2(6^{12}\cdot8^3)$, as determined with the program TOPOS,[44] and features 6- and 8-gons within the extended lattice. Crystallographically elucidated in 1913 by W. H. Bragg,[45] iron disulfide (pyrite, FeS_2)[46] is a mineral which now lends its name to a topology of many high-symmetry crystal systems with application in catalysis,[47] and recently demonstrated by Yaghi and O'Keefe, in the development of metal-organic frameworks (MOFs) for gas storage.[48] The ***pyr*** topology is relatively rare for 3,6-connected 3D networks [49] and the vast majority have rutile (***rtl***) topology.[50]

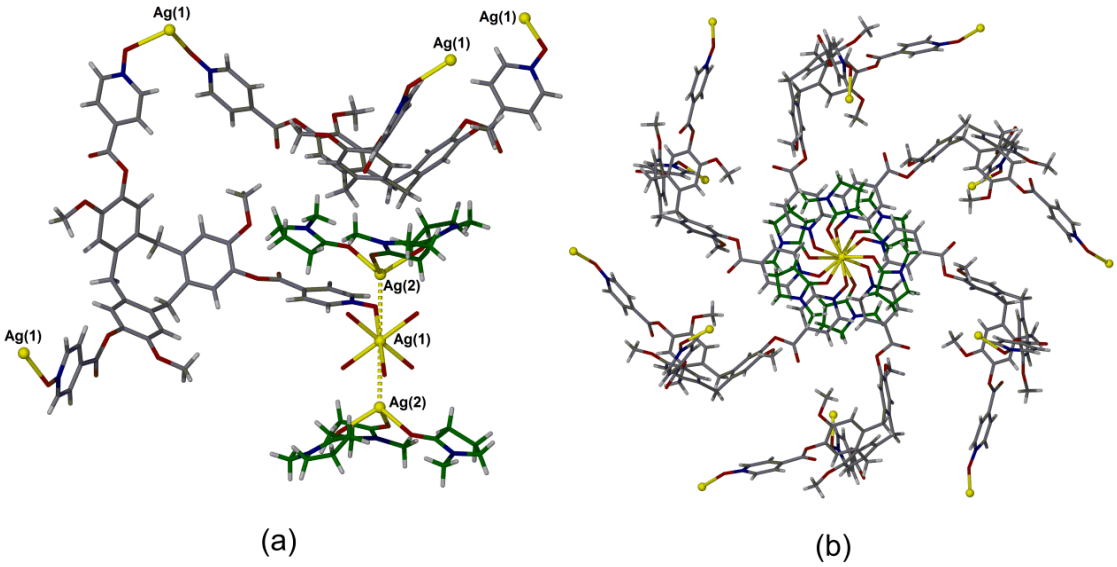

Figure 3.5 *From the crystal structure of complex* ***3.1****. (a) the ligand unsupported argentophilic trimer, coordinated by one* ***2.13*** *ligand and NMP-****2.13*** *lattice support; (b) displaying ligand growth from the central silver(I) centre, as viewed down the* Ag_3 *trimer, depicting the overall high-symmetry connectivity. NMP ligands are coloured green and perchlorate anions have been omitted for clarity.*

Although not included in the network connectivity or topology, the $[Ag(NMP)_3]$ units act as symmetry-matching supports within the lattice and interact with the underside of neighbouring **2.13** ligands in an inverted host-guest manner, whereby the underside of the [*a*,*d*,*g*]cyclononatriene unit is guest, as opposed to host, within the lattice. Aromatic separations are in the excess of 4.3 Å, and so there are no formal interactions present between such units, **Figure 3.5a**.

The extended lattice of complex **3.1** does not possess any channels and so may be considered as non-porous; however, there are relatively large voids present between the inwardly orientated ligands, **Figure 3.6a**. The distance between individual **2.13** ligands, measured from the centre of opposing ligands, measures approximately 30 Å. The cavity contains NMP solvent and

disordered perchlorate anions which could not be crystallographically modelled. Thermogravimetric analysis (TGA) indicated a net mass loss of 40% up to 210 ºC, which is consistent with eight molecules of NMP solvent *per* formula unit. This is complemented by combustion analysis which indicates higher levels of solvation than expected and is consistent with the calculated void space in the crystal lattice. Furthermore, IR spectroscopy confirms the inclusion of perchlorate anions in the crystalline material, and hence complex formation, with Cl-O bond stretches at 1090, 945 and 623 cm^{-1}. Once formed, complex **3.1** was observed to be completely insoluble and so solution-phase analysis was not undertaken.

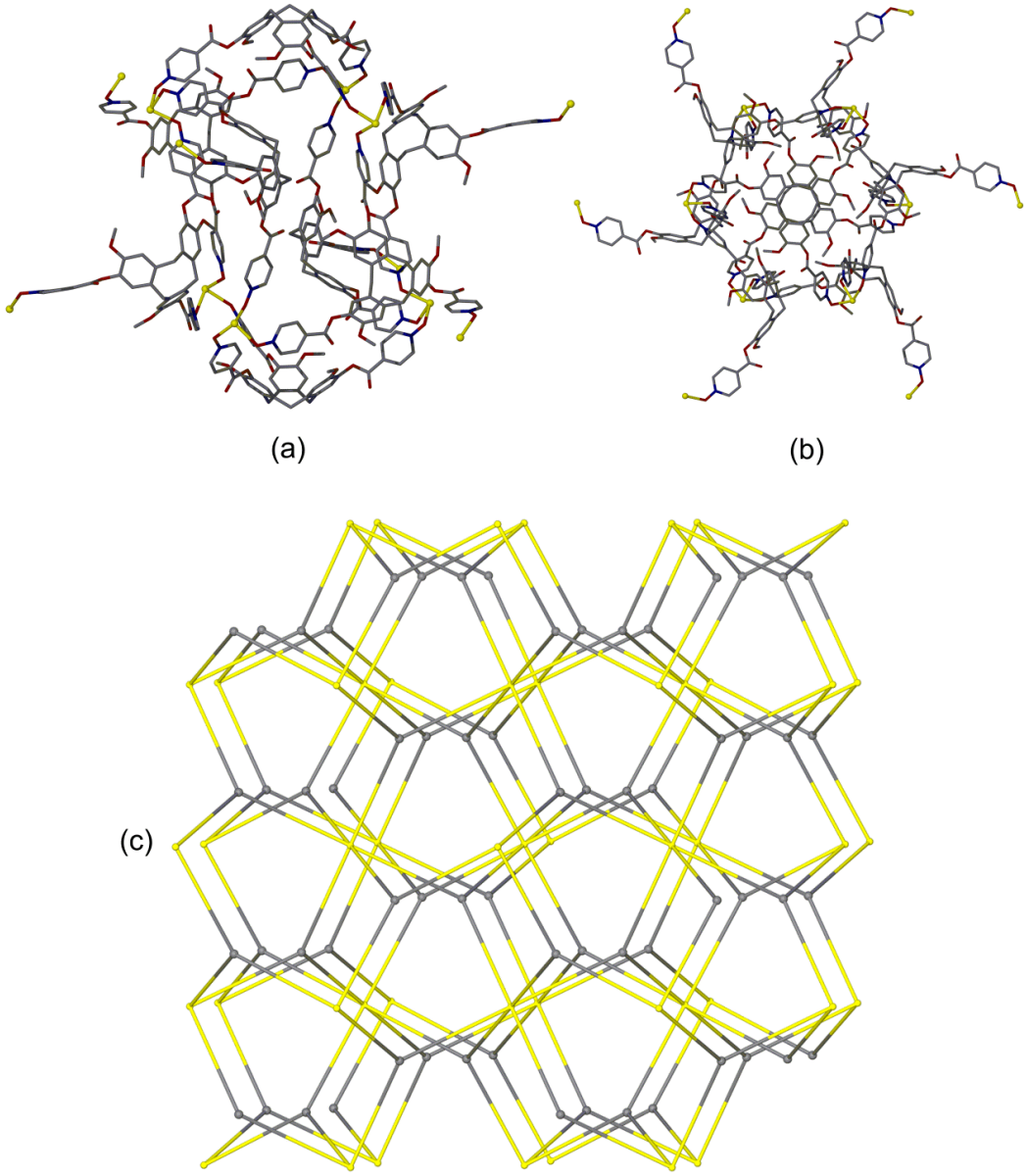

Figure 3.6 *From the crystal structure of complex* ***3.1****. The capsular motif present within the extended crystal lattice, as viewed from the side (a) and the top (b). Disordered NMP solvent and perchlorate anions are omitted for clarity. (c) The extended lattice of pyrite (****pyr****) topology. Silver centres and ligand centroids are represented as yellow and grey spheres, respectively.*

3.2.2 {[M(2.13)$_2$]·(BF$_4$)$_2$·*n*(solvent)}$_\infty$ 2D networks with kagome dual (*kgd*) topology

Independent reactions of ligand **2.13** with cobalt(II) and zinc(II) tetrafluoroborate (BF_4^-) salts afforded isostructural 2D coordination polymers of the relatively rare kagome dual (***kgd***) topology,[6c] complexes {[Co(**2.13**)$_2$]·(BF$_4$)$_2$·*n*(DMF)}$_\infty$ **3.2** and {[Zn(**2.13**)$_2$]·(BF$_4$)$_2$·*n*(NMP)}$_\infty$ **3.3**, respectively. Crystals of complexes **3.2** and **3.3** were fragile, small and very weakly diffracting, with complex **3.3** requiring synchrotron radiation for its structural elucidation. In addition, both complexes featured large voids within the lattice that were filled with disordered anions and solvents of crystallisation, with only the [M(**2.13**)$_2$]$^{2+}$ units being located crystallographically.

Small, orange crystals of complex **3.2** were grown from the diffusion of diethyl ether vapours into a NMP solution of the complex over a two week period. The structure was solved in the monoclinic space group *C*2/*c* to display the asymmetric unit as one molecule of ligand **2.13**, coordinating a Co(II) cation which is sited on an inversion centre, **Figure 3.7**.

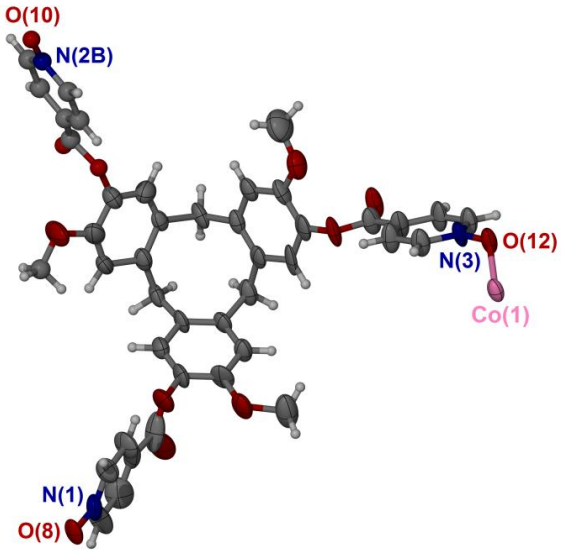

Figure 3.7 *The asymmetric unit of complex **3.2**, as viewed down the crystallographic a-b plane. Generally, all anisotropic displacement parameters are shown at the 35 % probability. Only one disordered orientation is shown when ligand arm N=2B and the corresponding atoms have been refined isotropically (atoms are shown as hard spheres).*

The ligand is desymmetrised, where one of the three 4-pyridyl-*N*-oxide ligand arms is orientated orthogonally to the others and is disordered over two positions. No tetrafluoroborate anions and NMP solvent molecules could be crystallographically located owing to large void spaces in the crystal lattice. The cobalt(II) centres have almost true octahedral geometry and are coordinated by six, symmetry equivalent **2.13** ligands that display Co-O bond lengths in the range 2.051(4)-2.113(5) Å. Other notable bond metrics for complex **3.2** are given below in **Table 3.2**.

Co(1)-O(12)	2.065(4)	O(12)-Co(1)-O(8^{v})	90.17(17)
Co(1)-O(12^{i})	2.065(4)	O(12^{i})-Co(1)-O(10^{i})	89.5(3)
Co(1)-O($10^{ii\text{-}iii}$)	2.113(5)	O(12i)-Co(1)-O(8^{v})	89.83(17)
Co(1)-O($8^{iv\text{-}v}$)	2.051(4)	O(10^{ii})-Co(1)-O(10^{iii})	180.00(17)
O(12)-Co(1)-O(12^{i})	180.0(2)	O(8^{iv})-Co(1)-O(8^{v})	180.0(2)
O(12)-Co(1)-O(10^{ii})	90.5(3)		

Symmetry operations: **i** $-x + ½, 1-y + ½, 1-z$; **ii** $x - ½, y + ½, z$; **iii** $1-x, 1-y, 1-z$; **iv** $1-x + ½, 1-y + ½, 1-z$; **v** $1-x, y, z$.

Table 3.2 *Selected bond lengths (Å) and angles (°) from the crystal structure of complex* ***3.2***

Symmetry expansion of the $[Co(\mathbf{2.13})_2]^{2+}$ unit results in a 3,6-connected 2D network, where ligand and metal represent 3- and 6-connecting nodes, respectively. The resultant two-tiered network features inwardly orientated **2.13** ligands in a head-to-head manner, **Figure 3.8a**. These 'upper' and 'lower' tiers of the 2D sheets incorporate the opposing enantiomer of **2.13** ligands, rendering the overall network a racemate. The rigidity of the ligands and their orientation with respect to one another may be attributed to there being no intrachain interactions within individual 2D sheets.

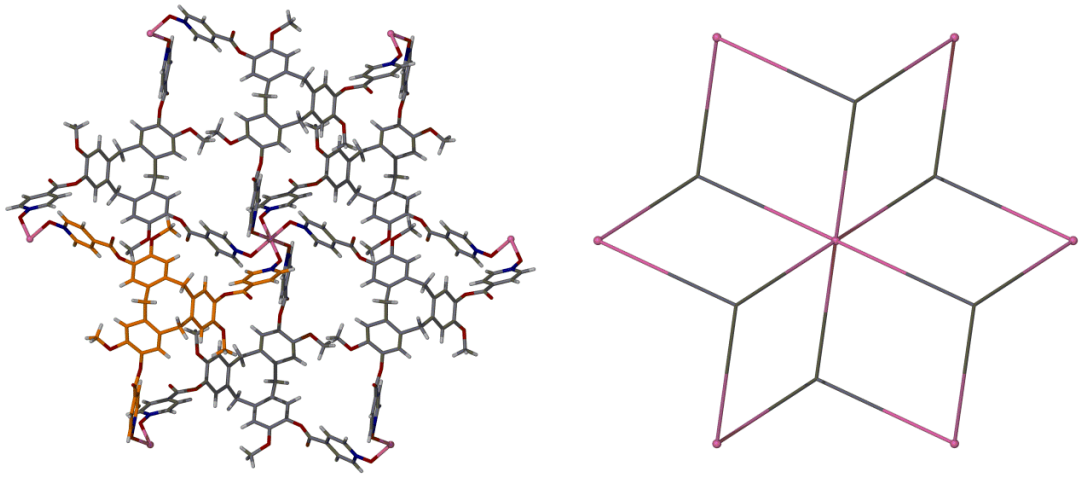

Figure 3.8 *From the crystal structure of complex* ***3.2****, as viewed down the crystallographic c axis. (a) Part of the resultant 2D sheet, showing the connectivity of metal and ligand, where one ligand is colour-coded orange for clarity; (b) wire frame of the 2D net showing network topology, where metal and ligand have been simplified to be pink and grey nodes, respectively.*

As for complex **3.1**, above, the network topology of complex **3.2** was determined using the program TOPOS,[44] by reducing the net into simplified nodes and examining the resultant connectivity against a pre-existing catalogue of polymeric structures.[6c] The kagome dual lattice (***kgd***) features a regular star-shaped tessellation of diamonds which result in the Schläfli symbol

$(4^3)\cdot(4^6\cdot6^6\cdot8^3)$, as described in the preamble, above.[6b, 51] The 3,6-connected ***kgd*** net of complex **3.2** is displayed graphically in **Figure 3.8b**.

A 3,6-connectivity within nets is common; in fact, many of Yaghi's iso-reticular metal-organic frameworks (IRMOF's) for hydrogen storage are a result of infinitely linked octahedral metallic nodes with bridging tricarboxylate linkers.[52] The kagome dual (***kgd***) net is much less common, however, and Biradha and co-workers have isolated examples which undergo dynamic exchange of guests in a single-crystal-to-single crystal (SCTSC) manner, **Figure 3.9a**,[53] as well as 'breathing' crystals which display intriguing sorption properties.[54] Similarly, the groups of Batten and Lu have constructed ***kgd*** networks which display luminescence [55] and gas storage abilities,[56] respectively. Whilst the archetypal ***kgd*** net is of cadmium(II) iodide, examples more closely related to our two-tiered lattice are Zheng's cadmium-containing 2D sheets which feature similarly orientated tripodal ligands, **Figure 3.9b**.[57]

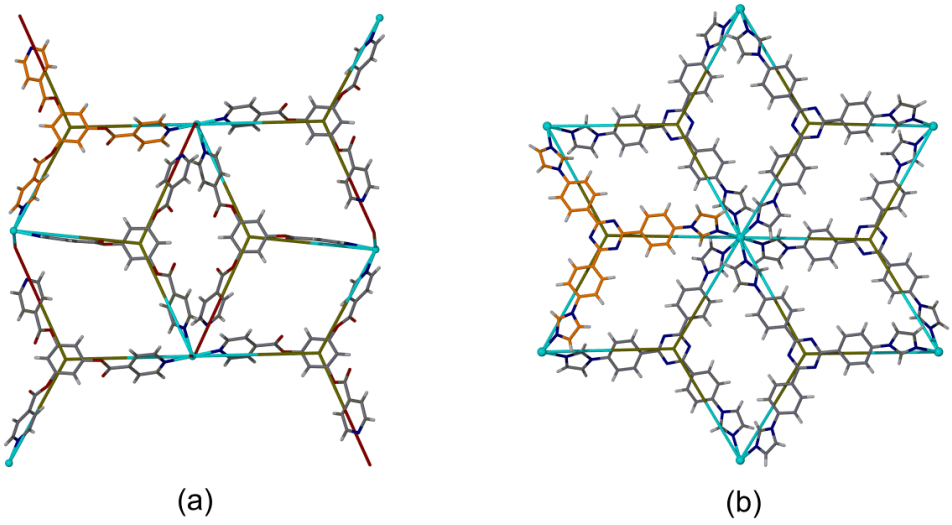

Figure 3.9 *From the crystal structures of Biradha's (a) and Zheng's (b) 3,6-connected* ***kgd*** *2D nets resulting from the metal-mediated polymerisation of tripodal ligands. The tessellation of diamonds for each example is shown by solid lines and indicates the network topology. One ligand in each example is colour coded for clarity.*[53, 57]

The inward-facing orientation of **2.13** ligands results in large bi-directional channels running through individual 2D sheets, **Figure 3.10**. These 'tubular' channels extend along the *a* and *b* unit cell axes and correspond to two thirds of the total cell volume. Whilst this may appear attractive for potential application in gas storage *etc.*, the crystals were seen to degrade rapidly upon desolvation, as indicated by powder X-ray diffraction measurements, and are therefore non-porous. In order to be considered porous, the network must retain its structure and crystallinity upon the removal of solvent. Unsurprisingly, most porous materials are isotropic 3D networks which display an increased stability and robustness; however, there are a handful

of 2D networks which display considerable porosity,[10a] but the majority of these examples are covalently linked.[58]

Individual 2D sheets are related to one another by a screw axis, and pack through back-to-back stacking of **2.13** ligands; however, centroid separations of 4.88 Å rule out aromatic interactions. This packing leads to additional void spaces in the extended crystal lattice that are again filled with disordered solvent and anions, **Figure 3.10**.

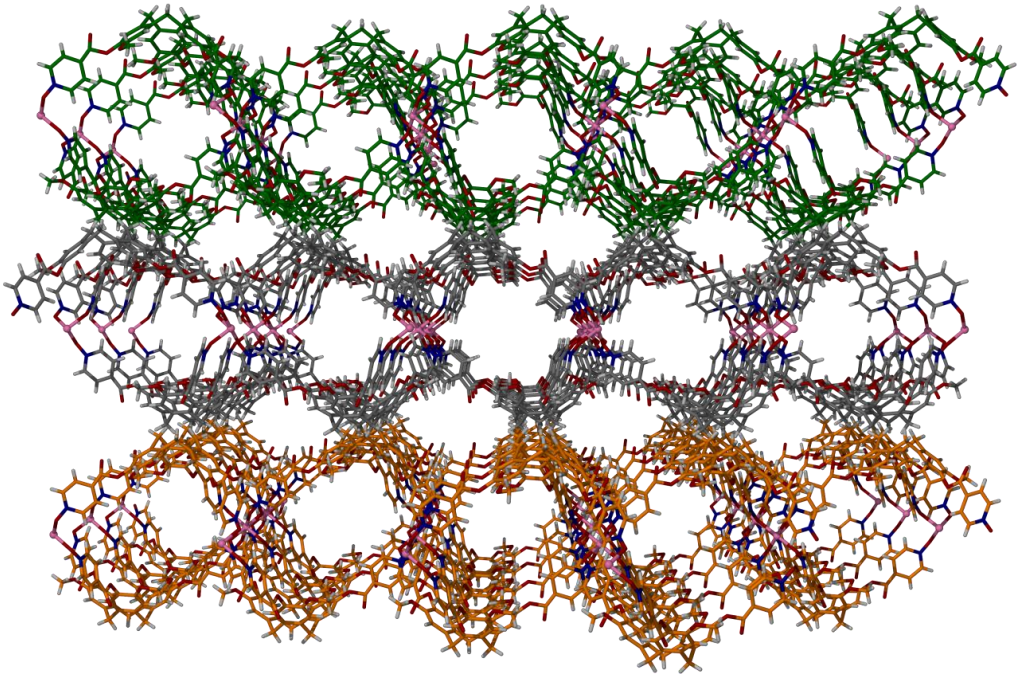

Figure 3.10 *From the crystal structure of complex* ***3.2****, as viewed down the crystallographic a axis, showing the two large void spaces within the crystal lattice. Individual 2D polymers are colour coded and the image has been rendered using a perspective tool for clarity.*

Colourless crystals of complex **3.3** were grown from an *N*-methylpyrrolidone (NMP) solution *via* the slow diffusion of diethyl ether co-solvent and analysed using synchrotron radiation. The structure was solved in the triclinic space group $P\bar{1}$ to display the asymmetric unit of composition $\{[Zn(\mathbf{2.13})_2]\cdot(BF_4)_2\}_\infty$, where the Zn(II) cation is sited on a crystallographic centre of inversion, **Figure 3.11**. Individual 2D nets are essentially analogous to those described for complex **3.2**, above, and feature the same star-shaped tessellation of diamonds that results in the Schlälfi symbol $(4^3)\cdot(4^6\cdot6^6\cdot8^3)$, as determined using the program TOPOS.[44] A key difference of complex **3.3**, however, is that individual 2D sheets are related by simple translation, owing to the lack of crystallographic symmetry.

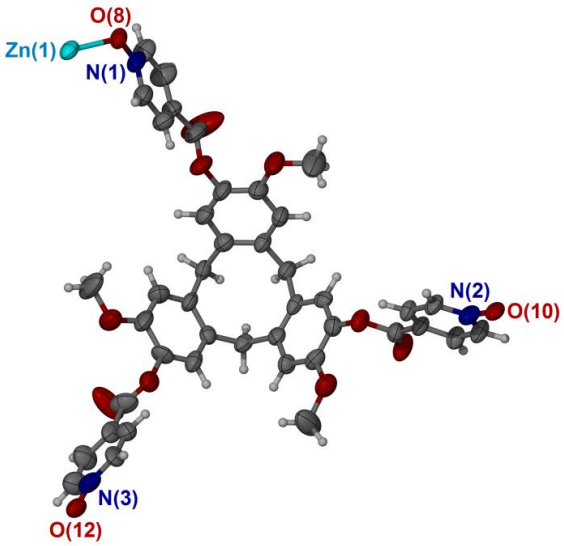

Figure 3.11 *The asymmetric unit of complex **3.3**, as viewed down the crystallographic a-b plane. All anisotropic displacement parameters are shown at the 35 % probability.*

The compositions of complexes **3.2** and **3.3** were confirmed using combustion analyses and IR spectroscopy; the latter being indicative of tetrafluoroborate inclusion, and thus complex formation, displaying a characteristic and broad B-F bond stretch at 1050 cm^{-1}. Additionally, thermogravimetric analyses (TGA) of complex **3.3** displayed a net weight loss of 35% up to 210 ^{o}C, which corresponds to ten molecules of NMP *per* formula unit. This is consistent with the cavity size present within the 2D net and further supported by elemental analysis. X-ray powder diffraction measurements of isolated and dried crystals displayed only broad, amorphous peaks, indicating a structural collapse and loss of crystallinity, which is likely due to the fragile crystals degrading through rapid loss of diethyl ether solvent from the network. As for complex **3.1**, above, complexes **3.2** and **3.3** were completely insoluble once formed and not analysed in the solution-phase.

3.2.3 {[Cu(2.13)$_2$]·(BF4)$_2$·*n*(NMP)}$_\infty$ 2D *kgd* network with solvated Cu(II) lattice guest

The reaction of ligand **2.13** and $Cu(BF_4)_2$ in NMP solvent afforded complex **3.4**, $\{[Cu(\mathbf{2.13})_2][Cu(NMP)_4(H_2O)]\cdot 4(BF_4)\cdot 8(NMP)\cdot 2(H_2O)\}_\infty$, that again features a 2D net of the kagome dual (***kgd***) topology.[6c] The 2D net is isostructural to those found in complexes **3.2** and **3.3** described above; however, in this instance the framework plays host to additional $[Cu(NMP)_4(H_2O)]^{2+}$ lattice guest in a similar manner to complex **2.22** of Chapter 2.

Crystals of complex **3.4** were grown by diffusing diethyl ether vapours into an NMP solution of the complex and isolated as small, green plates. The structure solved in the triclinic space group $P\bar{1}$ to display the asymmetric unit as the composition stated above, **Figure 3.12**.

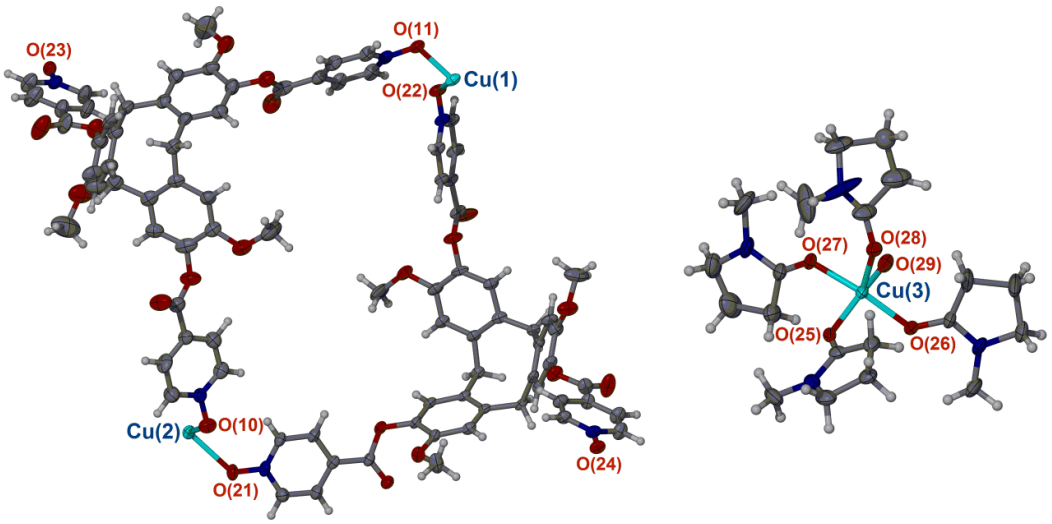

Figure 3.12 *The two copper(II)-containing units in the asymmetric unit of complex* ***3.4****. All anisotropic displacement parameters are at 35 % probability and solvent NMP and tetrafluoroborate anions have been omitted for clarity.*

Cu(1)-O(11)	1.978(5)	$O(22^{i})$-Cu(1)-O(22)	180.0(2)
Cu(1)-$O(24^{ii,iii})$	2.003(5)	O(10)-Cu(2)-$O(10^{v})$	179.998(1)
Cu(1)-O(22)	2.435(5)	O(10)-Cu(2)-$O(23^{v})$	93.1(3)
Cu(2)-O(10)	1.976(6)	$O(23^{v})$-Cu(2)-$O(23^{vi})$	179.998(2)
Cu(2)-O(21)	2.415(6)	O(10)-Cu(2)-O(21)	89.2(2)
Cu(2)-$O(23^{v,vii})$	1.984(6)	$O(23^{v})$-Cu(2)-O(21)	83.1(2)
Cu(3)-O(25)	1.991(7)	O(21)-Cu(2)-$O(21^{v})$	179.999(2)
Cu(3)-O(26)	1.955(5)	O(26)-Cu(3)-O(27)	169.2(3)
Cu(3)-O(27)	1.962(6)	O(26)-Cu(3)-O(29)	88.8(3)
Cu(3)-O(28)	2.193(6)	O(27)-Cu(3)-O(29)	87.1(3)
Cu(3)-O(29)	1.967(9)	O(26)-Cu(3)-O(25)	90.3(2)
O(11)-Cu(1)-$O(11^{i})$	179.997(2)	O(27)-Cu(3)-O(25)	89.6(3)
O(11)-Cu(1)-$O(24^{iv})$	92.3(2)	O(29)-Cu(3)-O(25)	157.3(3)
$O(24^{iv})$-Cu(1)-$O(24^{iii})$	179.998(2)	O(26)-Cu(3)-O(28)	102.2(2)
$O(24^{iv})$-Cu(1)-$O(22^{i})$	90.5(2)	O(27)-Cu(3)-O(28)	88.5(2)
O(11)-Cu(1)-O(22)	94.9(2)	O(29)-Cu(3)-O(28)	103.9(3)
$O(24^{iv})$-Cu(1)-O(22)	89.5(2)	O(25)-Cu(3)-O(28)	98.5(3)

Symmetry operations: **i** 1-*x*, -*y*, 1-*z*; **ii** 2-*x*, -*y*, 1-*z*; **iii** 1-*x*, *y*, *z*; **iv** 2-*x*, 1-*y*, -*z*; **v** 2*x*, *y*, *z*; **vi** 1-*x*, 1-*y*, -*z*.

Table 3.3 *Selected bond lengths (Å) and angles (°) from the crystal structure of complex* ***3.4***

The crystals were of considerably better quality than for complexes **3.2** and **3.3** and three of the four tetrafluoroborate anions and eight NMP solvents molecules could be crystallographically

located. The two octahedral copper(II) centres of the 2D net are each located on an inversion centre and have been refined at half occupancy. They display equatorial and axial Cu-O bond lengths of 1.978(5) and 2.435(5) Å, respectively, which is indicative of Jahn-Teller distortion along the coordination *z* axis.[59] Selected bond metrics are given below in **Table 3.3**. The two crystallographically independent **2.13** ligands in the asymmetric unit are differentiated by subtle symmetrical differences and display varied host-guest interactions within the 2D polymer.

The mononuclear complex, $[Cu(NMP)_4(H_2O)]^{2+}$, is five-coordinate and displays O-Cu-O bond angles of 169.2(3) and 157.3(3) º, which affords a τ value of 0.2. This value is indicative of a Cu(II) centre with square pyramidal geometry as opposed to trigonal bipyramidal.[60]

Host-guest interactions are present within individual 2D polymers, whereby the inwardly orientated and electron-rich [*a*,*d*,*g*]-cyclononatriene cores play host to NMP solvent molecules, as well as NMP solvent molecules of $[Cu(NMP)_4(H_2O)]^{2+}$ complexes. In both instances it is the non-polar methylene protons of the NMP molecules that are non-covalently bound in the ligand cavity, **Figure 3.13**. Such host-guest interactions are typical for functionalised CTV-based materials, especially in organically linked cryptophanes which are observed to bind various gases [61] and liquids,[36, 62] in both the solution and solid state. Other notable examples are de Mendoza's fullerene scavengers [63] and Holman's first reported example of the encapsulation of a trifluoromethane sulfonate anions into the π-acidic interior of a cryptophane.[64]

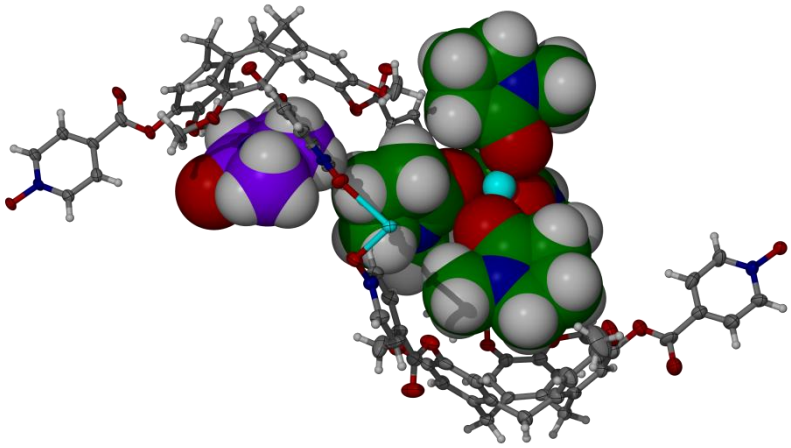

Figure 3.13 *From the crystal structure of complex **3.4**, displaying the two sites of host-guest interaction present within the asymmetric unit. Intracavity guest $[Cu(NMP)_4(H_2O)]^{2+}$ and solvent NMP are coloured green and purple, respectively, and displayed in space-filling view for clarity.*

Symmetry expansion of this $[Cu(\mathbf{2.13})_2]^{2+}$ unit generates the ***kgd*** net, as described for complexes **3.2** and **3.3** above, **Figure 3.14**. Complex **3.4** was considerably more stable than complexes **3.2** and **3.3** yet was non-porous owing to the presence of the mononuclear $[Cu(NMP)_4(H_2O)]^{2+}$

lattice guest. Interestingly, crystals of complex **3.4** could not be obtained in the absence of the $[Cu(NMP)_4(H_2O)]^{2+}$ complex, unlike complexes **3.2** and **3.3**, which may suggest a possible templating effect in its formation. The presence of an active template in supramolecular self-assembly is well documented. Nitschke and co-workers, for example, have described intricate examples based on sub-component self-assembly where the addition of a specific cation,[65] anion [66] or organic guest [67] can cause structural reconfiguration or allosterically modulate the systems properties.[68]

The extended lattice packs through back-to-back stacking of **2.13** ligands between the 2D sheets, as seen for complexes **3.2** and **3.3**, and again in the absence of π-interactions, with aromatic centroid separations of 4.45 Å. The extended structure of complex **3.4** can be seen graphically in **Figure 3.14**, below.

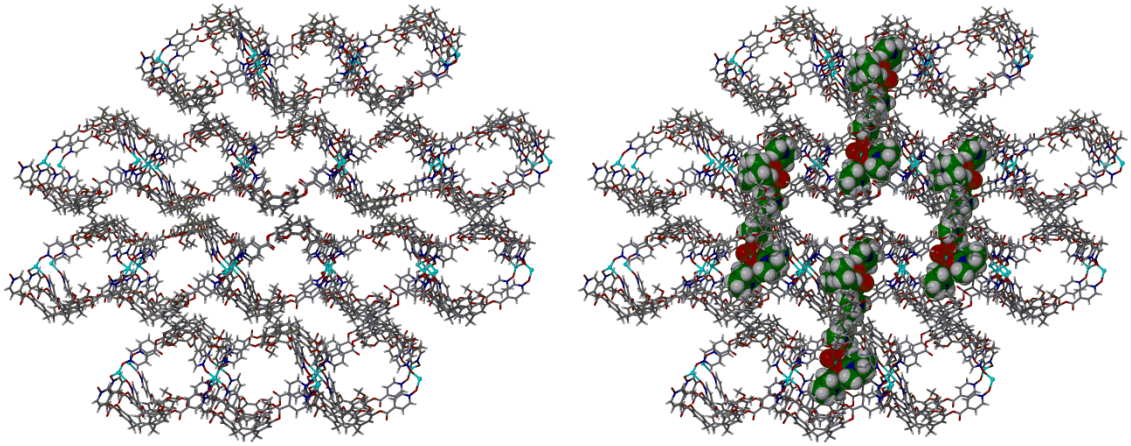

Figure 3.14 *From the crystal structure of complex **3.4**, as viewed down the crystallographic a axis. (a) The **kgd** 2D frameworks only, (b) the **kgd** 2D frameworks with added $[Cu(NMP)_4(H_2O)]^{2+}$ lattice guest, shown in green and space-filling for clarity.*

It was hoped that the increased stability of complex **3.4** over complexes **3.2** and **3.3** and the presence of a solvated copper(II) lattice guest may lead to potential application in catalysis; however, the crystals were not seen to withstand desolvation. Two independent review articles by Pinel [69] and Hupp [7e] outline the potential that MOFs and coordination polymers with pendant metal sites have in catalysis. Powder X-ray analysis was concordant with lattice degradation and showed only a loss of crystallinity upon loss of solvent. TGA analysis showed a step-wise weight loss that is consistent with the level of solvation found in the crystal structure. Irrespective of composition, complex **3.4** displayed the same 35% weight loss over 210 ºC as complex **3.2**, suggesting complete loss of the NMP ligands of the mononuclear $[Cu(NMP)_4(H_2O)]^{2+}$ complex, as well as additional solvent NMP. Infrared analysis was supportive of complex formation and displayed the characteristic B-F bond stretch of the

tetrafluoroborate anion at 1052 cm^{-1}. Furthermore, network purity and composition was confirmed by elemental analysis.

3.3 3-connected 2D coordination networks

A common feature of complexes **3.1**-**3.4** was weakly coordinating anions. The employment of coordinating anions, such as nitrate and chloride, as seen for complexes **3.5**-**3.7**, below, was observed to reduce the coordination at the metal centre and thus decrease the network connectivity.

Self-assembly of ligand **2.10** with the late transition metal salts affords 2D coordination polymers with a honeycomb (***hcb***) topology.[6] Here, network connectivity is determined by infinitely linked hexagons that results in a 6^3 connectivity.[6f, 51] The self-assembly of ligand **2.10** with copper(II) chloride in NMP affords a complex that features a 2D ***hcb*** lattice where the metal and ligand represent trivial and 3-connecting nodes, respectively, and packing of individual 2D sheets affords relatively large uni-directional channels. Self-assembly of ligand **2.10** with M(II) nitrate (where M=Zn, Cd) affords an analogous ***hcb*** lattice, where both ligand and metal centre are 3-connected nodes, that close-pack to afford a dense lattice with interstitial solvent guests.

3.3.1 $\{[Cu_5(\mathbf{2.10})_2Cl_{10}(NMP)_4]\cdot n(NMP)\}_\infty$ 2D coordination complex with decorated 6^3 honeycomb (*hcb*) topology

The reaction of ligand **2.10** with copper(II) chloride in NMP afforded complex **3.5**, $\{[Cu_5(\mathbf{2.10})_2Cl_{10}(NMP)_4]\cdot n(NMP)\}_\infty$, featuring a 2D coordination polymer. Crystals were grown by diffusing diethyl ether vapours into a solution of the complex in NMP, isolated as green blocks and structurally elucidated by single crystal diffraction measurements. The structure solved in the triclinic space group $P\bar{1}$ to display the asymmetric unit as half the stated composition, **Figure 3.15**.

The asymmetric unit comprises one **2.10** ligand that coordinates to three crystallographically distinct Cu(II) centres, **Figure 3.16**. One of the three Cu(II) centres is sited on an inversion centre, has square planar coordination geometry, and is also coordinated by two *trans* chloride ligands with Cu-Cl and Cu-O bond distances of 2.2524(10) and 2.1.962(3) Å, respectively, and an O-Cu-Cl bond angle of 93.74(8) º. Selected bond metrics for complex **3.5** are given in **Table 3.4**. The other two Cu(II) centres are sited on general positions and bridge symmetry generated **2.10** ligands through a centrosymmetric Cu(II) dimer, featuring *cis*-chlorides with Cu-Cl bond distances of 2.2200(10) and 2.2175(9) Å and Cl-Cu-Cl coordination angle of 100.16(11) º. The two symmetry generated Cu(II) centres in the centrosymmetric dimer are linked by symmetry

equivalent **2.10** ligands, through μ_2-coordinating *N*-oxide moieties, with Cu-O bond lengths of 2.002(2) and 2.046(2) Å. These Cu(II) centres are also each coordinated by an NMP ligand along the *z* axis at Cu-O bond length 2.336(2) Å that results in a distorted square pyramidal coordination geometry,[60] which may be attributable to the steric bulk of the *cis*-chlorides, **Figure 3.16a**.

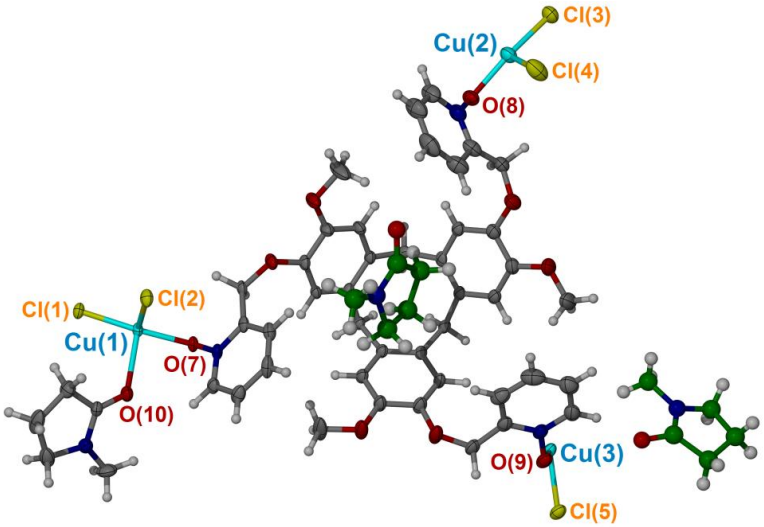

Figure 3.15 *The asymmetric unit, taken from the crystal structure of complex* ***3.5****. Anisotropic displacement parameters are shown at 35%. Intracavity and solvent NMP molecules are coloured green for clarity.*

Cu(1)-O(7)	2.002(2)	O(7)-Cu(1)-Cl(1)	93.29(7)
Cu(1)-O(7^{i})	2.046(2)	O(7)-Cu(1)-Cl(2)	162.17(7)
Cu(1)-Cl(1)	2.2200(10)	Cl(1)-Cu(1)-Cl(2)	100.16(11)
Cu(1)-Cl(2)	2.2175(9)	O(8)-Cu(2)-O(8^{ii})	180.0
Cu(1)-O(10)	2.336(2)	O(8)-Cu(2)-Cl(3)	93.74(8)
Cu(2)-O(8, 8^{ii})	1.962(3)	Cl(3)-Cu(2)-Cl(3^{ii})	180.0
Cu(2)-Cl(3, 3^{ii})	2.2524(10)	O(9)-Cu(3)-O(9^{iii})	69.98(14)
Cu(3)-O(9)	2.033(3)	O(9)-Cu(3)-Cl(4)	92.98(14)
Cu(3)-O(9^{iii})	2.000(3)	O(9)-Cu(3)-Cl(5)	161.28(9)
Cu(3)-Cl(4)	2.2173(12)	O(9)-Cu(3)-O(12^{iv})	87.94(13)
Cu(3)-Cl(5)	2.2199(16)	Cl(4)-Cu(3)-Cl(5)	100.78(5)
Cu(3)-O(12)	2.310(4)	O(9^{iii})-Cu(3)-Cl(4)	160.00(10)
O(7)-Cu(1)-O(7^{i})	70.48(10)	O(9^{iii})-Cu(3)-Cl(5)	93.94(10)
O(7)-Cu(1)-O(10)	86.05(9)	O(9^{iii})-Cu(3)-O(12^{iv})	86.84(12)

Symmetry operations: **i** 1-*x*, 1-*y*, -*z*; **ii** –*x* -1, -*y*, -*z*; **iii** –*x*, 1-*y*, 1-*z*; **iv** *x*-1, *y*, *z*.

Table 3.4 *Selected bond lengths (Å) and angles (°) from the crystal structure of complex* ***3.5***

Perhaps the first reported example of a copper(II) complex featuring a formally μ_2-bridging *N*-oxide ligand was reported by W. E. Hatfield in 1964, which remarked upon the spin-spin coupling of the complex but did not accurately determine its chemical structure.[70] Over the next two years Hatfield and co-workers reported the structure of $[Cu_2Cl_2$-μ_2-$(C_5H_5NO)]$ [71] and $[Cu_2Cl_2$-μ_2-$(C_9H_9NO)]$,[72] based upon magnetic and spectroscopic measurements only, yet mistook the square planar geometry about the Cu(II) centre for tetrahedral. The examples of pyridine-*N*-oxides acting as such μ_2-briding ligands that most closely resemble complex **3.5** are in the polymeric complex $\{[Cu_2Cl_4$-μ_2-$(C_5H_5NO)]\}_\infty$ [73] and mononuclear $[Cu_2Cl_4$-μ_2-$(C_5H_5NO)(C_5H_5NO)]$.[74] These complexes, reported by W. L. Watson and co-workers in 1968 and 1969, respectively, feature a centrosymmetric and square planar $[Cu_2Cl_2$-μ_2-$(C_5H_5NO)]$ dimer that is then further coordinated by another pyridine-*N*-oxide ligand in the apical plane. They too confirm similar bond metrics and a square pyramidal coordination geometry about the Cu(II) centre as for complex **3.5**, above.[73-74] Pyridine-*N*-oxides as μ_2-bridging ligands are somewhat less common than halides, carbonyls and oxides.[75] Zhang and co-workers have reported a MIL (Material Institute Lavoisier) comprising a bipyridine-*N*-oxide ligand which forms a networked structure with manganese(II) centres that is able to selectively uptake C_6-C_8 hydrocarbons, from solution, once evacuated.[76] More recently, Steel and Puttreddy have reported an example where the electron rich ligand, 4-methoxypyridine-*N*-oxide, μ_3-coordinates three silver(I) centres simultaneously in the formation of a 1D coordination chain.[77]

Additionally, there are three molecules of solvent NMP within the asymmetric unit of complex **3.5**, one of which associates with ligand **2.10** *via* host-guest interactions, where the methylene protons of the NMP molecule are directed into the electron rich [*a*,*d*,*g*]cyclononatriene core, **Figure 3.16c**.

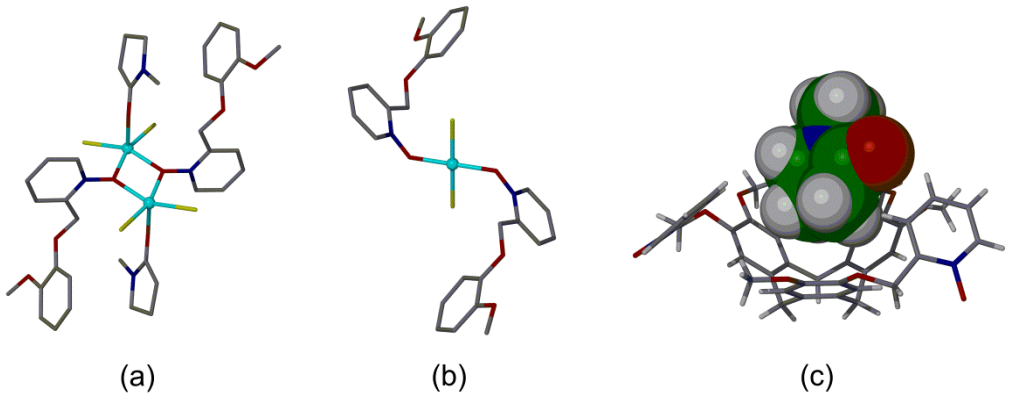

Figure 3.16 *From the crystal structure of complex* ***3.5****. (a) Centrosymmetric dinuclear copper(II) linker with* μ_2*-brinding* ***2.10*** *ligands; (b) mononuclear, square planar copper(II) centre; (c) displaying host-guest interactions between ligand* ***2.10*** *and intracavity NMP molecule. The NMP molecule is displayed in space-filling mode and coloured green for clarity.*

The 2-pyridyl substitution, alongside the flexibility provided by the ethereal linker, affords the propensity for ligand **2.10** to coordinate away from the ligand core. This is likely to prevent steric crowding upon metal coordination yet may also drive its 2D polymerisation. Additionally, it results in an increase in conformational freedom and therefore a decrease in molecular symmetry of individual **2.10** ligands, as opposed to **2.13** ligands in complexes **3.1**-**3.4**, above. Extension of the [Cu_3(**2.10**)] unit propagates two-dimensionally, where the metal and ligand represent trivial and 3-connecting nodes, respectively, resulting in a decorated 6^3 net with honeycomb (***hcb***) topology,[6c] **Figure 3.17b**.

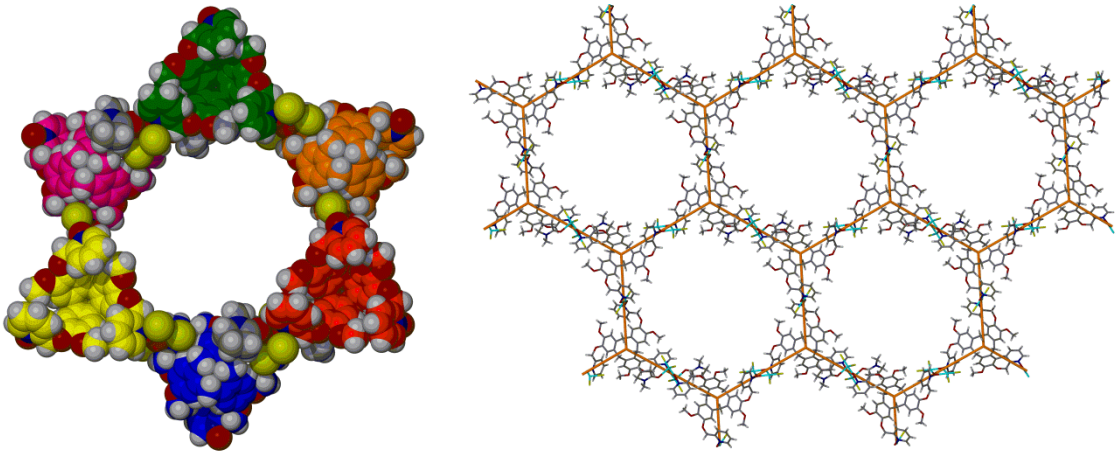

Figure 3.17 *From the crystal structure of complex* ***3.5****. (a) A resultant 6-gon formed through metal coordination. Individual ligands are distinguished by colour and shown in space-filling mode; (b) the decorated* 6^3 ***hcb*** *topology of the extended 2D sheet, as indicated by the solid, orange framework.*

The 6^3 ***hcb*** topology is commonplace amongst 2D coordination polymers and has been formed from alkali metal complexes of CTV,[78] as well as in complex {[Ag_3(**L**)$_2$Cl]·2(BF_4)·*n*(MeCN)}$_\infty$, where **L** represents a functionalised CTV derivative, *tris*(3-pyridyl-4-benzoxy)-CTG, **Figure 3.18**.[79] Other examples of 6^3 nets resulting from *N*-oxide complexation are Schröder's 'undulating' grid type structures.[16a] More closely related examples to complex **3.5** featuring tripodal ligands include Xia's porous networks which exhibit a solvent induced, single-crystal-to-single-crystal (SCTSC) transformation, in addition to gas sorption properties,[80] and Jacobsen's 'open net' frameworks formed through uranium(IV) coordination.[81]

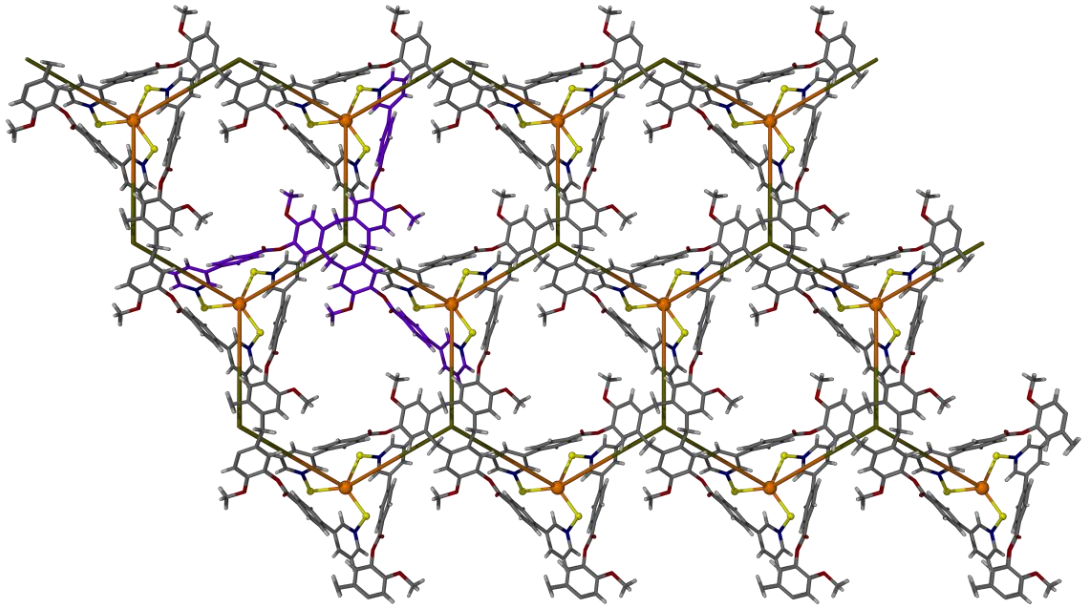

Figure 3.18 *The 6^3* ***hcb*** *net prepared by Ronson et.al. One ligand is distinguished in purple and the 'honeycomb' topology displayed by solid, orange lines.*[79]

Individual 2D sheets feature the inclusion of both ligand enantiomers and the complex is therefore a racemate. These sheets close pack in the absence of intermolecular interactions and in an off-set manner to yield large, unidirectional channels that run down the crystallographic *a* axis, **Figure 3.19**. Channels measure 12 × 16 Å in cross-section and account for approximately 40% of the total unit cell volume. The extended lattice also features small, interstitial voids between lattices that are filled with additional NMP solvent. These molecules do not form interactions with the network yet are aligned with the underside of **2.10** ligands.

The presence of large channels running through the structure did not permit the refinement of all NMP solvent molecules. Whilst they could not be located in the difference map, thermogravimetric analysis (TGA) indicated a step-wise, 40% mass loss up to 200 ºC that is supportive of an additional eight molecules of NMP within the lattice. This level of solvation was also supported by combustion analysis. As for complexes **3.2** and **3.3**, above, crystals of complex **3.5** were observed to rapidly degrade upon desolvation, as observed through powder X-ray diffraction analysis.

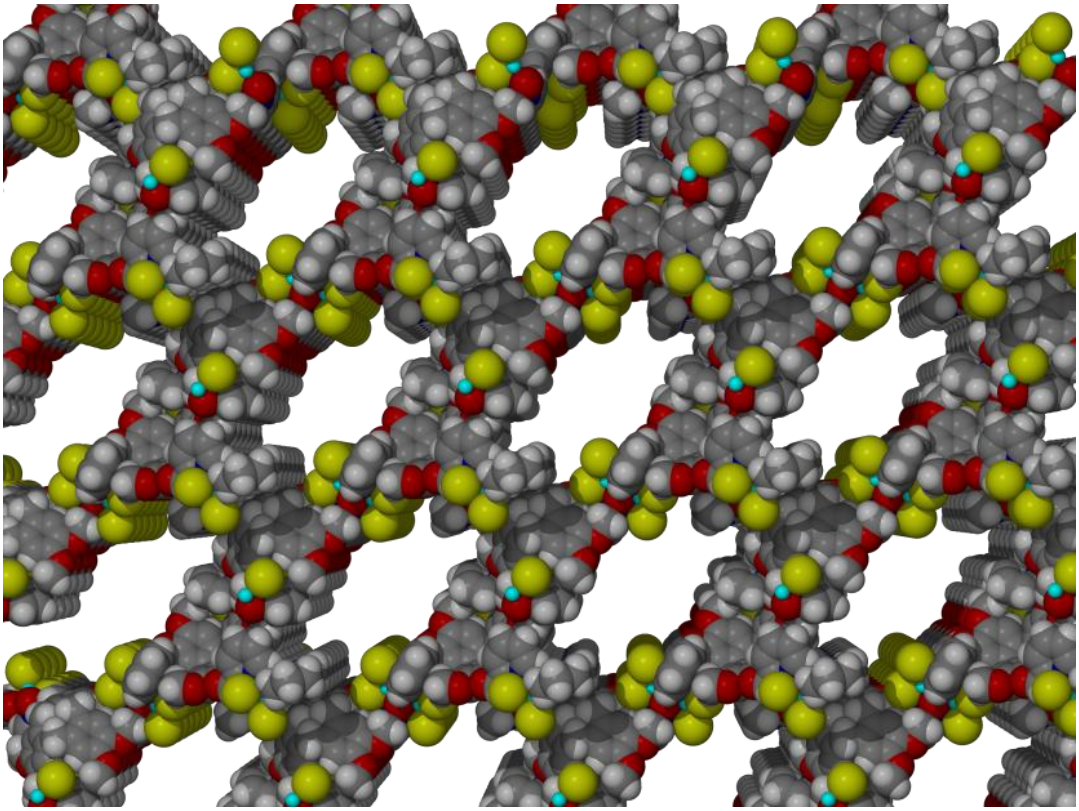

Figure 3.19 *From the crystal structure of complex* ***3.5****. A packing diagram, as viewed down the crystallographic a axis and in space-filling mode, displaying the 12 × 16 Å unidirectional channels. Solvent NMP has been omitted for clarity.*

3.3.2 {[Cd(2.10)$(NO_3)_2$]·2(DMF)}$_\infty$ 2D coordination complex with *hcb* topology

The stoichiometric reaction of ligand **2.10** and cadmium(II) nitrate in DMF solvent afforded complex **3.6**, featuring a 2D coordination polymer, of composition {[Cd(**2.10**)$(NO_3)_2$]·2(DMF)}$_\infty$. Crystals were grown from a DMF solution over a period of three weeks and elucidated by single crystal X-ray diffraction analysis. The complex solved in the chiral, monoclinic space group $P2_1$ to display the asymmetric unit contents as a Cd(II) centre, sited on a general position, that is coordinated by one **2.10** ligand and two chelating nitrate anions, **Figure 3.20**. There are also two molecules of DMF solvent, one of which has been refined with two-fold molecular disorder.

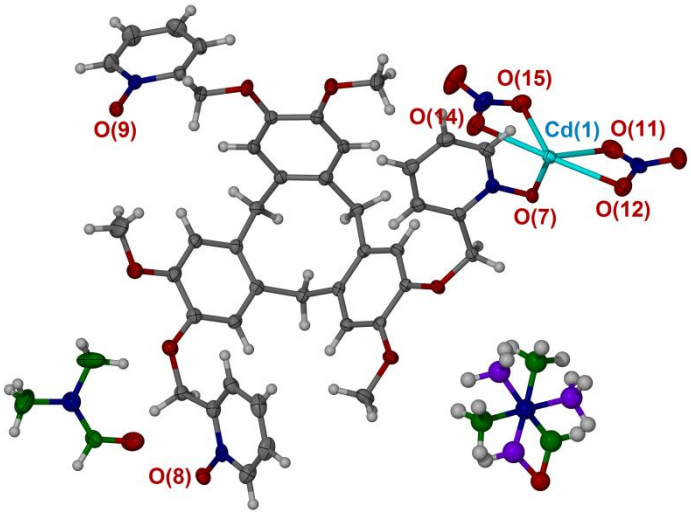

Figure 3.20 *The asymmetric unit, taken from the crystal structure of complex* ***3.6****. Anisotropic displacement parameters are shown at 40%. Solvent DMF is distinguished by colour and the two-fold molecular disorder colour coded and portrayed using hard spheres.*

Cd(1)-O(7)	2.255(4)	O(8^{i})-Cd(1)-O(9^{ii})	174.43(14)
Cd(1)-O(8^{i})	2.252(4)	O(7)-Cd(1)-O(11)	137.08(17)
Cd(1)-O(9^{ii})	2.283(4)	O(7)-Cd(1)-O(12)	84.78(17)
Cd(1)-O(11)	2.444(5)	O(7)-Cd(1)-O(14)	89.25(17)
Cd(1)-O(12)	2.454(5)	O(7)-Cd(1)-O(15)	142.55(15)
Cd(1)-O(14)	2.456(5)	O(8^{i})-Cd(1)-O(11)	90.86(16)
Cd(1)-O(15)	2.390(4)	O(8^{i})-Cd(1)-O(12)	100.04(17)
O(7)-Cd(1)-O(8^{i})	91.32(14)	O(9^{ii})-Cd(1)-O(11)	92.10(16)
O(7)-Cd(1)-O(9^{i})	89.73(14)	O(9^{ii})-Cd(1)-O(12)	85.51(16)

Symmetry operations: **i** 1-*x*, *y* + ½, 1-*z*; **ii** 1-*x*, *y* + ½, -*z*.

Table 3.5 *Selected bond lengths (Å) and angles (°) from the crystal structure of complex* ***3.6***

Ligand **2.10** retains approximate molecular C_3-symmetry and all 2-pyridyl-*N*-oxide moieties are orientated away from the ligand cavity. Ligand **2.10** coordinates the Cd(II) centre with bond lengths of 2.255(4) and 2.283(4) Å and displays O-Cd-O bond angles of 174.43(14) for two symmetry related and apically coordinated ligands and 91.32(14) º for two ligands in an apical-equitorial relationship. The Cd(II) centre is five-coordinate, approximating the chelating nitrates as single point donors, and possesses a distorted trigonal bipyramidal geometry. Two nitrate anions and one **2.10** ligand occupy equatorial coordination sites that results in O-Cd-O(nitrate) bond angles of 110.91 and 115.52 º and thus a O(nitrate)-Cd-O(nitrate) angle of 133.42 º. Additional bond metrics for complex **3.6** are summarised in **Table 3.5**, above.

Symmetry expansion of the asymmetric unit affords a 6^3 net of ***hcb*** topology where ligand and metal each represent 3-connecting nodes and the 2D tessellation of hexagons occurs in the *bc* plane, **Figure 3.21**. Complex **3.6** features the inclusion of only one ligand **2.10** enantiomer and is therefore chiral; however, the bulk crystalline mixture is a conglomerate.[82] The selective incorporation of one ligand enantiomer from a racemic mixture in the formation of a complex is known as 'spontaneous chiral resolution' and is commonplace amongst derivatised CTVs,[83] as well as other tripodal ligands such as *tris*(ureidobenzyl)amines [84] and trisubstituted carboxylic acid derivatives.[85]

Individual 2D sheets pack in an off-set manner that is facilitated by hydrogen bonding between the methylene protons of the [*a,d,g*]cyclononatriene core and the 3,4-diethereal moiety of an ligand beneath, with O···H-C separation of 2.540 Å. Additional face-to-face packing of sheets is in the absence of intermolecular interactions, with aromatic separations measured to be in the excess of 4 Å. Small, interstitial sites are generated through crystal packing and are filled with solvent DMF, which line up in a columnar manner down the crystallographic *a* axis, **Figure 3.21**. The result is a relatively dense extended lattice with no free space.

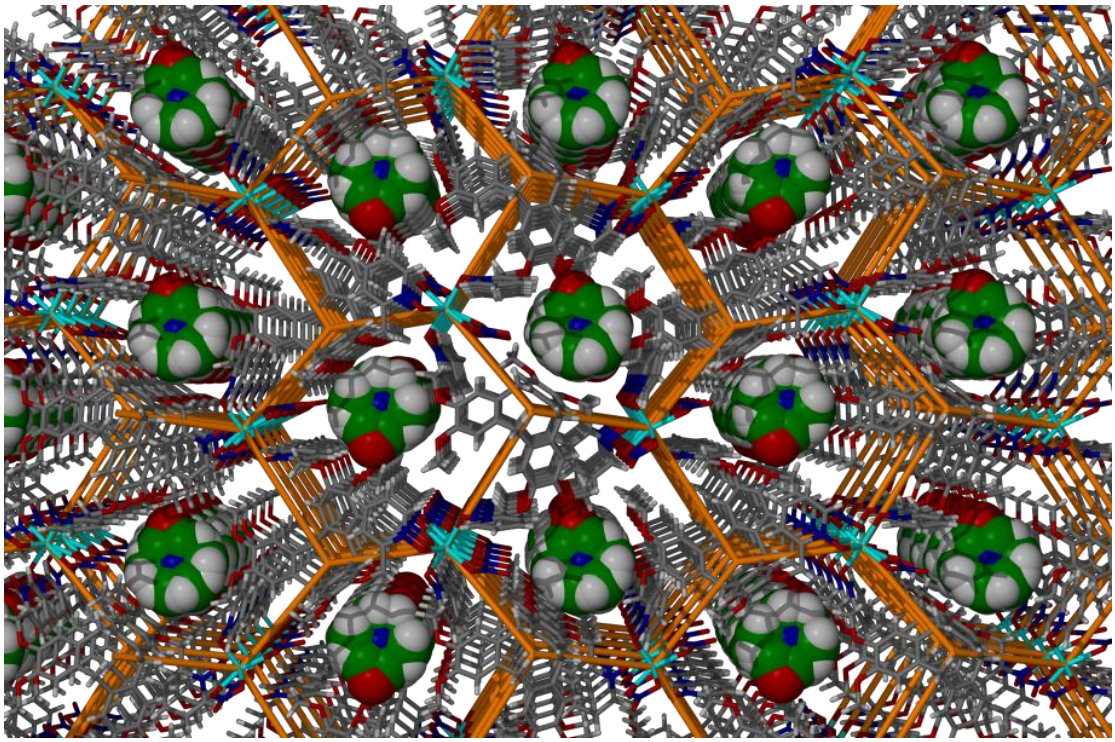

Figure 3.21 *From the crystal structure of complex* ***3.6****. The extended lattice, as viewed down the crystallographic a axis, highlighting the honeycomb topology and columnar stacking of solvent DMF. Solvent DMF are distinguished in green and have been shown in space-filling mode. The network topology is depicted as orange lines and bridges nodes within the 2D sheet.*

Complex **3.6** was further characterised by elemental analysis and IR spectroscopy. Both of which were fully concordant with the proposed composition from the crystal structure. Additionally, an isostructural complex was obtained when using $Zn(NO_3)_2$ in the place of $Cd(NO_3)_2$ for the crystallization; this structure, complex **3.7**, was identical to complex **3.6** and will not be discussed in this chapter.

3.4 Discrete and polymeric complexes featuring self-inclusion motifs

Self-inclusion is a common theme in CTV chemistry.[86] The electron rich [*a,d,g*]cyclononatriene core is a suitable host molecule for fullerenes,[63] carboranes [33,87] and other small molecules, such as in cryptophanes.[64,88] Additionally, and generally in the absence of additional guest molecules, derivatised CTVs show a propensity for self-inclusion, whereby self-recognition processes are energetically favourable.[89] Similar inclusion phenomena are observed for calix[*n*]arenes,[90] pillar[*n*]arenes [91] and other macrocyclic host molecules.[92] For a detailed review of host-guest chemistry, including noteworthy examples, see Chapter 1.

Complexes described herein comprise both discrete and polymeric examples that display both intra- and inter-species self-inclusion phenomena. Ligand **2.10** self-assembles with silver(I) centres to afford an 'imploded' capsule that arises due to host-guest interactions between ligand cavity and proximal ligand arm. Conversely, ligand **2.13** affords a monomeric copper(II) species which instead linearly assembles through inter-complex host-guest interdigitation to afford a *pseudo* 1D polymer. Ligand **2.12** displays a propensity for self-inclusion host-guest behaviour and affords both 1- and 2D coordination polymers with cobalt(II) and cadmium(II) centres, respectively. The 1D polymer afforded displays interstrand host-guest interdigitation, whereas the 2D ***sql*** net features reciprocal interactions within individual sheets.

3.4.1 Centrosymmetric M_2L_2 self-inclusion dimer, $[Ag_2(2.10)_2(NMP)_2]2(BF_4)$

The stoichiometric reaction of ligand **2.10** with silver(I) tetrafluoroborate in NMP solvent afforded an M_2L_2 centrosymmetric dimer, $[Ag_2(\mathbf{2.10})_2(NMP)_2]2(BF_4)$, complex **3.8**. Small, colourless crystals were isolated upon the diffusion of diethyl ether vapours into an NMP solution of the molecular components and analysed using single crystal X-ray diffraction measurements. The structure solved in the monoclinic space group $P2_1/c$ to display the asymmetric unit as half the overall complex, comprising one ligand **2.10** and two NMP ligands coordinating a silver(I) cation, alongside an additional NMP solvent molecule and a tetrafluoroborate anion, **Figure 3.22**. Selected bond metrics for complex **3.8** can be seen in **Table 3.6**.

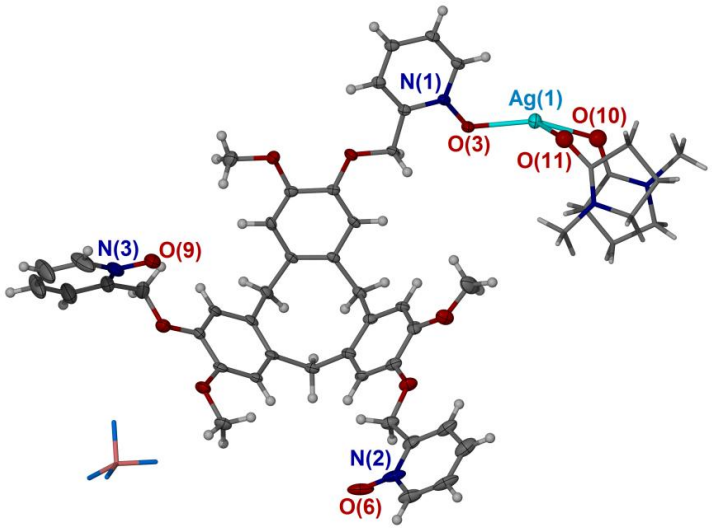

Figure 3.22 *From the crystal structure of complex* ***3.8****. Part of the asymmetric unit, as viewed down the crystallographic a-c plane. Solvent NMP omitted for clarity and anisotropic displacement parameters are shown at 35 % probability.*

Ag(1)-O(3)	2.224(5)	O(3)-Ag(1)-O(10)	153.3(2)
Ag(1)-O(10)	2.269(7)	O(3)-Ag(1)-O(11)	110.9(4)
Ag(1)-O(11)	2.546(18)	O(10)-Ag(1)-O(11)	81.8(5)

Table 3.6 *Selected bond lengths (Å) and angles (°) from the crystal structure of complex* ***3.8***

Each silver(I) centre lies on a general position and is four-coordinated by two symmetry related **2.10** ligands and two NMP ligands. The geometry about the silver(I) centre may be described as distorted tetrahedral and displays a ligand-to-metal O-Ag-O bond angle of 112.31 °. Thus, **2.10** ligands coordinate two symmetry generated silver(I) centres with one pyridyl-*N*-oxide moiety remaining uncoordinated. In doing so, the ligand loses its molecular C_3-symmetry and the capsule implodes somewhat to afford a synergistic self-inclusion motif, as seen for clathrate

complex **2.12**·2(NMP) of Chapter 2. This is supported through aromatic interactions between the pyridine ring and [*a*,*d*,*g*]cyclononatriene core, with π-π and C-H···π centroid separations of 3.78 Å and 2.67 Å, respectively, **Figure 3.23**.

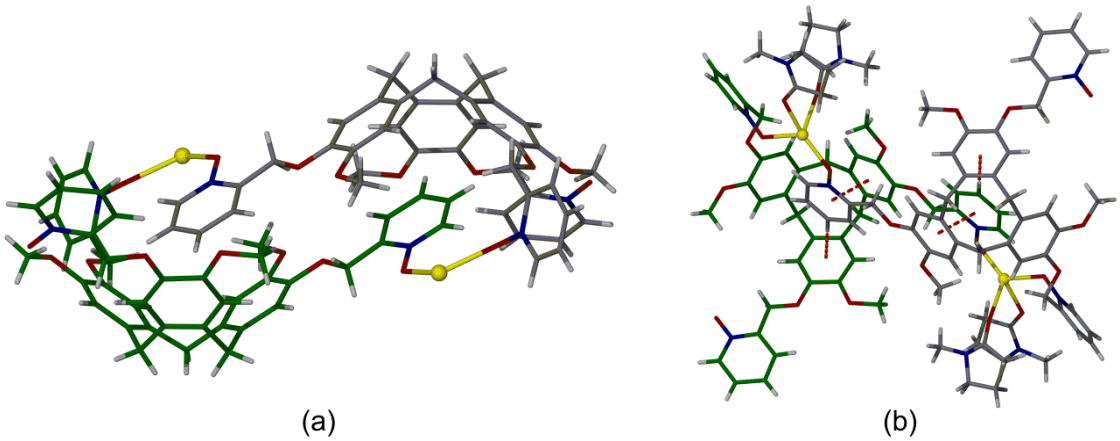

Figure 3.23 *From the crystal structure of complex* ***3.8****, highlighting the 'imploded' capsule with synergistic self-inclusion motif. (a) As viewed from side on, and (b) from above. Individual ligands are colour coded and counter anions and solvents of crystallization have been omitted for clarity. Aromatic π-π and π-H interactions are displayed with red, hashed lines.*

The solution-phase behaviour of complex **3.8** was investigated by ^{1}H NMR spectroscopy and mass spectrometry. The unavailability of d_9-NMP meant that all NMR studies were undertaken in d_6-DMSO; however, only broad resonances were observed which could not be meaningfully assigned. Electrospray mass spectrometric studies in NMP were indicative of the complex's existence in solution, whereby the weakly coordinated NMP ligands were lost before detection. The species $\{[Ag_2(\mathbf{2.10})_2]\cdot(BF_4)\}^+$ and $\{[Ag(\mathbf{2.10})]\}^+$ were observed at *m/z* of 1760.97 and 838.19, respectively.

The extended lattice develops through multiple π-π interactions, where individual M_2L_2 complexes form four face-to-face aromatic interactions with four neighbouring complexes. These occur between both uncoordinated and coordinated 2-pyridyl-*N*-oxide arms and the [*a*,*d*,*g*]-cyclononatriene core of two neighbouring complexes, with centroid separations of 3.55 and 3.61 Å, respectively. Furthermore, IR spectroscopy and elemental analysis were each consistent with the proposed structure of complex **3.8**.

This 'imploded' capsular motif has been previously observed with derivatised CTVs and all cases feature an analogous self-inclusion 'hand-shake' motif.[89] This shows the propensity for such species to reciprocally recognise one-an-other in the solid state and is testament to the hosting ability of the electron-rich CTV core.[33,86] Little *et al.* have prepared an organometallic $[Ag_2L_2]^{2+}$ capsule from the self-assembly of *tris*(allyl)CTG and silver(I) anions,[93] as well as an organically-linked, off-set disulfide capsule analogue, **Figure 3.24**.[88a] Other prominent

examples of $[M_2L_2]^{n+}$ complexes include Stang's [2+2] "molecular rectangles", formed from orthogonal bi-metallic building blocks,[94] and Fujita's palladium(II) ethylenediamine linked molecular rings, which undergo dynamic catenation in DMSO solution.[95]

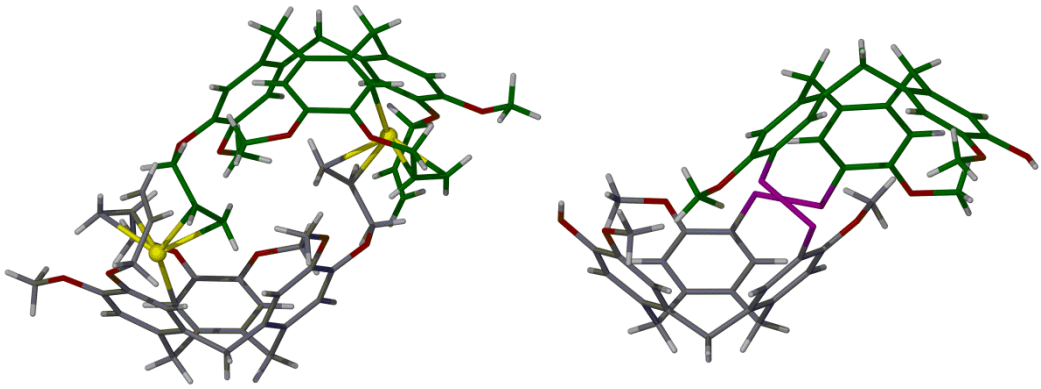

Figure 3.24 *Analogous off-set capsules reported by Little and co-workers. (a) From the crystal structure of the* $[Ag_2L_2]^{2+}$ *dimer, highlighting the* η^2 *coordination to the silver(I) centres (displayed as yellow spheres), and (b) from the crystal structure of the disulfide-linked organic dimer. For each example, individual CTV-based units have been colour-coded, and counter anions and solvents of crystallization have been omitted for clarity.*[88a, 93]

The elucidation of complex **3.8**, alongside complex **3.1** described above, shows the propensity for pyridine-*N*-oxide ligands to readily form complexes with silver(I) cations. Testament to this fact, Steel and co-workers have concluded that pyridine-*N*-oxide ligands represent 'hyperdentate argentophiles' that readily form coordination complexes with silver(I) centres.[77]

3.4.2 Mononuclear copper(II) complex, $[Cu(2.13)Cl_2(DMF)_2]\cdot 2(H_2O)$

The stoichiometric self-assembly of ligand **2.13** and copper(II) chloride in DMF solution afforded the mononuclear species $[Cu(\mathbf{2.13})Cl_2(DMF)_2]\cdot 2(H_2O)$, complex **3.9**. The use of different stoichiometries, or altering the reaction conditions, did not result in the formation of a different complex. Being mono-coordinated, complex **3.9** represents the simplest of all complexes gained with this particular ligand set and is mostly unremarkable in its molecular structure. Dark green crystals were isolated from the bulk solution after ten days, analysed by single crystal X-ray analysis and the structure solved in the triclinic space group $P\bar{1}$. The asymmetric unit comprises the entire complex, $[Cu(\mathbf{2.13})Cl_2(DMF)_2]\cdot 2(H_2O)$, which contains a central, 5-coordinate Cu(II) centre of disphenoidal,[60] or "see-saw" molecular geometry, **Figure 3.25**. It displays O-Cu-O(DMF) bond angles of 174.9(6) and 93.1(4) º and a Cl-Cu-Cl angle of 148.35(16) º. The DMF in the apical site displays a slightly longer O-Cu bond length of 2.218(8) º, when compared to the *trans*-DMF and *N*-oxide ligands, which display O-Cu bond

lengths of 2.006(15) and 1.974(9) º, respectively. A summary of selected bond metrics for complex **3.9** are given below in **Table 3.7**.

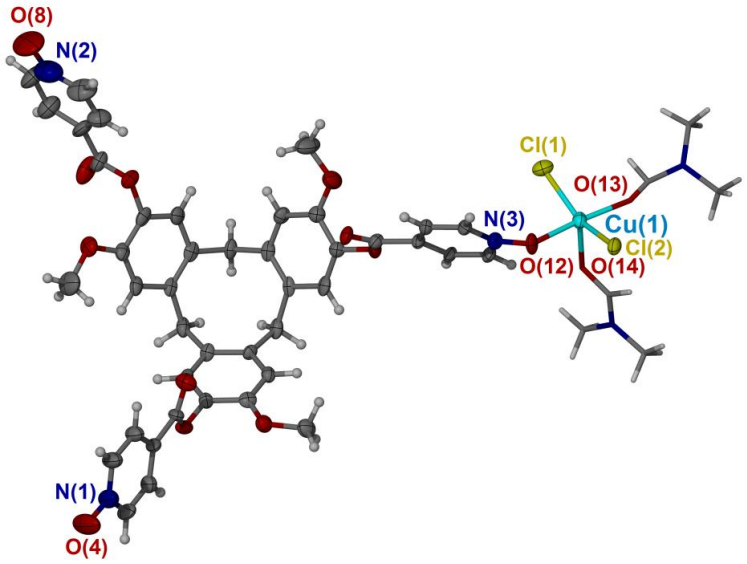

Figure 3.25 *From the crystal structure of complex **3.9**. Anisotropic displacement parameters are shown at 35% probability and water are molecules omitted for clarity.*

O(12)-Cu(1)	1.974(9)	O(12)-Cu(1)-O(13)	174.9(6)
O(13)-Cu(1)	2.006(15)	O(12)-Cu(1)-O(14)	93.1(4)
O(14)-Cu(1)	2.212(8)	O(12)-Cu(1)-Cl(1)	92.2(3)
Cl(1)-Cu(1)	2.287(4)	O(12)-Cu(1)-Cl(2)	85.5(3)
Cl(2)-Cu(1)	2.288(4)	Cl(1)-Cu(1)-Cl(2)	148.35(16)

Table 3.7 *Selected bond lengths (Å) and angles (°) from the crystal structure of complex **3.9***

Complex **3.9** was also observed to exist in the solution phase. Electrospray mass spectrometry of the complex in DMF afforded the mass peak 869.12, calculated for 869.10 and attributable to $\{[Cu(\mathbf{2.13})Cl]\}^{+}$, indicating formation of the complex, which loses the two weakly coordinated DMF ligands and a halide anion prior to its detection.

The extended structure of complex **3.9** is dependent on host-guest interactions, **Figure 3.26**; whereby the *N*,*N'*-dimethyl moiety of the apically coordinated DMF ligand is guest to a [*a*,*d*,*g*]cyclononatriene core of a neighbouring complex, which acts to link the molecular components in one-dimension. These complementary interspecies interactions have been previously observed to facilitate the formation and interlinking of 1D coordination polymers in the solid state.[96] Such 1D aggregates are linked two-dimensionally, along the crystallographic *ab* plane, by face-to-face π-π interactions between uncoordinated pyridyl-*N*-oxide ligand arms at

a centroid separation of 3.53 Å. The composition and purity of complex **3.9** was further determined by elemental analysis and IR spectroscopy.

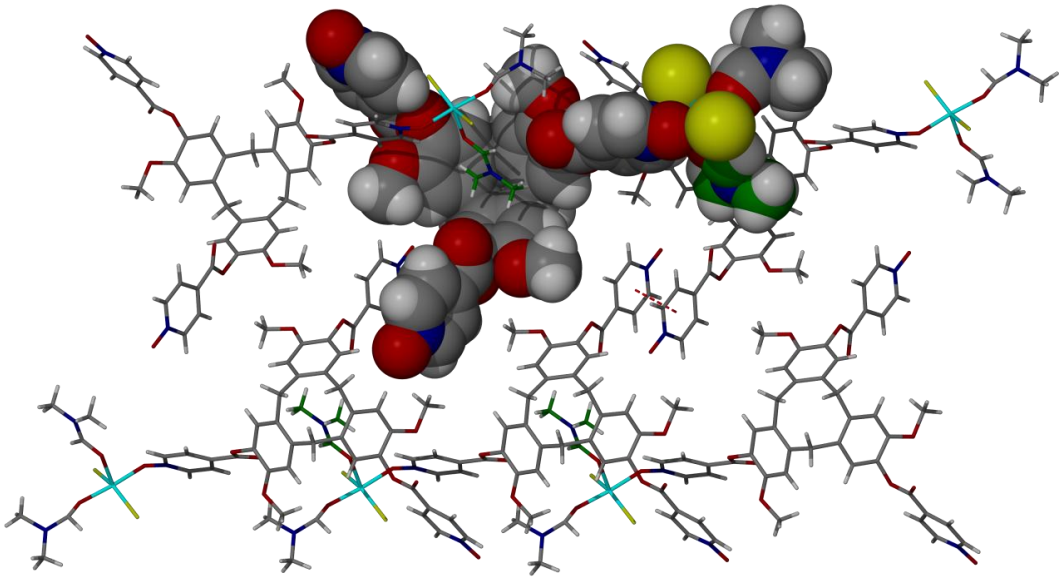

Figure 3.26 *From the crystal structure of complex* ***3.9****, as viewed down the crystallographic c axis, depicting the intermolecular interactions and host-guest inclusion between individual molecules. DMF ligands are shown in green and one complex molecule is shown in space-filling mode. Aromatic interactions between individual complexes are shown as red, hashed lines.*

3.4.3 {[Co(2.12)(DMF)]·$(NO_3)_2(DMF)_2(H_2O)$}$_\infty$ 1D coordination chain

The reaction of ligand **2.12** and cobalt(II) nitrate afforded complex **3.10**, featuring a 1D coordination polymer. Crystals of complex **3.10**, {[Co(**2.12**)(DMF)]·$(NO_3)_2(DMF)_2(H_2O)$}$_\infty$, were grown from a DMF solution, isolated as pale orange plates and elucidated crystallographically using synchrotron radiation. The structure solved in the triclinic space group $P\bar{1}$ to display the asymmetric unit as a central Co(II) centre, sited on an inversion centre and at half occupancy, which is coordinated by a molecule of both **2.12** and DMF ligands, alongside an uncoordinated nitrate anion, two additional molecules of solvent DMF and half a water molecule, **Figure 3.27**.

The cobalt(II) centres are coordinated by four symmetry equivalent **2.12** ligands and two DMF ligands, resulting in an approximately octahedral coordination geometry with coordination bond lengths of 2.129(3) and 2.094(4) Å, respectively, alongside a O(10)-Co(1)-O(13) coordination angle of 94.49(14) °. Selected bond metrics for complex **3.10** are given below in **Table 3.8**. Each **2.12** ligand is two-coordinate, with one arm remaining uncoordinated, acting to link the cobalt(II) centres in one-dimension along the crystallographic *b* axis.

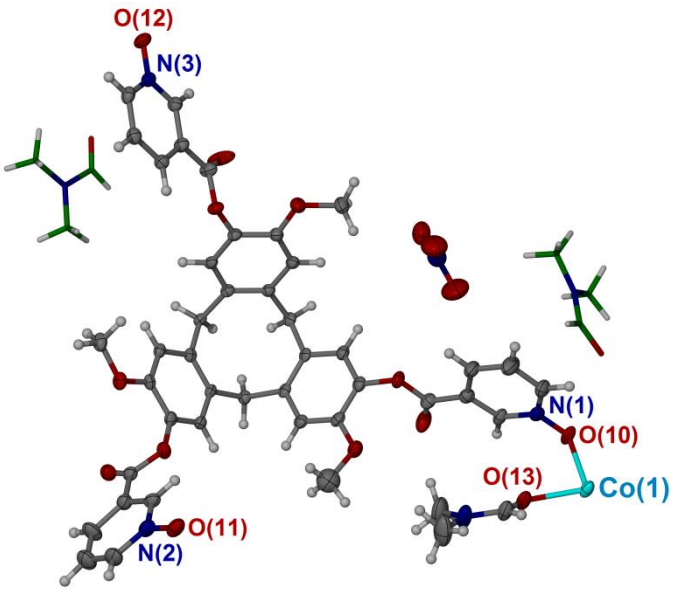

Figure 3.27 *From the crystal structure of complex* ***3.10****. Aside from two molecules of DMF solvent, coloured green, all anisotropic displacement parameters are shown at 35% probability.*

Co(1)-O(10)	2.129(3)	O(10)-Co(1)-O(13^{i})	94.49(14)
Co(1)-O(10^{i})	2.129(3)	O(13)-Co(1)-O(13^{i})	180.0(2)
Co(1)-O(11$^{ii\text{-}iii}$)	2.049(4)	O(10)-Co(1)-O(11^{iii})	88.95(15)
Co(1)-O(13)	2.094(4)	O(10)-Co(1)-O(11^{ii})	91.04(15)
Co(1)-O(13^{i})	2.094(4)	O(11^{ii})-Co(1)-O(11^{iii})	179.998(2)
O(10)-Cu(1)-O(10^{i})	179.999(2)	O(13^{i})-Co(1)-O(11^{ii})	92.55(16)
O(10)-Co(1)-O(13)	85.51(15)	O(13^{i})-Co(1)-O(11^{iii})	87.45(16)

Symmetry operations: **i** 1-*x*, 2-*y*, 1-*z*; **ii** 1-*x*, 1-*y*, 1-*z*; **iii** *x*, 1 + *y*, *z*.

Table 3.8 *Selected bond lengths (Å) and angles (°) from the crystal structure of complex* ***3.10***

Symmetry expansion of the [Co(**2.12**)(DMF)]$^{2+}$ unit proceeds 1-dimensionally in the absence of intermolecular interactions, **Figure 3.28**. There are two 'inverted' orientations of **2.12** ligands in the polymer chain, where each orientation is of the opposite molecular chirality to the other, rendering each 1D chain a racemate. Additionally, inwardly orientated methyl groups of **2.12** ligands and *N,N'*-dimethyl moieties of the DMF ligands create small, hydrophobic pockets within the 1D polymer. Individual 1D polymers associate through host-guest interactions through interdigitation, as opposed to the intrachain interactions seen for complexes **3.11** and **3.12**, below, and results in the formation of *pseudo*-2D sheets. This process is facilitated through reciprocal host-guest interactions between the uncoordinated 3-pyridyl-*N*-oxide ligand arm and a ligand cavity of a neighbouring 1D polymer, **Figure 3.28**. This 'hand-shake' motif is supported by aromatic π-π interactions at centroid separation of 3.64 Å, acting as a supramolecular 'zipper' between the 1D polymers. The crystal lattice contains uncoordinated

nitrate anions, alongside DMF and water solvents of crystallisation, which fill interstitial voids and form no interactions between the 1D chains or each other.

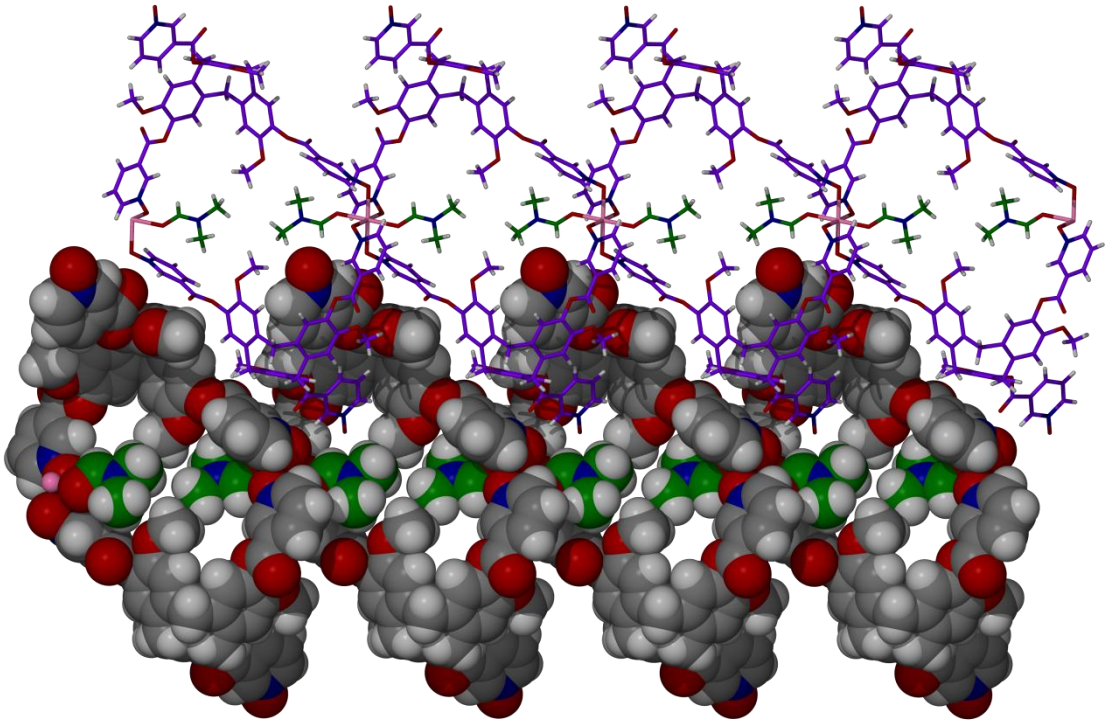

Figure 3.28 *From the crystal structure of complex* ***3.10****, depicting the packing and host-guest interactions between individual 1D polymers within the crystal lattice. Neighbouring 1D chains are colour-coded and DMF ligands are coloured green for clarity. One of the two 1D chains is shown in space-filling view.*

Interdigitation is a common motif found in coordination polymers of functionalised CTVs and has been noted in many three-connected ladder-type structures containing extended phenyl-pyridine ligands. These complexes echo the face-to-face aromatic interactions as seen in complex **3.10**, above, and display pyridyl-phenyl aromatic separations of ~3.8 Å.[96]

3.4.4 $\{[Cd(2.12)_2(DMF)_2]\cdot 2(ClO_4)\cdot 8(DMF)\}_\infty$ 2D coordination complex with *sql* topology

The reaction of ligand **2.12** and $Cd(ClO_4)_2$ in DMF solvent afforded complex **3.11**, $\{[Cd(\mathbf{2.12})_2(DMF)_2]\cdot 2(ClO_4)\cdot 8(DMF)\}_\infty$, featuring a 2D coordination polymer. Crystals suitable for X-ray diffraction were grown by diffusing diethyl vapours into solution of the complex in DMF and isolated as colourless blocks. The structure solved in the monoclinic space group $P2_1/n$ and the asymmetric unit was half that of the stated composition, **Figure 3.29**.

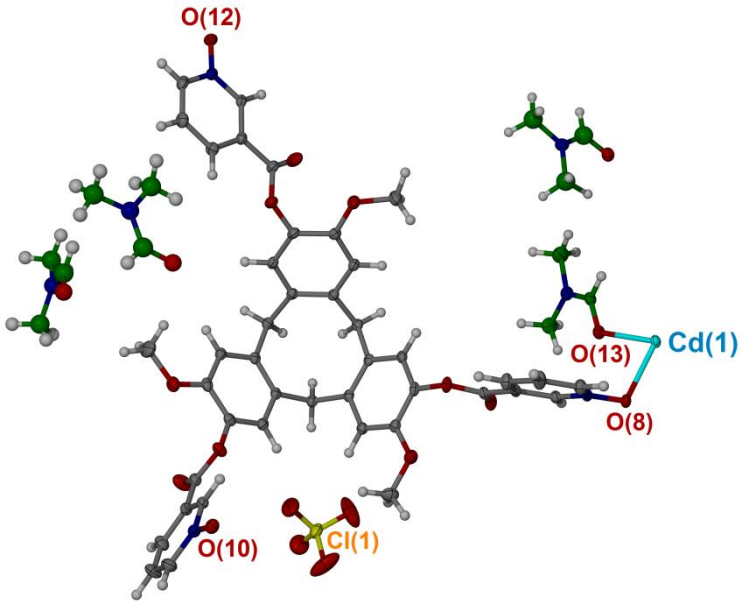

Figure 3.29 *The asymmetric unit, taken from the crystal structure of complex* ***3.11****. Anisotropic displacement parameters are shown at 35%. Intracavity and solvent NMP molecules are coloured green for clarity.*

Cd(1)-O(8)	2.3136(12)	O(8)-Cd(1)-O(10^{iv})	85.41(4)
Cd(1)-O(8^{i})	2.3137(12)	O(8)-Cd(1)-O(13)	87.08(4)
Cd(1)-O($10^{ii\text{-}iii}$)	2.3089(13)	O(8)-Cd(1)-O(13^{i})	92.91(4)
Cd(1)-O(13)	2.2681(11)	O(10^{ii})-Cd(1)-O(10^{iii})	180.0
Cd(1)-O(13^{i})	2.2681(11)	O(13)-Cd(1)-O(13^{i})	180.0
O(8)-Cd(1)-O(8^{i})	180.00(6)	O(10^{ii})-Cd(1)-O(13)	88.86(5)
O(8)-Cd(1)-O(10^{i})	84.59(4)	O(10^{ii})-Cd(1)-O(13^{i})	91.14(5)

Symmetry operations: **i** *-x*, 1-*y*, *-z*; **ii** *–x* – ½, *y* – ½, *-z* + ½; **iii** *x* + ½, 1-*y* + ½, *z* – ½.

Table 3.9 *Selected bond lengths (Å) and angles (°) from the crystal structure of complex* ***3.11***

The cadmium(II) centre in complex **3.11** is sited on an inversion centre and is octahedrally coordinated by four symmetry generated **2.12** ligands and two DMF ligands, in a similar manner to complex **3.10**, above, with O-Cd ligand bond distances of 2.316(12) and 2.2681(11)

measured, respectively. The **2.12** ligands are equatorially coordinated to the Cd(II) centre and the DMF ligands axially. Representative O-Cd-O bond angles are 84.59(4) and 180.00(6) for the *cis* and *trans* relationships, respectively. Selected bond metrics are listed above in **Table 3.9**. Individual **2.12** ligands are two-coordinate and thus afford a trivial, two-connecting node within the 2D sheet. Therefore the network topology is dictated by the four-connecting metallic nodes which results in a 4^4 square grid (***sql***) topology, **Figure 3.30**.[6c-e]

The ***sql*** topology is common in four-connecting 2D networks and is represented by the infinite tessellation of 4-gons across the sheet.[6c] The simplest examples of such nets are found in $\{[Pd(4,4'\text{-bipyridine})_n]\}_\infty$ [97] and its related complexes,[98] and interpenetrated variants.[99]

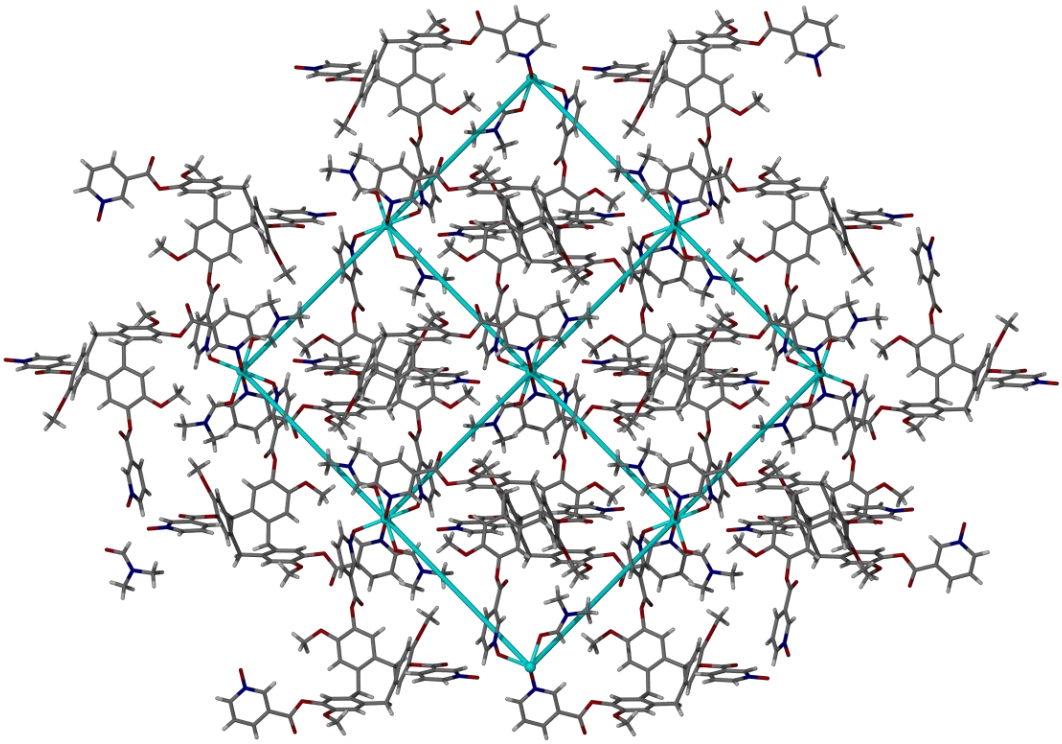

Figure 3.30 *From the crystal structure of complex* ***3.11****, displaying the resultant 2D sheet, as viewed down the crystallographic b axis. All anions and solvents are omitted for clarity and the* ***sql*** *topology is indicated by solid, blue lines which connect the metallic nodes within the network.*

The uncoordinated ligand arm of ligand **2.12** displays host-guest interactions with neighbouring ligands. This pair-wise and reciprocal motif is facilitated by face-to-face π-interactions between the aryl ring of the [*a*,*d*,*g*]cyclononatriene core and the pyridyl ring of the ligand arm, with aromatic centroid separation of 3.57 Å, **Figure 3.31**. This motif is common amongst derivatised CTVs [89a] and is also observed in complexes **3.8** and **3.10**, above. Individual 2D sheets close pack in a back-to-back manner in the absence of intermolecular interactions. This gives rise to small pockets which are filled with solvent DMF and well-ordered perchlorate counter anions.

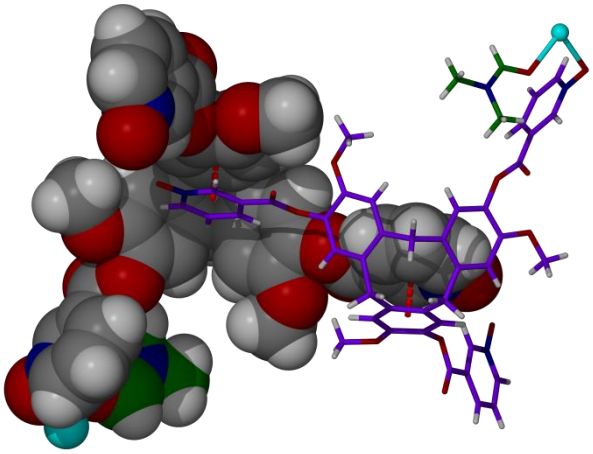

Figure 3.31 *From the crystal structure of complex* ***3.11****, depicting the host-guest self-inclusion motif present with individual 2D sheets. Ligands are distinguished by colour and one is shown in space-filling mode for clarity. Aromatic interactions are shown as hashed, red lines.*

Complex purity and composition were confirmed by combustion analysis and were consistent with the crystal structure model. Furthermore, IR spectroscopy confirms the inclusion of perchlorate anions in the crystalline material, and hence complex formation, with Cl-O bond stretches at 1094 and 944 cm^{-1}. Additionally, an isostructural complex was obtained when using $Cu(ClO_4)_2$ in the place of $Cd(ClO_4)_2$ for the crystallisation; this structure, complex **3.12**, was identical to complex **3.11** and will not be discussed in this chapter.

3.5 Conclusions and future work

Ligands **2.10**, **2.12** and **2.13** highlighted their versatile coordination chemistry with the transition metal cations and twelve complexes were isolated and fully characterised. These complexes described and summarised above comprise both discrete and polymeric structures and contain both topologically interesting features and host-guest self-inclusion motifs.

As expected, the coordination behaviour of these ligands was dissimilar to their corresponding parent, pyridyl congeners. For example, *tris*(isonicotinoyl)cyclotriguaiacylene and *tris*(2-pyridylmethyl)cyclotriguaiacylene afford an intertwined 2D network [100] and a four-fold interpenetrated (10,3)-a net [101] with silver(I) centres, respectively. This is in stark contrast to the structures gained as a result of *N*-oxide coordination seen for complexes **3.1** and **3.8**, respectively.

The first reported examples of transition metal coordination complexes with pyridine-*N*-oxide functionalised CTVs have been presented. Whilst complexes **3.1**-**3.12** are highly attractive in terms of their structural and topological diversity, the goal of constructing stable networks for further application was not realised. This was due, in part, to both crystalline fragility and a lack

of functionality control, whereby the orientation of host molecules within the complexes could not be efficiently controlled or predicted. All of these complexes possessed one of these attributes, but not both. For the above complexes to have post-synthetic application, they would need to posses the inwardly orientated and accessible [*a,d,g*]cyclononatriene core, whilst being able to withstand desolvation without a collapse of the crystalline lattice.

Future work should be focussed on the preparation of robust networks which possess the capsular arrangement of ligands and accessible void spaces. This may be achieved by preparing the desired materials in the presence of less volatile solvents which act to promote amorphisation due to rapid loss of solvent. Furthermore, isotropic 3D networks should be sought owing to their affinity for facile desolvation, which will help address this loss of crystallinity upon loss of solvent. Where potential candidates are isolated, gas sorption measurements should be targeted, with particular emphasis on methane, carbon dioxide and xenon. Additional experiments would perhaps address the materials ability to uptake molecules through a single-crystal-to-single-crystal (SCTSC) manner, which would negate the requirement of desorption and thus prevent amorphisation upon desolvation. If such materials displayed an ability to exchange guests in such a manner they could also be applied in areas that include molecular separations and catalysis, where the networks could be 'charged' with a reagent prior to the uptake of a second reactive species.

3.6 Experimental

Ligands **2.10**, **2.12** and **2.13** were prepared according to procedures listed in Chapter 2 of this thesis and employed as racemic mixtures for all complexation studies listed herein.

3.6.1 Instrumentation

High resolution mass spectrometric analyses of metal complexes were measured by Dr Lindsay P. Harding of the University of Huddersfield using a Bruker MicroTOF-Q or Bruker MaXis Impact spectrometer in either positive or negative ion mode. FT-IR spectra were recorded as solid phase samples on a Perkin-Elmer Spectrum One spectrophotometer. Samples for microanalysis were dried under vacuum before analysis and the elemental composition determined by Mr Ian Blakeley of the University of Leeds Microanalytical Service using a Carlo Erba elemental analyser MOD 1106 spectrometer. Thermogravimetric and energy dispersive X-ray analyses were performed by experimental officer Dr. Algy Kazlauciunas of the University of Leeds Colour Science department.

Crystals were mounted under inert oil on a MiTeGen tip and flash frozen to 150(1) K using an Oxford Cryosystems cryostream low temperature device. X-ray diffraction data were collected

using graphite-monochromated Mo-*K* radiation (λ = 0.71073 Å) using a Bruker-Nonius X-8 diffractometer with ApexII detector and FR591 rotating anode generator; or using synchrotron radiation (λ = 0.6889 Å) with a Crystal Logic 4-circle Kappa goniometer and Rigaku Saturn 724 CCD diffractometer at station i19 of Diamond Light Source. Data were corrected for Lorenztian and polarization effects and absorption corrections were applied using multi-scan methods. The structures were solved by direct methods using SHELXS-97 and refined by full-matrix on F^2 using SHELXL-97, interfaced through the X-seed interface.[102] Unless otherwise specified, all non-hydrogen atoms were refined as anisotropic, and hydrogen positions were included at geometrically estimated positions. Molecular graphics were obtained using POV-RAY through the X-Seed interface.[103] Additional details are given below and data collections and refinements summarised in Tables below.

3.6.2 Preparation of complexes

General procedure for the formation of metal complexes: ligand and metal salts were independently dissolved in 0.5 mL of the required solvents and combined at room temperature into a small vial. The vial was capped with a polythene plug and then punctured with a small hole to allow for the diffusion of diethyl ether vapours into the mixture and placed inside a larger vial containing the antisolvent. The samples were then sealed and left undisturbed for a period up to one month, or until crystals were observed to form, at which point analysis was sought.

Synthesis of $\{[Ag_3(NMP)_6(\mathbf{2.13})_2]\cdot 3(ClO_4)\cdot n(NMP)\}_\infty$, complex 3.1. $AgClO_4\cdot H_2O$ (5.07 mg, 0.0225 mmol) and ligand **2.13** (5.02 mg, 0.0075 mmol) were dissolved in NMP (~ 1 mL) and diethyl ether vapours were diffused into the solution, where small colourless crystals formed after 14 days that were analysed by X-ray diffraction. Yield 9.8 mg. As anticipated, microanalysis indicates a higher level of solvation than refined in the crystal structure, and additional solvent added to formula is consistent with analysis of crystal void space and TGA. Analysis for $[Ag_3(\mathbf{2.13})_2(NMP)_6]\cdot 3(ClO_4)\cdot NMP\cdot 2(H_2O)$ (% calculated, found) C (49.37, 49.30), H (4.63, 5.00), N (6.29, 6.55); Infrared analysis (FT-IR, cm^{-1}) 3463 (broad), 3107, 2938, 1746, 1659, 1510, 1445, 1252, 1166, 1066, 988, 927, 861, 764, 682, 630, 568, 490.

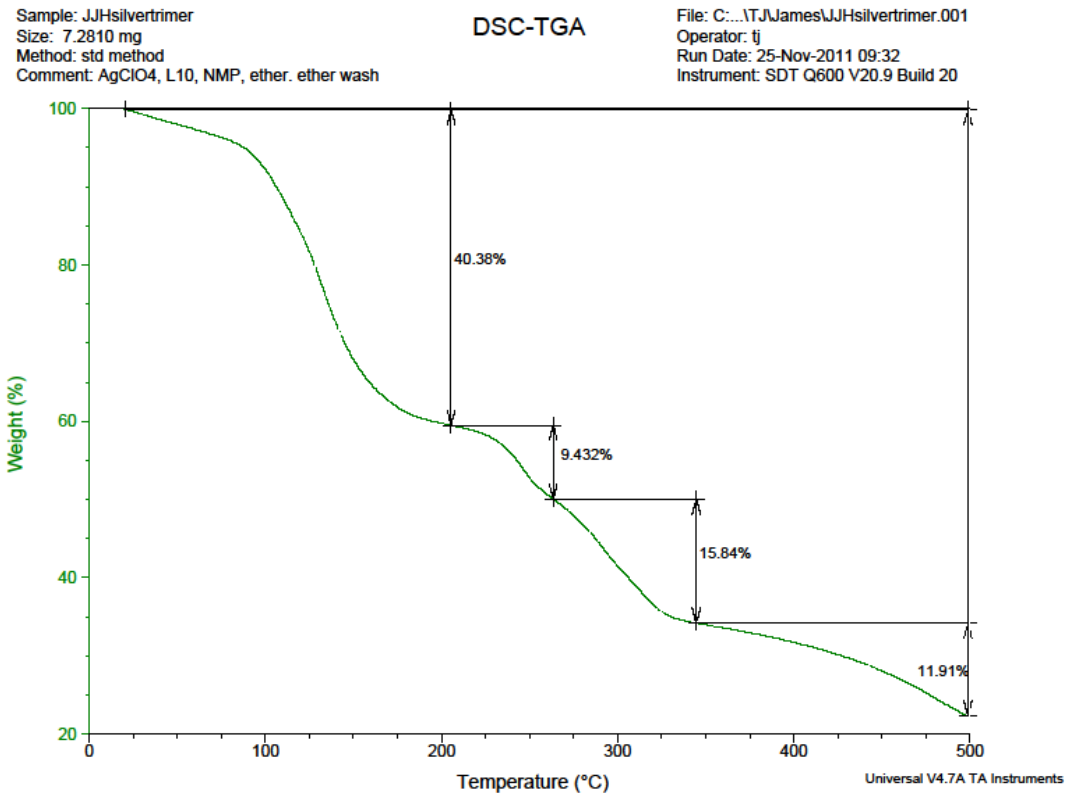

Synthesis of {[Co(2.13)$_2$]·2(BF$_4$)·*n*(DMF)}$_\infty$, complex 3.2. Co(BF$_4$)$_2$·6H$_2$O (7.66 mg, 0.0225 mmol) and ligand **2.13** (5.09 mg, 0.0075 mmol) were dissolved in DMF (~ 1 mL) and diethyl ether vapours were diffused into the solution, where orange plates formed after 14 days that were analysed by X-ray diffraction. Yield 7.1 mg. Analysis for {[Co(**2.13**)$_2$]·2(BF$_4$)·4(DMF)·2(H$_2$O)}$_\infty$ (% calculated, found) C (48.68, 48.70), H (4.92, 4.70), N (7.36, 7.40). Infrared analysis (FT-IR, cm^{-1}) 3333, 2936, 1735, 1634, 1505, 1415, 1254, 1051.

Synthesis of {[Zn(2.13)$_2$]·2(BF$_4$)·*n*(NMP)}$_\infty$, complex 3.3. Zn(BF$_4$)$_2$·6H$_2$O (7.81 mg, 0.0225 mmol) and ligand **2.13** (5.0 mg, 0.0075 mmol) were dissolved in NMP (~ 1 mL) and diethyl ether vapours were diffused into the solution, where small colorless plates formed after 18 days. Yield 8.3 mg that were analysed by X-ray diffraction using a synchrotron source. Analysis for {[Zn(**2.13**)$_2$]·2(BF$_4$)·3.5(NMP)·2(H$_2$O)}$_\infty$ (% calculated, found) C (53.11, 52.80), H (5.13, 5.20), N (6.77, 6.90). Infrared analysis (FT-IR, cm^{-1}) 3348 (broad), 1740, 1653, 1619, 1513, 1443, 1402, 1286, 1241, 1170, 1106, 1072, 942, 865, 764, 748, 677, 631.

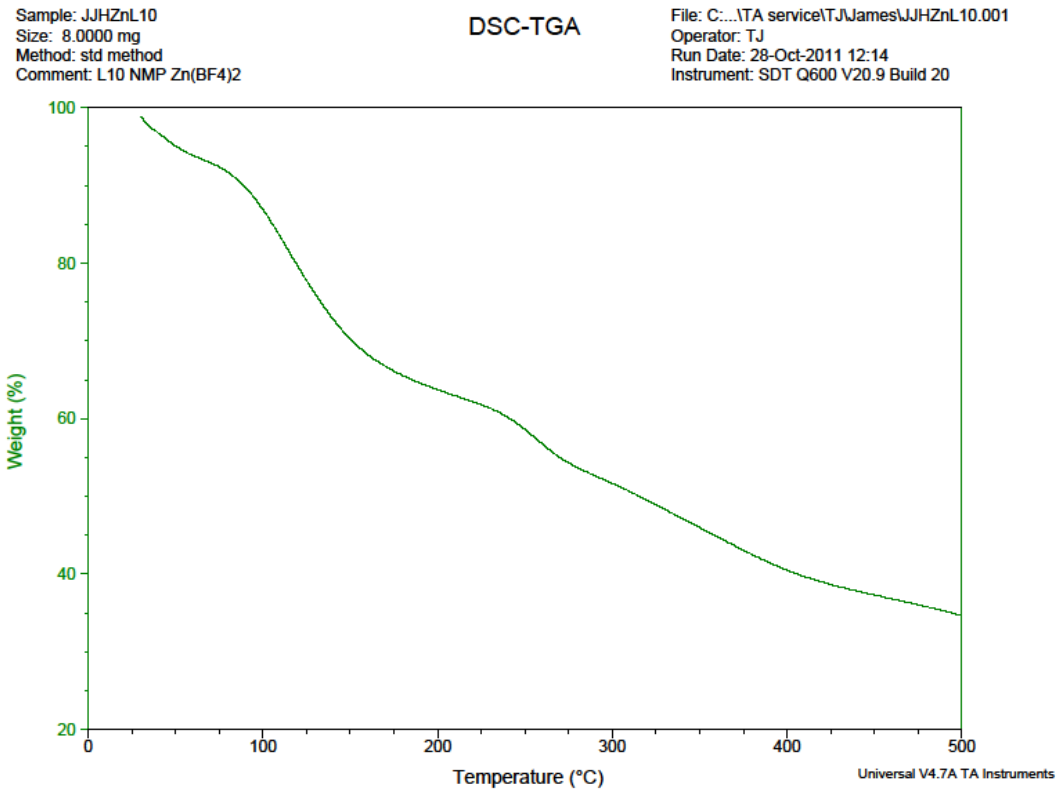

Synthesis of {[Cu(2.13)$_2$]·[Cu(H$_2$O)(NMP)$_4$]·4(BF$_4$)·8(NMP)·2(H$_2$O)}$_\infty$, complex 3.4. Cu(BF$_4$)$_2$·4H$_2$O (6.95 mg, 0.0225 mmol) and ligand **2.13** (5.0 mg, 0.0075 mmol) were dissolved in NMP (~ 1 mL) and diethyl ether vapours were diffused into the solution, where green plates formed after 14 days that were analysed by X-ray diffraction. Yield 6.3 mg. Analysis for {[Cu(**2.13**)$_2$]·[Cu(NMP)$_4$(H$_2$O)]·4(BF$_4$)·5(NMP)}$_\infty$ (% calculated, found) C (52.92, 52.95), H (5.13, 5.25), N (7.18, 7.20). Infrared analysis (FT-IR, cm^{-1}) 3119, 2938, 1745, 1628, 1505, 1484, 1443, 1404, 1252, 1163, 1139, 1052, 927, 861, 830, 746, 679, 630, 581, 497, 484, 470.

Synthesis of {[Cu$_5$(2.10)$_2$Cl$_{10}$(NMP)$_4$]·*n*(NMP)}$_\infty$, complex 3.5. CuCl$_2$·2H$_2$O (3.0 mg, 0.0225 mmol) and ligand **2.10** (5.0 mg, 0.0075 mmol) were dissolved in NMP (~ 1 mL) and diethyl-ether vapours were diffused into the solution, where small green needles formed after 14 days that were analysed by X-ray diffraction. Yield 8.3 mg. Analysis for {[Cu$_5$(**2.10**)$_2$Cl$_{10}$(NMP)$_4$]·6(NMP)}$_\infty$ (% calculated, found) C (51.51, 51.10), H (5.42, 5.00), N (7.18, 6.60). Infrared analysis (FT-IR, cm^{-1}) 3310 (broad), 2936, 1633, 1508, 1442, 1398, 1258, 1192, 1148, 1111, 1087, 1046, 993, 843, 781, 743, 694, 658, 619, 556.

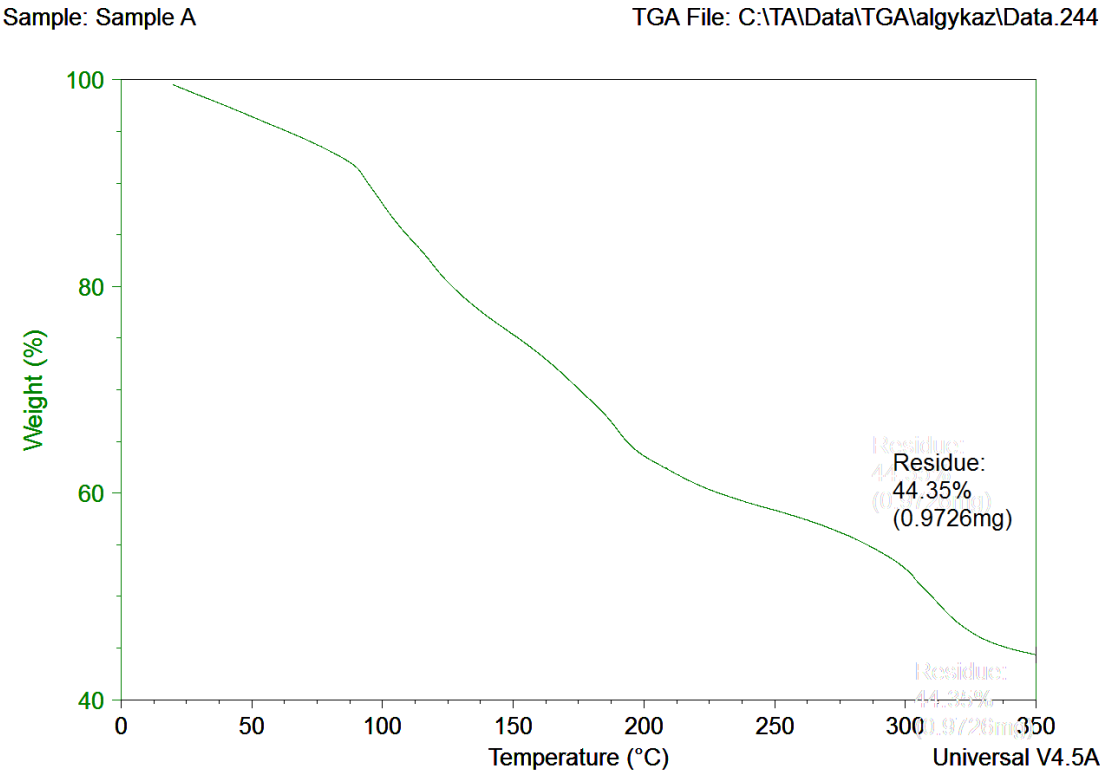

Synthesis of {[Cd(2.10)$(NO_3)_2$]·2(DMF)}$_\infty$, complex 3.6. $Cd(NO_3)_2{\cdot}4H_2O$ (6.9 mg, 0.0225 mmol) and ligand **2.10** (5.0 mg, 0.0075 mmol) were dissolved in DMF (~ 1 mL) and diethyl-ether vapours were diffused into the solution, where small colorless needles formed after 14 days that were analysed by X-ray diffraction. Yield 7.4 mg. Analysis for {[Cd(**2.10**)$(NO_3)_2$]·2(DMF)}$_\infty$ (% calculated, found) C (51.12, 51.30), H (4.58, 4.85), N (7.95, 7.50). Infrared analysis (FT-IR, cm^{-1}) 2902, 1674, 1608, 1511, 1441, 1265, 1203, 1150, 1111, 1089, 1050, 1026, 996, 884, 837, 775, 742, 697, 619, 547.

Synthesis of {[Zn(2.10)$(NO_3)_2$]·2(DMF)}$_\infty$, complex 3.7. $Zn(NO_3)_2{\cdot}6H_2O$ (6.7 mg, 0.0225 mmol) and ligand **2.10** (5.1 mg, 0.0075 mmol) were dissolved in DMF (~ 1 mL) and diethyl ether vapours were diffused into the solution, where small colourless needles formed after 14 days that were analysed by X-ray diffraction. Yield 11.8 mg. Analysis for {[Zn(**2.10**)$(NO_3)_2$]}$_\infty$ (% calculated, found) C (54.86, 55.00), H (4.28, 5.50), N (7.62, 8.00). Infrared analysis (FT-IR, cm^{-1}) 3421 (broad), 2928, 1670, 1608, 1511, 1439, 1400, 1262, 1203, 1149, 1088, 1028, 996, 947, 837, 775, 742, 698, 658, 619, 548.

Synthesis of [Ag_2(2.10)$_2$(NMP)$_4$]·2(BF_4), complex 3.8. $AgBF_4$ (4.3 mg, 0.02 mmol) and ligand **2.10** (7.5 mg, 0.017 mmol) were dissolved in NMP (~ 1 mL) and diethyl ether vapours were diffused into the solution, where small colourless blocks formed after 14 days that were analysed by single crystal X-ray diffraction analysis. Yield 6.9 mg. HRMS (ES^+): *m/z* 1760.97 {[Ag_2(**2.10**)$_2{\cdot}BF_4$]}$^+$ (calcd. 1760.36), 837.14 [Ag(**2.10**)]$^+$ (calcd. 836.68); Analysis for

$[Ag_2(\mathbf{2.10})_2(NMP)_4]\cdot 2(BF_4)\cdot H_2O$ (% calculated, found) C (53.52, 53.55), H (4.38, 4.50), N (4.46, 4.55); Infrared analysis (FT-IR, cm^{-1}) 3565 (broad), 2920, 1645, 1607, 1515, 1445, 1085 (s, broad, B-F).

Synthesis of $[Cu(\mathbf{2.13})Cl_2(DMF)_2]\cdot 2(H_2O)$, complex 3.9. $CuCl_2\cdot 2H_20$ (2.56 mg, 0.015 mmol) and ligand **2.13** (10.1 mg, 0.015 mmol) were dissolved in DMF (~ 1 mL) and diethyl ether vapours were diffused into the solution, where green block-shaped crystals formed after 14 days that were analysed by single crystal X-ray diffraction analysis. Yield: 7.76 mg. HRMS (ES^+): *m/z* 772.2 $\{\mathbf{2.13}\cdot H\}^+$ (calcd. 772.21), 869.1 $\{Cu(\mathbf{2.13})Cl\}^+$ (calcd. 869.10); Analysis for: $[Cu(\mathbf{2.13})(DMF)_2Cl_2]\cdot 2H_2O$ (% calculated, found) C (52.10, 52.23), H (4.20, 4.37), N (5.80, 5.52); Infrared analysis (FT-IR, cm^{-1}) 3421 (broad), 3509, 3111, 2925, 1733, 1635, 1505, 1440, 1249.

Synthesis of $\{[Co(\mathbf{2.12})_2(NO_3)_2(DMF)_2]\cdot 4(DMF\cdot H_2O)\}_\infty$, complex 3.10. $Co(NO_3)_2\cdot 6H_2O$ (4.25 mg, 0.0146 mmol) and ligand **2.12** (7.5 mg, 0.0103 mmol) were dissolved in DMF (~ 1 mL) and diethyl ether vapours were diffused into the solution, where orange needles formed after 14 days that were analysed by single crystal X-ray diffraction analysis using a synchrotron source. Yield: 7.76 mg. Analysis for: $\{[Co(\mathbf{2.12})_2(NO_3)_2]\cdot 3(DMF)\cdot 4(H_2O)\}_\infty$ (% calculated, found) C (54.87, 54.90), H (4.80, 4.65), N (7.57, 7.35). Infrared amalysis (FT-IR, cm^{-1}) 3402 (broad), 3476, 3044, 2914, 1747, 1648, 1508, 1443, 1375, 1322, 1278 (s), 1202, 1177, 1097, 1003, 939, 829, 742.

Synthesis of $\{[Cd(\mathbf{2.12})_2(DMF)_2]\cdot 2(ClO_4)\cdot 8(DMF)\}_\infty$, complex 3.11. $Cd(ClO_4)_2\cdot 6H_2O$ (6.31 mg, 0.015 mmol) and ligand **2.12** (10.1 mg, 0.015 mmol) were dissolved in NMP (~ 1 mL) and diethyl ether vapours were diffused into the solution, where off-white block crystals formed after 10 days that were analysed by single crystal X-ray diffraction analysis that were analysed by single crystal X-ray diffraction analysis. Yield: 7.76 mg. Analysis for: $\{[Cd(\mathbf{2.12})_2(DMF)_2]\cdot 2(ClO_4)\cdot 2(DMF)\cdot 2(H_2O)\}_\infty$ (% calculated, found) C (51.96, 52.15), H (4.63, 4.40), N (6.31, 6.15). Infrared analysis (FT-IR, cm^{-1}) 3421 (broad), 3476, 3104, 2928, 1749, 1667, 1508, 1432, 1283, 1128, 1140, 1094, 1007, 944, 831, 747.

Synthesis of $\{[Cu(\mathbf{2.12})_2(DMF)_2]\cdot 2(ClO_4)\cdot 8(DMF)\}_\infty$, complex 3.12. $Cu(ClO_4)_2\cdot 6H_2O$ (5.49 mg, 0.015 mmol) and ligand **2.12** (10.02 mg, 0.015 mmol) were dissolved in NMP (~ 1 mL) and diethyl ether vapours were diffused into the solution, where green obelisk crystals formed after 10 days that were analysed by single crystal X-ray diffraction analysis. Yield: 8.41 mg. Analysis for: $\{[Cu(\mathbf{2.12})_2(DMF)_2]\cdot 2(ClO_4)\cdot 6(DMF)\}_\infty$ (% calculated, found) C (53.06, 53.00), H (5.28, 5.20), N (8.12, 8.35). Infrared analysis (FT-IR, cm^{-1}) 3421 (broad), 3476, 3104, 2928, 1749, 1667, 1508, 1432, 1283, 1128, 1140, 1094, 1007, 944, 831, 747.

3.6.3 Supplementary crystallographic information

Crystals of complexes **3.2** and **3.3** were weakly diffracting and did not diffract at high angles. For complexes **3.1**-**3.3** and **3.5** the structures contained significant void space and residual electron density that could not be meaningfully refined as additional solvent, hence the SQUEEZE [104] routine of PLATON [104] was employed. For **3.3**, one ring was refined with a rigid body model, some bond lengths were restrained and one pyridine-*N*-oxide moiety was refined as disordered. Disordered groups and one methyl were refined isotropically. Complex **3.4** was refined with a block-matrix refinement and number of bond length and flat restraints. Additionally, some solvent was refined at half occupancy, one BF_4^- anion was refined with disordered F positions and some solvent and the anions were refined isotropically. In complex **3.6**, one DMF was refined isotropically and disordered over two positions with a shared N atom. Complex **3.7** was solved and refined as a twin. The bond lengths of both DMF solvent molecules were restrained to be chemically reasonable and one was modeled over two molecular positions and not refined anisotropically. One pyridine-*N*-oxide moiety and DMF solvent molecule were refined using planarity restraints using the FLAT command. Soft restraints were placed on the entire structure to make all thermal ellipsoid parameters chemically reasonable, using the SIMU, DELU and ISOR commands in ShelX. For complex **3.8** the B-F and some C-C and C-N distances of NMP molecules were restrained at chemically reasonable lengths and the BF_4^- and some NMP molecules were refined isotropically. Complexes **3.3** and **3.10** were analyzed using synchrotron data and one DMF of **3.10** was refined isotropically.

3.6.4 X-ray data tables for complexes 3.1-3.12

	3.1	**3.2**	**3.3***	**3.4**	**3.5**	**3.6**
Formula	$C_{114}H_{120}Ag_3Cl_3N_{12}O_{42}$	$C_{84}H_{66}BCoF_4N_6O_{24}$	$C_{84}H_{66}BF_4N_6O_{24}Zn$	$C_{144}H_{180}B_4Cu_2F_{16}N_{18}O_{39}$	$C_{124}H_{150}Cl_{10}Cu_5N_{14}O_{26}$	$C_{48}H_{53}CdN_7O_{17}$
Mr	2760.18	1689.17	1695.61	3261.38	2924.78	1112.37
Crystal colour and shape	Colourless, needle	Orange, plate	Colourless, plate	Green, plate	Green, needle	Colourless, needle
Crystal size (mm)	0.12 x 0.06 x 0.04	0.18 x 0.08 x 0.08	0.20 x 0.12 x 0.12	0.16 x 0.08 x 0.08	0.15 x 0.12 0.04	0.18 x 0.13 x 0.13
Crystal system	Cubic	Monoclinic	Triclinic	Triclinic	Triclinic	Monoclinic
Space group	$Pa\bar{3}$	$C2/c$	$P\bar{1}$	$P\bar{1}$	$P\bar{1}$	$P2_1$
a (Å)	25.9744(8)	17.5839(18)	17.44(3)	18.1713(19)	11.7843(8)	8.0052(7)
b (Å)	25.9744(8)	29.7518(18)	17.54(4)	21.487(2)	18.9058(12)	24.325(2)
c (Å)	25.9744(8)	34.404(3)	18.13(3)	24.177(2)	24.2187(16)	14.2675(12)
α (^{0})	90	90	100.28(8)	84.788(4)	100.396(3)	90.00
β (^{0})	90	99.609(3)	101.91(6)	80.734(4)	101.476(3)	100.117(3)
γ (^{0})	90	90	118.80(6)	80.361(4)	97.089(3)	90.00
V (Å^3)	17524.1(9)	17746(3)	4499(15)	9165.1(16)	5129.5(6)	2735.0(4)
Z	4	4	1	2	1	2
ρ_{calc} (g.cm^{-3})	1.046	0.632	0.626	1.182	0.947	1.351
θ range (^{0})	1.36 – 25.00	1.36 – 20.00	1.31– 22.69	1.33 – 25.00	4.08 – 24.93	1.67 – 29.36
No. data collected	70296	43822	30886	104252	61475	20183
No. unique data	5148	8276	12825	32232	17543	12571
R_{int}	0.0603	0.0976	0.0728	0.0536	0.0377	0.0279
No. obs. Data ($I > 2\sigma(I)$)	3178	3347	4800	18025	11995	10482
No. parameters	275	384	523	1768	815	654
No. restraints	1	3	0	23	0	1
R_1 (obs data)	0.0958	0.0909	0.0729	0.1643	0.0614	0.0583
wR_2 (all data)	0.2982	0.2605	0.1992	0.4894	0.1991	0.1705
S	1.074	0.881	0.805	1.751	1.032	1.036

	3.7[@]	**3.8**	**3.9**	**3.10***	**3.11**
Formula	$C_{48}H_{53}ZnN_7O_{17}$	$C_{114}H_{132}Ag_2B_2F_8N_{12}O_{24}$	$C_{48}H_{51}Cl_2CuN_5O_{16}$	$C_{102}H_{110}CoN_{14}O_{36}$	$C_{114}H_{136}CdCl_2N_{16}O_{42}$
Mr	1065.34	2443.68	1088.38	2166.97	2585.69
Crystal colour and shape	Colourless, needle	Colourless, block	Green, block	Orange, needle	Colourless, block
Crystal size (mm)	0.20 x 0.14 x 0.14	0.18 x 0.14 x 0.12	0.18 x 0.16 x 0.16	0.10 x 0.05 x 0.05	0.20 x 0.12 x 0.12
Crystal system	Monoclinic	Monoclinic	Triclinic	Triclinic	Monoclinic
Space group	$P2_1$	$P2_1/c$	$P\bar{1}$	$P\bar{1}$	$P2_1/n$
a (Å)	7.9869(14)	22.0843(11)	12.5748(18)	12.047(5)	16.2283(13)
b (Å)	24.435(5)	12.7697(7)	14.424(2)	14.724(6)	19.5779(17)
c (Å)	14.212(2)	21.5212(11)	18.045(3)	18.024(7)	20.2184(15)
α (^{0})	90.00	90.00	72.077(7)	97.0790(10)	90.00
β (^{0})	99.980(8)	111.184(2)	71.966(6)	107.478(5)	99.773(4)
γ (^{0})	90.00	90.00	88.086(7)	102.281(7)	90.00
V (Å^3)	2731.7(8)	5659.1(5)	2954.3(8)	2919(2)	6330.5(9)
Z	4	2	2	1	2
ρ_{calc} (g.cm^{-3})	1.295	1.434	1.224	1.233	1.356
θ range (^{0})	2.59-24.58	1.91 – 23.60	1.62 – 26.37	1.17 – 22.50	1.82 – 31.21
No. data collected	9114	19444	9681	33933	72930
No. unique data	5509	8388	6103	8349	20393
R_{int}	0.0279	0.0385	0.0433	0.0241	0.0426
No. obs. Data ($I > 2\sigma(I)$)	3664	5794	3394	7859	14902
No. parameters	655	641	646	649	803
No. restraints	204	12	0	0	0
R_1 (obs data)	0.1103	0.0941	0.1200	0.1207	0.0425
wR_2 (all data)	0.2891	0.3055	0.3887	0.4064	0.1227
S	1.145	1.043	1.343	1.995	1.020

***** data collection made using synchrotron radiation; [@] crystals were solved and refined as a twin.

3.7 Bibliography

[1] J. C. Bailar, Jr., *Prep. Inorg. React.* **1964**, *1*, 1-57.

[2] B. F. Hoskins, R. Robson, *J. Am. Chem. Soc.* **1989**, *111*, 5962-5964.

[3] O. M. Yaghi, H. Li, *J. Am. Chem. Soc.* **1995**, *117*, 10401-10402.

[4] S. Kitagawa, R. Kitaura, S.-i. Noro, *Angew. Chem. Int. Ed.* **2004**, *43*, 2334-2375.

[5] S. R. Batten, N. R. Champness, X.-M. Chen, J. Garcia-Martinez, S. Kitagawa, L. Ohrstrom, M. O'Keeffe, M. P. Suh, J. Reedijk, *Pure Appl. Chem.* **2013**, *85*, 1715-1724.

[6] (a) V. A. Blatov, M. O'Keeffe, D. M. Proserpio, *CrystEngComm* **2010**, *12*, 44-48; (b) S. T. Hyde, M. O'Keeffe, D. M. Proserpio, *Angew. Chem. Int. Ed.* **2008**, *47*, 7996-8000; (c) M. O'Keeffe, M. A. Peskov, S. J. Ramsden, O. M. Yaghi, *Acc. Chem. Res.* **2008**, *41*, 1782-1789; (d) O. Delgado-Friedrichs, M. O'Keeffe, O. M. Yaghi, *Phys. Chem. Chem. Phys.* **2007**, *9*, 1035-1043; (e) N. W. Ockwig, O. Delgado-Friedrichs, M. O'Keeffe, O. M. Yaghi, *Acc. Chem. Res.* **2005**, *38*, 176-182; (f) O. Delgado-Friedrichs, M. O'Keeffe, *J. Solid State Chem.* **2005**, *178*, 2480-2485.

[7] (a) H.-C. Zhou, J. R. Long, O. M. Yaghi, *Chem. Rev.* **2012**, *112*, 673-674; (b) T. R. Cook, Y.-R. Zheng, P. J. Stang, *Chem. Rev.* **2012**, *113*, 734-777; (c) R. Chakrabarty, P. S. Mukherjee, P. J. Stang, *Chem. Rev.* **2011**, *111*, 6810-6918; (d) J. R. Long, O. M. Yaghi, *Chem. Soc. Rev.* **2009**, *38*, 1213-1214; (e) J. Lee, O. K. Farha, J. Roberts, K. A. Scheidt, S. T. Nguyen, J. T. Hupp, *Chem. Soc. Rev.* **2009**, *38*, 1450-1459.

[8] J. An, N. L. Rosi, *J. Am. Chem. Soc.* **2010**, *132*, 5578-5579.

[9] (a) R. A. Smaldone, R. S. Forgan, H. Furukawa, J. J. Gassensmith, A. M. Z. Slawin, O. M. Yaghi, J. F. Stoddart, *Angew. Chem. Int. Ed.* **2010**, *49*, 8630-8634; (b) B. Panella, M. Hirscher, *Adv. Mater.* **2005**, *17*, 538-541; (c) H. Deng, S. Grunder, K. E. Cordova, C. Valente, H. Furukawa, M. Hmadeh, F. Gándara, A. C. Whalley, Z. Liu, S. Asahina, H. Kazumori, M. O'Keeffe, O. Terasaki, J. F. Stoddart, O. M. Yaghi, *Science* **2012**, *336*, 1018-1023; (d) S. S. Han, H. Furukawa, O. M. Yaghi, W. A. Goddard, *J. Am. Chem. Soc.* **2008**, *130*, 11580-11581; (e) N. L. Rosi, J. Eckert, M. Eddaoudi, D. T. Vodak, J. Kim, M. O'Keeffe, O. M. Yaghi, *Science* **2003**, *300*, 1127-1129.

[10] (a) J. S. Seo, D. Whang, H. Lee, S. I. Jun, J. Oh, Y. J. Jeon, K. Kim, *Nature* **2000**, *404*, 982-986; (b) Y. Inokuma, G.-H. Ning, M. Fujita, *Angew. Chem. Int. Ed.* **2012**, *51*, 2379-2381; (c) T. Kawamichi, T. Kodama, M. Kawano, M. Fujita, *Angew. Chem. Int. Ed.* **2008**, *47*, 8030-8032.

[11] M. D. Ward, *Nat. Chem.* **2010**, *2*, 610-611.

[12] (a) Q. W. Li, C. H. Sue, S. Basu, A. K. Shveyd, W. Y. Zhang, G. Barin, L. Fang, A. A. Sarjeant, J. F. Stoddart, O. M. Yaghi, *Angew. Chem. Int. Ed.* **2010**, *49*, 6751-6755; (b)

Q. Li, W. Zhang, O. Š. Miljanić, C.-H. Sue, Y.-L. Zhao, L. Liu, C. B. Knobler, J. F. Stoddart, O. M. Yaghi, *Science* **2009**, *325*, 855-859.

[13] O. M. Yaghi, M. O'Keeffe, N. W. Ockwig, H. K. Chae, M. Eddaoudi, J. Kim, *Nature* **2003**, *423*, 705-714.

[14] (a) F. Pointillart, T. Cauchy, O. Maury, Y. Le Gal, S. Golhen, O. Cador, L. Ouahab, *Chem. Eur. J.* **2010**, *16*, 11926-11941; (b) L. J. Zhang, D. H. Xu, Y. S. Zhou, F. Jiang, *New J. Chem.* **2010**, *34*, 2470-2478; (c) I. Binyamin, S. Pailloux, E. N. Duesler, B. M. Rapko, R. T. Paine, *Inorg. Chem.* **2006**, *45*, 5886-5892.

[15] L. L. Wen, D. B. Dang, C. Y. Duan, Y. Z. Li, Z. F. Tian, Q. J. Meng, *Inorg. Chem.* **2005**, *44*, 7161-7170.

[16] (a) J. Jia, A. J. Blake, N. R. Champness, P. Hubberstey, C. Wilson, M. Schröder, *Inorg. Chem.* **2008**, *47*, 8652-8664; (b) R. J. Hill, D.-L. Long, M. S. Turvey, A. J. Blake, N. R. Champness, P. Hubberstey, C. Wilson, M. Schroder, *Chem. Commun.* **2004**, 1792-1793; (c) D.-L. Long, R. J. Hill, A. J. Blake, N. R. Champness, P. Hubberstey, D. M. Proserpio, C. Wilson, M. Schröder, *Angew. Chem. Int. Ed.* **2004**, *43*, 1851-1854.

[17] V. N. Vukotic, K. J. Harris, K. Zhu, R. W. Schurko, S. J. Loeb, *Nat. Chem.* **2012**, *4*, 456-460.

[18] (a) D. J. Mercer, S. J. Loeb, *Dalton Trans.* **2011**, *40*, 6385-6887; (b) S. J. Loeb, *Chem. Commun.* **2005**, 1511-1518.

[19] D. J. Hoffart, S. J. Loeb, *Supramol. Chem.* **2007**, *19*, 89-93.

[20] H. J. Shepherd, I. y. A. Gural'skiy, C. M. Quintero, S. Tricard, L. Salmon, G. Molnár, A. Bousseksou, *Nat. Commun.* **2013**, *4*, 2607.

[21] (a) A. Coskun, M. Banaszak, R. D. Astumian, J. F. Stoddart, B. A. Grzybowski, *Chem. Soc. Rev.* **2012**, *41*, 19-30; (b) M. M. Boyle, R. A. Smaldone, A. C. Whalley, M. W. Ambrogio, Y. Y. Botros, J. F. Stoddart, *Chem. Sci.* **2011**, *2*, 204-210; (c) G. Barin, A. Coskun, D. C. Friedman, M. A. Olson, M. T. Colvin, R. Carmielli, S. K. Dey, O. A. Bozdemir, M. R. Wasielewski, J. F. Stoddart, *Chem. Eur. J.* **2011**, *17*, 213-222.

[22] (a) J. K. Sprafke, D. V. Kondratuk, M. Wykes, A. L. Thompson, M. Hoffmann, R. Drevinskas, W.-H. Chen, C. K. Yong, J. Kärnbratt, J. E. Bullock, M. Malfois, M. R. Wasielewski, B. Albinsson, L. M. Herz, D. Zigmantas, D. Beljonne, H. L. Anderson, *J. Am. Chem. Soc.* **2011**, *133*, 17262-17273; (b) M. C. O'Sullivan, J. K. Sprafke, D. V. Kondratuk, C. Rinfray, T. D. W. Claridge, A. Saywell, M. O. Blunt, J. N. O'Shea, P. H. Beton, M. Malfois, H. L. Anderson, *Nature* **2011**, *469*, 72-75.

[23] T. Nakamura, H. Ube, M. Shiro, M. Shionoya, *Angew. Chem. Int. Ed.* **2012**, *52*, 720-723.

[24] (a) T. Nakamura, H. Ube, M. Shionoya, *Angew. Chem. Int. Ed.* **2013**, *52*, 12096-12100; (b) N. Fujita, K. Biradha, M. Fujita, S. Sakamoto, K. Yamaguchi, *Angew. Chem. Int. Ed.* **2001**, *40*, 1718-1721.

[25] M. W. Hosseini, *Acc. Chem. Res.* **2005**, *38*, 313-323.

[26] E. Deiters, V. Bulach, N. Kyritsakas, M. W. Hosseini, *New J. Chem.* **2005**, *29*, 1508-1513.

[27] E. Deiters, V. Bulach, M. W. Hosseini, *Dalton Trans.* **2007**, 4126-4131.

[28] Z. Liu, M. Frasconi, J. Lei, Z. J. Brown, Z. Zhu, D. Cao, J. Iehl, G. Liu, A. C. Fahrenbach, Y. Y. Botros, O. K. Farha, J. T. Hupp, C. A. Mirkin, J. Fraser Stoddart, *Nat. Commun.* **2013**, *4*, 1855.

[29] S. Kennedy, G. Karotsis, C. M. Beavers, S. J. Teat, E. K. Brechin, S. J. Dalgarno, *Angew. Chem. Int. Ed.* **2010**, *49*, 4205-4208.

[30] N. L. Strutt, D. Fairen-Jimenez, J. Iehl, M. B. Lalonde, R. Q. Snurr, O. K. Farha, J. T. Hupp, J. F. Stoddart, *J. Am. Chem. Soc.* **2012**, *134*, 17436-17439.

[31] J. W. Steed, H. Zhang, J. L. Atwood, *Supramol. Chem.* **1996**, *7*, 37-45.

[32] N. J. Cookson, J. J. Henkelis, R. J. Ansell, C. W. G. Fishwick, M. J. Hardie, J. Fisher, *Dalton Trans.* **2014**, *43*, 5657-5661.

[33] C. Carruthers, J. Fisher, L. P. Harding, M. J. Hardie, *Dalton Trans.* **2010**, *39*, 355-357.

[34] (a) B. F. Abrahams, N. J. FitzGerald, R. Robson, *Angew. Chem. Int. Ed.* **2010**, *49*, 2896-2899; (b) B. F. Abrahams, B. A. Boughton, N. J. FitzGerald, J. L. Holmes, R. Robson, *Chem. Commun.* **2011**, *47*, 7404-7406.

[35] J.-T. Yu, J. Sun, Z.-T. Huang, Q.-Y. Zheng, *CrystEngComm* **2012**, *14*, 112-115.

[36] S. T. Mough, K. T. Holman, *Chem. Commun.* **2008**, 1407-1409.

[37] T. K. Ronson, H. Nowell, A. Westcott, M. J. Hardie, *Chem. Commun.* **2010**, *47*, 176-178.

[38] (a) L. Koskinen, S. Jaaskelainen, L. Oresmaa, M. Haukka, *CrystEngComm* **2012**, *14*, 3509-3514; (b) K. Kumar Bisht, A. Cherian Kathalikkattil, E. Suresh, *RSC Adv.* **2012**, *2*, 8421-8428; (c) A. Serpe, F. Artizzu, L. Marchiò, M. L. Mercuri, L. Pilia, P. Deplano, *Cryst. Growth Des.* **2011**, *11*, 1278-1286; (d) M. Dennehy, O. V. Quinzani, R. A. Burrow, *Acta Crystallogr., Sect. C* **2007**, *C63*, m395-m397.

[39] X. Liu, Guo, M.-L. Fu, X.-H. Liu, M.-S. Wang, J.-S. Huang, *Inorg. Chem.* **2006**, *45*, 3679-3685.

[40] V. J. Catalano, M. A. Malwitz, *Inorg. Chem.* **2003**, *42*, 5483-5485.

[41] G. S. M. Tong, S. C. F. Kui, H.-Y. Chao, N. Zhu, C.-M. Che, *Chem. Eur. J.* **2009**, *15*, 10777-10789.

[42] J. J. Henkelis, C. A. Kilner, M. A. Halcrow, *Chem. Commun.* **2011**, *47*, 5187-5189.

[43] G. N. Khairallah, R. A. J. O'Hair, *Dalton Trans.* **2005**, 2702-2712.

[44] V. A. Blatov, A. P. Shevchenko, V. N. Serezhkin, *J. Appl. Crystallogr.* **2000**, *33*, 1193.

[45] (a) W. H. Bragg, W. L. Bragg, *Proc. R. Soc. A* **1913**, *88*, 428-438; (b) W. L. Bragg, *Proc. R. Soc. A* **1913**, *89*, 248-277.

[46] E. D. Stevens, M. L. DeLucia, P. Coppens, *Inorg. Chem.* **1980**, *19*, 813-820.

[47] Y. Aray, J. Rodriguez, D. Vega, E. N. Rodriguez-Arias, *Angew. Chem. Int. Ed.* **2000**, *39*, 3810-3813.

[48] H. K. Chae, J. Kim, O. D. Friedrichs, M. O'Keeffe, O. M. Yaghi, *Angew. Chem. Int. Ed.* **2003**, *42*, 3907-3909.

[49] (a) M. Du, Z.-H. Zhang, L.-F. Tang, X.-G. Wang, X.-J. Zhao, S. R. Batten, *Chem. Eur. J.* **2007**, *13*, 2578-2586; (b) S. R. Batten, B. F. Hoskins, R. Robson, *Angew. Chem. Int. Ed.* **1995**, *34*, 820-822.

[50] (a) Y. Jin, F. Luo, Y. X. Che, J. M. Zheng, *Inorg. Chem. Commun.* **2008**, *11*, 711-713; (b) O. D. Friedrichs, M. O'Keeffe, O. M. Yaghi, *Solid State Sci.* **2003**, *5*, 73-78.

[51] A. F. Wells, *Three Dimensional Nets and Polyhedra*, Wiley, Chichester, **1997**.

[52] (a) J. L. C. Rowsell, A. R. Millward, K. S. Park, O. M. Yaghi, *J. Am. Chem. Soc.* **2004**, *126*, 5666-5667; (b) H. Furukawa, N. Ko, Y. B. Go, N. Aratani, S. B. Choi, E. Choi, A. O. Yazaydin, R. Q. Snurr, M. O'Keeffe, J. Kim, O. M. Yaghi, *Science* **2010**, *329*, 424-428.

[53] G. Mukherjee, K. Biradha, *Chem. Commun.* **2012**, *48*, 4293-4295.

[54] G. Mukherjee, K. Biradha, *Chem. Commun.* **2014**, *50*, 670-672.

[55] G.-P. Yang, L. Hou, Y.-Y. Wang, Y.-N. Zhang, Q.-Z. Shi, S. R. Batten, *Cryst. Growth Des.* **2011**, *11*, 936-940.

[56] D.-C. Zhong, W.-G. Lu, L. Jiang, X.-L. Feng, T.-B. Lu, *Cryst. Growth Des.* **2009**, *10*, 739-746.

[57] S.-R. Zheng, Q.-Y. Yang, Y.-R. Liu, J.-Y. Zhang, Y.-X. Tong, C.-Y. Zhao, C.-Y. Su, *Chem. Commun.* **2008**, 356-358.

[58] (a) A. P. Côté, A. I. Benin, N. W. Ockwig, M. O'Keeffe, A. J. Matzger, O. M. Yaghi, *Science* **2005**, *310*, 1166-1170; (b) J. W. Colson, A. R. Woll, A. Mukherjee, M. P. Levendorf, E. L. Spitler, V. B. Shields, M. G. Spencer, J. Park, W. R. Dichtel, *Science* **2011**, *332*, 228-231.

[59] H. A. Jahn, E. Teller, *Proc. R. Soc. A* **1937**, *161*, 220-235.

[60] A. W. Addison, T. N. Rao, J. Reedijk, J. van Rijn, G. C. Verschoor, *J. Chem. Soc., Dalton Trans.* **1984**, 1349-1356.

[61] (a) M. A. Little, J. Donkin, J. Fisher, M. A. Halcrow, J. Loder, M. J. Hardie, *Angew. Chem. Int. Ed.* **2011**, *51*, 764-766; (b) P. Berthault, H. Desvaux, T. Wendlinger, M. Gyejacquot, A. Stopin, T. Brotin, J.-P. Dutasta, Y. Boulard, *Chem. Eur. J.* **2010**, *16*, 12941-12946.

[62] (a) O. Taratula, P. A. Hill, N. S. Khan, P. J. Carroll, I. J. Dmochowski, *Nat. Commun.* **2010**, *1*, 148; (b) G. Haberhauer, Á. Pintér, S. Woitschetzki, *Nat. Commun.* **2013**, *4*, 2945.

[63] (a) E. Huerta, H. Isla, E. M. Perez, C. Bo, N. Martin, J. de Mendoza, *J. Am. Chem. Soc.* **2010**, *132*, 5351-5353; (b) E. Huerta, G. A. Metselaar, A. Fragoso, E. Santos, C. Bo, J. de Mendoza, *Angew. Chem. Int. Ed.* **2007**, *46*, 202-205; (c) E. Huerta, E. Cequier, J. de Mendoza, *Chem. Commun.* **2007**, 5016-5018.

[64] R. M. Fairchild, K. T. Holman, *J. Am. Chem. Soc.* **2005**, *127*, 16364-16365.

[65] S. Zarra, M. M. J. Smulders, Q. Lefebvre, J. K. Clegg, J. R. Nitschke, *Angew. Chem. Int. Ed.* **2012**, *51*, 6882-6885.

[66] I. A. Riddell, M. M. J. Smulders, J. K. Clegg, Y. R. Hristova, B. Breiner, J. D. Thoburn, J. R. Nitschke, *Nat. Chem.* **2012**, *4*, 751-756.

[67] A. Sørensen, A. M. Castilla, T. K. Ronson, M. Pittelkow, J. R. Nitschke, *Angew. Chem. Int. Ed.* **2013**, *52*, 11273-11277.

[68] J. Nitschke, T. Ronson, S. Zarra, S. P. Black, *Chem. Commun.* **2012**, *49*, 2476-2490.

[69] D. Farrusseng, S. Aguado, C. Pinel, *Angew. Chem. Int. Ed.* **2009**, *48*, 7502-7513.

[70] W. E. Hatfield, J. S. Paschal, *J. Am. Chem. Soc.* **1964**, *86*, 3888-3889.

[71] W. E. Hatfield, Y. Muto, H. B. Jonassen, J. S. Paschal, *Inorg. Chem.* **1965**, *4*, 97-99.

[72] R. Whyman, D. B. Copley, W. E. Hatfield, *J. Am. Chem. Soc.* **1967**, *89*, 3135-3141.

[73] R. S. Sager, R. J. Williams, W. H. Watson, *Inorg. Chem.* **1969**, *8*, 694-696.

[74] W. H. Watson, *Inorg. Chem.* **1969**, *8*, 1879-1886.

[75] J. C. Green, M. L. H. Green, G. Parkin, *Chem. Commun.* **2012**, *48*, 11481-11503.

[76] G. Xu, X. Zhang, P. Guo, C. Pan, H. Zhang, C. Wang, *J. Am. Chem. Soc.* **2010**, *132*, 3656-3657.

[77] R. Puttreddy, P. J. Steel, *CrystEngComm* **2014**, *16*, 556-560.

[78] M. J. Hardie, R. Ahmad, C. J. Sumby, *New J. Chem.* **2005**, *29*, 1231-1240.

[79] T. K. Ronson, M. J. Hardie, *CrystEngComm* **2008**, *10*, 1731-1734.

[80] X. Jiang, Z. Li, Y. Zhai, G. Yan, H. Xia, Z. Li, *CrystEngComm* **2014**, *16*, 805-813.

[81] Y. B. Go, X. Wang, A. J. Jacobson, *Inorg. Chem.* **2007**, *46*, 6594-6600.

[82] J. M. McBride, R. L. Carter, *Angew. Chem. Int. Ed.* **1991**, *30*, 293-295.

[83] (a) J. J. Henkelis, T. K. Ronson, L. P. Harding, M. J. Hardie, *Chem. Commun.* **2011**, *47*, 6560-6562; (b) T. K. Ronson, J. Fisher, L. P. Harding, M. J. Hardie, *Angew. Chem. Int. Ed.* **2007**, *46*, 9086-9088; (c) C. J. Sumby, M. J. Hardie, *Angew. Chem. Int. Ed.* **2005**, *44*, 6395-6399.

[84] M. Alajarin, R.-A. Orenes, J. W. Steed, A. Pastor, *Chem. Commun.* **2010**, *46*, 1394-1403.

[85] (a) J.-T. Yu, Y.-Y. Shi, J. Sun, J. Lin, Z.-T. Huang, Q.-Y. Zheng, *Sci. Rep.* **2013**, *3*, 2947; (b) K. K. Bisht, E. Suresh, *J. Am. Chem. Soc.* **2013**, *135*, 15690-15693.

[86] M. J. Hardie, *Chem. Soc. Rev.* **2010**, *39*, 516-527.

[87] (a) M. J. Hardie, C. L. Raston, *Chem. Commun.* **1999**, 1153-1163; (b) M. J. Hardie, C. L. Raston, *Cryst. Growth Des.* **2001**, *1*, 53-58.

[88] (a) M. A. Little, M. A. Halcrow, M. J. Hardie, *Chem. Commun.* **2013**, *49*, 1512-1514; (b) J. Canceill, L. Lacombe, A. Collet, *J. Chem. Soc., Chem. Commun.* **1987**, 219-221.

[89] (a) C. Carruthers, T. K. Ronson, C. J. Sumby, A. Westcott, L. P. Harding, T. J. Prior, P. Rizkallah, M. J. Hardie, *Chem. Eur. J.* **2008**, *14*, 10286-10296; (b) M. J. Hardie, R. M. Mills, C. J. Sumby, *J. Org. Biol. Chem.* **2004**, *2*, 2958-2964.

[90] (a) Y. Zhao, T. M. Swager, *J. Am. Chem. Soc.* **2013**, *135*, 18770-18773; (b) M. J. Hardie, C. L. Raston, *J. Chem. Soc., Dalton Trans.* **2000**, 2483-2492; (c) J. L. Atwood, L. J. Barbour, C. L. Raston, I. B. N. Sudria, *Angew. Chem. Int. Ed.* **1998**, *37*, 981-983.

[91] H. Zhang, Y. Zhao, *Chem. Eur. J.* **2013**, *19*, 16862-16879.

[92] (a) A. Szumna, *Chem. Soc. Rev.* **2010**, *39*, 4274-4285; (b) S. T. Schneebeli, C. Cheng, K. J. Hartlieb, N. L. Strutt, A. A. Sarjeant, C. L. Stern, J. F. Stoddart, *Chem. Eur. J.* **2013**, *19*, 3860-3868.

[93] M. A. Little, M. A. Halcrow, L. P. Harding, M. J. Hardie, *Inorg. Chem.* **2010**, *49*, 9486-9496.

[94] (a) S. Shanmugaraju, V. Vajpayee, S. Lee, K.-W. Chi, P. J. Stang, P. S. Mukherjee, *Inorg. Chem.* **2012**, *51*, 4817-4823; (b) C. J. Kuehl, S. D. Huang, P. J. Stang, *J. Am. Chem. Soc.* **2001**, *123*, 9634-9641; (c) C. J. Kuehl, C. L. Mayne, A. M. Arif, P. J. Stang, *Org. Lett.* **2000**, *2*, 3727-3729.

[95] M. Fujita, F. Ibukuro, H. Hagihara, K. Ogura, *Nature* **1994**, *367*, 720-723.

[96] M. A. Little, T. K. Ronson, M. J. Hardie, *Dalton Trans.* **2011**, *40*, 12217-12227.

[97] M. Fujita, M. Tominaga, A. Hori, B. Therrien, *Acc. Chem. Res.* **2005**, *38*, 369-378.

[98] X.-J. Kong, Y.-P. Ren, P.-Q. Zheng, Y.-X. Long, L.-S. Long, R.-B. Huang, L.-S. Zheng, *Inorg. Chem.* **2006**, *45*, 10702-10711.

[99] (a) D. Sun, Q.-J. Xu, C.-Y. Ma, N. Zhang, R.-B. Huang, L.-S. Zheng, *CrystEngComm* **2010**, *12*, 4161-4167; (b) Z.-H. Zhang, S.-C. Chen, J.-L. Mi, M.-Y. He, Q. Chen, M. Du, *Chem. Commun.* **2010**, *46*, 8427-8429.

[100] M. J. Hardie, C. J. Sumby, *Inorg. Chem.* **2004**, *43*, 6872-6874.

[101] C. J. Sumby, M. J. Hardie, *Cryst. Growth Des.* **2005**, *5*, 1321-1324.

[102] (a) G. Sheldrick, *Acta Crystallogr., Sect. A* **2008**, *A64*, 112-122; (b) L. J. Barbour, *Supramol. Chem.* **2001**, *1*, 189-191.

[103] Persistence of Vision Raytracer Pty. Ltd. Williamstown, 2004.

[104] A. L. Spek, *Acta Crystallogr. Sect. A.* **1990**, *A46*, 194-201.

Chapter 4

Towards the preparation of M_3L_2 metallo-cryptophanes

4.1 Introduction

Since the realisation of host-guest chemistry,[1] the preparation of synthetic receptors has remained an interesting challenge that spans the biological [2] and physical [3] sciences. Their ability for selective molecular recognition [4] has led to a variety of applications that include catalysis,[5] drug delivery [6] and small molecule separation,[7] to name a few.

Cryptophanes are organically-linked and C_3-symmetric capsules that are afforded through a head-to-head arrangement of cyclotriveratrylene (CTV) units.[8] In such species, the inherent hosting ability of the tribenzo[*a*,*d*,*g*]cyclononatriene core [9] is amplified by proximity and orientation effects, where guests bind by an 'induced fit' mechanism.[10] CTV is axially chiral and exists as a pair of enantiomers, ***M*** (minus) and ***P*** (plus), **Figure 4.1**.[11] Thus, cryptophanes possess two stereocentres, affording four possible stereoisomers (***MM***, ***MP***, ***PM*** and ***PP***) that are comprised of two diastereoisomers, *syn* (***MP*** and ***PM***) and *anti* (***MM*** and ***PP***). The *syn* diastereoisomer features the inclusion of both enantiomers of ligand and is therefore achiral (optically inactive). Irrespective of their relative orientation, ***MP*** and ***PM*** stereoisomers both display at least one plane of symmetry and are therefore *meso* (***m***) compounds. However, the *anti* stereoisomers ***MM*** and ***PP*** are each composed of a single ligand enantiomer and are therefore enantiomers. They may be described in terms of helical chirality, where the ***MM*** possesses right-handed helicity (***Δ***) and the ***PP*** enantiomer possesses left-handed helicity (***Λ***). Generally, the *syn* and *anti* cryptophane diastereoisomers possess C_{3h} and D_3 molecular symmetry,[12] respectively, **Figure 4.1**.

The hosting ability of cryptophanes is proportional to their size; where the smallest bind gases, such as methane [13] and xenon,[14] and the largest bind small organic molecules, such as chloroform, **Figure 4.1**.[15] However, a cryptophane capable of simultaneously binding two molecules, or having the ability to distinguish between guests, has yet to be identified.

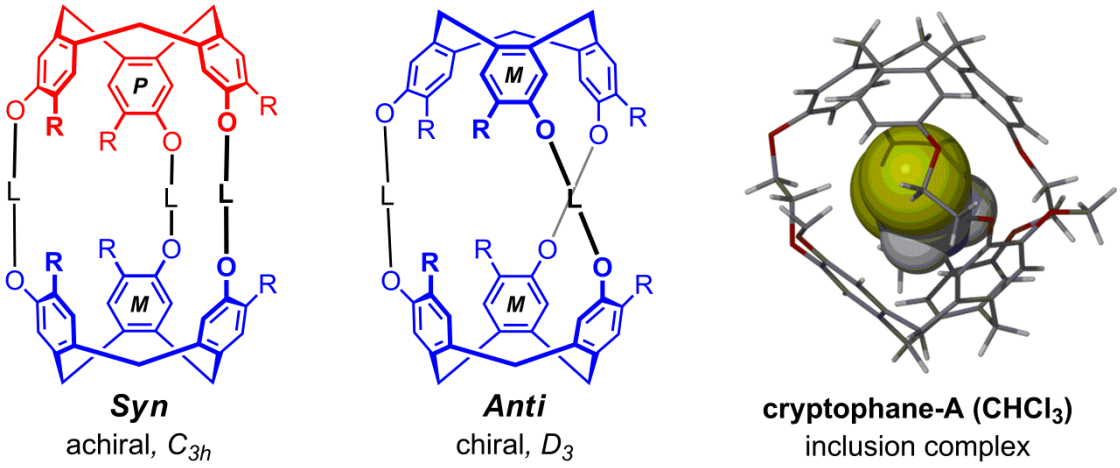

Figure 4.1 *The syn and anti cryptophane diastereoisomers, where L=organic linker and individual CTV enantiomers are colour-coded for clarity. Only the* ***Λ****-anti enantiomer is shown. The encapsulated chloroform molecule in the cryptophane-A ($CHCl_3$) inclusion complex is displayed in space-filling mode to indicate the 'induced fit'.*[16]

There is great potential, however, in $[M_3L_2]^{n+}$ metallo-cryptophanes as self-assembled 'nanohosts' for sophisticated host-guest and recognition chemistry.[17] These species have the same head-to-head orientation of CTV units as classical cryptophanes but are instead bridged with three metallic linkers.[18] Being trigonal bipyramidal in shape, they also possess a similarly well defined and hydrophobic internal cavity, although significantly larger, which greatly increases the scope for potential application. An attractive advantage of metallo-cryptophanes over their classical counterparts is their formation *via* metal mediated self-assembly, which negates the convoluted and often pyrrhic multistep syntheses that would be necessary to prepare classical cryptophanes of the same size.

The first metallo-cryptophane, reported by Shinkai and co-workers, features a head-to-head arrangement of *tris*(4-pyridyl)cyclotriguaiacylene (CTG) ligands, linked through metal coordination by three *cis*-protected palladium(II) metal centres.[19] Of the other metallo-cryptophanes prepared, none display the ability to host molecules. Ronson *et al.* have prepared a 'bow-tie' metallocryptophane from a carboxylate functionalised CTV,[20] where instead of dimerising to afford a hollow capsule, it is 'pinched' owing to the presence of a bridging metallic cluster. Two metallo-cryptophanes are then linked by the ligand 1,2-*bis*(4-pyridyl)ethylene to afford the 'bow-tie' motif, **Figure 4.2a**. Whilst this species may show magnetic properties, the lack of internal space limits host-guest application. Likewise, the *anti*-metallo-cryptophane afforded from the self-assembly of *tris*(4-phenyl-5-pyrimidyl)CTG with silver(I) cations was isolated upon crystallisation only, and not observed to exist in the solution-phase, **Figure 4.2b**.[21]

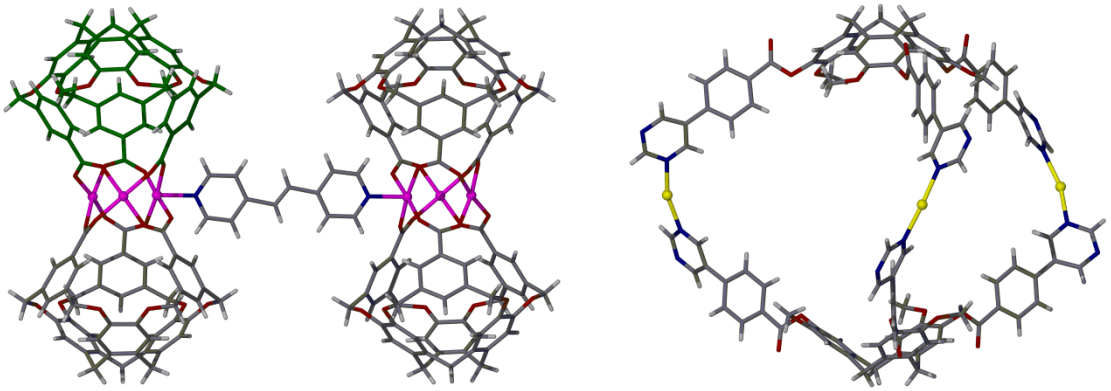

Figure 4.2 *Metallo-cryptophanes prepared by Ronson et al. (a) Two 1,2-bis(4-pyridyl)-ethylene bridged $[Cu_3(L)_2]$ syn-cryptophanes to afford the 'bow-tie' appearance. One functionalised CTV ligand is distinguished by colour;*[20] *(b) anti-cryptophane (Δ)-$[Ag_3(L)_2]\cdot 3(ClO_4)$.*[21]

Finally, although not strictly metallocryptophanes, Stang and co-workers have utilised the tripodal ligand *tris*(4-pyridyl)adamantane to prepare C_{3h} and D_{3h} $[M_3L_2]^{n+}$ trigonal bipyramidal cages using a *cis*-Pd(II) tecton [22] and a dinuclear organometallic Pt(II) 'metallic clip', respectively.[23] More recently, Scarso and co-workers have suggested a possible solution-phase structure of a chiral $[M_3L_2]^{n+}$ cage, formed *via* the self-assembly of an optically pure *tris*(4-pyridyl)benzotricamphor and *cis*-Pt(II) tecton, but have not remarked on its hosting abilities.[24]

In a similar approach to Shinkai and co-workers, ligands (±)-2,7,12-trimethoxy-3,8,13-*tris*(3-pyridylmethyloxy)-10,15-dihydro-5*H*-tribenzo[*a*,*d*,*g*]cyclononatriene (**2.6**), (±)-2,7,12-trimethoxy-3,8,13-*tris*(3-carboxypyridyl)-10,15-dihydro-5*H*-tribenzo[*a*,*d*,*g*]cyclononatriene (**2.7**) and (±)-2,7,12-trimethoxy-3,8,13-*tris*(4-carboxypyridyl)-10,15-dihydro-5*H*-tribenzo[*a*,*d*,*g*]cyclononatriene (**2.8**) of Chapter 2 were predicted to form $[M_3L_2]^{n+}$ metallo-cryptophanes with linear and 90 ° tectons, respectively, **Scheme 4.1**. Their potential hosting abilities were envisaged to be applicable in areas such as catalysis and molecular separations.

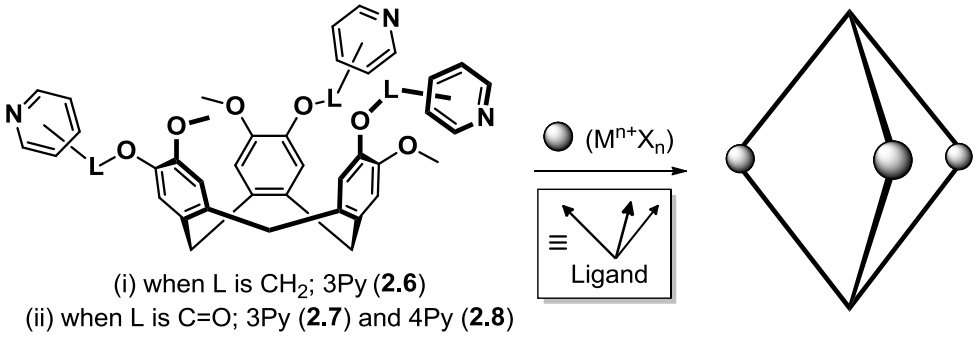

Scheme 4.1 *The predicted formation of $[M_3L_2]^{n+}$ metallo-cryptophanes from tripodal C_3-symmetric ligands(**2.6**-**2.8**) and metal cations.*

4.2 Isolation of a triply-interlocked [2]-catenane, $[Ag_6(\mathbf{2.6})_4]\cdot 6(ClO_4)\cdot n(DMF)$

The reaction of ligand **2.6** with silver(I) perchlorate (ClO_4^-) in *N,N'*-dimethylformamide (DMF) afforded a topologically complex and triply-interlocked [2]-catenane, $[Ag_6(\mathbf{2.6})_4]\cdot 6(ClO_4)\cdot n(DMF)$, complex **4.1**. Single crystals were obtained by diffusing diethyl ether vapours into a DMF solution of the complex and analysed by single crystal diffraction methods. The structure solved in the monoclinic space group *Cc* and displayed the asymmetric unit as the composition stated above, comprising two mechanically interlocked, but chemically independent, *anti*-$[Ag_3(\mathbf{2.6})_2]^{3+}$ metallo-cryptophanes, **Figure 4.3**.

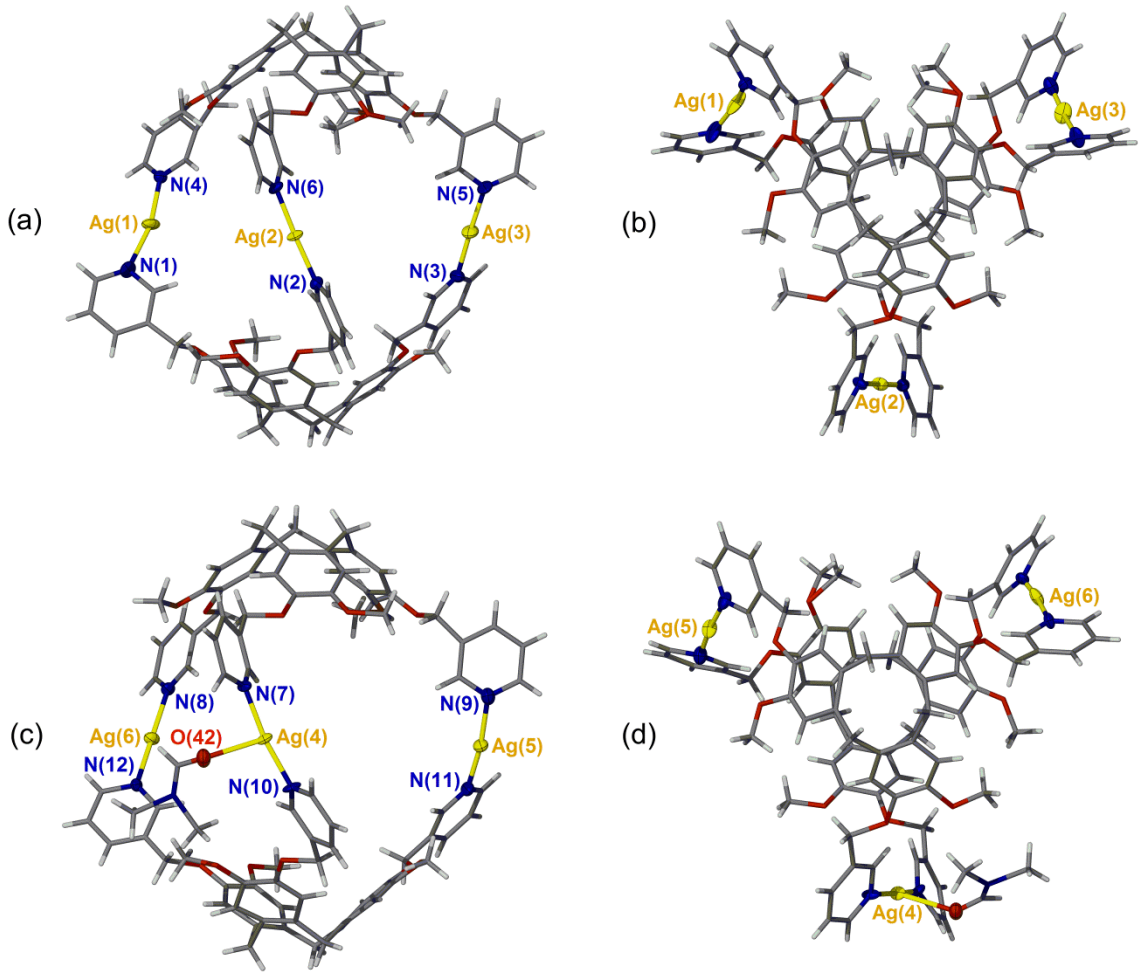

Figure 4.3 *Individual (Λ)-$[Ag_3(\mathbf{2.6})_2]^{3+}$ metallo-cryptophanes from the crystal structure of complex **4.1**. Identical cages, as viewed from the side (a, c), and above (b, d). All perchlorate anions and solvent DMF have been omitted for clarity.*

Each trigonal bipyramidal *anti*-$[Ag_3(\mathbf{2.6})_2]^{3+}$ cage is composed of two **2.6** ligands, bridged by approximately linear Ag(I) cations in a head-to-head orientation, with N-Ag-N bond angles and N-Ag bong lengths ranging 165.1(4) to 176.9(4) ° and 2.107(6) to 2.311(10) Å, respectively. One silver(I) centre also features a long contact to a DMF ligand at O-Ag separation 2.580(13)

Å. Selected bond metrics for complex **4.1** are given below in **Table 4.1**. In addition, there are six perchlorate anions, disordered across seven molecular positions, and three molecules of solvent DMF in the asymmetric unit. The inclusion of a single ligand enantiomer (***P***) affords two *anti*-metallo-cryptophanes which possess a left-handed (***M***) chirality, (***M***)-$[Ag_3(\mathbf{2.6})_2]^{3+}$.

Ag(1)-N(1)	2.363(10)	Ag(6)-N(8)	2.154(7)
Ag(1)-N(4)	2.117(8)	Ag(6)-N(12)	2.118(4)
Ag(2)-N(2)	2.131(7)	Ag(4)-O(42)	2.544(14)
Ag(2)-N(6)	2.102(5)	N(1)-Ag(1)-N(4)	164.2(4)
Ag(3)-N(3)	2.198(9)	N(2)-Ag(2)-N(6)	177.3(3)
Ag(3)-N(5)	2.161(9)	N(3)-Ag(3)-N(5)	177.0(4)
Ag(4)-N(7)	2.202(11)	N(7)-Ag(4)-N(10)	100.7(4)
Ag(4)-N(10)	2.172(6)	N(9)-Ag(5)-N(11)	171.6(4)
Ag(5)-N(9)	2.231(6)	N(8)-Ag(6)-N(12)	173.2(3)
Ag(5)-N(11)	2.123(7)		

Table 4.1 *Selected bond lengths (Å) and angles (°) from the crystal structure of complex* ***4.1***

Individual (***M***)-$[Ag_3(\mathbf{2.6})_2]^{3+}$ cryptophanes interlock to afford the [2]-catenane, $[Ag_6(\mathbf{2.6})_4]^{6+}$, **Figure 4.4**. This interlocking proceeds in the absence of a template, and there are no formal interactions between each metallo-cryptophane of the [2]-catenane. Despite their close proximity, aromatic and argentophilic separations are all outside of the 4 and 3.3 Å maxima, respectively.[25] This is unusual, as the majority of interlocked species are afforded *via* 'template directed' syntheses [26] which perhaps indicates a highly complex threading and interlocking mechanism. Catenation in this instance is likely entropically driven,[27] where the interlocking of each (***M***)-$[Ag_3(\mathbf{2.6})_2]^{3+}$ cage expels high energy solvent from within the cavity; however, symmetry-driven self-recognition is also observed.[28]

It is interesting that the [2]-catenane, (***M***,***M***)-$[Ag_6(\mathbf{2.6})_4]^{6+}$, is also enantiomerically pure and that the overall left-handed helical chirality and D_3-symmetry are conserved, especially given its formation without a template, **Figure 4.4**. Whilst spontaneous chiral resolution is an understood phenomenon, especially with derivatised CTVs,[29] it is usually as a result of additional directing factors. In this particular instance, a racemic mixture of **2.6** ligands has assembled into one interlocked species containing ten molecular components and with complete enantiomeric control. Similar phenomena have been noted by Nitschke and co-workers, where enantiopure metal complexes are afforded through stereochemical conservation and chiral induction; however, these are 'through-bond' examples and not mechanically interlocked.[30]

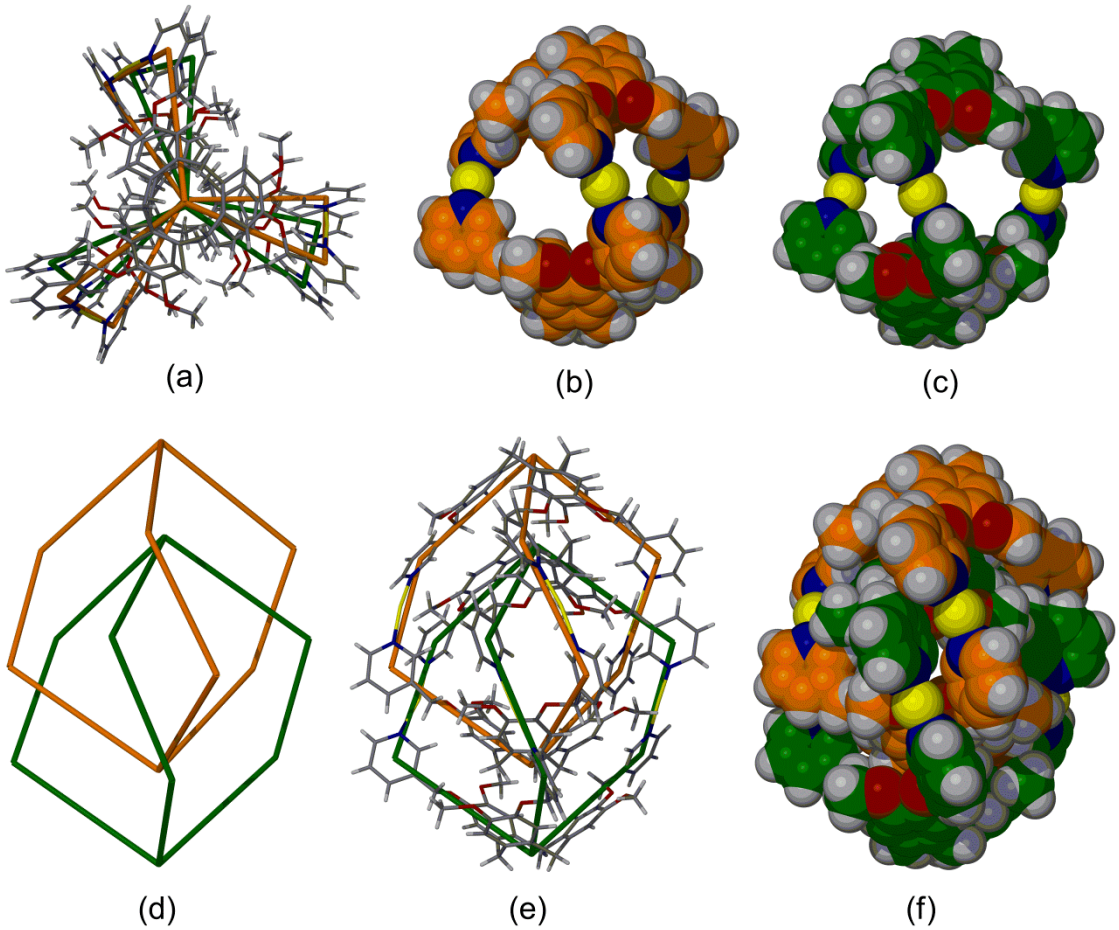

Figure 4.4 *From the crystal structure of complex* ***4.1****. The mutually left-handed (**Λ**, **Λ**) helical arrangement of both interlocked cages in the [2]-catenane, as viewed from the top (a) and side (e). Orange and green wire frames denote the independent metallo-cryptophanes. Individual (**Λ**)-[Ag$_3$(**2.6**)$_2$]$^{3+}$ cages of the [2]-catenane are shown in orange (b) and green (c) space-filling images, respectively. The [2]-catenane, (**Λ**,**Λ**)-[Ag$_6$(**2.6**)$_4$]$^{6+}$, is simplified by wire frames (d) and shown in space-filling mode (f). All perchlorate anions and solvent are omitted for clarity.*

Each [2]-catenane possesses four stereocentres and thus affords sixteen possible stereoisomers and eight diastereoisomers. The interlocking of any *anti* (**Δ** or **Λ**) metallo-cryptophane with a *syn* (***m***) metallo-cryptophane is always chiral, yet possesses no helical chirality and therefore has only C_1-symmetry; however, the interlocking of two chiral cages (**Δ** or **Λ**) affords enantiomers (**Δ**,**Δ**)-[Ag$_6$(**2.6**)$_4$]$^{6+}$ and (**Λ**,**Λ**)-[Ag$_6$(**2.6**)$_4$]$^{6+}$ where helical chirality and D_3-symmetry are conserved, **Figure 4.5**. Similar helical chirality is often shown in metal helicates [31] and mesocates.[32] Interestingly, the interlocking of (**Δ**)-[Ag$_3$(**2.6**)$_2$]$^{3+}$ and (**Λ**)-[Ag$_3$(**2.6**)$_2$]$^{3+}$ theoretically affords the [2]-catenane (**Δ**,**Λ**)-[Ag$_6$(**2.6**)$_4$]$^{6+}$, which is chemically achiral but rigidly chiral in every possible physical conformation, a phenomenon described by Mislow as a 'Euclidean rubber glove'.[33]

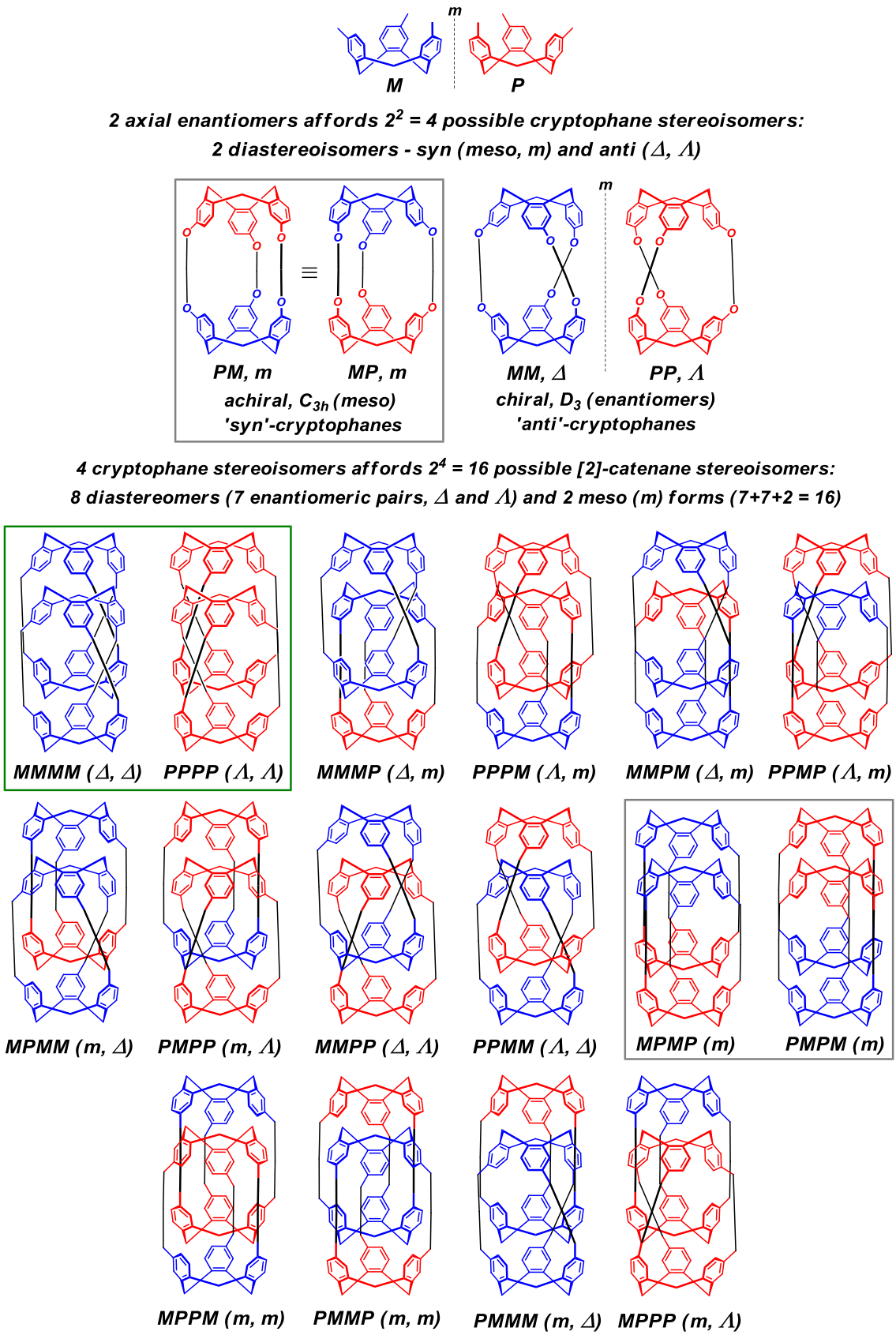

Figure 4.5 *All theoretical conformations of the [2]-catenane,* $[Ag_6(\mathbf{2.6})_4]^{6+}$. *Stereoisomers in grey boxes are meso (**m**) compounds and the homochiral enantiomers in the green box represent complex **4.1**.*

The depiction of all possible [2]-catenanes implies that conversion between various topological stereoisomers would require bond cleavage.[34] This is likely the case, and the lability of the Py-Ag bond and flexibility of the ethereal linkage may facilitate the formation of only one product, where the formation of all possible stereoisomers are removed by self-correction as self-assembly proceeds towards a thermodynamic sink.[27] This may be driven by the higher symmetry of both the *anti*-metallo-cryptophane and corresponding (***Δ***,***Δ***)- and (***Λ***,***Λ***)-[2]-catenanes, which are therefore favoured according to a more positive entropy of symmetry.[28]

Complexes of derivatised CTVs regularly display complementary self-recognition [35] between the tribenzo[*a*,*d*,*g*]cyclononatriene cores of the ligands, where they stack in a bowl-in-bowl manner. This is evident in the [2]-catenane, ***(Λ,Λ)***-$[Ag_6(\mathbf{2.6})_4]^{6+}$, where the hydrophobic core of one ligand plays host to the underside of another, with aromatic centroid separations of 4.723 Å, akin to the β-phase of CTV.[9] This intramolecular host-guest behaviour is pair-wise and occurs between the two chemically independent (***Λ***)-$[Ag_3(\mathbf{2.6})_2]^{3+}$ metallo-cryptophanes.

Whilst only the single enantiomer ***(Λ,Λ)***-$[Ag_6(\mathbf{2.6})_4]^{6+}$ was found in the asymmetric unit, the *c* glide plane within the monoclinic space group (*Cc*) generates a mirror plane; in doing so, the opposite enantiomer ***(Δ,Δ)***-$[Ag_6(\mathbf{2.6})_4]^{6+}$ is generated by symmetry in equal proportions to render complex **4.1** a racemate. The ***(Δ,Δ)***-$[Ag_6(\mathbf{2.6})_4]^{6+}$ and ***(Λ,Λ)***-$[Ag_6(\mathbf{2.6})_4]^{6+}$ enantiomers are identical, and differ only in their absolute stereochemical configuration. Additionally, whilst this is a phenomenon of crystallisation, there is no way of conclusively stating that only the enantiopure [2]-catenanes are afforded, or if there are other stereoisomers present in solution.[36] Crystals with similar unit cell parameters were also obtained from a DMSO solution, and when employing the similarly non-coordinating tetrafluoroborate (BF_4^-) and hexafluorophosphate (PF_6^-) anions. Likewise, alterations to reaction concentration did not change the self-assembly processes and spontaneous catenation was always observed. Regardless, the serendipitous formation of complex **4.1** suggests a self-assembly mechanism that is still not very well understood.

The internal volume of the [2]-catenane was estimated from its crystal structure [37] and calculated to be 197 $Å^3$; however, there are no solvent molecules located within the cavity and there are limited windows to allow for guest exchange. Interpenetration of the individual $[Ag_3(\mathbf{2.6})_2]^{3+}$ metallo-cryptophanes significantly reduces the internal space available to host molecules and, by considering the packing requirements according to Rebek and co-workers,[38] estimates an ideal guest size of 108 $Å^3$, which is too small for the applications discussed above.

Complex **4.1** represents the second triply-interlocked [2]-catenane composed of derivatised CTVs to date. The other example, (±)-$[Zn_6(\mathbf{L})_4(NO_3)_6]\cdot 6(NO_3)$, where L = *tris*(4-(4'-methyl-

2,2'-bipyridyl)-benzyloxy)cyclotriguaiacylene, features a similar 3D appearance and is comprised of two interlocking *syn*-metallo-cryptophanes, **Figure 4.6**.[39] This is a peculiar example, as each *syn*-$[Zn_3(\mathbf{L})_2(NO_3)_3]^{3+}$ cage is actually chiral, owing to the left-handed helical chirality (***Λ***) about the zinc(II) coordination environment, which removes the horizontal mirror plane expected for the *syn*-metallo-cryptophane. The resultant [2]-catenane is chiral, owing to the inequivalence of the ***PMMP*** and ***MPPM*** orientations of ligand enantiomers. However, by catenating, opposing helices are not constructive and generate both a mirror plane and C_2-rotation axis. This can be viewed graphically in **Figure 4.5**, above. This example again features self-inclusion motifs and displays a bowl-in-bowl stacking conformation of ligands, although between different enantiomers, and also features six instances of hydrogen bonding between nitrate anion and methyl moiety of the individual cages.

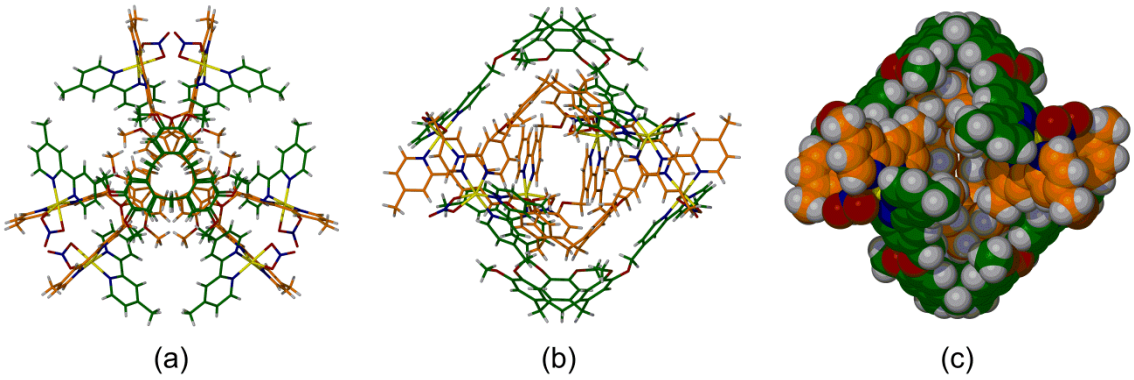

Figure 4.6 *Triply-interlocked [2]-catenane prepared by Westcott and co-workers, as viewed from above (a), the side (b) and in space-filling mode (c). The different enantiomers of ligand are distinguished by colour.*[39]

The first prominent example of a [2]-catenane was reported by Sauvage and co-workers in 1983.[40] It was constructed through templation, where two functionalised 1,10-phenanthroline ligands containing reactive termini were brought together through copper(I) coordination. Then, *via* a high-dilution cyclisation, the rings were clipped together to create an interlocked metal complex. The addition of acid or a suitable competing ligand removed the copper(I) centre to leave two mechanically interlocked and chemically independent rings. A labile metal as active template is not always necessary and the first examples of lanthanide(III)-containing [2]- and [3]-catenanes have been prepared by Gunnlaugsson and co-workers,[41] using ring closing metathesis to interlock the rings. A similar methodology has been used by Beer and co-workers [42] which uses chloride anions as the active template, **Figure 4.7a**.

An organic template methodology was developed by Stoddart and co-workers, utilising complementary aromatic interactions between interlocking species.[43] The electron rich *bis*-(*para*phenylene) macrocycle formed a host-guest complex with an electron poor and

bifunctionalised viologen, which was then cyclised to give the [2]-catenane. This approach has been utilised by Quintela and Peinador in the formation of a doubly-interlocked [2]-catenane,[44] where an electron poor diazapyrenium macrocycle is doubly interlocked by an electron rich crown ether, again facilitated by donor:acceptor aromatic interactions, **Figure 4.7b**. Similarly, Cooper and co-workers have prepared wholly-organic and triply interlocked [2]-catenanes using dynamic imine bond formation, which display host-guest properties in the solid state, **Figure 4.7c**.[49]

More similarly to the interlocking mechanics of complex **4.1**, Fujita and co-workers have demonstrated that a supramolecular palladacycle would spontaneously interlock to afford a [2]-catenane in DMSO solution.[45] This methodology was later exemplified in the construction of the first triply-interlocked [2]-catenane.[46] Here, two $[Pd_3(\mathbf{L})_2]^{6+}$ metallo-cages, where L = 1,3,5-*tris*(4-pyridylmethyl)triazine, spontaneously undergo a supramolecular reorganisation to afford the [2]-catenane, facilitated by the formation of four constructive aromatic interactions within the resultant complex. More recently, Clever and co-workers have succeeded in forming quadruply-interlocked [2]-catenanes from ditopic pyridyl-functionalised ligands and palladium(II) cations, **Figure 4.7d**.[47] In these examples, catenation can also be enhanced by anion binding and sequentially controlled through guest selectivity.[48]

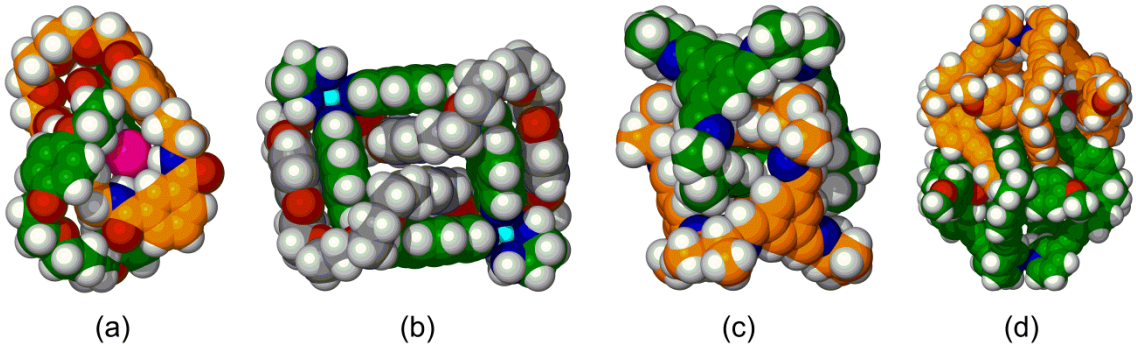

Figure 4.7 *Examples of other notable [2]-catenanes. Chemically independent components are distinguished by colour. (a) Beer's chloride-templated [2]-catenane;[42] (b) Quintela's doubly-interlocked [2]-catenane;[44] (c) Cooper's triply-interlocked organic [2]-catenane;[49] (d) Clever's quadruply-interlocked [2]-catenane.[47]*

Complex **4.1** was also identified to exist in the solution-phase, where the procured NMR and mass spectra were both symptomatic of catenation.[39] All ^{1}H NMR reactions of ligand **2.6** and silver(I) perchlorate in d_7-DMF afforded broad spectra that did not sharpen with time, **Figure 4.8**. Coordination-induced shifts were evident, yet well defined resonances were not observed. A simple metallo-cryptophane would be expected to have either C_{3h} or D_3 molecular symmetry, which would likely give rise to well-defined NMR spectra, and so its sole formation is unlikely. However, it is not clear whether the broadened resonances are attributable to multiple species in

solution or simply as a result of the chemically inequivalent protons of the [2]-catenane. Likewise, it is not possible to comment on the chirality of the [2]-catenane based on NMR measurements. Similarly to the solid state analysis, the solution-phase behaviour of complex **4.1** was seen to be consistent in d_6-DMSO and independent of the counter anion employed.

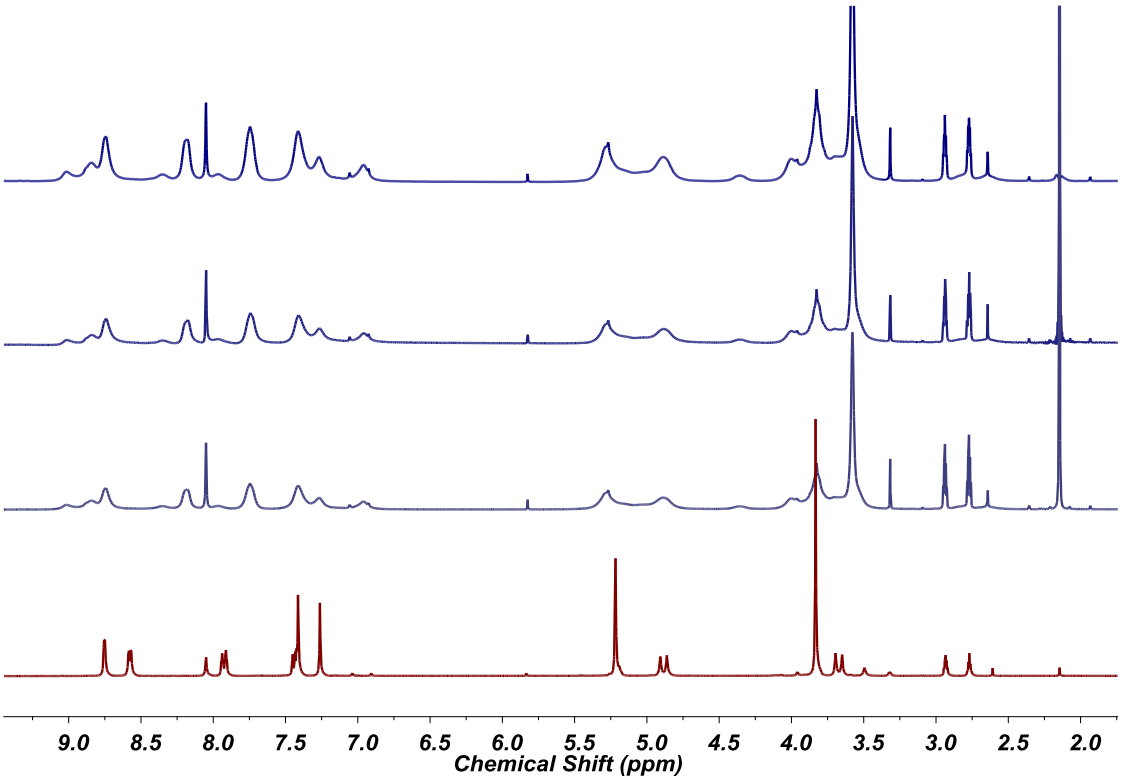

Figure 4.8 *^{1}H NMR spectra of ligand **2.6** (red) and timecourse formation of complex **4.1** (blue traces, increasing with time over one week) in d_7-DMF.*

Electrospray mass spectrometry of the complex mixture was indicative of multiple species present in the gas phase. Mass peaks of (*m/z*) 1887.2, 2567.5, 2774.3, 3457.6 and 3663.4 were identified and attributed to $\{Ag_3(\mathbf{2.6})_2(ClO_4)_2\}^+$, $\{Ag_3(\mathbf{2.6})_3(ClO_4)_2\}^+$, $\{Ag_4(\mathbf{2.6})_3(ClO_4)_3\}^+$, $\{Ag_4(\mathbf{2.6})_4(ClO_4)_3\}^+$, and $\{Ag_5(\mathbf{2.6})_4(ClO_4)_4\}^+$, respectively. Whilst this provides excellent evidence for catenation and the formation of higher order species in the gas phase, it is impossible to say whether the presence of $\{Ag_3(\mathbf{2.6})_2(ClO_4)_2\}^+$ in the mass spectrum is a stable metallo-cryptophane, as it could just as easily be a mass fragment or an intermediate of self-assembly.

The purity of complex **4.1** was confirmed by combustion analysis and consistent with the suggested composition obtained from the crystal structure. Furthermore, IR spectroscopy confirms the inclusion of perchlorate anions in the crystalline material, and hence complex formation, with Cl-O bond stretches at 1090, 945 and 623 cm^{-1}.

4.3 Synthesis of a novel, solubilised ligand library

It was believed that the flexibility of ligand **2.6** may be a contributing factor which facilitates the catenation observed in complex **4.1**. It was therefore predicted that ligand **2.7** (**Scheme 4.1**), which features the same 3-pyridyl functionality but linked through a rigid ester linkage, would afford the desired metallo-cryptophane, *sans*-catenation. Irrespective of the conditions employed, all attempts to form the metallo-cryptophane were quashed by high levels of insolubility and only oligomeric precipitates were isolated. It is likely to be the insolubility of the initial dynamic library that impedes self-correction and thus prevents the self-assembly processes required to reach a thermodynamic minimum.[50] Leaving no other options for a linearly coordinated metallo-cryptophane, attempts were focussed towards utilising the 4-pyridyl isomer **2.8** and *cis*-protected palladium(II) salts in a similar manner described by Shinkai and co-workers,[19] **Scheme 4.1**. Again, solubility was the major issue and no complexes were isolated.

The inability of ligands **2.6**-**2.8** to afford the desired metallo-cryptophane brought about the necessity for added solubility. Attempts were focussed towards bifunctionalising the tribenzo[*a*,*d*,*g*]cyclononatriene core in a manner which would simultaneously increase solubility and allow for the appendage of a donor moiety. The bifunctionalised CTV-derivative *tris*(propoxy)cyclotriveratrylene (*p*CTV, **4.3**)[51] was selected as a suitable starting material from which to subsequently demethylate and functionalise in order to prepare a solubilised ligand library. The addition of a propyl moiety to the CTV framework was considered a suitable compromise between solubility and sterics, and one which would not hinder their ability to crystallise. Literature compound *p*CTV (**4.3**) was prepared in a two-step procedure and isolated as a crystalline solid in low yield, **Scheme 4.2**.[51]

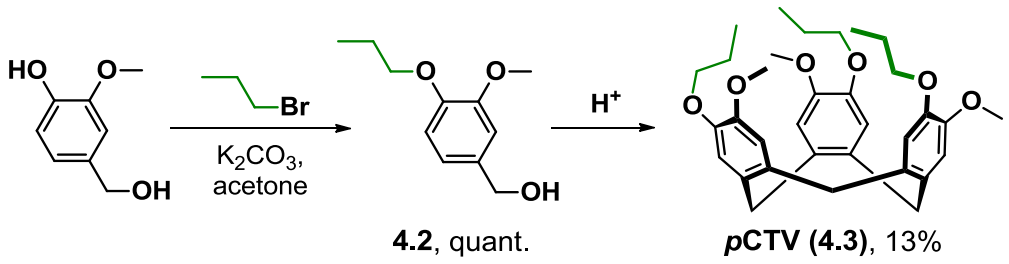

Scheme 4.2 *Preparation of tris(propoxy)cyclotriveratrylene,* ***4.3****.*[51]

Initial efforts to demethylate *p*CTG employed the Lewis acids BBr_3 and $AlCl_3$ under rigorously anhydrous conditions; however, selective demethylation was not achieved and mixtures of dealkylated products were consistently isolated, irrespective of the reaction conditions used. Reactions at low temperatures and with dropwise addition of the Lewis acid increased the

selectivity in favour of the depropylation. Whilst this approach is widely utilised for the demethylation of aryl-methyl ethers,[52] the inductive effect of the propyl moiety significantly increases the coefficient, and thus the Lewis basicity, of the corresponding ethereal lone pair, which ultimately promotes depropylation over demethylation, especially at lower temperatures, **Scheme 4.3a**. However, propyl induction generates a highly electron rich propyl α-carbon, whilst the opposing methyl group remains relatively electrophilic in comparison. Therefore, the reaction selectivity can be inverted in the presence of a strong nucleophile.

Lithium diphenyl phosphide represents a nucleophilic and highly selective reagent for the demethylation of aryl-methyl ethers, as any other alkylated ether would likely generate a more electropositive α-carbon. Testament to this, Collet and co-workers have used this methodology in preparing hetero-functionalised cryptophanes for use in binding lipophilic guests from an aqueous solution.[53]

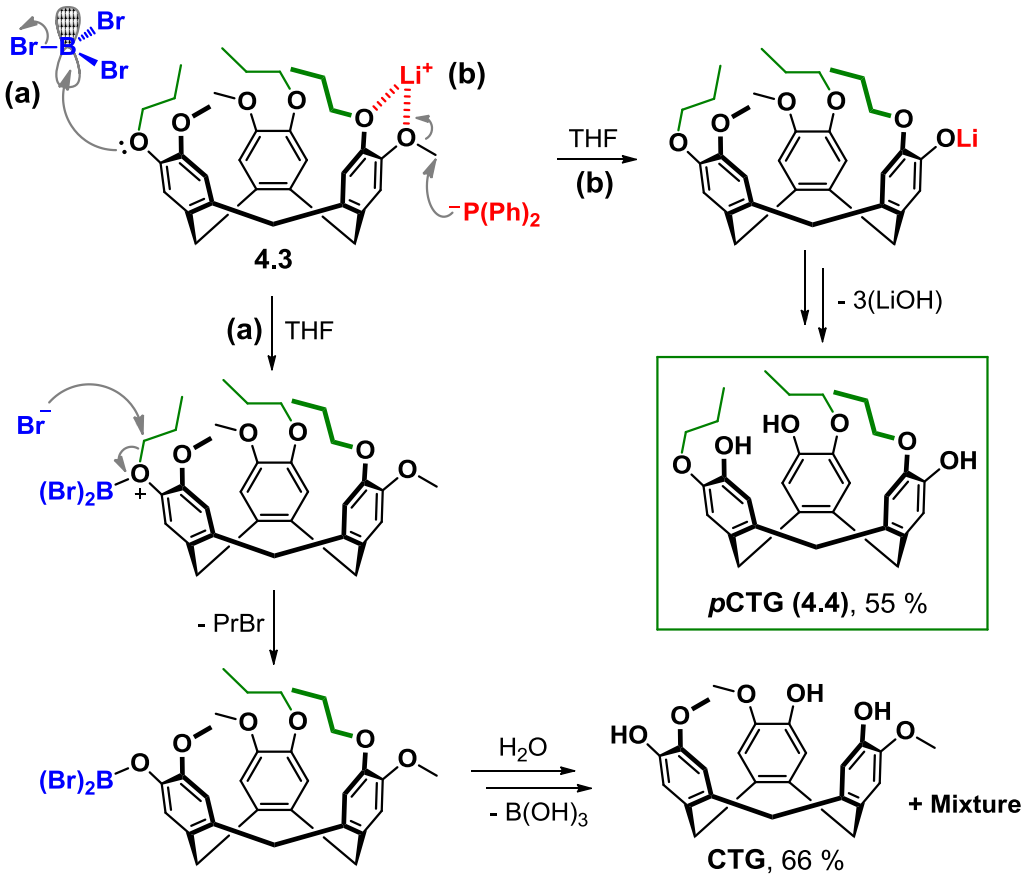

Scheme 4.3 *Towards the preparation of pCTG, **4.4**. (a) Initial and unsuccessful attempts using BBr_3;[54] (b) successful nucleophilic demethylation using $LiP(Ph)_2$.*[53]

Complete demethylation of **4.3** was effected using lithium diphenyl phosphide,[16] generated *in situ* by the lithiation of diphenylphosphine with *n*-butyllithium, and added dropwise in THF (tetrahydrofuran) solvent, **Scheme 4.3b**. The reaction was monitored by TLC until none of the

staring material remained and the resultant lithium phenoxide hydrolysed using aq. HCl to generate *p*CTG, **4.4**, which was then subjected to column chromatography (silica gel, chloroform solvent) and isolated as a colourless glass in 55% yield. The purity and composition of *p*CTG was confirmed by combustion analysis and infrared spectroscopy; the latter displaying a broad OH bond stretch at 3300 cm^{-1}, attributable to the hydrogen-bonded phenol. Electrospray mass spectrometry gave incontrovertible evidence for its formation with the mass peak at (*m/z*) 515.2410, corresponding to $\{\mathbf{4.4}\cdot Na\}^+$ (calcd. for 515.2410). Likewise, the ^1H NMR spectra of starting material **4.3** and the *tris*(hydroxy) product **4.4** were compared in $CDCl_3$ to confirm the loss of methyl group and addition of phenol functionality at 8.52 ppm, and thus a quantitative demethylation, alongside the characteristic *endo* and *exo* protons of the tribenzo[*a*,*d*,*g*]cyclononatriene core at 3.42 and 4.55 ppm, respectively, **Figure 4.9**.

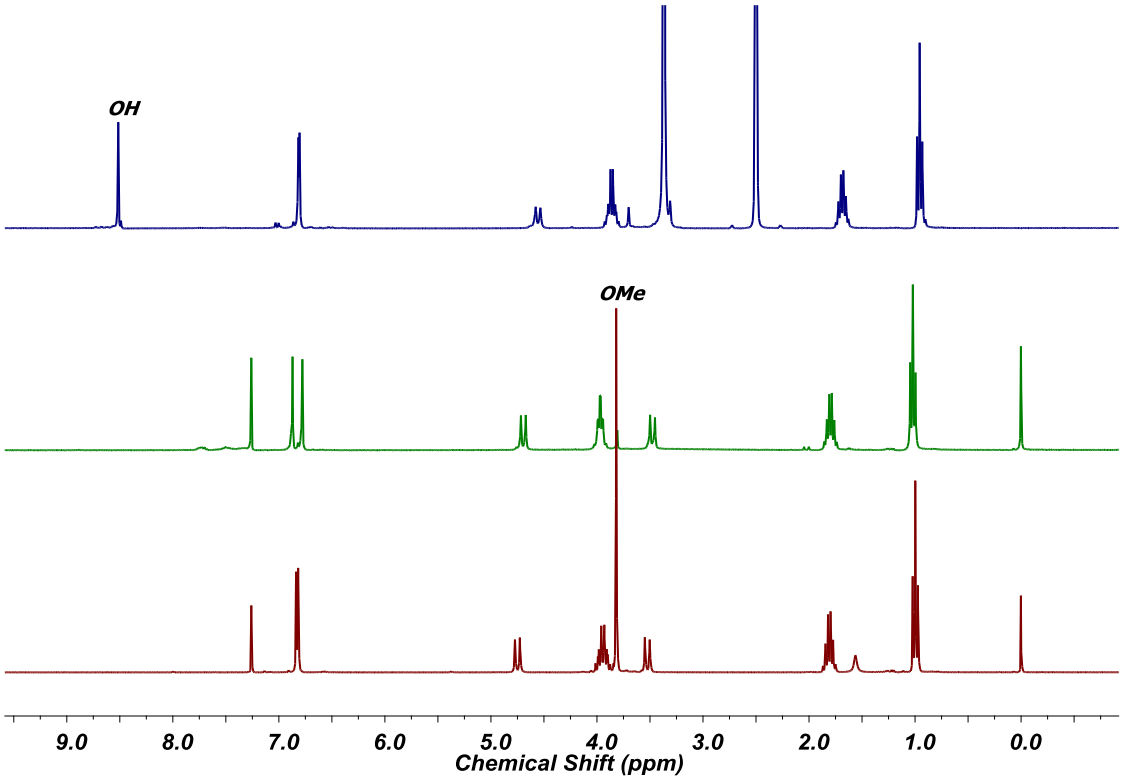

Figure 4.9 *Proton NMR spectra of starting material* ***4.3*** *(red trace, $CHCl_3$), noting the singlet at 3.82 ppm, corresponding to the methyl group, and its loss in the product* ***4.4*** *(green trace, $CHCl_3$). Product* ***4.4*** *(blue trace, d_6-DMSO) shown in order to confirm the presence of the phenolic proton at 8.52 ppm.*

Ligands (±)-*tris*(propoxy)-*tris*(3-pyridylcarboxy)cyclotricatechylene **4.5** and (±)-*tris*(propoxy)-*tris*(4-pyridylcarboxy)cyclotricatechylene **4.6** were subsequently prepared in high yields according to adapted literature procedures,[55] through reaction of *p*CTG with the corresponding pyridine carbonyl chloride, employing triethylamine as scavenger base and THF as solvent, **Scheme 4.4**. The electrospray mass spectra of ligands **4.5** and **4.6** affirmed their formation with

the mass peaks (*m/z*) 808.3229 and 808.3230, respectively, which were attributable to $\{M \cdot H\}^+$ in both instances and calculated for 808.3234. Their purity and composition were confirmed by combustion analysis and infrared spectroscopy; the latter indicating the inclusion of a *tris*(pyrdiylcarboxy) moiety with both C=O and C=N bond stretches at 1745 and 1605 cm^{-1}, respectively. The proton NMR spectra of ligands **4.5** and **4.6** displayed the splitting patterns expected for each pyridyl isomer and displayed the loss of the phenol proton. The ^1H NMR spectra for ligands **4.5** and **4.6** will be displayed below in the respective complexation studies.

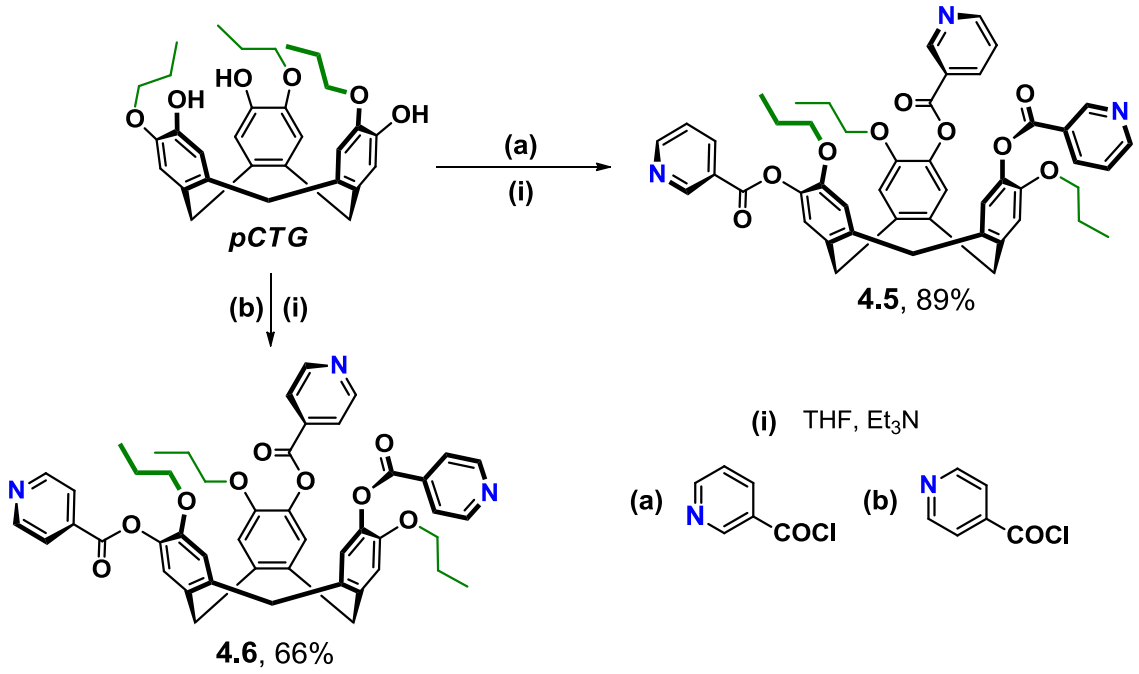

Scheme 4.4 *Preparation of ligands **4.5** and **4.6** from pCTG and the corresponding pyridine carbonyl chloride.*

Single crystals of ligands **4.5** and **4.6** were obtained from diffusion of the diethyl ether vapours into DMF and nitromethane solvent, respectively, and their clathrate complexes crystallographically determined. The structure of complex **4.5**·2(DMF)·(H_2O) solved in the triclinic space group $P\bar{1}$ to display the asymmetric unit as one molecule of **4.5**, one molecule of water and two molecules of DMF solvent, one of which displays host-guest interactions where a *N*-methyl moiety is orientated within the tribenzo[*a,d,g*]cyclononatriene core of ligand **4.5**, **Figure 4.10a**. One propyl arm of ligand **4.5** displays considerable disorder and one 3-pyridyl donor moiety is disordered over two positions. Individual ligands are arranged in an off-set head-to-head manner, facilitated by aggregation of propyl chains. The extended lattice is afforded without additional intermolecular interactions and close packs to afford interstitial sites that are filled with solvent DMF. Clathrate complex **4.5** features the inclusion of both enantiomers of ligand and is therefore a racemate.

The structure of clathrate complex **4.6**·0.5($MeNO_2$)·1.5(H_2O) solved in the triclinic space group $P\bar{1}$ to display the asymmetric unit as one molecule of ligand **4.6**, half a molecule of nitromethane solvent, disordered across a crystallographic inversion centre, and three molecules of water, all refined at half occupancy. Whilst they are not isomorphic, clathrate complexes **4.5** and **4.6** display similar unit cell parameters. Each **4.6** ligand has approximate C_3-molecular symmetry and has all propyl and ester carbonyl moieties arranged in the same orientation, **Figure 4.10b**. Individual ligands pack in a back-to-back manner, although centroid separations of 4.4 Å rule out any aromatic interactions.[25a] There are, however, aromatic π-H intermolecular interactions present between terminal γ-protons of the propyl chain and the π-cloud of a proximal pyridine group at separation of 3.06 Å. As for complex **4.5**, above, clathrate complex **4.6** is a racemate and features both enantiomers of ligand. Likewise, the extended lattice features a bilayer-like arrangement of ligands which are separated by nitromethane solvent.

The increased solubility of ligands **4.5** and **4.6** was expected to allow for the formation of $[M_3L_2]^{n+}$ metallo-cryptophanes with linear and *cis*-protected 90 ° tectons, respectively, by facilitating self-assembly and preventing the oligomerisation and precipitation observed for ligands **2.7** and **2.8**.

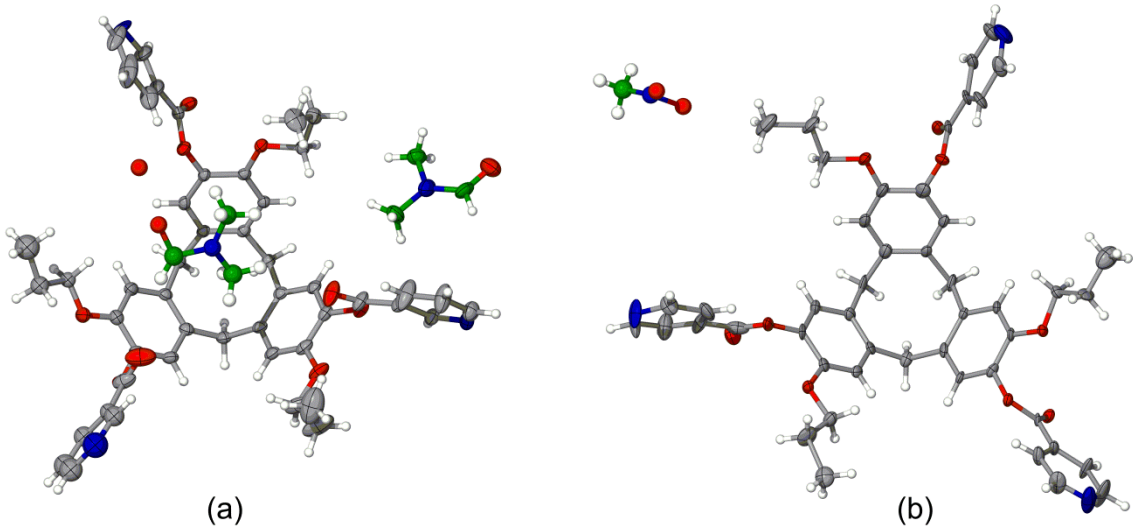

Figure 4.10 *From the crystal structure of clathrate complexes* ***4.5*** *(a) and* ***4.6*** *(b). Anisotropic displacement parameters are set at 40 % and DMF and nitromethane solvent molecules are coloured green for clarity.*

4.4 Preparation of an off-set metallo-cryptophane, $[Ag_2(4.5)_2]\cdot 2(PF_6)\cdot n$(MeCN)

Whilst methylated ligand **2.7** was not observed to afford complexes with transition metal salts, the reaction of its solubilised congener, ligand **4.5**, with silver(I) hexafluorophosphate (PF_6^-) in acetonitrile (MeCN) solvent afforded an 'off-set' metallo-cryptophane,

$[Ag_2(\mathbf{4.5})_2]\cdot 2(PF_6)\cdot n(MeCN)$, complex **4.7**. Single crystals were grown by diffusing diethyl ether vapours into an acetonitrile solution of the complex, isolated as colourless blocks, and structurally characterised by single crystal X-ray diffraction analysis.

The structure was solved in the triclinic space group $P\bar{1}$ and the asymmetric unit was determined as half of the overall complex, alongside one PF_6^- counter anion and three acetonitrile solvent molecules. There are host-guest interactions present between an acetonitrile solvent molecule and the complex, where the terminal methyl group is orientated within the shallow, hydrophobic bowl of the **4.5** ligand, **Figure 4.11**. The remaining acetonitrile solvent molecules and PF_6^- anions within the structure are also closely associated with the offset metallo-cryptophane, and one acetonitrile molecule displays a long association with a proximal Ag(I) centre at Ag···N distance 2.80 Å.

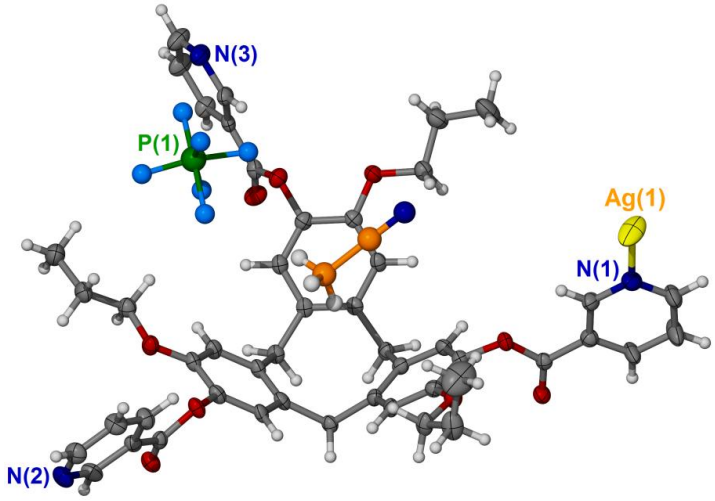

Figure 4.11 *From the asymmetric unit of complex* ***4.7****. All anisotropic displacement parameters set at 40 % probability, hexafluorophosphate anion and acetonitrile solvent shown as hard spheres, and non-covalently bound acetonitrile distinguished by colour.*

Silver(I) centres are approximately linearly coordinated by two symmetry related **4.5** ligands, each of which are associated by a crystallographic centre of inversion. The Ag-N bond distances and N-Ag-N bond angles were measured to be 2.166(6) and 2.181(7) Å, and 169.1(3) °, respectively. Each **4.5** ligand binds to the two silver(I) cations through only two of its three pyridyl groups to give the head-to-head, off-set appearance, **Figure 4.12**. The resultant 'off-set' metallo-cryptophane features both enantiomers of ligand **4.5** and is therefore achiral. It does not possess a well-defined and enclosed internal void space for further host-guest study. Upon closer inspection it becomes evident why the desired $[M_3L_2]^{n+}$ metallo-cryptophane is not accessible as a self-assembly product, as formation of both the *syn* and *anti* cryptophane diastereoisomers would result in structural penalty – either through steric clashes at the capsule

interface (*syn*) or unfavourable pyridine-ester bond conformations (*anti*). Other off-set metallo-cryptophanes have been prepared by Little and co-workers,[56] including an organometallic $[Ag_2(L)_2]^{2+}$ dimer, where L = *tris*(allyl)cyclotriguaiacylene, which is dependent on synergistic host-guest interactions.[57] Similarly, Holman and co-workers have prepared an off-set organic cryptophane that implodes upon the evacuation of solvent but subsequently regains its approximate C_3-symmetry upon the addition of a suitable solvent 'guest' molecule.[58]

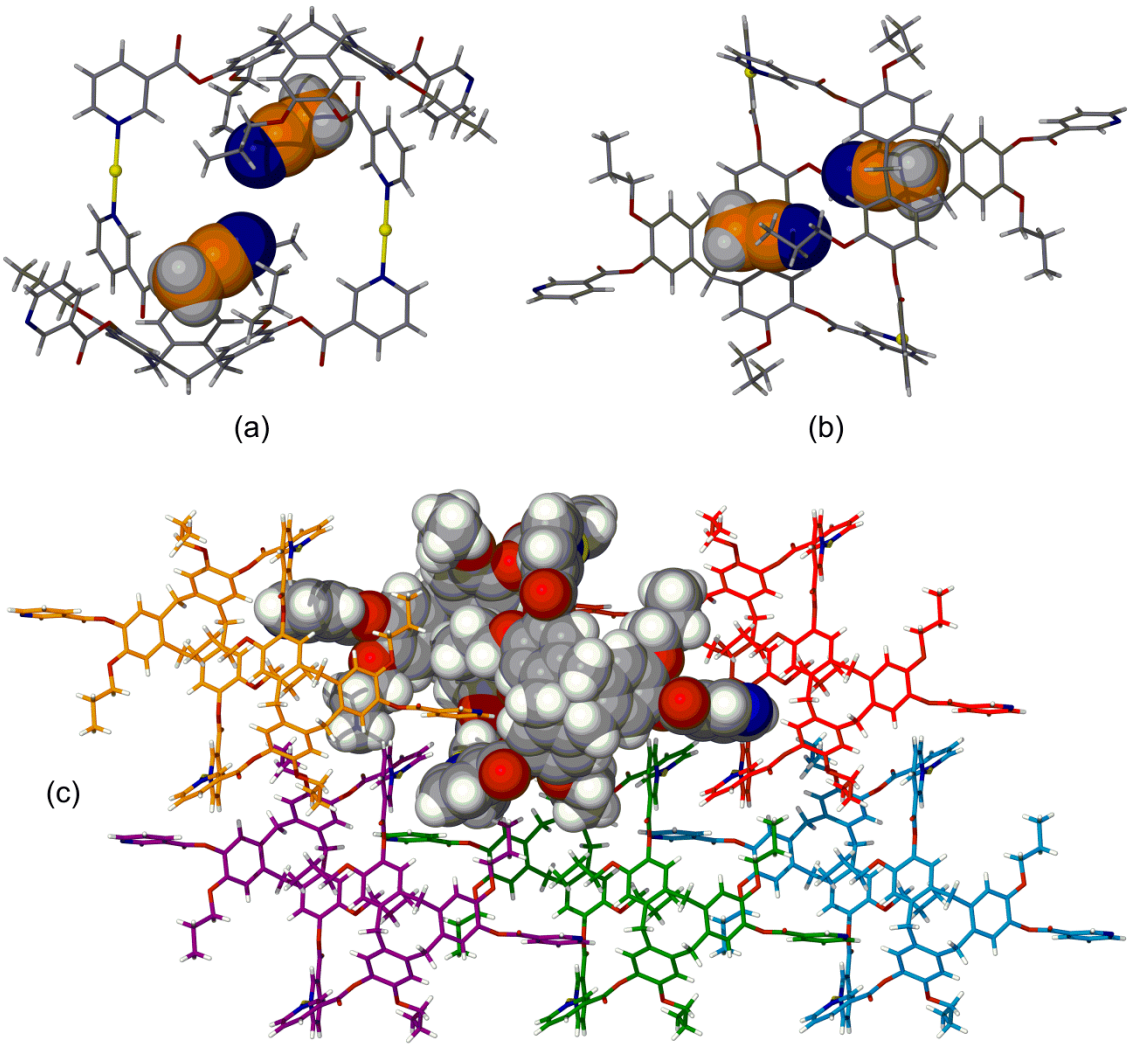

Figure 4.12 *From the crystal structure of complex* ***4.7****. The off-set metallo-cryptophane,* $[Ag_2(\mathbf{4.5})_2]^{2+}$*, as viewed from the side (a) and above (b). Non-covalently bound acetonitrile solvent is distinguished by colour and shown in space-filling mode. (c) The packing of individual* $[Ag_2(\mathbf{4.5})_2]^{2+}$ *complexes through interdigitation. One* $[Ag_2(\mathbf{4.5})_2]^{2+}$ *off-set capsule is shown in space-filling mode and the remainder are distinguished by colour.*

The uncoordinated ligand arm of each **4.5** ligand protrudes out to interdigitate the individual $[Ag_2(\mathbf{4.5})_2]^{2+}$ capsules into a *pseudo*-2D sheet, although no interactions are present between ligand arm and its neighbour, **Figure 4.12c**. This affords a bilayer of off-set metallo-cryptophanes within the crystal lattice with inter-species Ag···Ag separations of 4.19 Å, which

is too long to suggest argentophilic interactions. The 2-D sheets pack in a back-to-back manner with π-H interactions recorded between the γ-protons of a propyl arm and the π-cloud of a proximal tribenzo[*a,d,g*]cyclononatriene aromatic ring, with separations ranging 2.83-3.01 Å. The interdigitation of $[Ag_2(\mathbf{4.5})_2]^{2+}$ capsules is close-packed and the remaining interstitial lattice sites are filled with PF_6^- anions and acetonitrile solvent.

The solution-phase assembly of $[Ag_2(\mathbf{4.5})_2]^{2+}$ was investigated by proton NMR and electrospray mass spectrometry. Changes in the ^{1}H NMR spectra were subtle and only slight broadening of pyridyl resonances were observed, likely due to the desymmetrisation of the ligand upon formation of the complex, **Figure 4.13.** The ^{1}H NMR experiments were also consistent in d_6-DMSO and d_3-$MeNO_2$ (nitromethane), with no discernible changes evident in the spectra. Similarly, the addition of a templating guest, such as ferrocene or *ortho*-carborane did nothing to facilitate the self-assembly to the $[M_3L_2]^{n+}$ metallo-cryptophane. The mass spectra of complex **4.7** supported the formation of the $[Ag_2(\mathbf{4.5})_2]^{2+}$ cages with the mass peak (*m/z*) 1976.3330, corresponding to $\{[Ag_2(\mathbf{4.5})_2]\cdot PF_6\}^+$. There was no evidence of the desired $[Ag_3(\mathbf{4.5})_2]^{3+}$ by mass spectrometry, regardless of solvent or silver(I) salt employed.

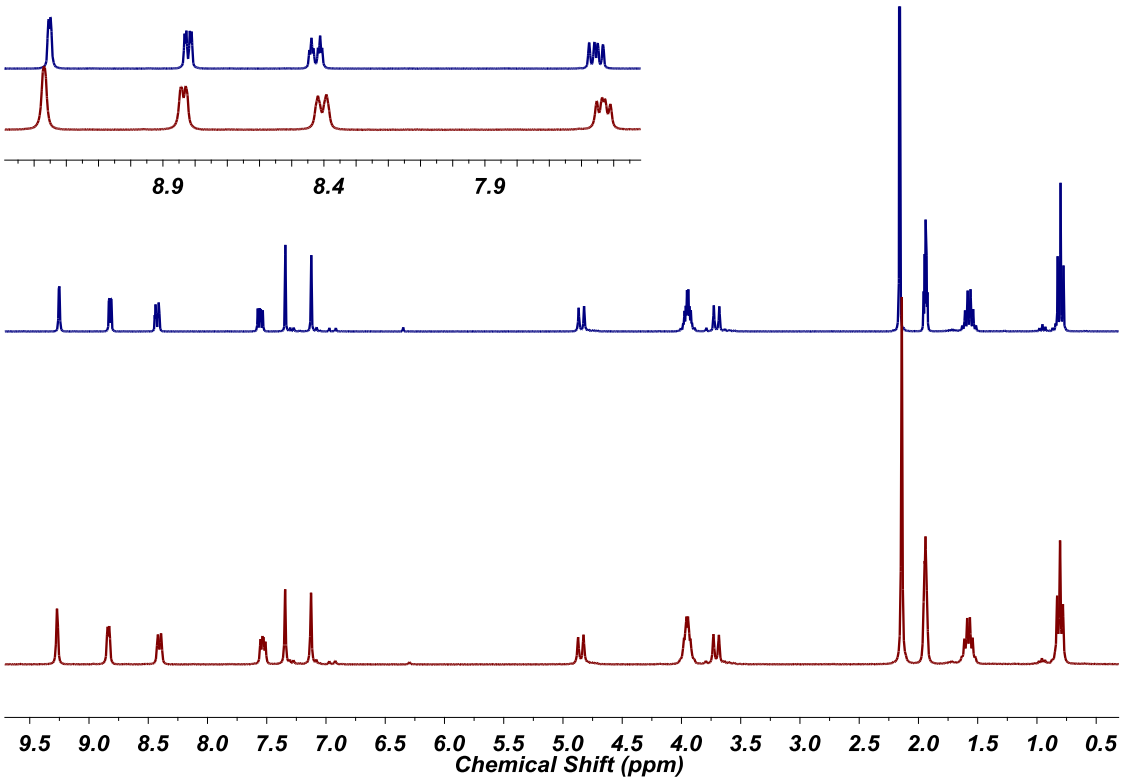

Figure 4.13 *Proton NMR spectra of ligand* ***4.5*** *(red trace) and complex* ***4.7*** *(blue trace). An expansion is provided above to display the subtle changes to the pyridyl resonances.*

Single crystals of complex **4.7** were isolated and their purity and composition were confirmed by combustion analysis and IR spectroscopy, respectively; the latter supporting the inclusion of

the PF_6^- anion, and hence complex formation, with P-F bond stretch at 839 cm^{-1}.

Whilst the solubility of ligand **4.5** did facilitate the solution-phase self-assembly with silver(I) cations, the desired $[M_3L_2]^{n+}$ metallo-cryptophane remains inaccessible due to sterics, despite the range of conditions employed. Interestingly, however, mass spectrometry does give evidence for the formation of a heteroleptic $[Ag_3(\mathbf{4.5})(\mathbf{2.7})_2]^{3+}$ assembly, likely to be a metallo-cryptophane, from a mixture of silver(I) hexafluorophosphate and ligands **4.5** and **2.7** in acetonitrile solvent. The mass spectrum indicated two heteroleptic species, namely $\{[Ag_2(\mathbf{4.5})(\mathbf{2.7})]\cdot PF_6\}^+$ and $\{[Ag_3(\mathbf{4.5})(\mathbf{2.7})]\cdot 2PF_6\}^+$, at mass peaks (*m/z*) 1891.2483 and 2145.0777, respectively. Whilst the accurate mass indicates the desired composition, it is impossible to suggest a possible structure. As a result of complex desymmetrisation, in addition to the broadening observed, the proton NMR spectra of the heteroleptic capsules were uninformative. It is interesting to note that whilst the methylated **2.7** ligand does not form stable, discrete complexes with Ag(I) cations, it is integral to the formation of the desired M_3L_2 metallo-cryptophane - which cannot be achieved as a homoleptic mixture with either **4.5** or **2.7**. This can be rationalised in terms of steric reduction, as the *syn*-cryptophane is no longer sterically unfavourable.

4.5 Solution-phase study of a metastable metallo-cryptophane, $[Pd_3(en)_3(\mathbf{4.6})_2]\cdot 6(NO_3)$

Whilst methylated ligand **2.8** was not observed to form a stable metallo-crytpophane with *cis*-protected transition metal salts, the reaction of ligand **4.6** with $[Pd(en)(NO_3)_2]$ (en = ethylenediamine), in DMSO solvent, afforded $[Pd_3(en)_3(\mathbf{4.6})_2]\cdot 6(NO_3)$, complex **4.8**. The formation of the metallo-cryptophane was monitored over time by various solution-phase techniques and observed to be structurally fluxional, **Figure 4.14**.

The solution-phase assembly of complex **4.8** was investigated by NMR spectroscopy and mass spectrometry. The ^1H NMR spectra in d_6-DMSO were indicative of complex formation, with the expected down-field shifting from 8.85 to 9.15 ppm identified for the *ortho*-pyridine resonances, **Figure 4.15b**. Likewise, NOESY (nuclear Overhauser effect spectroscopy) spectra were supportive of metallocryptophane formation and displayed the through-space coupling of *ortho*-pyridyl and ethylenediamine (N-H) protons required for a head-to-head complex. Furthermore, mass peaks of *m/z* 766.8358 and 1181.2535 were identified in the mass spectra and were attributed to the species $\{[Pd_3(en)_3(\mathbf{4.7})_2]\cdot 3(NO_3)\}^{3+}$ and $\{[Pd_3(en)_3(\mathbf{4.7})_2]\cdot 4(NO_3)\}^{2+}$, respectively.

Complex **4.8** was later determined to be a metastable product and underwent a significant structural reorganisation from the $[Pd_3(en)_3(\mathbf{4.6})_2]\cdot 6(NO_3)$ metallo-cryptophane to a

$[Pd_6(\mathbf{4.6})_8]\cdot 12(NO_3)$ octahedral coordination cage, complex **4.9**, assumed to be the thermodynamic product, **Figure 4.14**. Complex **4.9** represents a class of octahedral coordination cages that have been previously reported with 4-pyridyl functionalised CTVs,[59] and is a decorated but structurally analogous congener to $[Pd_6(\mathbf{2.8})_8]\cdot 12(NO_3)$, dubbed a 'stella octangula' cage.[60] The previously reported $[Pd_6(\mathbf{2.8})_8]\cdot 12(NO_3)$ stella octangula cage features an octahedral framework of palladium(II) cations, which is surrounded by eight face-capping **2.8** ligands to afford a 3 nm, high-symmetry cage with a large, internal void space. Each of the octahedrons faces are extended out to a point through ligand coordination, resulting in a spiked appearance that closely resembles the first stellation of an octahedron, **Figure 4.14**.

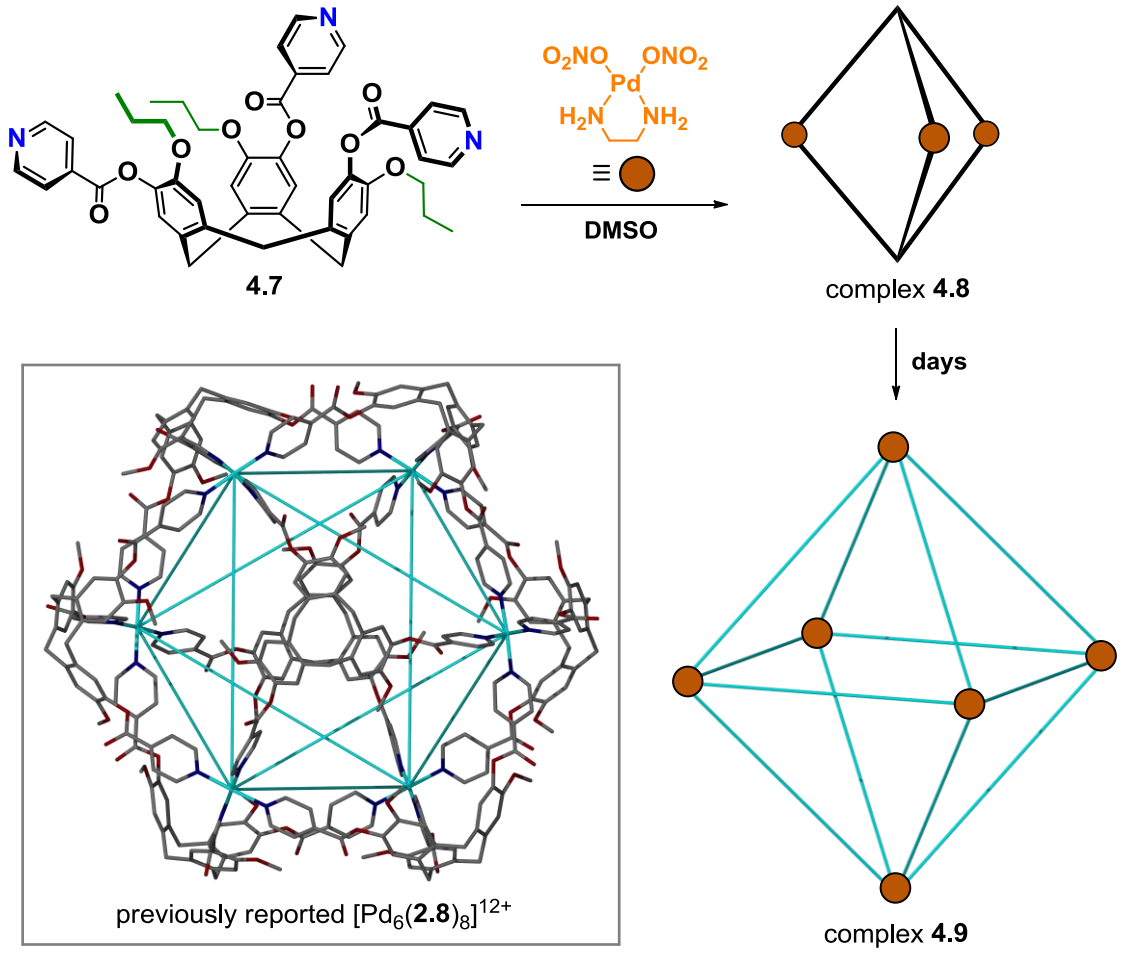

Figure 4.14 *The formation of complex **4.8** from ligand **4.7** and $[Pd(en)(NO_3)_2]$, followed by its subsequent degradation to complex **4.9**. The previously reported 'stella octangula' cage, $[Pd_6(\mathbf{2.8})_8]^{12+}$ is shown as reference.*[60]

The inter-cage conversion of complex **4.8** to complex **4.9** is thought to be entropically favourable according to the higher molecular symmetry of the stella octangula cage (O_h point group) over the trigonal bipyramidal metallo-cryptophane (C_{3h} or D_3 point group).[28] The process was continuously monitored by NMR spectroscopy and mass spectrometry until self-

reorganisation was complete. ^{1}H NMR resonances became increasingly broad, where desymmetrisation of the pyridyl protons was observed and a substantial upfield shift was noted in the ethylenediamine resonance, from 6.41 to 5.70 ppm, **Figure 4.15c-e**. During this time, mass peaks of *m/z* 724.8388 and 745.8361 became apparent in the mass spectra, which were identified as $\{[Pd_3(en)_1(\mathbf{4.6})_2]\cdot 3(NO_3)\}^{3+}$ and $\{[Pd_3(en)_2(\mathbf{4.6})_2]\cdot 3(NO_3)\}^{3+}$, respectively. The sequential loss of the inert ethylenediamine ligands from complex **4.8** supports the notion of symmetry-driven expansion and highlights the driving force towards the stella octangula cage, complex **4.9**. Furthermore, the mass peaks *m/z* 919.2482, 1058.8043, 1245.4923 and 1507.5749 were observed in the mass spectra, which correspond to $\{[Pd_6(\mathbf{4.6})_8]\cdot 5NO_3\}^{8+}$, $\{[Pd_6(\mathbf{4.6})_8]\cdot 6NO_3\}^{7+}$, $\{[Pd_6(\mathbf{4.6})_8]\cdot 7NO_3\}^{6+}$ and $\{[Pd_6(\mathbf{4.6})_8]\cdot 8NO_3\}^{5+}$ octahedral assemblies, respectively.

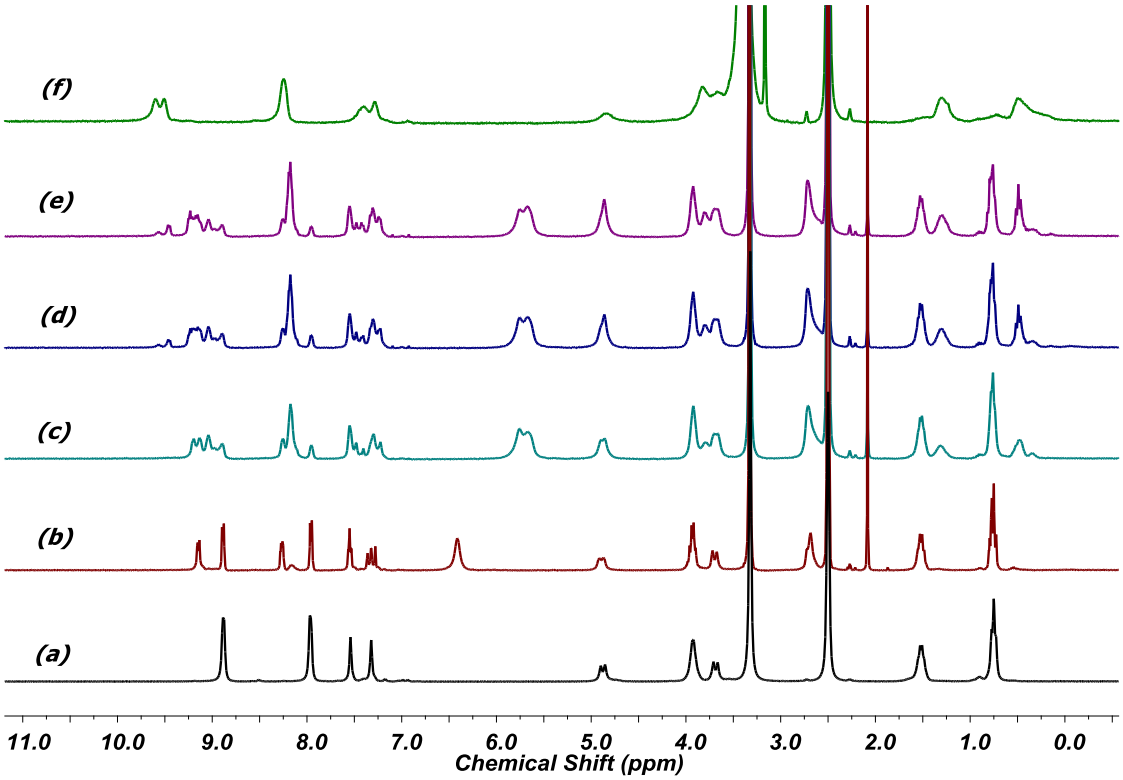

Figure 4.15 *Timecourse ^{1}H NMR experiment displaying the formation of complex **4.8** and its degradation to complex **4.9**, in d_6-DMSO solvent. (a) ligand **4.6**; (b) initial formation of complex **4.8**; (c-e) degradation of complex **4.8** to **4.9**, noting the desymmetrisation of pyridyl resonances and upfield shift of the ethylaminediamine resonances; (f) complex **4.9**, noting the absence of the ethylaminediamine resonances.*

An isolated sample of complex **4.9** indicated quantitative formation of the octahedral cage (with respect to the metal) and its subsequent dissolution in d_6-DMSO afforded the ^{1}H NMR spectrum of the stella octangula cage, with no evidence of ethylenediamine present in the complex, **Figure 4.15f**. The formation of complex **4.9** was also confirmed by 2D diffusion-ordered NMR

spectroscopy (DOSY), which identified only one large species present in solution with a diffusion coefficient (D) of 0.439×10^{-10} m^2 s^{-1}. Based on the diffusion coefficient of ligand **4.6**, 1.293×10^{-10} m^2 s^{-1}, a $D_{complex}/D_{ligand}$ ratio of 0.33:1 was established; which, *via* the Stokes-Einstein relationship, calculates the hydrodynamic radius (r) of the complex to be 23.4 Å.[61] This figure is slightly larger than the hydrodynamic radius of 19.4 Å obtained for complex $[Pd_6(\mathbf{2.8})_8]^{12+}$ and is likely to coincide with the presence of protruding propyl chains from the complex.[60] Similarly, this radius is far too large to correspond to complex **4.8**, confirming its quantitative conversion to complex **4.9**.

The use of $Pd(en)(NO_3)_2$ as a metallo-tecton is extremely well exemplified,[62] particularly in Fujita's archetypal cages,[63] where the ethylenediamine chelating ligand is almost always employed as a kinetically stable protecting group to ensure that all additional ligands bind only *cis* at the metal centre. Ultimately, its displacement in the conversion of complex **4.8** to complex **4.9** implies that the driving force of cage expansion exceeds the kinetic barrier for its dissociation from the palladium(II) centre.[64] The employment of 2,2'-bipyridine in place of ethelyenediamine as *cis*-protecting ligand did nothing to prevent the cage-to-cage conversion to complex **4.9**.

The majority of inter-cage transformations are initiated using a chemical trigger,[6] such as in Li's polyhedral metal-imidazolate cages, where the addition of methylamine to a preformed cage effects the transformation between two Ni_8L_{12} and $Ni_{14}L_{24}$ complexes.[65] Similarly, Nitschke and co-workers have described systems which undergo dynamic interconversion between helicates, tetrahedral and pentagonal prisms, based on labile imine and metal-ligand coordination bonds, again requiring use of a chemical trigger.[66] Examples which are more closely related to that of complex **4.8** and **4.9**, requiring no additional stimuli, are Mukherjee's organic cages, formed again through dynamic imine chemistry, which form a variety of covalent cages upon immediate mixing but self-sort with time to give only two species. Likewise, Wards's polyhedral coordination cages, formed from bidentate pyridine-pyrazolide ligands and cadmium(II) cations, undergo a structural reorganisation upon crystallisation and dissolution from a $Cd_{16}L_{24}$ truncated tetrahedron to Cd_6L_9 trigonal prism, respectively. Here, the trigonal prism is suggested to be the thermodynamic product and the larger truncated tetrahedron simply a phenomenon of the solid state.[65] Furthermore, Chand and co-workers have reported a trigonal bipyramidal $[Pd_3(en)_3L_2]^{6+}$ cage, where L = 1,3,5-*tris*(4-pyridylmethyl)benzene, which expands to the larger $[Pd_6L_8]^{12+}$ octahedral assembly upon heating in DMSO solvent.[67] However, it is likely that the heat stimulus labilises the Pd-N(en) coordination bond enough to facilitate the cage expansion. Nevertheless, inter-cage transformations remain relatively rare, and this represents the first example reported involving derivatised CTVs.

4.6 Conclusions and future work

Although perhaps the simplest metal complex accessible with functionalised CTVs, metallo-cryptophanes remain a relatively elusive product of their self-assembly. This chapter has discussed the difficulty in predicting their assembly from silver(I) and *cis*-protected palladium(II) salts, and highlights the challenges in being able to control how they self-assemble in solution.

The flexibility of ligand **2.6** was thought to be a contributing factor in forming the triply-interlocked [2]-catenane, complex **4.1**; however, its formation without an active template and the degree of overall enantiomeric purity perhaps indicates a process that is still not fully understood. Ultimately, the catenation of the metallo-cryptophanes significantly decreased the internal void space, and its accessible windows, and thus removed the possibility of hosting molecules.

Despite their suitable functionality, the inability of ligands **2.7** and **2.8** to afford metallo-cryptophanes was due to high levels of insolubility. The necessity of a soluble starting material was subsequently realised in propylated cyclotriguaiacylene (*p*CTG) and used to make solubilised congeners of the aforementioned ligands, ligands **4.5** and **4.6**, respectively. Metallo-cryptophane formation from the self-assembly of ligand **4.5** and silver(I) salts was prevented due to sterics and instead afforded an off-set metallo-cryptophane, complex **4.7**, which did not possess a well-defined internal cavity for further host-guest study. Whilst the metallo-cryptophane was thought to be accessible *via* heterolepticity, it could neither be isolated, nor fully characterised.

Finally, metallo-cryptophane formation was achieved through the self-assembly of ligand **4.6** and *cis*-protected palladium(II) salts, complex **4.8**; however, metastability resulted in an inter-cage expansion to a larger metallo-supramolecular assembly, complex **4.9**. In order to predictably afford stable metallo-cryptophanes with ligand **4.6**, and thus be able to explore their potential host-guest chemistry, future work must involve the utilisation of a suitably pre-functionalised *cis*-protecting metallo-tecton which would promote the formation of only one self-assembly product. This might be achieved by increasing the binding strength of the *cis*-protecting auxiliary ligand in order to increase the kinetic stability and barrier for its dissociation, incorporating ligands such as diphosphines. In doing so, it should be possible to prepare an analogous metallo-cryptophane which is indefinitely stable and thus capable of hosting molecules in the solution-phase. If a potential candidate were to be afforded, the interior void space of the cage could be modelled and its hosting ability systematically explored prior to the investigation into its catalytic activity or guest release properties.

4.7 Experimental

Ligands **2.6**-**2.8** were prepared according to procedures listed in Chapter 2 of this thesis and were employed as racemic mixtures for all complexation studies listed herein.

4.7.1 Instrumentation

NMR spectra were recorded by automated procedures on a Bruker Avance 500 or DPX 300 MHz NMR spectrometer. All deuterated solvents were purchased from Euriso-top. All ^{1}H and ^{13}C{^{1}H} spectra were referenced relative to an internal standard. High resolution DOSY and ROESY ^{1}H NMR spectra were recorded in collaboration with Dr. Julie Fisher of the University of Leeds. High resolution electrospray mass spectra (ESI-MS) were measured on a Bruker MicroTOF-Q or Bruker MaXis Impact spectrometer in either positive or negative ion mode by Ms. Tanya Marinko-Covell of the University of Leeds Mass Spectrometry Service and Dr Lindsay P. Harding of the University of Huddersfield. Low resolution mass spectra were recorded on an open-access Bruker Micromass LCT spectrometer with simultaneous HPLC using an acetonitrile/water eluent and sodium formate calibrant. FT-IR spectra were recorded as solid phase samples on a Perkin-Elmer Spectrum One spectrophotometer. Samples for microanalysis were dried under vacuum before analysis and the elemental composition determined by Mr Ian Blakeley of the University of Leeds Microanalytical Service using a Carlo Erba elemental analyser MOD 1106 spectrometer.

Crystals were mounted under inert oil on a MiTeGen tip and flash frozen to 150(1) K using an Oxford Cryosystems cryostream low temperature device. X-ray diffraction data were collected using graphite-monochromated Mo-*K* radiation (λ = 0.71073 Å) using a Bruker-Nonius X-8 diffractometer with ApexII detector and FR591 rotating anode generator; or using synchrotron radiation (λ = 0.6889 Å) with a Crystal Logic 4-circle Kappa goniometer and Rigaku Saturn 724 CCD diffractometer at station i19 of Diamond Light Source. Data were corrected for Lorenztian and polarization effects and absorption corrections were applied using multi-scan methods. The structures were solved by direct methods using SHELXS-97 and refined by full-matrix on F^2 using SHELXL-97, interfaced through the X-seed interface.[68] Unless otherwise specified, all non-hydrogen atoms were refined as anisotropic, and hydrogen positions were included at geometrically estimated positions. Molecular graphics were obtained using POV-RAY through the X-Seed interface.[69] Additional details are given below and data collections and refinements summarised in Tables below.

4.7.2 Synthesis of ligands and complexes

Synthesis of $[Ag_6(2.6)_4]\cdot 6(ClO_4)\cdot n$(DMF) (complex 4.1). $AgClO_4.H_2O$ (5.04 mg, 0.0225 mmol) and ligand **2.6** (10.01 mg, 0.0145 mmol) were dissolved in DMF (1 mL). Diethyl ether vapours were diffused into the solution, where small colourless crystals formed after 7 days that were analysed by single crystal X-ray analysis. Yield 2.1 mg. HR MS (ES^+): *m/z* 790.2 $\{[Ag(\mathbf{2.6})]\}^+$, 1887.2 $\{[Ag_3(\mathbf{2.6})_2(ClO_4)_2\}^+$, 2567.5 $\{[Ag_3(\mathbf{2.6})_3(ClO_4)_2\}^+$, 2774.3 $\{[Ag_4(\mathbf{2.6})_3(ClO_4)_3\}^+$, 3457.6 $\{[Ag_4(\mathbf{2.6})_4(ClO_4)_3\}^+$ and 3663.4 $\{[Ag_5(\mathbf{2.6})_4(ClO_4)_4\}^+$, calcd. for 789.2, 1885.0, 2566.3, 2773.6, 3454.9, 3662.3, respectively; ^{1}H NMR (300 MHz, d_6-DMF) δ (ppm) = 8.86 (bs, 3H, Py-H^2), 8.75 (bs, 3H, Py-H^6), 8.18 (bs, 3H, Py-H^5), 7.73 (bs, 3H, Py-H^4), 7.41 (s, 3H, Ar-H), 7.26 (s, 3H, Ar-H), 5.27 (s, 6H, Ar-OCH_2), 4.88 (d, 3H, CTG *exo*-H), 3.78 (s, 9H, Ar-OCH_3), 3.70 (d, 3H, CTG *endo*-H); As anticipated, microanalysis indicates a higher level of solvation than refined in the crystal structure; however, SQUEEZE [70] indicates that there is sufficient void space in the lattice for added solvent. The additional solvent added to the molecular formula accounts for 1280 electrons. Analysis for $[Ag_6(\mathbf{2.6})_4]\cdot 6(ClO_4)\cdot 6(DMF)\cdot 8(H_2O)$ (% calculated, found) C (49.04, 48.65), H (4.74, 4.63), N (5.54, 5.85); Infrared analysis (FT-IR, cm^{-1}) 3425 (broad), 2937, 1654, 1609, 1511, 1443, 1387, 1265, 1090, 945, 802, 678, 623.

Synthesis of 3-methoxy-4-propyloxy-benzylalcohol (4.2). 3-methoxy-4-phenoxy-benzylalcohol (5.01 g, 32.4 mmol), 1-bromopropane (3.60 mL, 40.0 mmol) and potassium carbonate (5.50 g, 40.0 mmol) were combined in acetone (80 mL) and held at reflux under an argon atmosphere for 24 hours. The reaction mixture was cooled to room temperature and the solvent was removed *in vacuo* to yield a yellow oil. The residue was taken up into dichloromethane (100 mL), washed with water (3 × 100 mL) and the chlorinated extracts dried over magnesium sulfate. The mixture was concentrated *in vacuo* to yield the target compound as a colourless oil. Yield 4.62 g, 73 % (Lit. 73 %). B.pt. 55 °C (Lit. 55 °C); ^{1}H NMR (300 MHz, $CDCl_3$) δ (ppm) = 6.90 (s, 1H, Ar-H^2), 6.84 (bs, 2H, Ar-H^5, Ar-H^6), 4.58 (s, 2H, C$\underline{H}_2$-OH), 3.96 (t, 2H, propyl α-H, J = 6.9 Hz), 3.85 (s, 3H, Ar-OCH_3), 1.85 (sext, 2H, propyl β-H, J = 7.1 Hz), 1.03 (t, 3H, propyl γ-H, J = 7.4 Hz); $^{13}C\{^1H\}$ NMR (75 MHz, $CDCl_3$) δ (ppm) = 149.5, 148.0, 146.7, 133.6, 119.4, 112.8, 110.9, 70.6, 65.2, 55.9, 53.5, 22.5, 10.4. All data are consistent with the literature.[51]

Synthesis of (±)-2,7,12-Tripropoxy-3,8,13-trihydroxy-10,15-dihydro-5*H*-tribenzo[*a,d,g*]cyclononatriene (4.3). Compound **4.2** (3.52 g, 0.018 mol) was heated to 90℃ with a catalytic amount of phosphoric acid (spatula tip) for three hours, during which time it solidified. The off-white solid was triturated in methanol and collected *via* filtration under

reduced pressure, washed with one portion ice-cold methanol (30 mL) and dried to give the target compound as a bright white solid. Yield 1.27 g, 13 % (Lit. 13 %). M.pt. 148 °C (Lit. 145 °C); ^{1}H NMR (300 MHz, $CDCl_3$) δ (ppm) = 6.84 (s, 3H, Ar-H), 6.82 (s, 3H, Ar-H), 4.76 (d, 3H, CTG *exo*-H, *J* = 13.8 Hz), 3.96 (m, 6H, propyl α-H), 3.83 (s, 9H, Ar-OCH_3), 3.54 (d, 3H, CTG *endo*-H, *J* = 13.8 Hz), 1.83 (sext, 6H, propyl β-H, *J* = 7.4 Hz), 1.00 (t, 9H, propyl γ-H, *J* = 7.4 Hz); ^{13}C{^{1}H} NMR (75 MHz, $CDCl_3$) δ (ppm) = 148.1, 147.1, 131.9, 115.0, 113.6, 70.7, 65.9, 56.2, 36.5, 22.4, 15.3, 10.5. All data are consistent with the literature.[51]

Synthesis of (±)-2,7,12-Tripropoxy-3,8,13-trihydroxy-10,15-dihydro-5*H*-tribenzo[*a,d,g*]cyclononatriene (4.4). Anhydrous tetrahydrofuran (10 mL) and **4.3** (1.02 g, 3.74 mmol) were added to a flame-dried Schlenk tube and stirred vigorously. Lithium diphenylphosphide was added dropwise *via* cannulae transfer over two hours, during which time it decolourised. The reaction mixture was stirred overnight and solidified. The resultant lithium phenoxide was hydrolysed with concentrated aq. HCl and volatiles removed *in vacuo*. Organics were extracted into dichloromethane (6 × 100 mL) and then back-extracted with 6M aqueous sodium hydroxide (6 × 100 mL). The sodium hydroxide layer was washed with dichloromethane (4 × 100 mL) and acidified with 6M aqueous HCl to precipitate the desired product as an off-white solid. The solid was allowed to stand for an hour before being filtered, washed with water (2 × 50 mL) and dried. Subsequent dissolution of the solid in chloroform, filtration through a silica pad and evaporation of the solution afforded the title compound as a colourless glass. Yield 974 mg, 55 %; M.pt. Decomposes > 270 °C; HR MS (ES^+): *m/z* 515.2410 $\{LNa\}^+$; calculated for $C_{30}H_{36}O_6Na$ 515.2410; ^{1}H NMR (300 MHz, $CDCl_3$) δ (ppm) = 8.52 (s, 3H, phenol), 6.82 (s, 3H, aryl-H), 6.80 (s, 3H, aryl-H), 4.55 (d, 3H, CTG *exo*-H, *J* = 13.4 Hz), 3.86 (t, 6H, propyl α-H, *J* = 6.6 Hz), 3.31 (d, 3H, CTG *endo*-H, *J* = 13.4 Hz), 1.69 (q, 6H, propyl β-H, *J* = 7.2 Hz), 0.96 (t, 9H, propyl γ-H, *J* = 7.4 Hz); ^{13}C{^{1}H} NMR (75 MHz, $CDCl_3$) δ (ppm) = 145.2, 145.0, 132.6, 130.4, 116.7, 115.3, 70.2, 35.0, 22.1, 10.4; Analysis for **4.4**·0.5(H_2O) (% calculated, found) C (71.83, 72.15), H (7.43, 7.35); Infrared analysis (FT-IR, cm^{-1}) = 3550-3110 (broad), 2945, 2910, 1645, 1485, 1390.

Synthesis of (±)-2,7,12-Tripropoxy-3,8,13-*tris*(3-pyridylcarboxy)-10,15-dihydro-5*H*-tribenzo[*a,d,g*]cyclononene (*tris*(nicotinoyl)-*tris*(propoxy)-cyclotricatechylene, 4.5). Anhydrous triethylamine (2.4 mL, 13.56 mmol) was added to a stirred solution of **4.4** (555 mg, 1.13 mmol) in dry THF (150 mL) at -78 °C, under an argon atmosphere. After one hour, nicotinoyl chloride hydrochloride (800 mg, 4.50 mmol) was added to the reaction mixture and stirred at -78 °C for a further two hours, before being left to stir at room temperature for 48 hours. A second portion of nicotinoyl chloride hydrochloride (800 mg, 4.50 mmol) was added

and left to stir for a further 48 hours, during which time the reaction mixture discoloured. The solvent was removed *in vacuo*, and the resultant residue triturated in ethanol to afford the target compound as a white solid. Yield 863 mg, 89 %; M.pt. Decomposes > 270 °C; HR MS (ES^+): *m/z* 808.3229 $(MH)^+$; calculated for $C_{48}H_{46}N_3O_9$ 808.3234; ^1H NMR (300Mhz, $CDCl_3$) δ (ppm) = 9.27 (s, 3H, Py-H^2), 8.83 (d, 3H, Py-H^6, *J* = 4.3 Hz), 8.40 (d, 3H, Py-H^4, *J* = 7.6 Hz), 7.52 (dd, 3H, Py-H^5, *J* = 5.3, 7.4 Hz), 7.17 (s, 3H, Ar-H), 6.95 (s, 3H, Ar-H), 4.82 (d, 3H, CTG *exo*-H, *J* = 13.6 Hz), 3.94 (t, 6H, propyl α-H, *J* = 6.4 Hz), 3.67 (d, 3H, CTG *endo*-H, *J* = 13.6 Hz), 1.65 (q, 6H, propyl β-H, *J* = 7.4 Hz), 0.86 (t, 9H, propyl γ-H, *J* = 7.4 Hz); $^{13}C\{^1H\}$ NMR (75 MHz, $CDCl_3$) δ (ppm) = 155.1, 151.6, 151.4, 149.2, 138.6, 138.2, 138.0, 137.6, 131.4, 123.8, 123.4, 115.3, 70.5, 36.5, 22.4, 10.3; Analysis for **4.5** (% calculated, found) C (71.36, 71.60), H (5.61, 5.40), N (5.08, 4.80); Infrared analysis (FT-IR, cm^{-1}) 2985 (w), 1735, 1604, 1511, 1269, 1099.

Synthesis of (±)-2,7,12-Tripropoxy-3,8,13-*tris*(4-pyridylcarboxy)-10,15-dihydro-5*H*-tribenzo[*a,d,g*]cyclononene (*tris*(isonicotinoyl)-*tris*(propoxy)-cyclotricatechylene, 4.6). Anhydrous triethylamine (2.4 mL, 13.56 mmol) was added to a stirred solution of **4.4** (555 mg, 1.13 mmol) in anhydrous THF (150 mL), at -78 °C, under an argon atmosphere. After one hour, isonicotinoyl chloride hydrochloride (800 mg, 4.50 mmol) was added to the reaction mixture and stirred at -78 °C for a further two hours before being left at room temperature for 48 hours. A second portion of isonicotinoyl chloride hydrochloride (800 mg, 4.50 mmol) was added, and left to stir for a further 48 hours, during which time the reaction mixture discoloured. The solvent was removed *in vacuo* and the resultant residue triturated in ethanol to afford the target compound as a white solid, which was isolated by filtration and dried *in vacuo*. Yield 640 mg, 66 %; M.pt. Decomposes > 270 °C; HR MS (ES^+): *m/z* 808.3232 $\{MH\}^+$; calculated for $C_{48}H_{46}N_3O_9$ 808.3234; ^1H NMR (500MHz, $CDCl_3$) δ (ppm) = 8.84 (d, 6H, Py-H^2, *J* = 6.0 Hz), 7.97 (d, 6H, Py-H^3, *J* = 6.0 Hz), 7.16 (s, 3H, aryl-H), 6.94 (s, 3H, aryl-H), 4.82 (d, 3H, CTG *exo*-H, *J* = 13.6 Hz), 3.93 (t, 6H, propyl α-H, *J* = 6.2 Hz), 3.67 (d, 3H, CTG *endo*-H, *J* = 13.6 Hz), 1.66 (q, 6H, propyl β-H, *J* = 7.4 Hz), 0.86 (t, 9H, propyl γ -H, *J* = 7.2 Hz); $^{13}C\{^1H\}$ NMR (75 MHz, $CDCl_3$) δ (ppm) = 162.6, 149.6, 148.2, 138.9, 137.9, 137.5, 131.9, 123.8, 123.6, 115.5, 69.8, 34.9, 21.7, 10.1; Analysis for **4.6**·H_2O (% calculated, found) C (69.80, 70.00), H (5.74, 5.55), N (5.09, 4.80); Infrared analysis (FT-IR, cm^{-1}) 3100, 2875, 1745 (strong), 1605, 1520.

Synthesis of $[Ag_2(4.5)_2]\cdot 2(PF_6)\cdot n$(MeCN) (complex 4.7). $AgPF_6$ (3.14 mg, 0.0224 mmol) and **4.5** (10.04 mg, 0.0125 mmol) were dissolved in acetonitrile (1 mL) and diethyl ether vapours were diffused into the solution, where small, colourless blocks formed after 14 days that were analyzed by single crystal X-ray analysis. Yield 5.1 mg. HR MS (ES^+): *m/z* 916.1713 $\{Ag(\mathbf{4.5})\}^+$, 1723.4090 $\{Ag(\mathbf{4.5})_2\}^+$ and 1976.3330 $\{[Ag_2(\mathbf{4.5})_2]\cdot(PF_6)\}^+$, calcd. for 915.2207,

1723.6394 and 1976.4085, respectively; ^{1}H NMR (300 MHz, d_3-MeCN) δ (ppm) = 9.25 (d, 6H, Py-H^2), 8.81 (dd, 6H, Py-H^6), 8.42 (dt, 6H, Py-H^4), 7.55 (dd, 6H, Py-H^5), 7.34 (s, 3H, Ar-H), 7.12 (s, 3H, Ar-H), 4.84 (d, 6H, CTG *exo*-H), 3.94 (oct, 12H, propyl α-H), 3.70 (d, 6H, CTG *endo*-H), 1.57 (sext, 12H, propyl β-H), 0.80 (t, 18H, propyl γ-H); Analysis for $[Ag_2(\mathbf{4.5})_2]\cdot 2(PF_6)\cdot 3(H_2O)$ (% calculated, found) C (53.00, 52.80), H (4.45, 4.30), N (3.86, 4.00); Infrared analysis (FT-IR, cm^{-1}) 2967, 1740, 1606, 1506, 1434, 1281, 1202, 1179, 1138, 1103, 971, 839, 736, 557.

Preparation of heteroleptic $[Ag_2(4.5)(2.7)]\cdot 2(PF_6)$ and $[Ag_3(4.5)(2.7)]\cdot 2(PF_6)$

$AgPF_6$ (3.14 mg, 0.0125 mmol), ligand **4.5** (5.04 mg, 0.0063 mmol) and ligand **2.7** (4.55 mg, 0.0063 mmol) were dissolved in acetonitrile (1 mL) and stirred at room temperature for six hours. HR MS (ES$^+$): *m/z* 1807.1603 $\{[Ag_2(\mathbf{2.7})_2]\cdot(PF_6)\}^+$, 1891.2483 $\{[Ag_2(\mathbf{2.7})(\mathbf{4.5})]\cdot(PF_6)\}^+$, 1975.3670 $\{[Ag_2(\mathbf{4.5})_2]\cdot(PF_6)\}^+$ and 2145.0777 $\{[Ag_3(\mathbf{2.7})(\mathbf{4.5})]\cdot 2(PF_6)\}^+$, calculated for 1807.2174, 1891.3113, 1976.4085 and 2144.1447, respectively; ^{1}H NMR (300 MHz, d_6-DMSO) δ (ppm) = 9.23 (bs, 6H, Py-H^2), 8.91 (bd, 6H, Py-H^6), 8.44 (m, 6H, Py-H^4), 7.66 (dd, 6H, Py-H^5), 7.54 (m, 6H, Ar-H), 7.32 (s, 6H, Ar-H), 4.88 (bs, 6H, CTG *exo*-H), 3.92 (m, 6H, **4.5** propyl α-H), 3.69 (bs, 6H, CTG *endo*-H), 1.53 (sext, 6H, **4.5** propyl β-H), 0.75 (t, 9H, **4.5** propyl γ-H).

Preparation of $[Pd_3(en)_3(4.6)_2]\cdot 6(NO_3)$ (complex 4.8). $Pd(en)(NO_3)_2$ (5.42 mg, 0.0186 mmol) was added to a solution of ligand **4.6** (10.04 mg, 0.0124 mmol) in d_6-DMSO and stirred at room temperature for 16 hours, during which time the solution decolourised. HR MS (ES$^+$): *m/z* 724.8388 $\{[Pd_3(en)_1(\mathbf{4.6})_2]\cdot 3(NO_3)\}^{3+}$, 745.8361 $\{[Pd_3(en)_2(\mathbf{4.6})_2]\cdot 3(NO_3)\}^{3+}$, 766.8358 $\{[Pd_3(en)_3(\mathbf{4.6})_2]\cdot 3(NO_3)\}^{3+}$, 792.8406 $\{[Pd_3(en)_3(\mathbf{4.6})_2]\cdot 3(NO_3)\subset(DMSO)\}^{3+}$, 1149.7511 $\{[Pd_3(en)_2(\mathbf{4.6})_2]\cdot 4(NO_3)\}^{2+}$ and 1181.2535 $\{[Pd_3(en)_3(\mathbf{4.6})_2]\cdot 4(NO_3)\}^{2+}$, calculated for 726.1246, 746.1475, 766.8389, 792.8435, 1151.2178 and 1181.2523 respectively; ^{1}H NMR (300 MHz, d_6-DMSO) δ (ppm) = 8.90-9.45 (bm, 12H, Py-H^2), 8.17 (s, 12H, Py-H^3), 7.41-7.54 (bm, 6H, Ar-H), 7.22-7.30 (bm, 6H, Ar-H), 5.75 (bs, 6H, en-NH_2), 5.67 (bs, 6H, en-NH_2), 4.86 (bs, 6H, CTG *exo*-H), 3.92 (bs, 9H, propyl α-H), 3.79 (bs, 4H, propyl α-H), 3.67 (bs, 6H, CTG *endo*-H), 2.70 (bs, 12H, en-CH_2), 1.51 (q, 8H, propyl β-H), 1.31 (bq, 3H, propyl β-H), 0.76 (t, 12H, propyl γ-H), 0.49 (t, 5H, propyl γ-H). Complex **4.8** was observed to degrade over time to afford complex **4.9** which was isolated as pale yellow block crystals. Yield 13 mg, quant.; HR MS (ES$^+$): *m/z* 919.2482 $\{[Pd_6(\mathbf{4.6})_8]\cdot 4NO_3\}^{8+}$, 1058.8043 $\{[Pd_6(\mathbf{4.6})_8]\cdot 5NO_3\}^{7+}$, 1245.4923 $\{[Pd_6(\mathbf{4.6})_8]\cdot 6NO_3\}^{6+}$ and 1507.0100 $\{[Pd_6(\mathbf{4.6})_8]\cdot 7NO_3\}^{5+}$ calculated for 918.9889, 1059.1284, 1245.9811 and 1507.5749 respectively; ^{1}H NMR (300 MHz, d_6-DMSO) δ (ppm) = 9.59 (s, 3H, Py-H^2), 9.48 (s, 3H, Py-H^2), 8.23 (s, 6H, Py-H^3), 7.44 (s, 3H, aryl-H), 7.28 (s, 3H, aryl-H), 4.87

(bs, 3H, CTG *exo*-H), 3.84 (bm, 6H, propyl α-H), 3.69 (bs, 3H, CTG *endo*-H), 1.32 (m, 6H, propyl β-H), 0.52 (m, 9H, propyl γ -H). A detailed characterisation of complex **4.9**, including both solution and solid-phase analysis will follow in Chapter 5.

4.7.3 Supplementary crystallographic information

Crystals of complex **4.1** diffracted poorly, and there were no observed data above 45 ^{o} in 2θ. The structure was refined as a merohedral twin in *Cc* with refined Flack parameter 0.58 (4), and there was no indication of higher symmetry. A number of pyridyl rings were treated with a rigid body refinement and some anisotropic displacement parameters were refined with restraints to be similar across the functional group. The ClO_4^- anions were all highly disordered, one was disordered across two sites, and the O positions were all highly disordered and should be regarded as unreliable. Solvent DMF and O positions on ClO_4^- were refined anisotropically. The structure contained significant solvent accessible voids and there was significant diffuse residual density which could not be adequately modelled as solvent. Hence the SQUEEZE routine of PLATON was employed,[70] which resulted in significant reduction in R_1 from ~18% to ~10%.

One pyridyl group of clathrate complex **4.5** was refined over two positions and one propyl moiety was modelled as disordered and its bonds restrained to be chemically reasonable. One DMF C-O bond was restrained to be chemically sensible. One pyridyl group of clathrate complex **4.6** was restrained to be flat and the three water molecules were refined at half occupancy. For complex **4.7**, one acetonitrile solvent molecule was refined at half occupancy and its bonds refined to be chemically reasonable.

4.7.4 X-ray data tables for complexes 4.1, 4.5-4.7

	4.1	**4.5**	**4.6**	**4.7**
Formula	$C_{177}H_{177}Ag_6Cl_6N_{15}O_{51}$	$C_{54}H_{61}N_5O_{12}$	$C_{48.5}H_{50.5}N_{3.5}O_{11.5}$	$C_{53}H_{52.5}AgF_6N_{5.5}O_9P$
Mr	4190.26	972.08	866.42	1163.34
Crystal colour and shape	Colourless, block	Colourless, block	Colourless, block	Colourless, needle
Crystal size (mm)	0.08 x 0.08 x 0.02	0.14 x 0.14 x 0.12	0.18 x 0.18 x 0.14	0.16 x 0.10 x 0.06
Crystal system	Monoclinic	Triclinic	Triclinic	Triclinic
Space group	*Cc*	*P*$\bar{1}$	*P*$\bar{1}$	*P*$\bar{1}$
a (Å)	33.352(3)	14.4759(16)	13.506(2)	14.3501(8)
b (Å)	19.288(2)	14.4859(17)	15.495(3)	14.5130(9)
c (Å)	40.328(3)	16.2902(17)	16.120(3)	15.3121(9)
α (^{0})	90.00	65.495(5)	62.596(8)	112.683(2)
β (^{0})	104.583(4)	63.930(5)	65.374(8)	91.710(2)
γ (^{0})	90.00	61.625(5)	64.841(8)	100.098(2)
V (Å^3)	25107(4)	2606.5(5)	2602.2(8)	2880.0(3)
Z	4	2	2	2
ρ_{calc} (g.cm^{-3})	1.109	1.239	1.104	1.342
θ range (^{0})	1.26 – 22.50	1.44 – 26.00	1.48 – 22.98	2.09 – 23.92
No. data collected	59610	50630	21791	42434
No. unique data	27816	9992	6798	8568
R_{int}	0.0885	0.0367	0.0511	0.0455
No. obs. Data ($I > 2\sigma(I)$)	15793	6179	3625	7416
No. parameters	1700	568	572	685
No. restraints	110	5	4	2
R_1 (obs data)	0.1066	0.1282	0.1777	0.0913
wR_2 (all data)	0.2685	0.3896	0.4876	0.2526
S	1.325	2.454	2.868	1.145

4.8 Bibliography

[1] D. J. Cram, *Angew. Chem. Int. Ed.* **1988**, *27*, 1009-1020.

[2] R. A. Brown, V. Diemer, S. J. Webb, J. Clayden, *Nat. Chem.* **2013**, *5*, 853-860.

[3] M. Juríček, N. L. Strutt, J. C. Barnes, A. M. Butterfield, E. J. Dale, K. K. Baldridge, J. F. Stoddart, J. S. Siegel, *Nat. Chem.* **2014**, *6*, 222-228.

[4] F. Hof, S. L. Craig, C. Nuckolls, J. J. Rebek, *Angew. Chem. Int. Ed.* **2002**, *41*, 1488-1508.

[5] Y. Inokuma, M. Kawano, M. Fujita, *Nat. Chem.* **2011**, *3*, 349-358.

[6] J. E. M. Lewis, E. L. Gavey, S. A. Cameron, J. D. Crowley, *Chem. Sci.* **2012**, *3*, 778-784.

[7] D. Ajami, J. Rebek, *Nat. Chem.* **2009**, *1*, 87-90.

[8] T. Brotin, J.-P. Dutasta, *Chem. Rev.* **2008**, *109*, 88-130.

[9] J. W. Steed, H. Zhang, J. L. Atwood, *Supramol. Chem.* **1996**, *7*, 37-45.

[10] O. Taratula, P. A. Hill, N. S. Khan, P. J. Carroll, I. J. Dmochowski, *Nat. Commun.* **2010**, *1*, 148.

[11] J. Costante, C. Garcia, A. Collet, *Chirality* **1997**, *9*, 446-453; A. Collet, J. Gabard, J. Jacques, M. Cesario, J. Guilhem, C. Pascard, *J. Chem. Soc., Perkin Trans.* **1981**, *1*, 1630-1638.

[12] K. T. Holman, *Encyclopedia of Supramolecular Chemistry. CRC Press* **2004**, 340-348.

[13] M. A. Little, J. Donkin, J. Fisher, M. A. Halcrow, J. Loder, M. J. Hardie, *Angew. Chem. Int. Ed.* **2011**, *51*, 764-766.

[14] L. Schröder, T. J. Lowery, C. Hilty, D. E. Wemmer, A. Pines, *Science* **2006**, *314*, 446-449.

[15] G. Haberhauer, Á. Pintér, S. Woitschetzki, *Nat. Commun.* **2014**, *5*, 3542.

[16] J. Canceill, A. Collet, J. Gabard, G. Gottarelli, G. P. Spada, *J. Am. Chem. Soc.* **1985**, *107*, 1299-1308.

[17] M. J. Hardie, *Chem. Soc. Rev.* **2010**, *39*, 516-527.

[18] M. J. Hardie, *Israel J. Chem.* **2011**, *51*, 807-816.

[19] Z. Zhong, A. Ikeda, S. Shinkai, S. Sakamoto, K. Yamaguchi, *Org. Lett.* **2001**, *3*, 1085-1087.

[20] T. K. Ronson, H. Nowell, A. Westcott, M. J. Hardie, *Chem. Commun.* **2010**, *47*, 176-178.

[21] J. J. Henkelis, T. K. Ronson, L. P. Harding, M. J. Hardie, *Chem. Commun.* **2011**, *47*, 6560-6562.

[22] U. Radhakrishnan, M. Schweiger, P. J. Stang, *Org. Lett.* **2001**, *3*, 3141-3143.

[23] C. J. Kuehl, Y. K. Kryschenko, U. Radhakrishnan, S. R. Seidel, S. D. Huang, P. J. Stang, *Proc. Natl. Acad. Sci. USA* **2002**, *99*, 4932-4936.

[24] S. Tartaggia, O. De Lucchi, A. Gambaro, R. Zangrando, F. Fabris, A. Scarso, *Chem. Eur. J.* **2013**, *18*, 5701-5714.

[25] S. L. Cockroft, C. A. Hunter, K. R. Lawson, J. Perkins, C. J. Urch, *J. Am. Chem. Soc.* **2005**, *127*, 8594-8595; C. A. Hunter, J. K. M. Sanders, *J. Am. Chem. Soc.* **1990**, *112*, 5525-5534.

[26] K. S. Chichak, S. J. Cantrill, A. R. Pease, S.-H. Chiu, G. W. V. Cave, J. L. Atwood, J. F. Stoddart, *Science* **2004**, *304*, 1308-1312.

[27] C. Piguet, *Dalton Trans.* **2011**, *40*, 8059-8071.

[28] S.-K. Lin, *J. Chem. Inf. Comp. Sci.* **1996**, *36*, 367-376.

[29] J.-T. Yu, Y.-Y. Shi, J. Sun, J. Lin, Z.-T. Huang, Q.-Y. Zheng, *Sci. Rep.* **2013**, *3*, 2947.

[30] A. M. Castilla, N. Ousaka, R. A. Bilbeisi, E. Valeri, T. K. Ronson, J. R. Nitschke, *J. Am. Chem. Soc.* **2013**, *135*, 17999-18006.

[31] J. E. Beves, C. J. Campbell, D. A. Leigh, R. G. Pritchard, *Angew. Chem. Int. Ed.* **2013**, *52*, 6464-6467.

[32] C. Jia, B. P. Hay, R. Custelcean, *Inorg. Chem.* **2014**, *53*, 3893-3898.

[33] K. Mislow, R. Bolstad, *J. Am. Chem. Soc.* **1955**, *77*, 6712-6713.

[34] O. Safarowsky, B. Windisch, A. Mohry, F. Vögtle, *Journal für praktische Chemie* **2000**, *342*, 437-444.

[35] C. Carruthers, T. K. Ronson, C. J. Sumby, A. Westcott, L. P. Harding, T. J. Prior, P. Rizkallah, M. J. Hardie, *Chem. Eur. J.* **2008**, *14*, 10286-10296.

[36] D. R. Link, G. Natale, R. Shao, J. E. Maclennan, N. A. Clark, E. Körblova, D. M. Walba, *Science* **1997**, *278*, 1924-1927.

[37] N. Guex, M. C. Peitsch, *Electrophoresis* **1997**, *18*, 2714

[38] S. Mecozzi, J. J. Rebek, *Chem. Eur. J.* **1998**, *4*, 1016-1022.

[39] A. Westcott, J. Fisher, L. P. Harding, P. Rizkallah, M. J. Hardie, *J. Am. Chem. Soc.* **2008**, *130*, 2950-2951.

[40] C. O. Dietrich-Buchecker, J. P. Sauvage, J. P. Kintzinger, *Tett. Lett.* **1983**, *24*, 5095-5098.

[41] C. Lincheneau, B. Jean-Denis, T. Gunnlaugsson, *Chem. Commun.* **2014**, *50*, 2857-2860.

[42] L. M. Hancock, L. C. Gilday, N. L. Kilah, C. J. Serpell, P. D. Beer, *Chem. Commun.* **2011**, *47*, 1725-1727.

[43] P. R. Ashton, T. T. Goodnow, A. E. Kaifer, M. V. Reddington, A. M. Z. Slawin, N. Spencer, J. F. Stoddart, C. Vicent, D. J. Williams, *Angew. Chem. Int. Ed.* **1989**, *28*, 1396-1399.

[44] C. Peinador, V. C. Blanco, J. M. Quintela, *J. Am. Chem. Soc.* **2008**, *131*, 920-921.

[45] M. Fujita, F. Ibukuro, H. Hagihara, K. Ogura, *Nature* **1994**, *367*, 720-723.

[46] M. Fujita, N. Fujita, K. Ogura, K. Yamaguchi, *Nature* **1999**, *400*, 52-55.

[47] S. Freye, R. Michel, D. Stalke, M. Pawliczek, H. Frauendorf, G. H. Clever, *J. Am. Chem. Soc.* **2013**, *135*, 8476-8479.

[48] M. Han, D. M. Engelhard, G. H. Clever, *Chem. Soc. Rev.* **2014**, *43*, 1848-1860.

[49] T. Hasell, X. Wu, T. A. JonesJames, J. Bacsa, A. Steiner, T. Mitra, A. Trewin, D. J. Adams, A. I. Cooper, *Nat. Chem.* **2010**, *2*, 750-755.

[50] C. Piguet, *Chem. Commun.* **2010**, *46*, 6209-6231.

[51] R. Ahmad, M. J. Hardie, *Supramol. Chem.* **2006**, *18*, 29-38.

[52] J. Canceill, J. Gabard, A. Collet, *J. Chem. Soc., Chem. Commun.* **1983**, 122-123.

[53] J. Canceill, L. Lacombe, A. Collet, *J. Chem. Soc., Chem. Commun.* **1987**, 219-221.

[54] J. L. Scott, D. R. MacFarlane, C. L. Raston, C. M. Teoh, *Green Chem.* **2000**, *2*, 123-126.

[55] M. J. Hardie, R. M. Mills, C. J. Sumby, *J. Org. Biol. Chem.* **2004**, *2*, 2958-2964.

[56] M. A. Little, M. A. Halcrow, M. J. Hardie, *Chem. Commun.* **2013**, *49*, 1512-1514.

[57] M. A. Little, M. A. Halcrow, L. P. Harding, M. J. Hardie, *Inorg. Chem.* **2010**, *49*, 9486-9496.

[58] S. T. Mough, J. C. Goeltz, K. T. Holman, *Angew. Che,m. Int. Ed.* **2004**, *43*, 5631-5635.

[59] T. K. Ronson, C. Carruthers, J. Fisher, T. Brotin, L. P. Harding, P. J. Rizkallah, M. J. Hardie, *Inorg. Chem.* **2010**, *49*, 675-685.

[60] T. K. Ronson, J. Fisher, L. P. Harding, M. J. Hardie, *Angew. Chem. Int. Ed.* **2007**, *46*, 9086-9088.

[61] M. Nilsson, *J. Mag. Resn.* **2009**, *200*, 296-302.

[62] M. Fujita, D. Oguro, M. Miyazawa, H. Oka, K. Yamaguchi, K. Ogura, *Nature* **1995**, *378*, 469-471.

[63] N. Takeda, K. Umemoto, K. Yamaguchi, M. Fujita, *Nature* **1999**, *398*, 794-796.

[64] J. Hamacek, M. Borkovec, C. Piguet, *Dalton Trans.* **2006**, 1473-1490.

[65] A. Stephenson, S. P. Argent, T. Riis-Johannessen, I. S. Tidmarsh, M. D. Ward, *J. Am. Chem. Soc.* **2010**, *133*, 858-870.

[66] W. Meng, T. K. Ronson, J. K. Clegg, J. R. Nitschke, *Angew. Chem. Int. Ed.* **2012**, *52*, 1017-1021.

[67] D. K. Chand, R. Manivannan, H. S. Sahoo, K. Jeyakumar, *Eur. J. Inorg. Chem.* **2005**, *2005*, 3346-3352.

[68] G. Sheldrick, *Acta. Crystallogr., Sect. A* **2008**, *A64*, 112-122; L. J. Barbour, *Supramol. Chem.* **2001**, *1*, 189-191.

[69] Persistence of Vision Raytracer Pty. Ltd. Williamstown, **2004**.

[70] A. L. Spek, *Acta. Crystallogr., Sect. A* **1990**, *A46*, 194-201.

Chapter 5

High fidelity self-assembly control of Pd_6L_8 metallo-supramolecular cages

5.1 Introduction

Control over the assembly, chirality and speciation of a supermolecule is a common goal across the biological and physical sciences,[1] and understanding the way in which complex biological systems structurally 'evolve' to perform a given function is highly important in the continuous development of synthetic supramolecular chemistry.[2] Darwinian evolution has of course perfected their structure and function [3] and synthetic supramolecular self-assembly remains in its relative infancy.[4] However, its growth will ultimately help bridge the gap between these natural and unnatural systems.[5]

Being able to control the self-assembly processes of synthetic systems is key to the predictable installation of desirable properties and required functionality.[6] Their properties are generally 'emergent' and are therefore only realised as the complex,[7] and not as the individual molecular components.[8] Achieving this with a high degree of control allows for their implementation in molecular switches [9] and information processing,[10] alongside cage-type constructs for guest incarceration,[11] cargo delivery [12] and catalysis.[13]

In metallo-supramolecular chemistry, careful tailoring of the molecular building blocks (generally ligands) allows for their self-assembly to be controlled.[14] The employment of sterically and interactionally similar ligand sets allows for the formation of either homo- or heteroleptic complexes,[15] which ultimately allows for the structural elucidation of complexes that are ordinarily inaccessible with a single ligand system.[16] Fujita and co-workers, for example, have reported a system where incremental expansions to ligand bite angle effect a considerable structural change between $M_{12}L_{24}$ and $M_{24}L_{48}$ polyhedra.[17] Likewise, the groups of Stang [18] and Yamaguchi [19] have shown that multi-ligand systems can undergo reversible exchange at room temperature to afford a variety of products. Alternatively, Ward and co-workers have shown how a sterically and interactionally similar ligand pair of multidentate pyridine-pyrazole ligands can each self-assemble into a tetrahedral complex when a templating tetrahedral anion is used; yet heteroleptic complexes are formed when largely different ligand systems are employed in direct competition.[20]

Reported within Chapter 4 of this thesis was a symmetry-driven cage-to-cage expansion of a metastable metallo-cryptophane, $[Pd(en)_3(\mathbf{4.6})_2]\cdot 6(NO_3)$ (complex **4.8**), to an octahedral 'stella octangula' coordination cage, $[Pd_6(\mathbf{4.6})_8]\cdot 12(NO_3)$ (complex **4.9**). Complex **4.9** was noted to possess increased solubility over its methylated congener, which should allow for detailed

solution-phase analysis and a thorough examination of its hosting abilities. Ultimately, ligands **2.8** and **4.6** represent a sterically and interactionally similar ligand pair that are each capable of affording structurally analogous $[Pd_6L_8]^{12+}$ metallo-supramolecular cages, **Scheme 5.1**. The following is a detailed examination into the chemistry, dynamics and controllability of these 'stella octangula' cages.

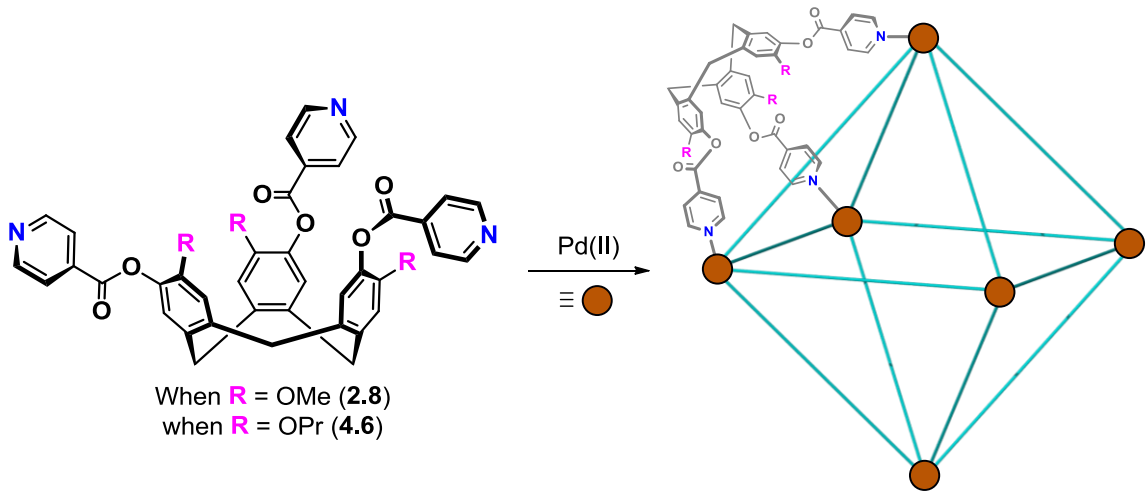

Scheme 5.1 *The sterically and interactionally ligand pair used in the following study and the generic formation of the* $[Pd_6L_8]^{12+}$ *stella octangula cages.*

5.2 Solvent-dependent chirality control and sterically-induced ligand scrambling

The reaction of eight equivalents of ligand (*rac*)-**4.6** with six equivalents of palladium(II) tetrafluoroborate (BF_4^-) saw the immediate and quantitative formation of the stella octangula cage $[Pd_6(\mathbf{4.6})_8]\cdot 12(BF_4)$, complex **5.1**, based on ^{1}H NMR spectroscopy and mass spectrometry. Employment of the BF_4^- anion over nitrate (NO_3^-) was to ensure complete dissociation from the cage and ensure consistency when comparing the solution-phase chemistry of individual stella octangula cages. Complex **5.1** was relatively soluble in organic solvents, in contrast with its methyl congener which only exists in DMSO solution at low concentrations.[21] Mass spectra were identical in DMSO, DMF, MeCN and $MeNO_2$ solvents, alongside a 9:1 mixture of MeCN and water. For example, the mass spectrum collected in DMSO solvent indicated the mass peaks (*m/z*) 1949.6343, 1542.0858, 1270.3947 and 1076.7391, which were attributable to $\{[Pd_6(\mathbf{4.6})_8]\cdot 8(BF_4)\}^{4+}$, $\{[Pd_6(\mathbf{4.6})_8]\cdot 7(BF_4)\}^{5+}$, $\{[Pd_6(\mathbf{4.6})_8]\cdot 6(BF_4)\}^{6+}$ and $\{[Pd_6(\mathbf{4.6})_8]\cdot 5(BF_4)\}^{7+}$, respectively. Cage-DMSO adducts were also identified in the mass spectra. The 4+ charge state, for example, included the mass peaks (*m/z*) 1968.5019 and 1988.5064 which corresponded to $\{[Pd_6(\mathbf{4.6})_8]\cdot 8(BF_4)\subset(DMSO)\}^{4+}$ and $\{[Pd_6(\mathbf{4.6})_8]\cdot 8(BF_4)\subset(DMSO)_2\}^{4+}$, respectively. A typical mass spectrum of complex **5.1** in DMSO solution is shown in **Figure 5.1**. It is important to note that the mass spectra of complex

5.1 do not alter with time (months) or heat and the $\{[Pd_6(\mathbf{4.6})_8]\cdot n(BF_4)\}^{(12-n+)}$ mass peaks are the only observable species present in the gas phase, with no other complexes identified.

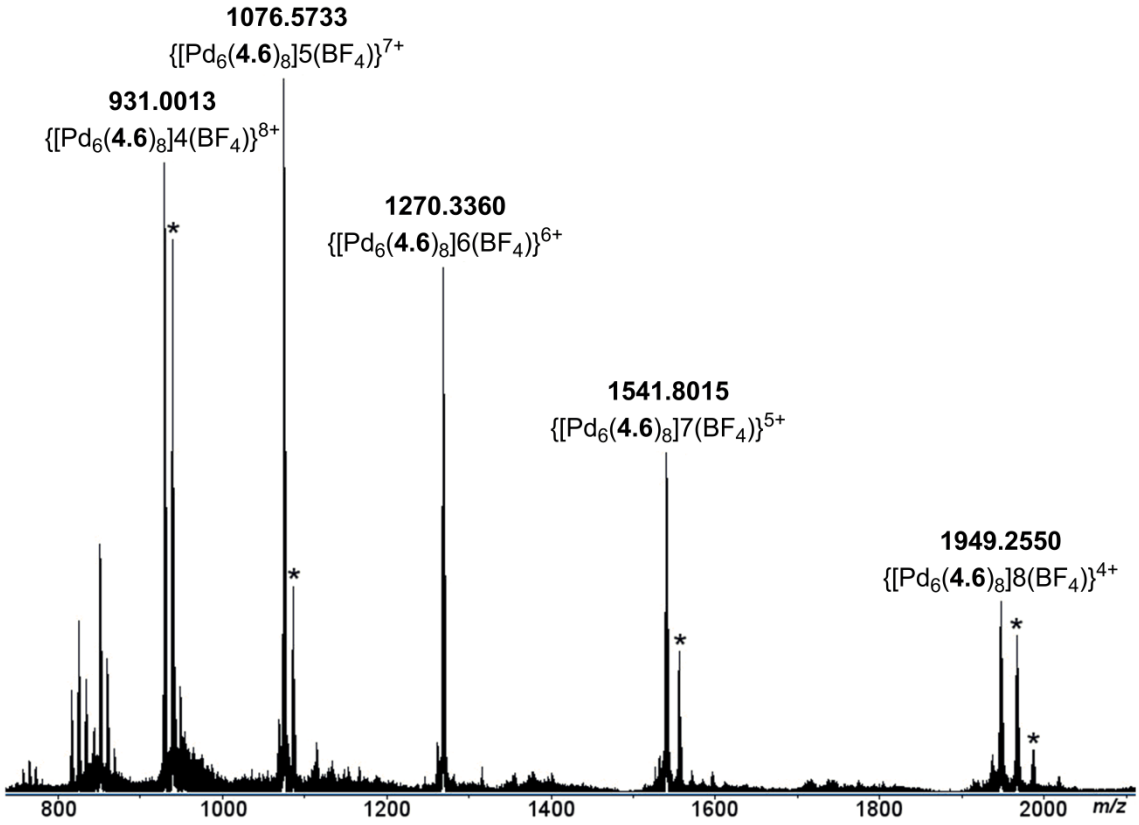

Figure 5.1 *Electrospray mass spectrum of complex* ***5.1*** *in DMSO solvent. Cage-DMSO adducts are indicated by asterisks.*

^{1}H NMR spectra of complex **5.1** were collected in d_6-DMSO, d_3-MeCN, d_7-DMF and d_3-$MeNO_2$ solvents and continuously monitored at regular intervals until fully equilibrated. Whilst the mass spectra of complex **5.1** were identical in all solvents, the corresponding proton NMR spectra indicated a solvent dependence. Strong coordination-induced down-field shifts were noted for the *ortho*-pyridyl protons in all solvents, as well as upfield shifting of the β- and γ-protons of the propyl chain. The propyl chains are situated at the windows of the stella octangula cage and therefore in close proximity with one another. The broadness and shielding of these protons is likely due to their fluxional movement between the internal, hydrophobic cavity and the external, bulk environments on the NMR timescale. Similarly, all ^{1}H NMR spectra were approximately symmetrical, and indicated the presence of only one large species according to diffusion ordered NMR spectroscopy (DOSY) with an approximate hydrodynamic radius (r) calculated to be 23.4 Å.

Whilst the $[Pd_6(\mathbf{4.6})_8]^{12+}$ cage assembles both rapidly and quantitatively, ligand exchange about the Pd_6 octahedral framework can continue to occur over a period of weeks, depending on the

solvent used. The ^{1}H NMR spectra of complex **5.1** in the polar aprotic solvents d_6-DMSO and d_7-DMF displayed identical and broad spectra that did not sharpen with time, **Figure 5.2**. The pyridyl proton resonances remained uncharacteristically broad and the *ortho*-protons were split into two broad singlets at 9.46 and 9.59 ppm. A true octahedral cage with O_h point group symmetry should afford only two equivalent pyridyl resonances for the *ortho* and *meta*-protons. Whilst the rest of the NMR spectrum remains relatively symmetric, this pyridyl asymmetry is indicative of ligand disorder about the Pd_6 framework.

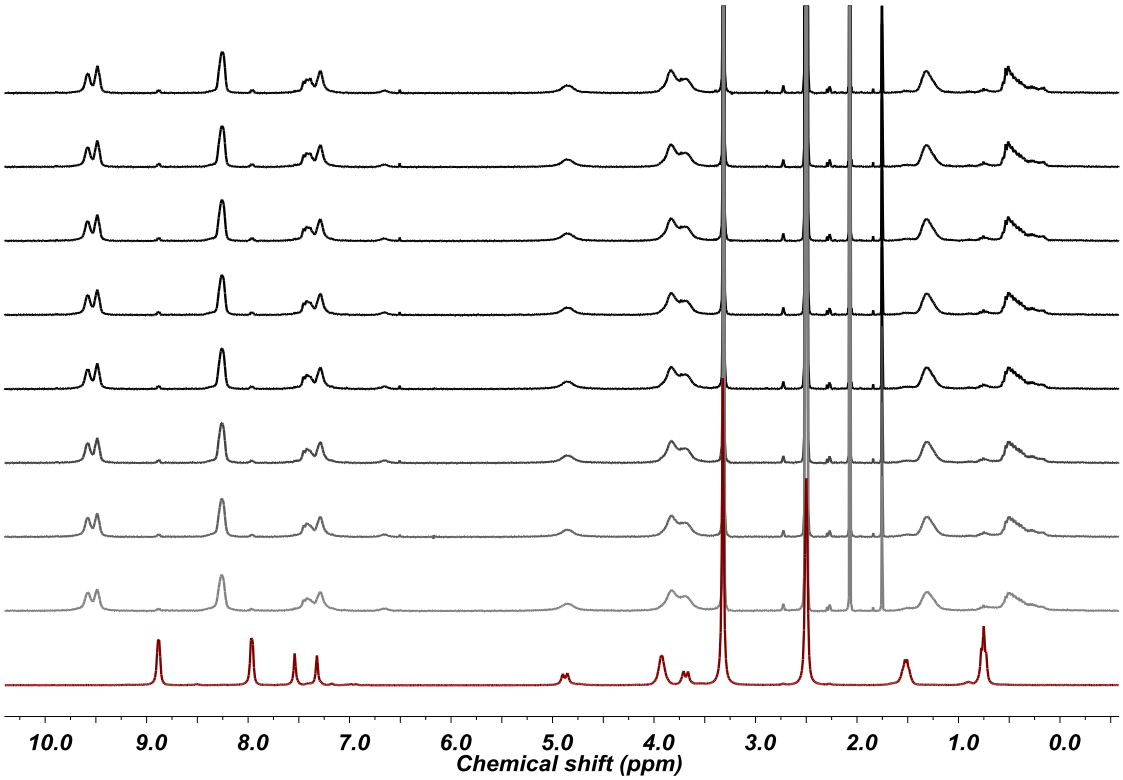

Figure 5.2 *Timecourse proton NMR spectra of ligand* ***4.6*** *(red trace) and complex* ***5.1*** *(black traces, increasing with time over two weeks) in d_6-DMSO.*

The ligand asymmetry about the Pd_6 framework is related to ligand chirality, where the broadness and inequivalence of the pyridyl resonances is due to the inclusion of both ***M*** and ***P*** ligand enantiomers into the cage complex. This hypothesis was supported through solution-phase measurements of complex **5.1** in d_3-MeCN and d_3-$MeNO_2$, which, unlike the measurements obtained in DMSO and DMF, did display further ligand exchange with time. The ^{1}H NMR spectra obtained in d_3-MeCN afforded broad resonances as for d_6-DMSO, which continued to sharpen over a period of weeks to give a well-resolved and down-field shifted doublet of the *ortho*-pyridyl proton at 9.14 ppm, **Figure 5.3**. The equilibrated resonances are believed to correspond to a higher symmetry, homochiral cage and the broadened spectra gained initially as a result of the inclusion of both ligand enantiomers about the Pd_6 framework. There

is, however, a minor component in the NMR spectrum which remains broadened and diffuses slightly slower than the homochiral cage, which is predicted to be a small proportion of unsorted cage that is unable to self-sort over any reasonable timescale. The immediate formation and subsequent equilibration of the $[Pd_6(\mathbf{4.6})_8]^{12+}$ cages suggests that they may be both the kinetic and thermodynamic products, although additional experiments are required to conclusively remark on the systems thermodynamics.[22] To convert between the 'unsorted' and homochiral enantiomers of the stella octangula cage ligands must completely dissociate, although it is likely to be a concerted and associative process. To do so they must break three Pd(II)-pyridyl coordination bonds, implying a considerable driving force to reach homochirality.[23] It is important to note that all mass spectra collected during the equilibration process identified only mass peaks pertaining to the $\{[Pd_6(\mathbf{4.6})_8]\cdot n(BF_4)\}^{(12-n+)}$ stella octangula complex, and were independent of equilibration time.

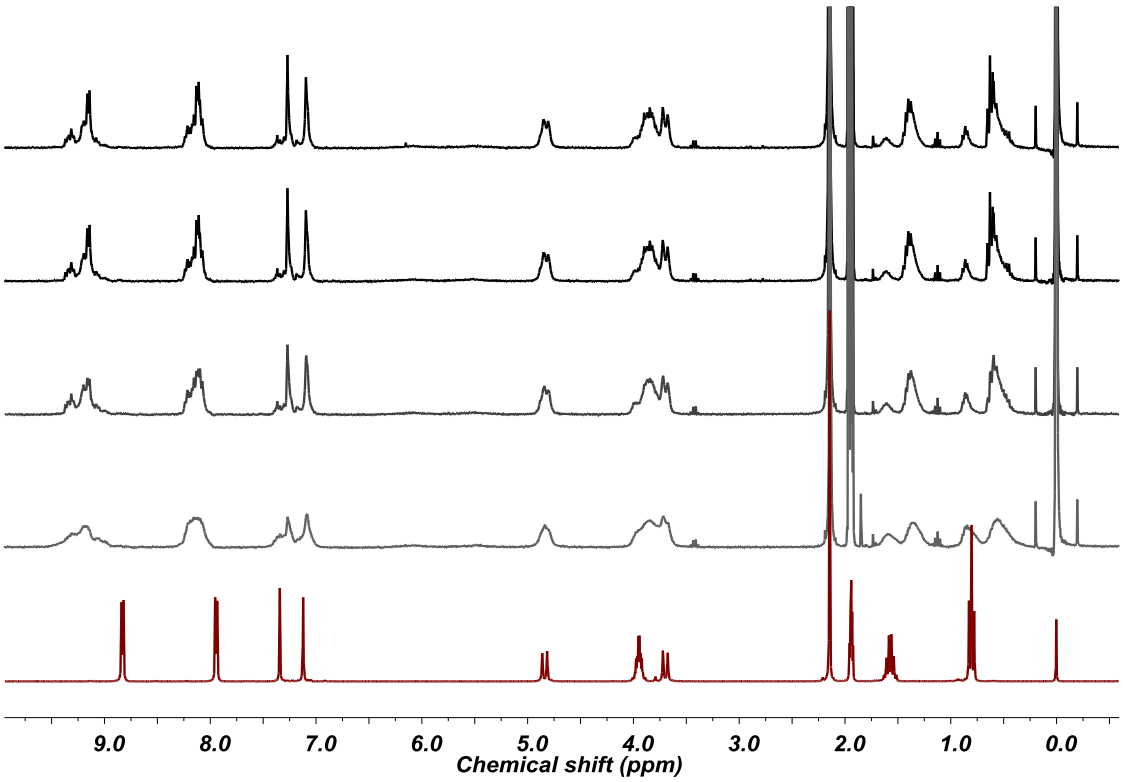

Figure 5.3 *Timecourse proton NMR spectra of ligand* ***4.6*** *(red trace) and complex* ***5.1*** *(black traces, increasing with time over two weeks) in d_3-MeCN.*

More interesting, are the ^{1}H NMR spectra recorded in d_3-$MeNO_2$, which indicate the rapid formation of the homochiral cage after only two hours; however, the $[Pd_6(\mathbf{4.6})_8]^{12+}$ stella octangula cage is never achieved quantitatively, in spite of the time frame or conditions employed, **Figure 5.4**. The ability to self-sort so rapidly (in low yield) in $MeNO_2$ solvent can be

rationalised in terms of its poor relative coordinating ability, whereas DMSO, DMF and MeCN solvents are well known to be coordinating solvents that facilitate self-assembly.[24]

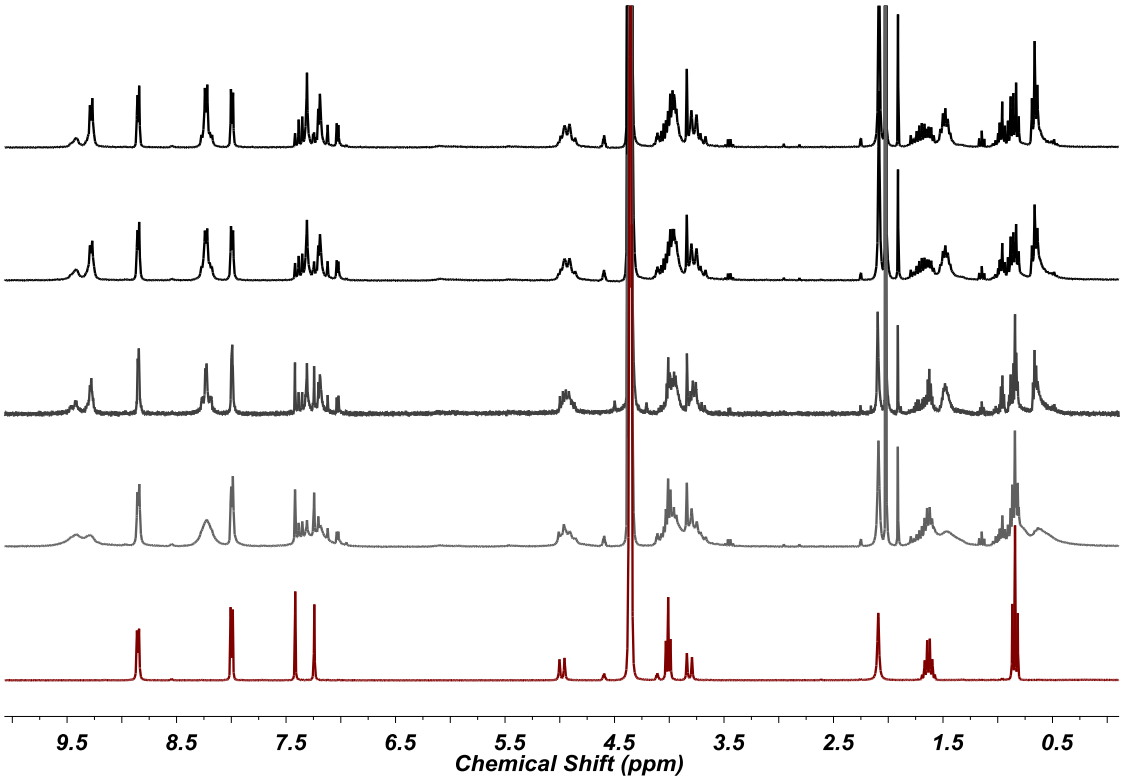

Figure 5.4 *Timecourse proton NMR spectra of ligand* ***4.6*** *(red trace) and complex* ***5.1*** *(black traces, increasing with time over two weeks) in d_3-$MeNO_2$. Note the broadened initial spectrum of the cage, followed by incomplete conversion to the homochiral species over two hours.*

The above data indicate that complex **5.1** forms rapidly and exists as a mixture of $[Pd_6(\mathbf{4.6})_8]^{12+}$ cages in solution, all built on the same Pd_6 framework, but are also controllable by the nature of the solvent employed. Thus, the stella octangula $[Pd_6(\mathbf{4.6})_8]^{12+}$ cage shows an inability to further self-sort in DMSO or DMF solvent, displays slow spontaneous chiral resolution in MeCN and rapid but incomplete self-sorting in $MeNO_2$.

To put this self-assembly behaviour into context, the methylated stella octangula cage $[Pd_6(\mathbf{2.8})_8]\cdot 12(BF_4)$, complex **5.2**, was prepared and subjected to the same solution and gas-phase studies. Complex **5.2** was prepared using ligand (*rac*)-**2.8** in place of ligand **4.6**, and observed to form immediately by NMR spectroscopy and mass spectrometry.[25] As already indicated, complexes **5.1** and **5.2** are essentially isostructural and differ only in their upper rim alkoxy substituents, and hence their solubility. The mass spectra of complex **5.2** in DMSO solution displayed the mass peaks of (*m/z*) 1158.1294, 1407.3632 and 1780.7396, which corresponded to $\{[Pd_6(\mathbf{2.8})_8]\cdot 6(BF_4)\}^{6+}$, $\{[Pd_6(\mathbf{2.8})_8]\cdot 7(BF_4)\}^{5+}$ and $\{[Pd_6(\mathbf{2.8})_8]\cdot 8(BF_4)\}^{4+}$, respectively. Conversely to the DMSO solvate of complex **5.1**, the ^1H NMR spectra of complex

5.2 in d_6-DMSO displayed a clear solvent dependence, **Figure 5.5**. The initial resonances were broad, which then sharpened over a two-week period to display the expected *meta* and *ortho*-pyridyl doublets at 8.19 and 9.48 ppm, respectively.

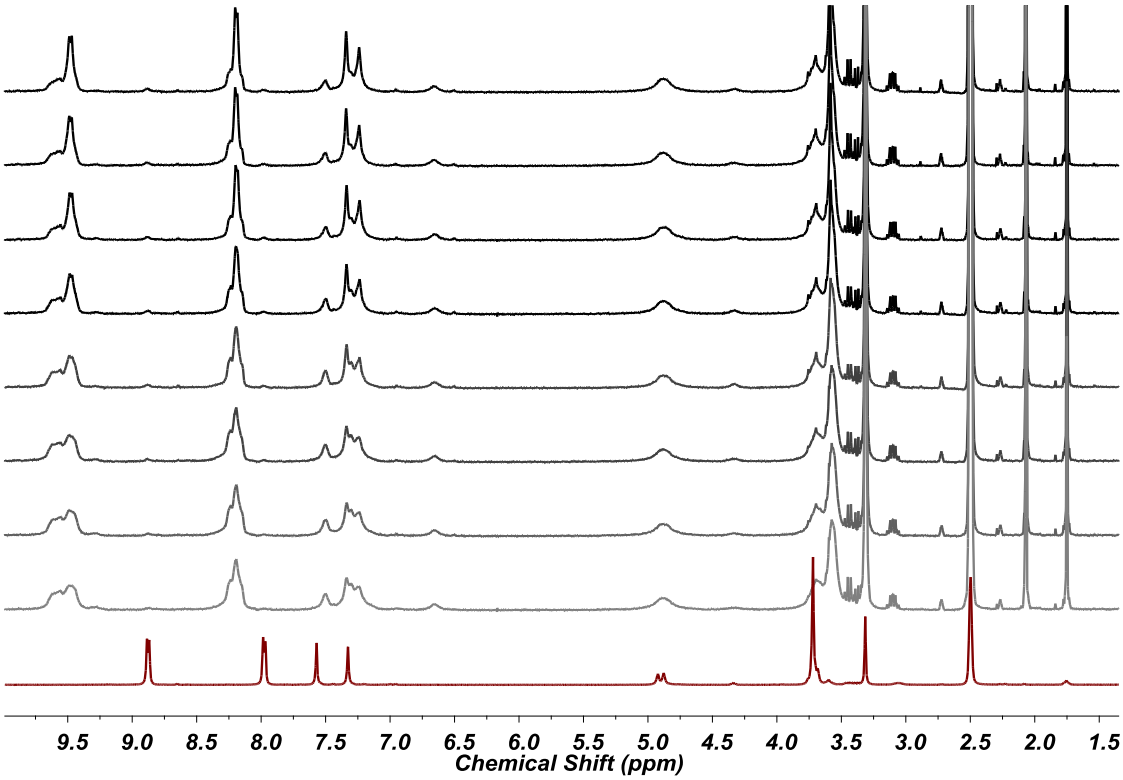

Figure 5.5 *Timecourse proton NMR spectra of ligand **2.8** (red trace) and complex **5.2** (black traces, increasing with time over two weeks) in d_6-DMSO.*

The ligand exchange noted for complex **5.2**, as evidenced by its ^{1}H NMR spectra, was verified through cross-examination of its crystal structure. The crystal structure of $[Pd_6(\mathbf{2.8})_8]\cdot 12(NO_3)$ displayed the inclusion of only one ligand enantiomer about the Pd_6 framework,[25] substantiating the notion that the well-resolved NMR spectra can indeed be related to their homochirality, **Figure 5.7b**. Complexes **5.1** and **5.2** therefore exhibit sterically-induced ligand scrambling behaviour, where it is likely to be the added steric bulk of the propyl chains situated at the cage windows which prevent this ligand exchange in complex **5.1** in DMSO.

In order to conclusively confirm the relative chirality of complex **5.1**, single crystals were grown by diffusing acetone vapours into a solution of the unsorted cage in DMSO solvent, isolated as large, truncated octahedral blocks and structurally elucidated using synchrotron radiation, **Figure 5.6**. The structure solved in the tetragonal space group *I*4/*mmm* to display the asymmetric unit as two thirds of a **4.6** ligand and two palladium(II) cations, both of which are sited on a special position, alongside two water molecules that are refined at partial occupancies. The diffraction data were weak and only the palladium(II) centres were refined anisotropically.

The Pd-N bond distances were measured at 1.981(6) and 2.144(8) Å, with N-Pd-N bond angles ranging 86.76(4) to 93.12(4) and 176.26(6) º for the *cis* and *trans* pyridyls, respectively. The Pd···Pd separations of the Pd_6 framework were measured at 16.3 Å, comparable to the inter-metallic distances of 16.6 Å recorded for complex **5.2**.[25]

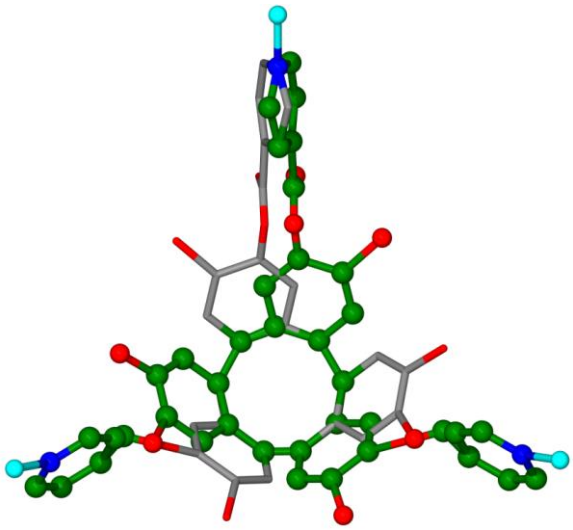

Figure 5.6 *From the crystal structure of complex **5.1**, indicating the two disordered enantiomers of **4.6** ligands in each $[Pd_6(\mathbf{4.6})_8]^{12+}$ cage. Individual ligand enantiomers are distinguished by colour.*

As predicted, the crystal structure of complex **5.1** displays substantial ligand disorder about the well-ordered octahedral Pd_6 framework. The disorder was modelled such that each full ligand position is a superposition of both **4.6** ligand enantiomers, **Figure 5.7a**. This implies that the broadened and relatively unsymmetrical NMR resonances obtained for complex **5.1** in d_6-DMSO can indeed be attributed to an 'unsorted' cage mixture. The crystals obtained were subsequently redissolved in d_6-DMSO and the proton NMR collected. The spectra displayed only the same broadened resonances, suggesting that the ligand disorder was not just a phenomenon of the solid state and they do indeed correspond to a mixture of cage stereoisomers. Whilst the crystal structures of complexes **5.1** and **5.2** solved in similar tetragonal cells, they are not isomorphic. Otherwise, each $[Pd_6L_8]^{12+}$ cage in complex **5.1** and **5.2** is approximately 3 nm in diameter and features a large and well-defined hydrophobic cavity.

The ligand exchange behaviour and the well-resolved NMR spectra of complex **5.1** in d_3-MeCN were therefore also believed to indicate a racemic mixture of enantiopure cages. In order to conclusively prove this fact, the acetonitrile solvate of complex **5.1** was subjected to reverse-phase chiral HPLC (high performance liquid chromatography) in order to separate the racemic mixture into the two enantiopure cages. Whilst the solubility of complex **5.1** was greatly

improved through use of propylated ligand **4.6**, chiral separation could not be achieved over a reasonable timescale without inducing precipitation.

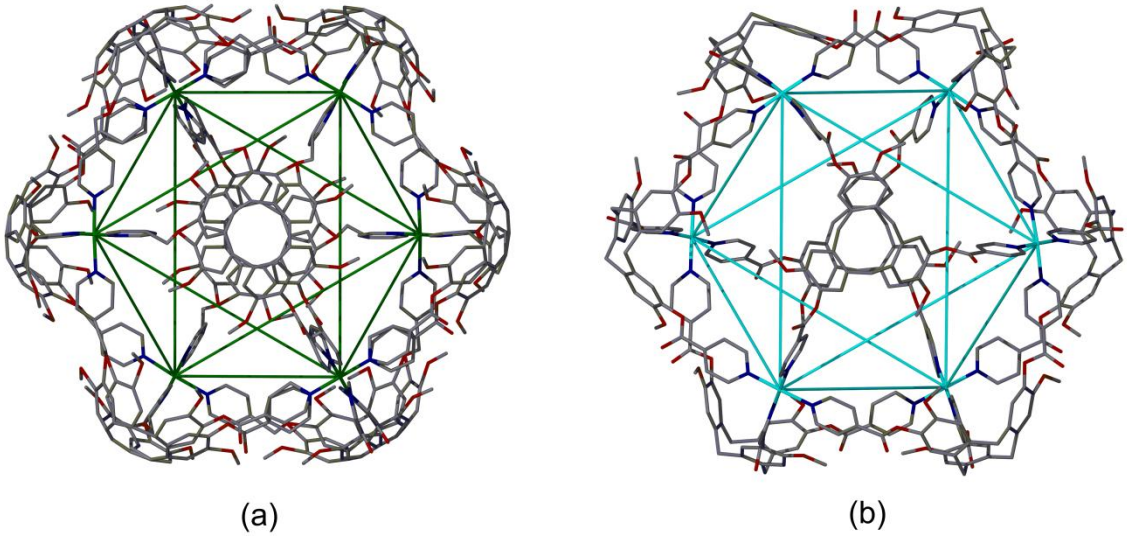

Figure 5.7 *From the crystal structures of complexes **5.1** (a) and **5.2** (b), noting the inclusion of both **M** and **P** ligand enantiomers in complex **5.1**. The Pd_6 framework is indicated by coloured lines in for each example.*

Single crystals of complex **5.1** were isolated from the bulk mixture and their composition and purity determined by combustion analysis and infrared spectroscopy. Combustion analysis suggests a high level of solvation and is consistent with the calculated void space within the crystal lattice. The size of the internal cavity also meant that this solvent could not be crystallographically modelled, hence the SQUEEZE [26] routine of PLATON [27] was employed. The BF_4^- anion was clearly evident in the infrared spectrum, with the broad B-F bond stretch at 1270 cm^{-1} confirming its inclusion into the crystal lattice.

Whilst it is of course impossible to conclusively state the exact composition of the DMSO solvated $[Pd_6(\mathbf{4.6})_8]^{12+}$ cages in terms of ligand enantiomer incorporation, the broadened NMR spectra certainly do relate to their being a mixture of such cages in solution. Another way to interpret the data is that they correspond to incomplete self-sorting of $[Pd_6(\mathbf{4.6})_8]^{12+}$ cages and that the data obtained relate to variants with the same stoichiometry.

Retrofitted molecular dynamics simulations performed by the Fujita group [28] suggest that lower symmetry constructs of the same stoichiometry are afforded *en route* to forming their final, spherical cage $[Pd_6L_8]^{12+}$, where L = 1,3,5-*tris*(methyl-4-pyridyl)benzene. Whilst their octahedral coordination cage is structurally similar to complex **5.1**, their model also suggests a very short intermediate lifetime of 50 – 80 ns, and therefore an improbable description of the ligand exchange described for complexes **5.1** and **5.2**.

In order to achieve enantiopurity in similar species, chiral resolution of the starting materials is generally required.[29] For example, the homochiral, octomeric CTV-based cube prepared through dynamic imine bond formation by Warmuth and co-workers was only realised by first chirally resolving the CTV starting materials, and was not seen to form from a racemic mixture.[30] Likewise, Lusby's enantiopure octahedral cage $[Ir_6(ppy)_{12}L_4]^{6+}$, where 'ppy' and L = 2-phenylatopyridine and 1,3,5-tricyanobenzene, respectively, was only achieved by chirally resolving and separating the $[Ir(ppy)_2]^+$ starting materials into the ***Δ*** and ***Λ*** enantiomers, prior to self-assembly.[31]

However, the spontaneous chiral resolution of metallo-supramolecular complexes from a racemic mixture of ligands is known,[32] as is the homochiral self-recognition of functionalised CTVs.[33] Ligand exchange towards enantiopurity, over a similar timescale as for the acetonitrile solvate of complex **5.1**, has also been noted in Torres' $[Pd_3L_2]^{6+}$ trigonal bipyramidal cages, where L = pyridyl-subphthalocyanin.[34] Lützen and co-workers have reported an example where a racemic mixture of 3-pyridyl-functionalised binapthol ligands display a narcissistic self-sorting to afford an enantiopure $[Pd_2L_4]^{4+}$ cage after 24 hours of equilibration at room temperature.[35] So whilst the sterically and interactionally similar ligand pair, **4.6** and **2.8** do self-assemble to afford structurally similar cages, complexes **5.1** and **5.2**, respectively, their solution-phase chemistry is highly dissimilar, despite only subtle differences between them.

To probe whether the labile pyridine-palladium(II) interaction was the determining factor in facilitating the aforementioned self-assembly behaviour, the platinum(II) congener, $[Pt_6(\mathbf{4.6})_8]\cdot 12(ClO_4)$, was prepared using $Pt(DMSO)_4(ClO_4)_2$ in place of $Pd(MeCN)_4(BF_4)_2$, although not in quantitative yields. Its ^{1}H NMR spectrum in d_6-DMSO was approximately symmetric and displayed characteristic down-field shifts to the pyridine protons, similar to complexes **5.1** and **5.2**, above. However, due to the decreased lability of the platinum(II) centres, conversion to the stella octangula cage complex was only 60 %, akin to the ^{1}H NMR spectrum of complex **5.1** in d_3-$MeNO_2$. Quantitative formation could not be achieved, despite heating at 70 ºC for 48 hours, and proton resonances were indicative of an 'unsorted' cage mixture with a smaller, homochiral component. The mass peaks of (*m/z*) 1371.6856, 1665. 9895 and 2107.4224 were observed in the mass spectrum and corresponded to $\{[Pt_6(\mathbf{4.6})_8]\cdot 6(ClO_4)\}^{6+}$, $\{[Pt_6(\mathbf{4.6})_8]\cdot 7(ClO_4)\}^{5+}$ and $\{[Pt_6(\mathbf{4.6})_8]\cdot 8(ClO_4)\}^{4+}$, respectively.

The sterically-induced ligand scrambling and solvent-induced chirality control displayed for the $[Pd_6(\mathbf{4.6})_8]^{12+}$ and $[Pd_6(\mathbf{2.8})_8]^{12+}$ stella octangula cages is uncommon, and the author is not aware of any examples in the literature, at present, which parallel this one.

5.3 Preliminary guest binding studies

It was envisaged that the heightened solubility of the $[Pd_6(\mathbf{4.6})_8]^{12+}$ cage would promote its ability to host molecules. Equilibrated solutions of complex **5.1** in various solvents were combined with an assortment of spherical and globular guests that included fullerenes, ferrocenes, carboranes and halogenated hydrocarbons; all of which have shown an ability to interact with functionalised CTVs.[36] Upon closer examination of the crystal structure, the incommensurate size of the windows to the cage cavity is thought to prevent the encapsulation and detection of guests.[37] The internal van der Waals volume of the cage was modelled to be approximately 2050 $Å^3$; which, according to the packing considerations described by Rebek and co-workers,[38] should be a perfect host for guests with a volume of 1128 $Å^3$. However, this is clearly not permissible with the size of windows which are approximately 7 × 11 Å, not including the ligand disorder about the octahedral framework of palladium(II) cations and the fluxional propyl moieties at the cage windows. The cage windows can therefore not allow for the diffusion of suitably large guests into the cavity, and the smaller guests which can diffuse into the cage do not create the ideal packing coefficient of 55% and are therefore not bound strongly enough to be detected by solution-phase measurements. This does not, however, take into account any cage permutations which can occur in solution upon the encapsulation of a guest and is merely an examination of the solid state structure of the $[Pd_6L_8]^{12+}$ cage.

Nevertheless, preliminary studies of the $[Pd_6(\mathbf{4.6})_8]^{12+}$ cage in the presence of *ortho*-carborane in DMF solution were indicative of host-guest behaviour. Electrospray mass spectra displayed the inclusion of variable numbers of carborane guests, *per* charge state. For example, the 5+ charge state envelope displayed mass peaks (*m/z*) 1541.8717, 1570.4850 and 1598.4942, which corresponded to $\{[Pd_6(\mathbf{4.6})_8]\cdot 7(BF_4)\}^{5+}$, $\{[Pd_6(\mathbf{4.6})_8]\cdot 7(BF_4)\subset(carb)\}^{5+}$, and $\{[Pd_6(\mathbf{4.6})_8]\cdot 7(BF_4)\subset(carb)_2\}^{5+}$, respectively. These inclusion phenomena are only observed between the *ortho*-carborane and $[Pd_6(\mathbf{4.6})_8]^{12+}$ cage and not between *ortho*-carborane and the individual molecular components, which suggests encapsulation as opposed to aggregation. Moreover, carboranes have demonstrated an ability to interact with the tribenzo[*a,d,g*]cyclononatriene core through C-H$\cdots\pi$ interactions from the relatively acidic C-H carborane donor.[39] In this study, however, there was no evidence for guest encapsulation by ^{1}H NMR spectroscopy.

The $[Pd_6(\mathbf{4.6})_8]^{12+}$ cage also displayed an ability to bind long chained surfactants, such as sodium dodecyl sulfate (SDS), in both solution and the gas-phase. In this instance the interaction between host and guest is enhanced due to coulombic interaction between the cage and dodecyl sulfate anion (SDS^-) and the stabilisation experienced by having the highly

hydrophobic alkyl chain situated within the cage cavity, as opposed to being solvated by the polar DMSO solvent.

The electrospray mass spectra indicated that the dodecyl sulfate anion (SDS^-) sequentially replaced the BF_4^- anion across each mass/charge envelope, creating a statistical mixture of $\{[Pd_6(\mathbf{4.6})_8]\cdot n(BF_4)\cdot m(SDS^-)\}^{(12-n-m)+}$ cages, *per* charge state. For example, in the 6+ charge state, mass peaks of (*m/z*) 1300.1009, 1329.8021, 1359.5119, 1389.4667 and 1419.4128 were attributed to $\{[Pd_6(\mathbf{4.6})_8]\cdot 5(BF_4)\cdot 1(SDS^-)\}^{6+}$, $\{[Pd_6(\mathbf{4.6})_8]\cdot 4(BF_4)\cdot 2(SDS^-)\}^{6+}$ $\{[Pd_6(\mathbf{4.6})_8]\cdot 3(BF_4)\cdot 3(SDS^-)\}^{6+}$, $\{[Pd_6(\mathbf{4.6})_8]\cdot 2(BF_4)\cdot 4(SDS^-)\}^{6+}$ and $\{[Pd_6(\mathbf{4.6})_8]\cdot 1(BF_4)\cdot 5(SDS^-)\}^{6+}$, respectively. ^1H NMR spectra in d_6-DMSO were indicative of guest interaction and displayed small upfield shifts to the SDS resonances, suggesting a fast and dynamic exchange on the NMR timescale. There were no observable changes to the cage resonances, suggesting that the binding of SDS through the cage windows does not permute the cage structure.

A detailed solution-phase examination of the encapsulation of various sodium alkyl sulphates has been the basis of a study by Fisher and co-workers,[40] who found that the methylated analogue $[Pd_6(\mathbf{2.8})_8]^{12+}$ bound two SDS molecules through a fast exchange mechanism with association constants of $3.7 \pm 0.076\ 10^4\ M^{-1}$ (K_1) and $6.0 \pm 0.132\ 10^2\ M^{-1}$ (K_2) for the first and second molecules of SDS, respectively. Simple molecular modelling calculations were in agreement with the encapsulation of two SDS molecules, where the long alkyl chains interact with the cage interior and the charged sulphate head groups interact in close proximity to the palladium(II) coordination site, possibly through a second-sphere interaction.[40]

5.4 Speciation control and cage dynamics

Combining the preformed $[Pd_6(\mathbf{4.6})_8]^{12+}$ and $[Pd_6(\mathbf{2.8})_8]^{12+}$ cages in DMSO solution resulted in a stable and co-existing mixture of homoleptic stella octangula cages. The cage mixture was continuously monitored over a four month period by electrospray mass spectrometry and ^{1}H NMR spectroscopy and there was no observable ligand exchange. The mass spectra procured during this time displayed only mass peaks pertaining to the individual cages $[Pd_6(\mathbf{4.6})_8]^{12+}$ and $[Pd_6(\mathbf{2.8})_8]^{12+}$ with no evidence for heteroleptic $[Pd_6(\mathbf{4.6})_{8-n}(\mathbf{2.8})_8]^{12+}$ species, **Figure 5.8**. The mass peaks of (*m/z*) 1158.1294, 1270.4061, 1407.3632, 1541.7124, 1780.7396 and 1948.9378 were identified and attributed to the homoleptic species $\{[Pd_6(\mathbf{2.8})_8]\cdot 6(BF_4)\}^{6+}$, $\{[Pd_6(\mathbf{4.6})_8]\cdot 6(BF_4)\}^{6+}$, $\{[Pd_6(\mathbf{2.8})_8]\cdot 7(BF_4)\}^{5+}$, $\{[Pd_6(\mathbf{4.6})_8]\cdot 7(BF_4)\}^{5+}$, $\{[Pd_6(\mathbf{2.8})_8]\cdot 8(BF_4)\}^{4+}$ and $\{[Pd_6(\mathbf{4.6})_8]\cdot 8(BF_4)\}^{4+}$, respectively. Furthermore, neither heating at 60 ºC overnight, nor standing for a further six month period produced observable changes to the mass spectra, suggesting that the two cages are indefinitely stable to one another under these conditions.

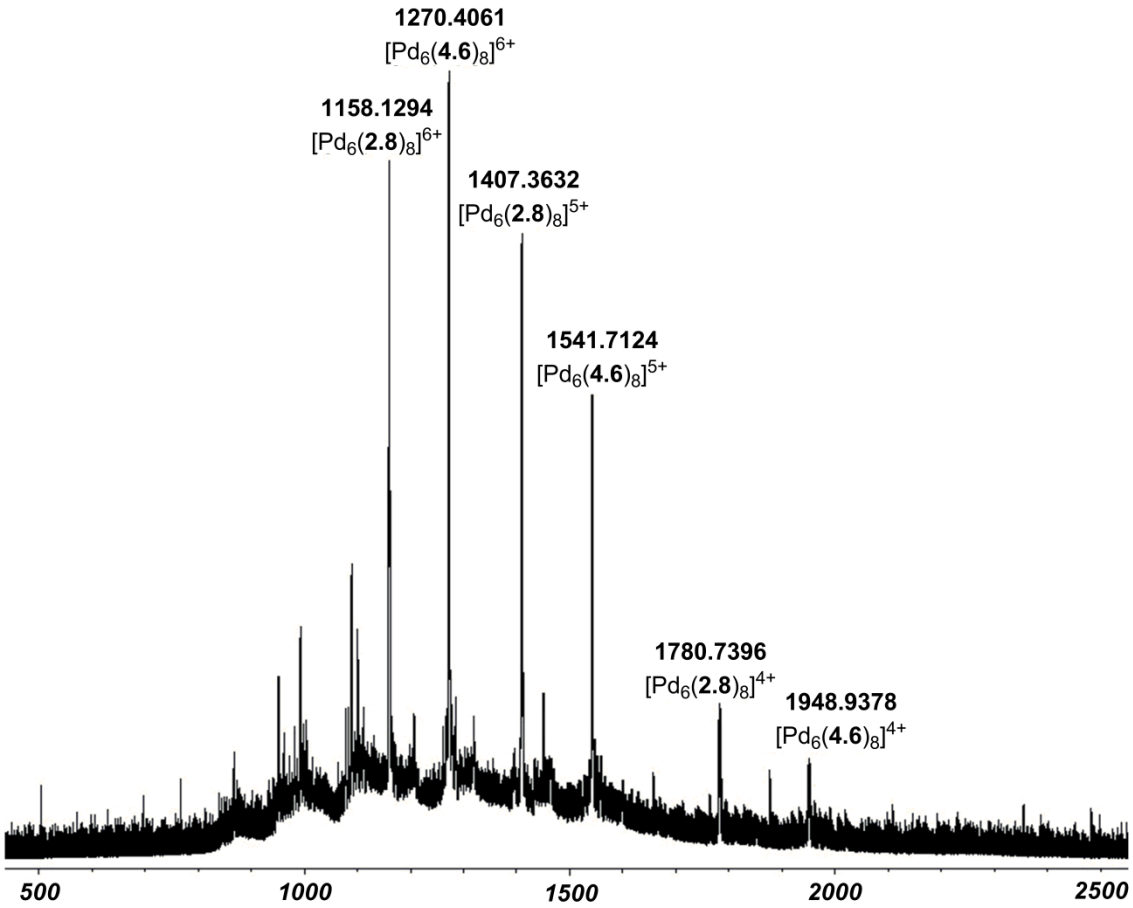

Figure 5.8 *Electrospray mass spectrum displaying a stable homoleptic mixture of* $[Pd_6(\mathbf{4.6})_8]^{12+}$ *and* $[Pd_6(\mathbf{2.8})_8]^{12+}$ *cages.*

This retained homolepticity was further supported by ^{1}H NMR spectroscopy, where the mixture of complexes **5.1** and **5.2** in d_6-DMSO displayed only a sum of the resonances for the two cages, with no variances observed over the four month timeframe, **Figure 5.9**.

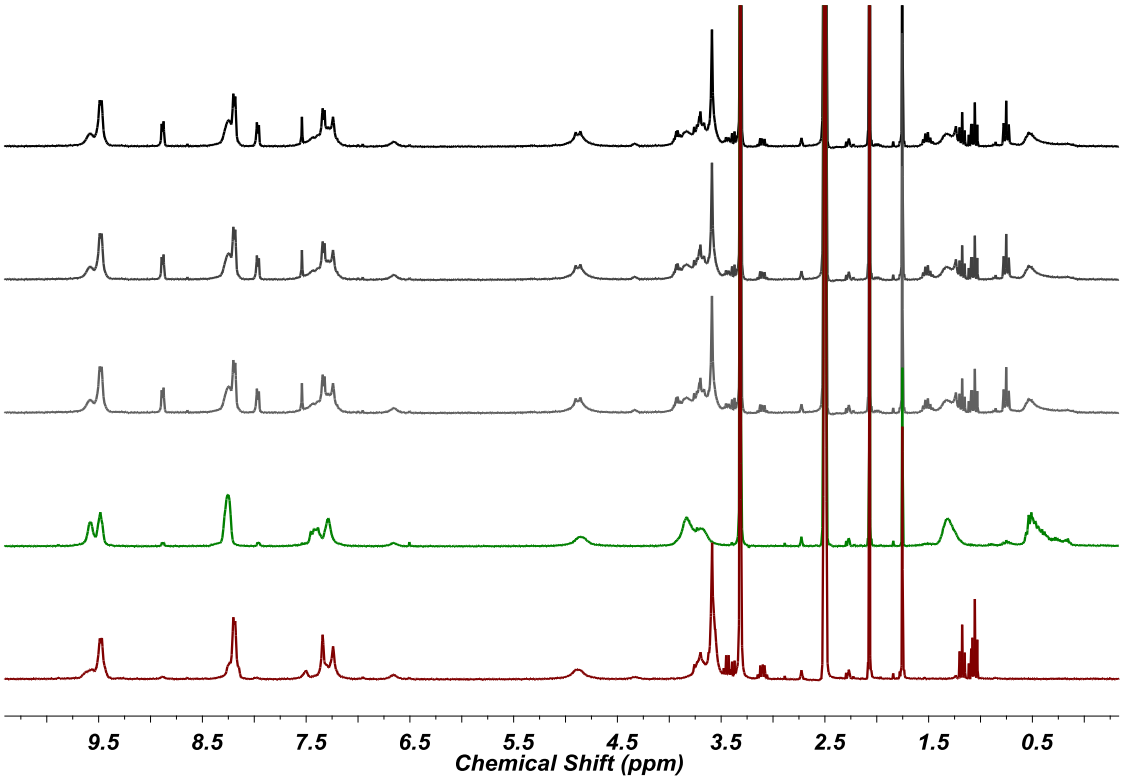

Figure 5.9 *Timecourse proton NMR spectra of individual complexes **5.1** and **5.2** (green and red traces, respectively) and the stable and co-existing mixture of homoleptic cages (black traces, increasing with time over two weeks) in d_6-DMSO.*

Likewise, stable and co-existing heteroleptic analogues could be prepared. The reaction of four equivalents of both ligands **4.6** and **2.8** with six equivalents of palladium(II) tetrafluoroborate in DMSO solution afford the cage mixture $[Pd_6(\mathbf{4.6})_{8-n}(\mathbf{2.8})_n]^{12+}$. Electrospray mass spectrometry indicated heteroleptic cage formation where each mass/charge envelope for a given charge state represented a near statistical mixture of ligand combinations, **Figure 5.10**. For example, the 5+ charge state displayed mass peaks of (*m/z*) 1424.7916, 1440.9024, 1457.9135, 1474.3383, 1491.3380 and 1510.6050, which corresponded to the species $\{[Pd_6(\mathbf{4.6})_1(\mathbf{2.8})_7]\cdot 7(BF_4)\}^{5+}$, $\{[Pd_6(\mathbf{4.6})_2(\mathbf{2.8})_6]\cdot 7(BF_4)\}^{5+}$, $\{[Pd_6(\mathbf{4.6})_3(\mathbf{2.8})_5]\cdot 7(BF_4)\}^{5+}$, $\{[Pd_6(\mathbf{4.6})_4(\mathbf{2.8})_4]\cdot 7(BF_4)\}^{5+}$, $\{[Pd_6(\mathbf{4.6})_5(\mathbf{2.8})_3]\cdot 7(BF_4)\}^{5+}$, and $\{[Pd_6(\mathbf{4.6})_6(\mathbf{2.8})_2]\cdot 7(BF_4)\}^{5+}$, respectively. In a similar manner to complexes **5.1** and **5.2**, the mass spectra obtained were independent of solvent employed and did not change with time.

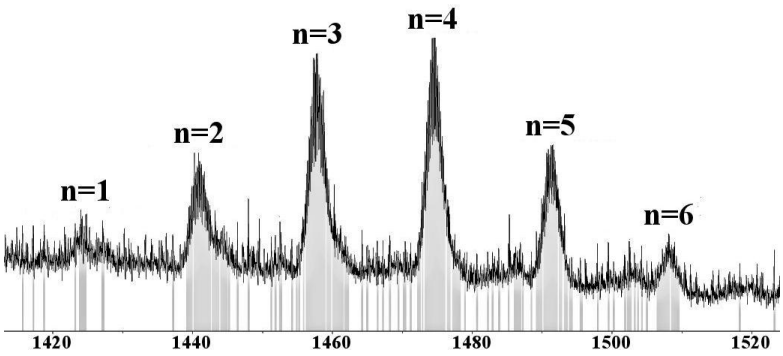

Figure 5.10 *Part of the mass spectrum (5+ charge state) of the heteroleptic cage mixture indicating the near statistical mixture of ligands in* $\{[Pd_6(\mathbf{4.6})_{8-n}(\mathbf{2.8})_n]\cdot 7(BF_4)\}^{5+}$.

The ^{1}H NMR spectrum of the heteroleptic cage mixture in d_6-DMSO was considerably broadened as a direct result of incorporating both **4.6** and **2.8** ligands about the Pd_6 octahedral framework, **Figure 5.11**. As for the homoleptic mixture of cages described above, the heteroleptic mixture was indefinitely stable once formed and there were no observable changes detected by NMR.

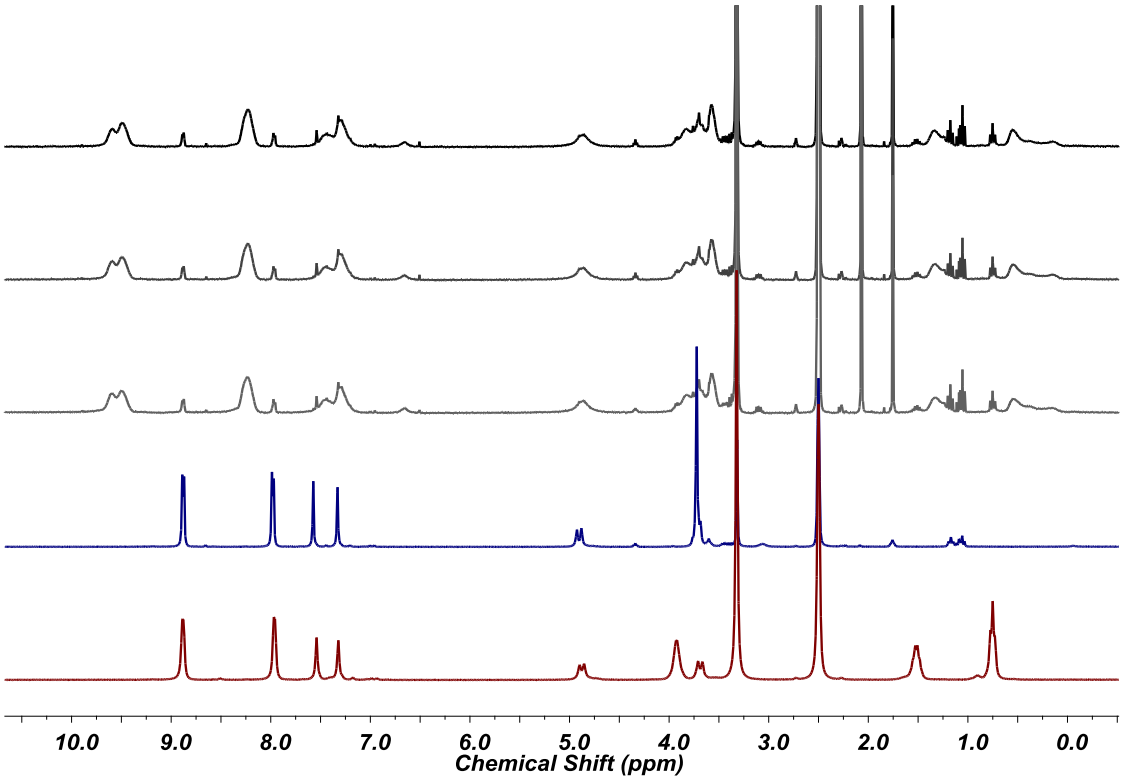

Figure 5.11 *Timecourse* ^{1}*H NMR spectra of ligands* ***4.6*** *and* ***2.8*** *(red and blue traces, respectively) and heteroleptic* $[Pd_6(\mathbf{4.6})_{8-n}(\mathbf{2.8})_n]^{n+}$ *(black traces, increasing with time over two weeks) in* d_6*-DMSO.*

The stable mixtures of homoleptic ($[Pd_6(\mathbf{4.6})_8]^{12+}$ and $[Pd_6(\mathbf{2.8})_8]^{12+}$) and the heteroleptic ($[Pd_6(\mathbf{4.6})_{8-n}(\mathbf{2.8})_n]^{12+}$) cages display contrasting behaviour to many in the literature. For

example, Dalcanale and co-workers have described a dynamic cage system utilising a pair of 4-pyridyl-functionalised calix[4]arene ligands, differing only in their lower rim alkoxy substitution, that afford structurally analogous $[Pt_4(L)_2]^{8+}$ and $[Pt_4(L')_2]^{8+}$ homoleptic cages that undergo rapid ligand exchange when combined to afford a mixture of heteroleptic $[Pt_4L_2]^{8+}$ cages.[41] Similar behaviour has been noted by Stang in the metal-directed formation of supramolecular polygons, where immediate equilibration of ligands was monitored in solution by mass spectrometry.[18] However, they found that they could control speciation to some extent if the ligands were highly dissimilar.[42] Moreover, by combining a four-component mixture of interactionally similar ligands with a mixture of copper(II) and zinc(II) metal cations, Schmittel and co-workers were able to determine a relationship between complexity and ligand exchange, invoking a mechanism of '2-fold completive self-sorting', where the self-assembly behaviour of the mixture is highly dissimilar to the self-assembly of the simple complexes.[43]

There are, however, examples which remark upon the high kinetic inertness of metallo-supramolecular cages. The stability of the $[Pd_6L_4]^{12+}$ and $[Pd_{12}L_{24}]^{24+}$ cages prepared by Fujita is testament to their predictable chemistry and hence their employment in many areas of chemistry, including molecular recognition,[44] guest binding [45] and catalysis.[46] Similarly, the slow ligand exchange in the gallium(III) tetrahedral cages reported by Raymond and co-workers allows for their employment in water-based catalysis, where enzyme-like catalytic behaviour has been achieved for the Nazarov cyclisation of various divinyl ketones [47] and in the C-H activation of ethene by the co-encapsulation of an iridium(III) complex.[48]

The predictable behaviour of the $[Pd_6L_8]^{12+}$ stella octangula cages described above closely resembles that of Fujita's and is likely attributable to their similar size and symmetry. In addition, ligand dissociation from the octahedral Pd_6 framework requires the cleavage of three coordination bonds which is energetically unfavourable. Ligand exchange could be effected, however, and the formation of the $[Pd_6(\mathbf{2.8})_8]^{12+}$ cage was observed to be substantially more favourable than the $[Pd_6(\mathbf{4.6})_8]^{12+}$ propylated congener. The addition of an excess of ligand **4.6** to the preformed $[Pd_6(\mathbf{2.8})_8]^{12+}$ cage in DMSO solvent had no observable effect, and the mass spectra displayed only mass peaks pertaining to the $\{[Pd_6(\mathbf{2.8})_8]\cdot n(BF_4)\}^{(12-n)+}$ species. Likewise, the ^{1}H NMR spectrum of the mixture in d_6-DMSO displayed only a sum of the $[Pd_6(\mathbf{2.8})_8]^{12+}$ cage and ligand **4.6** resonances. However, the addition of an excess of methylated ligand **2.8** to the preformed $[Pd_6(\mathbf{4.6})_8]^{12+}$ cage saw a rapid and quantitative degradation to the methylated $[Pd_6(\mathbf{2.8})_8]^{12+}$ cage. Electrospray mass spectra confirmed the ligand exchange by displaying the mass peaks for the $\{[Pd_6(\mathbf{2.8})_8]\cdot n(BF_4)\}^{(12-n)+}$ species, in addition to cage-ligand adducts. The ^{1}H NMR spectra of this mixture in d_6-DMSO saw the immediate inclusion of resonances attributable to ligand **4.6**, with the characteristic α-, β- and γ-protons of the propyl chain at 3.92,

1.51 and 0.73 ppm, respectively, **Figure 5.12**. Additionally, the broadened resonance corresponding to the *ortho*-proton of the $[Pd_6(\mathbf{2.8})_8]^{12+}$ cage at 9.46 ppm became apparent, which then underwent the same equilibration process to reach homochirality, as described in the preparation of complex **5.2**, above.

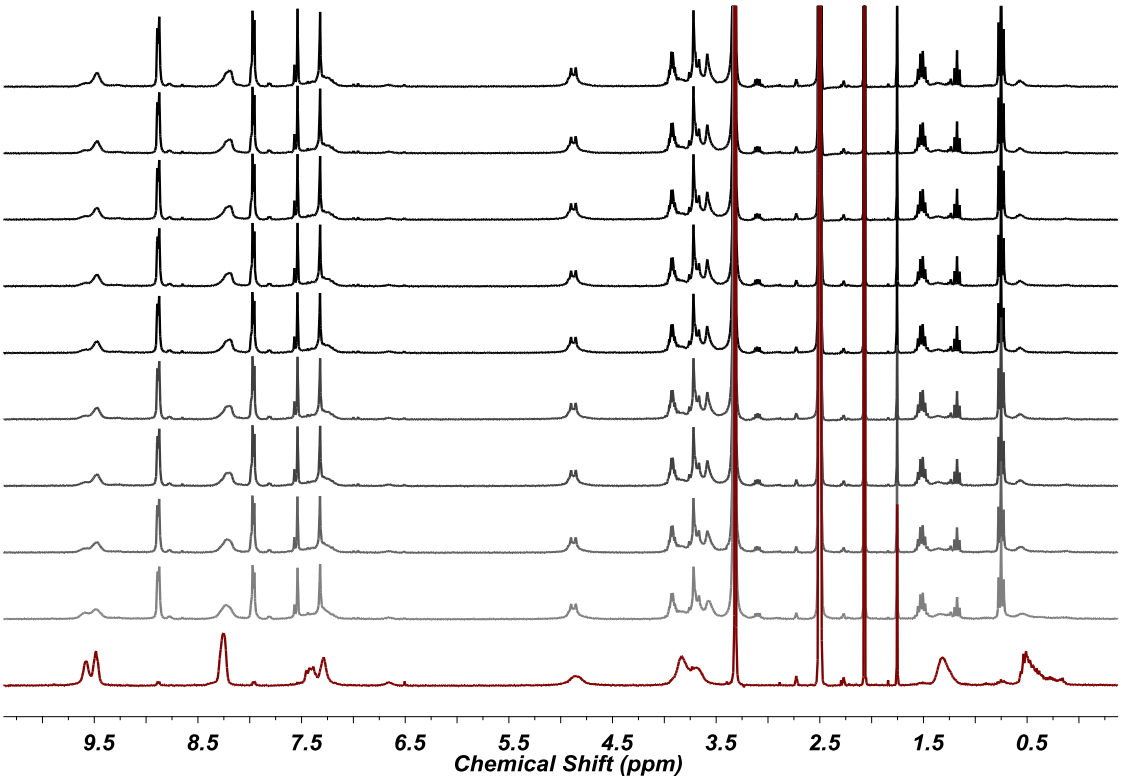

Figure 5.12 *Timecourse proton NMR spectra of complex **5.1** (red trace) and the conversion to complex **5.2** and ligand **4.6** (black traces, increasing with time over two weeks) in d_6-DMSO.*

The preferred formation of complex **5.2** over complex **5.1** may be related to the sterically-induced ligand scrambling discussed above, where the added symmetry of the homochiral $[Pd_6(\mathbf{2.8})_8]^{12+}$ cage drives its formation over the unsorted $[Pd_6(\mathbf{4.6})_8]^{12+}$ cage mixture.[23] The correlation of entropy with symmetry is a new phenomenon which has been noted by Skowronek [49] to be a determining factor that facilitates a thermodynamically-driven [8 + 12] cycloaddition to afford a large, covalent cage through dynamic imine bond formation.

5.5 Speciation control: An extended reference

There are currently no examples in the literature from which to help contextualise the behaviour of the homo- and heteroleptic cages described above. Therefore, the extended ligands (±)-2,7,12-tripropoxy-3,8,13-*tris*(4-pyridyl-4-phenylcarboxy)-10,15-dihydro-5*H*-tribenzo[*a*,*d*,*g*]cyclononatriene **5.3** and (±)-2,7,12-trimethoxy-3,8,13-*tris*(4-pyridyl-4-phenylcarboxy)-10,15-dihydro-5*H*-tribenzo[*a*,*d*,*g*]cyclononatriene **5.4**, were prepared as an

extended reference pair, **Figure 5.13**. Ligand **5.4** has been prepared previously and observed to form a stable stella octangula cage in DMSO solution,[21] and it was expected that novel ligand **5.3** would behave analogously.

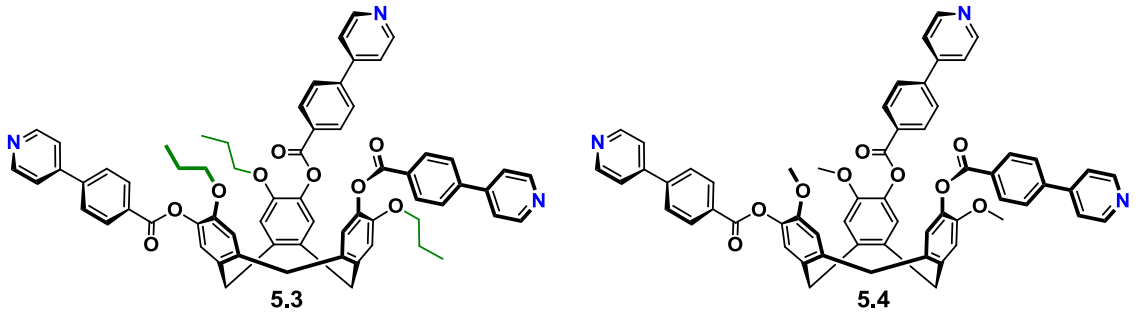

Figure 5.13 *Extended ligands **5.3** and **5.4** used to construct extended $[Pd_6L_8]^{12+}$ cages.*

Ligand **5.4** was prepared according to literature procedures and isolated in near quantitative yields.[21] The novel ligand **5.3** was synthesised using this adapted procedure from the reaction of propylated-CTG (*p*CTG, **4.4**) and 4-(4-pyridyl)benzoyl chloride hydrochloride, employing anhydrous tetrahydrofuran as solvent and triethylamine as scavenger base. The reactive electrophile 4-(4-pyridyl)benzoyl chloride hydrochloride was prepared from 4-bromopyridine and 4-carboxybenzene boronic acid using standard Suzuki conditions [50] and subsequently converted to the acid chloride using thionyl chloride. Ligand **5.3** was purified by flash chromatography (silica gel, chloroform solvent) and isolated as a crystalline white solid in 93% yield. The purity and composition of **5.3** were determined by combustion analysis and infrared spectroscopy, with electrospray mass spectrometry affording the mass peak (*m/z*) 1058.3941, which was attributed to $\{\mathbf{5.3}\cdot H\}^+$ and calculated for 1058.3993. Similarly, the ^1H and ^{13}C NMR spectra recorded in d_6-DMSO displayed the expected resonances and were concordant with the structure proposed. The ^1H NMR spectra recorded are displayed below in the formation of the corresponding $[Pd_6L_8]^{12+}$ stella octangula cages. Interestingly, propylation in this instance did little to improve the solubility of the large, rigid ligand, which was only soluble in DMSO solvent.

The reaction of ligand **5.3** with palladium(II) tetrafluoroborate in DMSO solvent afforded the stella octangula cage $[Pd_6(\mathbf{5.3})_8]\cdot 12(BF_4)$, complex **5.5**. Its formation was rapid and quantitative based on ^1H NMR spectroscopy and mass spectrometry measurements; however, and unlike complex **5.1**, it did continue to equilibrate with time. Electrospray mass spectrometry afforded the mass peaks (*m/z*) 1020.9683, 1159.3551, 1337.3494, 1574.9554 and 1906.9543, which corresponded to the species $\{[Pd_6(\mathbf{5.3})_8]\cdot 3(BF_4)\}^{9+}$, $\{[Pd_6(\mathbf{5.3})_8]\cdot 4(BF_4)\}^{8+}$, $\{[Pd_6(\mathbf{5.3})_8]\cdot 5(BF_4)\}^{7+}$, $\{[Pd_6(\mathbf{5.3})_8]\cdot 6(BF_4)\}^{6+}$ and $\{[Pd_6(\mathbf{5.3})_8]\cdot 7(BF_4)\}^{5+}$, respectively. The ^1H NMR spectra of the mixture were indicative of complex formation, with the *ortho* and *meta*-

pyridyl protons displaying the expected coordination-induced down-field shifting and the broadening of the propyl resonances due to added fluxionality on the NMR timescale. Diffusion-ordered NMR analysis (DOSY) of the $[Pd_6(\mathbf{5.3})_8]\cdot 12(BF_4)$ cage displayed the presence of one large species in solution and the diffusion constant (D_{cage}) was calculated to be 0.348×10^{-10} m^2s^{-1}; however, an accurate hydrodynamic radius (r) could not be determined due to the variable diffusion constants obtained for ligand **5.3**. Whilst the cage complex forms immediately, slight variances were noted upon continuous monitoring over a two-week period, **Figure 5.14**. Although sharpening of the pyridyl and propyl resonances were evident, a well-defined NMR spectrum indicative of a fully homochiral system was not obtained. Analogous behaviour was also noted for the previously reported methylated cage, $[Pd_6(\mathbf{5.4})_8]\cdot 12(BF_4)$.[21]

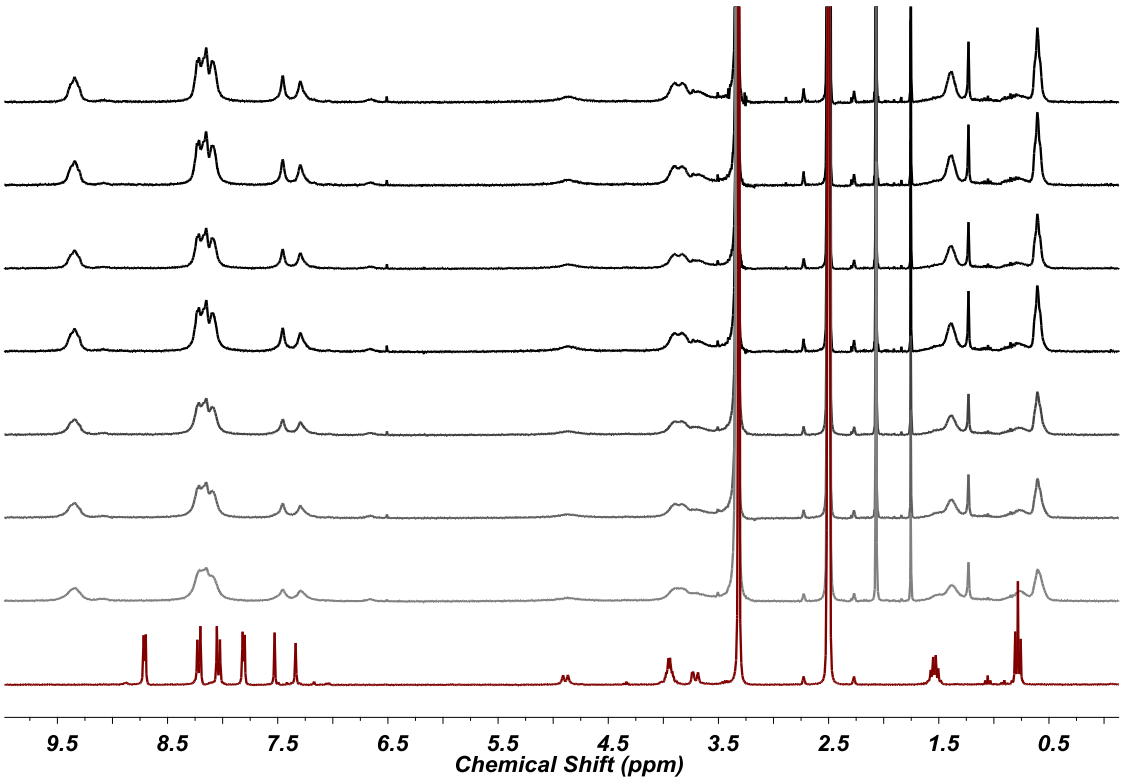

Figure 5.14 *Timecourse NMR spectra of ligand **5.3** (red trace) and complex **5.5** (black traces, increasing with time over two weeks) in d_6-DMSO.*

A solid sample of complex **5.5** was isolated by precipitation from the bulk solution with acetone; however, satisfactory combustion analyses could not be obtained owing to extremely high levels of solvation. Infrared spectroscopy was supportive of complex formation and indicated the presence of the BF_4^- anion with a strong and broad B-F bond stretch at 1024 cm^{-1}.

The reaction of four equivalents of ligands **5.3** and **5.4** with six equivalents of palladium(II) tetrafluoroborate in DMSO solvent afforded the cage mixture $[Pd_6(\mathbf{5.3})_{8-n}(\mathbf{5.4})_n]^{12+}$. Electrospray mass spectrometry of the cage mixture highlighted a clear heteroleptic mixture of cages and a

statistical mixture of ligands, *per* charge state, **Figure 5.15**. There were no observable changes in this heteroleptic mixture over time, based on ^{1}H NMR spectroscopy and mass spectrometry, which is in agreement with the $[Pd_6(\mathbf{4.6})_{8-n}(\mathbf{2.8})_n]^{12+}$ cage mixtures discussed above, where the limited relative proportion of ligand to metal prevents any preferential self-sorting behaviour.

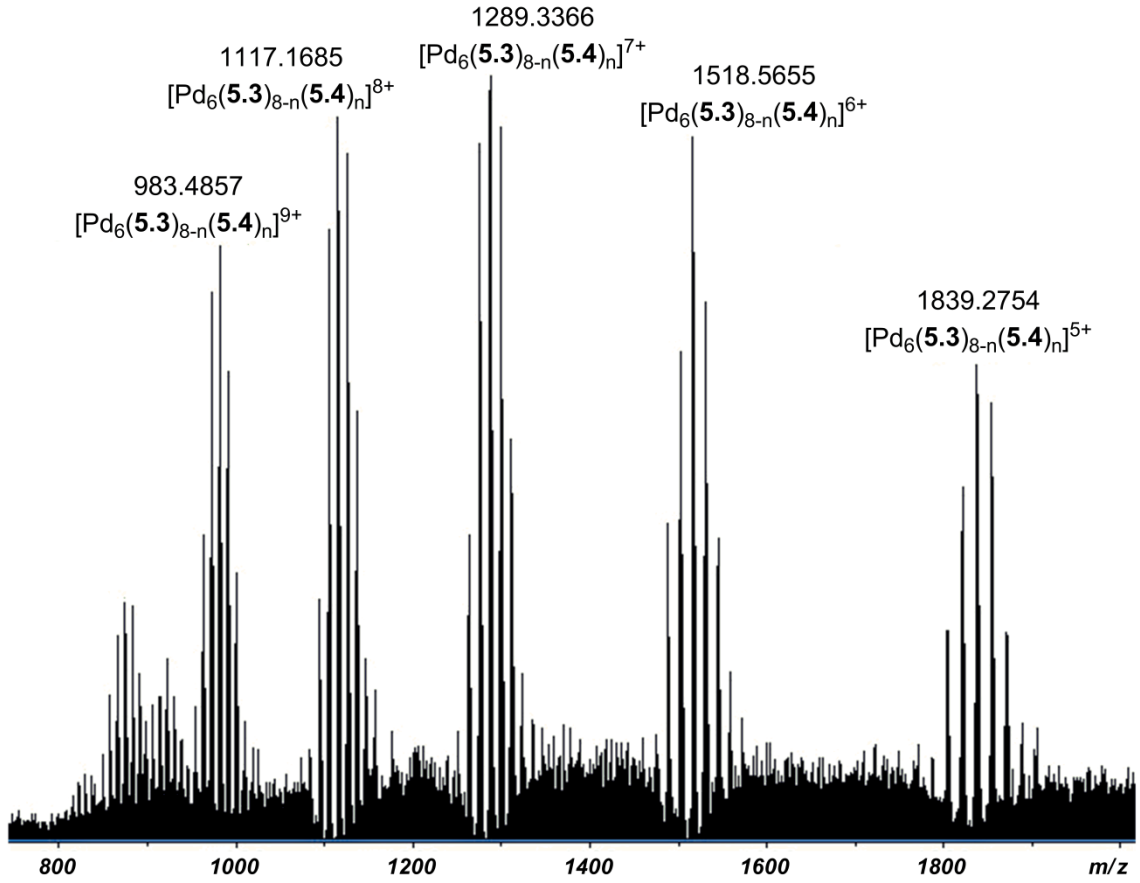

Figure 5.15 *The electrospray mass spectrum of the* $\{[Pd_6(\mathbf{5.3})_{8-n}(\mathbf{5.4})_n]\cdot x(BF_4)\}^{(12-x)+}$ *cage mixture in DMSO solution.*

Whereas the homoleptic $[Pd_6(\mathbf{4.6})_8]^{12+}$ and $[Pd_6(\mathbf{2.8})_8]^{12+}$ cages were indefinitely stable towards each other over any reasonable time frame, the extended analogues, $[Pd_6(\mathbf{5.3})_8]^{12+}$ and $[Pd_6(\mathbf{5.4})_8]^{12+}$, respectively, were not.

The two homoleptic $[Pd_6(\mathbf{5.3})_8]^{12+}$ and $[Pd_6(\mathbf{5.4})_8]^{12+}$ cages were combined in DMSO solvent and monitored continuously by ^{1}H NMR and mass spectrometry. Although limited, ligand exchange was observed to occur slowly over a two-month period. Further broadening of cage resonances were noted in the ^{1}H NMR spectra of the cage mixture, yet it was not possible to conclusively quantify any changes owing to the similar level of broadness of both $[Pd_6(\mathbf{5.3})_8]^{12+}$ and $[Pd_6(\mathbf{5.4})_8]^{12+}$ cages with the $[Pd_6(\mathbf{5.3})_{8-n}(\mathbf{5.4})_n]^{12+}$ cage mixture.

The electrospray mass spectra of this 'homoleptic' cage mixture displayed obvious ligand exchange, **Figure 5.16**. Ligand exchange about the octahedral Pd_6 framework is restricted, and up to three ligands were observed to exchange over the two-month period. It is not believed that true heterolepticity would ever be reached over any reasonable timescale without added input, such as heat or a chemical stimulus. This level of cage dynamics is minimal and not quite comparable to the rapid self-sorting behaviour observed by the likes of Stang [18] and Dalcanale.[41] They also appear less stable than the larger cages reported by Fujita,[28] despite their size and symmetry, which suggests that their dynamics cannot be accurately described by such empirical measurements and they may be both highly subtle and specific from system to system.

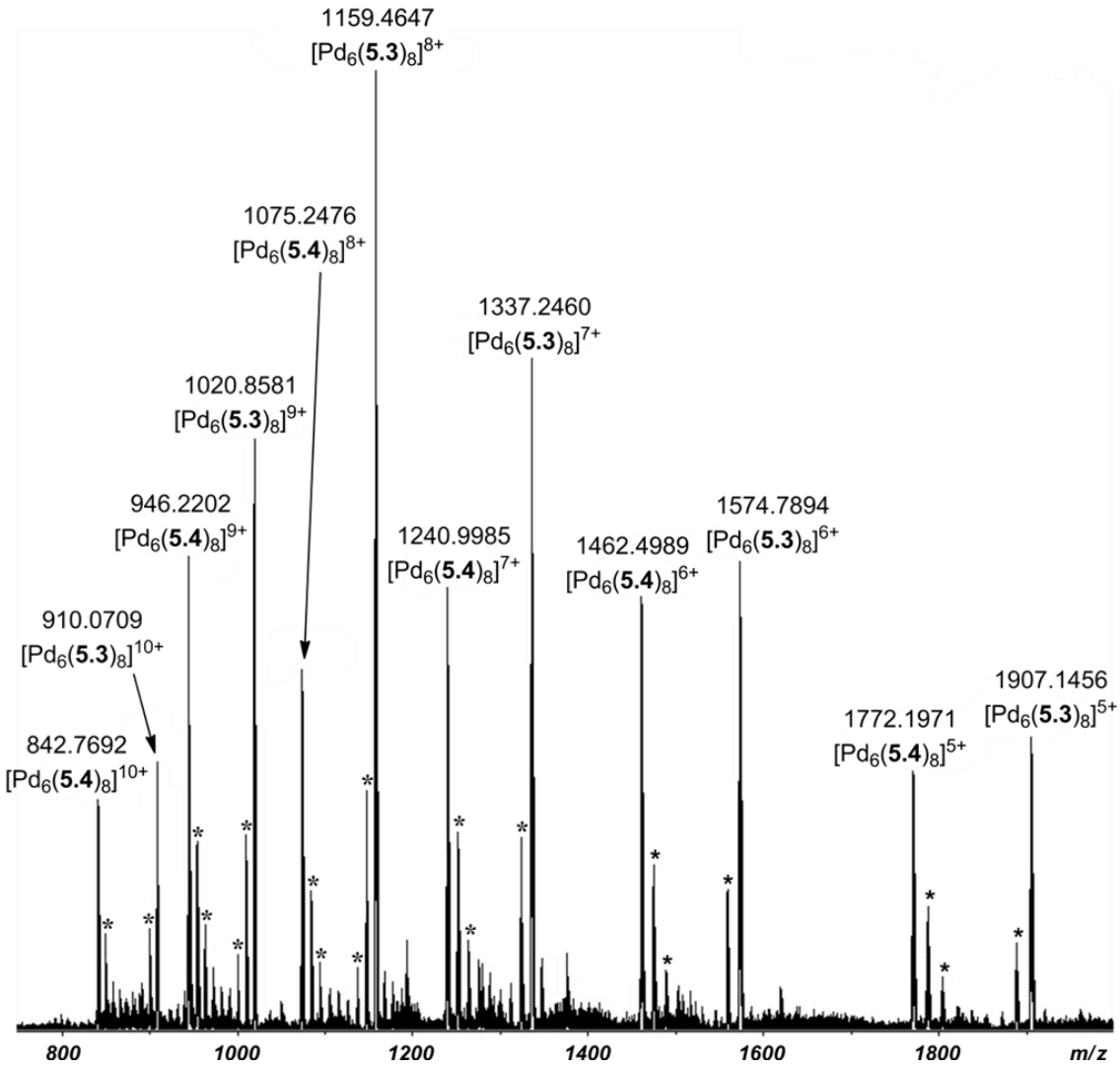

Figure 5.16 *Electrospray mass spectrum of the combined homoleptic* $[Pd_6(\mathbf{5.3})_8]^{12+}$ *and* $[Pd_6(\mathbf{5.4})_8]^{12+}$ *cages in DMSO solvent. The asterisks between homoleptic mass peaks pertain to the* $[Pd_6(\mathbf{5.3})_{8-n}(\mathbf{5.4})_n]^{12+}$ *cage mixtures of that given charge state.*

Any differences observed in the lability of the smaller ($[Pd_6(\mathbf{4.6})_8]^{12+}$ and $[Pd_6(\mathbf{2.8})_8]^{12+}$) and extended ($[Pd_6(\mathbf{5.3})_8]^{12+}$ and $[Pd_6(\mathbf{5.4})_8]^{12+}$) cages can be rationalised by the flexibility of the larger cages. It is well known that structural flexibility results in a decreased predictability with regards to self-assembly.[51] Their larger size, and hence increased conformational freedom, allows for entire structural permutations of the cage whilst in solution. This has been corroborated by preliminary molecular dynamics simulations on the larger $[Pd_6(\mathbf{5.4})_8]^{12+}$ cage,[52] which indicate that both the ligands and Pd_6 framework can substantially deform and, in doing so, that the individual palladium(II) coordination environments become increasingly strained, **Figure 5.17**. It is important to note that these permutations were not observed in the molecular dynamics simulations for the smaller $[Pd_6(\mathbf{2.8})_8]^{12+}$ stella octangula cage.

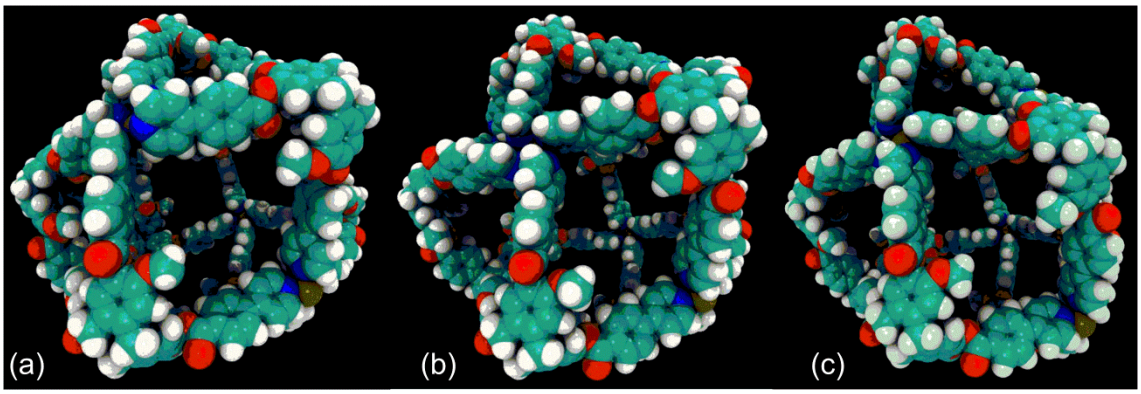

Figure 5.17 *Taken from the molecular dynamics simulations of $[Pd_6(\mathbf{5.4})_8]^{12+}$, showing the deformations within the Pd_6 framework (a), about the palladium(II) centres (b) and of individual **5.4** ligands (c).*

Structural deformations in CTV-type compounds have been described by Holman in an 'imploded cryptophane', where the flexibility of the linker which bridges the two organic CTV units allows for their conformational freedom.[53] Likewise, organic cages prepared by Cooper and co-workers have shown that their properties become unpredictable with increasing size,[54] and that as the cages get too large they attempt to close in on themselves as a response to increasing hydrostatic pressure, in order to reduce the high energy void space.[55] The extended $[Pd_6(\mathbf{5.3})_8]^{12+}$ and $[Pd_6(\mathbf{5.4})_8]^{12+}$ cages are too rigid too allow a complete structural collapse; however, the cage permutations suggested from the dynamics simulations are enough to facilitate ligand exchange at the cage surfaces by an associative mechanism.

5.6 High fidelity control over cage assembly and disassembly processes

Although mutually stable with respect to one another, the preferential formation of methylated $[Pd_6(\mathbf{2.8})_8]^{12+}$ over propylated $[Pd_6(\mathbf{4.6})_8]^{12+}$ allows for a high degree of control over their assembly, speciation and disassembly in DMSO solution, **Figure 5.18**.

A complex self-assembly cycle was determined by ^{1}H NMR and mass spectrometry, whereby the bulk mixture could be chemically switched between hetero- and homoleptic cage mixtures *via* a complete degradation process. This cycle was found to be near-quantitative at each step, and could afford the (i) molecular components, (ii) heteroleptic cage mixture, (iii) single cage species and (iv) homoleptic cage mixture, with high fidelity. This is described in detail below and summarised graphically in **Figure 5.18**.

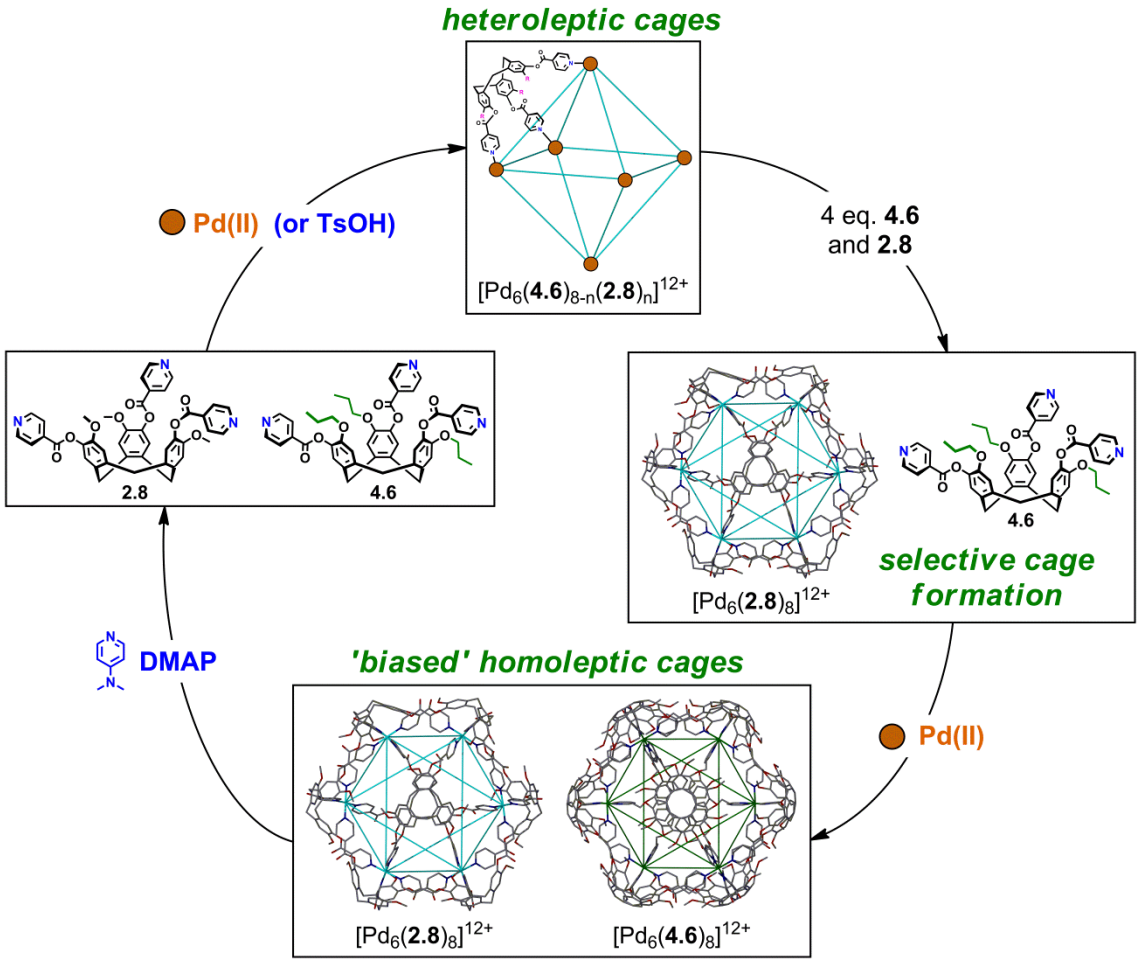

Figure 5.18 *The complex assembly/disassembly cycle between the* $[Pd_6(\mathbf{2.8})_8]^{12+}$, $[Pd_6(\mathbf{4.6})_8]^{12+}$ *and* $[Pd_6(\mathbf{4.6})_{8-n}(\mathbf{2.8})_n]^{12+}$ *cages via both stoichiometric and chemical control.*

The reaction of ligands **4.6** and **2.8** with palladium(II) tetrafluoroborate in DMSO solvent afforded the stable heteroleptic cage mixture, $[Pd_6(\mathbf{4.6})_{8-n}(\mathbf{2.8})_n]^{12+}$, as described above, **Figure 5.19c**. The addition of a further four equivalents of ligands **4.6** and **2.8** to this cage mixture saw the near-quantitative formation of methylated cage $[Pd_6(\mathbf{2.8})_8]^{12+}$, alongside free ligand **4.6**, as indicated by ^{1}H NMR and mass spectrometry, **Figure 5.19d**. Once equilibrated, the addition of a further six equivalents of $Pd(BF_4)_2$ to this mixture effected the formation of co-existing homoleptic $[Pd_6(\mathbf{4.6})_8]^{12+}$ and $[Pd_6(\mathbf{2.8})_8]^{12+}$ stella octangula cages, **Figure 5.19e**. The methylated cage, $[Pd_6(\mathbf{2.8})_8]^{12+}$, subsequently equilibrated to the homochiral species over a two-

week period, **Figure 5.19f**. The addition of 24 equivalents of *N,N'*-dimethylaminopyridine (DMAP) to this homoleptic mixture saw the quantitative degradation of both stella octangula cages and the formation of $Pd(DMAP)_4(BF_4)_2$, thus generating eight equivalents of ligands **4.6** and **2.8**, **Figure 5.19g**. The addition of *para*-toluenesulfonic acid (TsOH) to this reaction mixture protonated the DMAP and regenerated the heteroleptic cage mixture, $[Pd_6(\mathbf{4.6})_{8-n}(\mathbf{2.8})_n]^{12+}$, **Figure 5.19h**. Whilst the ^{1}H NMR spectra indicate that each step proceeds highly efficiently, there was evidence in the corresponding mass spectra to suggest that there are errors associated in the transformations, **Figure 5.20**. These imperfections were noted for the preferential formation of $[Pd_6(\mathbf{2.8})_8]^{12+}$ and the subsequent trapping of coexisting $[Pd_6(\mathbf{4.6})_8]^{12+}$ and $[Pd_6(\mathbf{2.8})_8]^{12+}$ stella octangula cages. Whilst these minor variances were not noted in the ^{1}H NMR spectra, it is likely that they arise due to experimental errors associated with the sub-micromolar scale at which the system operates.

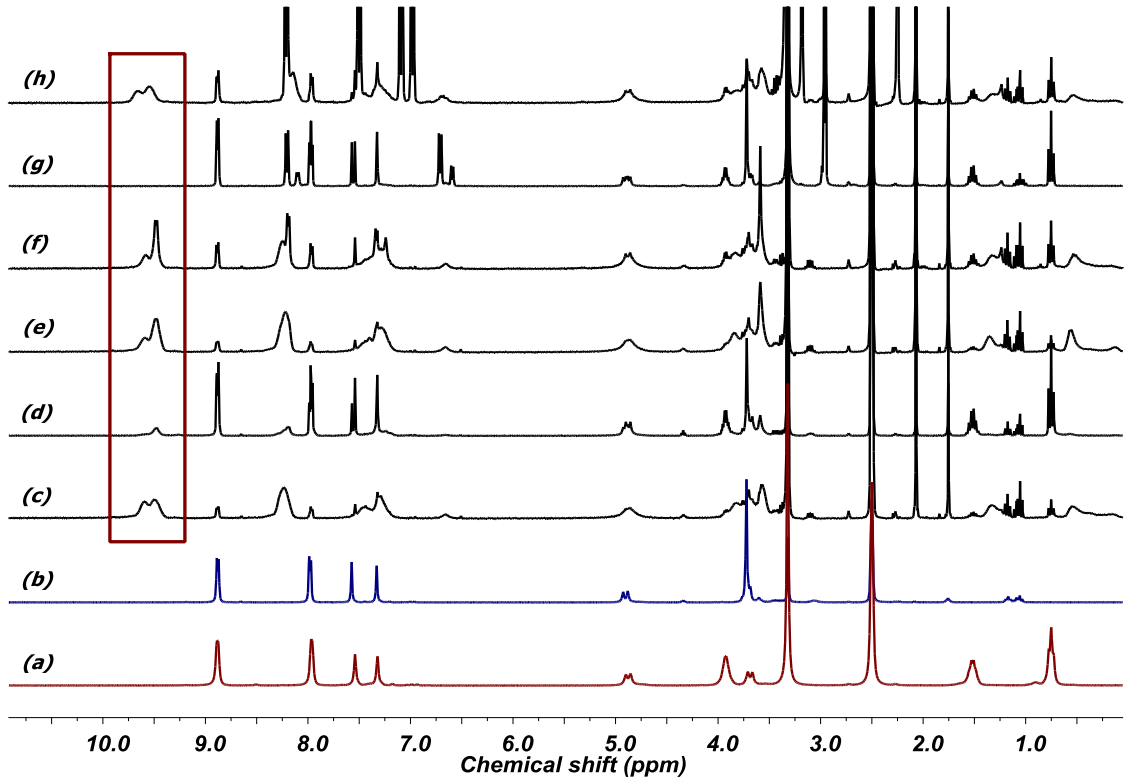

Figure 5.19 *Proton NMR study describing the assembly/disassembly processes in d_6-DMSO: (a) ligand **4.6**; (b) ligand **2.8**; (c) heteroleptic $[Pd_6(\mathbf{4.6})_{8-n}(\mathbf{2.8})_n]^{12+}$ cage mixture; (d) preferential formation of the $[Pd_6(\mathbf{2.8})_8]^{12+}$ cage; (e) coexisting homoleptic $[Pd_6(\mathbf{4.6})_8]^{12+}$ and $[Pd_6(\mathbf{2.8})_8]^{12+}$ cage mixture; (f) equilibrated homoleptic cage mixture; (g) chemical disassembly using DMAP; (h) regeneration of the heteroleptic $[Pd_6(\mathbf{4.6})_{8-n}(\mathbf{2.8})_n]^{12+}$ cages.*

The strong electronic induction of the *N,N'*-dimethylamine moiety greatly increases the lone pair coefficient on the pyridyl nitrogen, and thus DMAP is a stronger Lewis base than ligands **4.6** and **2.8**; hence, it effects the rapid degradation of the $[Pd_6(\mathbf{4.6})_8]^{12+}$ and $[Pd_6(\mathbf{2.8})_8]^{12+}$ cages

in DMSO solution. DMAP is also a much stronger Brønsted-Lowry base (pK_a of conjugate acid is 9.2) than either ligands **4.6** and **2.8** (pK_a's of conjugate acid calc. as 1.77) [56] and is therefore selectively protonated by the addition of the soluble organic acid, TsOH (pK_a is 2.1). This was evidenced in the ^{1}H NMR spectrum with a broad singlet at 13.15 ppm, corresponding to DMAP-H$^+$. It is likely that the electron withdrawing ester linkage present in ligands **4.6** and **2.8** will decrease the pK_a's of their corresponding conjugate acids such that they will not be protonated by TsOH in DMSO solution.[56]

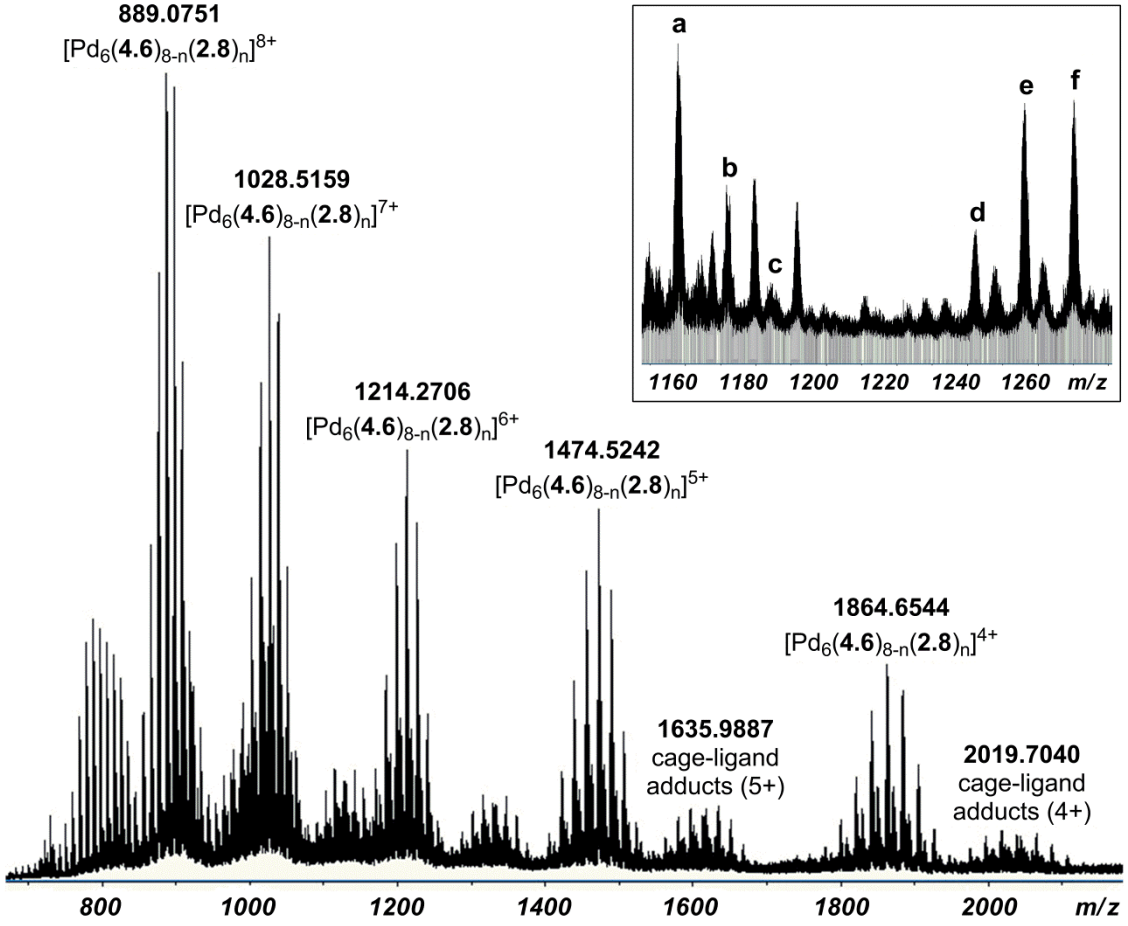

Figure 5.20 *Mass spectra taken from the reformation of {[Pd$_6$(**4.6**)$_{8-n}$(**2.8**)$_n$]·x(BF$_4$)}$^{(12-x)+}$ heteroleptic cages by the addition of TsOH (main figure, noting the cage-ligand adducts) and of the combined 'homoleptic' cage system (inset). True homoleptic cages **a** and **b** pertain to [Pd$_6$(**2.8**)$_8$]$^{12+}$ and [Pd$_6$(**4.6**)$_8$]$^{12+}$, respectively, whilst **b-e** correspond to minor, heteroleptic species formed through ligand exchange between reaction steps.*

The DMAP/TsOH chemical trigger is well-exemplified in bistable supramolecular systems, such as in molecular shuttles [57] and interlocked molecules,[58] and more recently, in the degradation of a metallo-supramolecular cage for the targeted release of cisplatin.[12] This shows that the high levels of control exhibited by the [Pd$_6$L$_8$]$^{12+}$ stella octangula cages, above, may allow for their application in areas such as cargo delivery.

5.7 Conclusions and future work

A family of $[Pd_6L_8]^{12+}$ and $[Pt_6L_8]^{12+}$ 'stella octangula' cages have been synthesised and discussed, including insight into their sophisticated solution-phase chemistry. As anticipated, use of the propylated ligand **4.6** in their construction resulted in a level of solubility that is inaccessible with the methylated ligand **2.8**.

This increased solubility of propylated cage $[Pd_6(\mathbf{4.6})_8]^{12+}$ allowed for an examination into their hosting capabilities, although an incommensurate size of windows to the cage interior limited their ability to form strong cage-guest interactions; nevertheless, preliminary studies displayed inclusion behaviour with the globular guest *ortho*-carborane and long-chained surfactant sodium dodecyl sulfate (SDS).

Solvent-dependent behaviour was noted for both propylated and methylated cages, $[Pd_6(\mathbf{4.6})_8]^{12+}$ and $[Pd_6(\mathbf{2.8})_8]^{12+}$, respectively. Chirality control could be effected in $[Pd_6(\mathbf{4.6})_8]^{12+}$, whereby acetonitrile and nitromethane solvents afforded homochiral cages, and DMSO and DMF solvents afforded only unsorted cages which were comprised of a mixture of ligand **4.6** enantiomers. Similarly, $[Pd_6(\mathbf{4.6})_8]^{12+}$ and $[Pd_6(\mathbf{2.8})_8]^{12+}$ displayed sterically-induced chirality control in DMSO solvent, whereby the methylated $[Pd_6(\mathbf{2.8})_8]^{12+}$ cage self-sorted with time to yield a homochiral cage species, owing to the less sterically demanding methyl groups at the cage windows. This was supported crystallographically, where examination of the static structures of $[Pd_6(\mathbf{4.6})_8]\cdot 12(BF_4)$ and $[Pd_6(\mathbf{2.8})_8]\cdot 12(NO_3)$ highlighted the 'unsorted' and homochiral cages, respectively.

The sterically and interactionally similar ligand pair **4.6**/**2.8** allowed for speciation control and the selective formation of coexisting and stable homoleptic cages, $[Pd_6(\mathbf{4.6})_8]^{12+}$ and $[Pd_6(\mathbf{2.8})_8]^{12+}$, and a heteroleptic cage mixture , $[Pd_6(\mathbf{4.6})_{8-n}(\mathbf{2.8})_n]^{12+}$. Ligand exchange could be effected by altering reaction stoichiometry, and $[Pd_6(\mathbf{2.8})_8]^{12+}$ was observed to be preferentially formed over the propylated analogue. Use of an extended ligand pair **5.3**/**5.4** allowed for the formation of homoleptic and heteroleptic 'stella octangula' cages $[Pd_6(\mathbf{5.3})_8]^{12+}$, $[Pd_6(\mathbf{5.4})_8]^{12+}$ and $[Pd_6(\mathbf{5.4})_{8-n}(\mathbf{5.3})_n]^{12+}$, respectively. These species were not as stable as their smaller analogues due to cage flexibility and limited ligand exchange was observed between cages, where it is assumed that ligand exchange proceeds *via* an associative mechanism.

Subtle variations in the stability and dynamics of the individual $[Pd_6(\mathbf{4.6})_8]^{12+}$ and $[Pd_6(\mathbf{2.8})_8]^{12+}$ cages has allowed for the determination of a cage assembly/disassembly relationship, which occurs cyclically and allows for the selective preparation of homoleptic and heteroleptic species by means of a well-established chemical trigger. Ultimately, the ability to control the

predominating species in solution gives potential application to these $[Pd_6L_8]^{12+}$ 'stella octangula' cages in areas such as cargo delivery, guest incarceration and catalysis.

Future work should involve an investigation into the cages ability to selectively bind molecules in the solution phase followed by a study of their release properties, either through use of a chemical trigger, or otherwise. The ability for the cages to associate with both globular guests and long chained surfactants affords the possibility for the binding of drug molecules, such as diclofenac and ibuprofen which each contain a non-polar moiety for interaction with the hydrophobic core of CTG and exist as anions in solution, providing coulombic stabilisation. If a host-guest relationship could be determined then an investigation into selective drug release could be realised by the addition of a weak acid or relevant chemical trigger, such as DMAP.

5.8 Experimental

Ligands **2.8** and **4.6** were prepared according to procedures listed in Chapter 2 and Chapter 4 of this thesis and were employed as racemic mixtures for all complexation studies listed herein.

Propylated-CTG (*p*CTG, **4.4**) was prepared according to procedures listed in Chapter 4 of this thesis and 4-(4-pyridyl)benzoyl chloride hydrochloride, ligand **5.4** [21] and complex **5.2** [25] were prepared according to literature procedures.

5.8.1 Instrumentation

NMR spectra were recorded by automated procedures on a Bruker Avance 500 or DPX 300 MHz NMR spectrometer. All deuterated solvents were purchased from Euriso-top. All ^{1}H and $^{13}C\{^{1}H\}$ spectra were referenced relative to an internal standard. High resolution DOSY and ROESY ^{1}H NMR spectra were recorded in collaboration with Dr. Julie Fisher of the University of Leeds. High resolution electrospray mass spectra (ESI-MS) were measured on a Bruker MicroTOF-Q or Bruker MaXis Impact spectrometer in either positive or negative ion mode by Ms. Tanya Marinko-Covell of the University of Leeds Mass Spectrometry Service and Dr Stuart L. Warriner of the University of Leeds. Low resolution mass spectra were recorded on an open-access Bruker Micromass LCT spectrometer with simultaneous HPLC using an acetonitrile/water eluent and sodium formate calibrant. FT-IR spectra were recorded as solid phase samples on a Perkin-Elmer Spectrum One spectrophotometer. Samples for microanalysis were dried under vacuum before analysis and the elemental composition determined by Mr Ian Blakeley of the University of Leeds Microanalytical Service using a Carlo Erba elemental analyser MOD 1106 spectrometer. Molecular dynamics calculations were performed by Dr Sarah Harris and Dr Geoff Wells of the School of Physics and Astronomy, University of Leeds.

Crystals were mounted under inert oil on a MiTeGen tip and flash frozen to 150(1) K using an Oxford Cryosystems cryostream low temperature device. X-ray diffraction data were collected using graphite-monochromated Mo-*K* radiation (λ = 0.71073 Å) using a Bruker-Nonius X-8 diffractometer with ApexII detector and FR591 rotating anode generator; or using synchrotron radiation (λ = 0.6889 Å) with a Crystal Logic 4-circle Kappa goniometer and Rigaku Saturn 724 CCD diffractometer at station i19 of Diamond Light Source. Data were corrected for Lorenztian and polarization effects and absorption corrections were applied using multi-scan methods. The structures were solved by direct methods using SHELXS-97 and refined by full-matrix on F^2 using SHELXL-97, interfaced through the X-seed interface.[59] Unless otherwise specified, all non-hydrogen atoms were refined as anisotropic, and hydrogen positions were included at geometrically estimated positions. Molecular graphics were obtained using POV-RAY through the X-Seed interface.[60] Additional details are given below and data collections and refinements summarised in the Table below.

5.8.2 Synthesis of ligands and complexes

Preparation of $[Pd_6(4.6)_8]\cdot12(BF_4)$ (complex 5.1). $Pd(MeCN)_4(BF_4)_2$ (5.0 mg, 0.0113 mmol) and ligand **4.6** (12.10 mg, 0.0150 mmol) were dissolved in d_3-MeCN (1 mL) and stirred for one hour, resulting in a pale-yellow solution, whereby ^{1}H NMR displayed quantitative cage formation. Diffusion of diethyl ether vapour into the solution afforded small, yellow prisms that were isolated, washed with a portion of diethyl ether and dried *in vacuo*. Quantitative. HR MS (ES^+): *m/z* 1076.7391 $\{[Pd_6L_8]\cdot5BF_4\}^{7+}$, 1270.3947 $\{[Pd_6L_8]\cdot6BF_4\}^{6+}$, 1542.0858$\{[Pd_6L_8]\cdot7BF_4\}^{5+}$ and 1949.6343 $\{[Pd_6L_8]\cdot8BF_4\}^{4+}$; calculated for 1076.5657, 1269.9968, 1542.5974 and 1949.9975, respectively; ^{1}H NMR (300 MHz, d_3-MeCN) δ (ppm) = 9.31 (m, 1H, Py-H^2, achiral cage), 9.16 (d, 5H, Py-H^2, chiral cage), 8.13 (d, 6H, Py-H^3), 7.27 (s, 3H, aryl-H), 7.10 (s, 3H aryl-H), 4.84 (d, 3H, CTG *exo*-H), 3.87 (m, 6H, propyl α-H), 3.69 (d, 3H, CTG *endo*-H), 1.62 (m, 1H, propyl β-H), 1.40 (m, 5H, propyl β-H), 0.85 (m, 2H, propyl γ-H), 0.60 (m, 7H, propyl γ -H); ^{1}H NMR (300 MHz, d_6-DMSO) δ (ppm) = 9.59 (s, 3H, Py-H^2), 9.48 (s, 3H, Py-H^2), 8.23 (s, 6H, Py-H^3), 7.44 (s, 3H, aryl-H), 7.28 (s, 3H, aryl-H), 4.87 (bs, 3H, CTG *exo*-H), 3.84 (bm, 6H, propyl α-H), 3.69 (bs, 3H, CTG *endo*-H), 1.32 (m, 6H, propyl β-H), 0.52 (m, 9H, propyl γ -H); ^{1}H NMR (300 MHz, d_3-$MeNO_2$) δ (ppm) = 9.42 (bs, 1H, Py-H^2, achiral cage), 9.27 (d, 5H, Py-H^2, chiral cage), 8.86 (d, Py-H^2, uncoordinated **4.6**), 8.24 (d, 6H, Py-H^3, chiral cage), 7.98 (d, Py-H^3, uncoordinated **4.6**), 7.31 (s, 3H, aryl-H), 7.19 (s, 3H, aryl-H), 4.95 (d, 3H, CTG *exo*-H), 3.99 (m, 6H, propyl α-H), 3.77 (d, 3H, CTG *endo*-H), 1.67 (m, 3H, propyl β-H), 1.48 (m, 3H, propyl β-H), 0.84 (m, 4H, propyl γ-H), 0.64 (m, 5H, propyl γ-H); Satisfactory elemental analysis could not be obtained owing to high levels of solvation.

Example for $[Pd_6(\mathbf{4.6})_8]\cdot 12(BF_4)$ (% calculated, found) C (56.64, 57.75), H (4.46, 5.35), N (4.13, 6.05); Infrared analysis (FT-IR, cm^{-1}) 3494, 2968, 2901, 1751, 1619, 1508, 1270 (s).

Diffusion Ordered (DOSY) NMR (500 MHz, d_6-DMSO): $D_{complex}$ = 0.439, D_{ligand} = 1.395×10^{-10} m^2s^{-1}; $D_{complex}/D_{ligand}$ = 0.33:1; Hydrodynamic radius (r) = 23.4 Å.[61]

$$\text{Where; } \frac{KBT}{D} = 6\pi\eta r$$

$D = 0.439\times10^{-10}\ m^2s^{-1}$; $K_B = 1.38065\times10^{-23}\ J\cdot K^{-1}$; T = 293.15 K; $\eta = 1.996\times10^{-3}$ Pa·s

Preparation of $[Pt_6(4.6)_8]\cdot 12(ClO_4)$. $Pt(ClO_4)_2$ (3.66 mg, 0.00928 mmol) was added to a solution ofligand **4.6** (10.12 mg, 0.0124 mmol) in d_6-DMSO (1 mL) and stirred at 70℃ overnight. ^{1}H NMR on the cooled solution displayed partial cage formation (~ 75 % based on relative integrals). HR MS (ES^+): *m/z* 1371.6856 $\{[Pt_6L_8]\cdot 6ClO_4\}^{6+}$, 1665.9895 $\{[Pt_6L_8]\cdot 7ClO_4\}^{5+}$ and 2107.4224 $\{[Pt_6L_8]\cdot 8ClO_4\}^{4+}$; calculated for 1371.1679, 1665.1912 and 2106.7254, respectively; ^{1}H NMR (300 MHz, d_6-DMSO) δ (ppm) 9.53-9.44 (bm, 3H, Py-H^2), 9.16 (d, 3H, Py-H^2), 8.88 (d, uncoordinated **4.6**), 8.33-8.25 (bm, 6H, Py-H^3), 7.96 (d, uncoordinated **4.6**), 7.55 (s, 3H, aryl-H), 7.32 (s, 3H, aryl-H), 4.89 (bd, 3H, CTG *exo*-H), 3.93 (bm, 6H, propyl α-H), 3.70 (bd, 3H, CTG *endo*-H), 1.53 (q, uncoordinated **4.6**), 1.30 (bq, 6H, propyl β-H), 0.75 (t, uncoordinated **4.6**), 0.53 (m, 9H, propyl γ-H).

Preparation of $[Pd_6(4.6)_8]\cdot 12(BF_4)\subset$ *o*-carborane. $Pd(MeCN)_4(BF_4)_2$ (2.51 mg, 0.00565 mmol) and ligand **4.6** (6.05 mg, 0.0075 mmol) were dissolved in d_7-DMF (0.6 mL) and equilibrated for one hour, resultanting in a pale-yellow solution, whereby ^{1}H NMR displayed quantitative cage formation. *O*-carborane (8 equivalents) was added to the preformed cage and was allowed to equilibrate for a further 16 hours. HR MS (ES^+): *m/z* 931.2771 $\{[Pd_6L_8]\cdot 4BF_4\}^{8+}$, 949.8336 $\{[Pd_6L_8]\cdot 4BF_4 \subset o\text{-carborane}\}^{8+}$, 966.6220 $\{[Pd_6L_8]\cdot 4BF_4 \subset 2(o\text{-carborane})\}^{8+}$, 1076.7391 $\{[Pd_6L_8]\cdot 5BF_4\}^{7+}$, 1096.7705 $\{[Pd_6L_8]\cdot 5BF_4 \subset o\text{-carborane}\}^{7+}$, 1270.3947 $\{[Pd_6L_8]\cdot 6BF_4\}^{6+}$, 1294.0441 $\{[Pd_6L_8]\cdot 6BF_4 \subset o\text{-carborane}\}^{6+}$, 1542.0858 $\{[Pd_6L_8]\cdot 7BF_4\}^{5+}$, 1570.4850 $\{[Pd_6L_8]\cdot 7BF_4 \subset o\text{-carborane}\}^{5+}$, 1598.4942 $\{[Pd_6L_8]\cdot 7BF_4 \subset 2(o\text{-carborane})\}^{5+}$ and 1949.6343 $\{[Pd_6L_8]\cdot 8BF_4\}^{4+}$; calculated for 931.4968, 949.5216, 966.9208, 1076.1397, 1097.7388, 1269.9968, 1294.8625, 1542.5974, 1570.4349, 1598.8752 and 1949.9975, respectively. ^{1}H NMR displayed only the sum of cage and guest resonances.

Disassembly and reassembly of $[Pd_6(4.6)_8]\cdot 12(BF_4)$. $Pd(MeCN)_4(BF_4)_2$ (2.51 mg, 0.00565 mmol) and **4.6** (6.05 mg, 0.0075 mmol) were dissolved in d_6-DMSO (0.6 mL) and equilibrated for one hour, resulting in a pale-yellow solution, whereby ^{1}H NMR displayed quantitative cage formation. 4-dimethylaminopyridine (DMAP, 24 equivalents) was then added to the reaction

mixture which resulted in rapid decolouration of the solution. ^{1}H NMR (300 MHz, d_6-DMSO) δ (ppm) = 8.88 (d, 6H, Py-H^2), 8.20 (d, 6H, DMAP Py-H^2), 7.96 (d, 6H, Py-H^3), 7.54 (s, 3H, aryl-H), 7.32 (s, 3H, aryl-H), 6.71 (d, 6H, DMAP Py-H^3), 4.88 (d, 3H, CTG *exo*-H), 3.92 (m, 6H, propyl α -H), 3.69 (d, 3H, CTG *endo*-H), 2.96 (s, 18H, DMAP Me), 1.52 (q, 6H, propyl β-H), 0.75 (t, 9H, propyl γ-H). The addition of *para*-toluenesulfonic acid (24 equivalents) to the reaction mixture resulted in recolourisation of the solution and reformation of the stella octangula cage. ^{1}H NMR (300 MHz, d_6-DMSO) δ (ppm) = 13.17 (s, 18H, DMAP N-H), 9.60 (bs, 3H, Py-H^2), 9.51 (bs, 3H, Py-H^2), 8.23 (bs, 12H, Py-H^3 and TsOH Ph-H^2), 7.52 (d, 6H, DMAP Py-H^2), 7.39 (s, 3H, aryl-H), 7.29 (s, 3H, aryl-H), 7.10 (d, 6H, DMAP Py-H^3), 6.97 (d, 6H, TsOH Ph-H^3), 4.82 (bd, 3H, CTG *exo*-H), 3.84 (bm, 6H, propyl α-H), 3.46 (s, 9H, TsOH Me), 2.07 (s, 18H, DMAP Me), 1.32 (bq, 6H, propyl β-H), 0.51 (bt, 9H, propyl γ-H).

Preparation of heteroleptic $[Pd_6(4.6)_{8-n}(2.8)_n]\cdot 12(BF_4)$ cages. $Pd(MeCN)_4(BF_4)_2$ (0.0113 mmol), **4.6** (6.05 mg, 0.0075 mmol) and **2.8** (5.47 mg, 0.0075 mmol) were dissolved in the required solvent (2 mL) and stirred for one hour, resulting in a pale-yellow solution. The reported HR MS (ES$^+$) data are representative for the solvents DMSO, DMF and MeCN and ratios correspond to **4.6**:**2.8**. HR MS (ES$^+$): *m/z* $[Pd_6L_8]^{5+}$ 1424.7916 (1:7), 1440.9024 (2:6), 1457.9135 (3:5), 1474.3380 (4:4), 1491.5342 (5:3) and 1510.6050 (6:2); $[Pd_6L_8]^{6+}$ 1171.7399 (1:7), 1186.2601 (2:6), 1200.4239 (3:5), 1214.4231 (4:4) and 1228.2939 (5:3); $[Pd_6L_8]^{7+}$ 1004.1753 (2:6), 1015.2259 (3:5), 1028.2081 (4:4), 1039.2467 (5:3) and 1051.2477 (6:2); $[Pd_6L_8]^{8+}$ 878.2324 (3:5), 888.2152 (4:4), 898.1935 (5:3), 909.4459 (6:2) and 920.1820 (7:1), calculated for 1424.6653, 1441.6847, 1458.5035, 1475.3223, 1492.1411, 1508.9599, 1171.8876, 1185.9026, 1199.9186, 1213.9342, 1227.9499, 1004.7735, 1016.7869, 1028.8003, 1040.8137, 1052.2562, 878.9377, 889.4495, 899.9612, 910.4730 and 920.9847, respectively; ^{1}H NMR (300 MHz, d_6-DMSO) δ (ppm) = 9.60 (bs, 6H, Py-H^2), 9.51 (bs, 6H, Py-H^2), 8.23 (bs, 12H, Py-H^3), 7.44 (bs, 6H, aryl-H), 7.29 (bs, 6H, aryl-H), 4.87 (bs, 6H, CTG *exo*-H), 3.84 (bm, 3H, **4.6** propyl α -H), 3.70 (bm, 3H, **4.6** propyl α-H), 3.57 (bs, 6H, **2.8** O-C$\underline{H}_3$), 1.34 (m, 6H, **4.6** propyl β-H), 0.55 (m, 9H, **4.6** propyl γ-H).

Preparation of coexisting homoleptic $[Pd_6(4.6)_8]^{12+}$ and $[Pd_6(2.8)_8]^{12+}$ cages. A 1:1 mixture of the pre-formed $[Pd_6(\mathbf{4.6})_8]\cdot 12(BF_4)$ and $[Pd_6(\mathbf{2.8})_8]\cdot 12(BF_4)$ cages were mixed at room temperature in DMSO and allowed to equilibrate overnight. HR MS (ES$^+$): *m/z* 1158.1294 $\{[Pd_6(\mathbf{2.8})_8]\cdot 6(BF_4)\}^{6+}$, 1270.4061 $\{[Pd_6(\mathbf{4.6})_8]\cdot 6(BF_4)\}^{6+}$, 1407.3632 $\{[Pd_6(\mathbf{2.8})_8]\cdot 7(BF_4)\}^{5+}$, 1541.7124 $\{[Pd_6(\mathbf{4.6})_8]\cdot 7(BF_4)\}^{5+}$, 1780.7396 $\{[Pd_6(\mathbf{2.8})_8]\cdot 8(BF_4)\}^{4+}$ and 1948.9379 $\{[Pd_6(\mathbf{4.6})_8]\cdot 8(BF_4)\}^{4+}$, calculated for 1157.8716, 1269.9986, 1407.8465, 1542.5974, 1781.5589 and 1949.9975, respectively. MS data were recollected and seen to be reproducible after heating and after an eight week standing period. ^{1}H NMR (300 MHz, d_6-DMSO) δ (ppm) = 9.56 (bs,

6H, Py-H^2), 9.48 (d, 6H, Py-H^2), 8.26 (bs, 6H, Py-H^3), 8.21 (d, 6H, Py-H^3), 7.46-7.25 (bs, 12H, 2 x aryl-H), 4.88 (bd, 6H, CTG *exo*-H), 3.83 (bm, 3H, **4.6** propyl α-H), 3.71 (bm, 3H, **4.6** propyl α-H), 3.58 (s, 6H, **2.8** ArO-C$\underline{H}_3$), 1.32 (m, 6H, **4.6** propyl β-H), 0.53 (m, 7H, **4.6** propyl γ-H), 0.13 (m, 2H, **4.6** propyl γ -H).

Reaction of $[Pd_6(4.6)_8]^{12+}$ and ligand 2.8. $[Pd_6(\mathbf{4.6})_8]^{12+}$ in d_6-DMSO was treated with 8 equivalents of methylated ligand **2.8** and allowed to stand at room temperature for one week. As soon as the components were mixed, propylated ligand **2.8** was observed in the NMR, with no free methylated ligand resonances seen, suggesting quantitative assembly of the methylated cage. HR MS (ES$^+$): *m/z* 1158.1294 $\{[Pd_6(\mathbf{2.8})_8]\cdot 6(BF_4)\}^{6+}$, 1407.3632 $\{[Pd_6(\mathbf{2.8})_8]\cdot 7(BF_4)\}^{5+}$ and 1780.7396 $\{[Pd_6(\mathbf{2.8})_8]\cdot 8(BF_4)\}^{4+}$, calculated for 1157.8716, 1407.8465 and 1781.5589, respectively; ^{1}H NMR (300 MHz, d_6-DMSO) δ (ppm) = 9.60 (bs, 2H, Py-H^2), 9.51 (bs, 10H, Py-H^2), 8.22 (bs, 12H, Py-H^3), 7.41 (bs, 6H, aryl-H), 7.28 (bs, 6H, aryl-H), 4.86 (bs, 6H, CTG *exo*-H), 3.84 (bm, 3H, **4.6** propyl -H), 3.70 (bm, 3H, **4.6** propyl α -H), 3.57 (s, 6H, **2.8** ArO-C$\underline{H}_3$), 1.36(m, 6H, **4.6** propyl β-H), 0.55 (m, 9H, **4.6** propyl γ-H).

Reaction of $[Pd_6(2.8)_8]^{12+}$ and ligand 4.6. $[Pd_6(\mathbf{2.8})_8]^{12+}$ in d_6-DMSO was treated with 8 equivalents of propylated ligand **4.6** and allowed to stand at room temperature for 1 week, where only the sum of methylated stella octangula $[Pd_6(\mathbf{2.8})_8]^{12+}$ and propylated ligand resonances **4.6** are observed and there is no change with time. HR MS (ES$^+$): *m/z* 1158.1294 $\{[Pd_6(\mathbf{2.8})_8]\cdot 6(BF_4)\}^{6+}$, 1407.3632 $\{[Pd_6(\mathbf{2.8})_8]\cdot 7(BF_4)\}^{5+}$ and 1780.7396 $\{[Pd_6(\mathbf{2.8})_8]\cdot 8(BF_4)\}^{4+}$, calculated for 1157.8716, 1407.8465 and 1781.5589, respectively; ^{1}H NMR (300 MHz, d_6-DMSO) δ (ppm) = 9.48 (bd, 6H, Py-H^2), 8.83 (d, uncoordinated **4.6**, Py-H^2), 8.18 (bd, 6H, Py-H^3), 7.96 (d, uncoordinated **4.6**, Py-H^3), 7.54 (s, 3H, aryl-H), 7.32 (s, 3H, aryl-H), 4.89 (bd, 6H, CTG *exo*-H and uncoordinated **4.6** *exo*-H), 3.93 (p, uncoordinated **4.6** propyl α-H), 3.72 (s, 6H, **2.8** ArO-C$\underline{H}_3$), 3.64 (bd, 6H, CTG *endo*-H and uncoordinated **4.6** *endo*-H), 1.53 (q, uncoordinated **4.6** propyl β-H), 0.78 (t, uncoordinated **4.6** propyl γ-H).

Preparation of (±)-2,7,12-Tripropoxy-3,8,13-*tris*(4-pyridyl-4-phenylcarboxy)-10,15-dihydro-5*H*-tribenzo[*a,d,g*]cyclononatriene (5.3). Anhydrous triethylamine (1.32 mL, 7.56 mmol) was added to a stirred solution of 4.4 (310 mg, 0.630 mmol) in anhydrous THF (50 mL), at -78 °C, under an argon atmosphere. After one hour, 4-(4-pyridyl)benzoyl chloride hydrochloride (960 mg, 3.78 mmol) was added to the reaction mixture and stirred at -78 °C for a further two hours before being left at room temperature for 48 hours. The solvent was removed *in vacuo* and the resultant residue triturated in ethanol to afford the target compound as a white solid, which was isolated by filtration and dried *in vacuo*. Yield 609 mg: 93 %; M.pt Decomposes > 270 °C; HR MS (ES$^+$): *m/z* 1058.3941 $\{5.3\cdot Na\}^+$; calculated for $C_{66}H_{57}N_3O_9Na$

1058.3993; ^{1}H NMR (300 MHz, d_6-DMSO) δ (ppm) = 8.70 (d, 6H, Py-H^{2}, *J* = 6.2 Hz), 8.20 (d, 6H, Ph-H^{3}, *J* = 8.5 Hz), 8.03 (d, 6H, Ph-H^{2}, *J* = 8.5 Hz), 7.81 (d, 6H, Py-H^{3}, *J* = 6.2 Hz), 7.53 (s, 3H, aryl-H), 7.34 (s, 3H, aryl-H), 4.87 (d, 3H, CTG *exo*-H, *J* = 12.5 Hz), 3.94 (t, 6H, propyl -H, *J* = 6.2 Hz), 3.73 (d, 3H, CTG *endo*-H, *J* = 12.5 Hz), 1.53 (q, 6H, propyl β-H, *J* = 6.6 Hz), 0.78 (t, 9H, propyl -H, *J* = 7.4 Hz); ^{13}C{^{1}H} NMR (75 MHz, d_6-DMSO) δ (ppm) = 184.2, 150.7, 148.6, 145.7, 142.2, 138.4, 136.6, 131.8, 130.3, 129.2, 127.2, 121.5, 69.7, 21.8, 9.9; Analysis for 5.3·0.5($CHCl_3$) (% calculated, found) C (72.88, 73.15), H (5.29, 5.40), N (3.83, 3.80); Infrared analysis (FT-IR, cm^{-1}) = 2960, 1734 (s), 1594, 1508, 1400, 1263 (s), 1181, 1093, 820, 762.

Preparation of $[Pd_6(5.3)_8]\cdot12(BF_4)$ (complex 5.5). $Pd(MeCN)_4(BF_4)_2$ (3.2 mg, 0.00725 mmol) and ligand **5.3** (10.00 mg, 0.00966 mmol) were dissolved in d_6-DMSO (1 mL) and stirred for one hour, resulting in a pale-yellow solution, where both 1D and 2D ^{1}H NMR displayed cage formation. Diffusion of acetone vapour into the solution afforded a microcrystalline solid which was isolated, washed with a portion of acetone and dried *in vacuo*. HR MS (ES^{+}): *m/z* 1020.9683 $\{[Pd_6L_8]\cdot3BF_4\}^{9+}$, 1159.3551 $\{[Pd_6L_8]\cdot4BF_4\}^{8+}$, 1337.3494 $\{[Pd_6L_8]\cdot5BF_4\}^{7+}$, 1574.9554 $\{[Pd_6L_8]\cdot6BF_4\}^{6+}$ and 1906.9543 $\{[Pd_6L_8]\cdot7BF_4\}^{5+}$; calculated for 1021.3029, 1159.8441, 1337.9659, 1575.4558 and 1907.9476, respectively; ^{1}H NMR (300 MHz, d_6-DMSO) δ (ppm) = 9.34 (bm, 6H, Py-H^{2}), 8.24-8.08 (bm, 18H, Py-H^{3}, Ph-H^{2}, Ph-H^{3}), 7.46 (s, 3H, aryl-H), 7.30 (s, 3H, aryl-H), 4.82 (bd, 3H, CTG *exo*-H), 3.84 (bm, 6H, propyl α-H), 3.69 (bd, 3H, CTG *endo*-H), 1.38 (bq, 6H, propyl β-H), 0.61 (bt, 9H, propyl γ-H). Satisfactory elemental analysis could not be obtained due to high levels of solvation; Infrared analysis (FT-IR, cm^{-1}) 3384 (broad), 1742 (weak), 1622 (weak), 1024 (weak). 2D DOSY NMR (500 MHz, d_6-DMSO) $D = 0.348 \times 10^{-10}$ m^{2}s^{-1}.

Preparation of heteroleptic $[Pd_6(5.3)_n(5.4)_m]\cdot12(BF_4)$ cages. $Pd(MeCN)_4(BF_4)_2$ (0.0113 mmol), ligand **5.4** (6.05 mg, 0.0075 mmol) and ligand **5.4** (5.47 mg, 0.0075 mmol) were dissolved in DMSO (1 mL) and stirred for one hour, resulting in a pale-yellow solution. The reported HR MS (ES^{+}) ratios correspond to **5.3**:**5.4**. HR MS (ES^{+}): *m/z* $[Pd_6L_8]^{9+}$ 964.3977 (2:6), 974.4185 (3:5), 983.3334 (4:4), 992.3270 (5:3), 1000.9031 (6:2), 1010.8867 (7:1), 1020.7853 (8:0); $[Pd_6L_8]^{8+}$ 1096.1697 (2:6), 1106.8121 (3:5), 1117.3817 (4:4), 1127.4205 (5:3), 1138.1523 (6:2), 1147.8401 (7:1); $[Pd_6L_8]^{7+}$ 1265.1132 (2:6), 1277.1484 (3:5), 1289.2449 (4:4), 1301.4740 (5:3), 1313.3052 (6:2), 1323.7125 (7:1); $[Pd_6L_8]^{6+}$ 1475.8295 (1:7), 1490.2005 (2:6), 1504.7537 (3:5), 1518.8601 (4:4), 1532.5273 (5:3), 1546.7584 (6:2), 1561.2863 (7:1); $[Pd_6L_8]^{5+}$ 1806.4309 (2:6), 1822.4428 (3:5), 1839.5668 (4:4), 1856.0725 (5:3), 1871.5294 (6:2).

Preparation of coexisting homoleptic $[Pd_6(5.3)_8]\cdot12(BF_4)$ and $[Pd_6(5.4)_8]\cdot12(BF_4)$ cages. A 1:1 mixture of the pre-formed $[Pd_6(\mathbf{5.3})_8]\cdot12(BF_4)$ and $[Pd_6(\mathbf{5.4})_8]\cdot12(BF_4)$ stella octangulas were mixed at room temperature and allowed to equilibrate overnight. HR MS (ES^+): *m/z* 946.0922 $\{[Pd_6(\mathbf{5.4})_8]\cdot3BF_4\}^{9+}$, 1020.7993 $\{[Pd_6(\mathbf{5.3})_8]\cdot3BF_4\}^{9+}$, 1075.3161 $\{[Pd_6(\mathbf{5.4})_8]\cdot4BF_4\}^{8+}$, 1159.3551 $\{[Pd_6(\mathbf{5.3})_8]\cdot4BF_4\}^{8+}$, 1241.1279 $\{[Pd_6(\mathbf{5.4})_8]\cdot5BF_4\}^{7+}$, 1337.3494 $\{[Pd_6(\mathbf{5.3})_8]\cdot5BF_4\}^{7+}$, 1462.4924 $\{[Pd_6(\mathbf{5.4})_8]\cdot6BF_4\}^{6+}$, 1574.9554 $\{[Pd_6(\mathbf{5.3})_8]\cdot6BF_4\}^{6+}$, 1772.5636 $\{[Pd_6(\mathbf{5.4})_8]\cdot7BF_4\}^{5+}$ and 1907.1185 $\{[Pd_6(\mathbf{5.3})_8]\cdot7BF_4\}^{5+}$, calculated for 946.5528, 1021.3029, 1075.7473, 1159.8441, 1241.8544, 1337.9659, 1463.3306, 1575.4553, 1773.3973 and 1907.9476, respectively. The sample was allowed to stand for a further eight weeks and reanalysed under the same conditions. The reported HR MS (ES^+) ratios correspond to **5.3**: **5.4**. HR MS (ES^+): *m/z* $[Pd_6L_8]^{10+}$ 842.7962 (8:1), 851.2043 (7:1), 859.4148 (6:2), 893.0513 (2:6), 901.6593 (1:7), 910.0709 (0:8); $[Pd_6L_8]^{9+}$ 946.2201 (8:1), 955.6739 (7:1), 964.5744 (6:2), 974.2492 (5:3), 983.4076 (4:4), 993.1514 (3:5), 1002.0600 (2:6), 1011.6249 (1:7), 1020.8581 (0:8); $[Pd_6L_8]^{8+}$ 1075.2478 (0:8), 1085.8834 (7:1), 1096.0231 (6:2), 1107.0224 (5:3), 1116.8033 (4:4), 1127.8173 (3:5), 1138.4280 (2:6), 1148.6996 (1:7), 1158.4648 (0:8); $[Pd_6L_8]^{7+}$ 1240.9985 (8:0), 1253.0090 (7:1), 1265.0251 (6:2), 1277.1850 (5:3), 1313.6404 (2:6), 1325.2294 (1:7), 1337.2459 (0:8); $[Pd_6L_8]^{6+}$ 1462.4989 (8:0), 1476.6771 (7:1), 1490.2000 (6:2), 1560.4347 (1:7), 1574.7895 (0:8); $[Pd_6L_8]^{5+}$ 1772.1971 (8:0), 1789.2190 (7:1), 1806.0316 (6:2), 1890.5309 (1:7), 1907.1460 (0:8).

Experiments in cage speciation control. A heteroleptic $[Pd_6(\mathbf{4.6})_{8-n}(\mathbf{2.8})_n]\cdot12BF_4$ cage mixture was generated from $Pd(MeCN)_4(BF_4)_2$ (0.0113 mmol), ligand **4.6** (6.05 mg, 0.0075 mmol) and ligand **2.8** (5.47 mg, 0.0075 mmol) as described above. The heteroleptic mixture was treated with a further four equivalents of both methylated **2.8** and propylated **4.6** ligands and allowed to stand. As soon as the reagents were added, resonances attributable to the free propylated ligand were seen in the NMR spectra which did not change with time. ^{1}H NMR (300 MHz, d_6-DMSO) δ (ppm) = 9.48 (s, 6H, Py-H^2), 8.89 (d, uncoordinated **4.6** Py-H^2), 8.21 (bs, 6H, Py-H^3), 7.95 (d, uncoordinated **4.6** Py-H^3), 7.54 (s, 3H, aryl-H), 7.29 (s, 3H, aryl-H), 4.88 (d, 3H, CTG *exo*-H), 3.94 (m, uncoordinated **4.6** propyl α-H), 3.80 (s, 9H, **2.8** ArO-C$\underline{H}_3$), 3.62 (d, 3H, CTG *endo*-H), 1.53 (m, uncoordinated **4.6** propyl β-H), 0.71 (t, uncoordinated **4.6** propyl γ-H).

A further six equivalents of palladium (II) were added to generate coexisting homoleptic $[Pd_6(\mathbf{4.6})_8]^{12+}$ and $[Pd_6(\mathbf{2.8})_8]^{12+}$ cages. Free propylated ligand resonances were consumed and resonances attributable to the propylated cage (particularly in the propyl moiety region) were formed. NMR shows a bias towards homoleptic cages, and ESI-MS also indicate a strong bias towards homoleptic cages along with some heteroleptic cages present along with ligand⊂cage

adducts. ^{1}H NMR (300 MHz, d_6-DMSO) δ (ppm) = 9.60 (bs, 2H, Py-H^{2}), 9.51 (bs, 10H, Py-H^{2}), 8.22 (bs, 12H, Py-H^{3}), 7.41 (bs, 6H, aryl-H), 7.28 (bs, 6H, aryl-H), 4.86 (bs, 6H, CTG *exo*-H), 3.84 (bm, 3H, **4.6** propyl α-H), 3.70 (bm, 3H, **4.6** propyl α -H), 3.57 (s, 6H, **2.8** ArO-C$\underline{H}_3$), 1.36 (m, 6H, **4.6** propyl β-H), 0.55 (m, 9H, **4.6** propyl γ-H).

The addition of DMAP (24 equivs.) to this mixture quantitatively disassembles the cages into the individual substituents. ^{1}H NMR (300 MHz, d_6-DMSO) δ (ppm) = 8.88 (m, 6H, **4.6** and **2.8** Py-H^{2}), 8.20 (d, 6H, DMAP Py-H^{2}), 7.96 (m, 6H, **4.6** and **2.8** Py-H^{3}), 7.57 (s, 1.5H, **2.8** aryl-H), 7.54 (s, 1.5H, **4.6** aryl-H), 7.32 (s, 3H, aryl-H), 6.71 (d, 6H, DMAP Py-H^{3}), 4.88 (m, 3H, **4.6** and **2.8** CTG *exo*-H), 3.92 (m, 6H, **4.6** propyl α-H), 3.72 (s, 4.5H, **2.8** ArO-CH$_3$), 3.69 (m, 3H, **4.6** and **2.8** CTG *endo*-H), 2.96 (s, 18H, DMAP Me), 1.52 (q, 6H, **4.6** propyl β-H), 0.75 (t, 9H, **4.6** propyl γ-H).

The addition of TsOH (24 equivs.) quantitatively and rapidly regenerates the heteroleptic [Pd$_6$(**4.6**)$_{8-n}$(**2.8**)$_n$]·12BF$_4$ cage mixture. The corresponding ratios represent **4.6**:**2.8**. HR MS (ES$^+$): *m/z* [Pd$_6$L$_8$]$^{5+}$ 1424.7916 (1:7), 1440.9024 (2:6), 1457.9135 (3:5), 1474.3380 (4:4), 1491.5342 (5:3) and 1510.6050 (6:2); [Pd$_6$L$_8$]$^{6+}$ 1171.7399 (1:7), 1186.2601 (2:6), 1200.4239 (3:5), 1214.4231 (4:4) and 1228.2939 (5:3); [Pd$_6$L$_8$]$^{7+}$ 1004.1753 (2:6), 1015.2259 (3:5), 1028.2081 (4:4), 1039.2467 (5:3) and 1051.2477 (6:2); [Pd$_6$L$_8$]$^{8+}$ 878.2324 (3:5), 888.2152 (4:4), 898.1935 (5:3), 909.4459 (6:2) and 920.1820 (7:1), calculated for 1424.6653, 1441.6847, 1458.5035, 1475.3223, 1492.1411, 1508.9599, 1171.8876, 1185.9026, 1199.9186, 1213.9342, 1227.9499, 1004.7735, 1016.7869, 1028.8003, 1040.8137, 1052.2562, 878.9377, 889.4495, 899.9612, 910.4730 and 920.9847, respectively; ^{1}H NMR (300 MHz, d_6-DMSO) δ (ppm) = 13.17 (s, 18H, DMAP N-H), 9.60 (bs, 3H, Py-H^{2}), 9.51 (bs, 3H, Py-H^{2}), 8.23 (bs, 12H, Py-H^{3} and TsOH Ph-H^{2}), 7.52 (d, 6H, DMAP Py-H^{2}), 7.39 (s, 3H, aryl-H), 7.29 (s, 3H, aryl-H), 7.10 (d, 6H, DMAP Py-H^{3}), 6.97 (d, 6H, TsOH Ph-H^{3}), 4.82 (bd, 3H, CTG *exo*-H), 3.84 (bm, 6H, **4.6** propyl α-H), 3.57 (s, 6H, **2.8** ArO-C$\underline{H}_3$), 3.46 (s, 9H, TsOH Me), 2.07 (s, 18H, DMAP Me), 1.32 (bq, 6H, **4.6** propyl β-H), 0.51 (bt, 9H, **4.6** propyl γ-H).

5.8.3 Supplementary crystallographic information

Crystals of complex **5.1** diffracted poorly, and despite their large size there was no observable diffraction at high angles (data cut off at 2θ = 20 º) using synchrotron radiation. Poor crystal quality was indicated by high levels of internal inconsistencies (R_{int} = 0.1422). Many crystals were trialled, from multiple crystallisation batches, but improved diffraction data were not obtained. Weak diffraction is due to large void spaces within the lattice (~ 70 %) and the inherent molecular disorder within the structure. Only the two palladium(II) centres were refined anisotropically and hydrogen atoms were not modelled. Each **4.6** ligand was modelled with complete molecular disorder, corresponding to the inclusion of two enantiomers into the structure. One ligand arm was disordered over two positions in accordance with the symmetry restriction imposed by the two ligand enantiomers. Both the pyridyl rings and aryl rings of the tribenzo[*a*,*d*,*g*]cyclononatriene ligand core were refined using rigid body restraints (AFIX 66 command). The weak data meant that the propyl moieties could not be crystallographically located in the difference map. Likewise, all tetrafluoroborate anions and solvents could not be crystallographically located owing to the large void spaces within the structure; hence, the SQUEEZE [26] routine of PLATON was employed.[27]

5.8.4 X-ray data table for complex 5.1

	5.1*
Formula	$C_{228}H_{288}B_{12}F_{48}N_{24}O_{54}Pd_6$
Mr	6629.54
Crystal colour and shape	Pale yellow, cube
Crystal size (mm)	0.2 x 0.2 x 0.2
Crystal system	Tetragonal
Space group	*I*4/*mmm*
a (Å)	30.688(5)
b (Å)	30.688(5)
c (Å)	45.906(11)
α (^{0})	90.00
β (^{0})	90.00
γ (^{0})	90.00
V (Å^3)	43234(15)
Z	2
ρ_{calc} (g.cm^{-3})	0.509
θ range (^{0})	0.77-20.00
No. data collected	105938
No. unique data	6101
R_{int}	0.1422
No. obs. Data ($I > 2\sigma(I)$)	3142
No. parameters	90
No. restraints	0
R_1 (obs data)	0.1577
wR_2 (all data)	0.3880
S	1.320

***** Data were collected using synchrotron radiation.

5.9 Bibliography

[1] G. M. Whitesides, B. Grzybowski, *Science* **2002**, *295*, 2418-2421.

[2] (a) M. C. O'Sullivan, J. K. Sprafke, D. V. Kondratuk, C. Rinfray, T. D. W. Claridge, A. Saywell, M. O. Blunt, J. N. O'Shea, P. H. Beton, M. Malfois, H. L. Anderson, *Nature* **2011**, *469*, 72-75; (b) B. Lewandowski, G. De Bo, J. W. Ward, M. Papmeyer, S. Kuschel, M. J. Aldegunde, P. M. E. Gramlich, D. Heckmann, S. M. Goldup, D. M. D'Souza, A. E. Fernandes, D. A. Leigh, *Science* **2013**, *339*, 189-193.

[3] N. Ichihashi, K. Usui, Y. Kazuta, T. Sunami, T. Matsuura, T. Yomo, *Nat. Commun.* **2013**, *4*, 2494.

[4] J. F. Stoddart, *Nat. Chem.* **2009**, *1*, 14-15.

[5] F. Stoddart, *Nature* **1988**, *334*, 10-11.

[6] J.-M. Lehn, *Science* **2002**, *295*, 2400-2403.

[7] J. R. Nitschke, *Nature* **2009**, *462*, 736-738.

[8] P. Mal, B. Breiner, K. Rissanen, J. R. Nitschke, *Science* **2009**, *324*, 1697-1699.

[9] A. C. Fahrenbach, Z. Zhu, D. Cao, W.-G. Liu, H. Li, S. K. Dey, S. Basu, A. Trabolsi, Y. Y. Botros, W. A. Goddard, J. F. Stoddart, *J. Am. Chem. Soc.* **2012**, *134*, 16275-16288.

[10] R. A. Brown, V. Diemer, S. J. Webb, J. Clayden, *Nat. Chem.* **2013**, *5*, 853.860.

[11] O. Taratula, P. A. Hill, N. S. Khan, P. J. Carroll, I. J. Dmochowski, *Nat. Commun.* **2010**, *1*, 148.

[12] J. E. M. Lewis, E. L. Gavey, S. A. Cameron, J. D. Crowley, *Chem. Sci.* **2012**, *3*, 778-784.

[13] M. Juríček, N. L. Strutt, J. C. Barnes, A. M. Butterfield, E. J. Dale, K. K. Baldridge, J. F. Stoddart, J. S. Siegel, *Nat. Chem.* **2014**, *6*, 222-228.

[14] M. D. Levin, P. J. Stang, *J. Am. Chem. Soc.* **2000**, *122*, 7428-7429.

[15] S. De, K. Mahata, M. Schmittel, *Chem. Soc. Rev.* **2010**, *39*, 1555-1575.

[16] M. M. J. Smulders, I. A. Riddell, C. Browne, J. R. Nitschke, *Chem. Soc. Rev.* **2013**, *42*, 1728-1754.

[17] Q.-F. Sun, J. Iwasa, D. Ogawa, Y. Ishido, S. Sato, T. Ozeki, Y. Sei, K. Yamaguchi, M. Fujita, *Science* **2010**, *328*, 1144-1147.

[18] Y.-R. Zheng, P. J. Stang, *J. Am. Chem. Soc.* **2009**, *131*, 3487-3489.

[19] S. J. Park, D. M. Shin, S. Sakamoto, K. Yamaguchi, Y. K. Chung, M. S. Lah, J.-I. Hong, *Chem. Eur. J.* **2005**, *11*, 235-241.

[20] R. L. Paul, Z. R. Bell, J. C. Jeffery, J. A. McCleverty, M. D. Ward, *Proc. Natl. Acad. Sci. USA* **2002**, *99*, 4883-4888.

[21] T. K. Ronson, C. Carruthers, J. Fisher, T. Brotin, L. P. Harding, P. J. Rizkallah, M. J. Hardie, *Inorg. Chem.* **2010**, *49*, 675-685.

[22] C. Piguet, *Chem. Commun.* **2010**, *46*, 6209-6231.

[23] S.-K. Lin, *J. Chem. Inf. Comp. Sci.* **1996**, *36*, 367-376.

[24] K. Mahata, M. Schmittel, *Beilstein J. Org. Chem.* **2011**, *7*, 1555-1561.

[25] T. K. Ronson, J. Fisher, L. P. Harding, M. J. Hardie, *Angew. Chem. Int. Ed.* **2007**, *46*, 9086-9088.

[26] A. L. Spek, *Acta. Crystallogr., Sect. D* **2009**, *D65*, 148-155.

[27] A. L. Spek, *Acta Crystallogr. Sect. A* **1990**, *A46*, 194-201.

[28] M. Yoneya, T. Yamaguchi, S. Sato, M. Fujita, *J. Am. Chem. Soc.* **2012**, *134*, 14401-14407.

[29] J. Canceill, A. Collet, G. Gottarelli, *J. Am. Chem. Soc.* **1984**, *106*, 5997-6003.

[30] D. Xu, R. Warmuth, *J. Am. Chem. Soc.* **2008**, *130*, 7520-7521.

[31] O. Chepelin, J. Ujma, X. Wu, A. M. Z. Slawin, M. B. Pitak, S. J. Coles, J. Michel, A. C. Jones, P. E. Barran, P. J. Lusby, *J. Am. Chem. Soc.* **2012**, *134*, 19334-19337.

[32] M. M. Safont-Sempere, G. Fernández, F. Würthner, *Chem. Rev.* **2011**, *111*, 5784-5814.

[33] J.-T. Yu, Y.-Y. Shi, J. Sun, J. Lin, Z.-T. Huang, Q.-Y. Zheng, *Sci. Rep.* **2013**, *3*, 2947.

[34] C. G. Claessens, I. Sánchez-Molina, T. Torres, *Supramol. Chem.* **2009**, *21*, 44-47.

[35] C. Gütz, R. Hovorka, G. Schnakenburg, A. Lützen, *Chem. Eur. J.* **2013**, *19*, 10890-10894.

[36] (a) C. Carruthers, J. Fisher, L. P. Harding, M. J. Hardie, *Dalton Trans.* **2010**, *39*, 355-357; (b) E. Huerta, H. Isla, E. M. Perez, C. Bo, N. Martin, J. de Mendoza, *J. Am. Chem. Soc.* **2010**, *132*, 5351-5353; (c) J. Canceill, L. Lacombe, A. Collet, *J. Chem. Soc., Chem. Commun.* **1987**, 219-221.

[37] F. Hof, S. L. Craig, C. Nuckolls, J. J. Rebek, *Angew. Chem. Int. Ed.* **2002**, *41*, 1488-1508.

[38] S. Mecozzi, J. J. Rebek, *Chem. Eur. J.* **1998**, *4*, 1016-1022.

[39] M. J. Hardie, C. L. Raston, *Chem. Commun.* **1999**, 1153-1163.

[40] N. J. Cookson, J. J. Henkelis, R. J. Ansell, C. W. G. Fishwick, M. J. Hardie, J. Fisher, *Dalton Trans.* **2014**, *43*, 5657-5661.

[41] L. Pirondini, F. Bertolini, B. Cantadori, F. Ugozzoli, C. Massera, E. Dalcanale, *Proc. Natl. Acad. Sci. USA* **2002**, *99*, 4911-4915.

[42] J. Lee, K. Ghosh, P. J. Stang, *J. Am. Chem. Soc.* **2009**, *131*, 12028-12029.

[43] K. Mahata, M. Schmittel, *J. Am. Chem. Soc.* **2009**, *131*, 16544-16554.

[44] Y. Inokuma, T. Arai, M. Fujita, *Nat. Chem.* **2011**, *2*, 780-783.

[45] D. Fujita, K. Suzuki, S. Sato, M. Yagi-Utsumi, Y. Yamaguchi, N. Mizuno, T. Kumasaka, M. Takata, M. Noda, S. Uchiyama, K. Kato, M. Fujita, *Nat. Commun.* **2012**, *3*, 1093.

[46] Y. Kohyama, T. Murase, M. Fujita, *J. Am. Chem. Soc.* **2014**, *136*, 2966-2969.

[47] C. J. Hastings, M. D. Pluth, R. G. Bergman, K. N. Raymond, *J. Am. Chem. Soc.* **2010**, *132*, 6938-6940.

[48] D. H. Leung, R. G. Bergman, K. N. Raymond, *J. Am. Chem. Soc.* **2006**, *128*, 9781-9797.

[49] P. Skowronek, B. Warzajtis, U. Rychlewska, J. Gawronski, *Chem. Commun.* **2013**, *49*, 2524-2526.

[50] N. Kudo, M. Perseghini, G. C. Fu, *Angew. Chem. Int. Ed.* **2006**, *45*, 1282-1284.

[51] N. J. Young, B. P. Hay, *Chem. Commun.* **2013**, *49*, 1354-1379.

[52] Molecular dynamics calculations performed by Sarah Harris and Geoff Wells, School of Physics and Astronomy, University of Leeds.

[53] S. T. Mough, J. C. Goeltz, K. T. Holman, *Angew. Chem. Int. Ed.* **2004**, *43*, 5631-5635.

[54] T. Tozawa, J. T. A. Jones, S. I. Swamy, S. Jiang, D. J. Adams, S. Shakespeare, R. Clowes, D. Bradshaw, T. Hasell, S. Y. Chong, C. Tang, S. Thompson, J. Parker, A. Trewin, J. Bacsa, A. M. Z. Slawin, A. Steiner, A. I. Cooper, *Nat. Mater.* **2009**, *8*, 973-978.

[55] T. Hasell, J. L. Culshaw, S. Y. Chong, M. Schmidtmann, M. A. Little, K. E. Jelfs, E. O. Pyzer-Knapp, H. Shepherd, D. J. Adams, G. M. Day, A. I. Cooper, *J. Am. Chem. Soc.* **2014**, *136*, 1438-1448.

[56] R. Casasnovas, J. Frau, J. Ortega-Castro, A. Salva, J. Donoso, F. Munos, *J. Mol. Struct.* **2009**, *912*, 5-12.

[57] J. D. Crowley, D. A. Leigh, P. J. Lusby, R. T. McBurney, L.-E. Perret-Aebi, C. Petzold, A. M. Z. Slawin, M. D. Symes, *J. Am. Chem. Soc.* **2007**, *129*, 15085-15090.

[58] J. F. Stoddart, *Chem. Soc. Rev.* **2009**, *38*, 1802-1820.

[59] (a) G. Sheldrick, *Acta Crystallogr., Sect. A* **2008**, *A64*, 112-122; (b) L. J. Barbour, *Supramol. Chem.* **2001**, *1*, 189-191.

[60] A. Persistence of Vision Raytracer Pty. Ltd. Williamstown, 2004.

[61] M. Nilsson, *J. Mag. Resn.* **2009**, *200*, 296-302.

Chapter 6

The host-guest chemistry of stable M_3L_2 metallo-cryptophanes

6.1 Introduction

The attractive properties associated with cryptophanes,[1] such as their ability to discriminate between and selectively bind small molecules,[2] were introduced in Chapter 4 of this thesis. The preparation of their metallo-supramolecular analogues, $[M_3L_2]^{n+}$ metallo-cryptophanes, remains synthetically challenging, in spite of their structural simplicity.[3] Of the handful of metallo-cryptophanes isolated,[4] none display the desirable properties associated with their organic counterparts, despite possessing a similarly well-defined and hydrophobic internal cavity.[5] For these species to have application in catalysis,[6] cargo delivery [7] and molecular recognition,[8] the inherent unpredictability and instability associated with their construction must be addressed.

As described in Chapter 4, the reaction of 4-pyridyl-derived ligand **4.6** and $Pd(en)(NO_3)_2$ (en = ethylenediamine) afforded the metastable metallo-cryptophane, $[Pd_3(en)_3(\mathbf{4.6})_2]\cdot 6(NO_3)$. Although unstable, its fleeting formation did indicate the suitability of ligand, and so $[M_3L_2]^{n+}$ metallocryptophanes may be accessible if a suitable *cis*-protected metallo-tecton can be found. Ethylenediamine has proven a suitable auxiliary ligand in the construction of a wealth of complexes, including $[Pd_4L_4]^{8+}$ squares,[9] $[Pd_6L_3]^{12+}$ trigonal prisms [10] and $[Pd_6L_4]^{12+}$ octahedra.[11] Fujita's well-known $[Pd_6L_5]^{12+}$ hexagonal prism, where L = 4,4'-bipyridine and 1,3,5-*tris*(4-pyridyl)triazine, has been further exemplified in its ability to bind a variety of guests, including ferrocenes, carboranes and aromatic hydrocarbons, such as triphenylene, **Figure 6.1a**.[12] In fact, the extent of palladium(II) complexes afforded using ethylenediamine as a *cis*-protecting ligand have been the subject of a recent review article by Fujita and Therrien.[13]

The more strongly coordinating *N,N,N',N'*-tetramethylethylenediamine (TMEDA) [14] and chelating heterocycles, such as 2,2'-bipyridine and its derivatives,[15] have been successfully employed as auxiliary ligands in metallo-supramolecular systems; however, the *N*-Pd(II) coordination bond remains relatively labile. Conversely, the diphosphines 1,2-*bis*(diphenylphosphino)ethane (dppe) [16] and 1,1'-*bis*(diphenylphosphino)ferrocene (dppf) [17] have been used as *cis*-protecting ancillaries that display high kinetic stability. Stang and co-workers have used a $[Pd(dppf)]^{2+}$ tecton to prepare a $[Pd_2L_2]^{4+}$ metallo-rectangle, where L = 3,6-di(4-pyridylethynyl)carbazole, which was observed to bind fullerenes in acetone solution, **Figure 6.1b**. Yet, whilst they remain strongly coordinated to the palladium(II) centre, there are questions regarding the oxygen sensitivity of diphosphines as auxiliaries.[16]

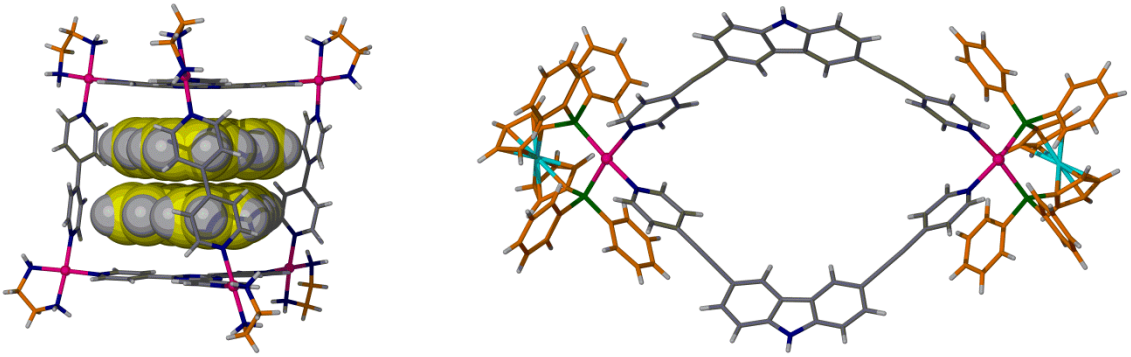

Figure 6.1 *Complexes prepared using cis-protected palladium(II) metal centres (pink spheres). (a) Fujita's* $[Pd_6L_5]^{12+}$ *hexagonal prism.*[13] *Ethylenediamine auxiliary ligands are coloured orange and encapsulated triphenylene molecules coloured yellow and shown in space-filling mode for clarity; (b) Stang's* $[Pd_2L_2]^{4+}$ *metallo-rectangle.*[17] *The dppf auxiliary and iron(II) centre of the ferrocene moiety are distinguished by colour.*

The use of *N*-heterocyclic carbenes (NHCs) as ligands offers a suitable alternative to diphosphines.[18] Like phosphines, they represent neutral, two-electron donors that are capable of forming strong coordination bonds to a metal centre. NHCs are generated from the corresponding imidazolium or dihydroimidazolium salts, through deprotonation or otherwise, and are not usually isolated.[19] The 1,3-nitrogen substitution within the heterocycle electronically stabilises the carbenic centre through σ-withdrawal and π-donation. Induction of π-electron density into the carbon p_z orbital forces the carbenic lone pair to occupy the sp^2 orbital, where they adopt the singlet state.[20] This π-induction is so strong that the NHC may be described as being carbanionic, with *pseudo*-zwitterionic resonance character. Consequently, they are extremely strong σ-donors with relatively low π-acidity, and therefore do not readily partake in synergistic back-bonding when bound to a metal centre. Although free carbenes may be highly sensitive to both water and oxygen mediated degradation,[21] their complexes are often uncommonly stable. As a direct result of their high kinetic stability, a wide range of silver(I), copper(I), palladium(II), ruthenium(II) and iridium(I/III) complexes have been prepared.[22] Much of the research focus in metal-NHC complexes is in catalysis,[23] where they have been found to facilitate the transformation of many organic substrates, such as in olefin metathesis using the archetypal Hoveyda-Grubbs 2nd generation catalyst and its analogues.[24]

Despite their wide-ranging application, metal complexes of NHCs have not been widely exemplified as supramolecular metallo-tectons, despite their suitability to the role.[25] The strong σ-donating ability of the NHC induces a *trans*-labilising effect at the metal centre which should therefore facilitate the self-assembly of ligands into a supramolecular complex. Common examples of NHCs in supramolecular self-assembly employ the NHC as a metallo-ligand, which undergo self-complexation or aggregation to afford a superstructure.[26] For example,

Reek and co-workers have prepared a heterotopic silver(I)-NHC complex, appended with a 3-pyridyl donor moiety, which undergoes self-polymerisation to afford a variety of coordination polymers, **Figure 6.2**.[27]

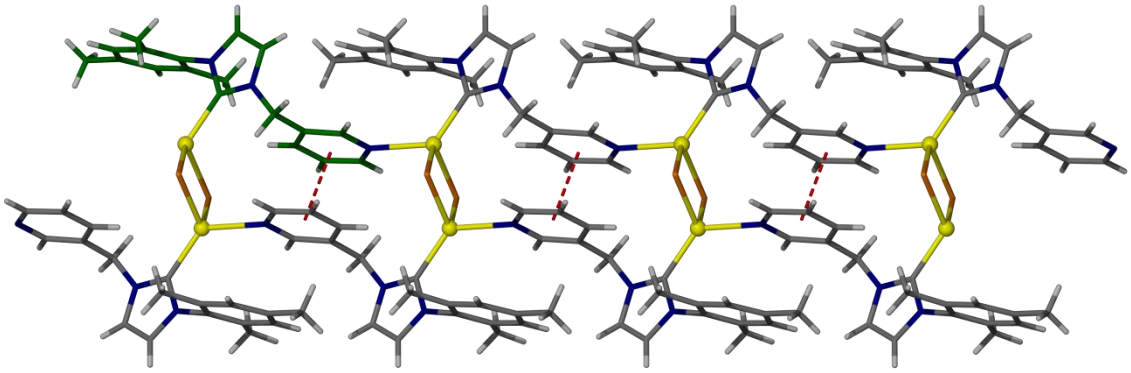

Figure 6.2 *The 1D coordination polymer prepared by Reek and co-workers.[27] Silver centres are displayed as yellow spheres and aromatic interactions between ligands indicated by hashed, red lines. The μ_2-bridging chloride ligands and one NHC ligand are coloured orange and green, respectively.*

There is, however, only one example which utilises a metallated NHC as a supramolecular tecton, in the formation of a $[M_4L_4]^{4+}$ molecular square, where L = 4,4'-bipyridine and tetra-*N*-substituted benzo-*bis*-benzimidazolium.[28] Hahn and co-workers have illustrated that the metallation of the benzo-*bis*-benzimidazolium salt with nickelocene affords a *bis*-carbene bridged binuclear metal complex which, following halide abstraction with silver(I) hexafluorophosphate and subsequent treatment with 4,4'-bypyridine, yields the $[M_4L_4]^{4+}$ molecular square complex, **Scheme 6.1**. This is a rather elegant example that combines traditional organometallic chemistry with supramolecular self-assembly.

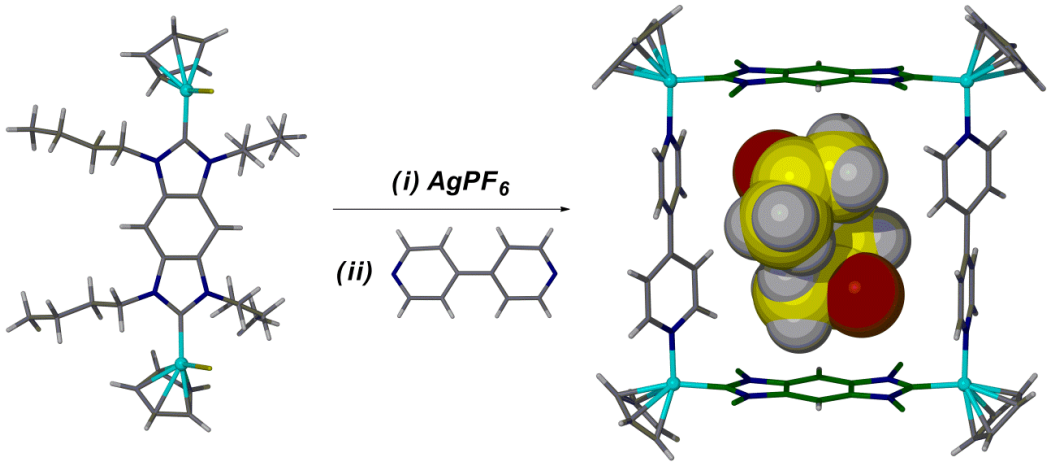

Scheme 6.1 *Preparation of the $[M_4L_4]^{4+}$ molecular square complex by Hahn and co-workers.[28] Nickel(II) centres are shown as blue spheres and encapsulated acetone molecules displayed in yellow and in space-filling mode.*

It was envisaged that suitably prefunctionalised *bis*-(NHC) ligands may offer an attractive alternative to other commonplace auxiliaries, such as ethylenediamine and related diphosphines, in the construction of well-defined and stable $[M_3L_2]^{n+}$ metallo-cryptophanes with suitable 4-pyridyl-functionalised CTVs, such as ligand **4.6**.

6.2 Preparation of novel *bis*-(NHC)-palladium(II) metallo-tectons

The precursor 1,1'-methylenebis-1*H*-imidazole (**6.1**) was prepared according to adapted procedures developed by Diez-Barra and co-workers, **Scheme 6.2**.[29] The substitution of dibromomethane with the imidazolide nucleophile, generated from the deprotonation of 1*H*-imidazole with hydroxide base, afforded **6.1** in high yield. The reaction did not proceed with dichloromethane electrophile, and the phase-transfer reagent tetra-*n*-butylammonium bromide (TBAB) was necessary in facilitating the reaction between the immiscible aqueous imidazolide and dibromomethane. The ^{1}H NMR spectrum of **6.1** is given below as reference in **Figure 6.3a**.

Compound **6.1** is easily *N*-substituted, which allows access to a range of functionalised metallo-tectons. The importance of functionalised ancillary ligands has been noted by Fujita and co-workers in tailoring the host-guest properties of $[Pd_6L_4]^{12+}$ octahedral coordination cages, where L = 2,4,6-*tris*(4-pyridyl)triazine.[30] They demonstrated that the size and relative hydrophobicity of the cage cavity could be controlled by manipulating the sterics at the palladium(II) centre.

Thus, compound **6.1** was used to prepare the *N*-functionalised *bis*-imidazolium salts, 1,1'-methylenebis(3-benzyl-1*H*-imidazolium)bromide (**6.2**) and 1,1'-methylenebis(3-(naphthalen-2-ylmethyl)-1*H*-imidazolium)bromide (**6.3**), **Scheme 6.2**.

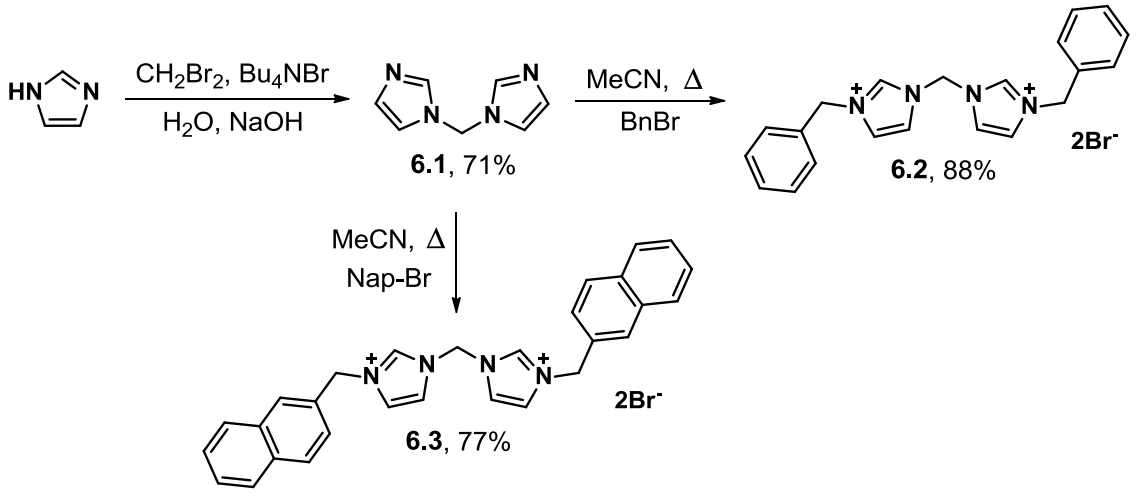

Scheme 6.2 *The preparation of N-substituted bis-imidazolium salts* ***6.2*** *and* ***6.3****.*

Compound **6.1** was treated with two equivalents of benzyl bromide (**6.2**) [31] or 2-chloromethylnaphthalene (**6.3**) in acetonitrile at reflux to afford the polar salts in 88 and 77%

isolated yields, respectively. Compounds **6.2** and **6.3** precipitated from solution with time and required elevated temperatures and extended reaction times to ensure disubstitution.

Their formation was supported through solution-phase and solid state analysis and concordant with the proposed structures. Most notable were their characteristic ^{1}H NMR spectra which displayed the strongly deshielded imidazolium protons of **6.2** and **6.3** at 9.64 and 9.69 ppm, respectively. The ^{1}H NMR spectrum of compound **6.3** is given below in **Figure 6.3b**. Moreover, formation of the imidazolium salts were evidenced by mass spectrometry, which highlighted the mass peaks (*m/z*) 409.1017 and 429.2157 for {**6.2**-Br}$^{+}$ and {**6.3**-2Br-H}$^{+}$, respectively.

The *bis*-imidazolium salts **6.2** and **6.3** were subsequently metallated at the C2 position to afford 1,1'-methylenebis(3-benzyl-imidazol-2-ylidene)palladium(II) bromide (**6.4**) and 1,1'-methylenebis(3-(naphthalen-2-ylmethyl)-imidazol-2-ylidene)palladium(II) bromide (**6.5**). The use of palladium(II) acetate in acetonitrile at reflux drives a ligand-assisted C-H activation pathway,[32] which proceeds through either a four- (**TSa**) or six-membered ring (**TSb**) transition state, **Scheme 6.3**.[33] Glorius, Fagnou and Sanford have each postulated that the mechanism is both associative and concerted, where abstraction of the imidazolium proton (pK_a range of 21-24) is facilitated by the acetate ligand (pK_a of acetic acid is 4.8) at the palladium(II) centre.[34] Proton abstraction occurs simultaneously with palladium(II) insertion, which is supported by an agostic interaction from the C-H σ-bond. The cycle is redox neutral and driven by the formation of acetic acid (HOAc).

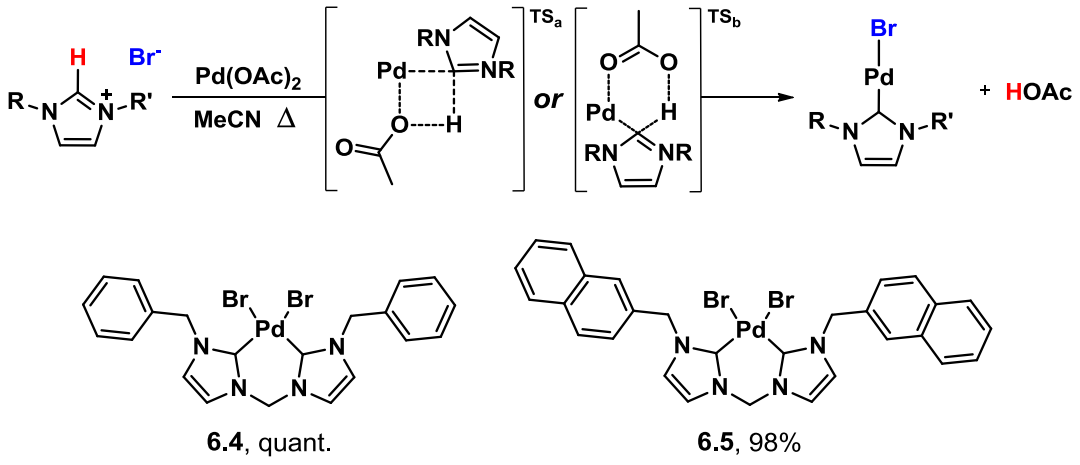

Scheme 6.3 *The proposed ligand-assisted C-H activation pathway to compounds **6.4** and **6.5**.*

The formation of compounds **6.4** and **6.5** was evidenced by mass spectrometry and ^{1}H NMR spectroscopy and their purity and composition confirmed through combustion analysis and infrared spectroscopy. The electrospray mass spectra of DMSO solutions of **6.4** and **6.5** highlighted the mass peaks (*m/z*) 515.0061 and 613.0218, which corresponded to {**6.4**-Br}$^{+}$ and {**6.5**-Br}$^{+}$, respectively. Loss of the imidazolium proton was noted for both **6.4** and **6.5**,

alongside the generation of diastereotopic protons for the now inequivalent protons of the 1,1'-methylene bridge, as observed in their ^{1}H NMR spectra. This is suggestive of restricted rotation of the *bis*-(NHC) ligand about the palladium(II) centre and arises due to a decrease in molecular symmetry as planarity is lost. The ^{1}H NMR spectrum of **6.5** is given below in **Figure 6.3c**.

Compounds **6.4** and **6.5** were subsequently treated with silver(I) tetrafluoroborate (BF_4^-) in acetonitrile solvent to generate the corresponding acetonitrile adducts 1,1'-methylenebis(3-benzyl-imidazol-2-ylidene)palladium(II) tetrafluoroborate (**6.6**) and 1,1'-methylenebis(3-(naphthalen-2-ylmethyl)-imidazol-2-ylidene)palladium(II) tetrafluoroborate (**6.7**), **Scheme 6.4**. The abstraction of halide ligands from a metal centre to generate a supramolecular synthon is well exemplified [35] and driven by the formation of highly insoluble silver(I) halide salt.

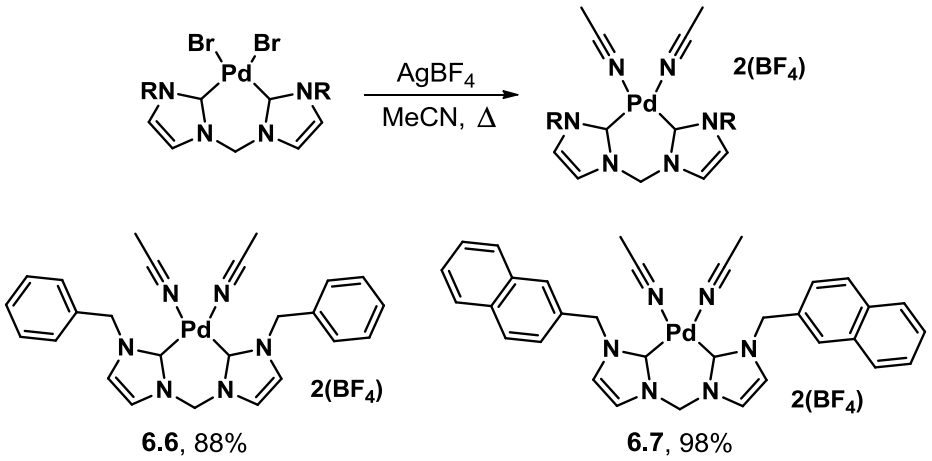

Scheme 6.4 *The preparation of acetonitrile adducts* ***6.6*** *and* ***6.7****.*

The mass peaks (*m/z*) 461.0832 and 268.0592 noted in the mass spectra were attributable to $\{$**6.6**(CN)-2(BF_4)$\}^+$ and $\{$**6.7**-2(BF_4)$\}^{2+}$, respectively, displaying that both species lose the weakly coordinating BF_4^- anions prior to detection. The ^{1}H NMR spectra of **6.6** and **6.7** were similar to the parent bromide complexes, with the diastereotopic resonances of the 1,1'-methylene protons being retained, with minor chemical shift changes. The proton NMR spectrum of compound **6.7** is given in **Figure 6.3d**. The purity of **6.6** and **6.7** was confirmed through combustion analysis and composition determined by infrared spectroscopy. The latter being particularly diagnostic, highlighting the inclusion of both tetrafluoroborate anion and acetonitrile ligand into the bulk solid, with the characteristic B-F and CN bond stretches at 1050 and 2330 cm^{-1}, respectively.

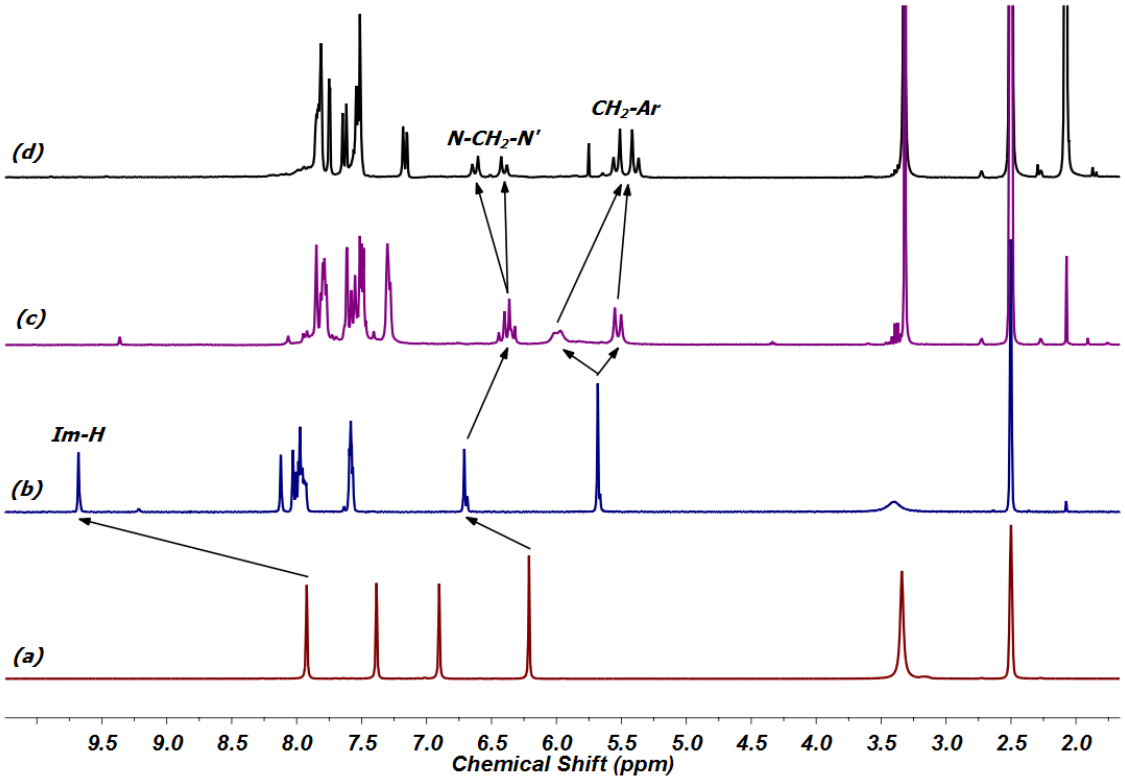

Figure 6.3 *Interpreted ^{1}H NMR spectra evidencing the step-wise preparation of metallo-tecton* ***6.7****. Spectral traces correspond to compounds* ***6.1*** *(a),* ***6.3*** *(b),* ***6.5*** *(c) and* ***6.7*** *(d). All spectra were acquired in d_6-DMSO solvent.*

Single crystals of **6.6** were grown from the diffusion of diethyl ether vapours into an acetonitrile (MeCN) solution of the compound and isolated as large, pale yellow blocks. The structure solved in the orthorhombic space group *Pna*2_1 to display the asymmetric unit as a single molecule of **6.6**, $[Pd(NHC)(MeCN)_2]\cdot 2(BF_4)$, where NHC = *bis*-(NHC) ligand, **Figure 6.4**.

As predicted by ^{1}H NMR spectroscopy, the *bis*-(NHC) ligand is *cis*-coordinated to the palladium(II) centre and deviates from planarity due to steric restrictions. The Pd(II) coordination environment is approximately square planar and features a somewhat constricted C-Pd-C coordination angle of 83.4(4) º and C-Pd bond lengths at 1.968(6) and 1.964(8) Å. As a result, the 1,1'-methylene linker remains unstrained, with a N-C-N' angle of 108.6(5) º.

The acetonitrile ligands are mutually *cis*, with a N-Pd-N bond angle of 88.3(3) º and N-Pd bond lengths of 2.068(6) and 2.092(6) Å. Selected bond metrics for **6.6** are displayed below in **Table 6.1**. The two benzyl arms of **6.6** are orientated orthogonally to one another and the tetrafluoroborate (BF_4^-) anions display close associations, but do not interact with, the cationic $[Pd(NHC)(MeCN)_2]^{2+}$ unit, **Figure 6.4**. The extended lattice features close-packed molecules of **6.6** that are not supported by intermolecular interactions.

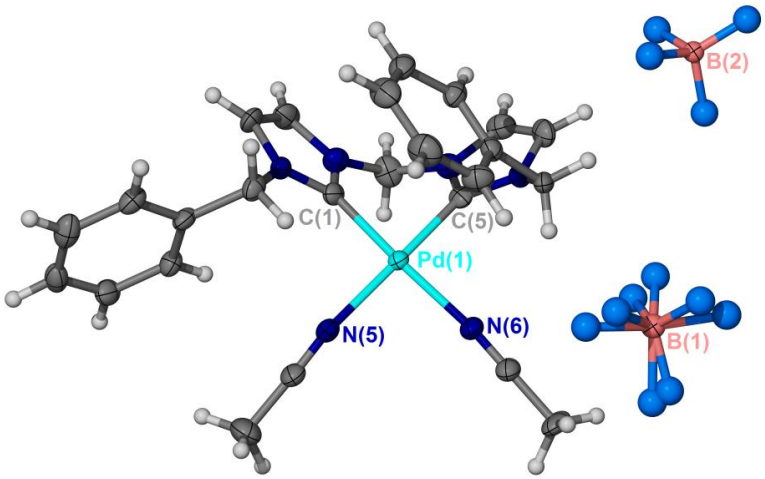

Figure 6.4 *The crystal structure of* ***6.6****, displaying the asymmetric unit. Anisotropic displacement parameters are shown at 40% probability and one BF_4^- anion displays two-fold molecular disorder. Fluorine atoms are refined isotropically.*

Pd(1)-C(1)	1.968(6)	N(5)-Pd(1)-N(6)	88.3(3)
Pd(1)-C(5)	1.964(8)	C(1)-Pd(1)-N(5)	93.4(3)
Pd(1)-N(5)	2.068(6)	C(1)-Pd(1)-N(6)	176.8(3)
Pd(1)-N(6)	2.092(6)	C(5)-Pd(1)-N(6)	94.9(3)
C(1)-Pd(1)-C(5)	83.4(4)	C(5)-Pd(1)-N(5)	173.6(2)

Table 6.1 *Selected bond lengths (Å) and angles (°) from the crystal structure of* ***6.6***

Single crystals of **6.7** were grown as described for **6.6** and analysed by single crystal diffraction methods. A structure was obtained in the monoclinic space group $P2_1/n$ to display the asymmetric unit as $[Pd(NHC)(MeCN)_2]\cdot 2(BF_4)\cdot(MeCN)$, **Figure 6.5**.

The palladium(II) coordination environment is again distorted square planar and the *bis*-(NHC) ligand is *cis*-coordinated with a C-Pd-C coordination angle of 83.8(2) º. The Pd-C bond lengths are 1.975(6) and 1.974(6) Å and the 1,1'-methylene linker remains unstrained with a N-C-N' bond angle of 107.3(8) º. Additional bond metrics for **6.7** are given in **Table 6.2**.

The naphthyl ligand arms are in the same approximate orientation and each display two-fold molecular disorder, **Figure 6.5**. There are no supramolecular interactions within the $[Pd(NHC)(MeCN)_2]^{2+}$ cationic unit, nor between it and the two BF_4^- anions or additional acetonitrile solvent molecule, despite their close proximity. The extended lattice is supported by aromatic interactions, where individual naphthyl arms form π-π interactions with centroid separation of 3.60 Å. There are additional π-H interactions between the same naphthyl arm and proximal proton of a bound acetonitrile ligand of a neighbouring **6.7** molecule, with C-H···centroid separation of 2.43 Å.

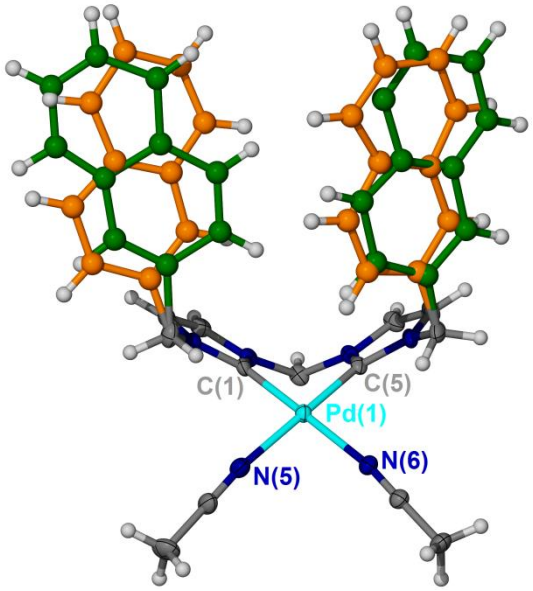

Figure 6.5 *The crystal structure of* ***6.7****, displaying the cationic portion of the asymmetric unit. Anisotropic displacement parameters are shown at 35% probability and both* BF_4^- *anions have been omitted for clarity. The naphthyl ligand arms are refined isotropically and their positional disorder is distinguished by colour.*

Pd(1)-C(1)	1.975(6)	N(5)-Pd(1)-N(6)	87.7(2)
Pd(1)-C(5)	1.974(6)	C(1)-Pd(1)-N(5)	92.9(2)
Pd(1)-N(5)	2.070(5)	C(1)-Pd(1)-N(6)	173.7(2)
Pd(1)-N(6)	2.072(5)	C(5)-Pd(1)-N(6)	95.3(2)
C(1)-Pd(1)-C(5)	83.8(2)	C(5)-Pd(1)-N(5)	177.2(2)

Table 6.2 *Selected bond lengths (Å) and angles (°) from the crystal structure of* ***6.7***

The *bis*-(NHC)-Pd(II) metal complexes **6.6** and **6.7** were observed to be highly stable to both oxygen, water and other polar, coordinating solvents at reflux, with no degradation or dissociation of the *bis*-(NHC) ligand from the palladium(II) centre. Their high levels of kinetic stability and increased solubility highlight their suitability as metallo-tectons for supramolecular self-assembly. Moreover, the strong σ-donating ability of the *bis*-(NHC) ligand and installation of labile and mutually *cis* acetonitrile ligands should facilitate the self-assembly towards a single, predetermined product – the $[M_3L_2]^{n+}$ metallo-cryptophane.

Tectons **6.6** and **6.7** were designed to further facilitate the self-assembly to the desired metallo-cryptophane through complementary aromatic interactions of the electron rich benzyl (**6.6**) and naphthyl (**6.7**) functions and the electron poor pyridine-ester moiety of ligand **4.6** upon coordination to the palladium(II) metal centre.

6.3 Nanometer-sized $[M_3L_2]^{n+}$ metallo-cryptophanes of C_{3h}-symmetry

The metallo-tectons **6.6** and **6.7** were used to prepare stable metallo-cryptophanes with solubilised ligand **4.6**, **Scheme 6.5**. The resultant complexes were of higher solubility than expected and were successfully and quantitatively prepared in nitromethane ($MeNO_2$) solvent. Only partial self-assembly was observed in dimethylsulfoxide (DMSO), acetonitrile (MeCN) or *N,N'*-dimethylformamide (DMF) solvents, which is likely to coincide with their ability to act as competing ligands.

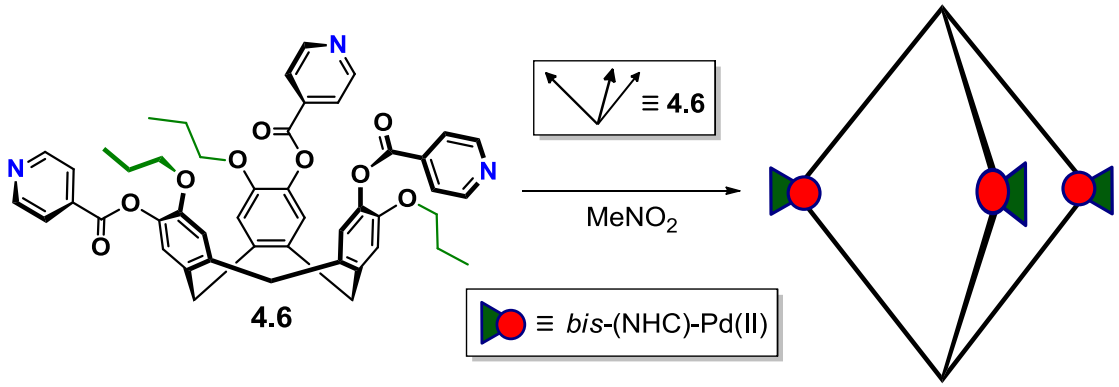

Scheme 6.5 *The preparation of stable $[M_3L_2]^{n+}$ metallo-cryptophanes using solubilised ligand* ***4.6*** *and novel bis-(NHC)-Pd(II) supramolecular tectons* ***6.6*** *and* ***6.7****.*

The reaction of ligand **4.6** and metallo-tecton **6.6** in nitromethane solvent saw quantitative formation of metallo-cryptophane $[Pd_3(NHC)_3(\mathbf{4.6})_2]\cdot 6(BF_4)\cdot n(MeNO_2)$, where NHC = *bis*-(NHC) ligand, complex **6.8**.

The electrospray mass spectrum of the complex mixture supported metallo-cryptophane formation, where the mass peaks (*m/z*) 1024.8, 1329.4 and 1633.4 were each identified and attributed to the species $\{[Pd(NHC)(\mathbf{4.6})_2]\}^{2+}$, $\{[Pd_2(NHC)_2(\mathbf{4.6})_2]\cdot 2(BF_4)\}^{2+}$ and $\{[Pd_3(NHC)_3(\mathbf{4.6})_2]\cdot 4(BF_4)\}^{2+}$, respectively. There were no observable changes to the mass spectra of complex **6.8** over any reasonable timescale, nor was there evidence for further equilibration or degradation during this time.

The formation of complex **6.8** was also evidenced in solution through various ^1H NMR experiments, recorded in d_3-$MeNO_2$ solvent. Subtle coordination-induced shifts were observed for the pyridyl *ortho*-proton, which shifted downfield from 8.85 to 9.06 ppm. More interestingly, were the pyridyl *meta*-protons which shifted upfield from 7.97 to 7.78 ppm, **Figure 6.6**. This is not typical behaviour,[36] and supports the hypothesis of additional stabilisation through aromatic interactions, where the pyridyl protons of ligand **4.6** are shielded as a direct result of constructive π-overlap from the benzyl moiety of tecton **6.6**.

A significant broadening and desymmetrisation of ligand **4.6** and tecton **6.6** resonances was observed, which perhaps indicates the presence of both *syn*- and *anti*-cryptophane diastereomeric forms in solution, although not in equal (~ 35:65) proportions, **Figure 6.6**. However, as both the *syn*- (achiral, C_{3h}) and *anti*- (chiral, D_3) diastereoisomers would each possess a minimum of molecular C_3-symmetry, it is impossible to assign the stereochemistry without further experiments.

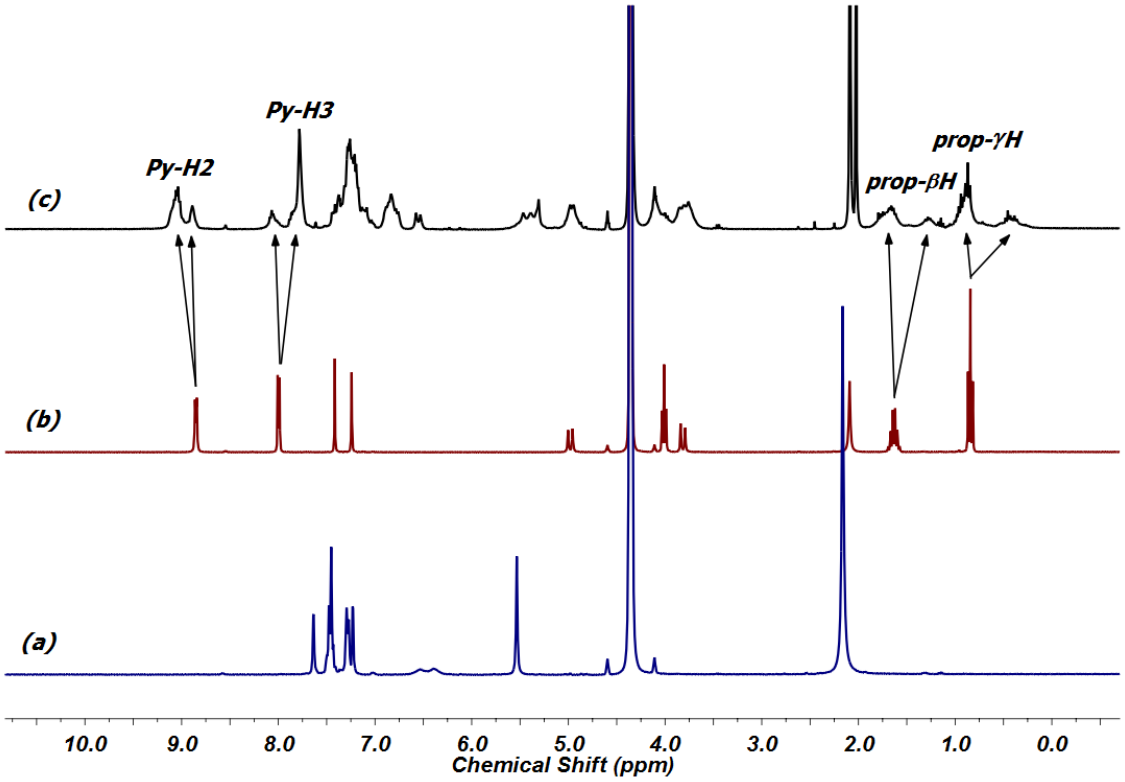

Figure 6.6 *Interpreted ^{1}H NMR spectra displaying the formation of complex* ***6.8*** *(black trace, c) from the self-assembly of ligand* ***4.6*** *(red trace, b) and metallo-tecton* ***6.6*** *(blue trace, a) in d_3-$MeNO_2$ solvent.*

There were no further changes to the ^{1}H NMR spectrum of complex **6.8** with time, suggesting that the two diastereoisomers are similar in energy and in an equilibrium which slightly favours one particular stereoisomer over the other, as indicated by the 35:65 ratio of corresponding resonances. Another interpretation of this desymmetrisation could be due to incomplete self-assembly to the metallo-cryptophane or the existence of other ligand-tecton adducts, although the author believes this to be improbable.[37]

The formation of complex **6.8** was further supported by 2D nuclear Overhauser effect spectroscopy (NOESY). The coordination of tecton **6.6** by ligand **4.6** was confirmed by the strong nOe's between the benzylic and pyridyl *ortho*-protons at 5.42 and 9.06 ppm, respectively, **Figure 6.7**. Furthermore, the strong nOe's observed between the benzyl protons of

tecton **6.6** and both the pyridyl and tribenzo[*a,d,g*]cyclononatriene protons of ligand **4.6** are indicative of an overlap of the benzyl and pyridyl π-surfaces, **Figure 6.7**.

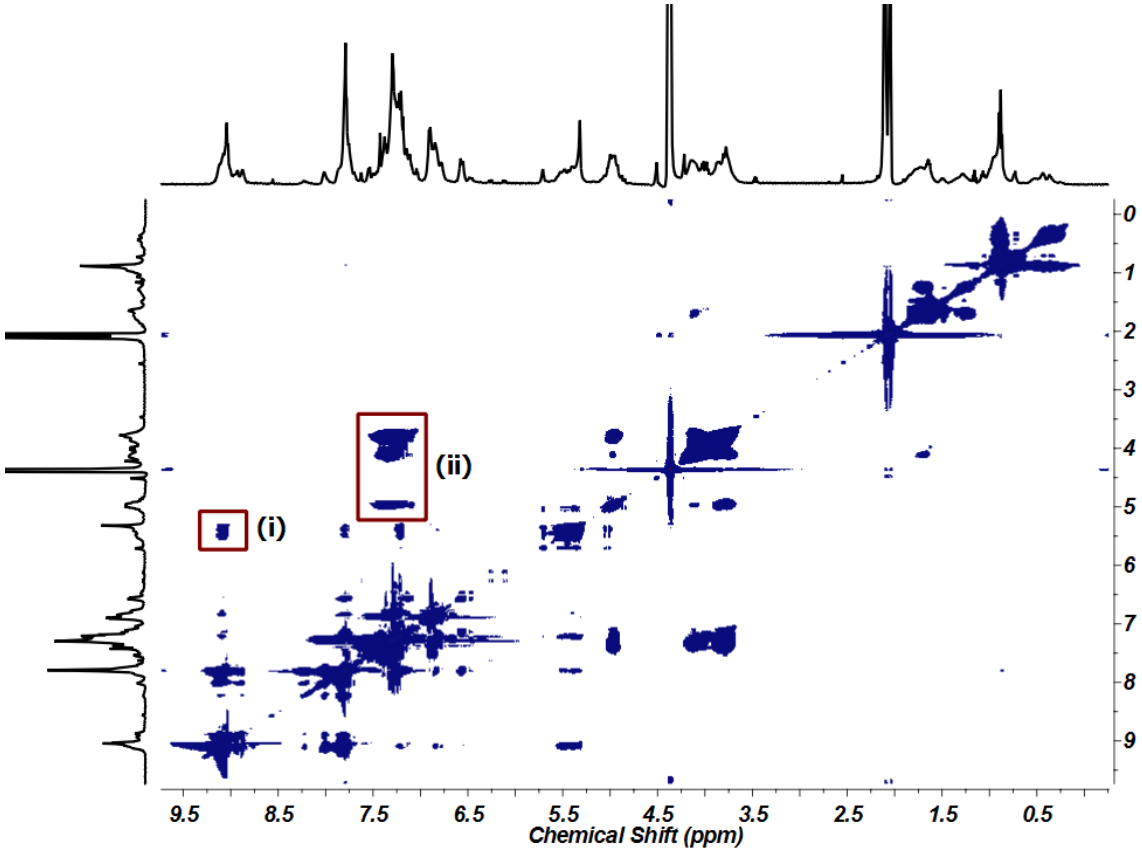

Figure 6.7 *Interpreted 2D NOESY spectrum of complex* ***6.8****, noting the strong nOe's between ortho-pyridyl and benzylic protons (i) and between the benzyl and tribenzo[a,d,g]cyclononatriene protons (ii). Spectrum recorded in* d_3*-*$MeNO_2$*.*

All attempts to gain crystals suitable for single crystal diffraction analysis were unsuccessful; nevertheless, a microcrystalline solid was obtained from the diffusion of diethyl ether vapours into a solution of complex **6.8** in nitromethane solvent and analysed in the solid state by combustion analysis and infrared spectroscopy. Combustion analysis was consistent with the suggested composition of $[Pd_3(NHC)_3(\mathbf{4.6})_2]\cdot 6(BF_4)\cdot(MeNO_2)\cdot(H_2O)$ and the IR spectrum highlighted the characteristic B-F bond stretch at 1056 cm^{-1}, confirming the inclusion of the tetrafluoroborate anion into the bulk solid. Furthermore, there was no evidence for acetonitrile in the IR spectrum, confirming its successful displacement from the metal centre.

It was envisaged that the larger aromatic surface of naphthylated tecton **6.7** would allow for a stronger donor-acceptor interaction with the electron poor π-surface of ligand **4.6**. It was also assumed that this would further stabilise the metallo-cryptophane and allow for its structural elucidation, crystallographically.

The reaction of ligand **4.6** with naphthylated tecton **6.7** in nitromethane solvent afforded the metallo-cryptophane $[Pd_3(NHC)_3(\mathbf{4.6})_2]\cdot 6(BF_4)\cdot n(MeNO_2)$, where L = *bis*-(NHC) ligand, complex **6.9**. Complex **6.9** was observed in the gas phase by electrospray mass spectrometry, where the mass peaks (*m/z*) 848.2383, 1159.9853 and 1783.4759 were observed and each attributed to the species $\{[Pd_3(NHC)_3(\mathbf{4.6})_2]\cdot 2(BF_4)\}^{4+}$, $\{[Pd_3(NHC)_3(\mathbf{4.6})_2]\cdot 3(BF_4)\}^{3+}$ and $\{[Pd_3(NHC)_3(\mathbf{4.6})_2]\cdot 4(BF_4)\}^{2+}$, respectively. Again, the mass spectra procured were independent of time and complex **6.9** was observed to be stable over the four month period that followed.

The solution-phase chemistry of complex **6.9** was somewhat dissimilar to complex **6.8**. Whilst the metallo-cryptophane was observed to form rapidly, quantitatively and not undergo further equilibration, the resonances observed in its ^{1}H NMR spectrum were well-resolved and indicative of only one cage diastereoisomer in solution, **Figure 6.8**.

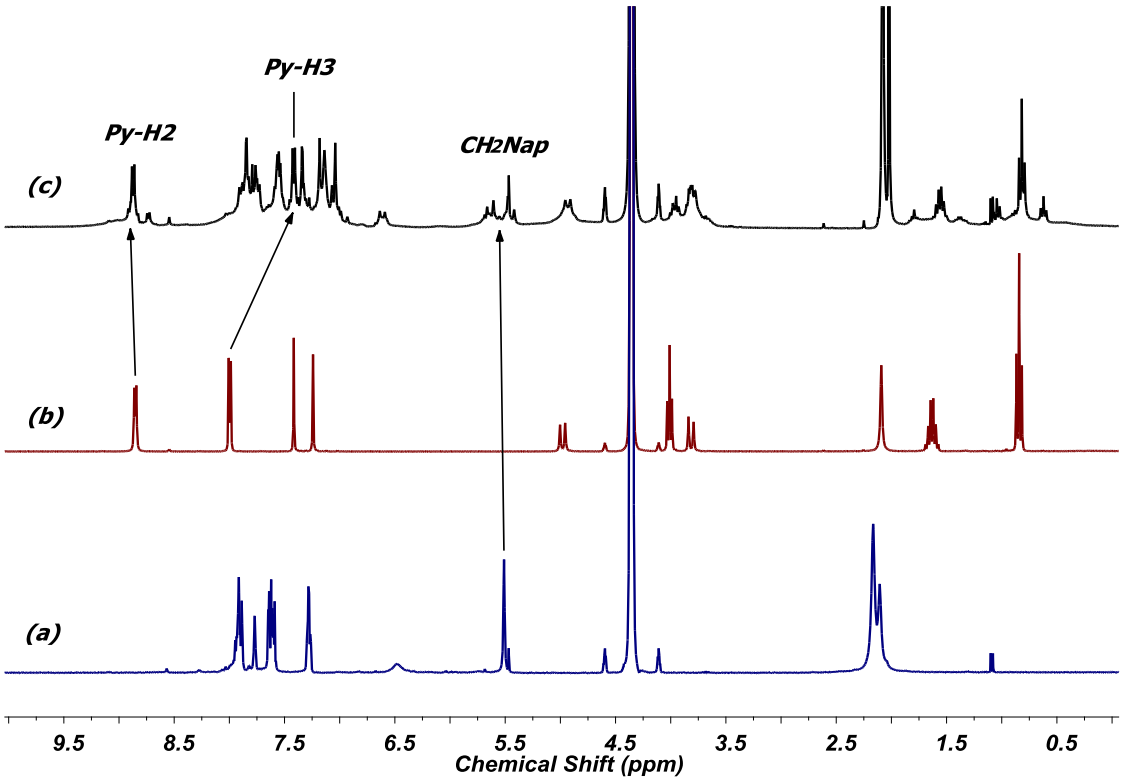

Figure 6.8 *Interpreted ^{1}H NMR spectra evidencing the formation of complex* ***6.9*** *(black trace, c) from the self-assembly of ligand* ***4.6*** *(red trace, b) and metallo-tecton* ***6.7*** *(blue trace, a) in d_3-$MeNO_2$ solvent.*

The chemical shift of the pyridine *ortho*-proton remained relatively unchanged, whilst the pyridyl *meta*-proton was shifted upfield from 7.99 to 7.41 ppm. This significant shielding is strong evidence for solution-phase aromatic interaction between the electron poor and electron rich π-surfaces of ligand **4.6** and tecton **6.7**, respectively. The 2D NOESY spectrum of complex **6.9** provides incontrovertible evidence for such an interaction, with strong nOe's observed

between the naphthyl H^6 and H^7 protons of tecton **6.7** and the *exo*-proton of the tribenzo[*a*,*d*,*g*]cyclononatriene ligand core at 7.56 and 4.95 ppm, respectively.

This aromatic interaction can be envisaged as a 'supramolecular embrace', where the naphthyl arms of tecton **6.7** wrap around the edges of the metallo-cryptophane to effectively lock it into a single conformation. The formation of a single diastereoisomer and a distinct set of well-defined cage resonances is testament to this interaction, which results in a stable and relatively static cage complex. Variable temperature ^{1}H NMR measurements indicated that this 'embrace' is relatively strong, with the diastereotopic naphthylic resonances at 5.64 and 5.42 ppm remaining unchanged up to 80 ºC, with no evidence for its dissociation.

The use of donor-acceptor aromatic interactions [38] between electron rich and electron poor π-surfaces is well exemplified in the literature and has been used to construct various catenanes, rotaxanes and other host-guest complexes, particularly by Stoddart and co-workers.[39] Similarly, donor-acceptor chemistry has been utilised by Nitschke and Sanders in the construction of a polycatenated tetrahedral assembly, where the interaction between electron rich crown ether and electron poor naphthalenediimide (NDI) drives assembly of the catenated struts.[40] More recently, the employment of π-cations and π-radicals (radical cations) in supramolecular chemistry has allowed for the realisation of the 'pimer'.[41] Molecular recognition using 'pimerisation' has allowed for the preparation of mechanically-interlocked and electronically-frustrated compounds for application in switching, sensing and in the preparation of compounds which exhibit room-temperature ferroelectricity.[42]

Formation of the metallo-cryptophane was corroborated by diffusion-ordered NMR spectroscopy (DOSY), which indicated the presence of a single large species in solution with a diffusion constant (D_{cage}) of 2.406×10^{-10} m^2s^{-1}. Based on the diffusion coefficient of ligand **4.6**, 4.549×10^{-10} m^2s^{-1}, a D_{cage}:D_{ligand} ratio of 0.53:1 was established which, through the Stokes-Einstein relationship, was estimated to give a hydrodynamic radius (*r*) of 14.4 Å, which is slightly smaller, but consistent, with the proposed size of the cage complex.

Single crystals were grown by diffusing diethyl ether vapours into a nitromethane solution of complex **6.9** and isolated as small, yellow needles. The crystals were weakly diffracting and multiple data collections, utilising both synchrotron and conventional X-ray sources, were necessary to obtain data of sufficient resolution. The structure was solved in the hexagonal space group $P6_3/m$ to display the asymmetric unit as one third of a molecule of ligand **4.6** and half a molecule of tecton **6.7**, alongside two molecules of nitromethane solvent and three partially occupied tetrafluoroborate anions, **Figure 6.9**.

The bond metrics of the *bis*-(NHC) ligand are relatively unchanged from those determined for complex **6.7**, above, with the C-Pd-C bond lengths and angles measured at 1.975(11) Å and 84.0(7) º, respectively. Complex formation affords no evidence for molecular strain within the *bis*-(NHC) ligand and the N-C-N' bond angle of 106.5(9) º is maintained. The pyridyl N-Pd bond lengths were measured at 2.113 Å, which is slightly lengthened from the ~ 2.0 Å recorded for palladium(II) complexes featuring only ligand **4.6**,[43] and in accordance with the *trans*-labilising effects of the *bis*-(NHC) ligand. The N-Pd-N coordination angle is also somewhat expanded at 98.4(9) º which likely arises due to an inflexibility of the coordinating **4.6** ligand. Selected bond metrics for complex **6.9** are given in **Table 6.3**.

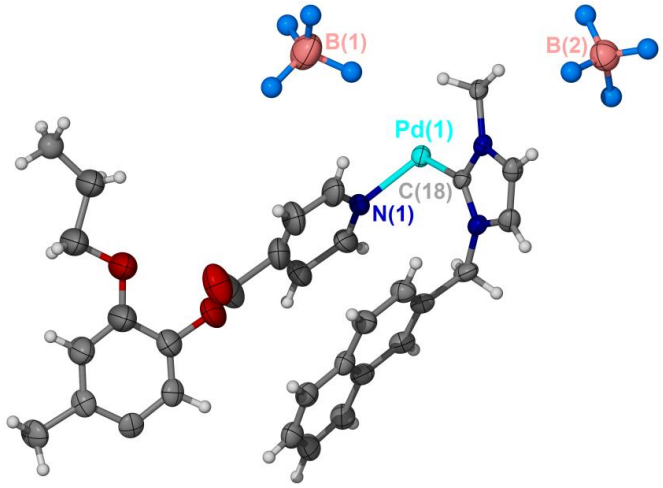

Figure 6.9 *From the crystal structure of complex* ***6.9****, displaying part of the asymmetric unit. Aside from all fluorine atoms of the* BF_4^- *anions and propyl γ-carbon, all anisotropic displacement parameters are set at 35% probability.*

Pd(1)-C(18)	1.975(11)	N(1)-Pd(1)-C(18*)	169.2(6)
Pd(1)-N(1)	2.110(11)	C(18)-Pd(1)-C(18*)	84.0(7)
N(1)-Pd(1)-C(18)	88.3(6)	N(1)-Pd(1)-N(1*)	98.4(9)

Table 6.3 *Selected bond lengths (Å) and angles (°) from the crystal structure of complex* ***6.9***

Symmetry expansion of the asymmetric unit affords the metallo-cryptophane, $[Pd_3(NHC)_3(\mathbf{4.6})_2]\cdot 6(BF_4)\cdot 2(MeNO_2)$, which is comprised of two **4.6** ligands in a head-to-head orientation that are mutually *cis*-coordinated to the three, symmetry-generated **6.6** tectons, **Figure 6.10**. The inter-metallic Pd···Pd distances were measured to be 16.29 Å which affords static cage dimensions of 17.91 × 23.86 Å, as measured between the basal protons of ligand **4.6** and the outermost naphthylic protons of tecton **6.7**, respectively.

The tetrafluoroborate anions form electrostatic associations with the palladium(II) centres at Pd···F separations 3.18 and 3.30 Å, through second-sphere interactions. There is evidence for

hydrogen bonding between a tetrafluoroborate anion and the backbone protons of the *bis*-(NHC) ligand, with F···C-H separation of 2.216 Å. Furthermore, and as expected, the naphthyl arms of tecton **6.7** form face-to-face aromatic interactions with the pyridyl-ester moiety of ligand **4.6** with centroid separation of 3.50 Å.

The 2 nm $[Pd_3(NHC)_3(\mathbf{4.6})_2]^{6+}$ cage is achiral and comprised of both ***P*** and ***M*** ligand enantiomers. Thus, this *syn*-diastereoisomer has perfect molecular C_{3h}-symmetry and is optically inactive, **Figure 6.10b**. Examination of the crystal structure indicates why the *syn*-$[Pd_3(NHC)_3(\mathbf{4.6})_2]^{6+}$ metallo-cryptophane is formed as the sole product, as the *anti*-diastereoisomer would result in significant torsional strain of the pyridyl-ester bond and would not allow for the aromatic interactions between ligand **4.6** and naphthyl moiety of tecton **6.7**.

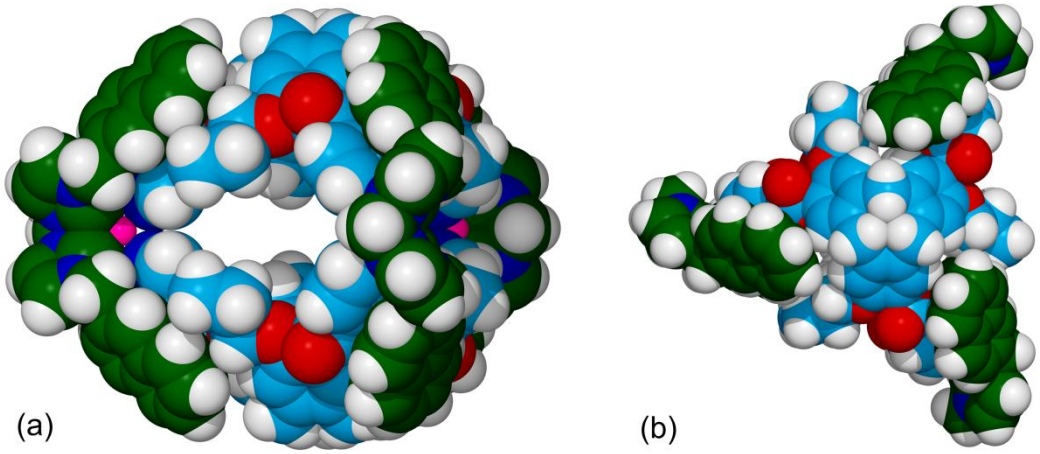

Figure 6.10 *From the crystal structure of complex* ***6.9****. The 2 nm syn-*$[Pd_3(NHC)_3(\mathbf{4.6})_2]^{6+}$ *metallo-cryptophane as viewed from the side (a), indicating the large and well-defined internal cavity and the 'naphthyl embrace'; and above (b), highlighting the* C_{3h}*-symmetry. The cryptophane is displayed in space-filling mode and the ligand and bis-(NHC) ligand are distinguished in pale blue and green, respectively. Nitromethane solvent and* BF_4^- *anions are omitted for clarity.*

It was possible to retrofit the ^{1}H NMR and NOESY spectral analysis based on crystallographic observations. The formation of a single set of well-defined resonances can be attributed to the formation of a single (*syn*) diastereoisomer, based on the inaccessibility of the *anti*-diastereomeric form. It can therefore be assumed that a racemic mixture of ligand **4.6** is necessary in affording a $[Pd_3(NHC)_3(\mathbf{4.6})_2]^{6+}$ metallo-cryptophane and that such complexes will be inaccessible from an optically resolved ligand. Likewise, the strong nOe's observed in the NOESY spectrum for the terminal naphthyl protons and the *exo*-protons of the tribenzo[*a,d,g*]cyclononatriene core can be attributed to the 'supramolecular embrace' between interacting aromatics, **Figure 6.11a**.

To verify, the sample was redissolved in d_3-$MeNO_2$ and the ^1H NMR spectrum re-recorded, where an identical spectrum, as can be seen in **Figure 6.8c**, was obtained. This suggests that the solution-phase and solid state configurations of the *syn*-$[Pd_3(NHC)_3(\mathbf{4.6})_2]^{6+}$ metallo-cryptophane are identical.

The *syn*-$[Pd_3(NHC)_3(\mathbf{4.6})_2]^{6+}$ metallo-cryptophane possesses a well-defined and hydrophobic internal cavity with a calculated static volume of 697 $Å^3$, **Figure 6.11b**. Whilst there were no solvent molecules crystallographically located within the cavity, the nitromethane and diethyl ether solvents are considered to be too disordered to be detected. Based on the packing considerations proposed by Rebek and Mecozzi,[44] for a non-polar guest to form strong interactions with a host it must occupy 55% of its internal volume. This phenomenon holds true only if the host-guest formation is only supported by van der Waals interactions.[45] Therefore, and according to these considerations, the ideal volume of hydrophobic guest for encapsulation would be 383 $Å^3$. The hosting abilities of such *syn*-$[Pd_3(NHC)_3(\mathbf{4.6})_2]^{6+}$ cages will form the basis of discussion in the latter sections of this chapter.

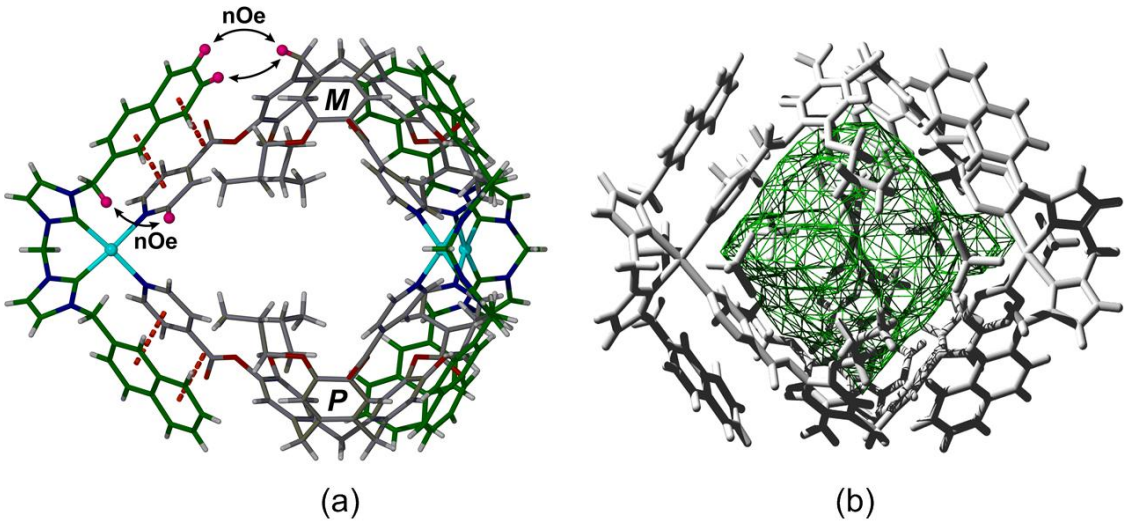

Figure 6.11 *(a) From the crystal structure of complex* ***6.9****, evidencing the solution-phase interactions based on crystallographic observations. Aromatic interactions between naphthyl moiety and pyridine-ester are shown as red, hashed lines and the arrows between the pink protons highlight the nOe's that can only be afforded in this particular cryptophane conformation. The chiral descriptors* ***M*** *and* ***P*** *denote the relative chirality of each* ***4.6*** *ligand. (b) Green mesh depicting the 697 $Å^3$ well-defined internal volume of the cryptophane, as calculated using SwissPDB-viewer.*[46]

Despite their large, external π-surfaces, there are no aromatic interactions between individual *syn*-$[Pd_3(NHC)_3(\mathbf{4.6})_2]^{6+}$ metallo-cryptophanes in the extended lattice. Rather, the lattice is supported by extensive hydrogen bonding between BF_4^- anions and the H^4 protons of six, symmetry-generated *bis*-(NHC) ligands, **Figure 6.12**. Although unexpected, there is literature

precedent to indicate that imidazolium salts do interact with tetrafluoroborate anions as both ionic liquids and crystalline materials through F···H-C hydrogen bonding.[47]

The symmetry-generated F···H-C interactions were recorded at 2.216 Å and occur from a superposition of two individual BF_4^- anions, where each anion affords three hydrogen bonds to the proximal H^4 protons of tecton **6.6**. This *pseudo*-cubic disorder is likely imposed by the lattice as six equal hydrogen bonds cannot be formed from a single tetrahedral anion alone. Despite the high crystallographic symmetry, each anion position has a distorted tetrahedral geometry and displays an F-B-F bond angle of 104.6(5) º. Likewise, the B-F bond lengths are highly dissimilar at 1.365(12) and 1.53(2) Å. The lengthening of the B-F bonds occurs axially and from those which do not act as hydrogen bond acceptors.

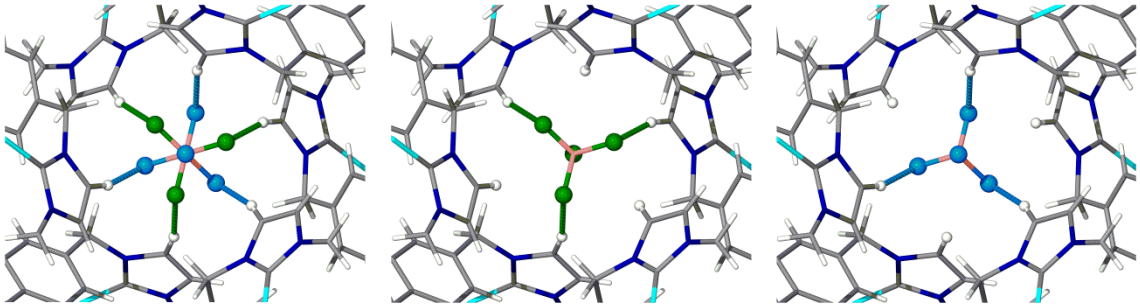

Figure 6.12 *From the crystal structure of complex **6.9**, depicting the hydrogen bonding between cubically-distorted BF_4^- anion and H^4 protons of the bis-(NHC) ligand (a). Individual orientations of the superposition are also shown (b and c). The F···H-C Interactions are displayed as green and blue hashed lines and correspond to the individual anion positions.*

The employment of tetrafluoroborate (BF_4^-) anion is critical for structural elucidation of the *syn*-$[Pd_3(NHC)_3(\mathbf{4.6})_2]^{6+}$ metallo-cryptophane. Use of hexafluorophosphate (PF_6^-) and nitrate (NO_3^-) anions did not afford crystals of the complex, which is to be expected given that neither can support six simultaneous hydrogen bonds, irrespective of their relative orientation. However, in spite of their geometrical suitability, the use perchlorate (ClO_4^-) and perrhenate (ReO_4^-) counter anions also inhibited crystallisation of the complex. Given their comparable size, the selectively for BF_4^- is likely due to the more electronegative fluorine atom being a stronger hydrogen bond acceptor.

Whilst the tetrafluoroborate anion is generally regarded as an 'innocent' and non-coordinating anion, the selectivity for the BF_4^- anion in the formation of complex **6.9** and the extent of hydrogen bonding within the lattice suggests a possible anion templation mechanism. Although not as pronounced as effect as is observed for other anions, such as chloride or nitrate,[48] the templating ability of the tetrafluoroborate anion has been noted in the formation of metallo-

supramolecular assembles, such as Ward's $[Co_4L_6]^{8+}$ and Custelcean's $[Zn_4L_6]^{8+}$ tetrahedra.[49]

Template directed syntheses allow for the predictable and controlled construction of highly complex architectures. Particularly notable accounts include Leigh's pentafoil knot and Nitschke's pentagonal prism, each of which are only accessible when using chloride anions as the active template.[50] Anion templation in metallo-supramolecular chemistry has been the basis of a recent and extensive review by Custelcean.[51]

The aforementioned F···H-C intermolecular interactions propagate the *syn*-$[Pd_3(NHC)_3(\mathbf{4.6})_2]^{6+}$ metallo-cryptophanes two-dimensionally in the crystallographic *ab* plane. This results in a network of linked cages, where the individual $[Pd_3(NHC)_3(\mathbf{4.6})_2]^{6+}$ cage cavities represent periodic voids within a lattice that are linked at the cage windows by smaller, interstitial voids, **Figure 6.13**.

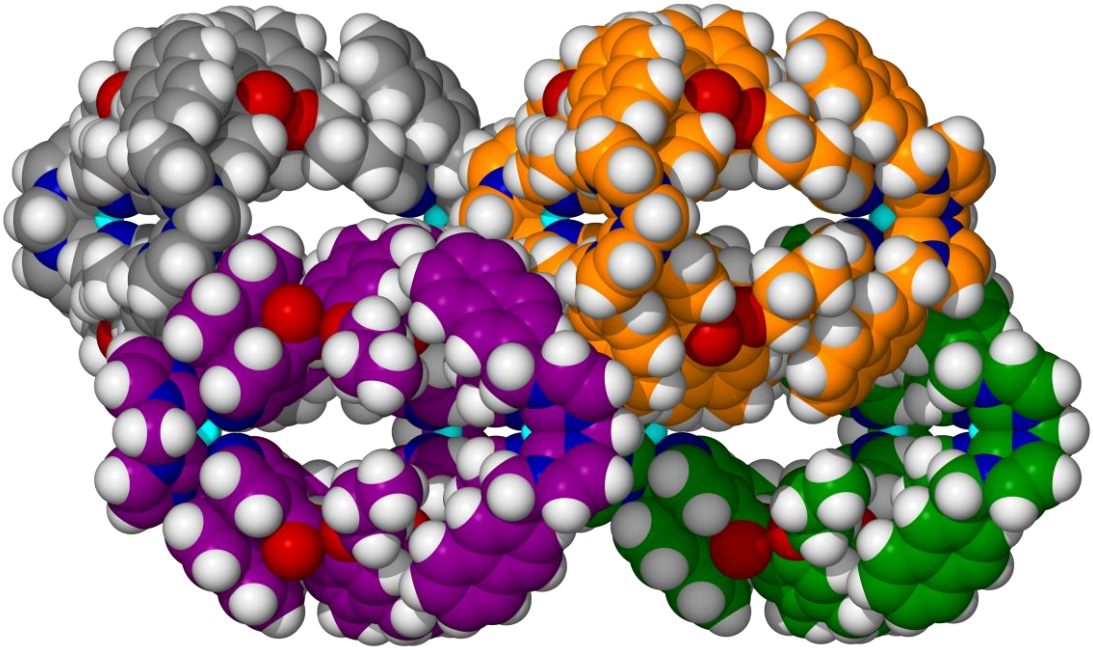

Figure 6.13 *From the crystal structure of complex* ***6.9*** *depicting the 'networked cages' as viewed down the crystallographic a-axis. Individual syn-*$[Pd_3(NHC)_3(\mathbf{4.6})_2]^{6+}$ *metallo-cryptophanes are distinguished by colour and displayed in space-filling mode.*

Such 'networked cages' represent a class of crystalline compounds where the hosting abilities of the molecular components are transferred to the bulk solid.[52] For this to be achieved the individual molecular components, be they cages or otherwise, must be arranged coherently as to allow the transport of guests through the crystalline solid, so that the cavities of the molecular cages can be readily accessed.[53] Their properties are analogous to many porous coordination polymers and they therefore exhibit similar chemical behaviour.

Examples include Fujita's $[Pd_6L_4]^{12+}$ octahedral assemblies, where L = *tris*(4-pyridyl)triazine,

which crystallise to allow access to the cage cavities by interconnected cage windows.[54] Single crystals of the networked cage have been shown to uptake fullerenes and other small organic guests from solution by simple diffusion, with no degradation to the cage network. Likewise, Cooper and co-workers have selectively crystallised their small, organic cages to create porous networks with application in gas storage and small molecule separations.[55]

The interstitial void spaces between the cages contain the nitromethane solvent molecules and there are no solvent molecules located within the cage cavity. However, thermogravimetric analysis (TGA) indicates a step-wise mass loss of 13.5% up to 230 ºC which corresponds to three additional molecules of nitromethane solvent, *per* cage, that could not be located crystallographically. This level of solvation is in accordance with the calculated void space within the lattice and consistent with the combustion analysis obtained. Finally, the composition of complex **6.9** was supported by infrared spectroscopy, which highlighted the inclusion of tetrafluoroborate anion into the crystal lattice with B-F bond stretch at 1062 cm^{-1}.

6.4 A general route for the preparation of $[Pd_3(NHC)_3(L)_2]^{6+}$ metallo-cryptophanes

Contrary to previous statements, the preparation of stable $[M_3L_2]^{n+}$ metallo-cryptophanes is actually rather general and can be achieved with a wide range of 4-pyridyl-derived CTVs, irrespective of solubility or sterics, provided that naphthylated tecton **6.7** is employed. The ability of tecton **6.7** to facilitate self-assembly whilst simultaneously increasing the solubility and stability of the resultant complex has allowed for a 'family' of $[Pd_3(NHC)_3(L)_2]^{6+}$ metallo-cryptophanes to be prepared, **Figure 6.14**.

To prove the concept, ligands **2.8**, **6.10** and **6.11** were each prepared and reacted with tecton **6.7** under conditions analogous to those described for complex **6.9**; where, in each case, the desired $[Pd_3(NHC)_3(L)_2]^{6+}$ metallo-cryptophane was generated both rapidly and quantitatively. It is important to note that each ligand differs from ligand **4.6** in at least one way which should prevent the formation of $[Pd_3(NHC)_3(L)_2]^{6+}$ metallo-cryptophanes, given that there was no evidence, fleeting or otherwise, for the formation of $[M_3L_2]^{n+}$ metallo-cryptophanes from their self-assembly with other *cis*-protected metallo-tectons, such as $Pd(en)(NO_3)_2$.

Ligand **2.8** was prepared according to syntheses described in Chapter 2 of this thesis and differs from ligand **4.6** only in its upper-rim alkoxy substitution and thus its solubility, particularly in nitromethane solvent. Ligands **6.10** and **6.11** were each prepared according to literature procedures, through reaction of CTG (**4.6**) with 2-methyl-isonicotinoylchloride hydrochloride (**6.10**) [56] and 4-chloromethylquinoline (**6.11**),[57] respectively. Each was obtained as a racemic mixture in high yields and the corresponding analyses consistent with the literature. Ligand **6.10**

is both relatively insoluble and sterically encumbering, owing to the methyl moiety sited *ortho* to the pyridyl nitrogen, and ligand **6.11** is both conformationally flexible and sterically demanding due to the ethereally-linked 4-quinalyl donor.

Nevertheless, the independent reactions of ligands **2.8**, **6.10** and **6.11** and tecton **6.7** in nitromethane solvent afforded the metallo-cryptophanes $[Pd_3(NHC)_3(\mathbf{2.8})_2]\cdot 6(BF_4)$, $[Pd_3(NHC)_3(\mathbf{6.10})_2]\cdot 6(BF_4)$ and $[Pd_3(NHC)_3(\mathbf{6.11})_2]\cdot 6(BF_4)$, complexes **6.12**, **6.13** and **6.14** respectively. Their formation was evidenced in the gas phase by electrospray mass spectrometry, where the species $\{[Pd_3(NHC)_3(\mathbf{2.8})_2]\}^{n+}$ $\{[Pd_3(NHC)_3(\mathbf{6.10})_2]\}^{n+}$ and $\{[Pd_3(NHC)_3(\mathbf{6.11})_2]\}^{n+}$ were each identified. For example, the mass peaks (*m/z*) 860.4655, 1175.6625 and 1807.4992 were observed in the mass spectrum of complex **6.14** and attributed to the species $\{[Pd_3(NHC)_3(\mathbf{6.11})_2]\cdot 2(BF_4)\}^{4+}$, $\{[Pd_3(NHC)_3(\mathbf{6.11})_2]\cdot 3(BF_4)\}^{3+}$ and $\{[Pd_3(NHC)_3(\mathbf{6.11})_2]\cdot 4(BF_4)\}^{2+}$, respectively. It is clear that the added flexibility, insolubility and increased steric bulk of ligand **4.11** do not impede the formation of complex **6.14**, despite the disparity from ligand **4.6**. Similar mass spectra were also obtained for **6.12** and **6.13**.

The ^{1}H NMR spectra of complexes **6.12-6.14** were recorded in d_3-$MeNO_2$ and were comparable to the spectrum of complex **6.9**. Again, subtle coordination-induced shifts were observed and the spectra were symptomatic for the presence of a single diastereoisomer in solution. Likewise, the corresponding NOESY spectra supported metallo-cryptophane formation and the expected nOe's between ligand and tecton were observed for all examples.

In order to display the generality of $[Pd_3(NHC)_3(L)_2]^{6+}$ formation, complexes **6.12-6.14** were each prepared in bulk (> 100 mg) and precipitated quantitatively from a nitromethane solution using diethyl ether solvent. The bulk powders each analysed for $[Pd_3(NHC)_3(L)_2]\cdot 6(BF_4)\cdot n(MeNO_2)$ and their compositions were supported by infrared spectroscopy, which highlighted the B-F bond stretch of the tetrafluoroborate (BF_4^-) anions at 1050 cm^{-1}. The subsequent dissolution of complexes **6.12-6.14** in d_3-$MeNO_2$ generated identical ^{1}H NMR and mass spectra to those obtained from the initial self-assembly, indicating no changes to their speciation or composition. Single crystals of each complex were grown as described for complex **6.9** and analysed crystallographically using a synchrotron X-ray source.

Complexes **6.12-6.14** crystallised in the hexagonal grace group $P6_3/m$ with identical unit cell parameters (hexagonal: a,b = 24.7, c = 20.1 Å; α,β = 90, γ = 120 º) as for complex **6.9**, above, and display analogous bond metrics and interactions within their crystal structures. Symmetry expansion generates the three structurally analogous and achiral metallo-cryptophanes, **Figure 6.13**. Despite their molecular differences, each ligand adopts an identical conformation within the complex that generates the *syn*-$[Pd_3(NHC)_3(L)_2]$ metallo-cryptophane, with no exception.

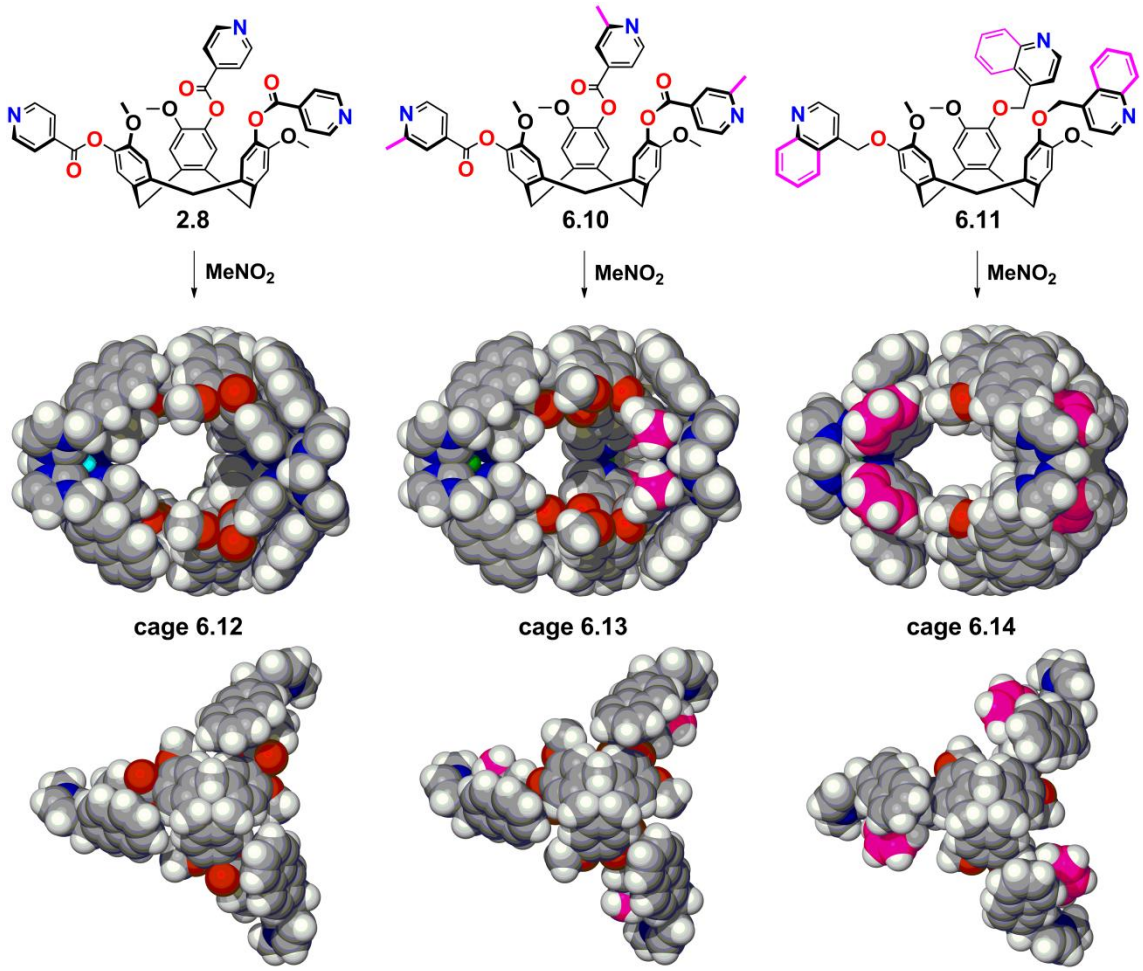

Figure 6.14 *The 'family' of syn-$[Pd_3(NHC)_3(L)_2]^{6+}$ metallo-cryptophanes prepared from the self-assembly of 4-pyridyl-derived CTV ligands **2.8**, **6.10** and **6.11** and tecton **6.7**. The corresponding metallo-cryptophanes **6.12**, **6.13** and **6.14** are shown in space-filling mode and the structural differences of ligand and cage distinguished in pink.*

6.5 The host-guest chemistry of networked-cage 'crystalline sponges'

In spite of possessing a well-defined and suitably hydrophobic internal cavity, complex **6.9** was not observed to form host-guest complexes in solution. Typical guests, including a variety of hydrocarbons and conjugated aromatics, ferrocenes and carboranes were systematically trialled, yet there was no evidence of guest binding by ^{1}H NMR spectroscopy or mass spectrometry.

The reason for which may lie in the similar hydrophobicity of the interior and exterior of the $[Pd_3(NHC)_3(\mathbf{4.6})_2]^{6+}$ cage complex. Despite having a net positive charge, the interior and exterior are both relatively non-polar which affords a high solubility in nitromethane solvent. However, it also eliminates the driving force for guest encapsulation, as the small and non-polar guests are equally solubilised by the bulk solution as they are inside the cage cavity.[58] To overcome this, and to drive the equilibrium towards the formation of a host-guest complex, the

construction of a water-soluble analogue would be advantageous, as the solvophobic nature of the guests would facilitate their encapsulation.[59]

Another contributing factor is the incommensurate volume of the $[Pd_3(NHC)_3(\mathbf{4.6})_2]^{6+}$ metallo-cryptophane cavity (697 $Å^3$) to that of the molecular volume of guests trialled. It has been noted that the specificity of guest to host, with respect to both size and geometry, must be perfect for encapsulation to occur.[60] However, to the best of the author's knowledge, there are no globular guests with a molecular volume of 383 $Å^3$ and so the ideal packing coefficient which would result in the formation of meaningful host-guest interactions cannot be achieved.

Nevertheless, complex **6.9** represents a remarkably stable and potentially porous crystalline lattice of infinitely linked $[Pd_3(NHC)_3(\mathbf{4.6})_2]^{6+}$ metallo-cryptophanes with which to uptake and bind guests. Thus, the solvent 1,2-dichlorobenzene was chosen as a suitable guest with which to examine the exchange properties of complex **6.9**. It was predicted that the relative hydrophobicity of the liquid would facilitate diffusion through the crystalline lattice and that the 1,2-substitution of heavy chlorine atoms would allow for its location in the difference map.[61] Similarly, complexes of CTV and organically-linked cryptophanes have each demonstrated an affinity for chlorinated guests, such as dichloromethane and chloroform, due to the formation of strong host-guest interactions with the electron-rich tribenzo[*a*,*d*,*g*]cyclononatriene core.[62]

Suitable single crystals of complex **6.9** were isolated, submerged in 1,2-dichlorobenzene and allowed to equilibrate for two weeks, during which time they yellowed. The crystals were isolated from the mother liquor and structurally characterised by X-ray diffraction analysis using a synchrotron source. The unit cell parameters remained unchanged from those of complex **6.9**, confirming that the crystal lattice had neither degraded nor undergone a structural reorganisation. Thus, if guest uptake had occurred, it must have proceeded *via* molecular diffusion through the crystal lattice.

The structure solved in the hexagonal space group $P6_3/m$ to confirm the uptake of 1,2-dichlorobenzene by the crystal. The asymmetric unit was the same as observed for complex **6.9**, in addition to half a molecule of 1,2-dichlorobenzene which is sited on a crystallographic mirror plane, **Figure 6.15**. The bond metrics are unchanged from those in complex **6.9** and the 1,2-dichlorobenzene guest molecule forms no interaction with either the cage framework or tetrafluoroborate anions.

Symmetry expansion generates the metallo-cryptophane exclusion complex, $[Pd_3(NHC)_3(\mathbf{4.6})_2]\cdot 6(BF_4)\subset 3(1,2\text{-DCB})$, complex **6.15**. Whilst the 1,2-dichlorobenzene molecules must access the metallo-cryptophane voids in order to diffuse through the crystal

lattice, there are no solvent molecules located within the *syn*-$[Pd_3(NHC)_3(\mathbf{4.6})_2]^{6+}$ cavity. Rather, the solvent molecules are sited within the small, hydrophobic interstitial sites between the cages, **Figure 6.14**. The interactions between guest and lattice are through weak London dispersion forces only, yet the high binding specificity allows for their structural elucidation.[63]

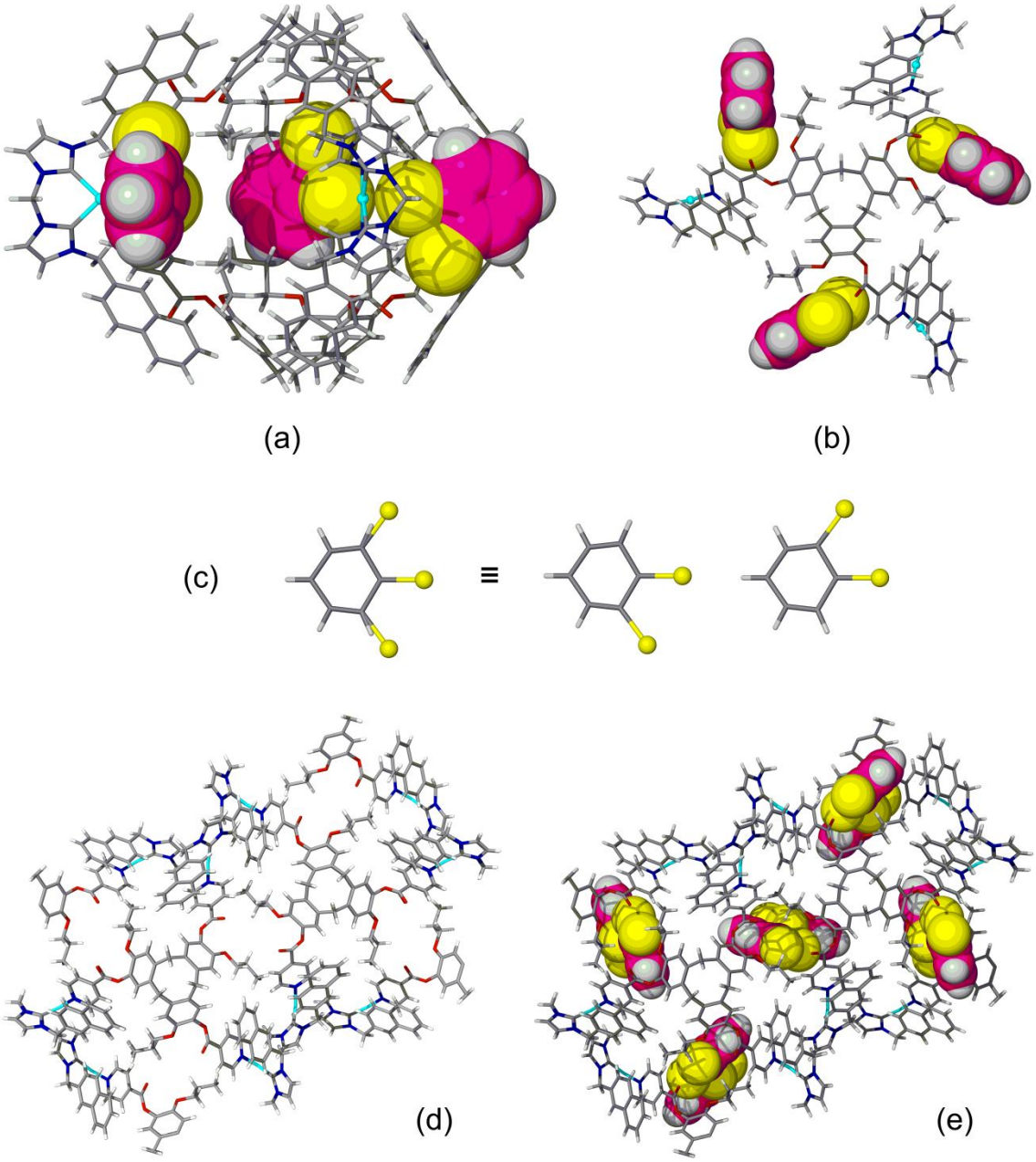

Figure 6.15 *From the crystal structure of exclusion complex* ***6.15****. The individual syn-*$[Pd_3(NHC)_3(\mathbf{4.6})_2] \subset 3$*(1,2-DCB) cages as viewed from the side (a) and from above (b). The 1,2-dichlorobenzene molecules are shown in space-filling mode and distinguished by colour, with only one disordered position shown. The two-fold molecular disorder of 1,2-dichlorobenzene present within the crystal lattice is also shown (c). The networked-cages, as viewed down the crystallographic c-axis, with and without 1,2-dichlorobenzene guest are shown as reference (d and e).*

Crystals of complex **6.15** were isolated and washed thoroughly with diethyl ether before being subjected to thermogravimetric analysis (TGA) and energy-dispersive X-ray spectroscopy (EDX) to quantify the 1,2-dichlorobenzene uptake. The TGA analyses of complexes **6.15** and **6.9** were compared and each displayed a net mass loss of 16% up to 250 ºC, after which they degraded. However, up to 175 ºC, complexes **6.15** and **6.9** indicated mass losses of 7 and 13%, respectively, which is consistent with the higher boiling point 1,2-dichlorobenzene (180.5 ºC) not being removed until heating past 210 ºC. The EDX spectra of complex **6.15** were consistent with the model obtained from the crystal structure and analysed for three molecules of 1,2-dichlorobenzene *per* $[Pd_3(NHC)_3(\mathbf{4.6})_2]^{6+}$ metallo-cryptophane unit. The two independent crystals probed each analysed for a 4.94 and 5.73% mass of chlorine, which is concordant with the calculated value of 5.09%.

The observations made from TGA and EDX analyses were validated by solution-phase measurements. The crystals of complex **6.15** were redissolved in d_3-$MeNO_2$ and the ^{1}H NMR spectrum recorded, indicating the presence of 1,2-dichlorobenzene in the complex mixture by the additional two resonances at 7.57 and 7.34 ppm, **Figure 6.16**. The relative integrations of guest to cage were determined and consistent with there being three to four molecules of 1,2-dichlorobenzene *per* $[Pd_3(NHC)_3(\mathbf{4.6})_2]^{6+}$ metallo-cryptophane unit.

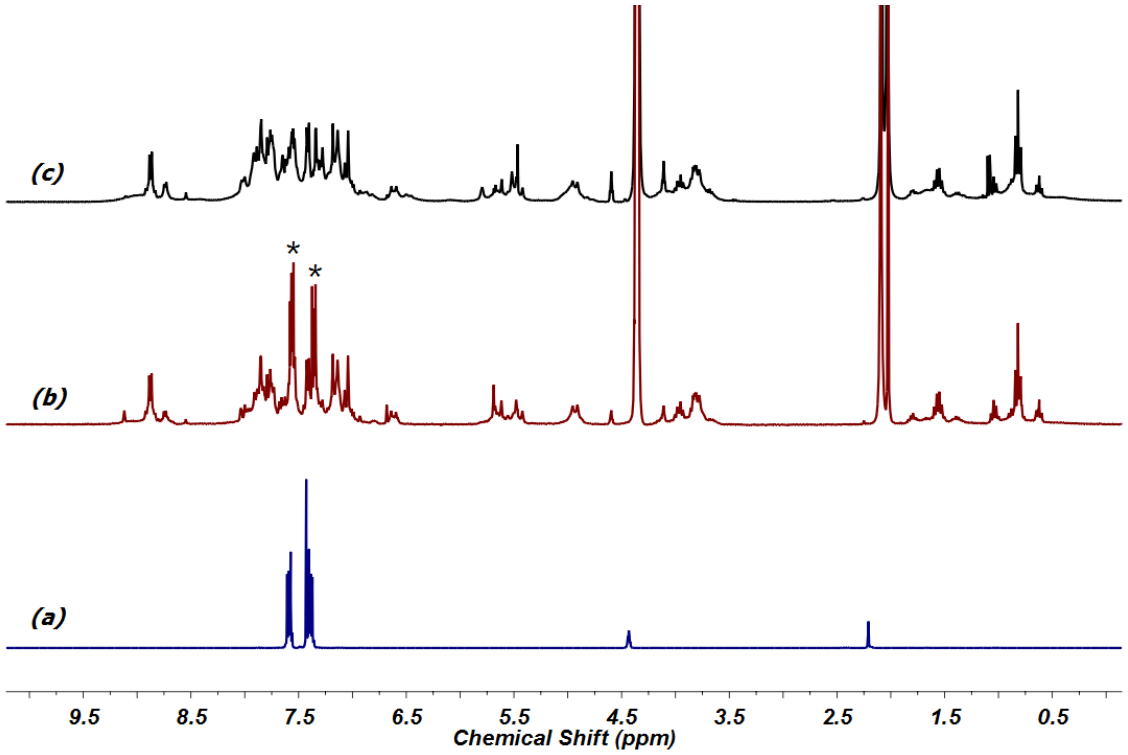

Figure 6.16 *Interpreted ^{1}H NMR spectra evidencing the formation of exclusion complex* ***6.15*** *(red trace, b) from the uptake of 1,2-dichlorobenzene (blue trace, a) by complex* ***6.9*** *(black trace, c) in d_3-$MeNO_2$ solvent.*

The ability to exchange lattice guests whilst retaining crystallinity is an attractive feature of the networked cages and indicates their suitability for the potential uptake of other molecular guests. Similar solvent exchange phenomena have been reported by Barbour and co-workers, where a porous lattice of metallocycles which crystallises with two molecules of acetonitrile solvent within its molecular cavity can undergo a single-crystal-to-single-crystal (SCTSC) solvent exchange for acetone, chloroform and toluene solvents.[64]

This builds on the seminal research by Atwood and colleagues in the field of porous molecular crystals, particularly of those containing derivatives of the molecular host calix[4]arene. It was found that by controlling the crystallisation of the *para*-sulfonatocalix[4]arene^{5-} anion they could engineer void spaces within the lattice, owing to the anti-parallel bilayers of molecular host within the crystal lattice.[65] They later realised that freshly sublimed crystals of *para*-tertiarybutylcalix[4]arene possessed small, interstitial voids of 235 Å^3 within the crystal lattice.[66] Whilst the crystals were classically non-porous, they could uptake vinyl bromide by cooperative van der Waals confinement, where the lattice underwent a SCTSC expansion to allow for the diffusion of guest into the voids within. This was later extended by Barbour and Atwood to various liquid and gaseous chlorofluorocarbons (CFCs, or 'Freons'),[67] methane [68] and even hydrogen,[69] evidencing that there can indeed be "porosity without pores".[70] There has since been a number of reviews detailing the engineering of porosity in molecular crystals and their SCTSC uptake of guests.[71]

The uptake of 1,2-dichlorobenzene described above for complex **6.15** is more in keeping with the chemistry of Fujita's 'crystalline sponges'.[54] Whilst they are not strictly molecular crystals, and are instead 'cage-type' cavities that are linked in 3D, they display similar properties to the metallo-cryptophane complex **6.15**. It was observed that in a crystal with two possible binding sites, simple size exclusion could be used to control the binding of guests. They observed that smaller guests such as tetrathiafulvalene (TTF) would occupy the comparatively smaller cage cavity, whereas the larger fullerene guests were too large to pass through the cage pores and so were crystallographically located within the channels between them. They went on to exemplify this phenomenon with the uptake of various chiral small molecules and even the natural products Santonin and Miyakosyne A.[61] Therefore, by confinement within a crystalline lattice, they were able to determine the structures of compounds that are extremely reluctant to crystallise themselves. The SCTSC uptake of guests remains relatively rare and is normally reserved for robust polymeric materials and not discrete, molecular entities.[72]

It was predicted that the substrate scope for SCTSC guest uptake by complex **6.9** could be extended to larger halogenated compounds, globular guests and even the molecular halogens. However, complex **6.9** is only accessible on small scales due to the synthetic difficulty in

preparing ligand **4.6**. Thus, the structurally analogous metallo-cryptophane $[Pd_3(NHC)_3(\mathbf{2.8})_2]\cdot 6(BF_4)$, complex **6.12**, was chosen as a suitable replacement. As discussed above, complex **6.12** is readily prepared in large quantities (> 100 mg) and its behaviour is almost indistinguishable from complex **6.9**, particularly in the solid state.

Molecular iodine (I_2) was chosen as a suitable guest due to its hydrophobicity and relatively large molecular volume. The encapsulation of iodine is an area of interest in radiochemistry, where its incarceration into a crystalline network is thought to prevent the radioactive degradation of ^{129}I to ^{129}Xe by β-decay.[73] There is a literature precedent for the uptake of molecular iodine by crystalline materials; however, the vast majority of these examples are not analysed using single crystal diffraction analysis and are instead subject to gas sorption isotherms and powder X-ray diffraction measurements.[74] Conversely, Barbour and co-workers have successfully used single crystal diffraction analysis to demonstrate how a molecular crystal of copper(II)-containing metallocycles will uptake molecular iodine when the crystals are subjected to an atmosphere of gaseous iodine vapours.[75] Over a 24 hour period the crystals turned from green to brown, providing visual evidence for guest uptake.

It was believed that crystals of complex **6.12** would display similar hosting behaviour to those described by Barbour, and that the hydrophobic bowl of the tribenzo[*a*,*d*,*g*]cyclononatriene core of ligand **2.8** would provide a suitable binding platform for the iodine guests. Portions of the work presented herein have been conducted in collaboration with MChem student Scott E. Chambers and the resultant data are included for sake of completeness.

Suitable single crystals of complex **6.12** were placed in a vial containing an ethereal solution of iodine and allowed to equilibrate for one week, during which time they turned from colourless to brown. The crystals were isolated from the mother liquor and analysed by single crystal diffraction measurements to determine whether the colour change was due to iodine uptake or simply a surface effect. The unit cell parameters were consistent with those of complex **6.12** and there was no evidence for sample degradation. The structure solved in the hexagonal space group $P6_3/m$ to display the asymmetric unit as that determined for complex **6.12**, in addition to three crystallographic sites of molecular iodine, **Figure 6.17a**.

Symmetry expansion affords the metallo-cryptophane inclusion complex $[Pd_3(NHC)_3(\mathbf{2.8})_2]\cdot 6(BF_4)\subset n(I_2)$, complex **6.16**. The bond metrics of the metallo-cryptophane remain unchanged from the parent complex **6.12** and there are no close contacts between the iodine molecules and the *syn*-$[Pd_3(NHC)_3(\mathbf{2.8})_2]^{6+}$ metallo-cryptophane. The iodine positions within the asymmetric unit were refined with partial occupancies and the I(2)-I(3) and I(4)-I(5)

bond lengths recorded at 2.71(3) and 2.82(2) Å, respectively. Such values are consistent with the experimental bond length of molecular iodine at 2.72 Å.

As predicted, inclusion phenomena were observed for the networked $[Pd_3(NHC)_3(\mathbf{2.8})_2]^{6+}$ metallo-cryptophanes. Twelve partially occupied, disordered and symmetry related iodine positions were generated, *per* cage cavity, from the two unique iodine molecules of the asymmetric unit. One crystallographically unique iodine molecule forms host-guest interactions with the tribenzo[*a*,*d*,*g*]cyclononatriene core at I···C(phenyl) separation 3.77 Å, **Figure 6.17b**. This close van der Waals separation is comparable to the intermolecular Xe···C(phenyl) separation of 3.86 Å reported by Taratula and co-workers and in accordance with the slightly larger atomic radius of xenon over iodine.[2] The short intermolecular distance observed is indicative of guest recognition and related to the balance of steric repulsion and favourable induced dipole interaction. In spite of guest inclusion, an accurate packing coefficient of guest to host could not be determined due to the aforementioned disorder and variable site occupancy of the iodine molecules.

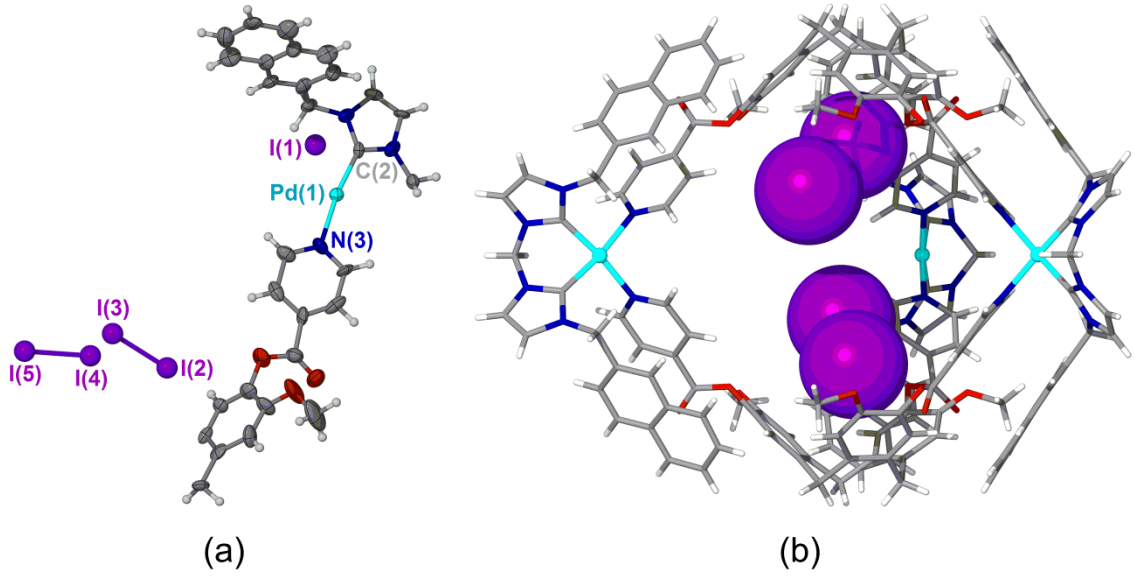

Figure 6.17 *From the crystal structure of inclusion complex* ***6.16****, displaying part of the asymmetric unit (a). Other than the three sites of I_2, all anisotropic displacement parameters are set at 35% probability. Host-guest behaviour in the metallo-cryptophane unit $[Pd_3(NHC)_3(\mathbf{2.8})_2] \subset 2(I_2)$ is shown (b), where the I_2 molecules are displayed in space-filling mode and in one disordered position for the sake of clarity.*

The third lattice position of iodine is realised upon symmetry expansion of the $[Pd_3(NHC)_3(\mathbf{2.8})_2]^{6+}$ cage network and is non-covalently bound in the small, interstitial sites between the cages, **Figure 6.18**. It is sited on a 6_3-rotation axis and disordered equally over three positions with an I-I bond length of 2.509(13). This decreased bond length likely arises due to positional disorder with a nitromethane molecule which is sited on the same lattice

position but at lesser proportions. Halogen bonding interactions are evident between the disordered iodine molecule and a proximal tetrafluoroborate anion, with B-F···I separation of 2.53 Å. This is shorter than the sum of their van der Waals radii but in agreement with the studies of Metrangelo and Resnati, who have employed prefunctionalised halogen bond acceptor/donors to construct various supramolecular architectures.[76] Although parent complex **6.12** contains a large proportion of free lattice space, inclusion complex **6.16** does not, with the molecular iodine filling the available pores. This is particularly apparent when viewing the extended lattice down the crystallographic *c*-axis, which appropriately illustrates the SCTSC guest uptake, **Figure 6.18**.

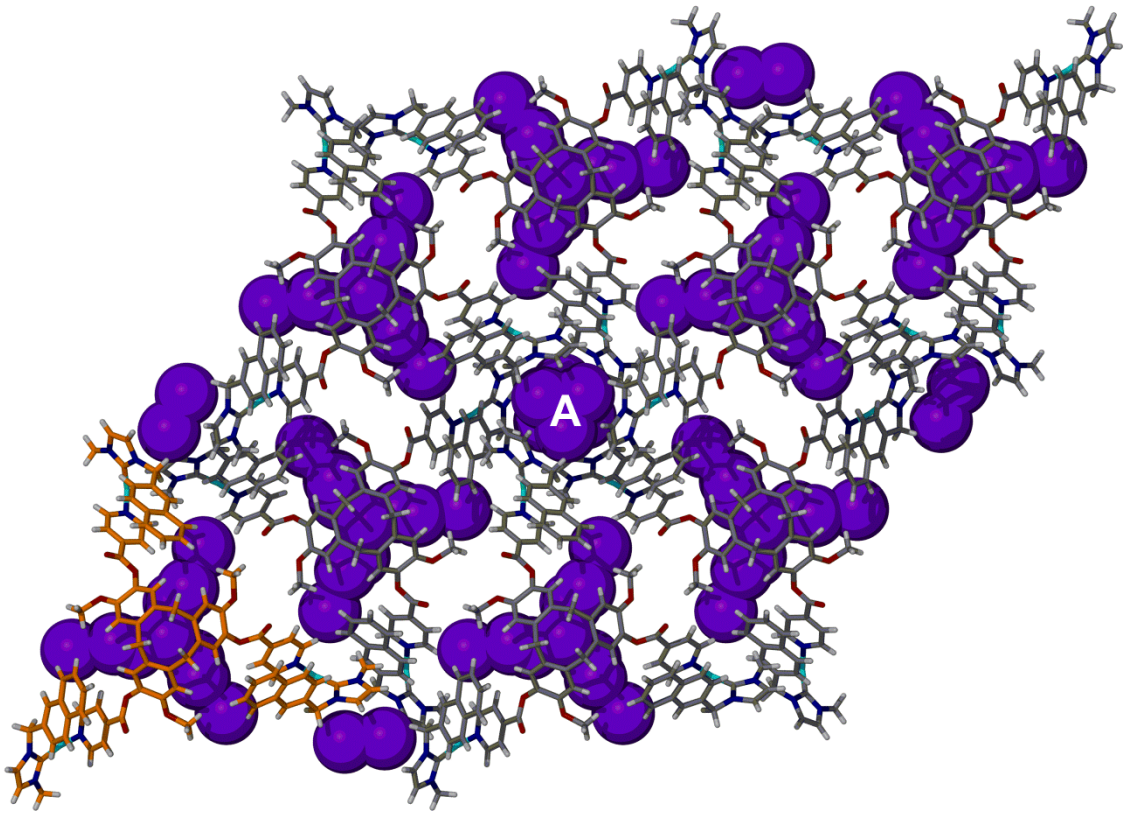

Figure 6.18 *From the crystal structure of inclusion complex* ***6.16****, displaying the distribution of molecular iodine throughout the crystal lattice, as viewed down the crystallographic c-axis. The descriptor 'A' is to indicate the three-fold molecular disorder of iodine within the smaller, meso sites between individual cages. All* BF_4^- *anions and omitted and one* $[Pd_3(NHC)_3(\mathbf{2.8})_2]^{6+}$ *metallo-cryptophane unit is coloured orange for clarity. The iodine molecules are shown in purple and displayed in space-filling mode.*

Crystals of complex **6.16** were isolated and washed throughly with diethyl ether before being subjected to EDX analysis. Each crystal analysed for a relative 23.68% mass of iodine, which is consistent with there being 4-5 molecules of I_2 *per* $[Pd_3(NHC)_3(\mathbf{2.8})_2]^{6+}$ metallo-cryptophane unit (calc. 23.39%). This is in agreement with the crystal structure model, in which the total number of iodine molecules was refined to be approximately five, *per* cage.

Given the stability of parent complex **6.12** and the ability of iodine to readily sublime under vacuum, gas phase SCTSC uptake studies were undertaken. Suitable crystals of complex **6.12** were isolated and placed in a sealed vessel alongside iodine solid. The sample was evacuated at room temperature to activate the crystals of complex **6.12**, with no amorphisation observed. Following, an atmosphere of gaseous iodine was introduced and the vessel returned to a positive pressure, during which time the crystals immediately turned from colourless to brown as iodine uptake occurred. All analyses gained authenticated the SCTSC uptake of gaseous iodine and were in agreement with the data obtained from the solution-phase experiments for complex **6.16**. Furthermore, optical microscopy images were obtained of the sample both before and after iodine exposure to provide visual evidence for successful iodine uptake, **Figure 6.19**.

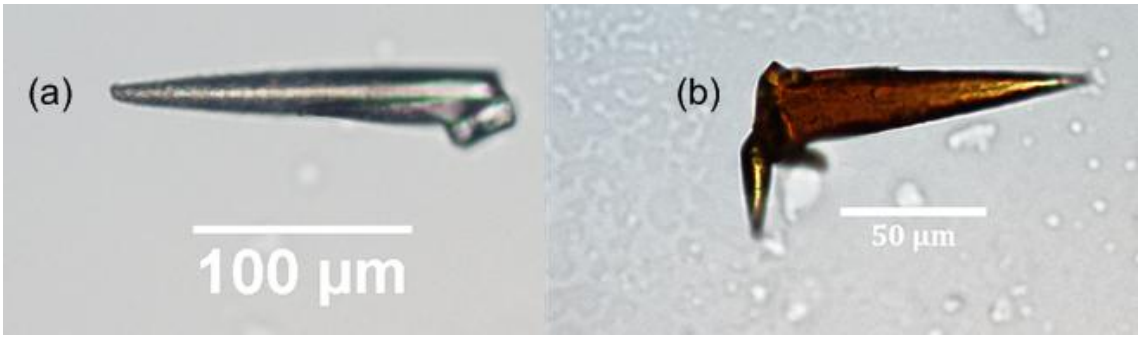

Figure 6.19 *Optical microscopy images displaying the before (complex **6.12**, a) and after (inclusion complex **6.16**, b) results of the single-crystal-to-single-crystal (SCTSC) uptake of iodine vapours.*

The crystals of complex **6.12** highlight remarkable stability to both heat and vacuum, with no loss of crystallinity observed during the evacuation/uptake cycles. Currently, surface area measurements and gas sorption isotherms are being studied in collaboration with researchers at the University of Liverpool, where it is predicted that other relatively non-polar gases will reversibly and hysteretically adsorb to the hydrophobic interior of the networked cages.

6.6 Conclusions and future work

A route towards the rational design and preparation of stable $[Pd_3(NHC)_3(L)_2]^{6+}$ metallo-cryptophanes has finally been realised, employing novel *bis*-(NHC)-Pd(II) supramolecular tectons over the conventional *cis*-protected metal salts. As far the author is aware, these are the first metallo-supramolecular cages that have been prepared that utilise classical organometallic chemistry and supramolecular syntheses. The functionalised *bis*-(NHC) ligands prepared were observed to both facilitate the formation of the metallo-cryptophane and afford further stabilisation through complementary aromatic interactions.

The $[Pd_3(NHC)_3(L)_2]^{6+}$ metallo-cryptophanes were crystallographically elucidated and observed to possess an internal, hydrophobic internal cavity of ~ 700 $Å^3$. Such species represent the first reported examples of metallo-cryptophanes which possess a stable and well-defined internal cavity which is free from either interpenetration or interdigitation. Furthermore, the directing nature of the *bis*-(NHC)-Pd(II) supramolecular tectons has provided a general synthetic procedure for the preparation of a 'family' of structurally analogous *syn*-$[Pd_3(NHC)_3(L)_2]^{6+}$ metallo-cryptophanes.

The solution phase host-guest chemistry of the $[Pd_3(NHC)_3(L)_2]^{6+}$ metallo-cryptophanes was somewhat impeded by their solubility and the incommensurate cavity volume to that of the guests trialled. Nevertheless, a highly robust crystallinity allowed for guest inclusion by single-crystal-to-single-crystal (SCTSC) uptake. Such inclusion phenomena were tolerated by both liquids and gases, including 1,2-dichlorobenzene and molecular iodine. This is unprecedented behaviour for cyclotriveratrylenes (CTVs) and remains particularly rare for discrete metallo-supramolecular cages, in general.

Future work is to be focussed towards molecular separations and catalysis, whereby the selective uptake of two molecules into the confines of the cage cavity may alter a given reaction pathway or allow for the enablement of unusual reactivity, akin to that of an enzyme. Additionally, the ability for the crystalline material to take up gaseous guests without degrading highlights potential in gas storage, where it would be hoped that gas sorption isotherms would show hysteretic behaviour with gases such as methane, carbon dioxide and xenon. Further work should be focussed towards the preparation of water soluble metallo-cryptophanes as a way to promote guest binding in the solution phase. This could be achieved either by synthesising a metallo-tecton bearing highly polar groups, such as sulfate or polyethyleneglycol, or by increasing the number of polar groups on the ligand core. A water solubilised metallo-cryptophane would enable the selective encapsulation of non-polar or hydrophobic guests by virtue of the hydrophobic effect, which cannot be exploited in other laboratory solvents.

6.7 Experimental

Ligands **2.8** and **4.6** were prepared according to procedures listed in Chapters 2 and 4 of this thesis, respectively, and ligands **6.10** and **6.11** were synthesised in reference to literature procedures.[56-57] All ligands were employed as racemic mixtures for the coordination studies listed herein.

6.7.1 Instrumentation

NMR spectra were recorded by automated procedures on a Bruker Avance 500 or DPX 300 MHz NMR spectrometer. All deuterated solvents were purchased from Euriso-top. All ^{1}H and $^{13}C\{^{1}H\}$ spectra were referenced relative to an internal standard. High resolution DOSY and ROESY ^{1}H NMR spectra were recorded in collaboration with Dr. Julie Fisher of the University of Leeds. High resolution electrospray mass spectra (ESI-MS) were measured on a Bruker MicroTOF-Q or Bruker MaXis Impact spectrometer in either positive or negative ion mode by Ms. Tanya Marinko-Covell of the University of Leeds Mass Spectrometry Service and Dr Stuart L. Warriner of the University of Leeds. Low resolution mass spectra were recorded on an open-access Bruker Micromass LCT spectrometer with simultaneous HPLC using an acetonitrile/water eluent and sodium formate calibrant. FT-IR spectra were recorded as solid phase samples on a Perkin-Elmer Spectrum One spectrophotometer. Samples for microanalysis were dried under vacuum before analysis and the elemental composition determined by Mr Ian Blakeley of the University of Leeds Microanalytical Service using a Carlo Erba elemental analyser MOD 1106 spectrometer. Thermogravimetric and energy dispersive X-ray analyses were performed by experimental officer Dr. Algy Kazlauciunas of the University of Leeds Colour Science department. Optical microscopy images were obtained in collaboration with Professor Fiona Meldrum and Dr Alexander Kulak of the University of Leeds.

Crystals were mounted under inert oil on a MiTeGen tip and flash frozen to 150(1) K using an Oxford Cryosystems cryostream low temperature device. X-ray diffraction data were collected using graphite-monochromated Mo-*K* radiation (λ = 0.71073 Å) using a Bruker-Nonius X-8 diffractometer with ApexII detector and FR591 rotating anode generator; or mirror-monochromated Mo-*K* (λ = 0.71073 Å) or Cu-*K* radiation (λ = 1.54184 Å) using an Agilent Supernova dual-source diffractometer with Atlas S2 CCD detector and fine-focus sealed tube generator; or using synchrotron radiation (λ = 0.6889 Å) with a Crystal Logic 4-circle Kappa goniometer and Rigaku Saturn 724 CCD diffractometer at station i19 of Diamond Light Source. Data were corrected for Lorenztian and polarization effects and absorption corrections were applied using multi-scan methods. The structures were solved by direct methods using SHELXS-97 and refined by full-matrix on F^2 using SHELXL-97, interfaced through the X-seed

interface.[77] Unless otherwise specified, all non-hydrogen atoms were refined as anisotropic, and hydrogen positions were included at geometrically estimated positions. Molecular graphics were obtained using POV-RAY through the X-Seed interface.[78] Additional details are given below and data collections and refinements tabulated below.

6.7.2 Preparation of organic compounds and metal complexes

Synthesis of 1,1'-methylenebis-1*H*-imidazole (6.1). 1*H*-imidazole (1.369 g, 20.08 mmol), potassium hydroxide (2.248 g, 41.05 mmol) and tetra-*n*-butylammonium bromide (0.1987 g, 0.612 mmol) were suspended in water (1 mL) and dissolved by aid of sonication. Dibromomethane (1.48 mL, 21.22 mmol) was added dropwise *via* syringe and the reaction mixture stirred overnight, during which time a white crystalline precipitate formed. The crude solid was collected and purified by column chromatography (SiO_2, ethyl acetate) to give the title product as a colourless crystalline solid. Yield 640 mg, 71% (Lit. 66%); HRMS (ES^+): *m/z* 149.0845 $\{MH\}^+$, calculated for $C_7H_9N_4$ 149.0822; ^1H NMR (300MHz, d_6-DMSO) δ (ppm) = 7.92 (s, 2H, H^2), 7.39 (s, 2H, H^5), 6.90 (s, 2H, H^4), 6.21 (s, 2H, N-CH_2-N'); $^{13}C\{^1H\}$ NMR (75 MHz, d_6-DMSO) δ (ppm) = 137.4, 128.8, 122.8, 51.7. All data are consistent with the literature.[29]

Synthesis of 1,1'-methylenebis(3-benzyl-1*H*-imidazolium)bromide (6.2). Compound **6.1** (1.56 g, 10.53 mmol) was dissolved in acetonitrile (100 mL) at 60℃ and benzyl bromide (2.68 mL, 22.60 mmol) added *via* syringe. The reaction was stirred overnight, during which time a white, crystalline solid was afforded. The solid was collected *via* filtration, washed with a small portion of acetonitrile (10 mL), diethyl ether (30 mL) and dried *in vacuo* to yield the title compound as a white, crystalline solid. Yield 4.15 g, 88 % (Lit. 81 %); M.pt. 278-280 °C (Lit. n/a); HRMS (ES^+): *m/z* 409.1024 $\{M\text{-}Br\}^+$; calculated for $C_{21}H_{22}N_4Br$ 409.1022; ^1H NMR (300MHz, d_6-DMSO) δ (ppm) = 9.64 (s, 2H, Im-H^2), 8.09 (s, 2H, Im-H^5), 7.91 (s, 2H, Im-H^4), 7.46-7.43 (m, 10H, Bn-H), 6.69 (s, 2H, N-CH_2-N'), 5.51 (s, 4H, CH_2-Bn); $^{13}C\{^1H\}$ NMR (75 MHz, d_6-DMSO) δ (ppm) = 137.7, 134.2, 129.0, 128.9, 128.7, 123.2, 122.5, 58.3, 52.3. All data are consistent with the literature.[31]

Synthesis of 1,1'-methylenebis(3-(naphthalen-2-ylmethyl)-1*H*-imidazolium)bromide (6.3). Compound **6.1** (1.23 g, 8.321 mmol) was dissolved in acetonitrile (100 mL) at 60℃ and 2-(chloromethyl)naphthalene (4.05 g, 18.31 mmol) added. The reaction was stirred overnight, during which time a white, crystalline solid was afforded. The solid was collected *via* filtration, washed with a small portion of acetonitrile (10 mL), diethyl ether (30 mL) and dried *in vacuo* to yield the title compound as a pure-white, crystalline solid. Yield 3.76 g, 77 %; M.pt. > 300 ºC; HRMS (ES^+): *m/z* 429.2 $\{M\text{-}2Br\text{-}H\}^+$; calculated for $C_{29}H_{25}N_4$ 429.2157; ^1H NMR (300MHz,

d_6-DMSO) δ (ppm) = 9.68 (s, 2H, Im-H^2), 8.12 (s, 2H, Im-H^5), 8.03 (s, 2H, Im-H^4), 7.97 (m, 8H, Nap-H), 7.58 (m, 6H, Nap-H), 6.71 (s, 2H, N-CH_2-N'), 5.68 (s, 4H, CH_2-Nap); $^{13}C\{^1H\}$ NMR (75 MHz, d_6-DMSO) δ (ppm) = 137.9, 132.8, 132.7, 131.5, 128.8, 128.0, 127.9, 127.7, 126.9, 126.7, 125.9, 123.3, 122.6, 58.4, 52.5; Analysis for **6.3**·0.5(H_2O)·0.5(CH_3CN) (% calculated, found) C (57.71, 57.50), H (4.68, 4.30), N (10.09, 10.00); Infrared analysis (FT-IR, cm^{-1}) = 3051, 1573 (w), 1442 (w), 1360 (w), 1151, 861, 758, 620.

Preparation of 1,1'-methylenebis(3-benzyl-imidazol-2-ylidene)palladium(II) bromide (6.4). Compound **6.2** (432 mg, 0.881 mmol) and palladium(II) acetate (201 mg, 0.882 mmol) were dissolved in acetonitrile (10 mL), under argon. The temperature was increased to 70℃ and the reaction stirred for 48 hours, during which time the solution bleached and product precipitated. The white solid was collected *via* filtration, washed with a small portion of dichloromethane (10 mL), diethyl ether (30 mL) and dried *in vacuo* to yield the title compound as an off-white solid. Yield 531 mg, quant. (Lit. 99 %); HRMS (ES$^+$): *m/z* 461.0832 {M(CN)-2Br}$^+$; calculated for $C_{22}H_{21}N_5Pd$ 461.0566; ^1H NMR (300MHz, d_6-DMSO) δ (ppm) = 7.60 (d, 2H, Im-H^5, *J* = 1.3 Hz), 7.30 (bs, 10H, Bn-H), 7.25 (bs, 2H, Im-H^4), 6.35 (q, 2H, CH_2-Bn, *J* = 13.1 Hz), 6.00 (bd, 2H, N-CH_2-N', *J* = 11.8 Hz), 5.35 (d, 2H, N-CH_2-N', *J* = 14.7 Hz); $^{13}C\{^1H\}$ NMR (75 MHz, d_6-DMSO) δ (ppm) = 137.7, 134.2, 129.0, 128.9, 128.7, 123.2, 122.5, 58.3, 52.3. All data are consistent with the literature.[31]

Preparation of 1,1'-methylenebis(3-(naphthalen-2-ylmethyl)-imidazol-2-ylidene)palladium(II) bromide (6.5). Compound **6.3** (400 mg, 0.6776 mmol) and palladium(II) acetate (152 mg, 0.6776 mmol) were dissolved in acetonitrile (14 mL), under argon. The temperature was slowly increased to 70℃ and the reaction stirred for 48 hours, during which time the solution bleached and product precipitated. The white solid was collected *via* filtration, washed with dichloromethane (10 mL) and dried *in vacuo* to yield the title compound as a pale yellow solid. Yield 332 mg, 71 %; M.pt. decomposes > 270℃; HRMS (ES$^+$): *m/z* 613.0218 {M-Br}$^+$; calculated for $C_{29}H_{24}N_4PdBr$ 613.0219; ^1H NMR (300MHz, d_6-DMSO) δ (ppm) = 7.85 (bd, 2H, Im-H^5, *J* = 1.8 Hz), 7.79 (dd, 4H, Nap-H, *J* = 8.6, 4.8 Hz), 7.62 (d, 2H, Im-H^4, *J* = 1.8 Hz), 7.48-7.58 (bm, 6H, Nap-H), 7.29 (bm, 4H, Nap-H), 6.38 (q, 2H, N-CH_2-N', *J* = 13.2 Hz), 5.99 (bd, 2H, CH_2-Nap, *J* = 13.8 Hz), 5.53 (d, 2H, CH_2-Nap, *J* = 14.5 Hz); $^{13}C\{^1H\}$ NMR (75 MHz, d_6-DMSO) δ (ppm) = 133.9, 132.6, 132.4, 128.3, 127.7, 127.6, 127.1, 126.5, 126.3, 125.5, 122.1, 122.0, 62.7, 53.6 (carbenic C2 resonance not found); Analysis for **6.5**·0.5(CH_3CN)·0.5(CH_2Cl_2) (% calculated, found) C (48.34, 48.00), H (3.52, 3.25), N (8.32, 8.20); Infrared analysis (FT-IR, cm^{-1}) = 3089, 1599, 1509 1425, 1235, 1188, 1106, 863, 827, 807, 778, 760, 742, 478.

Preparation of 1,1'-methylenebis(3-benzyl-imidazol-2-ylidene)palladium(II) tetrafluoroborate (6.6). Compound **6.4** (202 mg, 0.339 mmol) and silver(I) tetrafluoroborate (132 mg, 0.677 mmol) were suspended in acetonitrile (12 mL), under argon and the reaction mixture protected from light. The temperature was increased to 80℃ and the reaction mixture stirred for 18 hours, during which time silver(I) bromide precipitated from solution. The mixture was filtered through celite, the solvent removed *in vacuo* and the residue triturated in dichloromethane to afford the title compound as a white solid, which was collected *via* filtration, washed with diethyl ether and dried. Yield 205 mg, 88 %; M.pt. decomposes > 140℃; HRMS (ES^+): *m/z* 461.0832 $\{M(CN)\text{-}2(BF_4)\}^+$; calculated for $C_{22}H_{21}N_5Pd$ 461.0566; ^1H NMR (300MHz, d_3-MeCN) δ (ppm) = 7.51 (d, 2H, Im-H^5, *J* = 2.0 Hz), 7.39 (m, 6H, Bn-$H^{3,4}$), 7.21 (m, 4H, Bn-H^2), 7.11 (d, 2H, Im-H^4, *J* = 2.0 Hz), 6.31 (d, 1H, N-CH_2-N', *J* = 13.3 Hz), 6.16 (d, 1H, N-CH_2-N', *J* = 13.3 Hz), 5.39 (dd, 4H, CH_2-Bn, *J* = 15.6, 8.6 Hz); $^{13}C\{^1H\}$ NMR (75 MHz, d_3-MeCN) δ (ppm) = 146.8, 135.3, 128.8, 128.2, 127.2, 123.4, 122.6, 62.7, 53.6; Analysis for **6.6**·(H_2O) (% calculated, found) C (42.38, 42.35), H (3.98, 3.60), N (11.86, 11.75); Infrared analysis (FT-IR, cm^{-1}) = 3143, 2332 (bound CH_3CN), 1572, 1438, 1364, 1324, 1248, 1166, 1055 (B-F), 741, 521.

Preparation of 1,1'-methylenebis(3-(naphthalen-2-ylmethyl)-imidazol-2-ylidene)palladium(II) tetrafluoroborate (6.7). Compound **6.5** (298 mg, 0.4288 mmol) and silver(I) tetrafluoroborate (167 mg, 0.8576 mmol) were suspended in acetonitrile (12 mL), under argon and the reaction mixture protected from light. The temperature was increased to 80℃ and the reaction mixture stirred for 18 hours, during which time silver(I) bromide precipitated from solution. The mixture was filtered through celite, the solvent removed *in vacuo* and the residue triturated in dichloromethane to afford the title compound as a white solid, which was collected *via* filtration, washed with dichloromethane and dried. Yield 333 mg, 98 %; M.pt. decomposes > 140℃; HRMS (ES^+): *m/z* 268.0592 $\{M\text{-}2(BF_4)\}^{2+}$, 560.1 $\{M(CN)\text{-}2(BF_4)\}^+$, 579.1 $\{M(OAc)\text{-}2(BF_4)\}^+$; calculated for $C_{29}H_{26}N_4Pd$ 268.0596, $C_{30}H_{24}N_5Pd$ 560.1067 and $C_{30}H_{26}N_4O_2Pd$ 579.1091, respectively; ^1H NMR (300MHz, d_6-DMSO) δ (ppm) = 7.83 (bm, 6H, Nap-$H^{5\text{-}7}$), 7.75 (d, 2H, Im-H^5, *J* = 1.9 Hz), 7.63 (d, 2H, Nap-H^3, *J* = 8.5 Hz), 7.56-7.50 (m, 6H, Nap-H), 7.17 (dd, 2H, Nap-H^4, *J* = 8.5, 1.2 Hz), 6.63 (d, 1H, N-CH_2-N', *J* = 12.7Hz), 6.41 (d, 1H, N-CH_2-N', *J* = 12.7 Hz), 5.54 (d, 2H, CH_2-Nap, *J* = 14.6 Hz), 5.39 (d, 2H, CH_2-Nap, *J* = 14.8Hz); $^{13}C\{^1H\}$ NMR (75 MHz, d_6-DMSO) δ (ppm) = 145.0, 132.5, 131.5, 131.3, 127.4, 126.6, 126.5, 125.8, 125.6, 125.4, 124.1, 122.2, 122.0, 61.3, 51.5; Analysis for **6.7**·(H_2O)·0.5(CH_2Cl_2) (% calculated, found) C (47.27, 46.95), H (3.91, 3.65), N (9.87, 10.10); Infrared analysis (FT-IR, cm^{-1}) = 3143, 2329 (bound CH_3CN), 1431, 1239, 1054 (strong, B-F), 761, 474.

Preparation of $[Pd_3(NHC)_3(4.6)_2]\cdot 6(BF_4)$ (complex 6.8). Tecton **6.7** (64.1 mg, 0.0941 mmol) was added to a solution of ligand **4.6** (50.1 mg, 0.0627 mmol) in nitromethane (7.15 mL) and stirred at room temperature for 16 hours, during which time the solution decolourised. The product was precipitated by the addition of diethyl ether and collected on a sintered frit, washed with diethyl ether and dried *in vacuo* to afford complex **6.8** as a pale yellow solid. Yield 92 mg, 93 %; HRMS (ES^+): *m/z* 1024.3 $\{[Pd(NHC)(\mathbf{6.4})_2]\}^{2+}$, 1328.4 $\{[Pd_2(NHC)_2(\mathbf{6.4})_2]\cdot 2(BF_4)\}^{2+}$, 1633.4 $\{[Pd_3(NHC)_3(\mathbf{6.4})_2]\cdot 4(BF_4)\}^{2+}$; calculated for 1024.8534, 1329.8927 and 1633.4325, respectively; ^{1}H NMR (300 MHz, d_3-$MeNO_2$) δ (ppm) = 9.06 (m, 4H, Py-H^2), 8.89 (bs, 2H, Py-H^2), 8.07 (bm, 2H, Py-H^3), 7.78 (s, 4H, Py-H^3), 7.26 (bm, 15H, Bn-H), 6.83 (m, 4H, N-CH_2-N'), 6.58 (m, 2H, N-CH_2-N'), 5.40 (bs, 6H, CH_2-Bn), 4.96 (bd, 3H, CTG *exo*-H), 4.11 (m, 6H, propyl α-H), 3.80 (bm, 3H, CTG *endo*-H), 1.66 (m, 4H, propyl β-H), 1.28 (m, 2H, propyl β-H), 0.87 (m, 6H, propyl γ-H), 0.43 (m, 3H, propyl γ-H); Analysis for $\mathbf{6.8}\cdot(MeNO_2)\cdot 2(H_2O)$ (% calculated, found) C (54.31, 54.20), H (4.47, 4.35), N (7.52, 7.20); Infrared analysis (FT-IR, cm^{-1}) = 3124, 2968, 1752, 1615, 1508, 1425, 1278, 1056 (strong, tetrafluoroborate anion), 857, 734, 520.

Preparation of $[Pd_3(NHC)_3(4.6)_2]\cdot 6(BF_4)$ (complex 6.9). Tecton **6.7** (73.4 mg, 0.0941 mmol) was added to a solution of ligand **4.6** (50.1 mg, 0.0627 mmol) in nitromethane (8 mL) and stirred at room temperature for 16 hours, during which time the solution decolourised. The product was precipitated by the addition of diethyl ether and collected on a sintered frit, washed with diethyl ether and dried *in vacuo*. Yield 113 mg, 98 %; HRMS (ES^+): *m/z* 848.2383 $\{[Pd_3(NHC)_3(\mathbf{4.6})_2]\cdot 2(BF_4)\}^{4+}$, 1159.9853 $\{[Pd_3(NHC)_3(\mathbf{4.6})_2]\cdot 3(BF_4)\}^{3+}$ and 1783.4795 $\{[Pd_3(NHC)_3(\mathbf{4.6})_2]\cdot 4(BF_4)\}^{2+}$; calculated for 848.2209, 1159.9905 and 1783.9812, respectively; ^{1}H NMR (300 MHz, d_3-$MeNO_2$) δ (ppm) = 8.86 (d, 6H, Py-H^2, *J* = 6.5 Hz), 7.84 (d, 3H, Im-H^5, *J* = 1.9 Hz), 7.76 (m, 8H, Nap-H), 7.56 (m, 8H, Nap-H), 7.43 (d, 6H, Py-H^3, *J* = 6.6 Hz), 7.34 (d, 3H, Im-H^4, *J* = 2.0 Hz), 7.18 (s, 3H, CTG Ar-H), 7.14 (s, 5H, Nap-H), 7.04 (s, 3H, CTG Ar-H), 6.59 (d, 3H, N-CH_2-N', *J* = 13.7 Hz), 5.64 (d, 3H, CH_2Ar, *J* = 17.2 Hz), 5.42 (d, 3H, CH_2Ar, *J* = 17.2 Hz), 4.93 (d, 3H, CTG *exo*-H, *J* = 13.6 Hz), 3.93 (q, 4H, propyl α-H, *J* = 13.6 Hz), 3.80 (m, 5H, propyl α-H and CTG endo-H), 1.77 (m, 1H, propyl β-H), 1.55 (td, 4H, propyl β-H, *J* = 14.1, 7.1 Hz), 1.39 (m, 1H, propyl β-H), 1.04 (t, 2H, propyl γ-H, *J* = 7.4 Hz), 0.82 (t, 5H, propyl γ-H, *J* = 7.4 Hz), 0.62 (t, 2H, propyl γ-H, *J* = 7.4 Hz); $^{13}C\{^1H\}$ NMR (75 MHz, d_3-$MeNO_2$) δ (ppm) = 160.5, 154.4, 151.8, 148.7, 139.4, 132.8, 132.6, 131.5, 128.5, 127.7, 127.6, 126.9, 126.6, 125.4, 124.1, 123.8, 123.7, 123.5, 123.3, 117.7, 115.1, 34.9, 22.1, 9.5; Analysis for $\mathbf{6.9}\cdot(H_2O)\cdot(MeNO_2)$ (% calculated, found) C (57.85, 57.65), H (4.41, 4.35), N (6.97, 6.60); Infrared analysis (FT-IR, cm^{-1}) = 2970, 1754, 1616, 1506, 1428, 1326, 1279 (s), 1062 (strong, tetrafluoroborate anion), 857, 816, 751, 477.

Diffusion Ordered (DOSY) NMR (500 MHz, d_3-$MeNO_2$): $D_{complex}$ = 2.406, D_{ligand} = 4.549×10^{-10} m^2s^{-1}; $D_{complex}/D_{ligand}$ = 0.53:1; Hydrodynamic radius (r) = 14.4 Å.[80]

$$\text{Where; } \frac{KBT}{D} = 6\pi\eta r$$

$D = 0.439\times10^{-10}\ m^2s^{-1}$; $K_B = 1.38065\times10^{-23}\ J\cdot K^{-1}$; T = 293.15 K; $\eta = 0.620\times10^{-3}$ Pa·s

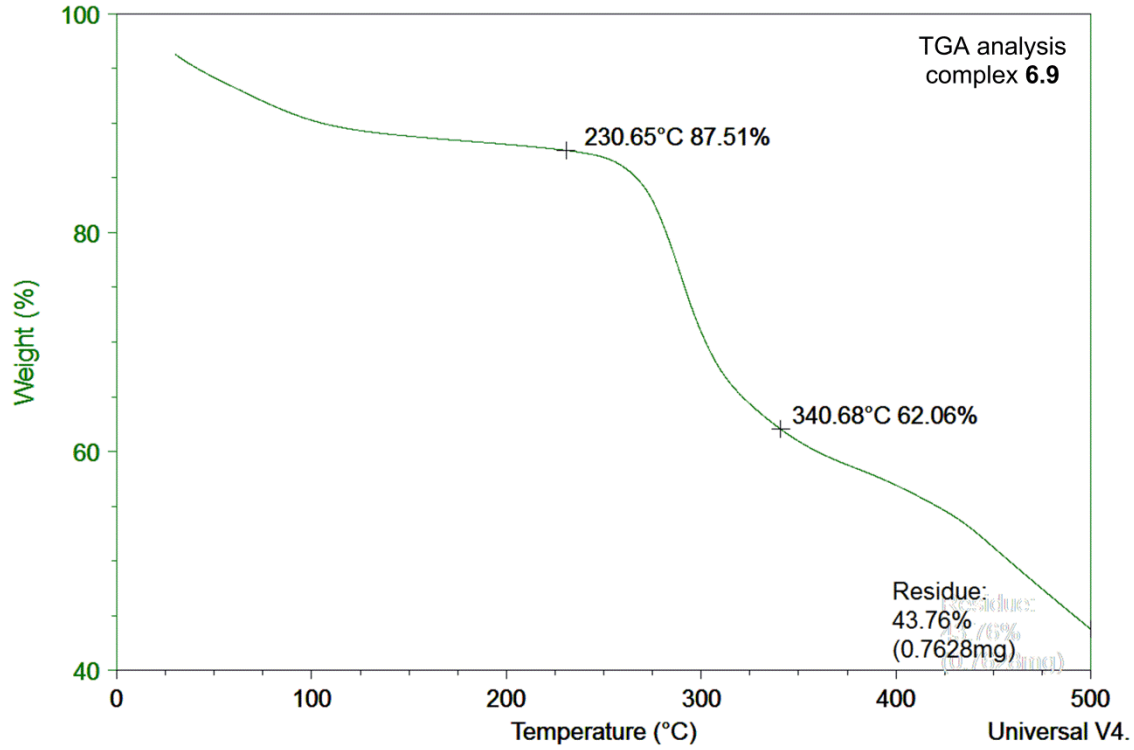

Preparation of $[Pd_3(NHC)_3(2.8)_2]\cdot6(BF_4)$ (complex 6.12). Tecton **6.7** (73.4 mg, 0.0941 mmol) was added to a solution of ligand **2.8** (45.3 mg, 0.0627 mmol) in nitromethane (8 mL) and stirred at room temperature for 16 hours, during which time the solution decolourised. The product was precipitated by the addition of diethyl ether and collected on a sintered frit, washed with diethyl ether and dried *in vacuo*. Yield 104 mg, 96 %; HRMS (ES^+): *m/z* 990.3 $\{[Pd(NHC)(\mathbf{2.8})_2]\}^{2+}$, 1345.3 $\{[Pd_2(NHC)_2(\mathbf{2.8})_2]\cdot2(BF_4)\}^{2+}$ and 1132.6 $\{[Pd_3(NHC)_3(\mathbf{2.8})_2]\cdot4(BF_4)\}^{2+}$; calculated for 990.7752, 1345.8301 and 1132.9237, respectively; ^{1}H NMR (300 MHz, d_3-$MeNO_2$) δ (ppm) = 8.91 (d, 6H, Py-H^2, *J* = 6.5 Hz), 7.85 (d, 3H, Im-H^5, *J* = 2.0 Hz), 7.75 (m, 8H, Nap-H), 7.54 (m, 8H, Nap-H), 7.46 (d, 6H, Py-H^3, *J* = 6.6 Hz), 7.34 (d, 3H, Im-H^4, *J* = 1.9 Hz), 7.20 (s, 3H, CTG Ar-H), 7.15 (s, 3H, CTG Ar-H), 7.04 (m, 5H, Nap-H), 6.61 (d, 3H, N-CH_2-N', *J* = 13.4 Hz), 5.66 (d, 3H, CH_2Ar, *J* = 16.9 Hz), 5.49 (d, 3H, CH_2Ar, *J* = 16.9 Hz), 4.94 (d, 3H, CTG *exo*-H, *J* = 14.3 Hz), 3.89-3.69 (m, 12H, ArO-CH_3 and CTG *endo*-H); Analysis for **6.12**·2(H_2O)·1.5($MeNO_2$) (% calculated, found) C (55.71,

55.60), H (4.03, 3.90), N (7.34, 7.00); Infrared analysis (FT-IR, cm^{-1}) = 3140, 1751, 1616, 1509, 1424, 1327, 1276, 1058 (strong, tetrafluoroborate anion), 758, 476.

Preparation of $[Pd_3(NHC)_3(\mathbf{6.10})_2]\cdot 6(BF_4)$ (complex 6.13). Tecton **6.7** (73.4 mg, 0.0941 mmol) was added to a solution of ligand **6.10** (48.0 mg, 0.0627 mmol) in nitromethane (8 mL) and stirred at room temperature for 16 hours, during which time the solution decolourised. The product was precipitated by the addition of diethyl ether and collected on a sintered frit, washed with diethyl ether and dried *in vacuo*. Yield 108 mg, 99 %; HRMS (ES^+): *m/z* 1032.3226 $\{[Pd(NHC)(\mathbf{6.10})_2]\cdot(BF_4)\}^{2+}$, 1386.3759 $\{[Pd(NHC)(\mathbf{6.10})]\cdot(BF_4)\}^{+}$ and 1741.4210 $\{[Pd_3(NHC)_3(\mathbf{6.10})_2]\cdot 4BF_4\}^{2+}$; calculated for 1032.8221, 1386.3711 and 1741.4325, respectively; ^{1}H NMR (300 MHz, d_3-$MeNO_2$) δ (ppm) = 9.31 (d, 3H, Py-H^2, *J* = 5.9 Hz), 7.98-7.55 (m, 14 H, overlapping Nap-H and Im-H), 7.45 (s, 3H, Py-H^3), 7.36 (s, 3H, Py-H^5), 7.31 (m, 8H, Nap-H), 7.20 (s, 3H, CTG Ar-H), 7.16 (s, 3H, CTG Ar-H), 7.10-7.05 (m, 5H, Nap-H), 6.75 (m, 3H, N-CH_2-N'), 5.65 (d, 3H, CH_2Ar, *J* = 16.8 Hz), 5.53 (d, 3H, CH_2Ar, *J* = 16.8 Hz), 4.94 (d, 3H, CTG *exo*-H, *J* = 14.2 Hz), 3.86 (m, 3H, CTG *endo*-H), 3.69 (s, 9H, CTG ArO-CH_3), 2.93 (s, 9H, Py-CH_3); Satisfactory elemental analysis could not be obtained; Infrared analysis (FT-IR, cm^{-1}) = 3624, 3144, 1748, 1621, 1566, 1506, 1428, 1284, 1205, 1065 (strong, tetrafluoroborate anion), 857, 818, 758.

Preparation of $[Pd_3(NHC)_3(\mathbf{6.11})_2]\cdot 6(BF_4)$ (complex 6.14). Tecton **6.7** (73.4 mg, 0.0941 mmol) was added to a solution of ligand **6.11** (52.2 mg, 0.0627 mmol) in nitromethane (8 mL) and stirred at room temperature for 16 hours, during which time the solution decolourised. The product was precipitated by the addition of diethyl ether and collected on a sintered frit, washed with diethyl ether and dried *in vacuo*. Yield 120 mg, 99 %; HRMS (ES^+): *m/z* 860.4955 $\{[Pd_3(NHC)_3(\mathbf{2.11})_2]\cdot 2BF_4\}^{4+}$, 1175.6625 $\{[Pd_3(NHC)_3(\mathbf{2.11})_2]\cdot 3BF_4\}^{3+}$ and 1807.4992 $\{[Pd_3(NHC)_3(\mathbf{2.11})_2]\cdot 4BF_4\}^{2+}$; calculated for 860.4955, 1175.6624 and 1807.4982, respectively; ^{1}H NMR (300 MHz, d_3-$MeNO_2$) δ (ppm) = 9.80 (s, 3H, Quin-H), 9.54 (s, 3H, Quin-H), 9.24 (s, 3H, Quin-H), 7.97 (m, 8H, Nap-H), 7.63 (m, 3H, Quin-H), 7.49 (m, 8H, Nap-H), 7.30 (m, 6H, Quin-H and CTG Ar-H), 7.13 (m, 6H, Quin-H and CTG Ar-H), 6.93 (m, 3H, N-CH_2-N'), 6.46 (bs, 3H, CH_2-Quin), 6.24 (bs, 3H, CH_2-Quin), 5.91 (bs, 3H, CH_2Ar), 5.58 (bs, 3H, CH_2Ar), 4.95 (bs, 3H, CTG *exo*-H), 3.81 (m, 12H, CTG ArO-CH_3 and *endo*-H); Satisfactory elemental analysis could not be obtained; Infrared analysis (FT-IR, cm^{-1}) = 3617, 3140, 1596, 1509, 1467, 1263, 1215, 1058 (strong, tetrafluoroborate anion), 853, 815, 762.

Preparation of $[Pd_3(NHC)_3(\mathbf{4.6})_2]\cdot 6(BF_4)\subset 3$(1,2-DCB) (complex 6.15). Single crystals of complex **6.9** were placed in a vial containing 1,2-dichlorobenzene and allowed to equilibrate for two weeks, during which time they turned yellow (from colourless). The crystals were isolated from the mother liquor and analysed using single crystal diffraction analysis using a synchrotron

source. Thermogravimetric analysis provided below. ^{1}H NMR (300 MHz, d_3-$MeNO_2$) δ (ppm) = 8.86 (d, 6H, Py-H^{2}, *J* = 6.5 Hz), 7.84 (d, 3H, Im-H^{5}, *J* = 1.9 Hz), 7.76 (m, 8H, Nap-H), 7.59 (dd, 3H, DCB-H^{3}, *J* = 6.0, 3.6 Hz), 7.56 (m, 8H, Nap-H), 7.43 (d, 6H, Py-H^{3}, *J* = 6.6 Hz), 7.39 (dd, 3H, DCB-H^{4}, *J* = 6.0, 3.6 Hz), 7.34 (d, 3H, Im-H^{4}, *J* = 2.0 Hz), 7.18 (s, 3H, CTG Ar-H), 7.14 (s, 5H, Nap-H), 7.04 (s, 3H, CTG Ar-H), 6.59 (d, 3H, N-CH_2-N', *J* = 13.7 Hz), 5.64 (d, 3H, CH_2Ar, *J* = 17.2 Hz), 5.42 (d, 3H, CH_2Ar, *J* = 17.2 Hz), 4.93 (d, 3H, CTG *exo*-H, *J* = 13.6 Hz), 3.93 (q, 4H, propyl α-H, *J* = 13.6 Hz), 3.80 (m, 5H, propyl α-H and CTG endo-H), 1.77 (m, 1H, propyl β-H), 1.55 (td, 4H, propyl β-H, *J* = 14.1, 7.1 Hz), 1.39 (m, 1H, propyl β-H), 1.04 (t, 2H, propyl γ-H, *J* = 7.4 Hz), 0.82 (t, 5H, propyl γ-H, *J* = 7.4 Hz), 0.62 (t, 2H, propyl γ-H, *J* = 7.4 Hz); EDX analysis for **6.15** (Wt. % calculated, found) = Cl (5.09, 5.73), Pd (7.63, 8.13).

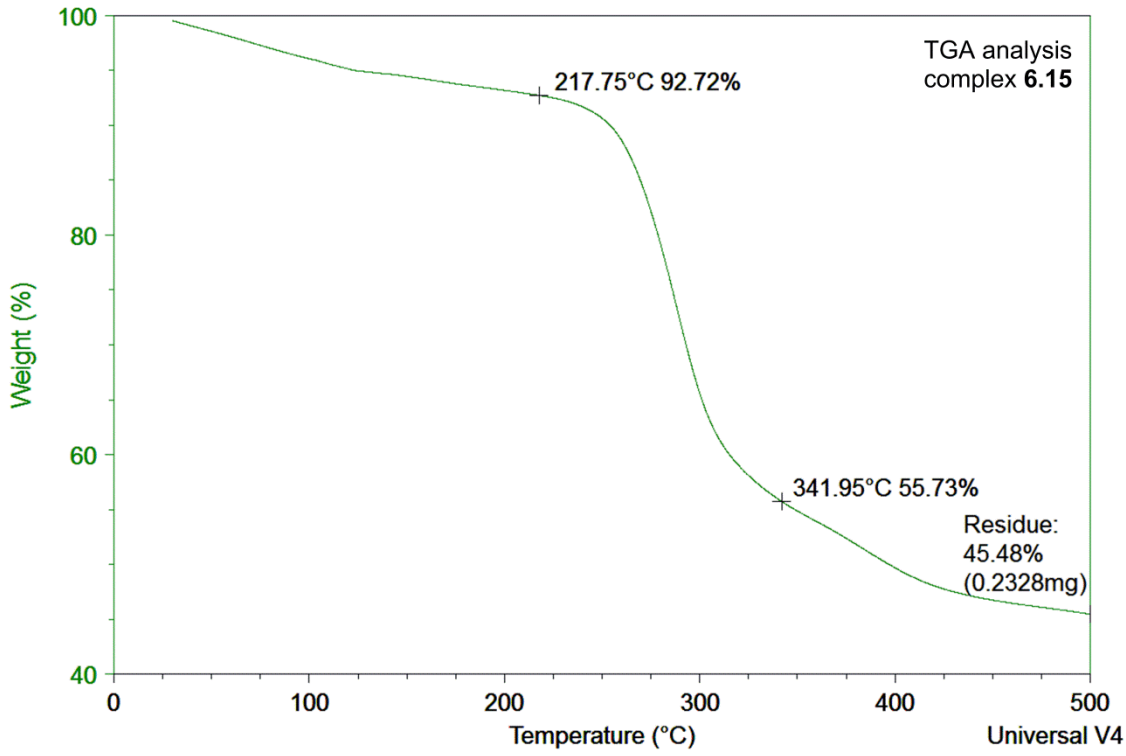

Preparation of [$Pd_3(NHC)_3(2.8)_2$]·6(BF_4)⊂*n*(I_2) (complex 6.16). Procedure 1: Single crystals of complex **6.12** were placed in a vial containing an ethereal solution of iodine and allowed to equilibrate for one week, during which time they turned from colourless to dark brown. Procedure 2: Single crystals of complex **6.12** were placed in one side of an H-tube with molecular iodine in the other. The sample was placed under vacuum and the iodine sublimed with heating, after which the system was returned to atmospheric pressure and the vessel sealed. Iodine vapours were taken up by the crystals immediately, which turned from colourless to dark brown. The crystals were isolated and pictures of the sample were taken using an optical microscope, followed by single crystal X-ray analysis. EDX analysis for **6.15** (Wt. % calculated, found) = F (9.34, 9.75), Pd (6.54, 9.77), I (23.39, 23.68).

6.7.3 Supplementary crystallographic information

Compound **6.6** was refined with general ADP similarity restraints (SIMU and DELU) and one tetrafluoroborate anion was refined as isotropic and over two positions. The naphthyl arms of **6.7** were each refined isotropically and modelled over two positions with a 50:50 occupancy and the bond lengths of one naphthyl moiety were refined to be chemically reasonable. One tetrafluoroborate anion was refined isotropically and as disordered and the uncoordinated acetonitrile solvent molecule was refined isotropically.

Crystals of complexes **6.9**, **6.12-6.16** did not diffract to high angles and the SQUEEZE routine of PLATON was employed for all samples.[79] Complex **6.9**: The pyridyl arm was refined isotropically and over two molecular positions with a 50:50 occupancy. The γ-carbon of the propyl chain was refined isotropically and the bond lengths restrained to be chemically reasonable. A nitromethane molecule was refined at half occupancy and isotropically with the N-C bond length restrained to be chemically reasonable.

Complex **6.12**: The methoxy group of ligand **2.8** was modelled as disordered over two positions at 75:25 occupancies and refined isotropically. One of the corresponding C-O bond lengths was restrained to be chemically reasonable and anisotropic displacement parameters restrained to be similar using the EADP command. One of the two nitromethane molecules was refined isotropically at half occupancy and refined isotropically.

Complex **6.13**: One of the three partially occupied BF_4^- anions was modelled as disordered and none of the anions were refined anisotropically.

Complex **6.14**: Crystals did not diffract to high angles and the reflection data were poor. No BF_4^- anions or nitromethane solvent molecules were located in the difference map and the naphthyl and 4-quinolyl groups were refined with a rigid body restraint (AFIX66). Only the palladium(II) position was refined anisotropically. The structure is not of publishable quality.

Complex **6.15**: One BF_4^- anion was refined as disordered across two positions, refined isotropically and the B-F bond lengths restrained to be chemically reasonable. The propyl moiety was refined isotropically. The 1,2-dichlorobenzene molecule was sited on, and disordered across, a mirror plane. The entire unit was refined with a planarity restraint (FLAT) and isotropically. The nitromethane molecule was modelled as disordered and its thermal ellipsoid parameters restrained to be similar.

Complex **6.16**: Two of the three BF_4^- anions were refined isotropically and the B-F bond lengths were restrained to be chemically reasonable. Three water molecules were included in the

refinement at quarter occupancies. None of the iodine atoms were refined anisotropically and the bond lengths of the two complete iodine molecules were restrained. All iodine atoms were refined at partial occupancies and their thermal parameters restrained to be chemically reasonable.

6.7.4 X-ray data tables for compounds 6.6 and 6.7 and complexes 6.9 and 6.12-6.16

	6.6[a]	**6.7**[a]	**6.9**[b]	**6.12**[c]
Formula	$C_{25}H_{26}B_2F_8N_6Pd$	$C_{35}H_{33}B_2F_8N_7Pd$	$C_{187}H_{174}B_6F_{24}N_{22}O_{26}Pd_3$	$C_{175}H_{150}B_6F_{24}N_{22}O_{26}Pd_3$
Mr	690.54	832.71	3985.54	3817.23
Crystal colour and shape	Yellow, block	Yellow, block	Yellow, needle	Yellow, needle
Crystal size (mm)	0.28 x 0.26 x 0.24	0.18 x 0.18 x 0.16	0.24 x 0.12 x 0.12	0.24 x 0.14 x 0.14
Crystal system	Orthorhombic	Monoclinic	Hexagonal	Hexagonal
Space group	$Pna2_1$	$P2_1/n$	$P6_3/m$	$P6_3/m$
a (Å)	11.1200(6)	12.2792(3)	24.6118(19)	24.6185(14)
b (Å)	17.3098(9)	14.3456(4)	24.6118(19)	24.6185(14)
c (Å)	15.0454(8)	20.8758(6)	20.272(3)	20.3337(12)
α (^{0})	90.00	90.00	90.00	90.00
β (^{0})	90.00	69.3210(10)	90.00	90.00
γ (^{0})	90.00	90.00	120.00	120.00
V (Å^3)	2896.0(3)	3654.97(17)	10634.4(18)	10672.6(11)
Z	4	6	2	2
ρ_{calc} (g.cm^{-3})	1.584	1.578	1.245	1.188
θ range (^{0})	1.79 – 26.48	1.73 – 26.37	3.01 – 45.00	1.60 – 20.17
No. data collected	11642	20954	10244	56227
No. unique data	4898	7458	2988	3862
R_{int}	0.0202	0.0375	0.0531	0.0872
No. obs. Data ($I > 2\sigma(I)$)	4497	5543	2172	2995
No. parameters	331	4216	361	397
No. restraints	288	17	3	1
R_1 (obs data)	0.0579	0.0730	0.0960	0.1082
wR_2 (all data)	0.1727	0.2234	0.2935	0.3312
S	1.003	1.531	1.186	1.373

Radiation sources: ***a*** (Mo), ***b*** (Cu) and ***c*** (Synchrotron)

	6.13[c]	**6.14**[c]	**6.15**[c]	**6.16**[b]
Formula	$C_{177}H_{150}B_6F_{24}N_{18}O_{18}Pd_3$	$C_{195}H_{162}B_6F_{24}N_{18}O_{12}Pd_3$	$C_{202}H_{177}B_6Cl_6F_{24}N_{19}O_{22}Pd_3$	$C_{171}H_{138}B_6F_{24}I_{4.5}N_{18}O_{22.5}Pd_3$
Mr	3657.21	3789.49	4275	4216.10
Crystal colour and shape	Yellow, needle	Yellow, needle	Yellow, needle	Brown, needle
Crystal size (mm)	0.20 x 0.13 x 0.13	0.18 x 0.08 x 0.08	0.22 x 0.15 x 0.15	0.21 x 0.14 x 0.14
Crystal system	Hexagonal	Hexagonal	Hexagonal	Hexagonal
Space group	$P6_3/m$	$P6_3/m$	$P6_3/m$	$P6_3/m$
a (Å)	25.2100(12)	24.755(15)	24.7360(8)	24.7016(8)
b (Å)	25.2100(12)	24.755(15)	24.7360(8)	24.7016(8)
c (Å)	20.5293(7)	19.387(16)	20.0595(7)	20.3905(7)
α (^{0})	90.00	90.00	90.00	90.00
β (^{0})	90.00	90.00	90.00	90.00
γ (^{0})	120.00	120.00	120.00	120.00
V (Å^3)	11299.3(9)	10289(12)	10629.4(6)	10774.8(6)
Z	2	2	2	2
ρ_{calc} (g.cm^{-3})	1.075	1.223	1.336	1.330
θ range (^{0})	0.90 – 26.35	0.92 – 17.50	1.60 – 21.25	2.99 – 44.99
No. data collected	95207	34497	64445	14403
No. unique data	8523	2492	4459	3029
R_{int}	0.1494	0.4008	0.0878	0.0536
No. obs. Data ($I > 2\sigma(I)$)	5684	1748	3669	208
No. parameters	360	113	395	385
No. restraints	0	0	6	8
R_1 (obs data)	0.1417	0.2920	0.1246	0.1489
wR_2 (all data)	0.3647	0.5413	0.3509	0.3967
S	1.927	2.348	2.619	2.769

Radiation sources: ***a*** (Mo), ***b*** (Cu) and ***c*** (Synchrotron)

6.8 Bibliography

[1] T. Brotin, J.-P. Dutasta, *Chem. Rev.* **2008**, *109*, 88-130.

[2] O. Taratula, P. A. Hill, N. S. Khan, P. J. Carroll, I. J. Dmochowski, *Nat. Commun.* **2010**, *1*, 148.

[3] M. J. Hardie, *Chem. Soc. Rev.* **2010**, *39*, 516-527.

[4] (a) Z. Zhong, A. Ikeda, S. Shinkai, S. Sakamoto, K. Yamaguchi, *Org. Lett.* **2001**, *3*, 1085-1087; (b) T. K. Ronson, H. Nowell, A. Westcott, M. J. Hardie, *Chem. Commun.* **2010**, *47*, 176-178; (c) J. J. Henkelis, T. K. Ronson, L. P. Harding, M. J. Hardie, *Chem. Commun.* **2011**, *47*, 6560-6562.

[5] K. T. Holman, *Encyclopedia of Supramolecular Chemistry. CRC Press* **2004**, 340-348.

[6] C. J. Hastings, M. D. Pluth, R. G. Bergman, K. N. Raymond, *J. Am. Chem. Soc.* **2010**, *132*, 6938-6940.

[7] J. E. M. Lewis, E. L. Gavey, S. A. Cameron, J. D. Crowley, *Chem. Sci.* **2012**, *3*, 778-784.

[8] F. Hof, S. L. Craig, C. Nuckolls, J. J. Rebek, *Angew. Chem. Int. Ed.* **2002**, *41*, 1488-1508.

[9] M. Fujita, O. Sasaki, T. Mitsuhashi, T. Fujita, J. Yazaki, K. Yamaguchi, K. Ogura, *Chem. Commun.* **1996**, 1535-1536.

[10] N. Fujita, K. Biradha, M. Fujita, S. Sakamoto, K. Yamaguchi, *Angew. Chem. Int. Edit.* **2001**, *40*, 1718-1721.

[11] M. Fujita, D. Oguro, M. Miyazawa, H. Oka, K. Yamaguchi, K. Ogura, *Nature* **1995**, *378*, 469-471.

[12] M. Yoshizawa, J. K. Klosterman, M. Fujita, *Angew. Chem. Int. Edit.* **2009**, *48*, 3418-3438.

[13] M. Fujita, M. Tominaga, A. Hori, B. Therrien, *Acc. Chem. Res.* **2005**, *38*, 369-378.

[14] Y. Inokuma, M. Kawano, M. Fujita, *Nat. Chem.* **2011**, *3*, 349-358.

[15] S. G. Baca, H. Adams, C. S. Grange, A. P. Smith, I. Sazanovich, M. D. Ward, *Inorg. Chem.* **2007**, *46*, 9779-9789.

[16] J. J. Loughrey, S. Sproules, E. J. L. McInnes, M. J. Hardie, M. A. Halcrow, *Chem. Eur. J.* **2014**, *20*, 6272-6276.

[17] S. Shanmugaraju, V. Vajpayee, S. Lee, K.-W. Chi, P. J. Stang, P. S. Mukherjee, *Inorg. Chem.* **2012**, *51*, 4817-4823.

[18] D. Bourissou, O. Guerret, F. P. Gabbaï, G. Bertrand, *Chem. Rev.* **1999**, *100*, 39-92.

[19] L. Benhamou, E. Chardon, G. Lavigne, S. Bellemin-Laponnaz, V. César, *Chem. Rev.* **2011**, *111*, 2705-2733.

[20] A. J. Arduengo, H. V. R. Dias, R. L. Harlow, M. Kline, *J. Am. Chem. Soc.* **1992**, *114*, 5530-5534.

[21] A. J. Arduengo, R. L. Harlow, M. Kline, *J. Am. Chem. Soc.* **1991**, *113*, 361-363.

[22] B. R. M. Lake, C. E. Willans, *Chem. Eur. J.* **2013**, *19*, 16780-16790.

[23] S. Díez-González, N. Marion, S. P. Nolan, *Chem. Rev.* **2009**, *109*, 3612-3676.

[24] G. C. Vougioukalakis, R. H. Grubbs, *Chem. Rev.* **2009**, *110*, 1746-1787.

[25] R. Visbal, M. C. Gimeno, *Chem. Soc. Rev.* **2014**, *43*, 3551-3574.

[26] (a) M. Rubio, E. Jellema, M. A. Siegler, A. L. Spek, J. N. H. Reek, B. de Bruin, *Dalton Trans.* **2009**, 8970-8976; (b) C.-X. Lin, X.-F. Kong, Q. Li, Z.-Z. Zhang, Y. Yuan, F.-B. Xu, *Crystengcomm* **2013**, *15*, 6948-6962.

[27] M. Rubio, M. A. Siegler, A. L. Spek, J. N. H. Reek, *Dalton Trans.* **2010**, *39*, 5432-5435.

[28] C. Radloff, F. E. Hahn, T. Pape, R. Frohlich, *Dalton Trans.* **2009**, 7215-7222.

[29] E. Diez-Barra, A. Sanchez-Migallon, A. Tejeda, *Heterocycles* **1970**, *34*, 1365-1373.

[30] Y. Fang, T. Murase, S. Sato, M. Fujita, *J. Am. Chem. Soc.* **2012**, *135*, 613-615.

[31] H. M. Lee, C. Y. Lu, C. Y. Chen, W. L. Chen, H. C. Lin, P. L. Chiu, P. Y. Cheng, *Tetrahedron* **2004**, *60*, 5807-5825.

[32] J. Wencel-Delord, T. Droge, F. Liu, F. Glorius, *Chem. Soc. Rev.* **2011**, *40*, 4740-4761.

[33] (a) A. Maleckis, J. W. Kampf, M. S. Sanford, *J. Am. Chem. Soc.* **2013**, *135*, 6618-6625; (b) M. Anand, R. B. Sunoj, H. F. Schaefer, *J. Am. Chem. Soc.* **2014**, *136*, 5535-5538; (c) K. M. Engle, D.-H. Wang, J.-Q. Yu, *J. Am. Chem. Soc.* **2010**, *132*, 14137-14151.

[34] L. C. Campeau, D. R. Stuart, J. P. Leclerc, M. Bertrand-Laperle, E. Villemure, H. Y. Sun, S. Lasserre, N. Guimond, M. Lecavallier, K. Fagnou, *J. Am. Chem. Soc.* **2009**, *131*, 3291-3306.

[35] (a) T. G. Larocque, A. C. Badaj, G. G. Lavoie, *Dalton Trans.* **2013**, *42*, 14955-14958; (b) B. M. Mattson, W. A. G. Graham, *Inorg. Chem.* **1981**, *20*, 3186-3189.

[36] (a) N. J. Cookson, J. J. Henkelis, R. J. Ansell, C. W. G. Fishwick, M. J. Hardie, J. Fisher, *Dalton Trans.* **2014**, *43*, 5657-5661; (b) T. K. Ronson, C. Carruthers, J. Fisher, T. Brotin, L. P. Harding, P. J. Rizkallah, M. J. Hardie, *Inorg. Chem.* **2010**, *49*, 675-685.

[37] M. Yoneya, T. Yamaguchi, S. Sato, M. Fujita, *J. Am. Chem. Soc.* **2012**, *134*, 14401-14407.

[38] (a) M. O. Sinnokrot, E. F. Valeev, C. D. Sherrill, *J. Am. Chem. Soc.* **2002**, *124*, 10887-10893; (b) S. L. Cockroft, C. A. Hunter, K. R. Lawson, J. Perkins, C. J. Urch, *J. Am. Chem. Soc.* **2005**, *127*, 8594-8595; (c) C. A. Hunter, J. K. M. Sanders, *J. Am. Chem. Soc.* **1990**, *112*, 5525-5534.

[39] (a) Z. Zhu, C. J. Bruns, H. Li, J. Lei, C. Ke, Z. Liu, S. Shafaie, H. M. Colquhoun, J. F. Stoddart, *Chem. Sci.* **2013**, *4*, 1470-1483; (b) J.-F. Ayme, J. E. Beves, C. J. Campbell,

D. A. Leigh, *Chem. Soc. Rev.* **2012**, *42*, 1700-1712; (c) Z. Zhu, A. C. Fahrenbach, H. Li, J. C. Barnes, Z. Liu, S. M. Dyar, H. Zhang, J. Lei, R. Carmieli, A. A. Sarjeant, C. L. Stern, M. R. Wasielewski, J. F. Stoddart, *J. Am. Chem. Soc.* **2012**, *134*, 11709-11720.

[40] S. P. Black, A. R. Stefankiewicz, M. M. J. Smulders, D. Sattler, C. A. Schalley, J. R. Nitschke, J. K. M. Sanders, *Angew. Chem. Int. Ed.* **2013**, *52*, 5749-5752.

[41] (a) D. Small, V. Zaitsev, Y. Jung, S. V. Rosokha, M. Head-Gordon, J. K. Kochi, *J. Am. Chem. Soc.* **2004**, *126*, 13850-13858; (b) J. M. Spruell, A. Coskun, D. C. Friedman, R. S. Forgan, A. A. Sarjeant, A. Trabolsi, A. C. Fahrenbach, G. Barin, W. F. Paxton, S. K. Dey, M. A. Olson, D. Benítez, E. Tkatchouk, M. T. Colvin, R. Carmielli, S. T. Caldwell, G. M. Rosair, S. G. Hewage, F. Duclairoir, J. L. Seymour, A. M. Z. Slawin, W. A. Goddard, M. R. Wasielewski, G. Cooke, J. F. Stoddart, *Nat. Chem.* **2010**, *2*, 870-879; (c) J. M. Spruell, *Pure Appl. Chem.* **2010**, *82*, 2281-2294.

[42] (a) A. S. Tayi, A. K. Shveyd, A. C. H. Sue, J. M. Szarko, B. S. Rolczynski, D. Cao, T. J. Kennedy, A. A. Sarjeant, C. L. Stern, W. F. Paxton, W. Wu, S. K. Dey, A. C. Fahrenbach, J. R. Guest, H. Mohseni, L. X. Chen, K. L. Wang, J. F. Stoddart, S. I. Stupp, *Nature* **2012**, *488*, 485-489; (b) J. C. Barnes, A. C. Fahrenbach, D. Cao, S. M. Dyar, M. Frasconi, M. A. Giesener, D. Benítez, E. Tkatchouk, O. Chernyashevskyy, W. H. Shin, H. Li, S. Sampath, C. L. Stern, A. A. Sarjeant, K. J. Hartlieb, Z. Liu, R. Carmieli, Y. Y. Botros, J. W. Choi, A. M. Z. Slawin, J. B. Ketterson, M. R. Wasielewski, W. A. Goddard, J. F. Stoddart, *Science* **2013**, *339*, 429-433; (c) A. C. Fahrenbach, Z. Zhu, D. Cao, W.-G. Liu, H. Li, S. K. Dey, S. Basu, A. Trabolsi, Y. Y. Botros, W. A. Goddard, J. F. Stoddart, *J. Am. Chem. Soc.* **2012**, *134*, 16275-16288; (d) A. Trabolsi, N. Khashab, A. C. Fahrenbach, D. C. Friedman, M. T. Colvin, K. K. Cotí, D. Benítez, E. Tkatchouk, J.-C. Olsen, M. E. Belowich, R. Carmielli, H. A. Khatib, W. A. Goddard, M. R. Wasielewski, J. F. Stoddart, *Nat. Chem.* **2010**, *2*, 42-49.

[43] J. J. Henkelis, J. Fisher, S. L. Warriner, M. J. Hardie, *Chem. Eur. J.* **2014**, *20*, 4117-4125.

[44] S. Mecozzi, J. J. Rebek, *Chem. Eur. J.* **1998**, *4*, 1016-1022.

[45] D. Ajami, J. Rebek, *Nat. Chem.* **2009**, *1*, 87-90.

[46] Swiss-PDB Viewer: *spdbv.vital-it.ch.*

[47] (a) H. Roohi, R. Salehi, *J. Mol. Liq.* **2011**, *161*, 63-71; (b) X. Hu, Q. Lin, J. Gao, Y. Wu, Z. Zhang, *Chem. Phys. Lett.* **2011**, *516*, 35-39.

[48] C. J. Kuehl, Y. K. Kryschenko, U. Radhakrishnan, S. R. Seidel, S. D. Huang, P. J. Stang, *Proc. Natl. Acad. Sci. USA* **2002**, *99*, 4932-4936.

[49] (a) H. Fenton, I. S. Tidmarsh, M. D. Ward, *Dalton Trans.* **2009**, 4199-4207; (b) R. L. Paul, Z. R. Bell, J. C. Jeffery, J. A. McCleverty, M. D. Ward, *Proc. Natl. Acad. Sci. USA* **2002**, *99*, 4883-4888; (c) J. S. Fleming, K. L. V. Mann, C. A. Carraz, E. Psillakis,

J. C. Jeffery, J. A. McCleverty, M. D. Ward, *Angew. Chem. Int. Edit.* **1998**, *37*, 1279-1281; (d) R. Custelcean, P. V. Bonnesen, N. C. Duncan, X. Zhang, L. A. Watson, G. Van Berkel, W. B. Parson, B. P. Hay, *J. Am. Chem. Soc.* **2012**, *134*, 8525-8534.

[50] (a) J.-F. Ayme, J. E. Beves, D. A. Leigh, R. T. McBurney, K. Rissanen, D. Schultz, *Nat. Chem.* **2012**, *4*, 15-20; (b) I. A. Riddell, M. M. J. Smulders, J. K. Clegg, Y. R. Hristova, B. Breiner, J. D. Thoburn, J. R. Nitschke, *Nat. Chem.* **2012**, *4*, 751-756.

[51] R. Custelcean, *Chem. Soc. Rev.* **2014**, *43*, 1813-1824.

[52] S. J. Dalgarno, N. P. Power, J. L. Atwood, *Coord. Chem. Rev.* **2008**, *252*, 825-841.

[53] Y. Z. Liu, M. D. Ward, *Cryst. Growth Des.* **2009**, *9*, 3859-3861.

[54] Y. Inokuma, T. Arai, M. Fujita, *Nat. Chem.* **2011**, *2*, 780-783.

[55] (a) T. Mitra, K. E. Jelfs, M. Schmidtmann, A. Ahmed, S. Y. Chong, D. J. Adams, A. I. Cooper, *Nat. Chem.* **2013**, *5*, 276-281; (b) T. Hasell, X. Wu, T. A. JonesJames, J. Bacsa, A. Steiner, T. Mitra, A. Trewin, D. J. Adams, A. I. Cooper, *Nat. Chem.* **2010**, *2*, 750-755; (c) T. Hasell, J. L. Culshaw, S. Y. Chong, M. Schmidtmann, M. A. Little, K. E. Jelfs, E. O. Pyzer-Knapp, H. Shepherd, D. J. Adams, G. M. Day, A. I. Cooper, *J. Am. Chem. Soc.* **2014**, *136*, 1438-1448.

[56] C. Carruthers, *University of Leeds, PhD Thesis* **2010**.

[57] C. Carruthers, T. K. Ronson, C. J. Sumby, A. Westcott, L. P. Harding, T. J. Prior, P. Rizkallah, M. J. Hardie, *Chem. Eur. J.* **2008**, *14*, 10286-10296.

[58] D. Chandler, *Nature* **2005**, *437*, 640-647.

[59] M. Whitehead, S. Turega, A. Stephenson, C. A. Hunter, M. D. Ward, *Chem. Sci.* **2013**, *4*, 2744-2751.

[60] (a) P. Mal, B. Breiner, K. Rissanen, J. R. Nitschke, *Science* **2009**, *324*, 1697-1699; (b) T. K. Ronson, C. Giri, N. Kodiah Beyeh, A. Minkkinen, F. Topić, J. J. Holstein, K. Rissanen, J. R. Nitschke, *Chem. Eur. J.* **2013**, *19*, 3374-3382.

[61] Y. Inokuma, S. Yoshioka, J. Ariyoshi, T. Arai, Y. Hitora, K. Takada, S. Matsunaga, K. Rissanen, M. Fujita, *Nature* **2013**, *495*, 461-466.

[62] J. Canceill, L. Lacombe, A. Collet, *J. Chem. Soc., Chem. Commun.* **1987**, 219-221.

[63] (a) F. London, *J. Chem. Soc., Faraday Trans.* **1937**, *33*, 8b-26; (b) L. Yang, C. Adam, G. S. Nichol, S. L. Cockroft, *Nat. Chem.* **2013**, *5*, 1006-1010.

[64] M. du Plessis, V. Smith, L. Barbour, *CrystEngComm* **2014**, *16*, 4126-4132.

[65] G. W. Orr, L. J. Barbour, J. L. Atwood, *Science* **1999**, *285*, 1049-1052.

[66] J. L. Atwood, L. J. Barbour, A. Jerga, B. L. Schottel, *Science* **2002**, *298*, 1000-1002.

[67] J. L. Atwood, L. J. Barbour, A. Jerga, *Science* **2002**, *296*, 2367-2369.

[68] J. L. Atwood, L. J. Barbour, P. K. Thallapally, T. B. Wirsig, *Chem. Commun.* **2005**, 51-53.

[69] J. L. Atwood, L. J. Barbour, A. Jerga, *Angew. Chem. Int. Ed.* **2004**, *43*, 2948-2950.

[70] L. J. Barbour, *Chem. Commun.* **2006**, 1163-1168.

[71] S. J. Dalgarno, P. K. Thallapally, L. J. Barbour, J. L. Atwood, *Chem. Soc. Rev.* **2007**, *36*, 236-245.

[72] T. Jacobs, L. J. Barbour, *New J. Chem.* **2013**, *37*, 71-74.

[73] D. F. Sava, M. A. Rodriguez, K. W. Chapman, P. J. Chupas, J. A. Greathouse, P. S. Crozier, T. M. Nenoff, *J. Am. Chem. Soc.* **2011**, *133*, 12398-12401.

[74] (a) G. Massasso, J. Long, J. Haines, S. Devautour-Vinot, G. Maurin, A. Grandjean, B. Onida, B. Donnadieu, J. Larionova, C. Guérin, Y. Guari, *Inorg. Chem.* **2014**, *53*, 4269-4271; (b) M.-H. Zeng, Q.-X. Wang, Y.-X. Tan, S. Hu, H.-X. Zhao, L.-S. Long, M. Kurmoo, *J. Am. Chem. Soc.* **2010**, *132*, 2561-2563.

[75] L. Dobrzańska, G. O. Lloyd, H. G. Raubenheimer, L. J. Barbour, *J. Am. Chem. Soc.* **2005**, *128*, 698-699.

[76] (a) P. Metrangolo, G. Resnati, *Science* **2008**, *321*, 918-919; (b) J. Marti-Rujas, L. Colombo, J. Lu, A. Dey, G. Terraneo, P. Metrangolo, T. Pilati, G. Resnati, *Chem. Commun.* **2012**, *48*, 8207-8209.

[77] (a) G. Sheldrick, *Acta Crystallogr., Sect. A* **2008**, *A64*, 112-122; (b) L. J. Barbour, *Supramol. Chem.* **2001**, *1*, 189-191.

[78] Persistence of Vision Raytracer Pty. Ltd. Williamstown, 2004.

[79] (a) A. L. Spek, *Acta Crystallogr., Sect. A* **2009**, *A46*, 194-201; (b) A. L. Spek, *Acta Crystallogr., Sect. A* **1990**, *A46*, 194-201.

[80] M. Nillson, *J. Mag. Resn.* **2009**, *200*, 296-302.